

The
University
Of
Sheffield.

**Experimental Investigation and Mechanistic
Understanding of Granule Internal Microstructure
of Heterogeneous-Wetting Powder Blends**

The University of Sheffield

Faculty of Engineering

Department of Chemical and Biological Engineering

By

Duaa Khalid Ahmed Al-aaraj

Supervisors: Rachel Smith and Alan Dunbar

A thesis submitted to The University of Sheffield in partial fulfilment of the
requirement for the degree of Doctor of Philosophy

August 2020

Abstract

Research into the mechanisms of formation of granules produced from heterogeneous-wetting powder blends is still at an early stage. Granulation of non-wetting powders is a common problem in pharmaceutical applications. The discovery of liquid marbles by the spreading of non-wetting powder over a liquid droplet is a promising way to solve the wettability problem of non-wetting powder. Hollow granules are formed upon drying of liquid marbles. In this work experimental investigations using different formulation and process parameters were designed to understand the mechanism of liquid marble and hollow granule formation. This work has helped to produce a qualitative and semi-quantitative prediction of internal microstructure behaviour of new formulations from fundamental properties. This research investigated the required conditions to form stable, spherical, hollow granules that form from liquid marbles in the nucleation stage.

Wetting and non-wetting model powder mixtures (glass beads silanised to give different wetting properties) with different types and viscosities of liquid binder (polyethylene glycol) were used. Nucleation experiments were performed outside the mixer where drops of liquid binder were placed on a powder bed. Different mixing time, primary particle size and shearing forces were investigated. Different granule size and internal microstructure were produced using different formulation and process parameters. Studies concluded that the binder viscosity and shearing force are critical factors in producing spherical hollow granules.

Mixtures of wetting and non-wetting pharmaceutical powder (red iron oxide/efavirenz) were granulated with different concentrations of liquid binder (dextran). Different operational conditions were applied by changing mixing time and shearing forces. Granule size, morphology, internal microstructure and ingredients distribution inside the granules were identified. The effect of binder viscosity and shearing forces were found to be essential parameters in controlling granule size, internal microstructure and ingredient distribution.

Two novel regime maps were developed. A mechanistic understanding of internal microstructure of granules produced using wettable powders (contact angle $< 90^\circ$) was proposed. It was found that solid granule internal structure is produced with a decrease of the immersion time of powder particles into the liquid droplet. The immersion time of low wettability particles (contact angle $> 90^\circ$) into the liquid droplet is infinite, and the only way the particles can move through the droplet surface is by high impact forces. Therefore, for the

first time, a mechanistic understanding of internal microstructure behaviour of granules produced using low wettability powders is introduced. A hollow granule internal microstructure was produced with decrease inertial force, which led to decrease in the immersion rate of powder particles inside the liquid droplet.

This research has established that longer immersion time and lower level of inertial forces applied are successful in producing hollow granules. This is expected to facilitate progress in creating hollow granules as both products and precursors for a wide range of structured powder-liquid products in the pharmaceutical, detergents, food and other advanced materials industries.

Acknowledgments

I would like to thank my supervisor Dr. Rachel Smith, for all her kind guidance, help and support during my research project. Rachel has shown enthusiasm, direction and assistance for which I am really thankful. My thanks also extend to my industrial supervisor Dr. Leon Farber, for his kind guidance and support throughout my research study at MSD, and beyond. Many thanks to Dr. Michael Gentzler, who has contributed toward my understanding and thought. I would also like to express gratitude to my second supervisor Dr. Alan Dunbar, for his advice on my doctoral development program. Many thanks go to Dr. Kate Pitt whose feedback on my writing has been invaluable, and Dr. Omid Tash, who put me in the right direction to develop the regime maps.

Thanks must also go to the fabulous members of particle Technology Group. Thank you for all your support, for your feedback, for providing a great working environment, and for all the wonderful activities we have did. Thanks also extend to staff at the Formulation department of MSD for their kindness and support. Special thanks go to Victoria Kitching for giving feedback on my thesis. I would also like to thank the awesome technical staff at the University of Sheffield.

I am grateful to the Higher Committee for Education Development in Iraq for providing the funding of my study.

Finally, but most importantly, my deepest gratitude also goes to my mother, husband, sister and to my children for their moral support and love.

List of contents

Abstract.....	i
Acknowledgments	iii
List of contents	v
List of Figures.....	xi
List of Tables	xvii
Nomenclature	xix
CHAPTER 1. Introduction	1
1.1 Research Background.....	2
1.1.1 Granulation	2
1.2 Thesis objectives	3
1.3 Thesis outline	4
CHAPTER 2. Literature review	7
2.1 Introduction	8
2.2 Application.....	9
2.3 Granulation techniques	9
2.4 Granulation equipment	11
2.4.1 Tumbling drum granulator.....	11
2.4.2 High shear mixer	12
2.4.3 Fluidised bed granulator	13
2.4.4 Twin screw granulator	13
2.5 Granulation processes (wet granulation).....	14
2.5.1 Wetting, nucleation and binder distribution	15
2.5.2 Consolidation and Growth.....	20
2.5.2.1 Consolidation	20
2.5.2.2 Granule growth	21
2.5.2.2.1 Non-deformable particle systems	21
2.5.2.2.2 Deformable particle systems.....	22
2.5.2.2.3 Regime maps.....	24
2.5.3 Breakage and attrition.....	27
2.6 Granulation of non-wetting powder: theory and mechanism.....	27
2.7 Powder wettability-Theory.....	30
2.7.1 Methods for determining the wettability of powder	34
2.8 Characterisation and uses of liquid marbles	36
2.9 Liquid marbles in granulation	40
2.9.1 Regime maps	47
2.10 Conclusions and thesis objectives	52
CHAPTER 3. Materials and Methods	55
3.1 Introduction	56
3.2 Characterisation methods.....	56
3.2.1 Particle size distribution	57
3.2.1.1 Laser diffraction.....	57

3.2.1.2 Sieve analysis	59
3.2.2 Contact angle measurements	60
3.2.3 Interfacial tension measurements	62
3.2.4 Viscosity measurements	63
3.2.5 True density measurements	64
3.2.6 Liquid density measurements	65
3.2.7 Liquid droplet size measurements	65
3.2.8 Scanning electron microscopy and energy dispersive X-ray spectroscopy for morphological analysis and elemental composition	66
3.2.9 X-ray computed tomography for internal structural analysis	67
3.3 Powders	69
3.3.1 Glass beads	71
3.3.1.1 Hydrophobisation of glass beads powder	72
3.3.2 Efavirenz	73
3.3.3 Red iron oxide	73
3.4 Liquids	74
3.4.1 Aqueous polyethylene glycol solutions	74
3.4.2 Aqueous dextran 70000 solutions	76
3.5 Powder-binder systems	77
3.6 Methods	80
3.6.1 Pre-nucleation experiments	80
3.6.2 Granulation of model particles in a low shear mixer	83
3.6.3 Granulation of model particles in a high shear mixer	85
3.6.4 Granulation of pharmaceutical powder	87
CHAPTER 4. Granulation of model particles in a low shear mixer	91
4.1 Introduction	92
4.2 Materials and Methods	93
4.3 Results and discussion	96
4.3.1 The effect of binder viscosity and powder wettability	98
4.3.1.1 Granule size distribution	98
4.3.1.1.1 Low powder wettability	98
4.3.1.1.2 Medium powder wettability	100
4.3.1.1.3 High powder wettability	102
4.3.1.2 Internal structural analysis	105
4.3.1.2.1 Porosity	107
4.3.2 The effect of tumbling speed and powder wettability	108
4.3.2.1 Granule size distribution	109
4.3.2.2 Internal structural analysis	111
4.3.2.2.1 Porosity	113
4.3.3 The effect of powder particle size and wettability	114
4.3.3.1 Granule size distribution	115
4.3.3.1.1 Low powder wettability	115
4.3.3.1.2 Medium powder wettability	117
4.3.3.1.3 High powder wettability	119
4.3.3.2 Internal structural analysis	121

4.3.3.2.1 Porosity	122
4.3.4 The effect of mixing time	124
4.3.4.1 Granule size distribution	124
4.3.4.2 Internal structural analysis	126
4.3.4.2.1 Porosity	128
4.5 Summary and further discussion.....	130
4.5.1 Effect of binder viscosity on granule size	130
4.5.2 Effect of primary particle size on granule size	131
4.5.3 Effect of mixing time on granule size	133
4.5.4 Effect of binder viscosity and primary particle size on granule porosity	133
4.6 Conclusions	134
CHAPTER 5. Granulation of model particles in a high shear mixer	137
5.1 Introduction	138
5.2 Materials and Methods	139
5.3 Results and Discussion	142
5.3.1 The effect of impeller speed and powder wettability	143
5.3.1.1 Granule size distribution	143
5.3.1.1.1 Low powder wettability	143
5.3.1.1.2 Medium powder wettability	145
5.3.1.1.2 High powder wettability	147
5.3.1.2 Internal structural analysis	149
5.3.1.2.1 Porosity	152
5.3.2 The effect of impeller design and powder wettability	153
5.3.2.1 Granule size distribution	153
5.3.2.1.1 Low powder wettability	154
5.3.2.1.2 Medium powder wettability	155
5.3.2.1.3 High powder wettability	157
5.3.2.2 Internal structural analysis	159
5.3.2.2.1 Porosity	161
5.3.3 The effect of powder wettability	162
5.3.3.1 Granule size distribution	163
5.3.3.1.1 Flat plate impeller	163
5.3.3.1.2 2-Bladed impeller.....	165
5.3.3.1.3 3-Bladed impeller.....	167
5.3.3.2 Internal microstructural analysis	168
5.3.3.2.1 Porosity	170
5.4 Summary and further discussion.....	171
5.5.1 The effect impeller speed on granule size and internal structure	171
5.5.2 Effect of impeller design on granule size	172
5.5.3 Effect of powder wettability	173
5.5.4 Effect of impeller speed and powder wettability on granule porosity	174
5.5 Conclusions	175

CHAPTER 6. Granulation of pharmaceutical powder	177
6.1 Introduction	178
6.2 Materials and Methods	179
6.3 Results and Discussion	184
6.3.1 Analysis of the powder blends.....	186
6.3.2 Single drop nucleation	191
6.3.2.1 Internal structural analysis	194
6.3.3 Granulation in a low shear mixer	197
6.3.3.1 Internal structural analysis	200
6.3.3.1.1 XRCT analysis	200
6.3.3.1.1.1 Porosity	202
6.3.3.1.1.2 SEM analysis	204
6.3.3.1.2.1 EDX analysis	205
6.3.4 Granulation as a function of time	212
6.3.4.1 Internal structural analysis	215
6.3.4.1.1 XRCT analysis	215
6.3.4.1.2 SEM analysis	218
6.3.5 Granulation in a high shear mixer	221
6.3.5.1 Internal structural analysis	224
6.3.5.1.1 XRCT analysis	225
6.3.5.1.2 SEM analysis	228
6.4 Summary and further discussion.....	233
6.4.1 Effect of binder viscosity and shear forces on granule size and shape.....	233
6.4.2 Effect of binder viscosity on intra-granular materials distribution.....	235
6.4.3 Formation of hollow granules.....	236
6.5 Conclusions	237
 CHAPTER 7. Mechanistic behaviour of internal granules microstructure.....	 239
7.1 Introduction	240
7.2 Granule kinetic behaviour using powder of medium and high wettability	241
7.2.1 Background.....	241
7.2.3 Kinetic analysis: Theory	242
7.2.4 Regime maps of granule behaviour of medium and high powder wettabilities	244
7.3 Granule kinetic behaviour using low powder wettability	251
7.3.1 Background.....	252
7.3.2 Kinetic analysis: Theory	253
7.3.3 Regime maps of granule behaviour of low powder wettability.....	257
7.4 Conclusions	263
 CHAPTER 8. Conclusions and recommendations	 265
8.1 Introduction	266
8.2 Conclusions	266
8.3 Recommendation for future work	269

Appendix.....	271
Appendix A.1: The volume moment mean diameter d43 (µm) of all granules produced in Chapter 4:	272
A.1.1 The effect of binder viscosity and powder wettability	272
A.1.2 The effect of powder particle size and wettability.....	274
A.1.3 The effect of mixing time	276
Appendix A.2: XRCT cross sectional images	277
A.2.1: Effect of binder viscosity and powder wettability.....	277
A.2.2: Effect of tumbling speed and powder wettability.....	292
A.2.3: Effect of powder particle size and powder wettability	297
A.2.4: Effect of mixing time.....	306
Appendix B.1: the volume moment mean diameter d43 (µm) of all granules produced in Chapter 5:	311
B.1.1 The effect of impeller speed and powder wettability.....	311
B.1.2 The effect of impeller design and powder wettability	313
Appendix B.2: XRCT-3D images.....	315
B.2.1. Effect of impeller speed and powder wettability	315
B.2.2 Effect of impeller design and powder wettability.....	326
References.....	331

List of Figures

Figure 2.1: Schematic of an example of a high shear granulator with a vertical axis shaft. ...	13
Figure 2.2: Components of a typical screw granulation.	14
Figure 2.3: Modern approach on wet granulation processes.	15
Figure 2.4: Nucleation mechanism, a: distribution b: immersion.....	16
Figure 2.5: Schematic diagram of tunnelling mechanism.	17
Figure 2.6: Schematic diagram of crater formation mechanism.....	17
Figure 2.7: Schematic diagram of spreading mechanism.	18
Figure 2.8: Nucleation regime map developed by Hapgood et al.....	19
Figure 2.9: Coalescence regime map in terms of deformation stokes number and viscous stokes number (Liu et al. 2000).	23
Figure 2.10: Proposed growth regime map by Iveson and Litster 1998.....	25
Figure 2.11: Contact angle on a powder surface.....	31
Figure 2.12: Schematic of advancing and receding contact angles.	32
Figure 2.13: (a) Cassie-Baxter (b) Wenzel models for wettability states.....	33
Figure 2.14: Liquid marbles of a mixture of 75% salicylic acid and 25% microcrystalline cellulose with 5 % polyethylene glycol 200.	36
Figure 2.15: Phase inversion of foams (air in water) to liquid marbles (water in air).....	39
Figure 2.16: SEM images of granules produced at 70 % and 78 % liquid/solid ratio and at 1 and 7 minutes mixing time.....	42
Figure 2.17: XRCT images of granules produced at different mixing times.....	43
Figure 2.18: Granule size and morphology as a function of increasing amount of salicylic acid (non-wetting) powder.....	45
Figure 2.19: Hollow granules formed at 100 °C from Aerosil R974 and (a) 12% HPMC, and (b) 18% HPMC.	46
Figure 2.20: Regime map for liquid marble formation.....	48
Figure 2.21: Verified regime map for liquid marble formation.....	49
Figure 2.22: Schematic chart for the formation of liquid marbles by a droplet template regime.	51
Figure 3.1: Principle of laser diffraction (Malvern Instrument handbook).	58
Figure 3.2: Contact angle measurement by goniometer.	62
Figure 3.3: Rheometer for measuring viscosity.....	64
Figure 3.4: SEM images of all powders used in this study.....	70
Figure 3.5: Particle size distribution of glass beads obtained via laser diffraction.....	71
Figure 3.6: Preparation of the non-wetting glass beads.....	72
Figure 3.7: Viscosities of PEGs solutions as a function of shear rate in the range between 1-300 s ⁻¹	75
Figure 3.8: Viscosities of PEGs solutions as a function of shear rate the same as Figure 3.7 but in range between 1-16 s ⁻¹	75
Figure 3.9: Viscosities of 10%, 30% and 50% dextran solutions as a function of shear rate..	76
Figure 3.10: Viscosities of 10%, 30% and 50% dextran solutions as a function of shear rate the same as Figure 3.9 but in the range between 1-12 s ⁻¹	77
Figure 3.11: Microscope images of 60%-40% Efavirenz-IROX with 50% dextran solution. The contact angle is stable over the time of the measurements.	79
Figure 3.12: schematic diagram of liquid marble formation.	80
Figure 3.13: Schematic diagram of immersion nuclei formation (Hapgood, Litster and Smith, 2003).	81
Figure 3.14: Tumbling drum granulation procedure.....	84

Figure 3.15: High shear mixer.	86
Figure 3.16: Impeller designs.	87
Figure 4.1: Particle size distribution of granules produced using low powder wettability and different binder viscosities, obtained via sieve analysis. Error bars are the standard deviation of three measurements.	99
Figure 4.2: Comparison of granules produced using low powder wettability and different binder viscosities.	100
Figure 4.3: Particle size distribution of granules produced using medium powder wettability and different binder viscosities, obtained via sieve analysis. Error bars are the standard deviation of three measurements.	101
Figure 4.4: Comparison of granules produced using medium powder wettability and different binder viscosities.	102
Figure 4.5: Particle size distribution of granules produced using high powder wettability and different binder viscosities, obtained via sieve analysis. Error bars are the standard deviation three measurements.	103
Figure 4.6: Comparison of granules produced using high powder wettability and different binder viscosities.	104
Figure 4.7: Images of granules produced using different powder wettabilities and binder viscosities. The outer rings are part of the sample container. (Reconstructed XRCT images; representative central cross-section).	106
Figure 4.8: Wall thickness as a function of binder viscosity and powder wettability. Error bars are the standard deviation of three measurements. Θ is liquid powder contact angle.	107
Figure 4.9: Total porosity as a function of binder viscosity and powder wettability. Error bars are the standard deviation of three measurements.	108
Figure 4.10: Particle size distributions of granules produced using low powder wettability and different tumbling speeds, obtained via sieve analysis. Error bars are the standard deviation of two or three measurements.	109
Figure 4.11: Particle size distributions of granules produced using medium powder wettability and different tumbling speeds, obtained via sieve analysis. Error bars are the standard deviation of two or three measurements.	110
Figure 4.12: Particle size distributions of granules produced using high powder wettability and different tumbling speeds, obtained via sieve analysis. Error bars are the standard deviation of two or three measurements.	111
Figure 4.13: Images of granules produced using different powder wettabilities and tumbling speeds. The outer rings are part of the sample container. (Reconstructed XRCT images; representative central cross-section).	112
Figure 4.14: Wall thickness as a function of tumbling speed and powder wettability. Error bars are the standard deviation of three measurements.	113
Figure 4.15: Total porosity as a function of tumbling speed and powder wettability Error bars are the standard deviation of three measurements.	114
Figure 4.16: Particle size distributions of granules produced using low powder wettability and different powder particles size, obtained via sieve analysis. Error bars are the standard deviation of two or three measurements.	116
Figure 4.17: Image comparison of granules produced using low powder wettability and different powder particle sizes.	117
Figure 4.18: Particle size distributions of granules produced using medium powder wettability and different powder particle sizes, obtained via sieve analysis. Error bars are the standard deviation of two or three measurements.	118
Figure 4.19: Comparison of granules produced using medium powder wettability and different powder particle size.	119

Figure 4.20: Particle size distributions of granules produced using high powder wettability and different powder particle size, obtained via sieve analysis. Error bars are the standard deviation of two or three measurements.	120
Figure 4.21: Image comparison of granules produced using high powder wettability and different powder particles size.	121
Figure 4.22: Images of granules produced using different powder wettabilities and primary particles size. The outer rings are part of the sample container. (Reconstructed XRCT images; representative central cross-section).	122
Figure 4.23: Total porosity as a function of powder particle size and powder wettability. Error bars are the standard deviation of three measurements.	123
Figure 4.24: Particle size distributions of granules produced using low powder wettability and different mixing times, obtained via sieve analysis.	125
Figure 4.25: Image comparison of granules produced using low powder wettability and different mixing times.	126
Figure 4.26: Images of granules produced using low powder wettability and different mixing times. The outer rings are part of the sample container. (Reconstructed XRCT images; representative central cross-section).	127
Figure 4.27: Wall thickness as a function of mixing time. Error bars are the standard deviation of three measurements.	128
Figure 4.28: Total porosity as a function of mixing time. Error bars are the standard deviation of three measurements.	129
Figure 5.1: Images of granules produced from different powder wettabilities and 700 rpm impeller speed.	141
Figure 5.2: Images of flakes produced from 100%-0% non wetting –wetting powders and at 150 rpm impeller speed.	141
Figure 5.3: Particle size distribution of granules produced using low powder wettability and different impeller speeds, obtained via sieve analysis. Error bars are the standard deviation of two or three measurements.	144
Figure 5.4: Comparison of granules using low powder wettability and different impeller speeds.	145
Figure 5.5: Particle size distribution of granules produced using medium powder wettability and different impeller speeds, obtained via sieve analysis. Error bars are the standard deviation of two or three measurements.	146
Figure 5.6: Comparison of granules using medium powder wettability and different impeller speeds.	147
Figure 5.7: Particle size distribution of granules produced using high powder wettability and different impeller speeds, obtained via sieve analysis. Error bars are the standard deviation of two or three measurements.	148
Figure 5.8: Comparison of granules using high powder wettability and different impeller speeds.	148
Figure 5.9: Images of granules produced using different powder wettabilities and impeller speeds. The outer rings are part of the sample container. (Reconstructed XRCT images; representative central cross-section).	150
Figure 5.10: Wall thickness as a function of impeller speed and powder wettability. Error bars are the standard deviation of three measurements. θ is liquid powder contact angle.	151
Figure 5.11: Total porosity as a function of impeller speed and powder wettability. Error bars are the standard deviation of three measurements. θ is liquid powder contact angle.	152
Figure 5.12: Particle size distribution of granules produced using low powder wettability and different impeller designs, obtained via sieve analysis. Error bars are the standard deviation of three measurements.	154

Figure 5.13: Comparison of granules using low powder wettability and different impeller designs.....	155
Figure 5.14: Particle size distribution of granules produced using medium powder wettability and different impeller designs, obtained via sieve analysis. Error bars are the standard deviation of three measurements.	156
Figure 5.15: Comparison of granules using medium powder wettability and different impeller designs.....	157
Figure 5.16: Particle size distribution of granules produced using high powder wettability and different impeller designs, obtained via sieve analysis. Error bars are the standard deviation of three measurements.....	158
Figure 5.17: Comparison of granules using high powder wettability and different impeller designs.....	158
Figure 5.18: Images of granules produced using different powder wettabilities and impeller designs. The outer rings are part of the sample container. (Reconstructed XRCT images; representative central cross-section).	160
Figure 5.19: Wall thickness as a function of impeller design and powder wettability. Error bars are the standard deviation of three measurements. θ is liquid powder contact angle.	161
Figure 5.20: Total porosity as a function of impeller design and powder wettability. Error bars are the standard deviation of three measurements. θ is liquid powder contact angle.	162
Figure 5.21: Particle size distribution of granules produced using the flat plate impeller and different powder wettabilities, obtained via sieve analysis. Error bars are the standard deviation of three measurements.	164
Figure 5.22: Comparison of granules using the flat plate impeller and different powder wettabilities.....	165
Figure 5.23: Particle size distribution of granules produced using the 2-bladed impeller and different powder wettabilities, obtained via sieve analysis. Error bars are the standard deviation of three measurements. θ is liquid powder contact angle.	166
Figure 5.24: Comparison of granules using the 2-bladed impeller and different powder wettabilities.....	166
Figure 5.25: Particle size distribution of granules produced using the 3-bladed impeller and different powder wettabilities, obtained via sieve analysis. Error bars are the standard deviation of three measurements. θ is liquid powder contact angle.	167
Figure 5.26: Comparison of granules using the 3- bladed impeller and different powder wettabilities.....	168
Figure 5.27: Images of granules produced using different powder wettabilities and impeller designs. The outer rings are part of the sample container. (Reconstructed XRCT images; representative central cross-section).	169
Figure 6.1: Mixing time of the dry mixture using the high shear mixer.....	180
Figure 6.2: Calibration curve of droplet diameter and binder concentration.....	186
Figure 6.3: SEM images of efavirenz and IROX and the different blends of the two ingredients; (a) efavirenz, (b) Red iron Oxide (IROX), (c) 60% Efavirenz-40% IROX, (d) 50% Efavirenz-50% IROX, (e) 30% Efavirenz-70% IROX.....	188
Figure 6.4: SEM images of compressed mixtures of (a) 60%-40% efavirenz-IROX, (b) 50%-50% efavirenz-IROX, (c) 30%-70% efavirenz-IROX.....	189
Figure 6.5: Images of primary blends of efavirenz-IROX in different ratios (a) 60%-40%, (b) 50%-50%, (c) 30%-70%. (Reconstructed XRCT images; representative central cross-section).	190
Figure 6.6: Particle size of dried liquid marbles or immersion nuclei of different powder wettabilities and binder viscosities, obtained via image analysis. The error bars are the standard deviation of the ten measurements. θ is liquid powder contact angle.....	191

Figure 6.7: Comparison of dried liquid marbles or immersion nuclei of different powder wettabilities and binder viscosities.	192
Figure 6.8: Images of dried liquid marbles or immersion nuclei of different powder wettabilities and binder viscosities. (Reconstructed XRCT images; representative central cross-section).	195
Figure 6.9: Images of immersion nuclei of powder of high wettability and low binder viscosity (a) wet immersion nuclei (b) dry immersion nuclei. (Reconstructed XRCT images, representative central cross-section).	196
Figure 6.10: Images of a liquid marble of powder of low wettability and high binder viscosity (a) wet liquid marble (b) after drying for 2 hr (c) after drying for 14 hr. (Reconstructed XRCT images; representative central cross-section).....	196
Figure 6.11: Particle size of granules produced using different powder wettabilities and binder viscosities, obtained via image analysis. The error bars are the standard deviation of the ten measurements. θ is liquid powder contact angle.....	197
Figure 6.12: Comparison of granules of different powder wettabilities and binder viscosities.	198
Figure 6.13: Images of granules of different wettabilities and different binder viscosities. The outer rings are part of the sample container. (Reconstructed XRCT images; representative central cross-section).	202
Figure 6.14: Total porosity as a function of binder viscosity and powder wettability. The error bars are the standard deviation of three measurements. θ is liquid powder contact angle. ...	203
Figure 6.15: SEM images of granules produced using different powder wettabilities and different binder viscosities.	205
Figure 6.16: Compositional analysis of granules produced using low powder wettability and different binder viscosities.	206
Figure 6.17: Compositional analysis of granules produced from medium powder wettability and different binder viscosities.	208
Figure 6.18: Compositional analysis of granules produced from high powder wettability and low binder viscosity.	210
Figure 6.19: Granule size of medium powder wettability and higher binder viscosity as a function of time, obtained via image analysis. The error bars are the standard deviation of the ten measurements.	213
Figure 6.20: Comparison of granules produced using medium powder wettability and different mixing times.....	214
Figure 6.21: Images of granules produced using medium powder wettability and different mixing times. The outer rings are part of the sample container. (Reconstructed XRCT images; representative central cross-section).	216
Figure 6.22: Total porosity as a function of mixing time. The error bars are the standard deviation of three measurements. θ is liquid powder contact angle.	217
Figure 6.23: SEM images of granules produced using medium powder wettability and different mixing times.....	218
Figure 6.24: Compositional analysis of granules produced using medium powder wettability and high binder viscosity at two different mixing times.....	219
Figure 6.25: Granule size of different powder wettabilities and binder viscosities obtained via image analysis. The error bars are the standard deviation of the ten measurements. θ is liquid powder contact angle.	222
Figure 6.26: Comparison of granules produced using different powder wettabilities and binder viscosities in a high shear.	223

Figure 6.27: Images of granules produced using different powder wettabilities and binder viscosities in a high shear mixer. (Reconstructed XRCT images; representative central cross-section).....	226
Figure 6.28: Total porosity as a function of powder wettability, binder viscosity and shear force. The error bars are the standard deviation of three measurements. θ is liquid powder contact angle.....	227
Figure 6.29: Comparison of SEM images of granules of produced using different powder wettabilities and binder viscosities in a high shear mixer.....	229
Figure 6.30: Compositional analysis of granules produced from low powder wettability and high binder viscosity using the high shear mixer.....	230
Figure 6.31: Compositional analysis of granules produced from medium powder wettability and medium binder viscosity using a high shear mixer.....	231
Figure 6.32: Compositional analysis of granules produced from high powder wettability and high binder viscosity using a high shear.....	232
Figure 7.1: Regime map of granule internal microstructure in terms of contact angle and St_v in low shear mixer.....	249
Figure 7.2: Regime map of granule internal microstructure in terms of contact angle and St_v in high shear mixer.....	251
Figure 7.3: Images of video sequence of the water entry of a hydrophobic sphere.....	256
Figure 7.4: Regime map of granule internal microstructure in low shear mixer.....	260
Figure 7.5: Regime map of granule internal microstructure in a high shear mixer.....	261
Figure A.1.1: Granules volume moment mean diameter (d_{43}) produced using different binder viscosity and powder wettability.....	273
Figure A.1.2: Granules volume moment mean diameter (d_{43}) produced using different powder particle size and powder wettability.....	275
Figure A.1.3: Granules volume moment mean diameter (d_{43}) produced using different mixing time and low powder wettability.....	276
Figure B.1.1: The volume moment mean diameter (d_{43}) of granules produced using different impeller speed and powder wettability.....	312
Figure B.1.2: The volume moment mean diameter (d_{43}) of granules produced using different impeller speed and powder wettability.....	314

List of Tables

Table 2.1: Methods for determining the wettability of a powder.	35
Table 3.1: Summary of powder properties.	69
Table 3.2: Liquid properties; Standard deviation are shown as (\pm).	74
Table 3.3: Overview of powder-PEG systems used in this study.	78
Table 3.4: Overview of powder-dextran systems used in this study.	79
Table 3.5: Summary of pre-nucleation experiments.	82
Table 4.1: PEG binder viscosities and powder-binder systems used and their contact angles.	94
Table 4.2: Experimental design.	95
Table 4.3: Summary of pre-nucleation experiments.	96
Table 4.4: PEG liquid droplet properties.	97
Table 4.5: Froude number of low shear mixer.	97
Table 5.1: Binder viscosity, powder binder systems and contact angle of liquid on powder.	139
Table 5.2: Experimental design of different impeller speeds and designs.	140
Table 5.3: Summary of pre-nucleation experiments.	142
Table 5.4: Liquid droplet properties.	142
Table 5.5: Froude number data of high shear mixer using flat plate impeller.	143
Table 6.1: Binder viscosity and powder-binder systems and contact angles.	182
Table 6.2: Experimental design.	183
Table 6.3: Overview of powder liquid combinations and their contact angle.	184
Table 6.4: Summary of pre-nucleation experiments.	185
Table 6.5: Liquid droplet properties.	185
Table 6.6: Froude number data of low and high shear mixer.	186
Table 6.7: Compositional analysis of efavirenz, IROX, dextran and different mixtures of powder blends.	190
Table 6.8: Summary of % change in size of dried liquid marbles or immersion nuclei in relation to the size of initial liquid droplets.	193
Table 6.9: Summary of % change in size of granule in relation to size of initial liquid droplet.	199
Table 6.10: Elemental ratio comparisons in powder blends and granules produced using low powder wettability and different binder viscosities.	207
Table 6.11: Elemental ratio comparisons in powder blends and granules produced using medium powder wettability and different binder viscosities.	209
Table 6.12: Elemental ratio comparisons in powder blends and granules produced using high powder wettability and low binder viscosity.	211
Table 6.13: Summary of % change in size of granules in relation to size of initial liquid droplet.	215
Table 6.14: Elemental ratio comparisons in powder blends and granules produced using medium powder wettability and high binder viscosity and at different mixing times.	220
Table 6.15: Summary of % change in size of granules in relation to size of initial liquid droplet.	224
Table 6.16: Elemental ratio comparisons in powder blends and granules produced using low powder wettability in a high shear.	230
Table 6.17: Elemental ratio comparisons in powder blends and granules produced using medium powder wettability and medium binder viscosity in a high shear mixer.	231
Table 6.18: Elemental ratio comparisons in powder blends and granules produced using high powder wettability and high binder viscosity in a high shear.	232

Table 7.1: Six different model systems for wet granulation with different formulation and process parameters along with the calculated timescales and dimensionless numbers.	246
Table 7.2: Six different model systems for wet granulation of different formulation and process parameters along with the calculated viscous Stokes numbers.	247
Table 7.3: Three different model systems of granules produced using low powder wettability with different formulation and process parameters along with the calculated parameters and dimensionless numbers.	258
Table A.1.1: Granule size distribution, q_3 in each size fraction for granule produced using low powder wettability and different binder viscosity.....	272
Table A.1.2: Granule size distribution, q_3 in each size fraction for granule produced using medium powder wettability and different binder viscosity.	272
Table A.1.3: Granule size distribution, q_3 in each size fraction for granule produced using high powder wettability and different binder viscosity.	272
Table A.1.4: d_{43} of granules produced using different binder viscosity and powder wettability.	273
Table A.1.5: Granule size distribution, q_3 in each size fraction for granule produced using low powder wettability and different primary particle size.	274
Table A.1.6: Granule size distribution, q_3 in each size fraction for granule produced using medium powder wettability and different primary particle size.	274
Table A.1.7: Granule size distribution, q_3 in each size fraction for granule produced using high powder wettability and different primary particle size.	274
Table A.1.8: d_{43} of granules produced using different powder particle size and powder wettability.	275
Table A.1.9: Granule size distribution, q_3 in each size fraction for granule produced using low powder wettability and different mixing time..	276
Table A.1.10: d_{43} of granules produced using different mixing times and low powder wettability.	276
Table B.1.1: Granule size distribution, q_3 in each size fraction for granule produced using low powder wettability and different impeller speed.....	311
Table B.1.2: Granule size distribution, q_3 in each size fraction for granule produced using medium powder wettability and different impeller speed.	311
Table B.1.3: Granule size distribution, q_3 in each size fraction for granule produced using medium powder wettability and different impeller speed.	311
Table B.1.4: The volume moment mean diameter (d_{43}) of granules produced using different impeller speed and powder wettability.	312
Table B.1.5: Granule size distribution, q_3 in each size fraction for granule produced using low powder wettability and different impeller design.	313
Table B.1.6: Granule size distribution, q_3 in each size fraction for granule produced using medium powder wettability and different impeller design.	313
Table B.1.7: Granule size distribution, q_3 in each size fraction for granule produced using high powder wettability and different impeller design.	313
Table B.1.8: The volume moment mean diameter (d_{43}) of granules produced using different impeller speed and powder wettability.	314

Nomenclature

Uppercase symbols

Symbol	Definition	Quantity
A	Area that passes through spray zone per time unit	area/time
B	Bond number	-
D_d	Droplet diameter	length
D_g	Granule diameter	length
E_{imm}	Energy of particle immersion	energy
F	Force	force
G	Granule size change	-
G_{Nu}	Granulation number	-
H	Contact angle hysteresis	angle
L	Liquid	volume
L	Wetted length	length
N_c	Number of capillary	-
Q_3	Cumulative frequency distribution	volume
R	Pore radius	length
R_c	Radius of the capillary	length
R_d	Radius of the liquid droplet	length
Re	Reynolds number	-
R_p	Radius of the particle	length
S	solid	volume
St_{def}	Stokes deformation number	-
S_{max}	Maximum granule pore saturation	-
St_v	Viscous stokes number	-
St_v^*	Critical stokes number	-
U_c	Granule collisional velocity	velocity
V	Vapour	volume

V	Volumetric binder spray rate	volume/time
V_d	Droplet volume	volume
W	Weber number	-
W_d	Mass of the droplet	mass
Y_g	Dynamic yield stress	pressure
Z_{max}	Maximum depth	length
Z_{pinch}	Pinch off depth	length

Lowercase symbol

Symbol	Definition	Quantity
a	Mixer diameter	length
d_{10}	10 th volume percentile size	length
$d_{3,2}$	Surface area mean diameter	length
$d_{4,3}$	Volume moment mean diameter	length
d_{50}	50 th volume percentile size	length
d_{90}	90 th volume percentile size	length
e	Coefficient of restitution	-
f_1, f_2	Fraction of powder mixture	-
g	Acceleration gravity	velocity
h	Liquid layer thickness	length
h	Height of the apex	length
h_a	Distance between two granules	length
k	Amount of powder build up	mass/time
k	Consolidation rate constant	-
m_p	Mass of particle	mass
q_3	Volume frequency distribution volume	volume
t	Time	time

t_{coll}	Collision time	time
t_{imm}	Immersion time	time
t_{pinch}	Time at pinch off depth	time
u	Final particle velocity	velocity
u_o	Initial particle velocity	velocity
v	Representative collision velocity	velocity
v_p	Relative granule velocity	velocity
w	Liquid to solid ratio	-

Greek symbol

Symbol	Definition	Quantity
γ	Liquid surface tension	Force/length
γ_{LV}	Liquid vapour interfacial tension	Force/length
λ_{SL}	Solid liquid spreading coefficient	Force/length
γ_{SL}	Solid-liquid interfacial tension	Force/length
γ_{SV}	Solid vapour interfacial tension	Force/length
ε	porosity	-
ε_b	Bed porosity	-
ε_g	Granule porosity	-
ε_{min}	Minimum porosity	-
Fr	Froude number	-
ζ	Proportion of non-wetting powder	-
μ	Dynamic liquid viscosity	Pressure*time
σ	Interfacial tension	Force/length
σ_t	Granule static strength	Pressure

Symbol	definition	Quantity
σ_v	Granule dynamic strength	Pressure
ρ_g	Granule density	Density
ρ_l	Liquid density	Density
ρ_s	Solid density	Density
ρ_{true}	True density	Density
θ	Contact angle	-
θ_a	Advancing contact angle	Angle
θ_{ave}	Average contact angle	Angle
θ_r	Receding contact angle	Angle
θ_y	Young's contact angle	Angle
ϕ	Particle shape factor	-
ϕ_{cp}	Critical packing liquid volume fraction	Volume
ϕ_{pb}	Particle volume fraction	Volume
τ_p	Dimensionless penetration time	-
\ddot{u}	Particle acceleration velocity	Velocity
ω	Mixer velocity	Velocity
ψ_a	Dimensionless spray flux	-

Abbreviations

Abbreviation	Definition
API	Active pharmaceutical ingredients
C	Carbon
Cl	Chlorine
EDX	Energy dispersive X-ray spectroscopy
Fe	Ferrous
HIV	Human immunodeficiency virus

HPC	Hydroxy propyl cellulose
HPMC	Hydroxy propyl methyl cellulose
ILD	Initial liquid droplet
IROX	Red iron oxide
MCC	Microcrystalline cellulose
min	Minute
PEG	Polyethylene glycol
PTFE	Poly tetra floro ethylene
PVP	Polyvinyl pyrrolidone
rpm	Round per minute
SEM	Scanning electron microscopy
sec	Second
XRCT	X-ray computed tomography

CHAPTER 1. Introduction

1.1 Research Background

Granulation is the size enlargement of small particles by the addition of a liquid binder to agglomerate the particles. Granulation plays an important role in the pharmaceutical, food, cosmetics and detergent industries and has an important influence on the properties and quality of the products (Iveson et al. 2001).

Granulation of non-wetting powders is a common problem in the pharmaceutical industry, which compromises a uniform distribution of drugs during granulation. The effects of non-wetting powder in wet granulation has been investigated by some studies, including observing the initial formation and stability of liquid marbles, liquid marbles morphology, examining the driving force of liquid marbles formation, and looking at hydrophobic powder distribution for different ranges of formulation wettability (K.Hapgood et al. 2009; N.Eshtiaghi 2012; C. Williams et al. 2013; N. Eshtiaghi et al. 2009).

The granulation growth behaviour of pure hydrophilic powder is becoming established but an understanding of the effect of heterogeneous-wetting powders on the granule size and internal microstructure in low and high shear granulation remains relatively unknown, and this forms the motivation of this study.

1.1.1 Granulation

Granulation is used to reduce dusting, improve product handling, increase or decrease bulk density, improve dissolution or dispersion, and is used prior to tableting (Knight, 2001). These desired properties can be achieved by the design of particles with a suitable combination of formulation and process parameters that control the characteristics of products. Wet granulation in high shear mixers and tumbling drums are popular methods for the size enlargement processes because they permit the production of uniformly shaped granules with a high level of compaction (Parikh, 2005). High and low shear granulators are used for a wide range of applications in pharmaceuticals, agricultural chemicals and detergents. These granulators work by causing powder motion using a mechanical impeller while the liquid binder is sprayed from above onto the moving powder bed (Litster, Ennis, & Liu, 2004); (Parikh, 2005) and (Salman et al. 2007, chapter 1).

A great advance in understanding the granulation mechanism and controlling the granules size has been made (Iveson & Litster 1998). For a wetting powder, the distribution of the liquid binder occurs homogeneously under suitable conditions (Charles-Williams, Wegeler, et al. 2013). However, if the mixture contains a high percentage of non-wetting powder, for example in pharmaceutical industries, the problems then begin. To solve the wettability problems, a surfactant may be added. However, this is not always the case, as the surfactant may be either incompatible or too expensive to use (Hapgood and Khanmohammadi, 2008).

Many studies investigate the granulation of non-wetting powder. The nucleation of non-wetting powder involves spreading of the powder over the liquid droplets to form liquid marbles. Hollow granules are produced after drying of the liquid marbles (Aussillous et al. 2006).

Tablets with good pharmaceutical characteristics, such as active ingredient and excipient uniformity, compressibility and flowability, are usually a function of the granulation process rather than the tableting process. Hollow granules with their porous structure provide good compression properties and excellent dissolution rates due to thin wall thickness (Hapgood et al. 2009). It may be possible to control the size distribution and the internal structure of the granules by monitoring the shell thickness of the hollow granules.

1.2 Thesis objectives

The aim of this thesis is to provide a mechanistic understanding of the internal microstructure of hollow granules formed from heterogeneous-wetting components using low and high shear wet granulation. Therefore, it is essential to develop an experimental method to investigate the effect of different formulation and process parameters on granule internal structure and granule size. The thesis aim can be subdivided into:

- A literature study on granulation, granulation processes, and the effect of powder wettability on the granulation process to highlight the novelty and impact of this work.
- Development of an experimental method to study granule size and internal microstructure.
- Using the developed experimental method to study the effect of different powder-binder systems on granule size and internal microstructure using model powders and PEG solutions binder, including the following factors:

- a. The effect of binder viscosity
 - b. The effect of powder wettability
 - c. The effect of powder particle size
 - d. The effect of shear force applied
 - e. The effect of mixing time
- Applying the understanding from the above investigations into a study using real industrial pharmaceutical powders and verify their applicability.
 - Developing novel regime maps that explain the kinetic behaviour of the internal microstructure of the granules produced using different powder wettabilities, binder viscosities and the shear forces applied.

1.3 Thesis outline

Chapter 2 gives a summary of the up-to-date understanding of granulation, which is relevant to this work. The review starts with an introduction to the general granulation process and then proceeds to focus on the phenomena of liquid marbles. The different parameters affecting the formation and stability of liquid marbles and hollow granules is reviewed. Finally, an insight into the different mechanisms controlling the growth of granules is presented.

Chapter 3 describes the properties of the raw materials used in this project, such as determination of their size distribution, density and powder-liquid contact angle. In addition, the set up for different equipment used to characterise the granules along with details of the granulation experiments is explained.

Chapter 4 describes the results obtained from low shear granulation experiments and discusses the effect of binder viscosity, powder wettability, mixing time and primary particle size on granule size and internal microstructure using model powder blends of various wettability. The aim is to investigate which condition result in formation of large hollow granules and explain the granule size behaviour for a range of powder wettabilities.

Chapter 5 describes the results obtained from high shear granulation experiments and discusses the effect of shear forces on granule size and internal microstructure on model

powder blends with different wettability. The level of shear force is determined to produce spherical hollow granules and investigate the granule size behaviour using different shear force and powder wettability.

Chapter 6 applies all the understanding and results from Chapters 4 and 5 into industrial pharmaceutical powder. Low and high shear granulation is used to verify the applicability of this work. This work was performed by the author of this thesis at MSD, PA, USA.

Chapter 7 contains details of novel regime maps developed to understand the mechanistic behaviour of internal microstructure formation of granules produced using different formulation and process parameters.

Chapter 8 summarises the results of the effect of different parameters on granule size and internal microstructure for a range of powder wettabilities. The overarching trends and themes are described and explained. A theoretical concept is described and the contribution of this work to the field of pharmaceutical granulation. Finally, recommendations for further research in this field are proposed.

CHAPTER 2. Literature review

2.1 Introduction

Granulation/agglomeration is the process in which small particles combine into a larger semi-permanent aggregate while the small particles are still distinguishable (Iveson et al. 2001). This process can occur by either wet or dry granulation methods. During wet granulation, liquid binders are sprayed onto powder particles and act as a linking material. This can be carried out by granulating in a tumbling drum (low shear), high shear, twin screw granulator or similar device. Dry granulation can also be used to produce granules by pressurization or by the cohesive characteristics of the material itself (Kumar et al. 2014; Tu et al. 2013). After the granulation process, the obtained granules can be used as an intermediate step process in the manufacture of the solid dosage form such as tablets and capsules (Yu et al. 2014).

There are many advantages of using granules instead of powder during production processes in many industries. It reduces dusting, caking, explosion, lump formation and powder losses. Granulation is used to increase bulk density, control dissolution, porosity and improve powder handling and metering. Furthermore, it improves product appearance and flowability and decreases segregation of powder blend ingredients. The latter is very important in tablet pharmaceutical manufacturing (Litster, Ennis, & Liu, 2004).

Despite many years of research, granulation has been more of an art rather than being based on science. More recently, there have been improvements in the understanding of the granulation process (Salman et al. 2007, Chapter 20). However, further experiments are still necessary to determine and predict which conditions result in granules with desired properties (Litster, Ennis, & Liu, 2004)

Here, a review of the basic considerations for a granulation process are described, with a focus on low and high shear wet granulation. The principles of granulation equipment are presented. Next, the current understanding of the mechanisms involved in the granulation process are presented. Finally, literature studies of granulation with a range of powder wettabilities and liquid marble formation are discussed. An understanding of the effect of heterogeneous-wetting components on the granule size and internal-microstructure in low and high shear granulation remains relatively unknown, and this forms the motivation of this study.

2.2 Application

In the pharmaceutical industry, it has been reported that 60% of products are synthesised as granules, and an additional 20% use powders as constituents. Granulation is also an essential and widely adopted process varying from pharmaceutical, food, detergent, catalyst manufacturing and agricultural chemical and minerals processing (Iveson et al, 1998). Some advantages that granulation provides are listed below:

- Improved flow properties:

It is very important for the homogeneous distribution of the particles and content uniformity of the drug in pharmaceutical manufacturing when using granulation as an intermediate step in tableting (Chang et al. 2014).

- Product design:

The granule properties such as surface area, hardness, bulk density, morphology, size distribution, etc. can be modified, achieving the desired manufacturing requirement with appropriate granulation equipment. It can improve medicines in terms of dissolution characteristics, release rates, or even taste can be controlled (Tu et al. 2009).

- Reducing dust:

Dust can cause many problems ranging from inhalation to the mass distribution, wastage of the ingredients and even dust explosion risk (Rhodes, 1998).

However, the granulation process is not without drawbacks. The main disadvantage is that the production process is relatively complex, and even with the knowledge of all the variables during this process, it is still impossible to predict the behaviour of the granules in an accurate way.

2.3 Granulation techniques

In the pharmaceutical industry, three types of granulation technology are employed: wet, dry and melt granulation. The use of this technology depends on physicochemical properties such as water and heat lability, melting point and glass transition temperature of the active pharmaceutical ingredient (API) in the formulation (Lackman & Liebermann, 2013).

During wet granulation, the liquid binders or adhesives are added to the excipient and active mixture, usually by agitating. The mixture is then dried, sized and compressed into tablets. The most common equipment used are high shear mixers, twin screw extruders and fluidised bed granulators. Some active pharmaceutical ingredients show moisture and heat sensitivity that can be problematic during wet granulation. Therefore, an alternative method needs to be used (Aulton, 2007).

In the dry granulation process, the powder mixture is compressed without the use of heat and liquid and is, therefore, suitable for ingredients that are heat and moisture sensitive. There are two basic intermediate procedures; the formation of large tablets where the powder is precompressed, in the process known as slugging. The other method is to precompress the powder with pressure rollers to produce a sheet or flakes by a process called roller compaction (Lackman & Liebermann, 2013). In both cases, the intermediate product is broken to produce granules using milling equipment. Then, these granules are sieved to separate the desired size fraction. Fines, friable and poorly compressible granules are produced using this method, which can be overcome by recycling the unused fine product to avoid waste.

Hot melt granulation methods are used for moisture sensitive drug formulations. During the process, the temperature stays below the melting point of the active ingredient but above the glass transition temperature of the binder. The powder mixture consists of low-melting binders, which typically melt or soften at relatively low temperatures (50-80°C) (Weatherley et al. 2013). Either the agglomerates are formed from the molten material in a powder mixture when the temperature decreases or the water of crystallization released from the powder bed acts as a binding agent.

Hot-melt extrusion (HME) is a continuous process that makes it useful in pharmaceutical formulations, which helps to decrease the number of manufacturing steps. It is primarily employed to improve the bioavailability of poorly soluble substances, but also shows a considerable benefit for different usages such as controlled release formulations and targeted drug delivery including taste masking systems (Pimparade et al. 2015). Twin screw extruders, high shear mixers and fluidized bed granulators can be used for melt granulation (Patil et al. 2015).

2.4 Granulation equipment

There are different types of granulation equipment, each of which has advantages and disadvantages. Four different wet granulation techniques are discussed in this chapter:

- Tumbling drum granulator
- High shear mixer granulator
- Fluidised bed granulator
- Twin screw granulator

2.4.1 Tumbling drum granulator

Tumbling drum granulation is a wet granulation process that granulates fine powders into large agglomerates using a cylindrical rotating drum in the presence of liquid binder (Walker et al. 2000). The granules in the tumbling granulator grow by layering or by crushing in which the granules abrade but still have sufficient energy to coalesce with other granules without breakage (Knight et al. 2000).

There are many types of tumbling granulator including rotating drums, pans and discs. In tumbling granulators, motion is imparted to the particles by tumbling action. Liquid binder can be added by a spray nozzle and a scraper is used to prevent build-up of powder on the tumbling wall. These types of granulator are used in the fertiliser and minerals industries and in particle coating (Litster, Ennis, & Liu, 2004).

Granule size produced from tumbling drums is in the range of 2-20 mm, and these granulators are not suitable to produce small granule sizes. In addition, highly dense and consolidated granules are produced using this granulator. Tumbling granulators are characterised by a very large throughputs (up to 100 tonne/hr) (Iveson et al. 1998a).

In disc granulation during continuous operation, the natural segregation of the particles can be useful to sort out and remove the largest particles. This can result in narrow particle size distributions and low recycling rates of off-size product (Litster, Ennis, & Liu, 2004).

2.4.2 High shear mixer

High shear mixer granulator consist of a bowl with different geometries and sometimes a chopper to break down large agglomerates. Here, an impeller is used to vigorously agitate the powder and produce high-density granules (Salman et al. 2007, Chapter 1). This type of granulator is usually more popular than the low shear force mixers.

They are widely used in pharmaceutical, agrochemical and detergent industries due to short processing times and the ability to manage difficult formulation properties, involving high viscosity binders and fine cohesive powders. However, an inconsistent result is sometimes obtained when scaling up from laboratory-sized (up to 15 kg per batch) to industrial sized (up to 100 kg per batch) high shear mixers (Litster, Ennis, & Liu, 2004).

At the same time, the high work rate can lead to an increase in the temperature, causing damage to heat labile ingredients. In addition, the binder may become less viscous at this elevated temperature. Consequently, it is difficult to determine a theoretical end point of high shear granulation due to complex growth behaviour as a result of more deformable granules (Parikh, 2005).

High shear mixer can be used for batch-wise or continuous wet granulation. Batch-wise high shear is widely used in the pharmaceutical industry due to their ease of enclosure and robustness. Dry mixing of the ingredients can be performed in this type of mixer. There can be differences in powder flow pattern and shear rate, which is mainly due to the difference in impeller and chopper geometry. For example, a chopper has a relatively small effect in a vertical-shaft mixer. In contrast, in horizontal-shaft design the chopper has a much larger effect (Litster, Ennis, & Liu, 2004). A schematic of a vertical-shaft mixer can be seen in Figure 2.1.

The impeller speed in high shear plays an important role in the granulation process. It has a major effect on the mixing quality between the powder and liquid binder, and the collisions between the particles or between the particles and the walls of the equipment. A controlled granulation with proper wetting is usually achieved by increasing impeller speed with good granule compaction and liquid binder dispersion. However, uncontrolled granulation with preferential growth and local wetting results from an inappropriate mixing between the powder and liquid binder due to a decrease in the impeller speed (Benali, Gerbaud and Hemati, 2009).

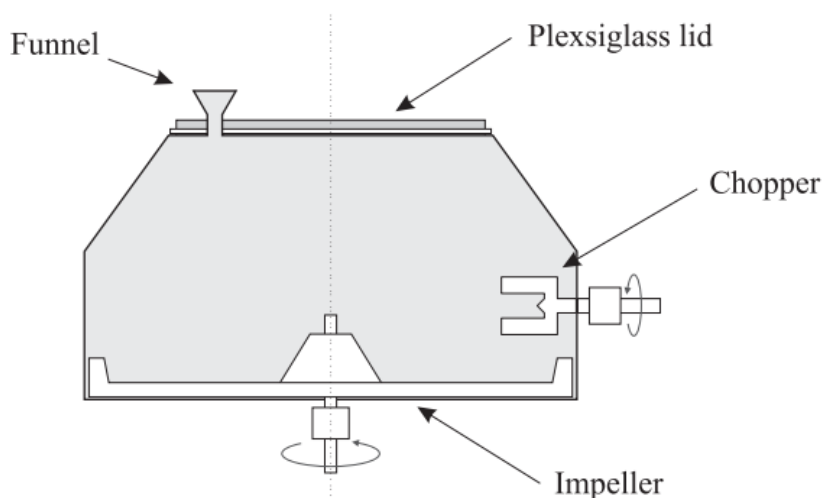


Figure 2.1: Schematic of an example of a high shear granulator with a vertical axis shaft.

Reprinted from Chemical Engineering Research and Design, Vol (91), Žižek, K., Hraste, M. & Gomzi, Z., High shear granulation of dolomite-I: Effect of shear regime on process kinetics, pp. 70-86., (2013), with permission from Elsevier.

2.4.3 Fluidised bed granulator

The particles in fluidised bed granulator are mixed in motion by air, rather than by mechanical agitation. This method is widely used in industries such as pharmaceutical, chemical, fertilizer, and can be operated as a batch or continuous granulation. The granule size produced using this equipment is typically in the range of 0.1-2 mm. This equipment, providing low shear forces, has the advantage of producing either high porosity agglomerates or high strength layered granules. It is a mechanically simple process with the removal of the drying step. However, the running costs are high and poor operation with fine powder and highly cohesive powder are the main disadvantages of the fluidised bed (Litster, Ennis, & Liu, 2004).

2.4.4 Twin screw granulator

The modification of a twin screw extruder for batch or continuous twin screw granulation has been carried out in the past few years. In some cases, twin screw extruder can replace high shear granulation, which may be desirable because the former can be continuously operated. Figure 2.2 shows a schematic diagram of twin-screw granulation; force is applied onto raw materials filled in the container from one end towards the opposite end by a pair of rotating

screws. The screw used are conveying and/or kneading elements (Keleb et al. 2004). Conveying elements design to impart low mechanical energy and act to transport material between mixing zone. Kneading design to impart high mechanical energy and act as a mixing zone. The granule size distribution and shape can be varied using different kneading elements. The particle size can be produced directly or after an extra step such as cutting or milling which depends on the granulation conditions used. The main disadvantages of this equipment are the complexity of process parameters which make the control and the optimisation of the granulation mechanism difficult (Seem et al. 2015).

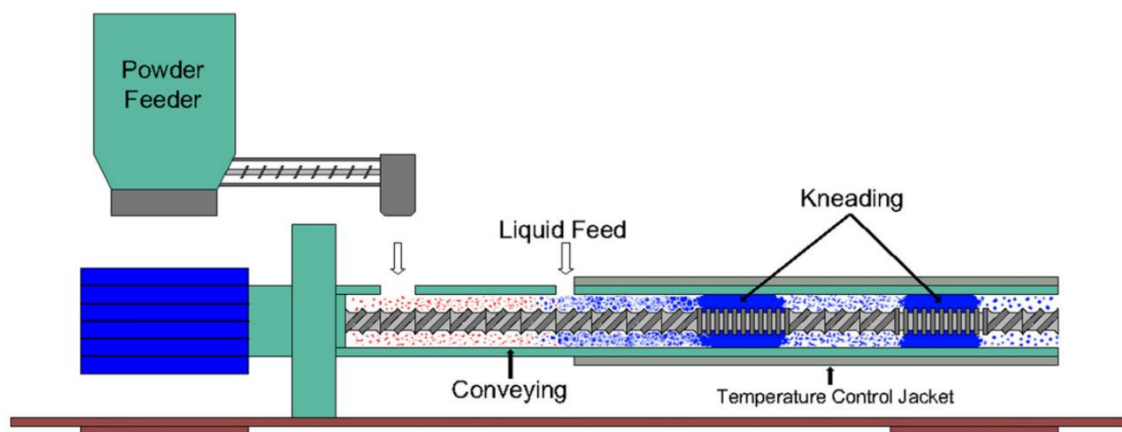


Figure 2.2: Components of a typical screw granulation.

Reprinted from Powder Technology, Vol (276), Seem, T.C. et al, Twin Screw Granulation – A Literature Review, pp. 89-102., (2015), with permission from Elsevier.

2.5 Granulation processes (wet granulation)

Wet granulation is a complex process that is usually composed of many competing physical phenomena occurring in the granulator. A thorough understanding of different phenomena during granulation is important to design granulation processes. Hence, it is becoming more popular to view granulation as a combination of only three groups of rate processes as shown in Figure 2.3 (Salman et al. 2017, Chapter 20), granule average length approximately between 0.2-4 mm:

- 1- Wetting, nucleation and binder distribution
- 2- Consolidation and growth
- 3- Breakage and attrition

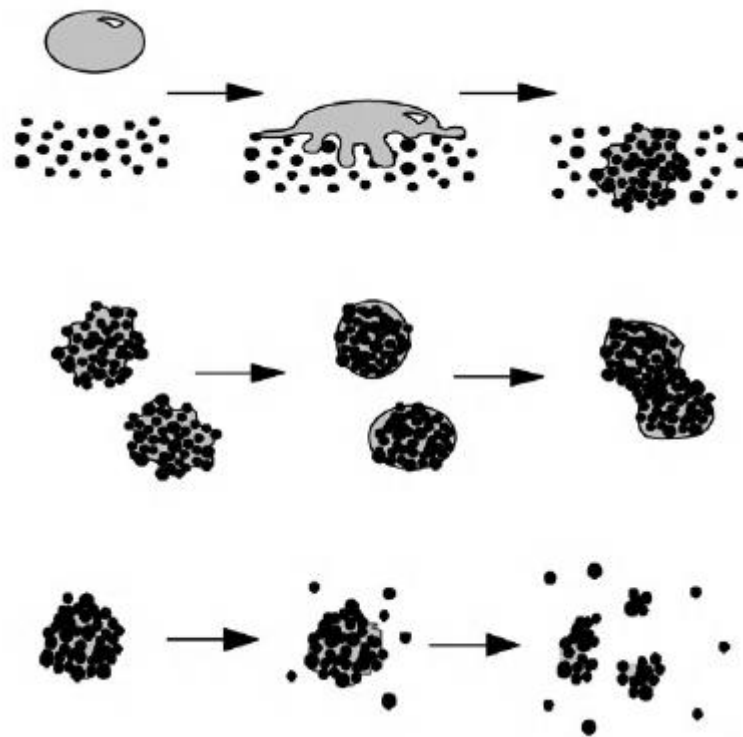


Figure 2.3: Modern approach on wet granulation processes.

Reprinted from Powder Technology, V (117), Iveson S., Litster J., Hapgood K., Ennis B., nucleation, growth breakage phenomena in agitated wet granulation processes: a review, pp. 3-39. (2001), with permission from Elsevier.

2.5.1 Wetting, nucleation and binder distribution

This is an essential step in the granulation process but is difficult to examine separately from other effects like agglomeration and attrition. During this process, the liquid binder is sprayed into a moving powder bed (Litster, Ennis, & Liu, 2004).

There are two different nuclei formation mechanisms: distribution or immersion, depending on the relative size of the liquid droplet to the primary particles. Nucleation with small binder droplets will occur by the distribution of the drop on a surface of the primary particle. When the binder droplets are bigger than the powder particles, they are immersed by the droplet, as shown in Figure 2.4 (Iveson et al. 2001), nuclei average length approximately between 0.2-4 mm.

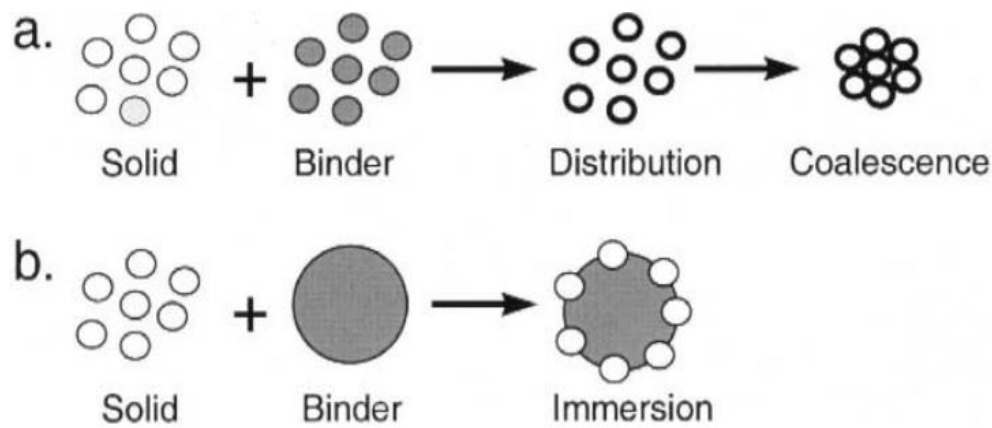


Figure 2.4: Nucleation mechanism, a: distribution b: immersion.

Reprinted from Powder Technology, V (117), Iveson S., Litster J., Hapgood K., Emis B., Nucleation, growth breakage phenomena in agitated wet granulation processes: a review, pp. 3-39., (2001), with permission from Elsevier.

In the immersion mechanism, when the droplet impacts the powder bed, different types of fragmentation of the droplet can occur, each resulting in different granules types. A tunnelling mechanism is observed when using fine cohesive powder and at low granular velocity. Cohesive powder formed large loose aggregates with high powder bed porosity. When the droplet first comes to contact with powder bed, it bounces and rolls, eventually ending in a stabilised position. The liquid penetration is driven by capillary action and penetrates through small pores of dry aggregates rather than in between large aggregates. Dry aggregates are sucked inside the droplet which then causes the bed to collapse by the weight of the drop which tunnels into the powder bed. This leads to collection up of new powder particles and dry aggregates from the new surface. The liquid droplet keeps its original spherical shape during nucleation leading to spherical granules (Figure 2.5) (Emady et al. 2011).

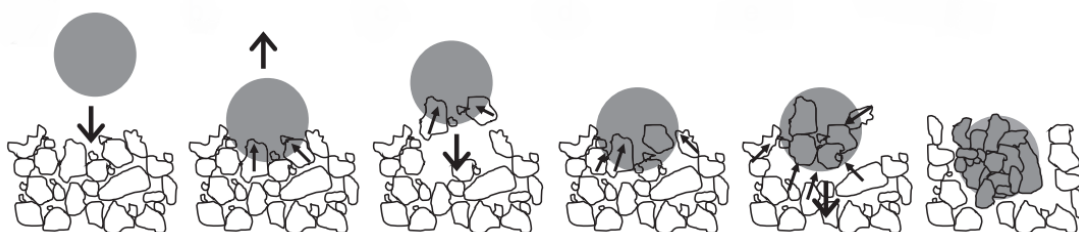


Figure 2.5: Schematic diagram of tunnelling mechanism.

Reprinted from Powder Technology, Vol (212), (Emady et al., 2011), Granule formation mechanisms and morphology from single drop impact on powder beds, P 69-79., Copyright (2011), with permission from Elsevier.

A spreading/crater formation mechanism is observed when using coarse and free flowing powder (Emady et al. 2011). A spreading formation mechanism occurred when the liquid droplets hit the smooth surface of free flowing powder. Then the droplet is deformed elastically, splashing a small amount of powder and making a shallow crater. After a very short time, a few powder particles are picked up by the liquid droplet which then retracts. If there is a low concentration of the gathered particles on the surface, they form a mobile layer on the liquid surface, allowing the droplet to spread on the powder surface over a longer time scale. The liquid spreads over the powder bed surface by capillary action while it is simultaneously penetrating into the powder bed. As the rate of penetration is slow compared to the rate of spreading, the resultant granules are disc shaped with a slightly higher rim (Figure 2.6) and (Figure 2.7) (Emady et al. 2011).

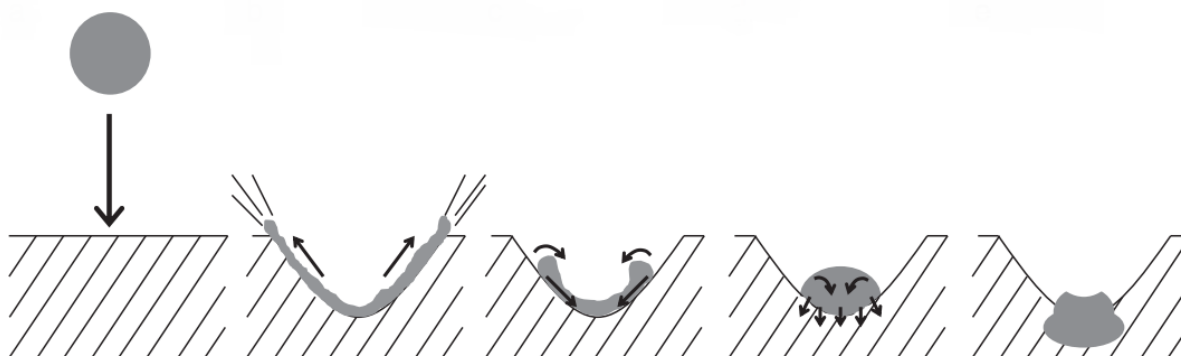


Figure 2.6: Schematic diagram of crater formation mechanism.

Reprinted from Powder Technology, Vol (212), (Emady et al., 2011), Granule formation mechanisms and morphology from single drop impact on powder beds, P 69-79., Copyright (2011), with permission from Elsevier.

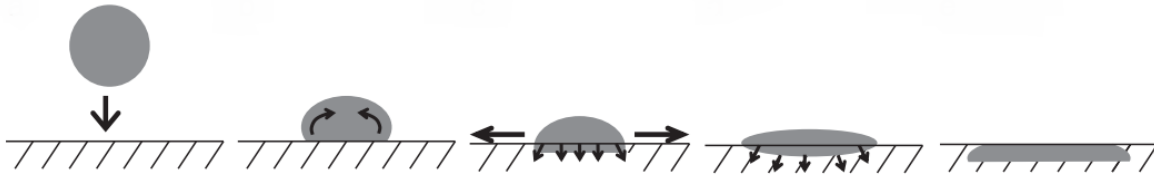


Figure 2.7: Schematic diagram of spreading mechanism.

Reprinted from Powder Technology, Vol (212), (Emady et al., 2011), Granule formation mechanisms and morphology from single drop impact on powder beds, P 69-79., Copyright (2011), with permission from Elsevier.

Charles-Williams et al. 2011 compared drop infiltration and spreading on a dry and pre-wetted particle powder bed. Infiltration time is longer in a pre-wetted powder, and the binder viscosity effects the spreading and infiltration time of the liquid droplet. For a liquid/powder contact angle greater than 90° , for example aqueous liquid with non-wetting powder, the liquid spreads on the liquid droplet and forms a layer around the droplet surface. The spreading of the non-wetting powder on the liquid droplet is forms a granule which is known the liquid marble, which upon drying form a hollow granule (Hapgood and Khanmohammadi, 2009).

Binder distribution is an important parameter in the control of granule properties and an indication of the effectiveness of mixing between the powder and binder fluid. A narrow granule size distribution is obtained when the liquid is distributed homogenously. If the binder is unequally distributed, then a bimodal nuclei size distribution is likely. The quality of the dispersion of the granulating liquid depends on the combination of the powder mixture, granulating liquid and the method of binder addition (Balashanmugam et al. 2015).

Spray flux ψ_a is the dimensionless group which is considered as an important development in wetting and nucleation process. ψ_a is defined as the ratio of the area wetted from drops by the nozzle to the renewal area of powder surface in the nucleation zone (Hapgood, Litster and Smith, 2003).

$$\psi_a = \frac{3V}{2AD_d} \quad \text{Equation (2.1)}$$

In Equation (2.1), V is the volumetric spray rate, and A is the area passes through the spray zone, D_d is the droplet diameter. At a low spray flux, $\psi_a < 1$, one drop forms one nuclei and drops do not overlap. At high spray flux, $\psi_a > 1$, a broader nucleation distribution is observed. This probably occurs during granulation when the liquid is poured into the granulator. The

spray area is equal to the cross sectional area of the liquid sprayed (Iveson, Wauters, et al. 2001).

The nuclei formation kinetics can be also be quantified by penetration time (Hapgood, Litster and Smith, 2003). The penetration time depends on the wetting characteristics of the powder and on binder viscosity. Drop penetration time can be calculated according to the following equation:

$$\tau_p = 1.35 \frac{V_d^{2/3} \mu}{\varepsilon_b^2 R \gamma \cos(\theta)} \quad \text{Equation (2.2)}$$

where V_d is the volume of the drop, μ is the binder viscosity, ε_b is the porosity of the powder bed, R is the powder pore radius, γ is the liquid surface tension, θ is the dynamic contact angle of powder/liquid.

Hapgood, Litster and Smith, 2003 developed a nucleation regime map for wetting powder using the concept of spray flux and liquid penetration time as shown in Figure 2.8.

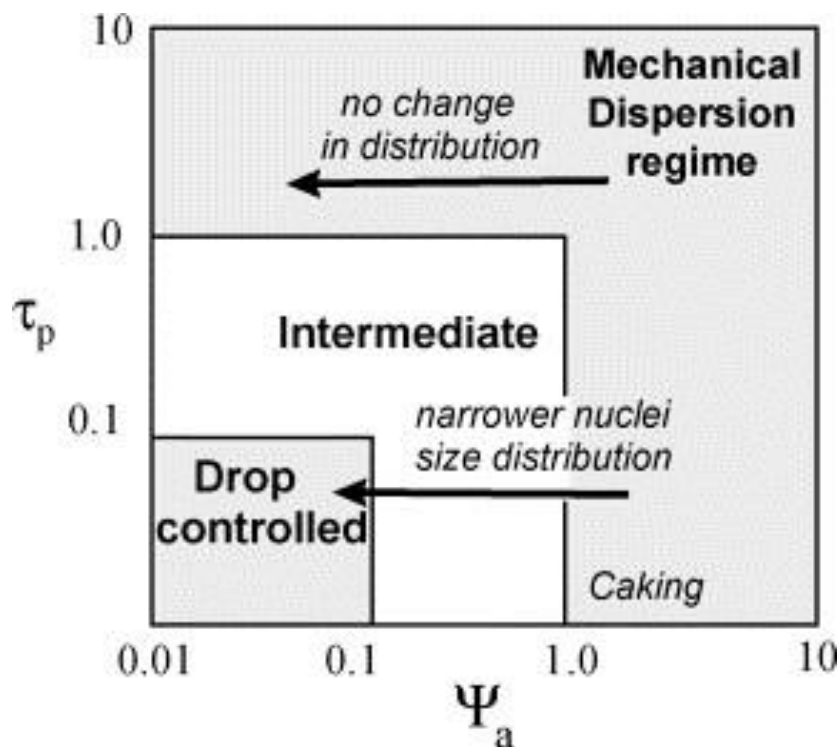


Figure 2.8: Nucleation regime map developed by Hapgood et al.

Reproduced with permission from Wiley Materials.

The nucleation regime map is divided into three regimes. Drop controlled nucleation regime obtained with low spray flux and fast drop penetration time. However, for high spray flux and long liquid penetration time, mostly occurred with poor wetting powder and high viscous binder, mechanical dispersion is obtained. There is also an intermediate regime in which the process is sensitive to changes in spray flux and penetration time. This regime map can be used to predict the nucleation behaviour using different formulations and process parameters.

2.5.2 Consolidation and Growth

Granules may consolidate and grow if successful wetting and nucleation are controlled. Understanding when and how growth occurs is essential in industry, since granulated products are often evaluated for size distribution and porosity or a related property (Parikh, 2005) Granules can undergo either slow or rapid growth, depending on the mechanics and how energy is absorbed on impact. Slow granule growth occurs by layering which is the formation of a fresh layer of powder around an existing granule. Rapid granule growth occurs by coalescence which involves the collision and sticking together of two or more granules. Growth by layering is often preferred over coalescence because it is more controllable. In the following sections, growth and consolidation are discussed.

2.5.2.1 Consolidation

Consolidation is the process during which granules experience numerous collisions between other granules and with the walls of the equipment. This will reduce the granule size and porosity, and consequently squeezes the interior granulating fluid and entrapped air to the granule surfaces. When the porosity decreases due to consolidation, the granules will be more robust (Pohlman et al. 2014).

Granule porosity also has a strong influence on granule growth due to its effect on liquid saturation and granule deformability. Rapid granule growth occurs if the consolidation permits more liquid to be squeezed to the granule surface after a period of little or no growth. Nevertheless, consolidation also reduces granule deformability, decreasing the area of contact formed between colliding granules and hence may reduce the probability of successful coalescence (Iveson & Litster 1998).

2.5.2.2 Granule growth

Granule growth is highly influenced by the powder particle size, width of powder size distribution and powder density, which ultimately affects the resulting properties of the granules. Granule growth is a complex process and many authors have studied its mechanism, but it is still not clear.

Granule growth is mainly divided into two systems based on a fundamental understanding of growth mechanism (Litster, Ennis, & Liu, 2004), and these are discussed in the following sections.

2.5.2.2.1 Non-deformable particle systems

When considering the growth of the granules in any mixer granulation, it is important to understand what happens when two surface wet granules collide with one another in the granulation equipment. Basically they are three types of collision can be seen, depending on the formulation and process parameters (Ennis et al. 1991).

For non-deformable or near elastic granules, only two phenomena can occur. This depends on the granule kinetic energy and collision of the granules can either result in rebounding or coalescence. Growth by coalescence occurs when the collisional kinetic energy is too small to overcome the resistance of viscous forces of the binder in the liquid layer. Rebound of the granules occurs when the granules have a high kinetic energy, and the formed liquid bridge is not enough to keep the granules together (Ennis et al. 1991).

Ennis et al. 1991 defined the granule coalescence by using the viscous Stokes number, St_v , for spherical, unequal sized particles. St_v is a ratio of initial granule kinetic energy to the viscous dissipation by binder lubrication force. St_v is highly influenced by impact collisional velocity and liquid binder viscosity and provides a suitable classification of the coalescence growth regime and according to Equation (2.3):

$$St_v = \frac{8 \rho_g v R_g}{9 \mu} \quad \text{Equation (2.3)}$$

where ρ is the granule density, v is relative collisional velocity, R_g is granule radius and μ is binder viscosity. By comparing the St_v to a critical value St_v^* a conclusion regarding the process

of granules collision can be obtained Equation (2.4). St_v^* is a function of the amount of liquid binder deposited on the powder bed:

$$st_v^* = \left(1 + \frac{1}{e}\right) \ln\left(\frac{h}{h_a}\right) \quad \text{Equation (2.4)}$$

where e is the restitution coefficient, h_a is the height of surface roughness, h is the thickness of liquid layer.

When the viscous Stokes number is smaller than critical viscous Stokes number, $St_v < St_v^*$, growth is in non-inertial regime, and all collisions are successful. Granules in this regime grow by coalescence or layering. When the viscous Stokes number increases and becomes equal the critical Stokes number, $St_v \sim St_v^*$, granule growth is in the inertial regime. There is a balance between granule growth by coalescence and granule rebound and overall reduction in granule size is observed. When the viscous Stokes number increases further and becomes much higher than the critical viscous Stokes number, $St_v > St_v^*$, in this regime granules enter the coating regime. In this case, all granules collisions result in rebound and layering which is the major granule growth mechanism (Ennis et al. 1991).

However, granules can be deformed during granulation which limits the applicability of the elastic assumption of the granule. This leads to another growth regime of plastic granule behaviour (Iveson & Litster 1998b), as described in the next section.

2.5.2.2 Deformable particle systems

Although the regime map developed by Ennis et al. 1991 provided a description of elastic and non-deformable granule, granules in high shear mixer can be deformable (Liu et al. 2000). When the kinetic energy is fully dissipated by the viscous forces between two colliding wet surface granules, then type I coalescence occurs. Either rebound or another type of coalescence occurred when the kinetic energy is high enough to make the granules collide. Type II coalescence occurs when the granule kinetic energy is slowed and keep the granules together. With a further increase in the kinetic energy, the liquid bridge breaks and the deformed granules rebound (Liu et al. 2000).

Liu et al. 2000 extended Ennis et al. 1991 study to include the probability of granule deformation during collision. The model is developed to include dimensionless group;

deformation stokes number St_{def} . St_{def} , is a function of the granule yield stress compared to kinetic energy (Equation (2.5) (Iveson, Wauters, et al. 2001):

$$St_{def} = \frac{\rho_g U_c^2}{2 Y_g} \quad \text{Equation (2.5)}$$

In Equation (2.5), ρ_g is the density of the granule, U_c^2 is the granule collisional velocity and Y_g is the dynamic yield stress. The regime map can be seen in Figure 2.9.

The collisional behaviour of the granules can be predicted using this proposed regime map by Liu et al. 2000. At a low granule velocity, minimal granule deformation is observed and granules show type I coalescence. At a high collisional velocity and low deformation number, rebound behaviour mostly observed. Type II coalescence mostly dominates at high velocity and with highly deformable granules (Liu et al. 2000).

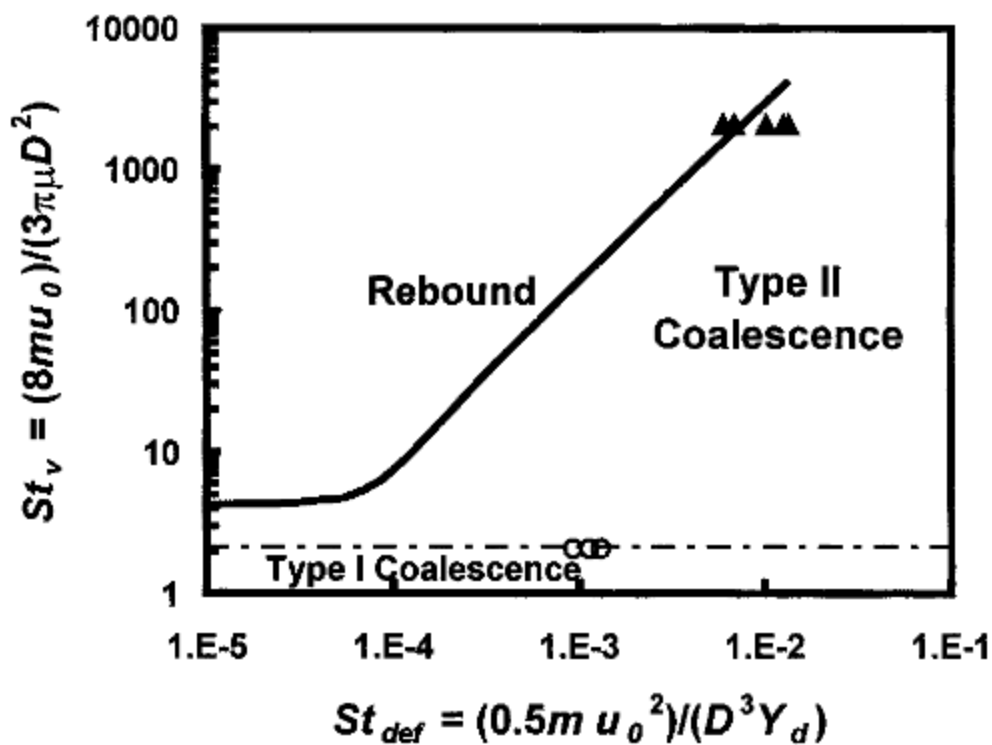


Figure 2.9: Coalescence regime map in terms of deformation stokes number and viscous stokes number (Liu et al. 2000).

Reproduced with permission from Wiley Materials.

2.5.2.2.3 Regime maps

In order to predict and identify all types of granule growth behaviour during granulation, Iveson and Litster 1998 proposed a regime map; an updated version can be seen in Figure 2.10. The map explains different regimes as a function of stokes deformation number, St_{def} , and maximum granule pore saturation, S_{max} , which gives the fraction of pores occupied by the liquid (Equation (2.6)):

$$S_{max} = \frac{w \rho_s (1 - \varepsilon_{min})}{\rho_l \varepsilon_{min}} \quad \text{Equation (2.6)}$$

where w is the liquid to solid mass ratio and ρ_s and ρ_l are the densities of the solid and liquid respectively and ε_{min} is the minimum powder pore saturation.

Granule growth behaviour depends on many variables such as deformability and consolidation rate of the granules (Litster, Ennis, & Liu, 2004). Narrowly sized, coarse particles and low viscosity liquid binders produce weak, deformable granules. This behaviour leads to steady growth by rapid coalescence. In contrast, for widely sized, fine particles and viscous liquid binders, there is initially a period of little or no growth known as the “induction” period. The duration of “induction” time decreases with increase in the saturation of the granules.

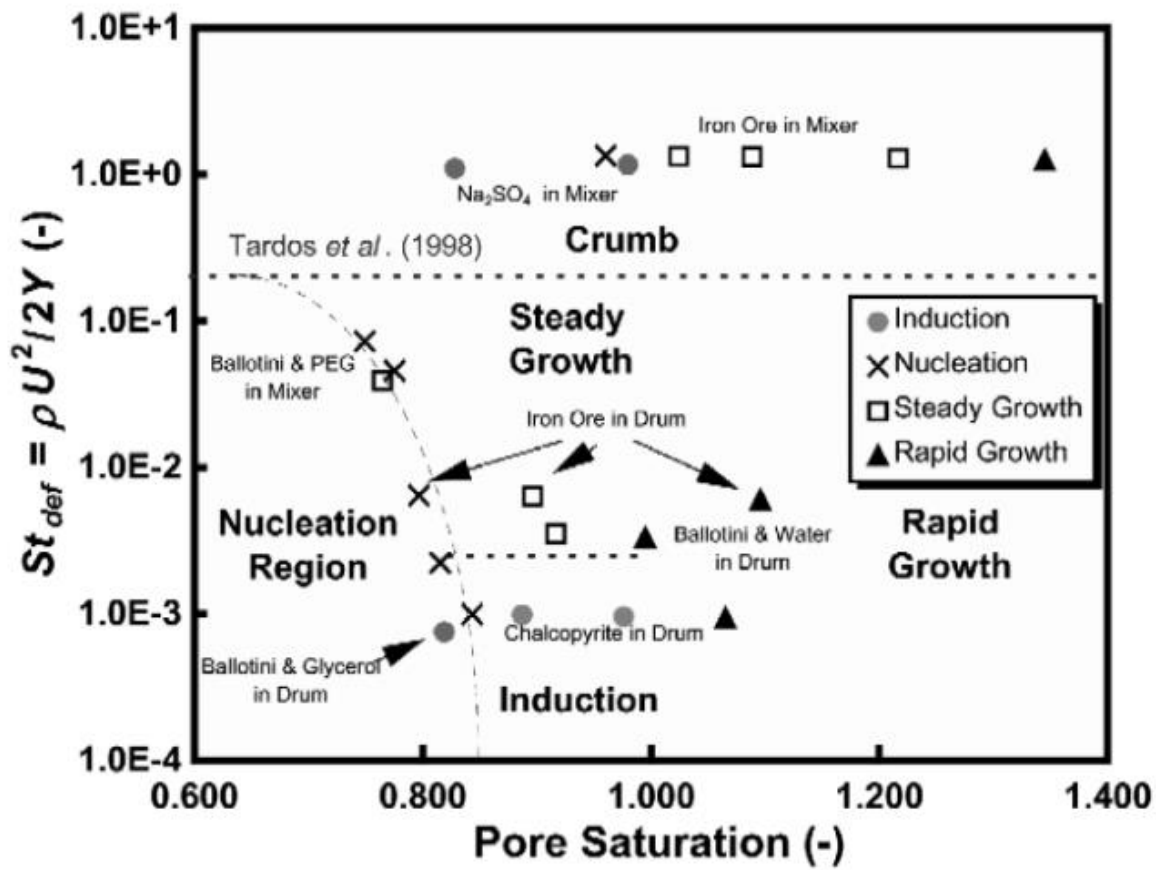


Figure 2.10: Proposed growth regime map by Iveson and Litster 1998.

Reprinted from *Powder Technology*, V (117), S. Iveson, Ph. Wauters S. Forrest J. Litster, G. Meesters B. Scarlet, *Growth regime map for liquid-bound granule: further development and experimental validation*, P (83-97), Copyright (2001), with permission from Elsevier.

The location of a system in terms of St_{def} and S_{max} , characterises the different behaviour of granule growth:

- At low S_{max} , nuclei are formed by Van der Waals interactions, and particles remain as a dry, free flowing powder.
- With an increase the S_{max} , the particle behaviour depends on the St_{def} ; at low St_{def} , nuclei are formed with no growth occurring, but at a high value of St_{def} , non-granular “crumb” material will be formed.
- At a medium level of granule saturation, with a moderate St_{def} , granules will grow steadily, but at low St_{def} slowly consolidated granules display an induction time behaviour.

- At high granule saturation, all granules will grow rapidly.
- At very high granule saturation, a slurry or over wet mass will be formed.

A regime map theory qualitatively or semi-quantitatively explains the difference in granulation behaviour during the granulation processes. By introducing a regime map, it becomes possible to correlate the input of processing variables and equipment with the granule properties, making it possible to envisage a formulation's growth behaviour without needing further laboratory or pilot scale testing. This would have enormous economic benefits (Kumar et al. 2014).

The proposed map was later experimentally validated by Iveson et al. 2001. They found a good fit with drum granulation data. However, it proved difficult to determine correctly the Stokes deformation number (St_{def}) for high shear mixing. However, the map gives some prediction and explanation of granulation behaviour.

Later, Tu et al. 2009 proposed the effect of processing parameters on the granulation regime map such as impeller speed and liquid to solid ratio, instead of Stokes deformation number and maximum pore saturation respectively, in high shear granulation. They found that increasing impeller speed leads to an increase in the rate of granule growth and finally larger granules, although sufficient binder is an essential requirement for granule growth. However, it is equally important for the distribution of this binder and that a low impeller speed is inadequate to achieve this.

Although, there have been significant advances in our understanding on the growth of granules from wetting powder, the addition of non-wetting material and the study of its effect on the nucleation behaviour and kinetics of growth remains to be considered. Charles-Williams et al. 2013 studied the effect of the increasing amounts of non-wetting substrate on the granulation mechanism. They used high shear granulation to investigate the effect of increasing non-wetting limestone on granulation growth behaviour. Lactose was used as base line data for the effect of increasing non-wetting ingredient. Rapid granulation was promoted with the decrease of the spraying droplet diameter. Non-wetting content had a strong effect on granule size and granulation behaviour. As the non-wetting powder increased there was a decrease in granule size at a given granulation time.

Yu et al. 2014 studied the effect of granulation behaviour in twin screw granulation for a formulation of increasing non-wetting content. Lactose was used as a wetting excipient and di-

calcium phosphate anhydrite was used as a non-wetting substrate. Hydroxypropyl methyl cellulose (HPC) was used over a range of viscosities as a liquid binder. They found that the liquid binder viscosity and powder wettability play an important role in controlling the granule size. The granulation liquid was easily distributed across the wetting powder bed, resulting in a higher granule size with a higher concentration of HPC binder. The effective liquid distribution was prohibited with an increase of non-wetting content in the powder, resulting in a decrease of granule growth. However, for a high binder viscosity, there was an overall increase in granule size due to an increase of the strength of liquid bridges which improves resistance to breakage.

It is clear that the non-wetting systems affect granule growth and internal microstructure and the properties of the resultant granules. The mechanism of granule growth in these systems will be different. This will be reviewed in section 2.6.

2.5.3 Breakage and attrition

Breakage may control and have an influence on the final granule size distribution, particularly in high shear granulation. In some cases, breakage can help the distribution of the granulating fluid or limit the maximum granule size (Ende, 2011).

Attrition leads to the formation of dust from the dry granules. This is generally an undesirable process, needed to be avoided in most granulation processes (Litster, Ennis, & Liu, 2004).

Limited studies have investigated wet granule breakage in granulation process. In tumbling drum some preferential granule growth may involve breakage and attrition of weak granules. However, breakage is much more likely in high agitation mixer such as high shear mixer (Litster, Ennis, & Liu, 2004).

2.6 Granulation of non-wetting powder: theory and mechanism

With 50 years of research, granulation is a major area of interest, and significant progress has been made in understanding the mechanisms of the granulation process (Hapgood et al. 2009). The majority of these studies have focused on the mechanism of granulation of wetting

systems. However, there have only been a few studies carried on non-wetting systems, despite the prevalence of these systems in the pharmaceutical industry.

For a wetting powder/liquid granulation process, the liquid binder wets and penetrates into the powder bed, which leads to formation of nuclei that, with agitation in suitable granulator, results in growth of the nuclei either by coating or coalescence. However, the situation is different with poorly or non-wetting powders; here, non-wetting powders spread over a liquid binder during agitation in a granulator (Hapgood et al. 2009).

Agglomeration of wetting powder typically involves the wetting of the powder particles with a liquid droplet. The liquid bridges are formed by the addition of liquid binder and bind the particles together. However, liquid binder cannot penetrate into poorly wetting powders. For non-wetting powder (high contact angle between powder and liquid), instead, particles spread over liquid droplets as the powder bed is agitated. Liquid marbles are formed, with encapsulation of the liquid droplets within the powder particles. These liquid marbles can bounce and move intact without leaking liquid. The dried form of these liquid marbles are called hollow granules (Whitby et al. 2013).

The spreading of fine non-wetting powder over a solid surface is generally known as “solid spreading nucleation”. In pharmaceutical manufacturing, the spreading coefficient has been used for many years to estimate the wettability of a given formulation. The spreading coefficient is usually referred as the difference between the work of adhesion and cohesion and gives an indication of whether the spreading of solid over a liquid is thermodynamically favourable. This is shown mathematically in Equation (2.7). In addition, the spreading coefficient has been used for many years by pharmaceutical companies to predict whether adequate wetting of pharmaceutical powders will occur (Hapgood et al. 2009).

$$\lambda_{SL} = \gamma_{SL} + \gamma_{Sv} - \gamma_{Lv} \quad \text{Equation (2.7)}$$

In Equation (2.7), λ_{SL} is a solid liquid spreading coefficient. γ is the interfacial adhesion of S solid, L liquid and V vapour.

Many researchers have studied the effect of spreading coefficient on wettability or other properties of non-wetting powder mixture (Planinsek et al. 2000; Zhang et al. 2002) and these generally have been performed on a large particle or compact powder.

The driving force for the spreading of non-wetting powder on a liquid drop has been investigated. Two mechanisms have been suggested, Firstly, the spreading of non-wetting powder is driven by a solid-over-liquid spreading coefficient (Eshtiaghi et al. 2009; Nguyen et al. 2010; Hapgood et al. 2009). Secondly, the kinetic energy is the driving force based on the examination of the role of mixing intensity through the production of liquid marbles (Forny et al. 2007).

Hapgood et al. 2009 suggested the use of a solid-liquid spreading coefficient, λ_{SL} , as a quantitative tool to predict whether a given combination of powder and liquid will result in the formation of liquid marbles. They found that by using different non-wetting powders and liquid binders, that the liquid marbles cannot be formed unless there is a solid liquid spreading coefficient more than $\lambda_{SL} > 0$.

Forny et al. 2007 studied encapsulation of water with fumed silica powder with various levels of wettability, and used two different mixers; a high and a low shear. Two alternative methods were used for adding water to the fumed silica powder; (i) direct loading of powder and liquid into the equipment, (ii) by atomization over 3-4 minutes. For a high shear with highly non-wetting fumed silica R812, successful liquid marbles were formed with direct addition of liquid within 10 seconds at a mixing rate above 12,000 rpm. 98% water encapsulation was obtained at a mixing rate of 18,000 rpm for 30 seconds. However, for a low mixing rate, between 4000 – 8000 rpm, liquid puddles of water were formed at the bottom of the mixing bowl, even with an increase in mixing time for up to 5 minutes. For low shear mixing, neither direct liquid addition nor atomization, with different mixing condition and agitation speeds resulted in a successful spreading of fumed silica R812 over a liquid droplet. From this study, one can conclude that with an increase in the agitation intensity such as impeller speed, the kinetic energy increased which plays a key role in liquid marble formation.

A study by Eshtiaghi et al. 2009 supports Forny's study. Here, they investigated in more detail the mechanism of non-wetting powder coverage on a liquid droplet to examine whether the solid over liquid spreading coefficient λ_{sL} or bulk motion is the responsible mechanism for liquid marble formation. This was done by releasing a single drop of different liquids (distilled water, glycerol, polyvinyl pyrrolidone (PVP), hydroxyl propyl methyl cellulose (HPMC) onto a loosely packed powder bed of different particle size powder. When the drop was placed directly and gently on the loosely packed non-wetting powder bed, no spreading occurred of the powder over a liquid droplet. However, a complete coverage of liquid marbles was formed

by releasing the drops from greater heights (10 cm to 25cm). This result indicated that the spreading coefficient alone could not predict the formation of liquid marbles, but there was a further contribution of kinetic energy or bulk motion for the spread of non-wetting powder over liquid.

More about liquid marble formation and characterisation can be found in Section 2.8. The next section will focus on powder wettability for understanding the solid-liquid contact angle, which gives an estimation of powder wettability.

2.7 Powder wettability-Theory

The wettability of powders is an important aspect during the production of pharmaceutical dosage forms. The wettability evaluation of the powders usually depends on a determination of the solid-liquid contact angle, which give an indication of their wettability. A completely wetting liquid has a contact angle of 0° . An incomplete powder/liquid wetting occurs with a contact angle of $0^\circ < \theta < 90^\circ$. A non-wetting system when the fluid comes in contact with powder without spreading across the surface is specified by a contact angle $\theta > 90^\circ$. A super non-wetting powder gives a complete non-wetting system with a contact angle greater than 150° (Hapgood, 2000).

In theory, the contact angle is expected to be a property for a given solid-liquid system in a particular environment. If you consider a static liquid droplet on a solid surface, the contact angle is the angle formed by the intersection of the liquid-solid interface and the liquid-vapour interface. The interface where liquid, solid and vapour intersect is known as the 3-phase contact line, where γ_{sv} , γ_{sl} , γ_{lv} are the solid-vapour, solid-liquid and liquid vapour interfacial energies respectively, and θ is the contact angle as shown in Figure 2.11. Determination of contact angle is not an easy task, but recently, efficient experimental methods have been described (Lazghab et al. 2005).

As described by Thomas Young in 1805, the contact angle is expressed by the mechanical equilibrium of the drop falling onto an ideal solid surface under the influence of the three interfacial tensions:

$$\gamma_{lv} \cos \theta_y = \gamma_{sv} - \gamma_{sl} \quad \text{Equation (2.8)}$$

where the subscripts l , v and s indicate liquid, vapour and solid respectively. γ represents the interfacial free energy of the surface at equilibrium and θ_y is the contact angle between the solid and liquid phase. This description of contact angle is usually referred to as Young's equation. This equation applies to a system at equilibrium (Snoeijer et al. 2008).

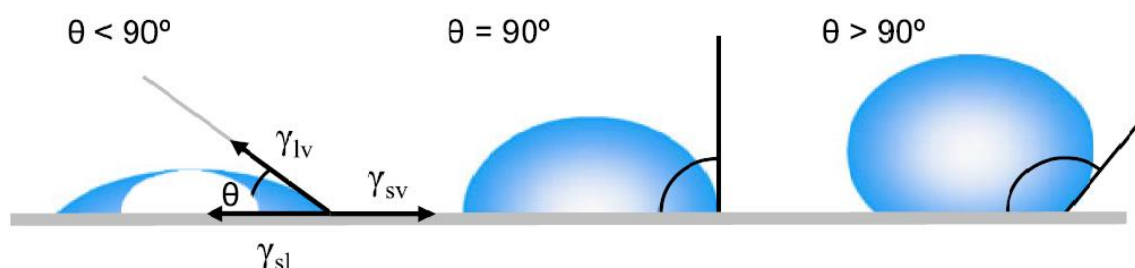


Figure 2.11: Contact angle on a powder surface.

Reprinted by permission from Springer Series in Surface Sciences, vol 51. Yuan Y., Lee T.R, Contact Angle and Wetting Properties. In: Bracco G., Holst B. (eds), Springer, Berlin, Heidelberg, (2013).

From Young's equation applied to a particular liquid-solid system, three thermodynamic parameters γ_{lv} , γ_{sv} , and γ_{sl} define a single and a unique contact angle θ_y . Practically, the process of wetting is more than just a stagnant state in which there are various metastable states of the droplet on a solid, and the contact angles are almost never equal to θ_y . When the three-phase contact line is in real motion, a single static contact angle θ_y is no longer adequate for describing the wetting behaviour. The angle at that time is called the "dynamic" contact angle. Particularly, the contact angles formed by expanding and contracting droplets are indicated as the advancing contact angle θ_a and the receding contact angle θ_r , respectively (Figure 2.12). These angles occur within a range, with the advancing angles approaching a largest reproducible value, and the receding angles approaching the smallest reproducible value. Dynamic contact angles can be determined at different ranges of shear. At low shear, it should be close or equal to a properly measured static contact angle. The difference between the advancing and receding angle is called the hysteresis (H) (Yuan & Lee 2013):

$$H = \theta_a + \theta_r \quad \text{Equation (2.9)}$$

The importance of contact angle hysteresis has been thoroughly investigated and it is assumed that it arises from surface roughness and/or heterogeneity. For surfaces that are heterogeneous, there are many barriers to the motion of the liquid droplets on the contact area. For instance, a

non-wetting surface will hinder the movement of the water front as it advances, leading to an increase in the observed contact angle; the same surface will restrain contracting movement of the water front when the water recedes, consequently causing a reduction in the observed contact angle. Young's equation fail to explain such contact angle data because it does not reflect surface topography (Timmons et al. 1966).

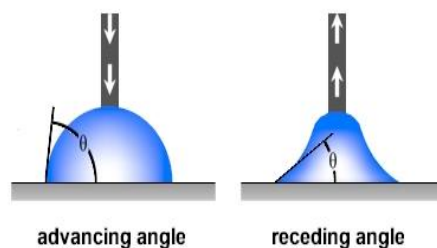


Figure 2.12: Schematic of advancing and receding contact angles.

Reprinted by permission from Springer Series in Surface Sciences, vol 51. Yuan Y., Lee T.R, Contact Angle and Wetting Properties. In: Bracco G., Holst B. (eds), Springer, Berlin, Heidelberg, (2013).

The determination of the contact angle is very intricate, as Young's contact angle θ_y might or might not reflect the experimentally determined contact angle. Nevertheless, Young's contact angle interprets the experimentally observed contact angle on ideal smooth solid surface when there is no contact angle hysteresis. While for non-homogenous solid surfaces, Young's contact θ_y angle might represent the advancing contact angle θ_a , but it is usually observed to be less consistent than the receding contact angle, θ_r , due to liquid sorption or solid swelling. There is no correlation between θ_a and θ_y on a rough solid surface as a Young's equation is inadequate to interpret contact angles on those types of surfaces (Yuan et al. 2013; Zhenyu et al. 2015). Two wetting states are generally defined, Wenzel and Cassie-Baxter, depending on whether the liquid droplet settles on a rough or heterogeneous surface respectively. The Wenzel model suggests that the droplet wets the entire rough substrate while the Cassie-Baxter model suggests that the liquid incompletely wets the rough substrate due to the air in the micro-structured surfaces (Wenzel, 1936; Cassie, 1944) as shown in Figure 2.13.

For a non-wetting powder, the Cassie and Baxter's approach can be used for estimating the average contact angle measurement, θ_{av} :

$$\cos \theta_{av} = f_1 \cos \theta_1 + f_2 \cos \theta_2 \quad \text{Equation (2.10)}$$

where f_1 is the fraction of the powder mixture with contact angle equal to θ_1 , and f_2 is the fraction of the powder mixture with contact angle equal to θ_2 . Experimentally, the measurement of the contact angle of neat pharmaceutical powders or a combination of powders with water was investigated by Lerk et al., 1976, cited in Hapgood et al. 2009, showed the contact angle directly affects the properties of a granulated batch and was unrelated to the particle size. However, for a combination of non-wetting drug powder and wetting ingredients, the contact angle depends on particle size. As a particle size increased, the non-wetting powder controlled the contact angle. Furthermore, there was a direct relationship between contact angle and the ratio of the components for a small particle size.

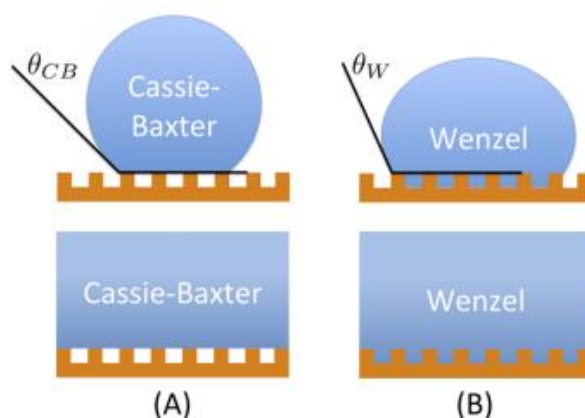


Figure 2.13: (a) Cassie-Baxter (b) Wenzel models for wettability states.

Reprinted with permission from Langmuir, 28(29), Giacomello, A. et al., Cassie-baxter and wenzel states on a nanostructured surface: Phase diagram, metastabilities, and transition mechanism by atomistic free energy calculations. pp.10764–10772, (2012). American Chemical Society.

The incorporation of non-wetting ingredients into the formulation decreases the extent of wetting between the liquid binder and the powder, which accordingly may lead to non-uniform distribution of the drug in the granulation mixture. Approximately 150000 new drugs have been investigated and showed to have a poor water solubility or non-wetting characteristics (Dimond et al. 2005; Straub et al. 2005), cited in (Nguyen et al. 2010). Hence, an understanding of the effects of the inclusion of non-wetting ingredients in wet granulation is becoming increasingly important for good granulation and particle design. The non-uniform distribution of the drug in the granulation mixture may partly be attributed to the difference in the particle size between the drug and ingredients in the granulation mixture (Nguyen et al. 2010).

Many authors have investigated the relationship between contact angle, wettability and the growth of non-wetting powders. Hemati et al. 2003 studied the effect of contact angle on granulation growth kinetics in a fluidized bed granulator through granulated sand powders with different wettability and 1% carboxy methyl cellulose solution with powder liquid contact angles ranging from 38.3°, 58.6°, 75.4°, > 90°. This study showed that as contact angle increased there was a decrease in agglomeration growth kinetics until no further growth occurred at a contact angle of more the 90°. Consequently, more studies are required to investigate the relationships between contact angle and the mechanism of growth of non-wetting powder mixtures.

2.7.1 Methods for determining the wettability of powder

The wettability of powders usually plays an enormous role in several applications such as powder processing, coating, dispersion and analytical techniques (contact angle analysis) to characterize surface properties (Öner et al. 2000). Such significance generates a continuous interest within the scientific community to develop methods to assess the wettability of powders by measuring the contact angle. In general, the wettability of the solid depends on the angle that is formed at the molecular interaction between solid and liquid coming into contact. The sessile drop technique is one of the most popular methods for measuring the contact angle. It can be measured directly through three-phase contact line of liquid, solid and gas formed when a liquid droplet is placed on a solid surface. However, it is only applicable for flat smooth and non-porous surfaces (Kwok et al. 1999).

Due to complex wetting behaviour of the powder system, new methods need to be developed for accurate measurement of the contact angle and wettability of the powder. This is a challenging task as they are many parameters which influence the measurement of contact angle on a solid surface apart from chemical and physical properties of the liquid, such as surface roughness, liquid penetration into the pores, surface heterogeneity and swelling (Alghunaim, Kirdponpattara and Newby, 2016).

Accordingly, there is no common test to estimate the wettability of the powder and every single powder-liquid pair must be investigated on a “case by case” basis to select the most suitable method for the contact angle measurement (Lazghab et al. 2005). Table 2.1, displays an

overview of some methods used for the determination of the wettability of powders with their advantages, disadvantages, and limitations.

Table 2.1: Methods for determining the wettability of a powder.

Studies	Methods	Benefits	Drawbacks
(Schuster, Schvezov and Rosenberger, 2015) (Puri et al. 2010)	Sessile drop	Easy and fast	It is generally applicable to smooth, flat surfaces regardless of chemical and physical properties of the solid-liquid contact area, such as surface roughness, surface heterogeneity, air encampment, and swelling.
(Buckton, 1990) (Pepin, Blanchon and Couarraze, 1997) (Chau, 2009)	Wilhelmy plate	Automated, does not require operator training	A very sensitive microbalance is required. Swelling occurs due to liquid penetration into the pores resulting in an underestimation of contact angle. A constant perimeter of the plate should be used, or a serious error could result.
(Shang et al. 2008) (Shi and Gardner, 2000)	Column wicking	Easy, reproducible	It requires the use of a referencing wetting liquid. Unsuitable for a powder containing extra pores or highly porous particles.
(Nowak et al. 2013) (Alghunaim, Kirdponpattara and Newby, 2016)	Thin layer method	Accurate and easily predicts the position of the liquid	Not applicable for a dense particle and a powder with a contact angle less than 50°.
(Lazghab et al. 2005a) (Nowak et al. 2013) (Alghunaim, Kirdponpattara and Newby, 2016)	Pressure compensation	Applicable for measuring a highly non-wetting powder with a contact angle greater than 90°	It cannot be considered as a robust method as liquid may diffuse between inter and intra-particles pores.
(Lazghab et al. 2005b) (Alghunaim, Kirdponpattara and Newby, 2016)	Environmental scanning electron microscopy	Direct measurement of the wettability of water droplets on a surface of fine powder	Inapplicable for powder with a lower contact angle. Failed to measure the wettability of fine and porous powder with a liquid other than water.

2.8 Characterisation and uses of liquid marbles

In section 2.6, the formation of liquid marbles from non-wetting systems is introduced. This is important as many pharmaceutical formulations use non-wetting powders. In this section, more details are given about the properties and uses of liquid marbles. Non-wetting powder can be used in combination with water or any liquid mixtures to produce spherical structures termed liquid marbles. They are formed from non-wetting powder covering water droplets and are able to roll and bounce as “glass” marbles but deform and flex like a liquid (Figure 2.14). Liquid marbles are characterised by distinctive physical and chemical properties which show a wide range of high value technological applications such as in the food, cosmetics, pharmaceutical, chemical, mechanical and biotechnology industries, which has attracted significant attention of researchers in the past decade (Eshtiaghi et al. 2012a; Anon et al. 2012; Eshtiaghi et al. 2009). There is a high demand for producing the chemically inert liquid marbles, which can be used in different industrial applications.

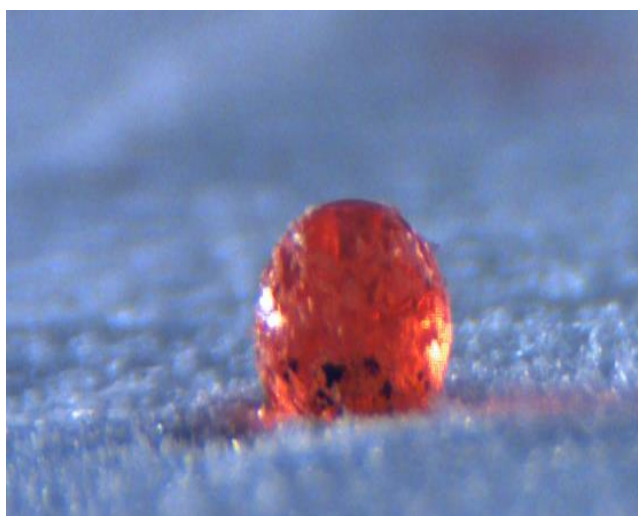


Figure 2.14: Liquid marbles of a mixture of 75% salicylic acid and 25% microcrystalline cellulose with 5 % polyethylene glycol 200.

Liquid marbles act as micro reservoirs of liquid that survive without leakage and are a potential candidate to be applied in genetic and biomedical analysis where lab-on-chip and 2D microfluidics methods are used. The evaporation rate of the liquid inside the marbles is an important parameter to ensure the stability of liquid marbles. If the liquid is quickly evaporated, the liquid marbles will collapse and deform easily. The lifetime of the liquid marbles depends

on the particle size of non-wetting powder and the chemical nature of the liquid used (Dandan et al. 2009; McHale et al. 2009).

The liquid marble phenomenon was first introduced in the pioneering works of Aussillous and Quéré (Aussillous, 2001) who have viewed that non-wetting lycopodium grain powder particles can spread over a liquid droplet creating a surface film or liquid marble. A high contact angle of non-wetting powder and lateral capillary force are responsible for the stabilization of non-wetting powder at the air-water interface. The wall of non-wetting powder around each liquid droplet acts as a protective shell to prevent leakage and coalescence of liquid marbles when they come into contact with each other (Forny et al. 2007).

Dandan et al. 2009 synthesized graphite liquid marbles. These graphite liquid marbles have an electrical conductivity which is promising to use in microfluidics, antifouling and genetic analysis. Liquid marbles were produced by encapsulating graphite powder on water droplets and the evaporation period and lifetime compared with pure water droplets. They found that the evaporation time for the graphite liquid marbles was twice the life-time of pure water droplets.

McHale et al. 2007 defined electro wetting liquid marbles which are widely used in 2D microfluidics. In biomedical and genetic analysis fields, liquid marbles are promising candidate to use, where very small quantities of materials must be analysed in a short duration of time. The electro wetting liquid marbles help to overcome contact angle hysteresis in order for a liquid droplet to move.

Ionic liquid marbles have received lots of attention over the last decade because of their excellent characteristics as a solvent, ionic conductivity, thermal stability, and low vapour pressure and evaporation rate. Ionic liquid marbles were produced by Gao and McCarthy, 2007, formed from perfluoroalkyl particles (OTFE) and polymeric (PTFE) tetrafluoroethylene, which were unreactive and fluoride containing polymers. The ionic liquid marbles with OTFE are much more robust and remained floating on the water surface for a week compared to those prepared with hydrophobized silica or lycopodium which coalesced after a minute of floating.

Bormashenko 2011 reviewed the properties and application of liquid marbles from over 10 years of experience gained from the study of liquid marbles. The study showed that liquid marbles could be used as “micro-reactors, micro-pumps and pH, gas, water pollution sensors. Arbatan et al. 2012 reported the usage of liquid marbles as a micro-bioreactor in biological and

analytical tests. Liquid marbles can be used to identify human blood groups by the formation of blood marbles. This may offer many advantages over traditional methods such as simplicity, safety, and cost effectiveness.

Liquid marbles are a promising tool for controlling the delivery of active ingredients from powdered drugs, food, detergents and fertilizers into solution. This can be achieved by assembling the particles in open and coarse aggregates (formed granules). The rate of the release depends on the granule size and porosity, and the granule microstructure (Whitby et al. 2013).

McEleney et al. 2009 studied the influence of formulation parameters rather than hydrophobicity on the formation and stability of liquid marbles, such as powder particle size, shape and density. They found the higher sphericity and low density powder particles lead to a complete spreading of the powder over the liquid, and more stable liquid marbles were produced. The sphericity contributes to the low contact of the spherical particles at the liquid-solid interface, while the lower density powder means lower energy is required to move over a liquid surface.

Bhosale et al. 2008 examined the formation of elasticity and strength of the shell of liquid marbles made from poly tetrafluoroethylene (PTFE) particle size of 7-12 μm and fumed silica powder with a surface treated with two different non-wetting chemicals; hexamethyldisilazane and dimethyldichlorosilane. Uniform wall coverage of the powder-liquid interface was formed with nanoparticle materials of non-wetting powder. They found that more “elastic” shells and mechanically robust liquid marbles were formed with nanoparticle sizes compared with the marbles formed from larger particle sizes. These robust liquid marbles were able to withstand the remaining process compression forces during drying and manufacturing.

Whitby et al. 2013 studied liquid marble behaviour by using liquids of different surface tensions by varying alcohol concentration in water. Three different sizes and shapes of non-wetting powder used; coarse spherical glass beads, irregular coarse coal particles, and irregular fine molybdenite particles. They found the droplet either easily wetted and penetrated the coarse powder bed (glass beads and coal dust) at low surface tension of the liquid, or spread over the liquid of high surface tension. Drops placed onto fine molybdenite powder bed do not penetrate, but instead roll away, even when deposited very carefully. They behave as a super non-wetting powder and collect much more non-wetting powder along their path. In addition,

they found that the evaporation of the liquid is slowed down on complete coating of the powder around the liquid droplet.

Nguyen, 2009 investigated the effect of powder particle sizes on the internal structure of the liquid marbles. It was found that the powder encapsulated the liquid droplet either as a monolayer or multi-layers of particles, which was mainly dependent on their size. Larger particle sizes, more than 50 μm , formed a monolayer, while a multi-layer powder shell was formed from a fine particle size. In addition, it was reported that the large particle size tended to float on the liquid surface with a decreasing extent of penetration into the liquid core compared with fine powder particles.

Binks et al. 2006 developed a novel method of phase inversion in a single system comprising water, air and fumed silica particles having different hydrophobicity. They described the phase inversion of particle stabilized aqueous foams into water in air powder (liquid marble) and vice versa (Figure 2.15). The transformation was achieved by either changing fumed silica wettability at constant air/water ratio or changing the air/water ratio at the same fumed silica hydrophobicity. A foam stabiliser was obtained with a contact angle of a fumed silica close to 90° , whereas antifoam formed at a contact angle more than 90° .

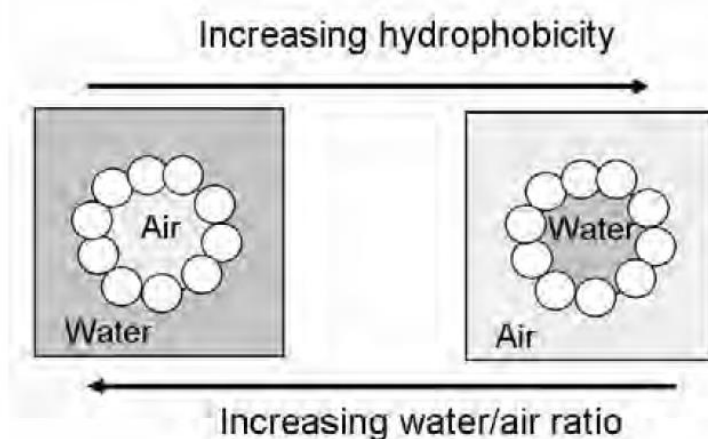


Figure 2.15: Phase inversion of foams (air in water) to liquid marbles (water in air).

Reprinted by permission from Nature Material, 5(11), Binks, B.P. & Murakami, R., Phase inversion of particle-stabilized materials from foams to dry water. pp.865–869., (2006).

Liquid marbles have attracted intensive experimental research and different industrial potential implementations. Many authors have focused on studying the effect of formulation or processing parameters on liquid marbles such as the drying temperature (Eshtiaghi et al. 2010,

Hapgood et al. 2009) or liquid marble properties such as strength, elasticity, etc (Bhosale, Panchagnula and Stretz, 2008). Others have studied liquid marbles with the aim of manufacturing designer particle configurations for pharmaceutical and industrial applications (Eshtiaghi et al. 2012; Hapgood et al. 2009; Forny et al. 2007). However, there are very limited studies on what is happening after liquid marble formation and the resulting hollow granule structure in low or high shear granulation. Studies in this area are reviewed in the following section.

2.9 Liquid marbles in granulation

In granulation, liquid marbles are a promising way to solve the problematic behaviour of non-wetting powder where the powder spreads around the liquid droplet in the nucleation stage and the interior liquid is subsequently dried to form hollow granules. Desirable granule properties can be produced from nuclei formed by the spreading of powder over a liquid droplet such as:

- Controlling granule size and structure. The size of granules is controlled by droplet size under low spray flux and hollow granule structure is self-assembled during the granulation, which depends on powder wettability (Eshtiaghi. et al. 2009).
- Ability to handle a high loading of a non-wetting powder (Eshtiaghi. et al. 2009).
- Improved flow properties with spherical granules (Hapgood et al. 2009).
- Good dissolution and compression properties for tableting with highly porous granule (Ansari et al. 2006).
- Reduction in the drying period due to thin wall powder structure (Eshtiaghi. et al. 2009).
- Potential to load both wetting and non-wetting drugs; soluble drug in liquid interior with a non-wetting one to form the outer shell (Hapgood et al. 2009).
- Economic advantages of producing light granules with minimum powder loading (Eshtiaghi. et al. 2009).

There are two reported experimental methods used in the production of liquid marbles resulting in hollow granules upon drying: melt granulation (Ansari et al. 2006) and high shear granulation (Hapgood et al. 2009; Eshtiaghi et al. 2009; Saleh et al. 2011).

Many researchers investigate the effect of different formulation and process parameters on granulation of liquid marbles in low or high shear mixers. These studies are aimed to better

understand the behaviour of decreasing powder wettabilities on the size, strength, shape, internal microstructure of resultant granules. In addition, researchers investigate the effect of different parameters on survivability (intact and spherical) of liquid marbles during granulation. They are described in the following sections:

- **Effect of process parameters (wet massing time, impeller speed and liquid/solid mass ratios):**

The effect of liquid to solid ratios (L/S) and wet massing time on granule size distribution and morphology was studied by Hapgood et al. 2009. L/S ratios of 70 wt. % and 78 wt. % for 1 and 7 minutes wet massing time were used. At 70 % liquid ratio, the granule size distribution was bimodal with a one mode at 300 μm and a second mode at 20 μm which is unrelated to wet massing time. However, granules deformed with an increase of wet massing time of 7 minutes. At 78 % liquid ratio, there was a significant change in granule microstructure and the granule size distributions were more dependent on wet massing time. Figure 2.16, shows granules deformation with prolonged mixing time. At 1 minute, a similar granule size distribution was produced but there was a decrease in the number of fines. After 7 minutes wet massing time, there was a unimodal granule size distribution.

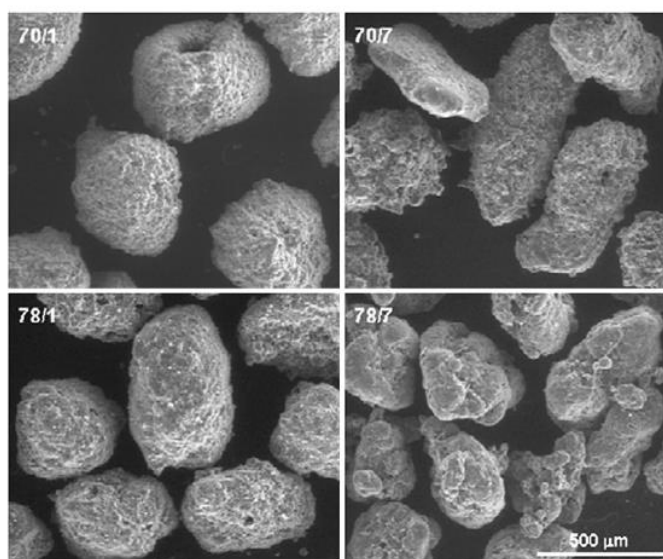


Figure 2.16: SEM images of granules produced at 70 % and 78 % liquid/solid ratio and at 1 and 7 minutes mixing time.

Reprinted from Powder Technology, Vol (188), Issue (3), K.P. Hapgood, Farber and Michaels, Agglomeration of hydrophobic powders via solid spreading nucleation, pp (248-254), Copyright (2009), with permission from Elsevier.

In addition, the effect of L/S on the formation of hollow granules of a fumed silica non-wetting powder in a high shear granulator was investigated by Eshtiaghi et al. 2009. Different ratios of hydroxypropyl cellulose solution were used. As the liquid to solid mass ratio increased, the granule size distribution increased with a decrease in the number of fines. Moreover, the number of stretched and flattened granules increased with increased liquid ratio. This highlights the importance of the use of an appropriate amount of liquid binder. It was concluded that the final granule size and shape was dependent on the liquid to solid ratio when nucleation of liquid marbles started with the nucleation droplet regime; one drop formed one nuclei. While in a mechanical dispersion regime, where there is a large bulk of fluid, the structure and morphology of the granules are independent of the liquid to solid mass ratio (Figure 2.8).

In addition, they found that the impeller speed had a significant effect on granulation growth behaviour of non-wetting powder. As the impeller speed increased with a mixture of a high non-wetting content, a better liquid distribution and greater extent of granulation was obtained at shorter granulation times. Under rigorous mixing conditions, a uniform distribution of wetting and non-wetting substituents inside the granules was obtained. The wetting material was initially nucleated followed by layering of the non-wetting substrate. As the impeller speed increased, the granules experienced more collisions leading to consolidation and became more

uniform in granule composition. During collisions, the structural rearrangement pushes the non-wetting particles at the surface into the centre of the granules (Charles-Williams et al. 2013).

The effect of granulation time was studied by Asada et al. 2018 who produced a sustained release formulation of non-wetting powder through the formation of hollow granules. phenytoin (non-wetting) and Eugragit (wetting) as powders and water as liquid binder were used. It was concluded that the granule size increases in a time dependent manner as the granulation proceeds. In addition, the wall thickness increased and the hollowness inside the granules decreases with granulation time. The roundness and smoothness of the granules also increased with granulation time (Figure 2.17).

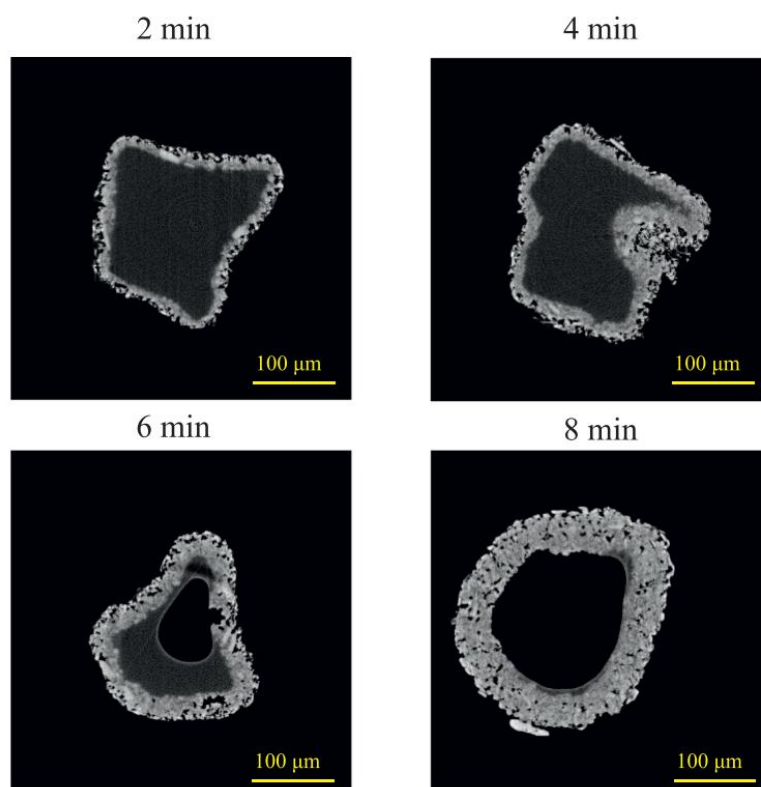


Figure 2.17: XRCT images of granules produced at different mixing times.

Reprinted from European Journal of Pharmaceutical Science, Vol (117), Asada et al., 2018, Mechanism of the formation of hollow spherical granules using a high shear granulator, pp (371-378), Copyright (2018), with permission from Elsevier.

- **Effect of formulation parameters (amount of non-wetting powder, binder viscosity and primary powder particle size):**

The effect of the presence of non-wetting powder in the powder mixture on the formation and stability of hollow granules was studied by Hapgood et al. 2009. They granulated a mixture of 70 wt. % non-wetting drug powder, 20 wt.% microcrystalline cellulose as a wetting diluent, 4% hydroxyl propyl cellulose powder as a binder. The presence of these wetting ingredient components did not affect liquid marble formation or movement of particles on the drop surface. In contrast, the existence of wetting ingredients helped to stabilize and preserve a hollow structure of liquid marbles during drying. Even the presence of 1% sodium lauryl sulfate as a surfactant did not affect the formation of liquid marbles since 70 wt. % (90% by volume) of the formulation is non-wetting powder. Stabilized hollow granules were produced by drying the liquid marbles to eliminate the interior drops. These hollow granules were strong enough to withstand further wet massing, milling during drying and additional pharmaceutical processes such as tableting. X-ray tomography of the dried granules was used to confirm the formation of hollow granules.

The increasing amount of non-wetting powder in the powder mixture is studied by Charles-Williams et al. 2013. Mixtures of wetting lactose and non-wetting limestone powders were used in their study. They found that the non-wetting content had a significant effect on granulation behaviour both for the size and granule compositional distribution. At the same granulation time, the granule size decreased as non-wetting powder content increased.

The effect of the amount of non-wetting powder in a mixture was also studied by Nguyen et al. 2010. This was conducted by granulating different ratios of salicylic acid (a non-wetting powder) and lactose (a wetting powder) with two different granulating liquids (water and 5 (w/v) % poly vinyl pyrrolidone (PVP)). They found that as the proportion of non-wetting powder increased, there was a decrease in granule size. A formulation with a lower proportion of salicylic acid produced granules that exhibit a morphology consisting of a large granule size with a saturated core surrounded by a semi-saturated shell powder. This suggested that the core-shell structure demonstrates high granule strength which was able to resist any deformation forces applied. As the proportion of salicylic acid increased the granule strength decreased. With 40 wt. % of the salicylic acid in the mixture, the outer semi-saturated shell was broken away from the saturated core. Increasing the proportion of the salicylic acid to 80

%, granules were composed of a saturated core only. This was because of the weak binding forces between salicylic acid particles and the weak resistance of the core to deformation forces that result in the loss of the all semi-saturated core during the granulation process. The saturated core only structure that was produced with the formulation that had a high proportion of salicylic acid can explain the decrease in the size of the granules due to breakage with an increase in the amount of non-wetting particles in the powder mixture (Figure 2.18). However, further studies are required to further investigate the mechanism behind the decrease in granule size with the use of more non-wetting powder.

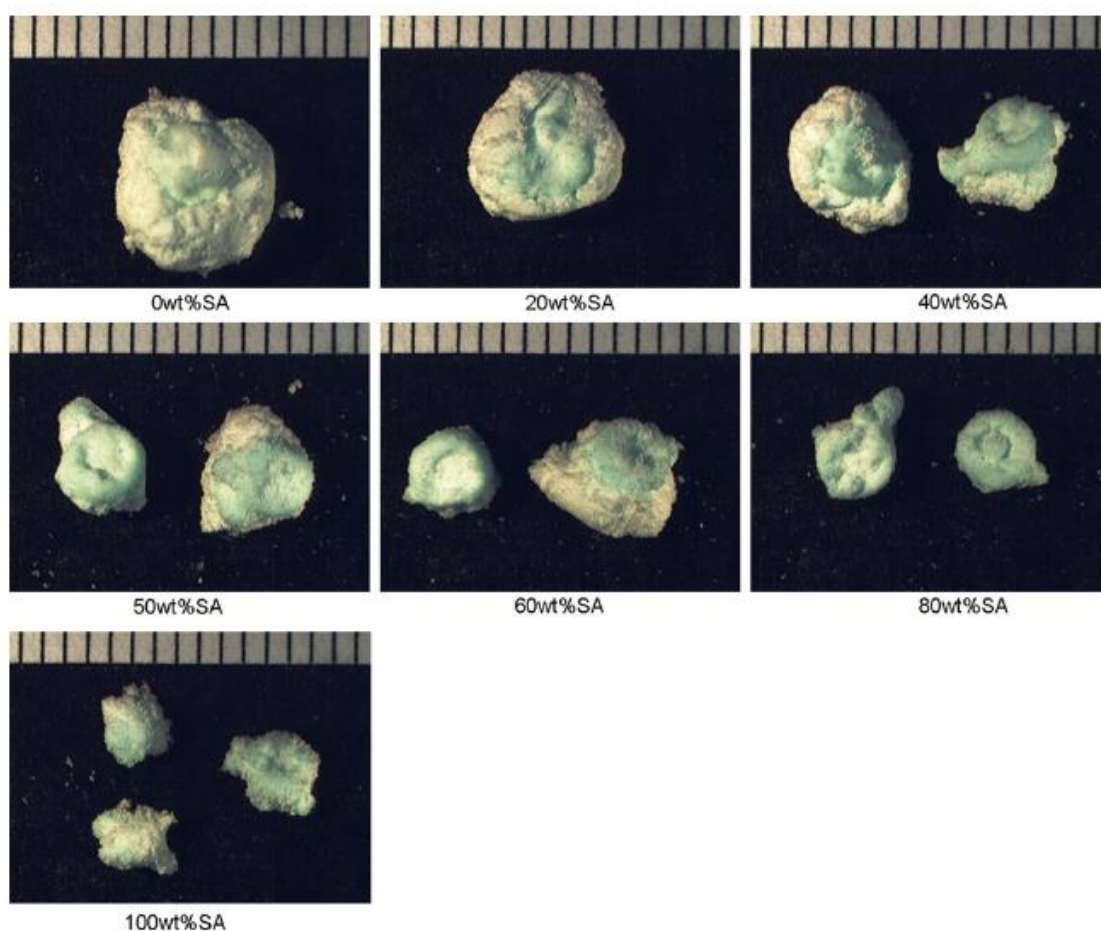


Figure 2.18: Granule size and morphology as a function of increasing amount of salicylic acid (non-wetting) powder.

Reprinted from Chemical Engineering Journal, Vol (164), T. H. Nguyen, W. Shen, K. Hapgood, Effect of formulation hydrophobicity on drug distribution in wet granulation, pp (330-339), Copyright (2010), with permission from Elsevier.

The effect of primary particle size on granule internal structure was studied by Davis et al. 2017. A quantitative method to study the variation in granule microstructure was developed. α -alumina powder with four different particle sizes were used. Water was used as a binder for

the ultra-fine powder particles, while water with 0.05 g of PVP was used for the larger particles size. Granules were prepared through single drop nucleation; liquid droplets were placed onto a static powder bed using a 22-gauge needle. The granule microstructure was obtained using X-ray tomography. Different primary powder particle size leads to differences in granule microstructure and the total volume of macro-voids. There were very few macro-voids in granules formed from coarser powders. Ultra-fine powder had the ability to form a complex structure and become stronger than other granules. This powder was capable of forming granules with large macro-voids of different shapes and sizes.

- **Combination of process and formulation parameters:**

The effect of binder viscosity, drying temperature and primary particle size on the formation and survivability of liquid marbles (liquid marble remain intact and spherical) was studied by Eshtiaghi, Liu and Hapgood, 2010. They found that at higher drying temperature, higher liquid viscosity, and smaller or nano-size particles, leads to the formation of a spherical liquid marble. It was found that there was a direct correlation between the survival rate (before collapsed) and the binder viscosity of hydroxy propyl methylcellulose (HPMC) (Figure 2.19) and polyvinyl pyrrolidone (PVP). However, for hydroxy propyl cellulose (HPC) binder, the survival rate was essentially constant regardless of HPC concentration. This may be due to decreasing solubility of HPC and precipitation of the polymer in water at higher temperature. Various combinations of drying temperature, binder type, binder concentration, and powder type/grade could result in major changes in survival rate, stressing the importance of careful formulation selection during hollow granule process development.

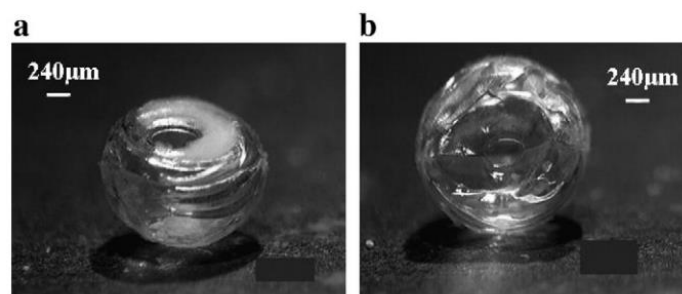


Figure 2.19: Hollow granules formed at 100 °C from Aerosil R974 and (a) 12% HPMC, and (b) 18% HPMC.

Reprinted from Powder Technology, Vol (197), Issue (3), N. Eshtiaghi, J. Liu and K. Hapgood, Formation of hollow granules from liquid marbles: small scale experiments, pp (184-195), Copyright (2010), with permission from Elsevier.

In addition, Ansari et al. 2006 studied the effect of binder particle size and liquid to solid ratio on granule internal microstructure using X-ray tomography. D-mannitol was used as a powder and polyethylene glycol was used as a binder using fluid bed in situ melt granulation. Binder size was found to have an effect on the formation of hollow granules. Formulations that have the binder particle size larger than the powder primary particle size tend to produce hollow granules. The hollowness inside the granules tends to increase as the binder particle size increased which, in turn, effects granule disintegration, dissolution and tableting.

Briens et al. 2019 studied the effect of tumbling speed and binder viscosity using different powder wettabilities on granule strength and size. They used three different powder wettabilities of biochar (low, medium and high) as a powder and different concentrations of aqueous HPMC solution as liquid binder. Two different tumbling speeds; 40 and 60 rpm were used. Granule strength was measured using Instron 8874. They found granules strength increased with increasing binder viscosity, tumbling speed and powder wettability. The granule size decreased with increasing binder viscosity because of increase droplet resistance to deformation and the viscous force inhibited the movement of the liquid through the granule voids. They suggested that the increasing binder viscosity produced a more hydrophobic liquid-powder interaction. The droplet penetration took longer time and became more difficult for the powder to penetrate into or around the liquid droplet to form a liquid marble. The granule size increased with increasing tumbling speed due to the increase the impact force and collision between granule with other granules and with the wall of the tumbling drum which contribute to particles coalescence.

2.9.1 Regime maps

A regime map was developed by Saleh et al. 2011 to described the primary mechanism responsible for hollow granule formation by examining the effect of several process parameters and a range of powder wettabilities on the formation of liquid marbles. The regime map was suggested to depend on the comparison between mechanical energy from mixing and the energy of particle immersion, ΔE_{Imm} , which differs linearly with wetting criterion, $\lambda_{LV} \cos \theta$, normalised with pure water surface tension as shown in Figure 2.20. In this diagram, the energetic impact of the mixing process is positioned qualitatively on the y-axis. For example, the energy of immersion, ΔE_{Imm} , is qualitatively described in this diagram and has a linear

correlation to the immersion parameter, $\lambda_{LV}\cos\theta$. For a wetting system, the energy of immersion is positive and a suspension can be obtained. In this region immersion takes place spontaneously without any mixing. For non-wetting powder, different systems can be seen depend on the effect of shearing forces and surface tensions forces. If the energy of mixing impacted to the particles is lower than the immersion energy, the biphasic system will be formed of water and silica. In contrast, if the mixing energy is high enough but does not exceed the immersion energy, a spreading of powder particles around a liquid droplet will occur and liquid marble will be formed. Finally, if the energy of mixing is higher than the energy of immersion the liquid will split into droplets and immerse the particles as a mousse can be seen.

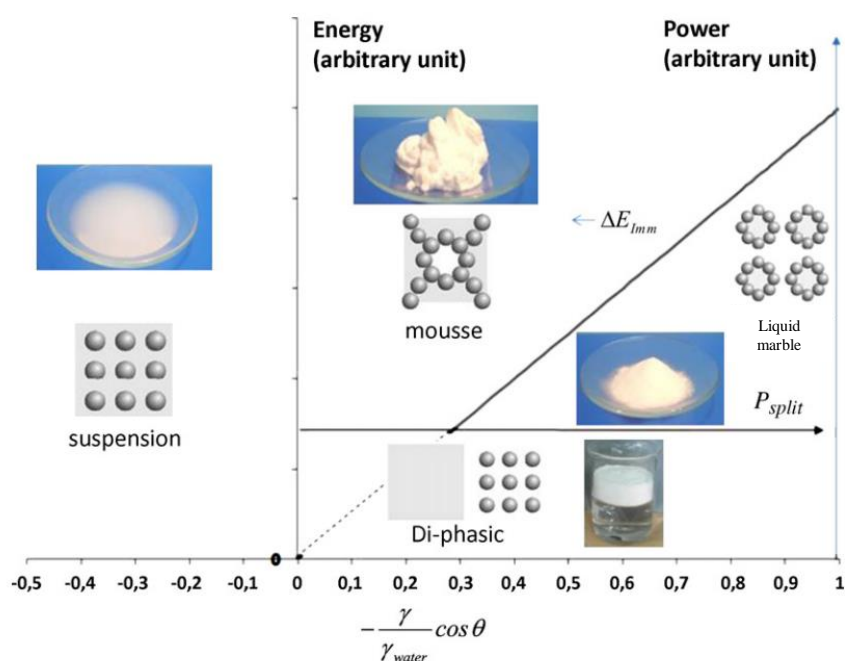


Figure 2.20: Regime map for liquid marble formation.

Reprinted from Chemical Engineering Research and Design, 89(5), Saleh, K. et al., Dry water: From physico-chemical aspects to process-related parameters, pp.537–544., (2011) with permission from Elsevier.

The regime map in Figure 2.20 was verified by Saleh et al. 2011. Under an extremely energetic process, only the highly non-wetting powder (Aerosil R812S) can produce liquid marbles. A mousse was formed with moderately non-wetting powder (Aerosil R972). The same finding was obtained with a decrease in surface tension of liquid. At point A (Figure 2.21) (water with

a highly non-wetting Aerosil R812S developing hollow granules) the power imparted into the system is high enough to split the liquid into droplets but does not exceed the energy of immersion, and solid particles will spread to the surface of the droplets and liquid marble will be obtained. With a decrease in hydrophobicity of Aerosil R972 or a decrease in surface tension of the liquid, points B and C are obtained. In addition, the power given to the system is high enough to split the liquid and to immerse the particles and a mousse will be formed.

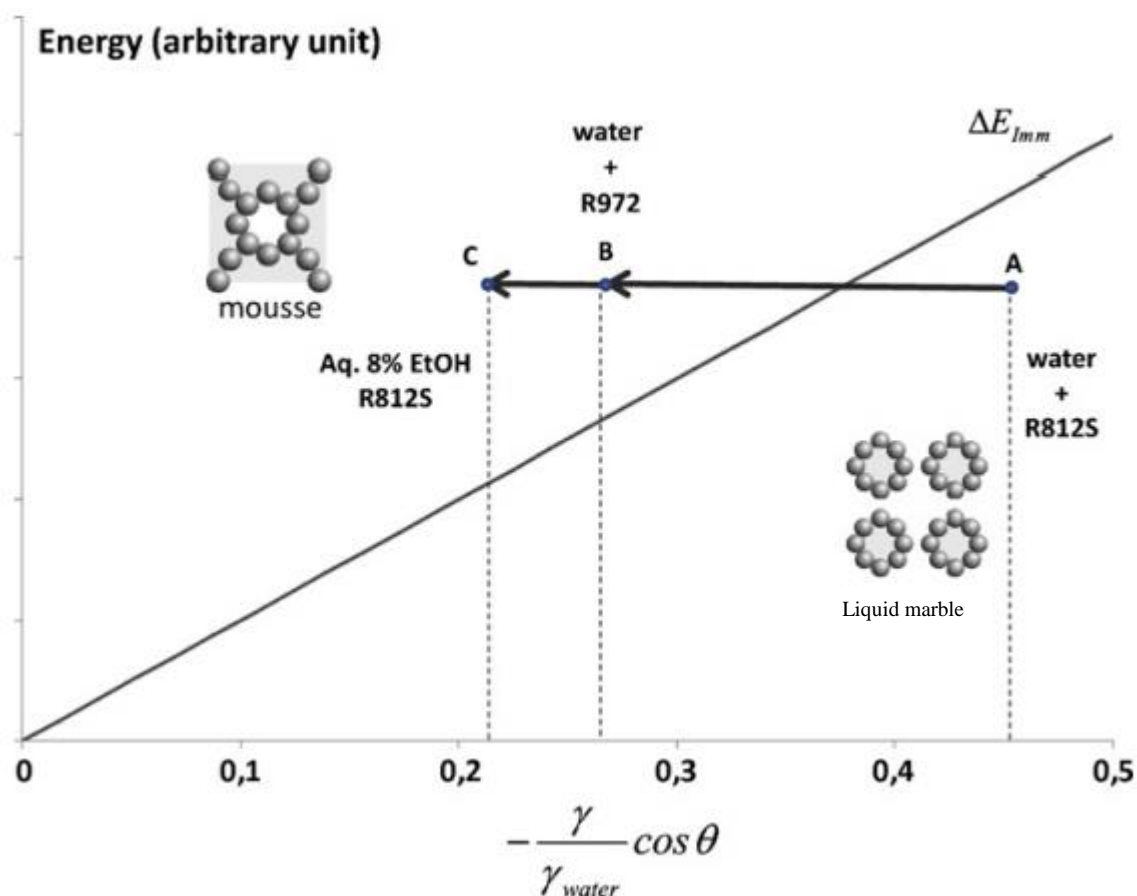


Figure 2.21: Verified regime map for liquid marble formation.

Reprinted from Chemical Engineering Research and Design, 89(5), Saleh, K. et al., Dry water: From physico-chemical aspects to process-related parameters, pp.537–544., (2011) with permission from Elsevier.

In addition, Eshtiaghi et al. 2012 revised and validated a preliminary flow chart for liquid marble formation proposed previously by Hapgood et al. 2009. A revised flow chart gives the opportunity for a better understanding of the mechanism of non-wetting powder granulation. This study showed the formation of liquid marbles by a "droplet template" regime; one drop forms one nuclei or liquid marble (Figure 2.22). They also developed a quantitative framework

for the formation of liquid marbles by a "mechanical dispersion regime", when a bulk of liquid is available during granulation. Contact angle and dimensionless spray flux, the measure of the area wetted the powder from the nozzle to the renewal flux of powder through the spray area, are among the important parameters in order to differentiate between the droplet template and mechanical dispersion regime, see nucleation regime map in Figure 2.8. They found that if the contact angle is above 110° , a successful liquid marble can form in the mechanical dispersion regime while an approximately 90° contact angle is essential for the droplet template regime. Consequently, in the mechanical dispersion regime, a more non-wetting powder is required than in the droplet template regime to prevent particle immersion and liquid marble destruction.

This framework has been achieved through many criteria;

- The liquid droplet size to be 25 times greater than the particles size ($d_d > d_p$).
- Bond number should be small to ensure the formation of spherical drop rather than distorted pool or puddle ($B < 1$).
- Weber number should be small, the drop must land on the powder and survive the impact without breaking or shattering ($W < 1000$).
- The contact angle of the binder on the powder bed needs to be $> 90^\circ$ to prevent the penetration of the drop into the powder bed.
- Dimensional spray flux should be small ($\psi_a < 1$), one drop form one nuclei.
- The kinetic energy should be enough to produce single spherical liquid marbles with spreading of the powder around liquid droplet.

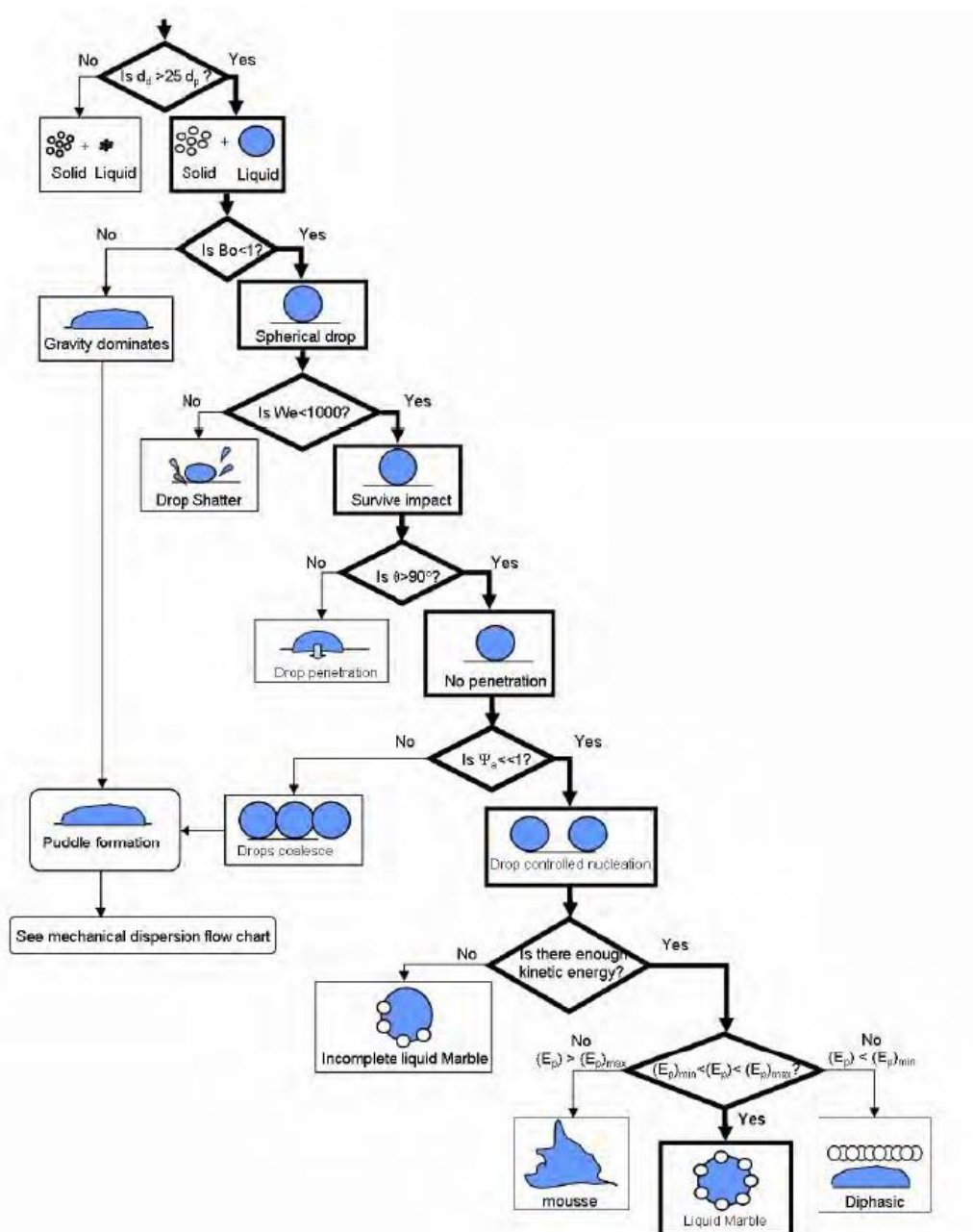


Figure 2.22: Schematic chart for the formation of liquid marbles by a droplet template regime.

Reprinted from Powder Technology, V (223), Eshtiaghi N., Hapgood K., P., A quantitative framework for the formation of liquid marbles and hollow granules from hydrophobic powders, pp.65-76, (2012), with permission from Elsevier.

2.10 Conclusions and thesis objectives

This literature review has summarised some of important studies relevant to this thesis. Until recently, there has been limited research on granulation of non-wetting powder, which is a major problem in the pharmaceutical industry, and how to control the granule size and microstructure of hollow granules. Little experimental data is available for the granulation growth mechanism of non-wetting powder, especially when compared to the data for wetting powders, or study the nucleation of non-wetting powders.

There have been several studies on the granulation and nucleation of non-wetting powder, and an approach proposed to transform the problematic non-wetting powder into a powerful tool for creating “designer pharmaceutical granules.” A framework for liquid marble formation by solid spreading nucleation has previously been proposed (Eshtiaghi et al. 2012).

Several methods for the study of the mechanism and driving force for liquid marble formation have been presented. Many researchers try to answer the question “Why are liquid marbles formed.” Based on experimental results, there is a relationship between increasing the kinetic energy and the percentage of coverage of a liquid marble. The liquid marble coverage percentage decreases as the binder viscosity increases and surface tension decreases. In addition, a complete coverage of powder around a liquid droplet is achieved with increase of powder particle size.

Furthermore, a framework for hollow granule formation has been developed. The framework emphasized the importance of using an optimum concentration of compatible polymeric binder. Liquid to solid ratio and drying temperature are an additional requirement for successful formation of hollow granules with single or multiple cavities. Many researchers have studied the growth of non-wetting powder granules and found that the granule size distribution decreases with an increase in the content of a non-wetting powder.

To conclude, liquid marble and hollow granules research is still in its infancy, and many essential properties of liquid marbles are yet to be explored. Studies on internal microstructure behaviour of heterogeneous-wetting powders are limited, requiring considerable further work.

Gaps in knowledge of liquid marble formation have been identified:

- A lack of systematic studies of the effect of formulation parameters over a wide range of conditions.
- Limited studies on growth of granules from non-wetting powder.
- Limited studies on the internal microstructure behaviour of hollow granules.
- Limited studies on the effect of shear force on size and internal microstructure of hollow granules.
- Most studies have focused on nucleation and mechanism of formation of liquid marbles. However, there is very limited work on the mechanism of growth and microstructure characteristics of the resulting hollow granules for range of wetting and non-wetting powders.

This thesis presents a unique approach to control the effect of formulation and process parameters on the granule size and internal microstructure of granules formed from non-wetting powders.

Consequently, a thorough understanding of the following questions is of great importance, and forms the basis of this thesis's objectives:

1. What is the effect of binder viscosity and powder properties (especially particle size) on the size and microstructure of hollow granules?
2. What is the effect of mixing conditions on granule size and microstructure in these systems?
3. What is the effect of changing wettability on the mechanism of granule size and microstructure?
4. What is the effect of powder and binder properties on the wall thickness of hollow granules?
5. What is the effect of powder particle size on the granulation of powder of different wettabilities on the size and microstructure of granules?

CHAPTER 3. Materials and Methods

3.1 Introduction

This chapter gives information of the materials used in all experiments, and the methods used for their characterisation. It also describes the experimental methodology and analysis of the products. This chapter acts as a reference for all the experiments described in the following chapters.

Section 3.2 explains the different characterisation methods used. Sections 3.3 and 3.4 describe the powders and liquid binders used, respectively. Section 3.5 describes the properties of the different powder-binder systems used in the experiments. Finally, the different experimental methods are explained in Section 3.6.

Three types of experiments were performed. The first type focuses on exploring the use of a low shear mixer (tumbling drum) for investigating the granule size and internal microstructure characterisation. The second type is an investigation of granule size and microstructure in a high shear mixer. Both these two methods employed a model material system. The final experimental part was performed to verify the applicability of the results obtained from the previous two methods into industrial pharmaceutical powder granulation. Here, similar methods using both low and high shear were employed, but in this case using a pharmaceutical formulation.

Although different types of methodologies are investigated to produce hollow granules, all of them are based on firstly pre-nucleated liquid marbles or immersion nuclei externally prior to granulation. Once the pre-nucleate liquid marbles or immersion nuclei are formed, there are then added to the different types of mixers for granulation.

3.2 Characterisation methods

Several methods are used to analyse and characterise the powder, liquid binder and the granules produced in this work. The principles of these methods and operation techniques are discussed in the following sections.

3.2.1 Particle size distribution

Particle size is an important property of particulate products. The measurement of particle size is usually performed in a wide range of industries and is an essential parameter in the manufacturing of many products. Particle size analysis gives information on the size distribution of particles. This can be used to calculate different properties of particles and how they will act under certain conditions. This information is critical in industries to achieve different goals (Litster, Ennis, & Liu, 2004).

The particle size distribution is a term used to represent the size of particles present and in what proportion. The length scale of particle size in industry can range from hundreds nanometres to several millimetres (Allen, 2003). Two methods of measuring the particle size distribution are used in this work and are described in the following sections.

3.2.1.1 Laser diffraction

All powders used in this work were analysed for their particle size distributions using dry and wet cell laser diffraction (Malvern Mastersizer 3000). Laser diffraction measures the particle size distribution by measuring the variation in intensity of light scattered as a laser beam passes through a dispersed particulate sample. Small particles scatter light at a large angle while large particles scatter light at a small angle, relative to the laser beam. The variation in angular intensity data is then analysed to calculate the particle size responsible for the scattered pattern, by the using Mie theory of light scattering (Ryzak et al. 2011) (Figure 3.1).

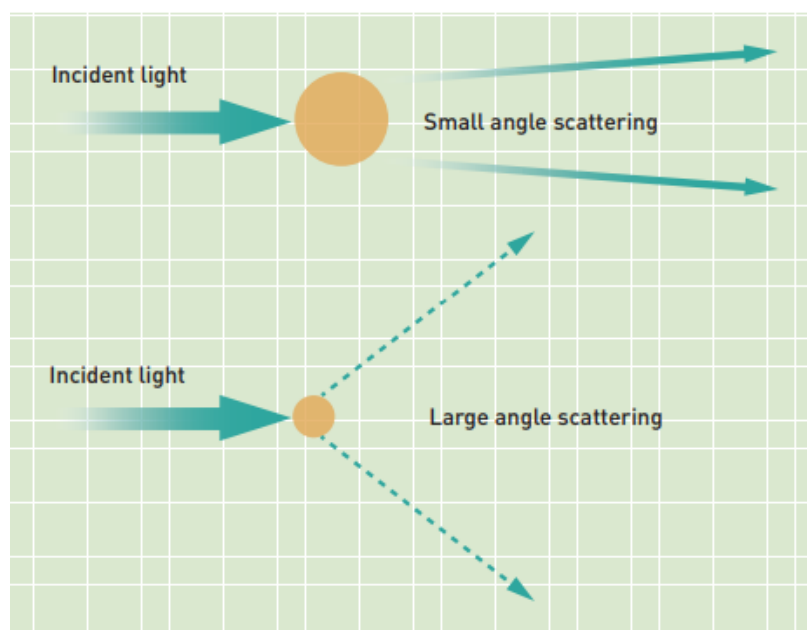


Figure 3.1: Principle of laser diffraction (Malvern Instrument handbook).

Laser diffraction is a widely used technique for determination of particle size for materials ranging from a nanometre to millimetre particle size range, which is the main reason for its success. In addition, there are other advantages such as rapid measurement, good repeatability when large numbers of particles are sampled in each measurement, instant feedback and, high sample throughput.

The output of the laser diffraction characterisation using the Malvern Mastersizer is a table with size classes, or bins, and the volume of the particles inside each bin. A plot of volume frequency distribution, q_3 , is obtained from this table; the volume percentage of particles in a bin divided by the bin width. The frequency distribution curve gives information on powder particle size uniformity, the surface area moment mean diameter or $d_{3,2}$, and the volume moment mean diameter or $d_{4,3}$. The $d_{3,2}$ is defined as the sphere diameter that has the same volume/surface area ratio of a particle of interest, and is mostly used when the surface area of the particles is important. The $d_{4,3}$ is more sensitive to the presence of a large particle size. It is relevant to the size of those particles which constitute the bulk volume of the sample.

The $d_{4,3}$ is most favourable because laser diffraction first isolates a distribution proportional to the volume of the particle. This volume distribution can be converted to a number distribution by matching some assumption on the size of the particles to each volume bin, and equally weighted all particles (Allen, 2003).

From the volume frequency distribution plot, the cumulative frequency distribution, Q_3 , by volume, can be calculated. This distribution yields three important percentile values (d-values). The d-values are the diameter when all particles in a sample are arranged in order of ascending mass, divided by the sample's mass into a specified percentage. The number expressed after the 'd' is the mass percentage below the diameter of interest. For example, d_{10} , is the diameter when 10% of the sample mass consists of particles smaller than this value. The d_{50} is the diameter when 50% of a sample's mass consists of particles smaller than this value. The d_{50} is also known as the mass median diameter. The d_{90} is the diameter when 90% of the sample mass of particles are smaller than that value.

In this work, the particle size distributions were measured give the $d_{4,3}$, $d_{3,2}$, d_{10} , d_{50} and d_{90} for all powders used. Additionally, the q_3 is shown for all samples. Measurements were carried out in triplicate. Equipment calibration was performed by the lab technician through verification using standard reference material.

3.2.1.2 Sieve analysis

The oldest and cheapest method of particle size determination is sieve analysis defined by the mass or volume. Sieve analysis is used to divide the particulate material into size fractions and then to determine the weight of this fraction. A Retsch sieve Shaker AS 200 is used in this work, and is a vibratory sieve shaker in which an electromagnetic drive sets a spring-mass system in motion and transfers oscillations to the sieve stack. The sample is subjected to 3-dimensional movement and is distributed uniformly across the whole area of the sieve. The probabilities of the particles passing through the sieve depend on particle size, particle orientation and the number of encounters between the particles and the mesh openings (GmbH, 2014).

In this research, the granule size distribution was measured by sieving using sieves (Retsch) with the following mesh sizes 4000, 3350, 2800, 1700, 1000, 500, 250, 180, and 106 μm . From visual inspection of the product, it appeared that there was no granular material present below a particle size of approximately 100 μm ; only ill-defined particles/fines were observed. Therefore, a 106 μm sieve was the smallest sieve size used. All material below this size was considered to be ungranulated and was not included in the granule size distribution.

These mesh sizes were arranged in a stack with the largest mesh opening at the top of the stack. The sample was placed on the top of the sieve and during the process the particles were separated into different size fractions through the sieves. Any remaining fine powder was collected in a collector pan at the bottom of the sieve stack. The sieving time was set for 2 minutes. The amplitude was chosen as 0.7 mm/g (Allen, 2003)).

Calibration of the sieves was performed by a visual check for broken wires or damaged mesh, confirmation that the tension was satisfactory, and excessive blinding and pegging. In addition, a visual check of solder joints for crevices was performed.

The frequency distribution curve, the number of particles between two sizes, was used to give the granule size distribution. The sample remaining on each sieve size was weighed and calculated as a percentage of the sum of the individual fractions. The mass frequency was obtained by dividing the percentage of the individual fraction by the width of each sieve size.

For the work that was performed at MSD, USA (Chapter 6), a Ro-Tap sieve shaker was used with sieves of the following mesh sizes; 1000, 500, 300, 180, 150, 106 μm . The sieving time was 1 minute. Here, the sieve analysis was performed to separate the granules from the fine powder. Light microscopy was done using SZX16 Olympus stereo microscope equipped with Infinity 3 color camera (Luminera, Canada). Granules were placed on a white plastic dish. Granule size was calculated from images acquired with SZX 16 microscope using ImagePro Premier software. Thresholding was done using build-in algorithm “dark object on white background”. For collapsed nuclei, the calculated size represents the diameter of the equivalent flat disk. Fifteen to eighteen granules were tested. A number median diameter (d_{50}) was measured and presented throughout Chapter 6. Median diameter was defined as the value where half of granule size resides above this point and half resides below this point.

3.2.2 Contact angle measurements

Contact angle measurements were used to characterise the wettability of different powders and liquid binder mixtures. Many different methods have been developed to measure the contact angle from the shape of drop. The shape of the drop depends on the combination effect of surface tension and the external force (gravity force).

The drop shape method is considered a recent development method for contact angle measurement. During an early stage of contact angle measurements, the $\theta/2$ method (Equation (3.1)) was widely used to analyse the shape of a sessile drop. In the shape analysis method, the liquid drop is assumed to be part of the sphere. Geometrically the contact angle can be measured by calculating the diameter of the drop and the height of the apex.

$$\frac{\theta}{2} = \tan^{-1} \left(\frac{h}{D_d} \right) \quad \text{Equation (3.1)}$$

where θ is the contact angle, h is the height of the apex and D_d is the drop diameter.

Contact angles of all powder-binder systems were measured using a First Ten Ångströms FTÅ200 goniometer (Figure 3.2). The instrument uses the “drop shape” analysis method, which describes the shape of a liquid drop in contact with a solid. It captures the images of liquid droplets on a CCD camera and analyses their shape and size by FTA software on a computer. 50 g of different powder mixtures were used after mixing with a spatula for 5 minutes. A thin layer of powder mixture was spread onto a microscope slide with double adhesive tape on top (Oostveen, Meesters and van Ommen, 2015). The contact angle was then measured through releasing the liquid droplet using a 22 G blunt needle onto the layer of powder (needle internal diameter = 0.41 mm). The drop detached from the needle before touching the powder surface. Single snapshots were taken over 20, 40, 60, 120, 300 and 600 secs, which was the expected duration of the measurement, and the time where the drops started to evaporate. From the images, the software automatically calculated the contact angle. The mean contact angle was calculated from three measurements for each powder/liquid combination.

For the work carried out at MSD (Chapter 6), the contact angle was measured manually at the intersection of the three-phase line (solid, liquid, gas) using light microscopy, Keyence VHX-6000 with 0.5X objective lens and 1X zoom lens with the same procedure and time duration as mentioned above. The mean contact angle was determined from three measurements for each powder/liquid combination using Keyence software.

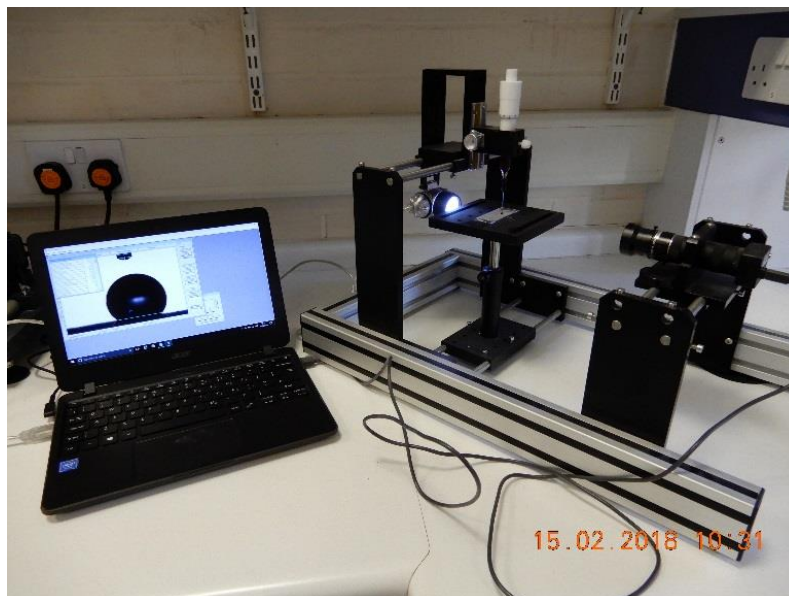


Figure 3.2: Contact angle measurement by goniometer.

3.2.3 Interfacial tension measurements

Interfacial tension is the elastic tendency of a liquid surface, which makes it acquire the least surface area possible. Interfacial tension is an important property affecting the wet granulation process. It controls solid flow pattern and relative motion of particles for controlling powder wetting and, therefore, the granulation mechanism (Torkkeli et al. 2003).

Interfacial tension was measured using a First Ten Ångströms FTÅ200 goniometer. For this measurement, the pendant drop shape method was used. The shape of the liquid droplet depends on the combined effect of interfacial and gravitational forces. Surface tension tends to make the drop spherical by minimizing the surface area, while the gravity tends to deform the liquid droplet by either elongating a pendant drop or flattening a sessile drop. The balance between interfacial tension and gravitational force was interpreted mathematically using the Laplace equation, which gives a chance to measure the surface tension by analysing the shape of the drop and the density of the liquid (Yuan et al. 2013).

A pendant droplet was produced using a 22 G blunt needle (0.41 mm internal diameter). A single snapshot was taken of the droplet, and then the image was analysed by the software. A mean average from ten interfacial tension measurements was calculated for each condition.

The interfacial tensions for liquids described in Chapter 6 were measured using a KRÜSS tensiometer based on the Wilhelmy plate method. A Wilhelmy plate was a thin plate that is

used to measure equilibrium surface or interfacial tension at an air-liquid or liquid-liquid interface. In this method, the plate was oriented perpendicular to the interface, and the force exerted on it was measured. When a vertically suspended plate touches a liquid surface or interface, then a force F was produced, which correlates with the interfacial tension σ and with the contact angle θ according to the following equation where L was the wetted length:

$$\sigma = \frac{F}{L \cdot \cos\theta} \quad \text{Equation (3.2)}$$

In this work, the plate was connected with a clamp to a microbalance force sensor. A liquid container on the platform was moved upwards at a specified constant speed to immerse the plate into the liquid container. During the immersion of the plate into the liquid pool, the microbalance force sensor measured the force applied on the moving plate and was recorded by built-in software in the tensiometer (Mohammad et al. 2018).

The calibrations for both types of equipment were performed by measuring the surface tension of a standard liquid.

3.2.4 Viscosity measurements

The viscosity of the liquids is determined using a Rheometer MCR 502 Anton Paar with a cone size of CP50-2/TG. Rheology is the study of flow and deformation of materials under applied forces. Viscosity is determined by shearing a sample and measuring its resistance to that shear, it is the ratio of shear stress to shear rate.

The liquid was placed on a stationary plate, and the upper moving plate was lowered onto the sample, which was attached to the rheometer's motor. The upper plate was moved at a specified velocity (shear rate), which was a function of the speed of the plate and the height of the gap between the stationary and rotating plate (Figure 3.3). The shear rate applied varied between 1-300 s⁻¹. A mean of three measurements was determined for each liquid.

For the work carried out at MSD (Chapter 6), the viscosity measurements were carried out using a rheometer (ARES G2) with the same principal as Rheometer MCR 502 Anton Paar.

The calibrations for both types of equipment were performed by measuring the viscosity of a standard liquid.



Figure 3.3: Rheometer for measuring viscosity.

3.2.5 True density measurements

The apparent density is the mass of substance divided by its volume, including open and closed pores. True density is similar to apparent density except the volume of closed pores is excluded. The true density of all powders were measured by helium pycnometry; AccuPyc 1340; Micromeritics (Norcross, Georgia, USA). Helium pycnometry is a non-destructive method as it uses the gas displacement method to measure the volume. Inert helium gas is used as a displacement medium. It is considered as the most reliable method for measuring the true volume and density (Micromeritics 2015; Nordström et al. 2015; Wade et al. 2015).

The samples were weighed and put in the instrument compartment of 10 cm³ volume. Helium gas flows into the sample chamber (purging stage) to remove all other gases, especially oxygen and nitrogen, in the chambers and pipes. Afterwards, the measuring stage was started, which consisted of 10 cycles. During this stage, helium flowed into sample chamber until a target pressure of 19 psi was reached. Helium molecules rapidly filled pores as small as one angstrom in diameter. Then, helium flowed into an additional second chamber of a known internal volume. The pressures were observed upon filling the sample chamber and then discharging it into a second empty chamber allowed computation of the sample solid phase volume. The volume obtained was divided by the sample weight to determine the gas displacement density. The pressure was then vented into the atmosphere. A mean of three measurements was determined for each powder or granule.

3.2.6 Liquid density measurements

Liquid density was determined using a measuring cylinder by weighing the specified volume of the liquid using the equation:

$$\rho_l = \frac{W_d}{V_d} \quad \text{Equation (3.3)}$$

where ρ_l is the density, W_d is the mass of the droplet, and V_d is the volume of the droplet.

Ten measurements for each liquid were performed for liquid density to ensure the reliability of the results.

3.2.7 Liquid droplet size measurements

The size of the droplets was measured through measuring the weight and the volume of the liquid droplet. The weight of each liquid droplet was measured individually using a microbalance (Mettler-Toledo XS3DU, 1 μg accuracy), and a mean of ten measurements was taken to measure the volume of the droplet using Equation (3.4):

$$V_d = \frac{W_d}{\rho_l} \quad \text{Equation (3.4)}$$

where V_d is the volume of the droplet in cm^3 , W_d is the mass of the droplet in g and ρ_l is the density of the liquid droplet in g/cm^3 .

Then, the radius of each liquid droplet was measured using Equation (3.5) by assuming the liquid droplet as a sphere:

$$R_d = \left(\left(\frac{V_d}{\pi} \right) \left(\frac{3}{4} \right) \right)^{\frac{1}{3}} \quad \text{Equation (3.5)}$$

where R_d (in cm) is the radius of the liquid droplet and V_d is the volume of the liquid droplet in (cm^3).

Equation (3.6) was used to calculate the % of Granule size change (G). This was performed by comparing the size of the wet liquid droplet to size of dried liquid marbles or immersion nuclei

for nucleation experiments and to size of the resultant granules after granulation in a low and a high shear mixer.

$$\% G = \left(\frac{D_g - ILD}{ILD} \right) \times 100 \quad \text{Equation (3.6)}$$

In Equation (3.6) D_g is the diameter of the granule after nucleation or granulation in μm , ILD is the initial liquid droplet diameter in μm . If the result of Equation (3.6) is a positive value, this gives a % of granule growth and indicates a percentage of granule increase in size compared to ILD . However, if the result is a negative value this gives a % of granule destruction and indicates a percentage of granule decrease in size compare to ILD value.

3.2.8 Scanning electron microscopy and energy dispersive X-ray spectroscopy for morphological analysis and elemental composition

A scanning electron microscope (SEM) and energy dispersive X-ray spectroscopy (EDX) were performed for all powders and some of the granules used in this study. SEM is a type of electron microscope that produces images of a sample by scanning it with a focused beam of electrons. The electrons interact with atoms in the sample, producing various signals that contain information about the sample's surface topography and composition. EDX can be used to obtain semi-quantitative elemental data about very specific locations within the area of interest. The powders used in Chapters 4 and 5 were scanned using a JEOL JSM-6010LA, with an accelerating voltage of 15 kV and 60 x magnification. For powder and granules produced in Chapter 6, a Quanta 250 F (Thermo) equipped with MAXX150 EDX detector (Oxford instruments), with an accelerating voltage of 10 kV and 10000 – 30000 x magnification, was used to obtain electron micrographs to identify the morphology and elemental composition of the primary powders and the granules.

All materials used in this study are not electrically conductive. For this reason, the samples were placed on metal stub and coated with a thin layer of gold of approximately 25 nm prior to any imaging.

3.2.9 X-ray computed tomography for internal structural analysis

The important characteristics of hollow granules are porosity and wall thickness as well as the size and distribution of the pores. The presence of voids inside the granules controls some important properties such as strength, disintegration, and dissolution for both granules and tablets. Mercury porosimetry is a common method used to measure the total porosity. However, it is a destructive method with handling problems, is time consuming and is a relatively costly apparatus. In addition, mercury is a toxic material. An alternative method to measure the porosity and wall thickness of granules is X-ray computed tomography (XRCT).

XRCT is a relatively new technology developed in the late 1970s, which is a non-destructive method that measures the difference in material density. XRCT is a very promising instrument to be able to characterise the porosity and morphology of granules with a length scale of 4 μm or larger. XRCT can provide qualitative morphological data about the pore shape and its spatial distribution. In addition, it can give a quantitative measure of total and local porosity, and wall thickness of granules (Farber, Tardos and Michaels, 2003).

In XRCT, the sample is rotated while the X-ray source and the detector are stationary (Zeitler et al. 2009). X-rays are emitted from a high power source towards an object that is placed in a special sample holder and collected on the detector on the opposite side. The sample holder is rotated around its z-axis with an angular increment (Perfetti et al., 2010).

After each rotation increment, the X-rays passing through the sample will attenuate depending on the atomic number and the density of the sample under examination, in addition to the energies of the X-rays used. The detector measures the intensities of the attenuated X-rays. Two-dimensional sectional images are available after complete revolution of the sample and under different angles by implementing mathematical algorithms. 3D visualization images with high resolution are obtained by the reconstruction techniques of the XRCT from different consecutive two-dimensional intensity slices (Sondej et al. 2015; Perfetti et al. 2010; Farber et al. 2003).

The equipment used for the experiments in Chapters 4 and 5 was a Skyscan 1172 device, Bruker, Belgium. Individual granules were mounted on the sample stage of the XRCT in a small cradle made of a plastic tube and stabilized on a plastic straw. Raw images were collected using a Skyscan 1172 X-ray micro tomograph with 3.8 $\mu\text{m}/\text{pixel}$ resolution. The X-ray source

was operated at 47 kV with a current of 132 μ A. Samples were scanned from 0-180° at intervals using a 0.7° rotation increment. A medium camera binning mode with 2000 x 1024 was used.

For work performed in Chapter 6, a Versa 500 XRM (Zeiss) was used. Many granules are mounted on the sample stage of the XRCT in a clear capsule shell and stabilized with blue tack on the stage. Granules were scanned at 80 kV, 1200 images/scan, 1 sec/image, using either 0.39X or 4X lens.

Images were reconstructed using dedicated software (NRecon v.1.6.3, Bruker-micro CT) that provided axial cross sections of the inner structure. The cross sectional, coronal and sagittal images of the granules are visualized using the reconstructed images and DataViewer software v 1.1.4 32 bit, Bruker-micro CT. Total porosity and wall thickness were measured using the reconstructed images and Micro-CT Analysis sky scan software (CTAn v1.14.4, Bruker-micro CT). Three representative granules from each sample were measured.

This study will focus on the measuring the wall thickness of hollow granules. Granules cross section wall thickness was measured by selecting the region of interest in the middle part of the granule approximately 300 – 500 μ m along, because the voids are mostly seen in the middle part. It is assumed that, it is more accurate to measure the wall thickness in the middle part of the granules than from the top or bottom, which might give false higher wall thickness results. The wall thickness was measured from the edge of internal void to the edge of the granule surface. Then, the mean of all measurements were shown on the screen.

For the first time, the porosity of granules was measured as the mean of the whole granule porosity. The granule was split into three main parts (bottom, middle and top) in Micro-CT Analysis software. Then, the porosity of each part was measured separately and the mean of the porosity of the all three parts was calculated. This way of measuring granule porosity is more accurate than measuring local or region of interest within the granules because it might give false higher or smaller porosity measurements. The top and bottom parts of the granule (wall) give lower porosity, while the middle part of the granule (empty space) give a high porosity measurement. It should be noted that the internal void in the middle part of the granules are considered for porosity measurement and ignored any voids that include in the granule powder shell.

3.3 Powders

Three different powders were used in the experiments performed in this work. Glass beads of three different sizes were used as a model powder. Efavirenz and red iron oxide were used as more realistic industrial materials. Glass bead powders were analysed for particle size distribution using dry cell laser diffraction. However, wet cell laser diffraction was used for efavirenz and iron oxide, because these two powders consisted of small particles and are very cohesive in nature. Helium pycnometry was used to measure the true density. A summary of all powders used, including some of their key properties, is shown in Table 3.1. SEM images for all powders are shown in Figure 3.4. Further details of the powders are given in the following sections, including the method of hydrophobisation of the glass beads to give different wetting properties.

Table 3.1: Summary of powder properties.

Powder	Glass beads (AQ)	Glass beads (AH)	Glass beads (AF)	Efavirenz	Red iron oxide
d_{3,2} (µm)	33.6 ± 1	65.9 ± 2.7	112.3 ± 2	3.4*	0.04**
d_{4,3} (µm)	35.5 ± 1	70.7 ± 1.9	115.3 ± 2	8.8*	0.06**
d₁₀ (µm)	25.3 ± 1	48.3 ± 1.7	91.3 ± 1.7	1.4*	0.04**
d₅₀ (µm)	34.6 ± 1	68.5 ± 2.0	114 ± 2.6	6.2*	0.05**
d₉₀ (µm)	47.3 ± 1	96.5 ± 1.5	141 ± 2.6	19.1*	0.09**
<i>ρ</i>_{true} (g/cm³)	2.54 ± 0.21	2.55 ± 0.35	2.54 ± 0.51	1.5*	5.242
Molecular formula	SiO ₂	SiO ₂	SiO ₂	C ₁₄ H ₉ ClF ₃ NO ₂	Fe ₂ O ₃

*data adapted from (Fandaruff et al., 2015); particle size distribution is measured using the wet mode of laser diffraction (Malvern Mastersizer 2000).

** data adapted from (Dengxin et al., 2008); Particle size distribution is measured using laser particle size analyser (LPSA).

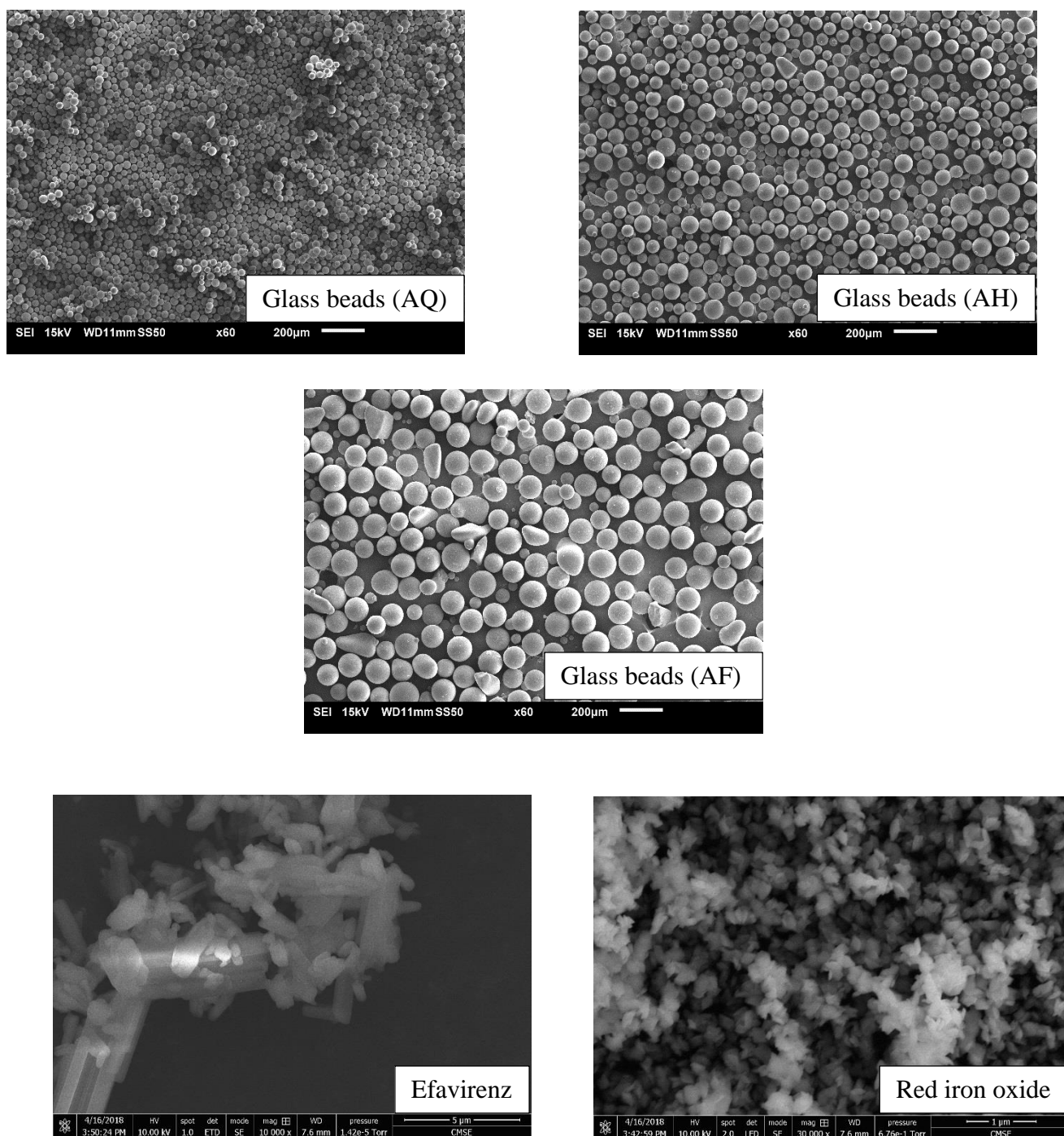


Figure 3.4: SEM images of all powders used in this study.

3.3.1 Glass beads

Glass beads of three different sizes, AQ, AH and AF, were provided by Potters Industries LLC Ltd. UK. Glass beads are powders consisting of spherical particles which are easy to use and characterise, and have been extensively used by many researchers (Hapgood et al. 2009; Iveson et al. 1998; Eshtiaghi et al. 2010). Beads were used as model wetting and non-wetting powders (by hydrophobisation Section 3.3.1.1) because of their nearly spherical shape, good flowability, and the rapid separation of powder and granules subsequent to granulation. Three different measurements of the particle size distribution of each glass bead size class were performed using dry cell laser diffraction. All grades of glass beads show a unimodal size distribution. Figure 3.5 shows the particle size distribution, q_3 , of all glass beads used in this work. The glass beads (AQ) are the smallest beads used with a $d_{50} \sim 35 \mu\text{m}$, while the glass beads (AF) are the largest beads used with a $d_{50} \sim 114 \mu\text{m}$. A triplicate series of helium pycnometry was used to determine the true density of the powder. The density was found to be approximately 2.54 g/cm^3 for all grades.

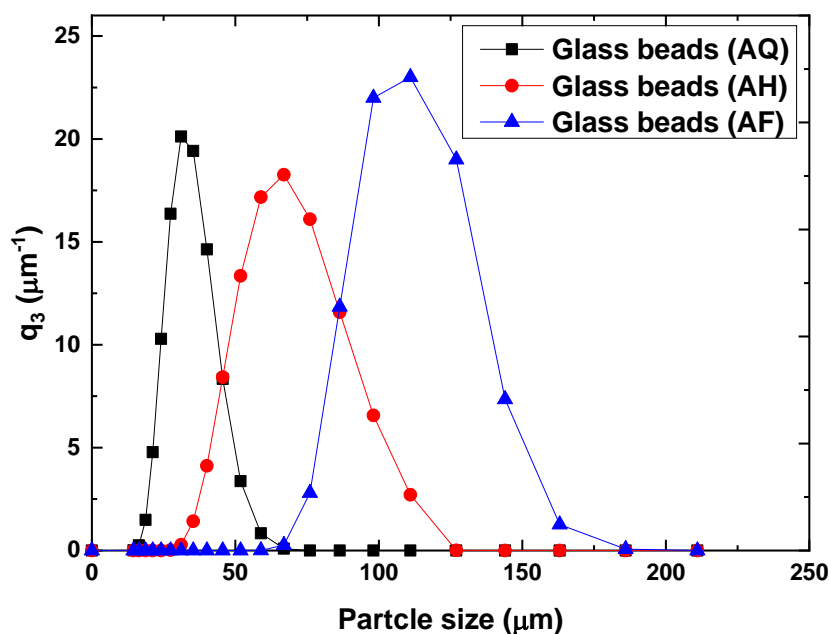


Figure 3.5: Particle size distribution of glass beads obtained via laser diffraction.

3.3.1.1 Hydrophobisation of glass beads powder

Hydrophobisation of the glass beads was carried out in this work to give a non-wetting powder. Granulation of non-wetting powder is a common problem in the pharmaceutical industry and understanding of the effect of heterogeneous-wetting components on the granule growth mechanism and internal microstructure remains relatively unknown, and this forms the motivation of this study.

Immersion of hydrophilic powder into chlorotrimethylsilane (Sigma Aldrich, company Ltd, Germany) was performed to produce hydrophobic powder. The immersion was performed as follows (Figure 3.6): (a) Firstly, hydrophilic powder was put inside a Pyrex bowl inside a fume cupboard. (b) Next, chlorotrimethyl silane was added until all the powders were covered sufficiently. (c) Then, the chlorotrimethyl silane was allowed to evaporate from the powder in the bowl overnight inside the fume cupboard. Finally, the resultant powders were put in an oven at 35° C for 5 hours to get rid of any remaining silane liquid.

This type of experiment permitted a modification of the glass beads surface properties and hence the wettability without changing any other glass beads properties (density, size, and surface roughness) (Saleh and Guigon, 2007).

It should be noted that many silane liquids were tried before chlorotrimethyl silane such as Sigmacot, dichlorodimethyl silane and tetraethylorthosilicate silane (Sigma Aldrich). Different exposure times with glass beads and mixtures of two of these liquid with different ratios were tried. All these trials failed to produce hydrophobic glass beads, that they were very difficult to dry.



Figure 3.6: Preparation of the non-wetting glass beads.

3.3.2 Efavirenz

In addition to using model powder, a realistic pharmaceutical powder was used for comparison with model materials (see Chapter 6). Efavirenz was acquired from Fabbrica Italiana Sintetici S.p.A, Vicenza, Italy. Efavirenz is a class of medication called non-nucleoside reverse transcriptase inhibitors. It works by decreasing the amount of human immunodeficiency virus (HIV) in the blood and used to treat HIV in humans. It is sold both as a solo API formulation or in combination with other antiretroviral medications (Pawar and Amin, 2016). Efavirenz was used as a non-wetting powder due to higher and stable contact angle with the liquid used over 15 minutes time (Table 3.4). Efavirenz show a narrow and unimodal size distribution with $d_{10} \sim 2.2 \mu\text{m}$, $d_{50} \sim 8.5 \mu\text{m}$ and $d_{90} \sim 22.8 \mu\text{m}$ (Table 3.1). Efavirenz is extremely cohesive. Compared to model powders, efavirenz has a smaller particle size at $d_{50} \sim 8.5 \mu\text{m}$ than the smallest glass beads powder (AQ) used in this work with $d_{50} \sim 35 \mu\text{m}$.

3.3.3 Red iron oxide

Red iron oxide is a real pharmaceutical excipient and was acquired from Ferroxiide Red 212P, Huntsman Pigments. This was used in this work as a wetting “real world” powder and will be referred as ‘IROX’. Red iron oxide or ferric oxide is an inorganic compound with the formula Fe_2O_3 . Red iron oxide was used as a wetting pharmaceutical excipient for various types of pills and film-coated tablets. IROX is a very fine powder and can be referred to as a self-agglomerating powder. It is the smallest powder particle size used in this work with $d_{50} \sim 0.4 \mu\text{m}$ compared to $d_{50} \sim 8.5 \mu\text{m}$ and $d_{50} \sim 35 \mu\text{m}$ of the efavirenz and smallest grade of beads powder particle size respectively (Table 3.1). Likewise, it has the same cohesive nature as efavirenz. The true density of iron oxide powder was found to be approximately 5.2 g/cm^3 , which is the highest density powder used in this work.

3.4 Liquids

The liquid binders used in this study were polyethylene glycol (PEG) and dextran aqueous solution. Viscosities were varied by using different molecular weight grades of PEG and different concentrations of dextran 70000, and spanned viscosities from ~ 8 mPa s to ~ 3067 mPa s. All liquids were analysed using a goniometer to determine their interfacial tension (Section 3.2.3). Liquid densities were determined using a measuring cylinder (Section 3.2.7); the liquid viscosities were determined using a rheometer (Section 3.2.4). A full list of solutions used and their properties is shown in Table 3.2.

Table 3.2: Liquid properties; Standard deviation are shown as (\pm).

Liquid	Density (g/cm ³)	Surface tension (mN/m)	Viscosity (mPa. s)
50 wt/wt % PEG 1500	1.0501 \pm 2	53.5 \pm 6	62.83 \pm 42
50 wt/wt % PEG 6000	1.0904 \pm 2	54.32 \pm 7	307.95 \pm 67
50 wt/wt % PEG 12000	1.0908 \pm 4	54.77 \pm 5	1267.2 \pm 22
50 wt/wt % PEG 20000	1.0944 \pm 1	55.82 \pm 5	3067.08 \pm 48
10 wt/v % Dextran	1.04 \pm 4	72.09 \pm 5	7.97 \pm 3
30 wt/v % Dextran	1.13 \pm 3	73.09 \pm 6	109.07 \pm 7
50 wt/v % Dextran	1.2 \pm 2	73.74 \pm 1	1039.21 \pm 1

3.4.1 Aqueous polyethylene glycol solutions

50 wt % aqueous solutions of different chain length polyethylene glycols (PEG) (Sigma Aldrich) were prepared with distilled water, and with acid red dye to allow better visualization of the resultant granules. First, a 1 wt % aqueous solution of acid red dye was prepared. Next, polyethylene glycol was dissolved in the dye solution in a 1:1 mass ratio. In this way, a 50 wt % PEG solution was produced. Four different molecular weight PEGs were used to produce solutions of different viscosities: PEG 1500, PEG 6000, PEG 12000 and PEG 20000. The liquids had approximately similar densities and surface tensions; all the data is presented in Table 3.2 after dye addition.

The viscosities of different PEGs solutions were analysed using a rheometer. The behaviour of the liquids showed constant viscosities (i.e. Newtonian) over the examined shear rate (1-300 s⁻¹), which is within the shear rate range for the granulation process (Figure 3.7).

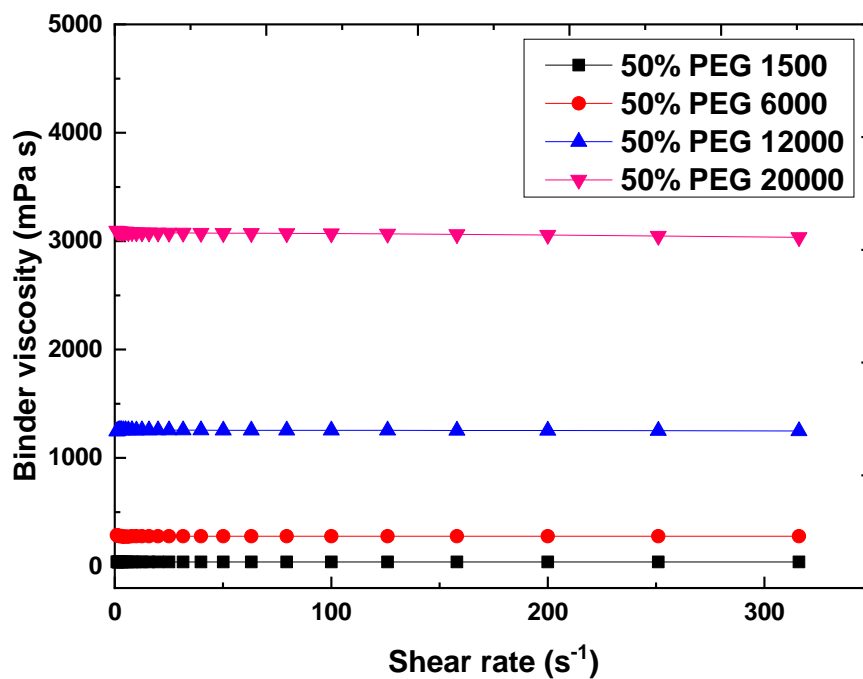


Figure 3.7: Viscosities of PEGs solutions as a function of shear rate in the range between 1-300 s⁻¹.

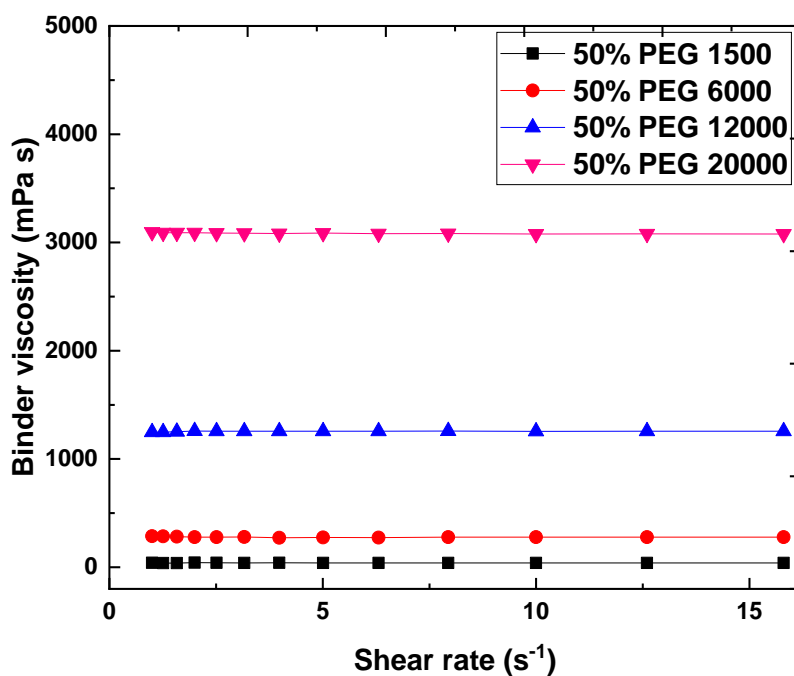


Figure 3.8: Viscosities of PEGs solutions as a function of shear rate the same as Figure 3.7 but in range between 1-16 s⁻¹.

3.4.2 Aqueous dextran 70000 solutions

Dextran 70000 solution (Sigma Aldrich), which will be referred as simply “dextran” in this work, was prepared with distilled water. Three different concentrations of dextran were prepared; 10 %, 30 % and 50 % dextran (wt/vol) to produced different liquid viscosities. The liquids had densities ranging from 1.004 to 1.2 g/cm⁻³, and surface tensions from 72.09 and 73.74 mN/m.

Overall, the curves in Figure 3.9 show linear behaviour, although the lines fluctuate more below a shear rate of 2 s⁻¹ using 50 % dextran. Measurements below this value are used to determine whether a liquid is shear-thickening or shear-thinning and, overall, measurements in this range show shear thinning. During the granulation experiments, shear is expected to be higher than this range.

However, there are linear behaviours for 30 % and 10 % dextran concentration over the shear force applied (Figure 3.9). The viscosities were 7.97, 109.7 and 1039.21 mPa s (mean values over whole range of shear rate) for 10 %, 30 % and 50 % dextran respectively.

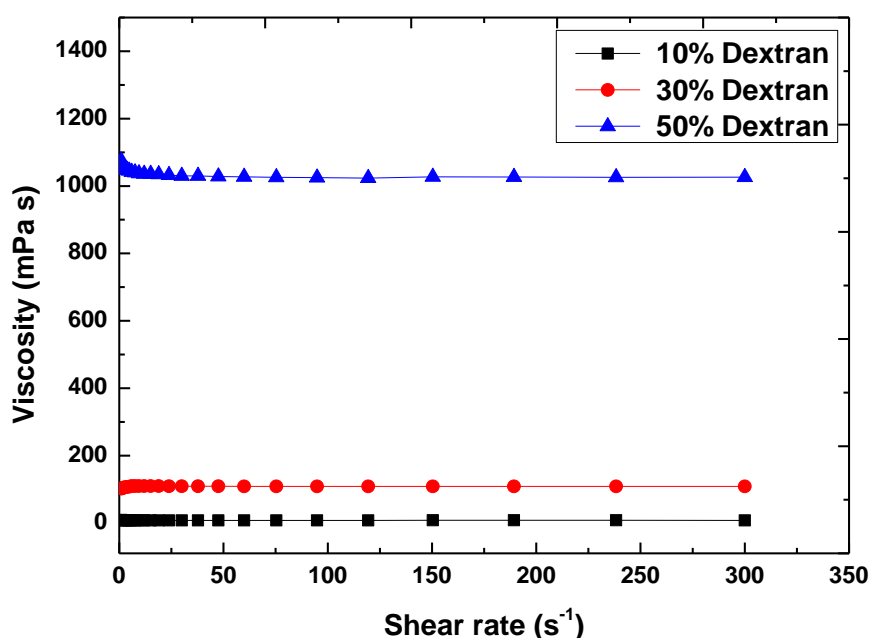


Figure 3.9: Viscosities of 10%, 30% and 50% dextran solutions as a function of shear rate.

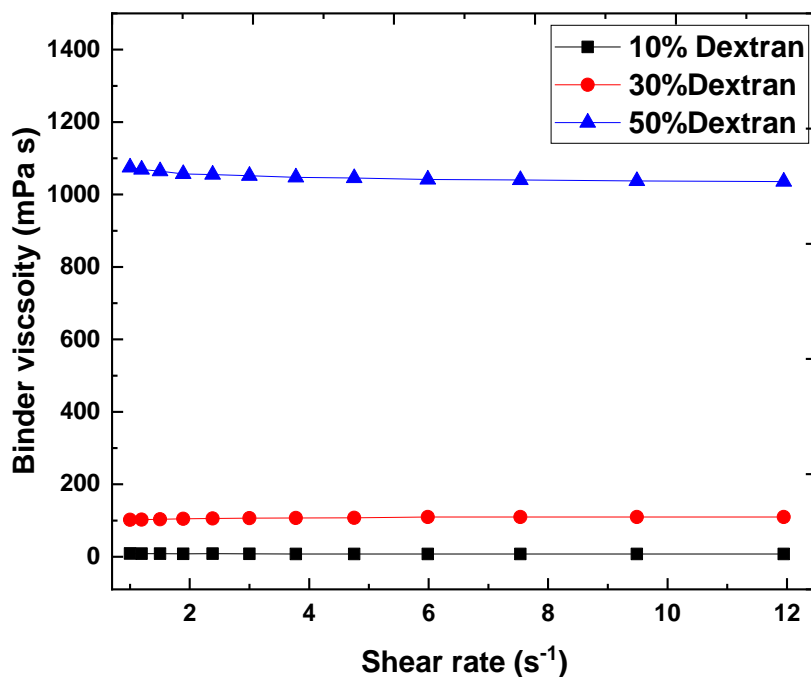


Figure 3.10: Viscosities of 10%, 30% and 50% dextran solutions as a function of shear rate the same as Figure 3.9 but in the range between 1-12 s⁻¹.

3.5 Powder-binder systems

Overall, 29 powder-binder systems will be investigated in this study. Non wetting % -wetting % glass beads systems, with powder mixtures of 100-0, 65-35, 25-75, 80-20, 0-100, in conjunction with four binders of different molecular weight PEGs were used in this study. Systems of beads-PEG are shown in Table 3.3. The contact angles of mixtures of 100%-0%, 80%-20% and 65%-35% non wetting- wetting powder mixtures were high and stable over time from 20 to 120 sec with different binder viscosities. Then, the contact angle decreased sharply after 300 secs.

Powder mixtures of 25%-75% and 0%-100% non wetting-wetting, can be classed as wetting powders. The liquid droplet spread quickly over time and a stable point was never reached, particularly with low binder viscosity such as 50 wt % PEG 1500 and 50 wt % PEG 6000. The liquid started to dry and evaporate after 10 minutes.

In addition, 60%-40%, 50%-50%, 30%-70% powder blends of efavirenz and IROX respectively were used. Table 3.4 shows the contact angle of all efavirenz-IROX blends with

different dextran solutions. These systems gave stable contact angles up to 600 sec with different dextran concentration; 10 %, 30 % and 50 % (Figure 3.11). The high percentage of efavirenz in the blends gave the higher contact angle; likewise, the lower percentage gave a lower contact angle and good wettability.

Table 3.3: Overview of powder-PEG systems used in this study.

Powder	Binder (PEG)	Binder viscosity (mPa s)	Contact angle ^o					
			20 sec	40 sec	60 sec	120 sec	300 sec	600 sec
Non-wetting	1500	60	114 ± 7	112 ± 1	107 ± 2	103 ± 1	91 ± 8	80 ± 4
	6000	300	115 ± 2	113 ± 3	109 ± 4	104 ± 5	95 ± 5	92 ± 3
	12000	1300	116 ± 3	113 ± 2	108 ± 5	105 ± 4	97 ± 4	96 ± 3
	20000	3000	116 ± 2	116 ± 1	110 ± 4	100 ± 5	98 ± 3	97 ± 6
Wetting	1500	60	29 ± 7	26 ± 8	24 ± 5	20 ± 3	18 ± 7	17 ± 7
	6000	300	33 ± 6	29 ± 8	25 ± 8	22 ± 7	19 ± 2	18 ± 6
	12000	1300	38 ± 3	35 ± 7	32 ± 8	30 ± 3	28 ± 1	26 ± 4
	20000	3000	40 ± 4	38 ± 5	36 ± 5	34 ± 4	32 ± 4	29 ± 9
80% - 20% Non-wetting - Wetting	1500	60	97 ± 3	96 ± 6	96 ± 4	95 ± 7	90 ± 6	89 ± 3
	6000	300	100 ± 4	100 ± 1	99 ± 9	97 ± 2	95 ± 4	90 ± 1
	12000	1300	102 ± 5	101 ± 2	99 ± 4	98 ± 1	96 ± 2	91 ± 7
	20000	3000	103 ± 1	101 ± 3	98 ± 5	97 ± 1	97 ± 1	92 ± 3
65% - 35% Non-wetting - Wetting	1500	60	90 ± 5	90 ± 7	89 ± 5	88 ± 1	84 ± 3	79 ± 3
	6000	300	92 ± 3	91 ± 6	90 ± 8	89 ± 4	85 ± 9	82 ± 2
	12000	1300	93 ± 3	92 ± 4	91 ± 5	90 ± 2	88 ± 3	85 ± 5
	20000	3000	93 ± 5	92 ± 1	91 ± 9	90 ± 3	89 ± 9	86 ± 3
25% - 75% Non-wetting - Wetting	1500	60	57 ± 4	49 ± 9	46 ± 1	42	32 ± 3	26 ± 3
	6000	300	59 ± 8	57 ± 2	56 ± 7	54 ± 7	48 ± 2	44 ± 4
	12000	1300	67 ± 8	64 ± 3	62 ± 2	60 ± 7	57 ± 7	55 ± 5
	20000	3000	68 ± 4	68 ± 3	68 ± 6	63 ± 5	62 ± 2	59 ± 4

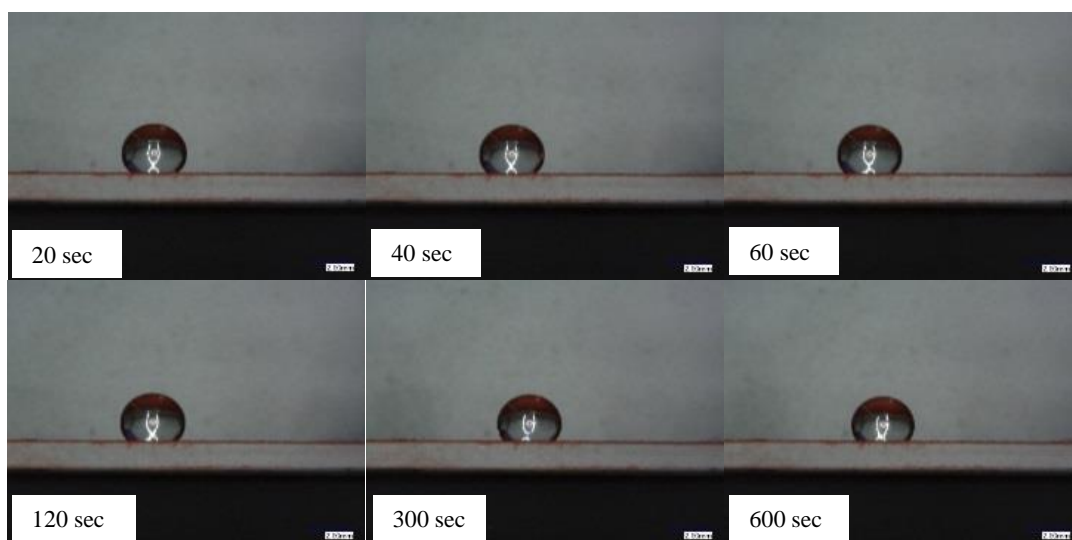


Figure 3.11: Microscope images of 60%-40% Efavirenz-IROX with 50% dextran solution. The contact angle is stable over the time of the measurements.

Table 3.4: Overview of powder-dextran systems used in this study.

Powder	Binder % Dextran	Binder viscosity (mPa s)	Contact angle ^o					
			20 sec	40 sec	60 sec	120 sec	300 sec	600 sec
Efavirenz	10	8	148 ±1	147±5	146±3	146±4	146±3	144±1
	30	100	148±3	147±4	147±2	146±2	146±9	145±3
	50	1000	152±1	148±7	147±3	147±8	146±4	145±3
IROX	10	8	64±3	63±8	62±3	62±2	61±1	59±6
	30	100	73±1	74± 6	74±2	73±3	70±5	69±5
	50	1000	79±9	79±2	79±4	77±9	74±1	72±5
60% - 40% Efavirenz- IROX	10	8	125±5	119±6	118±8	115±2	114±6	95±9
	30	100	130±5	128±5	128±6	127±3	117±3	117±9
	50	1000	141±3	135±3	133±3	132±3	132±1	128±5
50% - 50% Efavirenz- IROX	10	8	89±3	90±9	85± 8	76±2	69±4	61±5
	30	100	92±3	88±3	87±5	84±3	82±3	69±8
	50	1000	128±3	121±3	114±8	109±8	107±4	96±3
30% - 70% Efavirenz- IROX	10	8	63±5	61±3	57±5	54±7	50±6	49±6
	30	100	72±3	66±1	69±1	66±9	59±5	54±4
	50	1000	94±3	86±9	84±9	82±2	76±2	74±2

3.6 Methods

This section provides a description of all the experiments performed in this work. The section follows a chronological order; from early tumbling drum experiments (low shear) to high shear experiments using the model particles (glass beads), and finally the experimentation to apply the results obtained with the first two methods to pharmaceutical powders using a low and a high shear.

3.6.1 Pre-nucleation experiments

All the experiments performed in this thesis are based on the pre-nucleation of wet nuclei externally prior to granulation in a low or high shear granulation. Once the pre-nucleated wet nuclei were formed, these were then added to the granulator. The formation of immersion nuclei or liquid marbles depends on powder wettability. Liquid marbles are formed by solid spreading nucleation in which the powder spread on the liquid droplet. Liquid marbles are formed when the liquid/powder contact angle $> 90^\circ$ (Figure 3.12).

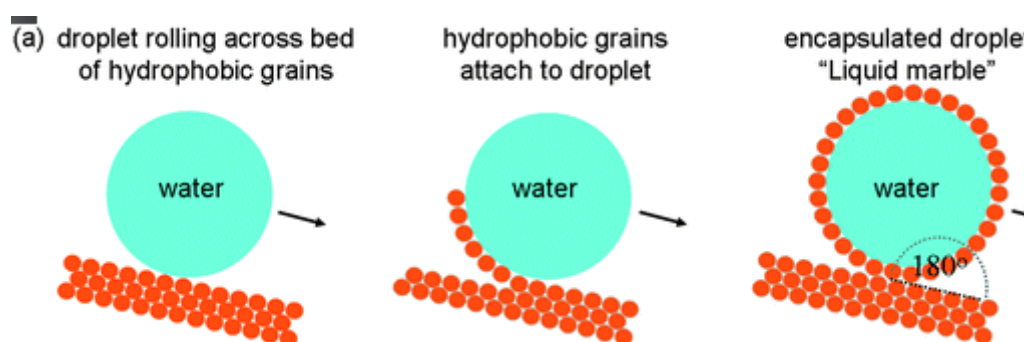


Figure 3.12: schematic diagram of liquid marble formation.

Reproduced from Soft Matter, V (12), Glen McHale and Michael I. Newton, Liquid marbles: principle and applications, pp. 5473-5481, (2011), with permission from the Royal Society of Chemistry.

The liquid marbles consist of a liquid core with a surrounding powder shell, which can be dried to form a hollow granule after granulation (Aussillous et al. 2001; Hapgood et al. 2009; Hapgood et al. 2009). However, drops interact with wetting powder with contact angle of less than 90° , and a different mechanism of pre-nucleation occurs; the droplet penetrates into the powder bed and a wet nucleus is formed (Figure 3.13).

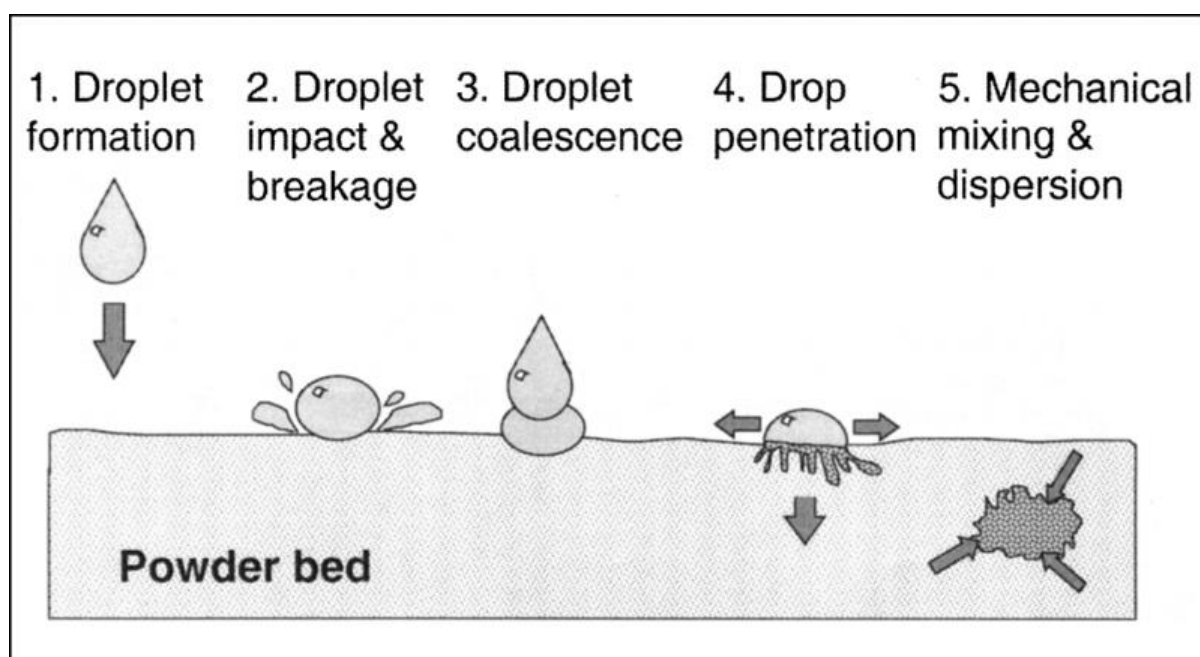


Figure 3.13: Schematic diagram of immersion nuclei formation (Hapgood, Litster and Smith, 2003).

Reproduced with permission from Wiley Materials.

Table 3.5 shows the identity of the initial product from pre-nucleation, prior to being added to the mixer. Liquid marbles are formed with a contact angle of powder/binder of 90° or more, such as powder mixtures of non wetting-wetting of 100%-0% and 65%-35% and efavirenz-IROX of 60%-40% and 50%-50% with different binder viscosity. Note that the contact angle of these powder mixtures with a range of binder viscosity shows contact angle equal or greater than 90° . Liquid marbles are formed when a powder of low wettability surrounds a liquid droplet by solid spreading nucleation.

On the other hand, wet nuclei are formed with powder/binder contact angle of less than 90° . Non wetting-wetting powder mixtures of 25%-75% and 0%-100% and efavirenz-IROX of 30%-70% having contact angle with a range of binder viscosity of less than 90° , produced immersion nuclei prior to granulation. During immersion nuclei formation, the droplet penetrates into the powder bed and a wet nucleus is formed.

Table 3.5: Summary of pre-nucleation experiments.

Conditions		Contact angle	Pre-nucleation product
Non wetting-wetting mixture	Binder viscosity (mPa s)(PEG)		
100%-0%	60	115	Liquid marble
100%-0%	300	115	Liquid marble
100%-0%	1300	116	Liquid marble
100%-0%	3000	117	Liquid marble
80%-20%	60	97	Liquid marble
80%-20%	300	100	Liquid marble
80%-20%	1300	102	Liquid marble
80%-20%	3000	103	Liquid marble
65%-35%	60	90	Liquid marble
65%-35%	300	92	Liquid marble
65%-35%	1300	93	Liquid marble
65%-35%	3000	94	Liquid marble
25%-75%	60	57	Immersion nuclei
25%-75%	300	59	Immersion nuclei
25%-75%	1300	68	Immersion nuclei
25%-75%	3000	68	Immersion nuclei
0%-100%	60	30	Immersion nuclei
0%-100%	300	34	Immersion nuclei
0%-100%	1300	39	Immersion nuclei
0%-100%	3000	40	Immersion nuclei
Conditions		Contact angle	Pre-nucleation product
Non wetting-wetting mixture (Efavirenz-IROX)	Binder viscosity (mPa s) (Dextran)		
60%-40%	8	125	Liquid marble
60%-40%	100	130	Liquid marble
60%-40%	1000	141	Liquid marble
50%-50%	8	89	Liquid marble
50%-50%	100	92	Liquid marble
50%-50%	1000	129	Liquid marble
30%-70%	8	64	Immersion nuclei
30%-70%	100	72	Immersion nuclei
30%-70%	1000	94	Immersion nuclei

3.6.2 Granulation of model particles in a low shear mixer

The initial investigation of granule size and internal microstructure focused on experiments in a low-shear mixer (tumbling drum). The drum has an internal diameter of 70 mm and is 100 mm in height. A powder bed for pre-nucleation was prepared in a small petri dish by sweeping the excess powder from the bed surface with a ruler to produce a smooth powder surface. Before granulation, the amount of the powder added to the low shear mixer was calculated by subtraction of the total amount of the powder from the amount of the powder added to the petri dish. A total amount of 100 g of powder was used. The powder fill level in the drum was 10% (Figure 3.14 a). The movement of the powder inside the drum was observed to be a rolling regime, which is the desired regime (Morrison et al. 2016). Rolling motion is characterised by static and uniform flow of a powder layer on the surface (Mellmann et al. 2001).

Liquid marbles or immersion nuclei were prepared through single droplet nucleation in the petri dish after the preparation of the powder bed and the low shear granulator (Figure 3.14). Pre-nucleation outside the low shear was performed to reduce the complexity of the granulation process that there was no need to add liquid binder during granulation (Figure 3.14 b and c). Twenty drops of 0.16:100 wt/wt L/S were used to increase the precision of the results. A higher number of drops was not used in order to decrease the probability of the coalescence of the liquid marbles or immersion nuclei inside the mixer. These drops were gently dropped ~ 5 cm over a loosely packed petri dish powder. Using a syringe pump (Harvard Apparatus PHD ULTRA I/W, USA). The close distance of liquid dropping was selected in order to minimize drop bouncing, rolling and splashing and to prevent crater formation). The needle was connected to a syringe through a tube and Luer lock connector. The syringe was operated at 4 $\mu\text{l/s}$ and at a constant speed, which gave an acceptable addition rate. The needle used was blunt with a 0.16 mm internal diameter (30 G). A simple shaking of the petri dish containing the formed liquid marbles was performed to ensure a full coverage of the droplet with a powder to prevent sticking of a liquid marbles to the wall of the drum during granulation (Figure 3.14 c). Then, the liquid marbles or immersion nuclei were removed from the petri dish using spatula once all the liquid marbles or immersion nuclei were formed and placed onto the powder bed surface inside the drum (Figure 3.14 d). The drum was then operated at 25 rpm for five minutes.

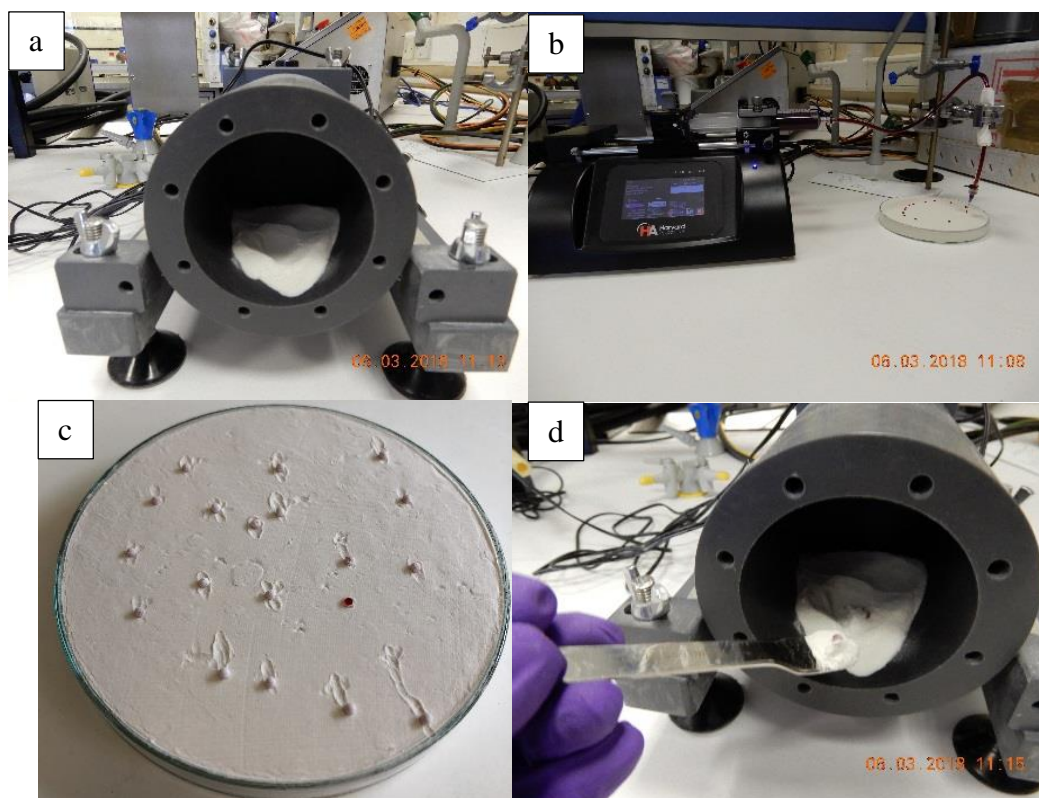


Figure 3.14: Tumbling drum granulation procedure.

After granulation, the whole powder mass from the drum was placed in a tray to dry overnight at room temperature (21°C). Granules, flakes or dyed fine particles were extracted using a stack of sieves as described in Section 3.2.1.2. Any remaining undyed fine powder in the tray in the pan was not included in the analysis, to allow a clear frequency size distribution of the granules. Then, the extracted granules, flakes or dyed fine particles were removed from the sieve cuts and stored in petri dishes at room temperature for XRCT analysis. The experiments were repeated after the end of each of the experiments using different powder wettabilities, binder viscosities, powder particle sizes and mixing times.

Three representative granules from each condition were selected for internal structure analysis using XRCT. Porosity and wall thickness of granules from all experiments were measured using XRCT software package. For more details of the methods and characterisation, see Chapter 4, Section 4.2.

3.6.3 Granulation of model particles in a high shear mixer

The purpose of experiments in a high shear mixer with a flat plate impeller is to investigate the effect of varying the shearing and impact forces and impacts on granule size and internal microstructure of granules formed from liquid marbles or immersion nuclei. A flat plate impeller was used to maximize shearing, but at the same time minimizing impact to liquid marbles or nuclei, which should reduce granule breakage. A stainless steel high shear mixer was used. The bowl has a capacity of 3 L, an internal diameter of 205 mm, and height of 125 mm (Figure 3.15). The impeller could rotate at speeds varying from 150 to 700 rpm. No chopper was used in these experiments. Furthermore, a 11° bevelled 2-bladed and a 3-bladed impeller were used to study the effect of various shearing and impact forces on granule size and internal microstructure (Figure 3.16). The use of 2-bladed and 3-bladed impellers was to vary the shearing force impacted to the granules as will be explained in detail in Chapter 5. In total, fifteen different systems were evaluated. The experimental procedure was the same as the low shear mixer described in Section 3.6.2. For all the impeller speeds, the motion of powder inside the high shear mixer was observed to be in a roping regime, which is the favourable regime for high shear mixer granulation. The roping regime provides a better mixing of the powder from top to the bottom in the mixer. Poor mixing results in accumulation of the liquid at the base of the bowl, which can occur if the powder runs in a bumping regime. Here, the powder loops around the wall of the granulator due to a lower powder content or higher rotational speed (Litster et al. 2002).

First, 500 g of powder was weighed. One portion of 100 mg was used to fill the petri dish, and the surface levelled by a ruler to obtain a smooth surface. The remaining powder was placed inside the high shear granulator. Liquid marbles or immersion nuclei were prepared through single droplet nucleation in a petri dish after the preparation of the powder bed in the petri dish and in the granulator. Fifty drops with 0.1:100 wt/wt L/S ratio were nucleated to extract a sufficient number of intact liquid marbles or immersion nuclei and increase the precision of the results. Drops were gently dropped over a loosely packed petri dish powder using syringe pump (Harvard Apparatus PHD ULTRA I/W, USA). A simple shaking of the petri dish containing the formed liquid marbles or immersion nuclei was performed to ensure a full coverage of the droplet with powder to prevent sticking of a liquid marbles to the wall of the bowl during granulation. Once all the liquid marbles or immersion nuclei were formed, they were extracted

by a spatula and placed onto the powder bed surface inside the high shear. The high shear mixer was then operated at different impeller speeds for twenty seconds.



Figure 3.15: High shear mixer.

After granulation, similar as mentioned in Section 3.6.2, the whole powder mass from the high shear mixer bowl was placed in tray to dry overnight at a room temperature. Granules, flakes or dyed fine particles were extracted by using a stack of sieves with cuts as mentioned in Section 3.2.1.2. Any remaining undyed fine powder in the pan at the bottom of the sieve stacks was not included in the analysis. Then, the extracted granules, flakes or dyed fine particles were removed from the sieve cuts and stored in a petri dish at room temperature (21°C) for XRCT analysis. The experiments were repeated after the end of each experiments using different impeller speeds, impeller designs and powder wettabilities.

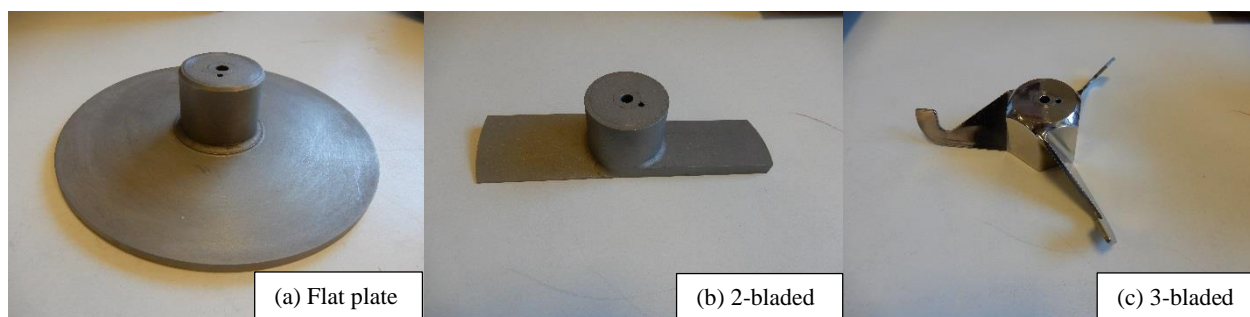


Figure 3.16: Impeller designs.

Five representative granules was selected from each condition for internal structural analysis using XRCT. The porosity and wall thickness was determined using XRCT software package. For more details of the methods and characterisation, see Chapter 5, Section 5.2.

3.6.4 Granulation of pharmaceutical powder

This work was performed by the author of this thesis at MSD, PA, USA. The aim of the experiments is to investigate the applicability of the results obtained using the previous two methods with model particles into industrial pharmaceutical powders. Efavirenz (non-wetting powder) as an active constituent and iron oxide (wetting powder) as an excipient were used. Dextran with three different concentrations (10 %, 30 %, 50 %) was used as a liquid binder. Both low and high shear granulations were performed in these studies. The low shear mixer was same as the specified in Section 3.6.1, while a 1L Diosna high shear granulator was used with a three-bladed impeller and built in chopper for high shear experiments.

The effect of varying the shearing force, binder viscosity and mixing time on granule size and internal microstructure of granules for a range of powder wettabilities was investigated. The experimental procedure was the same as for the low and high shear for the model systems (Section 3.6.2 and 3.6.3).

Liquid marbles or immersion nuclei were produced without further granulation to give data for comparison with granules formed after granulation in low and high shear granulators. Powder (15 g) was placed in a petri dish and the surface was levelled using a ruler. Liquids were allowed to drop on a powder surface using a 10 mL syringe and 21 G needle (0.51 mm in diameter). The formed liquid marbles or immersion nuclei in the petri dish were allowed to dry

overnight. The formed marbles or immersion nuclei were extracted by passing all the powder through 1 mm sieve. Sieving was performed manually by tapping the mesh with a spatula to allow the powder to pass through. The extracted liquid marbles or immersion nuclei were removed from the sieve and stored in plastic containers at room temperature (21°C) for internal microstructure and size analysis.

For low shear experiments, 20 g of powder was used, which was much lower than the amounts used in Section 3.6.2, because of the low powder bulk density. The 20 g of powder was divided into two. One portion (12 g) was placed in a petri dish and another inside the low shear mixer. Liquid marbles or immersion nuclei were prepared through single droplet nucleation after the preparation of the powder bed and the powder in granulator. Drops were introduced manually by hand, with a 10 mL syringe and a 21 G needle. Thirty drops with 0.3:20 wt/wt L/S were selected to increase the precision of the results; a higher number of drops was not performed in order to decrease the probability of the coalescence of the liquid marbles or immersion nuclei inside the mixer. Shaking of the petri dish was made to ensure spreading of powder around the droplet to prevent sticking of liquid marbles to the wall of the drum during granulation. Once all the liquid marbles or immersion nuclei were formed, they were extracted using a spatula and placed onto the powder bed surface inside the low shear mixer. The drum was then operated at 25 rpm for five minutes.

After granulation, similar as mentioned in Section 3.6.2, the whole powder mass from the drum was placed in tray to dry overnight at a room temperature (21° C). A Ro-tap sieve shaker was used for 1 minute with following mesh sizes; 1000, 500, 300, 180, 150 and 106 µm, to extract the formed granules. The granules and/or powder were removed from each sieve and put in small plastic containers for each sieve cut at room temperature for further analysis. The experiments were repeated using a different binder viscosity, mixing time/ speed and powder wettability.

For the high shear granulation, 200 g of the powder mixture was pre-loaded in 1 L bowl of the Diosna high-shear mixer first. The binder droplets with 0.3:200 wt/wt L/S ratio were deposited on the surface of the blend approximately at mid-radius position, distributed around the circumference and covered with some small amount of the powder. The run was initiated after approximately 30 secs after deposition. Granulation was performed for 20 secs, impeller speed 370 rpm, no chopper.

The shape and size of all resultant granules were analysed using light microscopy and image analysis. A select representative number of granules of 1000 μm mesh size were analysed with XRCT for internal structure and porosity using XRCT software package. Representative granules were selected for compositional analysis through SEM and EDX. For more details of the methods and characterisation, see Chapter 6, Section 6.2.

CHAPTER 4. Granulation of model particles in a low shear mixer

Granulation of non-wetting powders is a growing problem in the pharmaceutical industry. This creates considerable difficulty in understanding and controlling industrial granulation processes. Very limited studies have been reported in the literature on how different formulation and process parameters effect granule size and internal microstructure produced using heterogeneous-wetting powder blends and this forms the motivation of this work.

Three different mixtures of wetting and non-wetting powders were granulated with four different viscosities of PEG solutions in a tumbling drum. Tumbling speed, primary particle size and mixing time were investigated. The size and microstructure of the resultant granules were studied using sieve analysis and X-ray microcomputed tomography respectively.

The results show that granule size increased with increasing binder viscosity. Hollow granules were observed with varying average wall thicknesses using different binder viscosities and powder wettabilities.

Tumbling speed had a minimal effect on granule size using different powder wettabilities. It is suggested that this is because the impact force applied on the granules remained weak despite the difference in the tumbling speed. Hollow granules were produced with different average wall thickness using different powder wettabilities and tumbling speeds.

An increase in granule size was observed with increasing primary particle size. As the primary particle size increased, the granules became more consolidated. There was also a difference in the size of granules produced at different mixing times using powder of low wettability. Granule size increased with increasing mixing time. Hollow granules were produced at different mixing times with average wall thicknesses increasing with increasing mixing time.

This work shows that further research is required to identify the effect of impact and shearing forces on granule size and internal microstructure.

4.1 Introduction

It is clear from the literature review in Chapter 2, that there are gaps in knowledge of the mechanisms involve in the formation of hollow granules; what happens after initial liquid marble formation? One of these such gaps is the understanding of the change in granule size and the internal microstructure of the resulting granules using wetting and non-wetting powders.

The formation of hollow granules from liquid marbles is a developing field in the research of non-wetting granulation. A liquid marble is formed by the self-assembly of non-wetting powder around a liquid droplet. N. Eshtiaghi et al. 2009; Hapgood et al. 2009; N. Eshtiaghi et al. 2010; N. Eshtiaghi et al. 2009 investigated the different conditions required for hollow granule formation from liquid marble precursors.

In this chapter the work by Eshtiaghi and Hapgood has been extended to study granule size and internal structure for a range of wetting and non-wetting systems using varying parameters:

- Binder viscosity
- Powder wettability
- Powder particle size
- Mixing time

with a view to measuring properties relevant to granule size and hollow granule formation. In particular:

- Particle size distribution using sieve analysis
- Granule internal microstructure using X-ray tomography
- Calculation of the porosity and wall thickness of hollow granules which gives further insight of the internal structure of hollow granules

Studies have been conducted investigating the penetration time of liquid droplets into static powder beds of different wettabilities. However, there are very limited studies on the effect of different powder wettabilities on granule size and properties. These studies have focused on

wet granulation using high shear or twin screw granulation, but not wet tumbling drum granulation. In this chapter, a tumbling drum (low-shear) is employed to investigate these parameters and the properties of the resultant granules.

4.2 Materials and Methods

A short overview of materials and methods used is explained in this section. A more detailed description of the materials and methods can be found in Chapter 3. Experiments were performed with a low shear mixer (tumbling drum), with an internal diameter of 70 mm and 100 mm height, to granulate 100 g of powders. Pre-nucleation of liquid marbles or immersion nuclei was carried out externally prior to granulation; for more details see Section 3.6.1. Liquid marbles are formed when using low powder wettability of a contact angle with liquid of 90° or more. Immersion nuclei on the other hand occurs when using a wetting powder with a contact angle with liquid of less than 90° . The work performed in this chapter can be divided into four parts:

Firstly, the effect of varying powder wettabilities and binder viscosities were investigated. In this part, three different mixtures of 100%-0%, 65%-35%, and 25%-75% of non wetting-wetting powders were used, which will simply be denoted as low, medium and high powder wettability respectively, or by the contact angle of the liquid with powder. Four aqueous binder solutions were used: 50 w/w. % polyethylene glycol (PEG) with molecular weight of 1500, 6000, 12000, and 20000, which will be simply referred to by their viscosities. The tumbling speed was set at 25 rpm. The granulation time was five minutes.

Secondly, the effect of tumbling speed was investigated; 25 and 60 rpm using the three different powder mixtures of 100%-0%, 65%-35%, and 25%-75% of non wetting-wetting powders were used. One PEG solution was used; 50 w/w. % PEG 12000, with a viscosity of 1300 mPa s., which will be simply referred to by its viscosity. The granulation time was five minutes.

Thirdly, the effect of varying the powder wettabilities and primary particle size were investigated. In this part, three different mixtures of 100%-0%, 65%-35%, and 0%-100% of non wetting-wetting powders were used, which will also simply be denoted as low, medium and high powder wettability respectively or by their contact angle with the liquid. Three different primary particles size were used; AQ, AH and AF (the glass beads AQ are the smallest beads used with $d_{50} \sim 35\mu\text{m}$, while the glass beads AF are the largest beads with $d_{50} \sim 114\mu\text{m}$). They will be referred to by their d_{50} value throughout this work. The granulation time was five minutes. One PEG solution was used; 50 w/w % PEG 12000, with a viscosity of 1300 mPa s. The tumbling speed was set at 25 rpm.

Finally, varying the mixing times, 10, 300, 900 and 1800 s, was investigated. In this part, one powder of 100% non-wetting powder was used, which will also be simply denoted as a low powder wettability or by its contact angle with the liquid. One PEG solution was used; 50 w/w% PEG 12000, with a viscosity of 1300 mPa s. The tumbling speed was set at 25 rpm. For more details of the methods see Section 3.6.2.

A mixing time chosen of 5 minutes was chosen for most of the experiments performed in this chapter because it was expected that the granules at 5 minutes mixing time will start to grow and powder will layer around the liquid droplets, and they will start to consolidate.

All these parameters are used for the comparison of granule size and internal microstructure characterisation (total porosity and wall thickness). Table 4.1 shows the binder viscosity, blends of the powders and the liquid-powder contact angle. Table 4.2 summarises all the experiments performed in this chapter.

Table 4.1: PEG binder viscosities and powder-binder systems used and their contact angles.

Binder (molecular weight)	Binder viscosity (mPa s)	Powder			
		Non wetting – wetting			
		Contact angle ^o of binder/powder			
		100%-0%	65%-35%	25%-75%	0%-100%
1500	60	115	90	57	30
6000	300	115	92	59	34
12000	1300	116	93	68	39
20000	3000	117	94	68	40

Granule size distributions were measured by sieving with the following mesh sizes: 4000, 3350, 2800, 1700, 1000, 500, 250, 180, and 106 μm . The sieve fractions were reserved for

microstructural analysis by X-ray tomography (XRCT). Each experiment was repeated twice and the mean of particle size distribution was determined.

Images of granules were produced using digital microscope images (Lumenera Infinity 3 Camera, Navitar 12X zoom lenses).

Three representative granules were chosen from each experiment for XRCT imaging to examine and analyse the internal structure. Images were processed with Skyscan software DataViewer and CTAn. Three representative granules were measured for wall thickness and % total porosity and the average of three measurements was taken and presented throughout this chapter. More details of the procedure can be found in Chapter 3, Section 3.2.10.

Table 4.2: Experimental design.

Powder particle size d_{50} (μm)	Powder Non wetting-wetting	Binder viscosity (mPa s)			
		PEG 1500	PEG 6000	PEG 12000	PEG 20000
35	100%-0%	60	300	1300	3000
	65%-35%	60	300	1300	3000
	25%-75%	60	300	1300	3000
Powder particle size d_{50} (μm)	Powder Non wetting-wetting	Binder viscosity (mPa s)	Tumbling speed (rpm)		
35	100%-0%	1300	25	60	
	65%-35%	1300	25	60	
	25%-75%	1300	25	60	
Binder viscosity (mPa s)	Powder Non wetting-wetting	Powder particle size d_{50} (μm)			
1300	100%-0%	35	70	115	
	65%-35%	35	70	115	
	25%-75%	35	70	115	
Binder viscosity (mPa s)	Powder Non wetting-wetting	Mixing time (sec)			
1300	100%-0%	10	300	900	1300

4.3 Results and discussion

Over the last few decades, many studies have been performed on granulation of wetting powder. In contrast, there are very limited studies on granulation of non-wetting powder. Therefore, granule properties produced using heterogeneous-wetting powder mixtures are studied in this chapter using different process and formulation parameters.

Different powder wettabilities were produced by mixing non wetting and wetting powders in different percentages (100%-0%, 65%-35%, 25%-75%) respectively. From pre-nucleation, some of the mixtures formed immersion nuclei, while others formed liquid marbles, as can be seen in Table 4.3.

Table 4.3: Summary of pre-nucleation experiments.

Conditions		Contact angle ^o	Pre-nucleation product
Non wetting-wetting mixture	Binder viscosity (mPa s)(PEG)		
100%-0%	60	115	Liquid marble
100%-0%	300	115	Liquid marble
100%-0%	1300	116	Liquid marble
100%-0%	3000	117	Liquid marble
65%-35%	60	90	Liquid marble
65%-35%	300	92	Liquid marble
65%-35%	1300	93	Liquid marble
65%-35%	3000	94	Liquid marble
25%-75%	60	57	Immersion nuclei
25%-75%	300	59	Immersion nuclei
25%-75%	1300	68	Immersion nuclei
25%-75%	3000	68	Immersion nuclei

The measured diameter of all liquid droplets before nucleation and granulation used in this chapter can be seen in Table 4.4; for more details see Section 3.2.8. Droplets with higher binder viscosity had larger droplet radii compared to the droplets formed from lower binder viscosity. This is probably because that the higher binder viscosity tends to have higher mass and density, which in turn leads to the higher droplet diameter.

Table 4.4: PEG liquid droplet properties.

Binder viscosity (mPa s)	Droplet mass (g)	Density (g/cm³)	Droplet Volume (cm³)	Droplet Diameter (µm)
60	0.006645 ± 0.0013	1.0501 ± 0.023	0.006327	2345.42
300	0.00699 ± 0.0013	1.0904 ± 0.028	0.006410	2355.48
1300	0.00804 ± 0.0003	1.0908 ± 0.014	0.007345	2466.53
3000	0.008266 ± 0.0008	1.0944 ± 0.0001	0.007552	2486.45

The shear forces impacting on liquid marbles or immersion nuclei inside the drum were considered by calculating the Froude number (Equation 4.1). The Froude number, is a dimensionless number defined as the ratio of the flow inertia to the external field (the latter in many applications simply due to gravity). It has been described for powder blending and was suggested as a criterion for dynamic similarity and a scale-up parameter in wet granulation. The mechanics of the phenomenon has been described as an interplay of the centrifugal force (pushing the particles against the mixer wall) and the centripetal force produced by the wall, creating a “compaction zone” (Levin and Ph, 2013).

$$Fr = \frac{d \omega^2}{g} \quad \text{Equation (4.1)}$$

In Equation 4.1, Fr is the Froude number, d is the internal diameter of the drum, ω is the angular velocity (rad/s) and g is gravitational acceleration. Table 4.5, shows the Froude number data for two different drum speeds of 25 and 60 rpm. It can be seen the Froude number data is higher with the higher drum speed.

Table 4.5: Froude numbers of the low shear mixer.

Speed rate (rpm)	Drum internal diameter (m)	Gravitational acceleration (m/s²)	Angular velocity (radian/s)	Froude number
25	0.035	9.81	2.62	0.024
60	0.035	9.81	6.28	0.14

The results and discussion section is divided into four parts: the first section will explain the effect of binder viscosity and powder wettability. The second section will give an investigation of the effect of varying tumbling speeds on granule size for a range of powder wettabilities.

The third part will give details of the effect of primary particle size and powder wettability. Finally, the last section will show the effect of increasing mixing time on the granule size and internal microstructure of a non-wetting powder.

4.3.1 The effect of binder viscosity and powder wettability

In this section, different binder viscosities and powder wettabilities were investigated. The primary powder particle size was 35 μm , and the tumbling speed was set at 25 rpm with a 5 minutes mixing time.

4.3.1.1 Granule size distribution

The size distribution of the resultant granules produced from different powder wettabilities and binder viscosities for five minutes mixing time in low shear mixer granulation are discussed in this section.

4.3.1.1.1 Low powder wettability

Figure 4.1 shows the size distribution of the granules in the low shear mixer, using low powder wettability and different binder viscosities. After granulation and drying, small granules sizes were produced using 60 mPa s binder viscosity ($d_{43} = 726 \mu\text{m}$). An increase in the size of the granules was produced using 300, 1300 and 3000 mPa s binder viscosities ($d_{43} \approx 1300 \mu\text{m}$). A unimodal size distribution was obtained using 60 and 300 mPa s binder viscosities. A bimodal size distribution was obtained using 1300 and 3000 mPa s binder viscosities, with high frequency peak at 500 μm using 3000 mPa s binder viscosity. For more details of q_3 and d_{43} , see Appendix A.1.1.

At 60 mPa s binder viscosity, a fine powder was produced (Figure 4.2 a). At 300 mPa s binder viscosity, buckled, semi-spherical and elongated granules were produced (Figure 4.2 b). At 1300 mPa s and 3000 mPa s binder viscosities, mixtures of spherical, buckled, elongated granules and fine powder were produced (Figure 4.2 c and d).

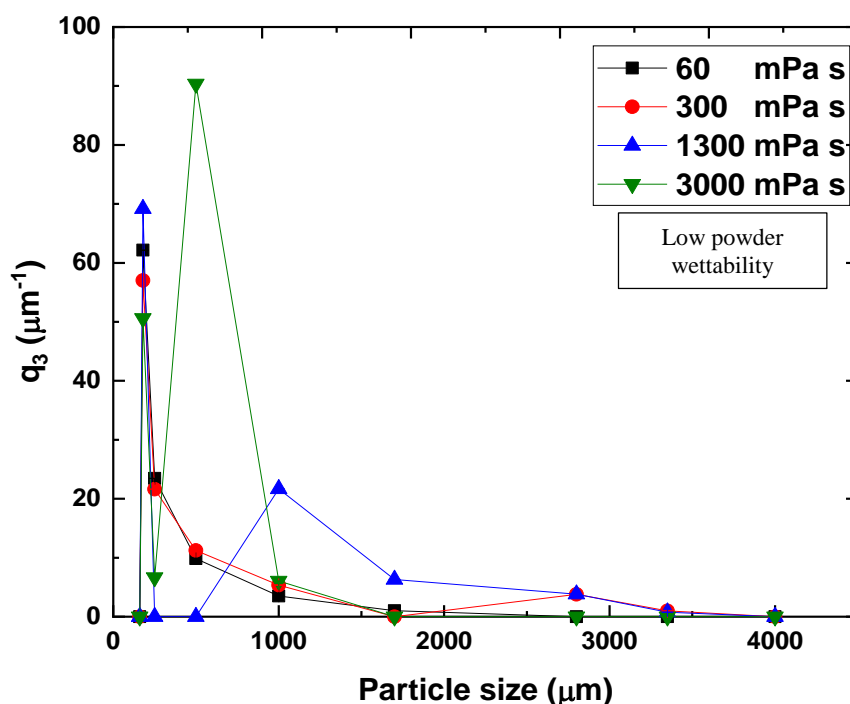


Figure 4.1: Particle size distribution of granules produced using low powder wettability and different binder viscosities, obtained via sieve analysis. Error bars are the standard deviation of three measurements.

The formation of fine powder using low viscosity binders might be due to wear as well as breakage of liquid marbles during granulation in the low shear mixer. It can be concluded that the percentage of ungranulated fine powder decreases gradually with increasing binder viscosity to 3000 mPa s binder viscosity. This is most likely due to the effect of viscous force; it is expected that the strength of liquid bridges increases with increasing binder viscosity. This results in the decrease of the breakage of liquid marbles during granulation.

The production of spherical granules with increasing binder viscosity is in agreement with Eshtiaghi et al. 2010. They studied the effect of binder viscosity on the shape of the resultant hollow granules using nucleation only experiments, in which a liquid droplet was released onto the static powder bed without subsequent granulation. Non-wetting glass beads powder and different aqueous concentrations of HPMC solution were used. They found that using higher binder viscosity led to the formation of a spherical hollow granules. Buckled hollow granules

were obtained using low HPMC concentration. They suggested that this might be due to the viscous forces effect, and the ability of high viscous binder to maintain the shape of the droplet during drying.

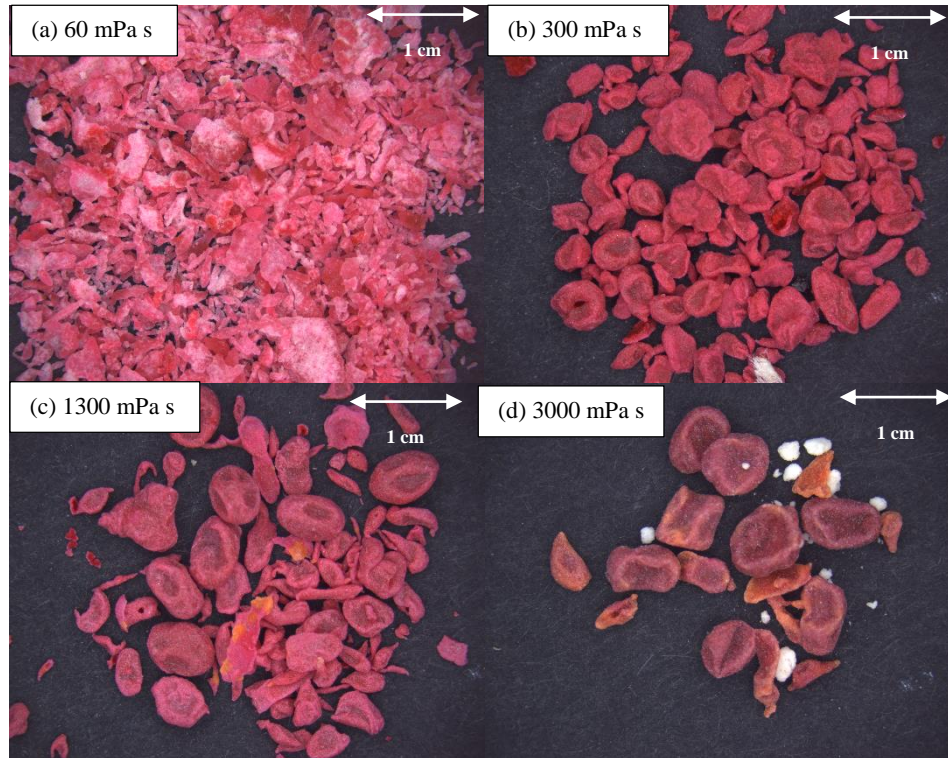


Figure 4.2: Comparison of granules produced using low powder wettability and different binder viscosities.

4.3.1.1.2 Medium powder wettability

Figure 4.3 shows the granule size distribution as a function of binder viscosity and medium powder wettability. Unlike the observations in Figure 4.1, this system produced smaller granule sizes with an increase in the binder viscosity. The use of 60 mPa s binder viscosity produced a larger granule size ($d_{43} = 2225 \mu\text{m}$), whereas the use of 3000 mPa s binder viscosity produced a smaller granule size ($d_{43} = 500 \mu\text{m}$). A unimodal size distribution was observed using 60, 1300 and 3000 mPa s binder viscosities. A bimodal size distribution with two different modes can be seen when using a 300 mPa s binder viscosity (Figure 4.3). For more details of q_3 and d_{43} , see Appendix A.1.1.

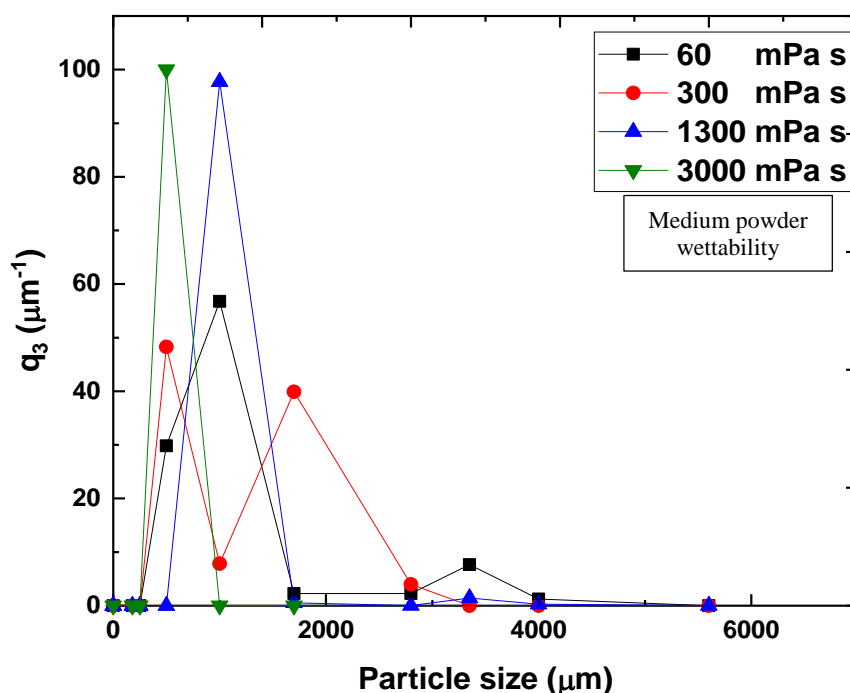


Figure 4.3: Particle size distribution of granules produced using medium powder wettability and different binder viscosities, obtained via sieve analysis. Error bars are the standard deviation of three measurements.

An additional interesting observation from the granules is the change in their shape with binder viscosity (Figure 4.4). At 60 and 300 mPa s binder viscosity, the granules were very flat and elongated (Figure 4.4 a and b). At 1300 mPa s binder viscosity, a mixture of flat, buckled and semi-spherical granules was obtained (Figure 4.4 c). Only semi-spherical buckled granules were obtained at 3000 mPa s binder viscosity (Figure 4.4 d). This is most likely the result of the binder viscous force. It is suggested that the ability of viscous action to keep the shape of the droplet intact during impact increased with increasing in the binder viscosity.

Most of the observations from Figure 4.3 and Figure 4.4 can be explained considering binder viscosity and powder wettability. In such a case, the combination of medium powder wettability and high binder viscosity leads to the production of spherical granules instead of flat and elongated granules.

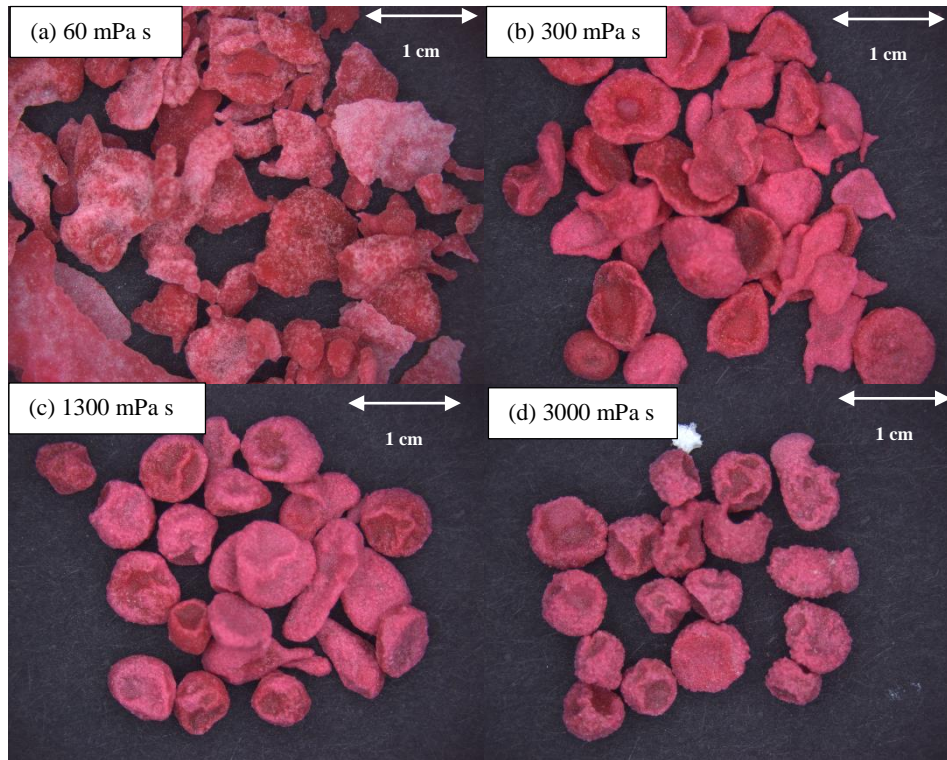


Figure 4.4: Comparison of granules produced using medium powder wettability and different binder viscosities.

4.3.1.1.3 High powder wettability

Figure 4.5 shows granule size distributions using high powder wettability and different binder viscosities. Approximately similar granule sizes were produced using 60, 300 and 1300 mPa s binder viscosities ($d_{43} \approx 2800 \mu\text{m}$). A larger granule size was produced using 3000 mPa s binder viscosity ($d_{43} = 4117 \mu\text{m}$). For more details of q_3 and d_{43} , see Appendix A.1.1.

At 60 mPa s binder viscosity, relatively flat shaped granules were produced (Figure 4.6 a). At 300, 1300 and 3000 mPa s binder viscosities, a mixture of spherical and buckled granules was produced (Figure 4.6 b, c and d).

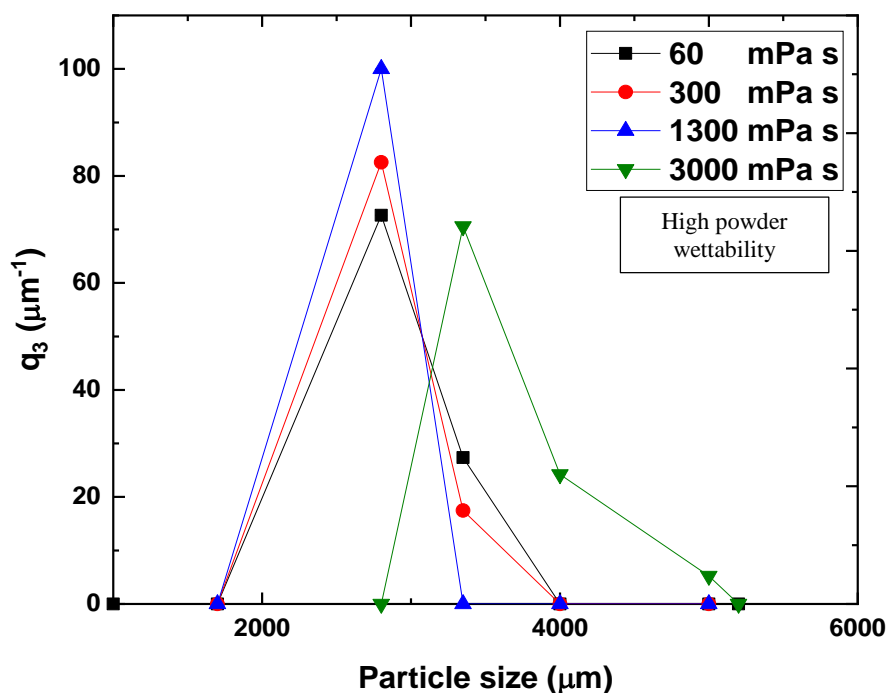


Figure 4.5: Particle size distribution of granules produced using high powder wettability and different binder viscosities, obtained via sieve analysis. Error bars are the standard deviation three measurements.

The small difference in the size of the granules produced using high powder wettability and 60, 300 and 1300 mPa s binder viscosities is consistent with Wade, Martin and Long, 2014. Aqueous polyvinyl pyrrolidone solution in different concentrations as a liquid binder and pharmaceutical grade hydroxyapatite as powder were granulated in a high shear mixer. Reverse phase wet granulation processes were used; all liquid binder was first added to the mixer bowl followed by the addition of all powders. They found that there was no difference in granule size using different binder viscosities and high powder wettability. They explained their results according Iveson, Litster and Ennis, 1996, who supposed the viscosity range used had a minimal difference in the contribution of the binder viscosity on interparticulate friction, viscous dissipation and capillary forces, resulting in similarities in granule size. It should be noted that Iveson, Litster and Ennis, 1996, suggested that the inter-particle friction and viscous dissipation contributed to the resistance to granule deformation. Increasing liquid content can either increase inter-particle friction due to lubrication or increase viscous force effects since more liquid is available within and on the granule surfaces. Either inter-particle friction or

viscous forces can be dominant depending on binder viscosity. The effect of inter-particulate friction will be dominant with an increase in the liquid content of low viscous binder, while viscous forces dominate with an increase in the liquid content of high viscous binder.

Granule coalescence was observed using a high binder viscosity of 3000 mPa s (Figure 4.6 d). These results are in accordance with Iveson et al. 1998, where it was reported that the binder viscosity was an essential parameter in agglomeration by coalescence. The coalescence occurred with increased binder viscosity and high powder wettability. Growth by coalescence occurs when the collisional kinetic energy is too small to overcome the resistance of viscous lubrication of the binder in the liquid layer.

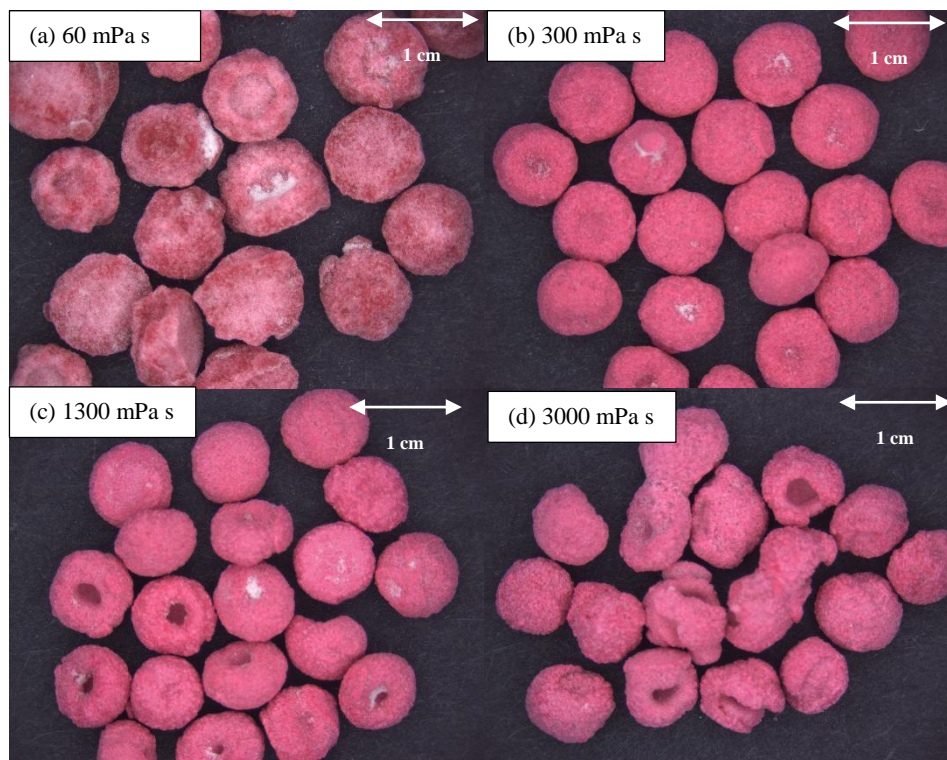


Figure 4.6: Comparison of granules produced using high powder wettability and different binder viscosities.

4.3.1.2 Internal structural analysis

Figure 4.7 presents 3D images of representative granules as a function of powder wettability and binder viscosity using XRCT. The observed white outer shell is the primary powder, the dark grey area is the dried liquid and the dark space in the middle of the granules is air.

For low powder wettability, fine powder was produced using low binder viscosity, which was difficult to scan using XRCT. Hollow granules were produced using different binder viscosities (Figure 4.7). The wall thickness of hollow granules increased from 34 μm using 300 mPa s binder viscosity to 36 μm and 38 μm using 1300 and 3000 mPa s binder viscosities respectively (Figure 4.8).

For medium powder wettability, flakes were produced using low binder viscosity, which were difficult to scan using XRCT. Hollow granules were produced using different binder viscosities (Figure 4.7). The wall thickness of hollow granules decreased in size from 1303 μm using 300 mPa s binder viscosity to 171 μm using 3000 mPa s binder viscosity (Figure 4.8).

For high powder wettability, single solid granules were produced using 60 mPa s and 300 mPa s binder viscosities. Hollow granules were observed using 1300 and 3000 mPa s binder viscosities. Hollow granules wall thickness decreased from 1000 μm to 742 μm using 1300 and 3000 mPa s binder viscosity respectively (Figure 4.8). More cross sectional XRCT images of granules can be found in Appendix A.2.1.

Single solid granules can be seen with powder of high wettability and low binder viscosity of 60 and 300 mPa s. This is probably because with increasing powder wettability and decreasing binder viscosity, the immersion of the powder particles inside the liquid droplet increased leading to formation of solid granules. For powders of medium and high wettabilities, a thin layer of powder was formed using higher binder viscosity compared with multi-layers of powder around the liquid droplet using low binder viscosity. It is hypothesized that the viscous force mostly dominates the binding force between the particles, which impairs the migration of liquid binder to the granule surface to allow binding of fresh powder particles, leading to the production of a thin layer of powder that covers the liquid droplet.

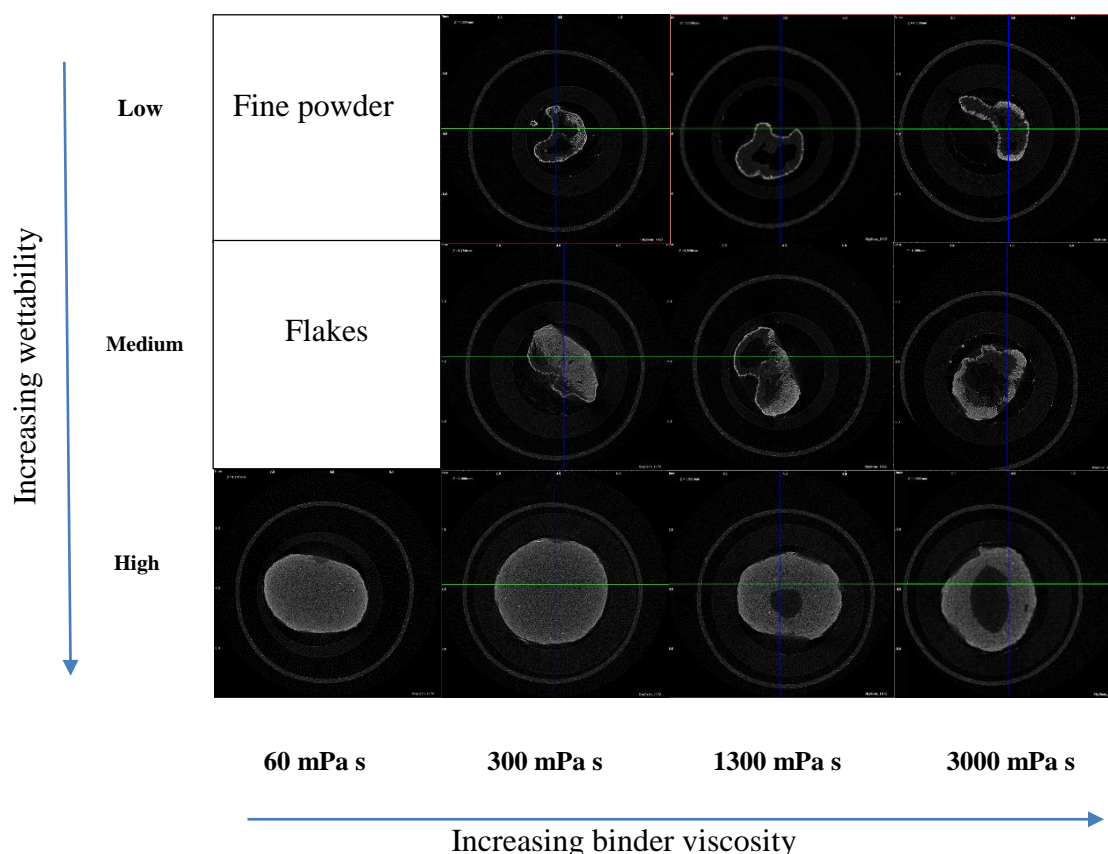


Figure 4.7: Images of granules produced using different powder wettabilities and binder viscosities. The outer rings are part of the sample container. (Reconstructed XRCT images; representative central cross-section).

The production of hollow granules using high binder viscosity and different powder wettabilities in this study is in accord with Eshtiaghi, Liu and Hapgood, 2010. Non-wetting glass beads as powder was used. Different concentrations of HPC and PVP were used as a liquid binder. They found that higher binder viscosity produced hollow granules. They suggested that the high binder viscosity impaired the process of deformation and drop recoil, which drove fluid flow upon impact and, therefore, enhanced liquid marble stability. They reported that the higher binder viscosity produced strong inter-particle bridges that decreased granule deformation.

Similarly, Eshtiaghi et al. 2009, studied the effect binder viscosity on the % of powder coverage around the liquid droplet. A non-wetting polytetrafluoro ethylene (PTFE) as a powder and water and different concentrations of glycerol as liquid binder were used. They found that increasing binder viscosity impaired drop deformation and drop recoil, which decreased powder coverage of the liquid droplet surface.

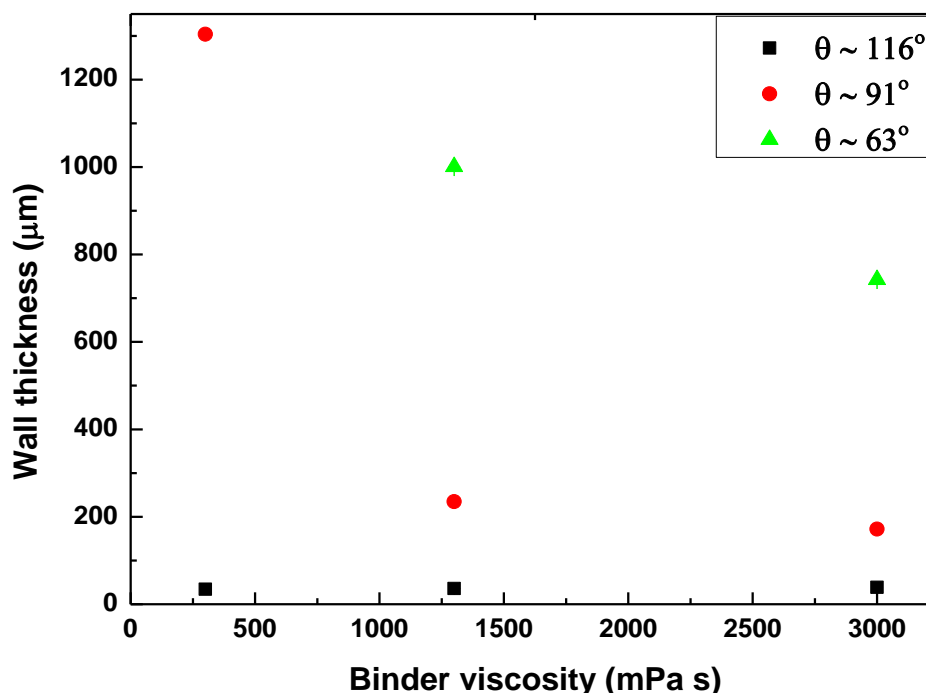


Figure 4.8: Wall thickness as a function of binder viscosity and powder wettability. Error bars are the standard deviation of three measurements. θ is liquid powder contact angle.

4.3.1.2.1 Porosity

Figure 4.9 presents the percentage (%) total porosity as a function of binder viscosity and powder wettability using XRCT software. For more details of XRCT software, see Section 3.2.10. For powders of low wettability, liquid marbles undergo breakage into fine powder at low binder viscosity of 60 mPa s and no porosity values were obtained. However, the porosity decreased slightly from 84 % to 75 % and 70 % using 300, 1300 and 3000 mPa s binder viscosities respectively. With powder of medium wettability, flakes produced using low binder viscosity which was difficult to scan using XRCT and no porosity values were obtained. Granule porosity increased from 31 % to 55 % and 57 % using 300, 1300 and mPa s binder viscosities respectively. For powders of high wettability, the porosity increased from 27 % to 36 % using 60 and 3000 mPa s binder viscosity respectively. However, the error bars for these values all overlap, and this is not conclusive.

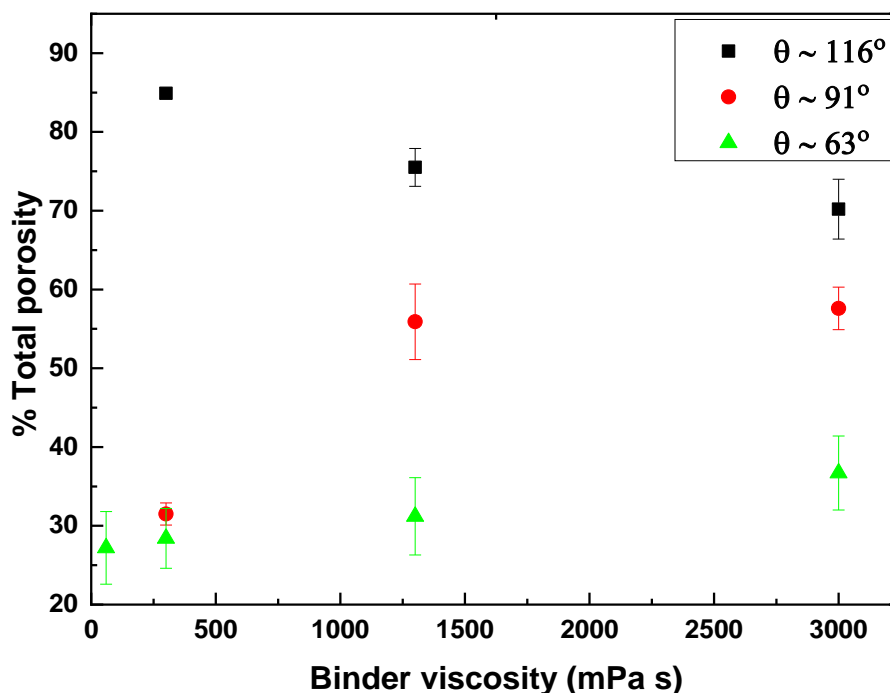


Figure 4.9: Total porosity as a function of binder viscosity and powder wettability. Error bars are the standard deviation of three measurements. θ is liquid powder contact angle.

These results are in agreement with Schæfer et al. 1996 who studied the effect of binder viscosity on granule porosity using melt granulation experiments in a high shear mixer. Lactose was used as a powder and different molecular weight PEGs (2000, 3000, 6000, 8000, 10000 and 20000) were used as a liquid binder. At a high liquid viscosity, the granule porosity was noticeably higher than with low binder viscosity. This was because the higher binder viscosity gives rise to a lower droplet deformation, consolidation and then lower granule porosity.

4.3.2 The effect of tumbling speed and powder wettability

The influence of two tumbling speeds, 25 and 60 rpm, on granule size and internal microstructure using powder of different wettabilities were investigated. Binder viscosity of 1300 mPa s, primary powder particle size of 35 μm and a mixing time of 5 minutes were used.

A binder viscosity of 1300 mPa s was chosen as it is not too highly viscous and, therefore, it is easy to handle. Additionally, it is not too low which could make it difficult to maintain stable liquid marbles.

4.3.2.1 Granule size distribution

For powder of low wettability, there was no significance difference in granule size produced using low tumbling speed from those produced using high tumbling speed (Figure 4.10). For powder of medium wettability, a minimal difference in granule size was observed using the two tumbling speeds (Figure 4.11). For powder of high wettability, an increase in granule size with increasing in tumbling speed was observed, in addition to broader size distribution (Figure 4.12).

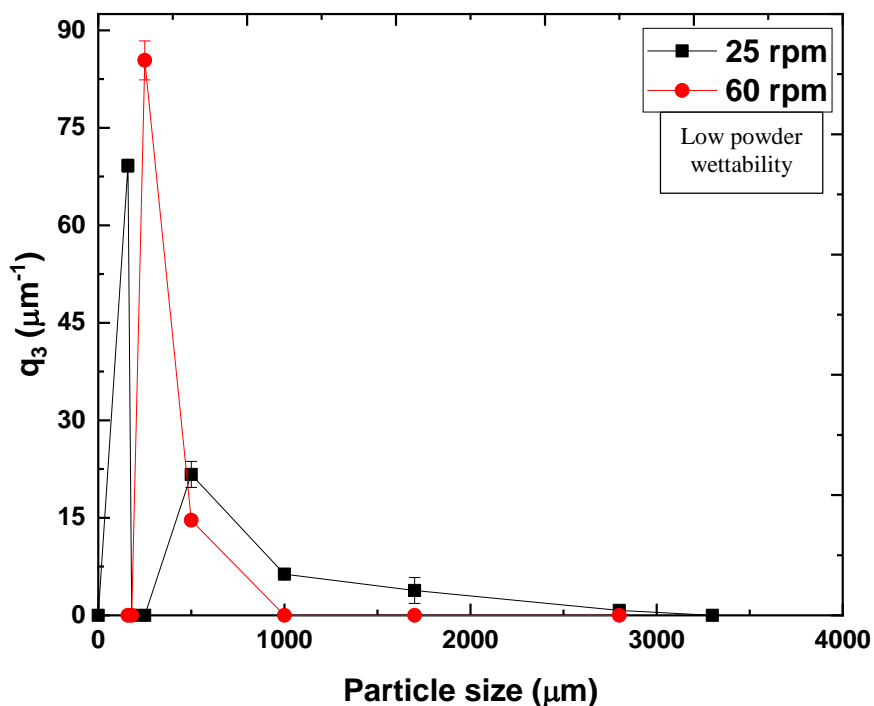


Figure 4.10: Particle size distributions of granules produced using low powder wettability and different tumbling speeds, obtained via sieve analysis. Error bars are the standard deviation of three measurements.

The similarity in granule size using powder of low and medium powder wettabilities, even with an increase in drum speed, may be because that the shearing forces applied on the granules remain weak despite the difference in tumbling speeds. The increase in granule size with increasing tumbling speed using high powder wettability is consistent with the results obtained by Bowden-Green et al. 2016 in spite of the different powder wettability used. They studied the effect of drum granulation on Biochar, a fertilizer powder which is very fine and difficult to control when applied on soil. Biochar behaves as a non-wetting powder, which forms liquid marbles with water. As the rotation speed of the tumbling increased, the agitation of the powder increased with better liquid binder distribution. This gives more opportunities for the granules to collide, consolidate and, hence, increase in granule size.

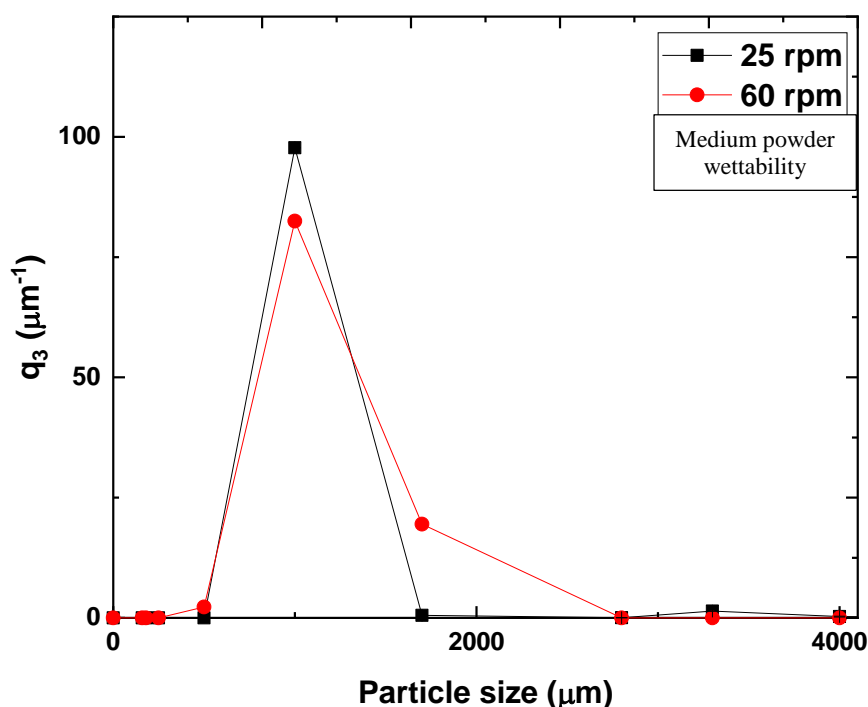


Figure 4.11: Particle size distributions of granules produced using medium powder wettability and different tumbling speeds, obtained via sieve analysis. Error bars are the standard deviation of three measurements.

Overall, the granulation behaviour of granules produced using two different tumbling speeds, showed growth by layering. These results are in accord with Mellmann et al. 2001, who found that the growth of granules inside a tumbling drum mainly occurred by layering. The contact between the powder and the liquid binder inside the tumbling drum, and the homogenous liquid

distribution, is essential to guarantee appropriate particle movement inside the tumbling drum. The particle collisions increased and the probability of powder-granule contact increased with higher drum speed giving more chance for the granules to consolidate and grow by layering.

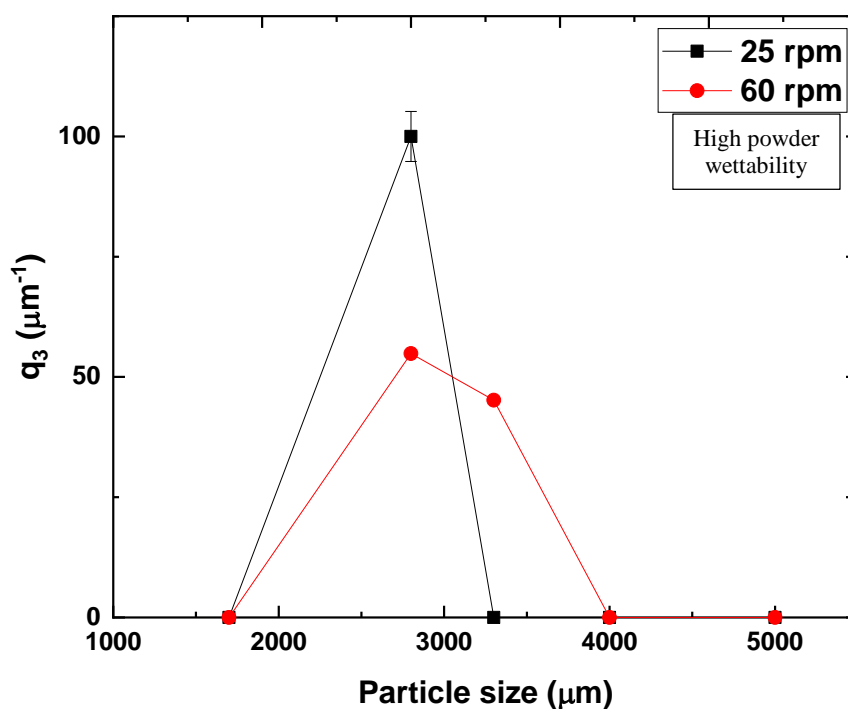


Figure 4.12: Particle size distributions of granules produced using high powder wettability and different tumbling speeds, obtained via sieve analysis. Error bars are the standard deviation of three measurements.

4.3.2.2 Internal structural analysis

Figure 4.13, shows cross sectional XRCT images as a function of powder wettability and tumbling speed. For powder of low wettability, hollow granules were produced with a thin wall thickness of 35.4 μm and 37.5 μm at 25 and 60 rpm tumbling speeds respectively (Figure 4.14). For powder of medium wettability, hollow granules were produced with wall thicknesses increasing from 234.5 μm to 326.5 μm at 25 and 60 rpm tumbling speeds respectively (Figure 4.14). With powder of high wettability, hollow granules were produced with wall thickness increasing from 1000.6 μm at 25 rpm to 1123.4 μm at 60 rpm tumbling speed (Figure 4.14). More cross sectional images of granules produced using 60 rpm tumbling speed can be found in Appendix A.2.2.

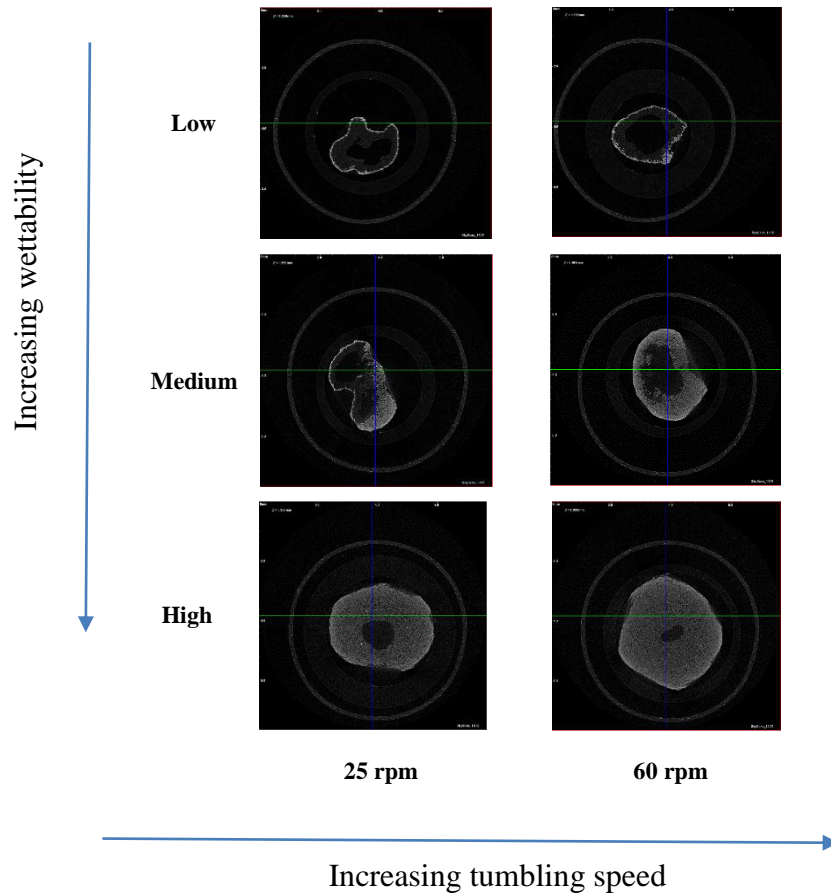


Figure 4.13: Images of granules produced using different powder wettabilities and tumbling speeds. The outer rings are part of the sample container. (Reconstructed XRCT images; representative central cross-section).

The increase in wall thickness at high tumbling speed can be explained by the fact that the granules are experiencing more force at a higher tumbling speed, which gives more chance for granules to collide resulting in more consolidated wall thickness, particularly for high wetting powder.

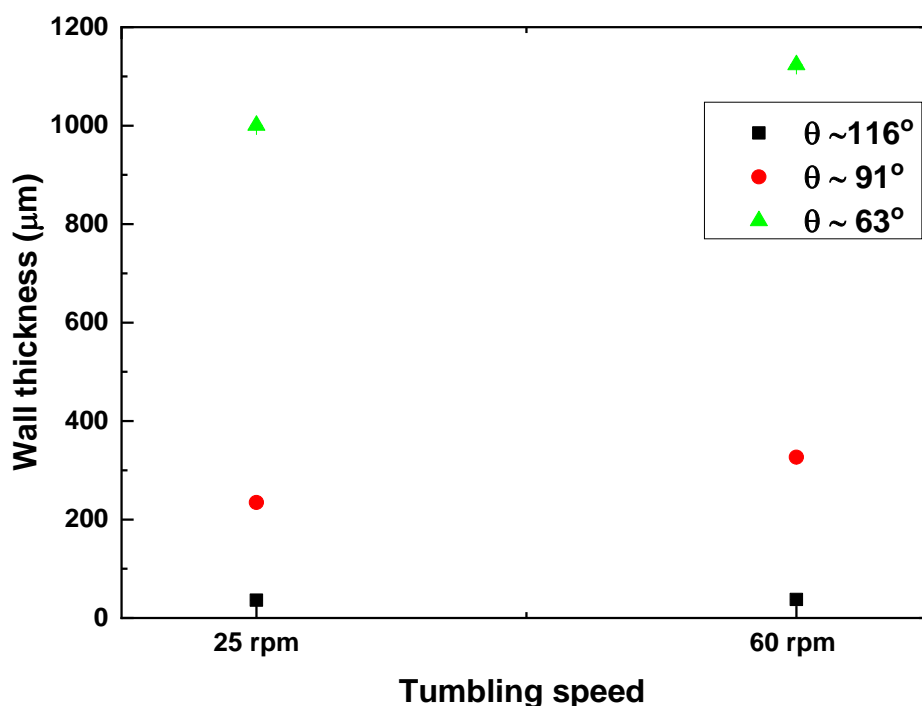


Figure 4.14: Wall thickness as a function of tumbling speed and powder wettability. Error bars are the standard deviation of three measurements. θ is liquid powder contact angle.

4.3.2.2.1 Porosity

Figure 4.15 shows granule porosity in terms of tumbling speed and powder wettability. For powder of low wettability, only a slight difference in porosity of the granules was observed at the two different tumbling speeds, especially when considering the error bars. The porosity decreased slightly from 75.5 % to 73.2 % at 25 and 60 rpm tumbling speeds respectively. With powder of medium wettability, a decrease in the porosity of the granules was observed at two different tumbling speeds. The porosity of granules decreased from 55.9 % to 37.9 % at 25 and 60 rpm tumbling speeds respectively. With powder of high wettability, a small decrease in the porosity of the granules was observed at two different tumbling speeds. The porosity of granules decreased from 31.2 % to 27.8 % at 25 and 60 rpm tumbling speeds respectively.

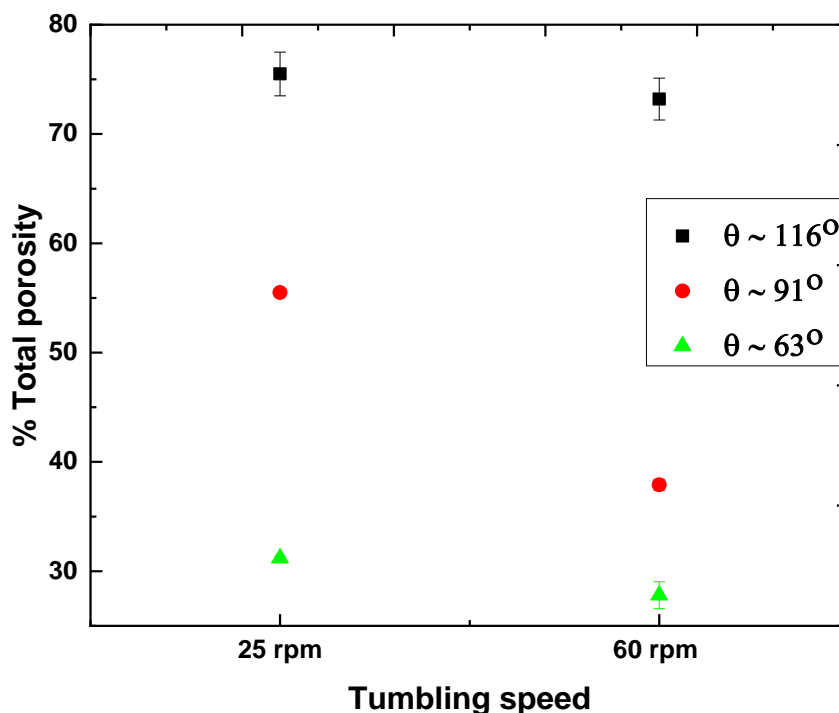


Figure 4.15: Total porosity as a function of tumbling speed and powder wettability
Error bars are the standard deviation of three measurements. θ is liquid powder contact angle.

These results of decreasing porosity with increasing tumbling speed agree with Rodrigues et al. 2017. In this study, phosphate powder was granulated with water in tumbling drum. They hypothesised that particle collisions increase with increasing drum speed, which increases the granule compaction. These collisions caused consolidation of the granules which decreased their porosity, squeezed out entrapped air and liquid binder to granule surface. Internal voids became smaller because of the compaction, and the granules became more consolidated due to an increase in the collisions, which results in decreased granule porosity.

4.3.3 The effect of powder particle size and wettability

The objective of this section is to contribute to the understanding of the effect of primary particle size and powder wettability on the granule size and internal microstructure produced in a low shear mixer. Here, binder viscosity of 1300 mPa s, tumbling speed of 25 rpm and mixing time of 5 minutes were used.

Many studies have been conducted investigating the effect of primary particle size of wetting powder on different granule properties such as (Schæfer and Mathiesen, 1996a; Knight et al. 1998; MacKaplow, Rosen and Michaels, 2000; Hassanpour et al. 2009; Cavinato et al. 2011). However, there is no study currently published on the effect of primary particle size of non-wetting powder on granule size and internal microstructure.

4.3.3.1 Granule size distribution

4.3.3.1.1 Low powder wettability

Figure 4.16 shows granule size distributions using low powder wettability and three different primary particle sizes. Small granules were obtained using a small primary particle size ($d_{43} = 1806 \mu\text{m}$). An increase in granule size was observed using a medium primary particle size, and the granule size continued to increase using a large primary particle size ($d_{43} = 2225 \mu\text{m}$). A bimodal granule size distribution was observed using a small primary particle size due to the breakage of liquid marbles during granulation. A unimodal granule size distribution was obtained using medium primary particle size with a peak at approximately $1000 \mu\text{m}$. Likewise, a unimodal granule size distribution was obtained using the large primary particle size. For more details of q_3 and d_{43} , see Appendix A.1.2.

Flakes and semi-spherical buckled granules were obtained using a small primary particle size (Figure 4.17 a). Buckled and semi-spherical granules were obtained using a medium primary particle size (Figure 4.17 b). However, buckled and elongated granules were obtained using powder of a large primary particle size (Figure 4.17 c). This is most likely the result of difficulty of the liquid droplet to keep the larger particles on the surface of the liquid droplet due to their weight during granulation in the tumbling drum.

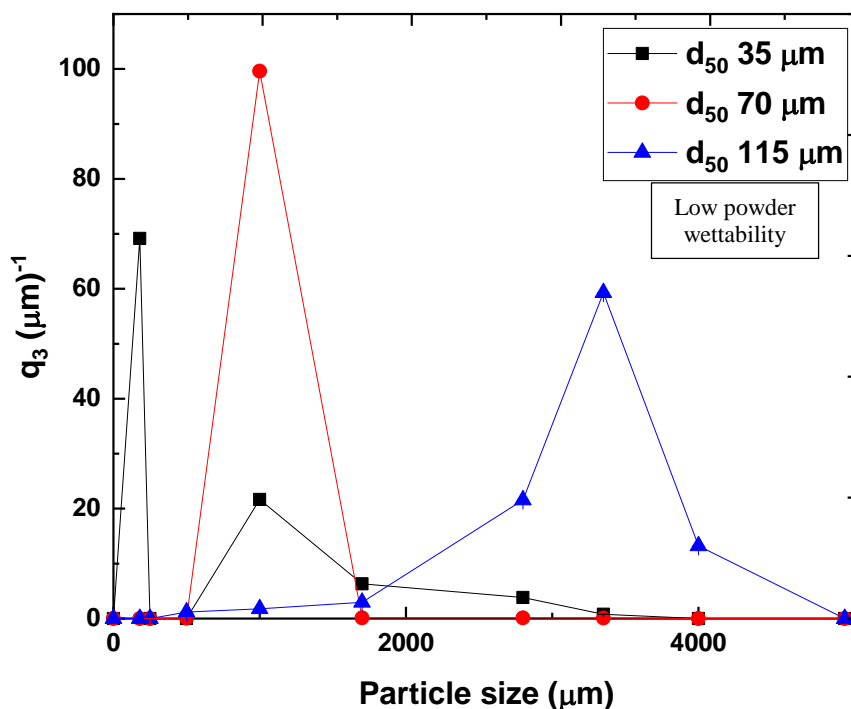


Figure 4.16: Particle size distributions of granules produced using low powder wettability and different powder particles size, obtained via sieve analysis. Error bars are the standard deviation of three measurements.

The results in this work of increased granule size with increasing primary particle size are in accord with Realpe and Velázquez, 2008. They studied the effect of primary particle size on granule size. Three different primary particles sizes of lactose monohydrate as a powder and 1 mPa s binder viscosity of aqueous povidone solution were used. They found that the large primary particle size produced larger granules, while the small primary particle size produced the smaller granules. They hypothesized that the small primary particle size had high cohesive force produced by the large surface area of contact. This produced a stronger, less deformable granules which results in a lower rate of granule growth.

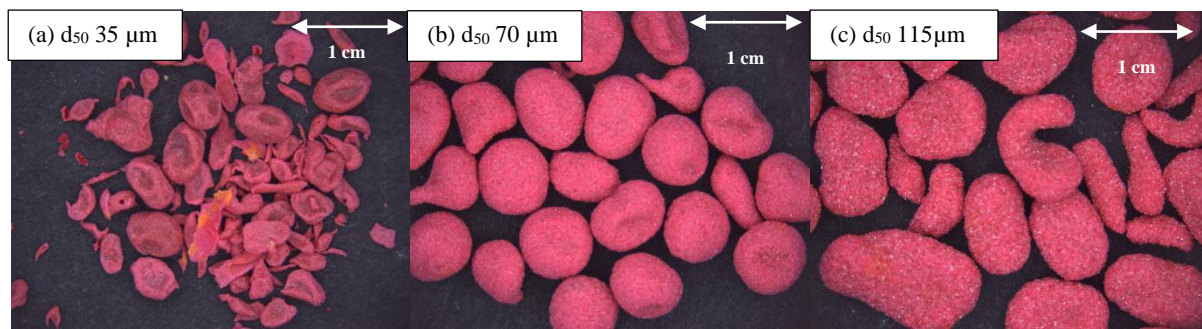


Figure 4.17: Image comparison of granules produced using low powder wettability and different powder particle sizes.

4.3.3.1.2 Medium powder wettability

Figure 4.18 shows granule size distributions using powder of medium wettability as a function of powder particle size. Consistent with the observations using powder of low wettability (Figure 4.16), a smaller granule size was obtained using powder of small primary particle size ($d_{43} \approx 2000 \mu\text{m}$). The granule size tends to increase with powder of medium primary particle size. Note, that the largest granules were obtained with powder of large primary particle size ($d_{43} \approx 3000 \mu\text{m}$). For more details of q_3 and d_{43} , see Appendix A.1.2.

Figure 4.19 shows images of granules using different primary particle sizes of medium powder wettability. Granules formed from small primary particle size were irregular in shape with elongated, buckled and elliptical granules (Figure 4.19 a). However, granules produced from medium and large primary particles were more uniform and semi-spherical in shape (Figure 4.19 b and c).

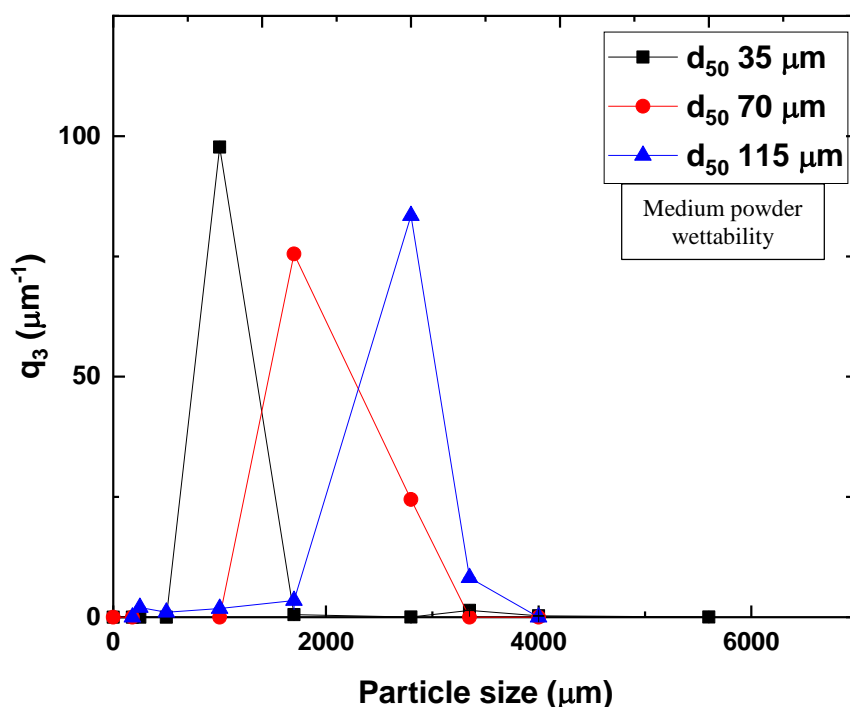


Figure 4.18: Particle size distributions of granules produced using medium powder wettability and different powder particle sizes, obtained via sieve analysis. Error bars are the standard deviation of three measurements.

The increase in the size of granules with increasing primary particle size is in accord with Johansen and Schafer, 2000. Six different mean particle sizes of calcium carbonate as a powder and PEG 1000 with a 2000 mPa s binder viscosity were granulated in a high shear mixer. The actual binder distributions in size fractions were measured by estimating the PEG concentration of a single size fraction using helium pycnometry. They found that an uneven liquid distribution in the granule produced using small primary particle size. They hypothesized that the higher cohesive forces between small primary particles impaired the uniform liquid distribution. This resulted in less deformable granules due to insufficient granule liquid saturation that limited the increase in the granule size. However, a uniform liquid distribution was obtained using powder of large primary particle size which led to more deformable granules and a larger granule size was obtained.

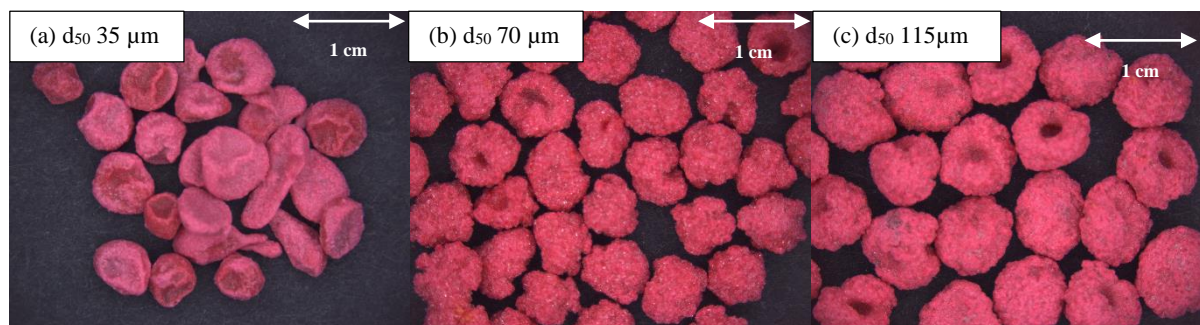


Figure 4.19: Comparison of granules produced using medium powder wettability and different powder particle size.

4.3.3.1.3 High powder wettability

Figure 4.20, shows the effect of primary particle size of high powder wettability. Small granules were produced using a small primary particle size. Larger granule sizes were produced using medium and large primary particles sizes ($d_{43} \approx 3000 \mu\text{m}$). Bowl-shape granules were obtained using a small primary particle size ($d_{43} = 2800 \mu\text{m}$) (Figure 4.21 a). Relatively flat granules with a slightly higher rim were obtained using medium and large primary particle sizes (Figure 4.21 b and c). A rough granule surface was observed with granules produced from powder of a large primary particle size (Figure 4.21c). For more details of q_3 and d_{43} , see Appendix A.1.2.

The shape of the granules produced using medium and large primary particle sizes can be explained by difference in the flowability properties of the powder used. In this study, glass beads powder was used which have free flowing properties. Emady et al. 2011. found that a spreading/crater formation mechanism was mainly observed for free flowing powder such as the glass beads that produced flat shape granules with a high rim. For more details of this mechanism, see Section 2.5.1.

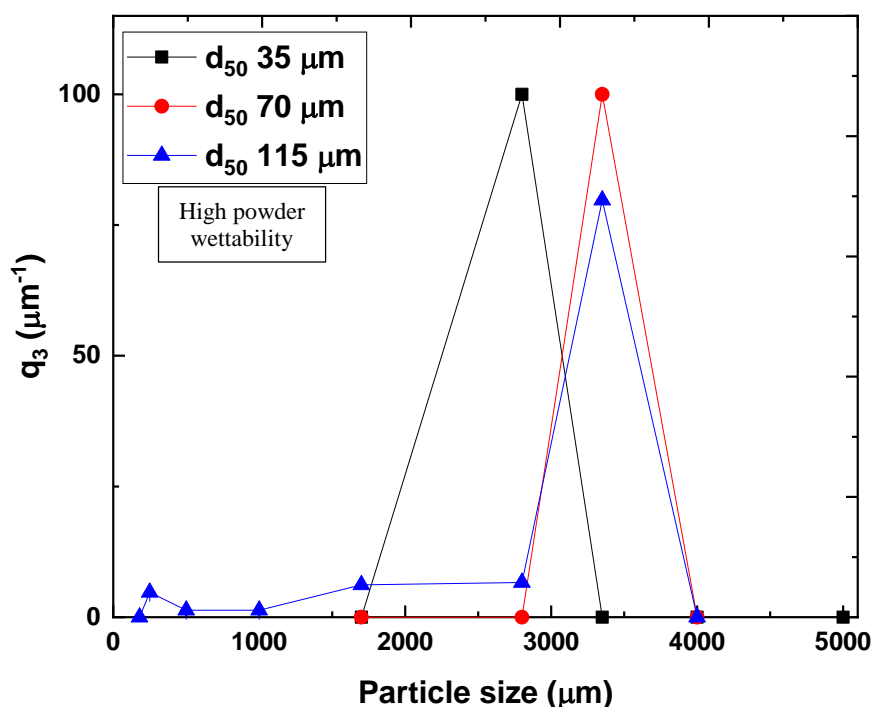


Figure 4.20: Particle size distributions of granules produced using high powder wettability and different powder particle size, obtained via sieve analysis. Error bars are the standard deviation of three measurements.

An increase in granule size with increasing in the primary particle size can be explained by differences particle packing with different sized particles. In a review by Schæfer, 2001 , it was explained that a small primary particle size had a lower particle packing ability. This lower packing ability causes higher inter-particle porosity and decreases granule liquid saturation. Then, less deformable granules will be obtained and, therefore, a smaller granule size.

Similarly, Tan et al. 2009 studied the effect of primary particle size on the nuclei size using hydroxyl propyl cellulose as a binder and lactose as a powder of two different sizes; 100 mesh (coarse primary particle) and 200 mesh (fine powder particle). For a given amount of binder, coarse lactose powder (100 mesh) produced larger nuclei. In other words, increasing primary particle size increases the size of the nuclei produced, because the fine lactose particle (200 mesh) did not pack as well as the coarse lactose particles. The poor packing of fine lactose

powder results in being more likely to contain more-macro voids which resist the liquid penetration through the powder bed and hence the extent of the nucleation.



Figure 4.21: Image comparison of granules produced using high powder wettability and different powder particles size.

An interesting observation of all the granules produced using different powder wettabilities (Figure 4.17, Figure 4.19 and Figure 4.21) is the surface texture. Granules formed from small primary particles have smooth surfaces compared to rough surfaces for granules produced from large primary particles. Schæfer, 1996, reported that a smoother granule surface was obtained when using a small primary particle size, which agrees with the results in this work.

4.3.3.2 Internal structural analysis

Figure 4.22 presents XRCT images of representative granules as a function of powder wettability and primary particle size. For powder of low wettability, hollow granules were obtained using different primary particle sizes. Hollow granules can be seen with very thin wall thickness using powder of small primary particle size. This wall thickness increased with granules produced using powder of medium and large primary particles size. For powder of medium wettability, hollow granules were obtained using powder of small and medium primary particles size. Single solid granules were obtained using powder of large primary particle size. A thin granule wall thickness was observed using powder of small primary particle size, and the wall thickness increased in size using powder of medium primary particle size. For powder of high wettability, hollow granules were produced using powder of small primary particle size. Single solid granules were produced using powder of medium and large primary particle size. More cross sectional images of the granules can be found in Appendix A.2.3.

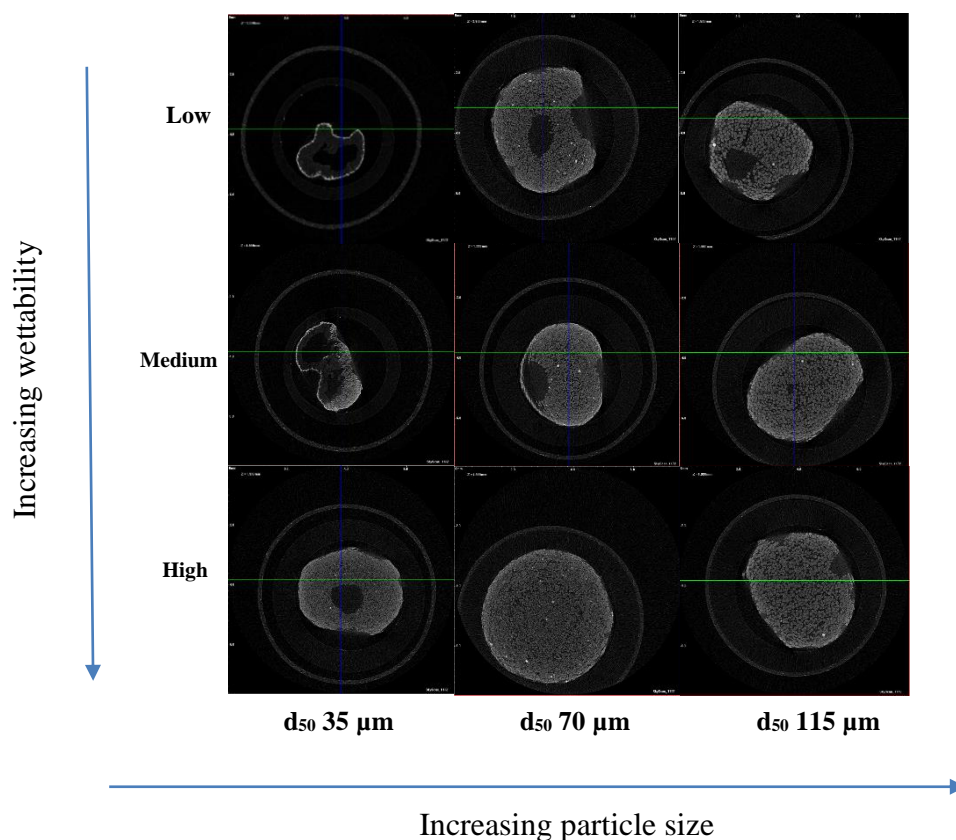


Figure 4.22: Images of granules produced using different powder wettabilities and primary particles size. The outer rings are part of the sample container. (Reconstructed XRCT images; representative central cross-section).

Thinner granule wall thickness was observed using small and medium primary particle sizes, than those produced using a large primary particle size (Figure 4.22). This is probably due to the lower packing ability of small primary particles leading to less deformable granules and a decrease the migration of the liquid to granule surface and therefore the ability to attach new powder particles.

4.3.3.2.1 Porosity

Figure 4.23 expresses the percentage total porosity as a function of different primary particle size and powder wettability. For powder of low wettability, there is a large decrease in granule porosity produced using powder of small primary particle size compared with granules produced using medium and large primary particle sizes. The porosity decreased from 75.5 % using the small primary particle size to 40.9 % using large primary particle size. For powder of medium wettability, the granule porosity decreased from 55.9 % to 36.8 % using small and

large primary particle sizes respectively. For powder of high wettability, minimal changes in granules porosity was observed especially when considering the error bars. The porosity decreased from 31.2 % to 28.2 % and 25.2 % using powder of small, medium and large primary particle sizes respectively.

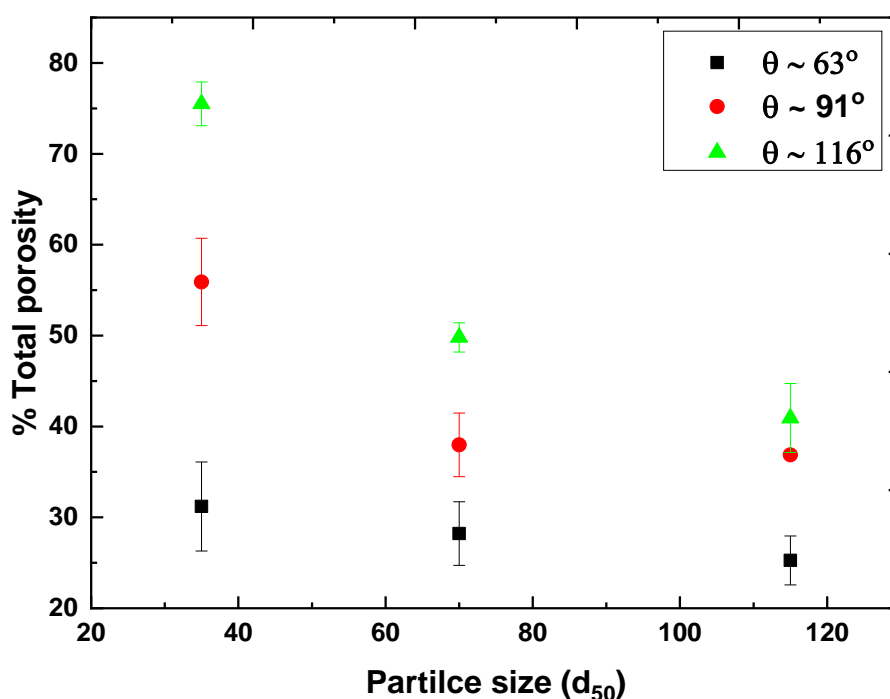


Figure 4.23: Total porosity as a function of powder particle size and powder wettability. Error bars are the standard deviation of three measurements. θ is liquid powder contact angle.

The decrease in the porosity of the granules with increasing primary particle size is in accord with Schæfer and Mathiesen, 1996. In their study, lactose monohydrate as a powder was melt pelletized with PEG of 3000, 6000 and 8000 as flakes, coarse powder and fine powder respectively. Granule density was measured using helium pycnometry. They hypothesized that the packing of small primary particle size was difficult, causing less deformable and highly porous granules.

4.3.4 The effect of mixing time

The objective of this part of the work is to study the effect of the increasing mixing time on granule size and internal microstructure using powder of low wettability in a low shear mixer. A low powder wettability was chosen because the effect of other parameters (binder viscosity and primary particle size) were more pronounced than the other types of powder wettabilities. In addition, very limited studies are currently published on the effect of mixing time on granule size and internal microstructure produced using non-wetting powder. Here, binder viscosity of 1300 mPa s, tumbling speed of 25 rpm and primary particle size of 35 μm were chosen throughout this work.

4.3.4.1 Granule size distribution

Figure 4.24 shows granule size distributions using four different mixing times. For the system using a 10 s mixing time, a smaller granule size was obtained ($d_{43} = 259 \mu\text{m}$). The granule size tends to increase with increasing mixing time to 300, 900 and 1800 s ($d_{43} \approx 1500 \mu\text{m}$). Semi-spherical buckled granules were obtained at 10 s mixing time (Figure 4.25 a). A mixture of flakes and buckled semi-spherical granules were obtained at 300 s mixing time (Figure 4.25 b). Relatively flat, buckled and elongated granules were obtained at 900 s and 1800 s mixing times (Figure 4.25 c and d). For more details of q_3 and d_{43} , see Appendix A.1.3.

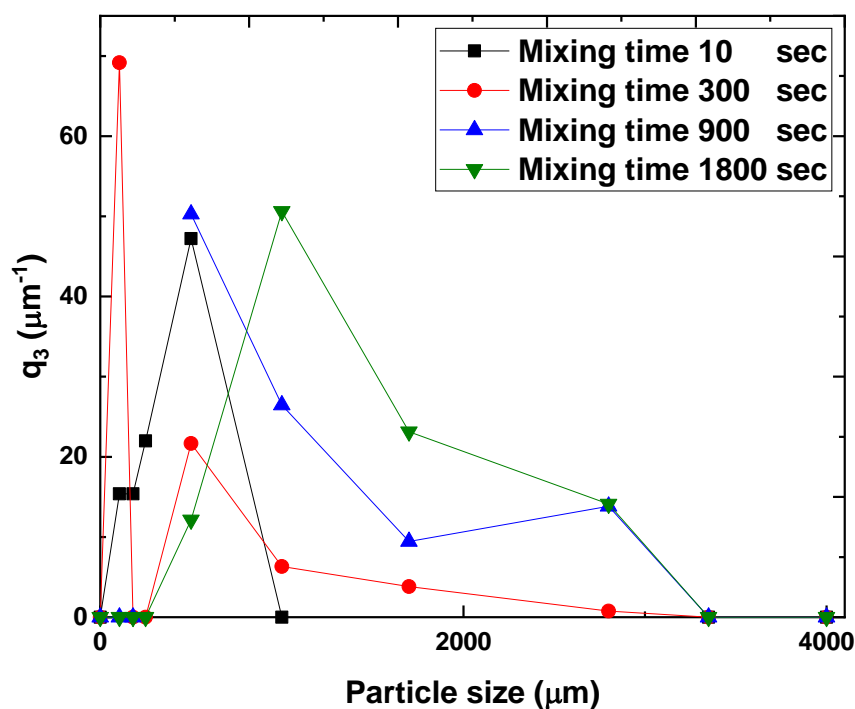


Figure 4.24: Particle size distributions of granules produced using low powder wettability and different mixing times, obtained via sieve analysis.

The production of spherical granules using 10 s mixing time is probably due to the low impact forces applied to the liquid marbles during this short granulation time. It is hypothesised that as the mixing time increases, the impact forces applied on the liquid marbles inside the mixer is increased. Therefore, liquid marbles undergo deformation which producing elongated granules.

The results in this work are in agreement with Hapgood, Farber and Michaels, 2009, who studied the granulation of a pharmaceutical formulation having 70% by weight of non-wetting powder. The effect of mixing time on granule shape was investigated. As the mixing time increased, the granules underwent more deformation leading to elongated granules. It was suggested that the prolonged mixing time imparted high impact forces leading to formation of elongated granules, see Figure 2.16.

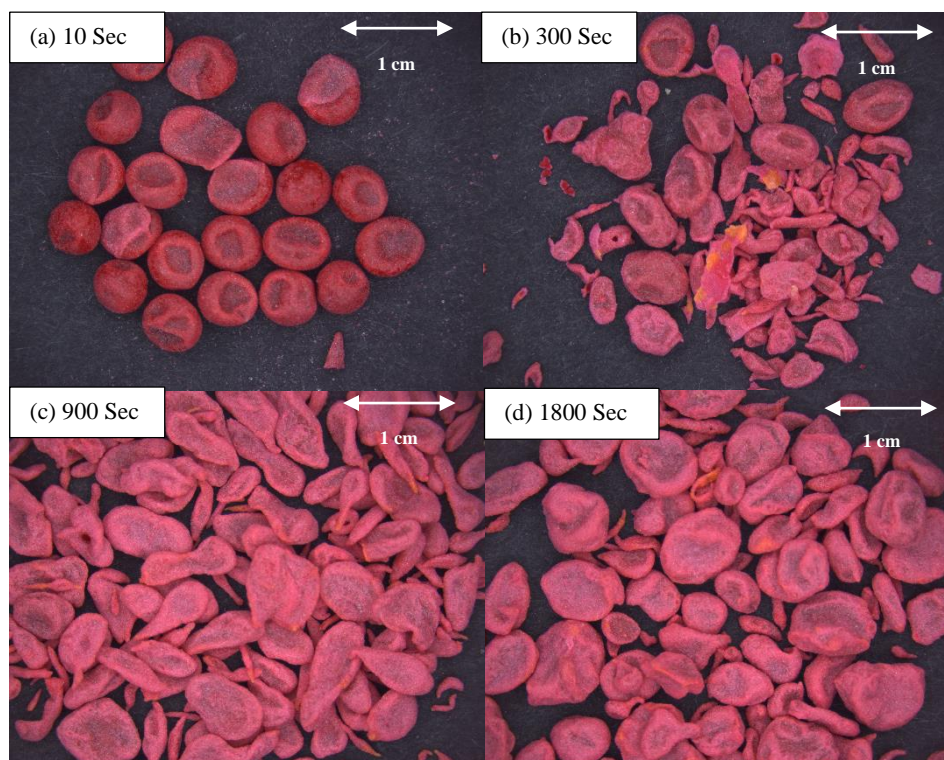


Figure 4.25: Image comparison of granules produced using low powder wettability and different mixing times.

However, the results in this thesis disagree with Oka et al. 2015 who studied the effect of mixing time on granule shape. Semi-fine acetaminophen and microcrystalline cellulose were granulated with water in high shear granulation. SEM was used to characterise granule shape. They found that there was no significant effect of mixing time on granule shape and surface roughness. They hypothesized that might be an indicator of well-mixed system with the high shear forces applied. The thesis results are different from the results in this work probably because of using different powder properties such as wettability and flowability and the use of a different shear mixer.

4.3.4.2 Internal structural analysis

Figure 4.26 presents XRCT images of representative granules as a function of mixing time. The images demonstrate that the granules formed across all mixing times have an internal void with a thin or a thick wall thickness (Figure 4.27).

Hollow granules were observed with a thin wall thickness of 34 μm at 10 s mixing time. A small increase in the average wall thickness to 36.1 μm was observed at 300 s mixing time. The hollow granule wall thickness increased to 42 μm and 44.5 μm at 900 and 1800 s mixing time. Although the error bars are large, there appears to be a clear trend of increasing wall thickness with time.

It is hypothesized that an increased mixing time led to an increase in the granule collisions with the drum's wall and with the powder bed. As a result of the increase in the granule collisions, the binder migrates to the surface of the granules, which increases the chance for particles sticking to granule surfaces and allows more layering of powder particles around the granules, and this expected to started at 300 sec mixing time. More cross sectional images of the granules can be found in Appendix A.2.4.

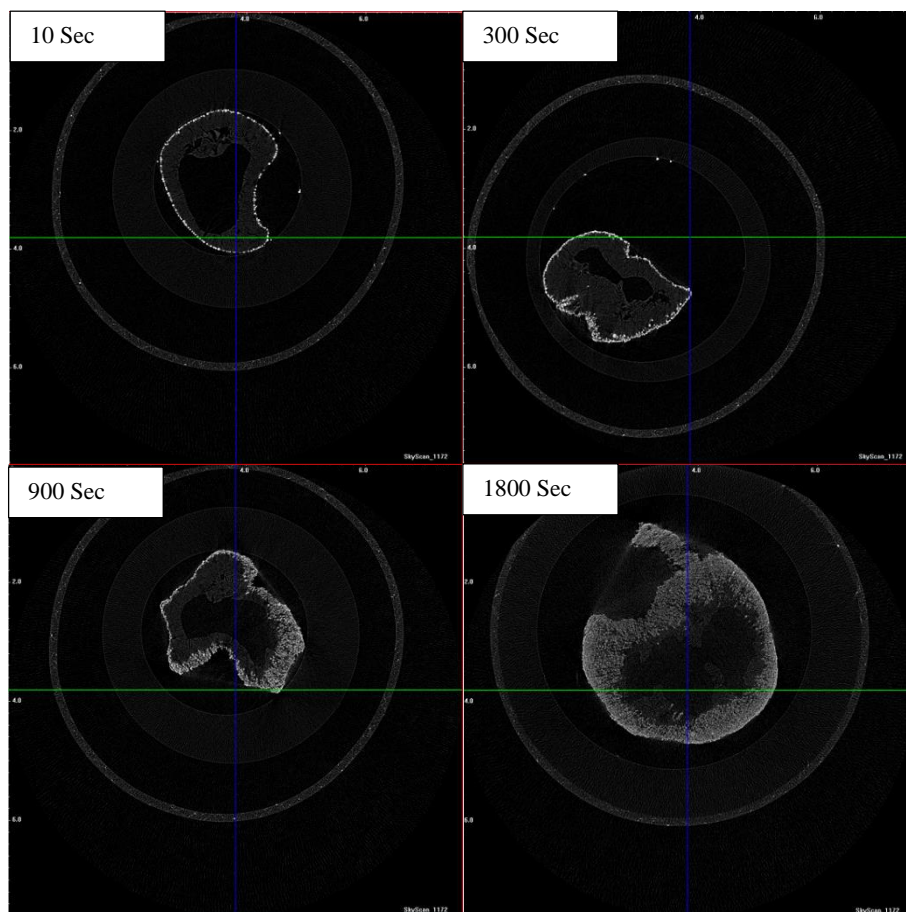


Figure 4.26: Images of granules produced using low powder wettability and different mixing times. The outer rings are part of the sample container. (Reconstructed XRCT images; representative central cross-section).

Asada et al. 2018 produced hollow granules by granulated different active constituents such as bromhexine hydrochloride, phenytoin and eugragit with HPC in high shear mixer. It was concluded that the granule size increased in a time dependent manner as the granulation proceeded. In addition, the wall thickness increased and the hollowness inside the granules decreased with granulation time. They suggested that this was because of an increase in the impact forces to the granules during the prolonged mixing time, see Figure 2.17.

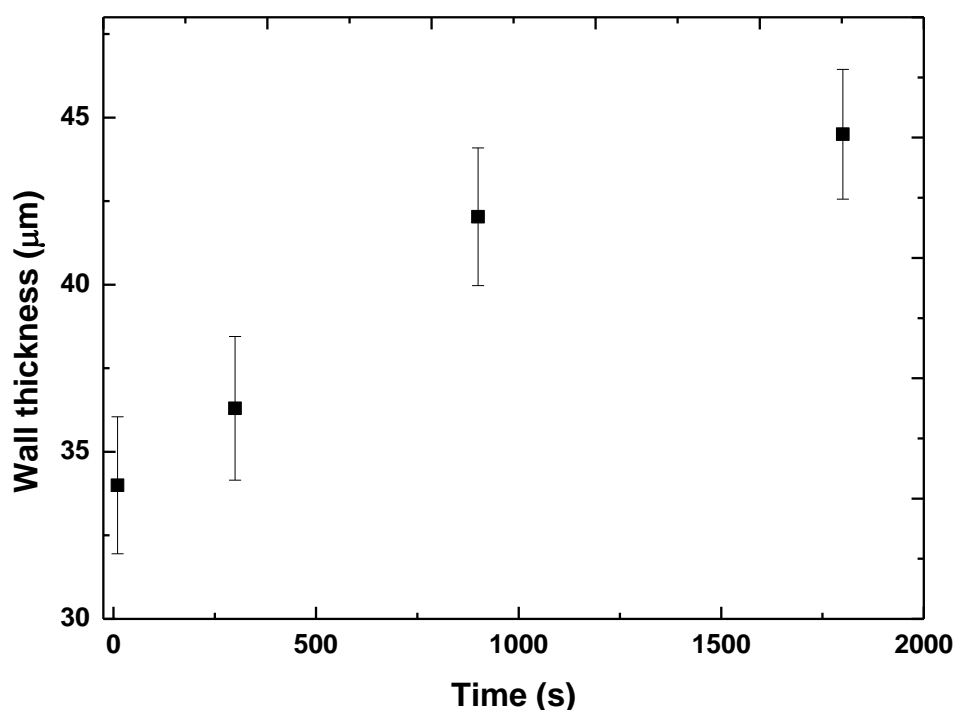


Figure 4.27: Wall thickness as a function of mixing time. Error bars are the standard deviation of three measurements.

4.3.4.2.1 Porosity

Figure 4.28 expresses the percentage total porosity as a function of different mixing times. Although the error bars are large, there appears to be a trend of porosity decreasing with increasing mixing time. The average porosity of granules at 10 s mixing time was 87.2 % and this porosity decreases to 75.5 %, 68.2 % and 59.7 % with 300, 900 and 1800 s mixing times respectively.

These results are in agreement with many researchers such as Schæfer et al. 2001 and Rahmanian, Naji and Ghadiri, 2011:

A review Schæfer et al. 2001 was based on the results of many researchers that studied the effect of granulation mixing time on granulation densification and consolidation. They found that the granule hardness and particle densification increased with increasing granulation time. They suggested that granule densification results from increasing shearing forces with increasing mixing time. Granule porosity reduced with this densification process and induced liquid migration to the granule surface which promoted further granule growth.

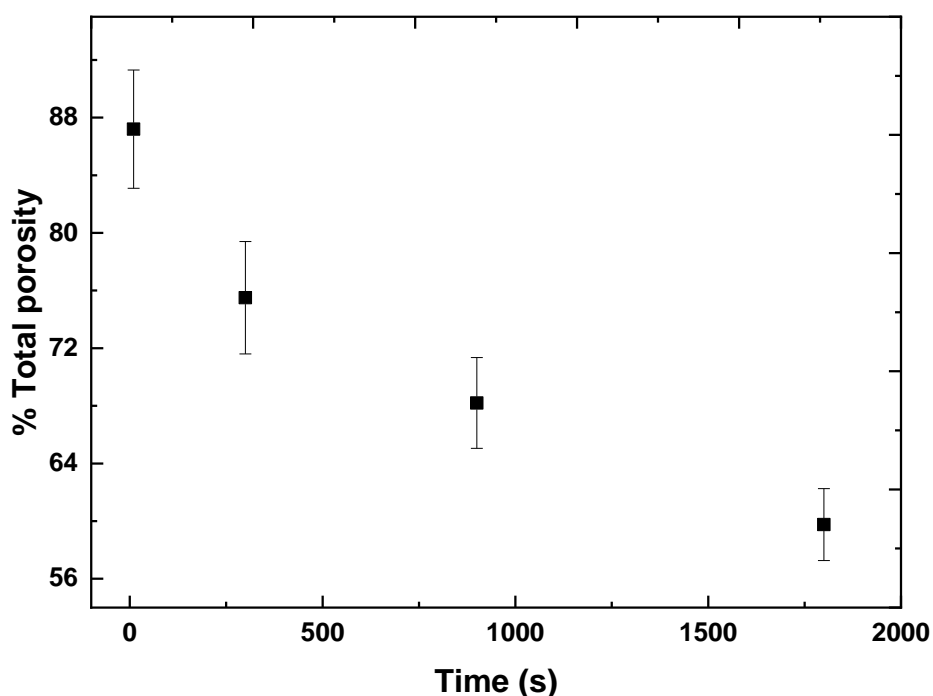


Figure 4.28: Total porosity as a function of mixing time. Error bars are the standard deviation of three measurements.

Rahmanian, Naji and Ghadiri, 2011 studied the effect of granulation time on granule strength and properties. Calcium carbonate as a powder was granulated with polyethylene glycol as a liquid binder in a high shear mixer. Granule strength was measured using a quasi-static side crushing test method. Granule porosity measurements was performed using Geopyc 1360. They found that increasing the mixing time has a significant effect on granule strength because

densified granules were produced with increasing granulation time. Granule porosity decreased with increasing granulation time due to granule consolidation.

4.5 Summary and further discussion

In this chapter, the following main experimental effects were measured and observed:

- Increasing the binder viscosity resulted in an increase in granule size for all powder wettability
- Increasing primary particle size resulted in increased granule size for all systems
- Increasing mixing time increased granule size for powder of low wettability
- Highly porous granules were produced using high binder viscosity and small primary particle size

The key results will be discussed in the following section.

4.5.1 Effect of binder viscosity on granule size

In this work, increasing binder viscosity resulting in increasing of granule size for most of the systems investigated in this chapter. The increasing granule size is probably due to a reduction in granule breakage with increasing binder viscosity. The destruction of liquid marbles using low powder wettability is probably due to the weak particles binding forces according to Rumpf 1962, who developed a widely used model for calculating static tensile strength. This model was developed assuming solid granules with uniform porosity, but may be applicable to granules that have a hollow internal structure. This model states that the granule static strength is linearly proportional to liquid powder contact angle:

$$\sigma_t = 6S \frac{1 - \varepsilon \gamma \cos\theta}{\varepsilon_g D_p} \quad \text{Equation (4.2)}$$

where S is the pore saturation of the liquid, ε is the granule porosity, D_p is the particles diameter, γ is the surface tension of the liquid and θ is the liquid powder contact angle. As the powder

wettability decreases, the $\cos \theta$ decreases, then granule static strength is assumed to decrease according to Equation (4.2). The low granule strength obtained by using low powder wettability was unable to withstand the impact forces applied leading to liquid marble destruction, most importantly when using low binder viscosity, which contributes to further a decrease in granule strength according to Van Den Dries et al., 2003 who developed a modified model of Rumpf 1962. This model predicts granule breakage behaviour after impact in a dynamic condition. According to this model, granules strength σ_v is related the liquid bridge viscous force:

$$\sigma_v = \frac{9}{8} \frac{(1-\varepsilon)^2}{\varepsilon^2} \frac{9\pi\mu v_p}{16 d_{3,2}} \quad \text{Equation (4.3)}$$

where ε is intragranular porosity, μ is liquid binder viscosity, v_p is moving particle relative velocity and $d_{3,2}$ is primary particle surface mean diameter. Van Den Dries et al., 2003 investigated experimentally the effect of binder viscosity on granule breakage. Lactose as a powder and different aqueous solution of hydroxypropylcellulose with viscosities range from 1 to 4000 mPa s as a binder were granulated in 10 L scale mixer granulator. They found that at a low binder viscosity considerable granule breakage was observed.

4.5.2 Effect of primary particle size on granule size

In this work, increasing primary powder particle size resulting in an increase of granule size for all systems investigated in this chapter. They are three theories that explain the effect of primary powder particle size on granule size:

- The penetration time developed by Hapgood et al., 2002 and Hapgood, Litster and Smith, 2003. For more details of the penetration time see Section 2.5.1. In order to describe drop penetration kinetics, Hapgood et al. 2002 developed dimensionless drop penetration time τ_p :

$$\tau_p = 1.35 \frac{V_d^{2/3} \mu}{\varepsilon_b^2 R \gamma \cos(\theta)} \quad \text{Equation (4.4)}$$

where V_d is the volume of the drop, μ is the binder viscosity, ε_b is the porosity of the powder bed, γ is the liquid surface tension, θ is the dynamic contact angle of powder/liquid. R is the powder pore radius:

$$R = \frac{\varphi d_{32}}{3} \left(\frac{\varepsilon_b}{1 - \varepsilon_b} \right) \quad \text{Equation (4.5)}$$

where ε_b is a function of the porosity of the powder bed, the surface-volume average size d_{32} and the particle shape φ . According to Hapgood et al., 2002 and Hapgood et al. 2003, poor liquid distribution occurred with a long liquid droplet penetration time inside the powder bed. Binder distribution is an important step for granule liquid saturation, deformation and granule growth.

According to Equation (4.4) and Equation (4.5), decreasing the powder primary particle size results in the decrease of the porosity of the powder bed and then increases the penetration time. It can be concluded that the penetration time of small primary particle sizes are higher than the medium and large primary particle sizes. The non-wetting effect of the powder used in this work leads to a further increase in the penetration time for powder of small primary particle size. The liquid distribution was impaired which limited the increase in the granule size.

- The lubrication analysis was developed by Ennis et al. 1991, and they reported that the capillary force was proportional to primary particle size, d . In addition, the viscous bridge force was also $\sim d$. Since the number of bridges per unit cross-sectional area differ as $1/d^2$, the total cohesive force in a granule differs as $1/d$. This scaling can be applied irrespective of which fluid force predominates. Therefore, the number of the bridges between particles was increased with decreasing primary particle size. This results in stronger, less deformable granules which then limits the granule growth.
- According to Equation (4.3), there is an inverse relationship between granule strength σ_v and primary powder particle size. This equation, therefore, predicts that the strength of the granules will increase with decreasing primary particle size, leading to less deformable granules obtained using a small primary particle size, which inhibits granule growth.

4.5.3 Effect of mixing time on granule size

The increase in the granule size with increasing mixing time can be explained by a mathematical model which expresses the amount of material transferred from powder to the agglomerated particles with time when the agglomerated particles are rolling on the powder bed in the rotating bowl as (Raj Kumar and Malayalamurthi, 2017):

$$k = \frac{d m_p}{dt} \quad \text{Equation (4.6)}$$

where m_p is the particle mass. From this mathematical equation, an increase in the mixing time results in an increasing the amount of powder builds up with the granule mass (k). Raj Kumar and Malayalamurthi, 2017 verified this mathematical model by experimental works. Sago powder (a staple food in Africa) was granulated with water from 20 to 600 s. The experimental results matched the mathematical results up to 360 s of the mixing time and then the experimental results showed a constant granule mass after this time. They suggested that with increasing mixing time, the granule growth became equal to the granule breakage (i.e. achieving an equilibrium) resulting in a constant granule size. Moreover, they suggested that the experimental results were more real considering atmospheric moisture conditions, air resistance and surface roughness of the bowl mixer.

4.5.4 Effect of binder viscosity and primary particle size on granule porosity

Iveson et al. 1998 described the relationship between binder viscosity (μ) and primary particle size (d_p) on consolidation rate (k):

$$k \propto \frac{D_p}{\mu} \quad \text{Equation (4.7)}$$

Increasing binder viscosity and decreasing primary particle size decrease the consolidation rate constant. This is in agreement with results in this thesis in which high granule porosity was obtained using high binder viscosity and small primary particle size.

Iveson and Litster, 1998 developed an exponential decay equation that described the change of porosity with time:

$$\exp(-kN) = \frac{\varepsilon - \varepsilon_{min}}{\varepsilon_0 - \varepsilon_{min}} \quad \text{Equation (4.8)}$$

where ε is the average granule porosity, ε_0 is the average porosity of primary particles, ε_{min} is the minimum granule porosity, N is the rotational drum speed and k is the consolidation rate constant. According to this equation, the porosity of the granules decreases as the rate of granule consolidation increases.

Granule consolidation also increased with increasing tumbling speed and mixing time, probably because of an increase in the collisions between the granule and powder bed and with wall of the drum with increasing tumbling speed or prolonged mixing time.

4.6 Conclusions

The effect of binder viscosity, powder wettability, shearing forces, powder particle size and mixing time in a low shear mixer were investigated in terms of granule size and internal microstructure.

The key conclusions of this chapter are:

- a- Granules size increases with:
 - Increasing binder viscosity
 - Increasing tumbling speed
 - Increasing primary particle size
 - Increasing mixing time

- b- Hollow granules are obtained using:
- High binder viscosity
 - Low and medium powder wettabilities
 - Small primary particle size
- c- Granule porosity increases with:
- Increasing binder viscosity
 - Decreasing tumbling speed
 - Increasing primary particle size

Overall, this chapter provides an understanding of the effects of different formulation and process parameters of wetting and non-wetting powders on granule size and internal microstructure. Different combinations of binder viscosity, powder wettability, primary particle size and mixing time result in large changes in characteristics of the resultant granules indicating the importance of these parameters which all need to be considered carefully to obtain the desired granule properties.

A full investigation of the effect of shearing forces on granule properties is not possible due to the limited tumbling speed of the low shear mixer. The following chapter will investigate granule size and internal microstructure under range of shear forces in high shear mixer using different impeller speeds and designs. This will allow for a more comprehensive study into the effect of shear on the granule size occurring and the granule internal microstructure during granulation using powders of different wettabilities.

CHAPTER 5. Granulation of model particles in a high shear mixer

Studies have been made in the last few decades to understand the fundamentals of granulation mechanisms using different operation conditions such as impeller speed and design. However, most of these studies have focused on granulation of wetting powders. No study is published on the impact of shearing forces on granule size and internal microstructure for a range of powder wettabilities, and this forms the motivation of this work.

Three different mixtures of wetting and non-wetting powders were granulated with polyethylene glycol solution in a high shear mixer. The effect of three different impeller speeds using a flat plate impeller, three different impeller designs and different powder wettabilities were investigated.

The results show that as the speed of flat plate impeller increased, the granule size decreased due to breakage of liquid marbles or immersion nuclei. Lower impeller speeds gave rise to more porous granules. A large granule size was produced using a flat plate impeller than granules produced using 2-bladed and 3-bladed impeller for powders of different wettabilities. Hollow granule wall thicknesses increased when changing the impeller from flat plate to 2-bladed and 3-bladed impeller. High porosities were seen using the flat plate impeller for low and medium powder wettabilities. The increase in the compaction force of 2-bladed and 3-bladed impellers results in more consolidated granules compared with the flat plate impeller. In addition, granule size increased with increasing powder wettability for all the impeller designs used. A transition from thin wall thicknesses to thick wall and finally to single solid granules with increasing powder wettability was observed.

The research demonstrates that the level of agitation applied is an important factor in controlling granule size and hollow granule formation. It is expected to facilitate progress in granulation of non-wetting powder in pharmaceuticals, cosmetics and other advanced materials.

5.1 Introduction

In the previous chapter, the effect of binder viscosity, powder wettability, tumbling speed, powder particle size and mixing time on granule size and internal microstructure were investigated in a low shear mixer. The range of tumbling speeds with this device was limited. The main aim of this chapter is to examine the granule size and internal microstructure of granules using a wider range of impact and shearing forces with different powder wettabilities. This is accomplished using a high shear mixer, which is capable of employing a large range of impeller speeds and accommodating different impeller designs.

Impeller design is one of most important process parameters in controlling the granule size, shape and size distribution. Controlling these parameters is problematic in the granulation process. Many studies on the effect of impeller design and how it affects the powder motion in the bowl to improve the granulation behaviour have been conducted (Knight et al. 2001; Smith et al. 2010; Schæfer et al. 1993b; Mirza et al. 2015; Campbell et al. 2011; Voinovich et al. 1999). All these previous studies were performed using a wetting powder. Despite these significant advances in understanding the behaviour of powder using different shear forces, more studies are needed to understand and improve the granulation performance and control granule size and size distribution particular for non-wetting powder.

The previous works of the effect of agitation forces on granulation of a non-wetting powder mainly focus on the formation and the stability of liquid marbles (Forny et al. 2007; Saleh et al. 2011; Forny et al. 2009). Charles-Williams et al. 2013 focused on studying the effect of increasing content of non-wetting powder on granule size in a high shear granulator using different parameters (spray droplet size and impeller speed).

This chapter is designed to study the granular behaviour in a high shear mixer using a range of powder wettabilities. The aims of these experiments are to investigate the granule size and internal microstructure under different conditions:

- Impeller speed
- Impeller design
- Powder wettability

Several parameters relevant to granule size and hollow granule formation will be analysed in particular:

- Particle size distribution using sieve analysis
- Granule internal structure using X-ray tomography
- Calculation of porosity and wall thickness of hollow granules which gives further insight of the internal microstructure of hollow granules

5.2 Materials and Methods

A more detailed description of materials and methods can be found in Chapter 3. An overview of materials and methods used in this chapter is given in this section. Salinized and un-salinized glass beads powder (AQ) with d_{50} of 35 μm are used. Three different mixtures of 80%-20%, 65%-35% and 0%-100% of non wetting-wetting powders were used, which will simply be denoted as low, medium and high powder wettability respectively or by their contact angle of liquid on powder. One PEG solution was used as binder; 50 w/w. % PEG 12000. The granulation time for all experiments was set at 20 seconds (s). Pre-nucleation of nuclei in a petri dish outside the granulator was performed before granulation in a high shear mixer. Binder viscosity and the blends of the powders used in this chapter and the liquid powder contact angle can be found in Table 5.1.

Table 5.1: Binder viscosity, powder binder systems and contact angle of liquid on powder.

Binder (PEG) Molecular weight	Viscosity (mPa s)	Powder (Non wetting – wetting)		
		Contact angle ° of binder/ powder		
		80%-20%	65%-35%	0%-100%
12000	1300	102	93	39

Experiments were divided into three parts. For the first part, a specially designed bowl with an internal diameter of 204 mm and a height of 130 mm and a flat plate impeller was used to granulate 500 g of powder mixture with a d_{50} of 35 μm . In this study different impeller speeds were investigated; 150, 350 and 550 rpm which will be simply denoted as low, medium and high impeller speed respectively. It should be noted that 150 rpm was the lowest speed that can be used with this equipment, while 700 rpm was the highest speed.

For the second part, different impact and shearing forces were investigated. A flat plate, 2-bladed (11° bevelled) impeller and 3-bladed (45° bevelled) impeller were used to vary the impact and shear forces on pre-nucleated liquid marbles or immersion nuclei. One impeller speed was used (350 rpm).

For the third part of this study, the effect of different powder wettability on granule size and internal microstructure were presented. Three different impeller designs; a flat plate, 2-bladed (11° bevelled) impeller and 3-bladed (45° bevelled) impeller were used. One impeller speed; 350 rpm was used. The experimental design is shown in Table 5.2. For more details of the method see Section 3.6.3.

A mixing time of 20 seconds was chosen for the all experiments performed in this chapter to prevent breakage of liquid marbles or immersion nuclei with prolonged mixing time during granulation.

Table 5.2: Experimental design of different impeller speeds and designs.

Impeller speed (rpm)	Powder (Non wetting-wetting)	Flat plate (number of repeats)	2-bladed (number of repeats)	3-bladed (number of repeats)
150	80%-0%	2	-	-
	65%-35%	2	-	-
	0%-100%	2	-	-
350	80%-0%	3	3	3
	65%-35%	3	3	3
	0%-100%	3	3	3
550	80%-0%	2	-	-
	65%-35%	2	-	-
	0%-100%	2	-	-

The granule size was characterised by sieving with mesh sizes of 4000, 3350, 2800, 1700, 1000, 500, 250, 180 and 106 μm . The volume frequency, q_3 (with a unit of μm^{-1}) was plotted as a function of particle size to give a size distribution. The sieve fractions were reserved for internal microstructural analysis by X-ray tomography (XRCT). Several formulations had one or more repeat experiments and the average of the experiments for each formulation are shown as a single point on size distribution figures. Error bars shown on all plots are the standard deviation of two or three measurements.

The images of all granules in this chapter were produced using a digital microscope (Lumenera Infinity 3 Camera, Navitar 12X zoom lenses).

Three representative granules were chosen from each experiment for XRCT imaging to examine and analyse the internal structure. Images were processed with Skyscan software DataViewer and CTAn. The representative granules were measured for wall thickness and % total porosity. More details of the procedure can be found in Chapter 3, Section 3.2.10.

Preliminary studies were carried out for 700 rpm using the flat plate impeller; and these experiments were excluded due to the high impact force applied to the liquid marbles or immersion nuclei; which led to significant breakage of the pre-formed liquid marbles using low powder wettability. In addition, flakes (Figure 5.1a) and irregular shaped granules (Figure 5.1 b and c) were produced at 700 rpm impeller speed using medium and high powder wettability respectively.

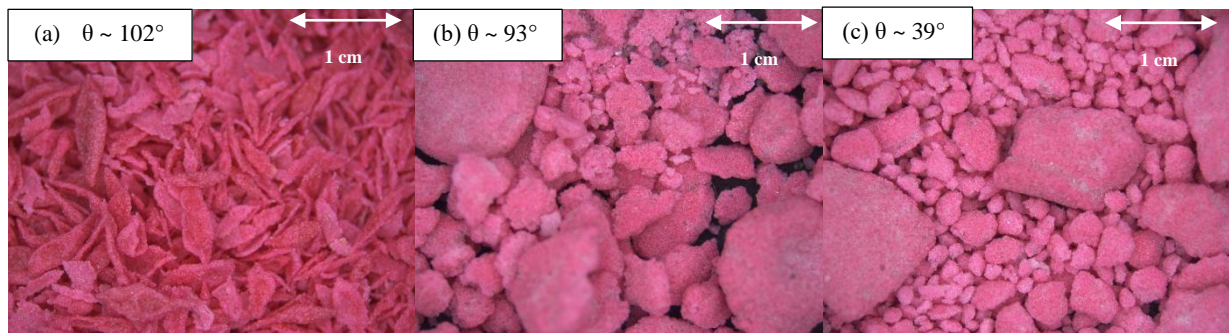


Figure 5.1: Images of granules produced from different powder wettabilities and 700 rpm impeller speed.

Preliminary studies were also carried out using 100% - 0% non wetting – wetting powders and 1300 mPa s binder viscosity with all different impeller designs, and at 150 rpm impeller speed. Here, flakes and fine powder were produced and it suggested that this was because of the weak binding forces between particles produced using low powder wettability which could not even withstand this low impact force applied. As a result, this mixture was excluded from the study (Figure 5.2).

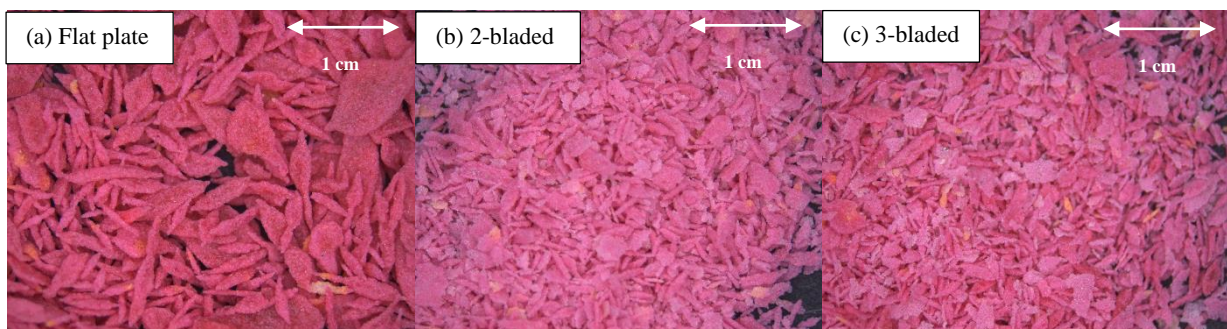


Figure 5.2: Images of flakes produced from 100%-0% non wetting – wetting powders and at 150 rpm impeller speed.

5.3 Results and Discussion

The aim of performing these experiments is to investigate the effect of different impact and shearing forces on the formation, size and internal microstructure of the resultant granules. Impeller speeds, impeller designs and powder wettabilities were investigated.

Different powder wettabilities were produced by mixing non-wetting and wetting powders in different percentages (80% - 20%, 65% - 35%, 0% - 100%). One mixture formed immersion nuclei, while others formed liquid marbles as can be seen in Table 5.3.

Table 5.3: Summary of pre-nucleation experiments.

Conditions		Contact angle ^o	Pre-nucleation product
Non wetting-wetting mixture	Binder (PEG) viscosity (mPa s)		
80%-20%	1300	102	Liquid marble
65%-35%	1300	93	Liquid marble
0%-100%	1300	39	Immersion nuclei

The measured diameters of liquid droplets before nucleation and granulation used in this chapter can be seen in Table 5.4.

Table 5.4: Liquid droplet properties.

Binder viscosity (mPa s)(PEG)	Droplet mass (g)	Density (g/cm ³)	Droplet Volume (cm ³)	Droplet Diameter (μm)
1300	0.00804 ± 0.0003	1.0908 ± 0.014	0.007345	2466.53

The Froude number data for the high shear mixer using the flat plate impeller are shown in Table 5.5. Froude number increases with impeller speed. For more details of Froude number definition see Section 4.3.

Table 5.5: Froude number data of high shear mixer using flat plate impeller.

Speed rate (rpm)	Drum internal diameter (m)	Gravitational acceleration (m/s)	Angular velocity (radian/s)	Froude number
150	0.7	9.81	15.7	17.6
350	0.7	9.81	36.65	95.85
550	0.7	9.81	52.36	236.7

The results and discussion section is divided into three parts. The first part will explain the effect of shearing forces (using different impeller speeds) and powder wettability. The second will give an investigation of the effect of varying impact and shearing forces, using different impeller designs on granule size and internal microstructure for a range of powder wettabilities.

Finally, the third part will give details of the effect of powder wettability on the granule size and internal microstructure.

5.3.1 The effect of impeller speed and powder wettability

The granule size and internal microstructure using different impeller speeds, ranging from 150 to 550 rpm using a flat plate impeller and different powder wettabilities were investigated.

5.3.1.1 Granule size distribution

The size distribution of the resultant granules produced from different impeller speeds and powder wettabilities for 20 s mixing time in high shear mixer are discussed in this section.

5.3.1.1.1 Low powder wettability

There was a difference in the size of granules produced using different impeller speeds and low powder wettability (Figure 5.3). The pre-nucleation experiments produced liquid marbles. After granulation and drying, large granule sizes were produced using 150 rpm impeller speed ($d_{43} = 1250 \mu\text{m}$). A decrease in the size of the granules was observed using 350 and 550 rpm

impeller speeds ($d_{43} = 726$ and $407 \mu\text{m}$ respectively). A unimodal size distribution was obtained using the 550 rpm impeller speed with the peak at $250 \mu\text{m}$. A bimodal size distributions were obtained using 150 and 350 rpm impeller speeds (Figure 5.3). For more details of q_3 and d_{43} , see Appendix B.1.1.

A mixture of both flakes and buckled semi-spherical granules were produced using low and medium impeller speeds (Figure 5.4 a and b), while only flakes were produced using high impeller speed (Figure 5.4 c). It is suggested that the liquid marbles experienced a high shearing leading to this granule shape.

It is observed that the percentage of flakes increases gradually with increasing impeller speed. This is most likely due to the effect of the shearing forces applied by the higher impeller speed which increases the probability of destruction of liquid marbles during granulation.

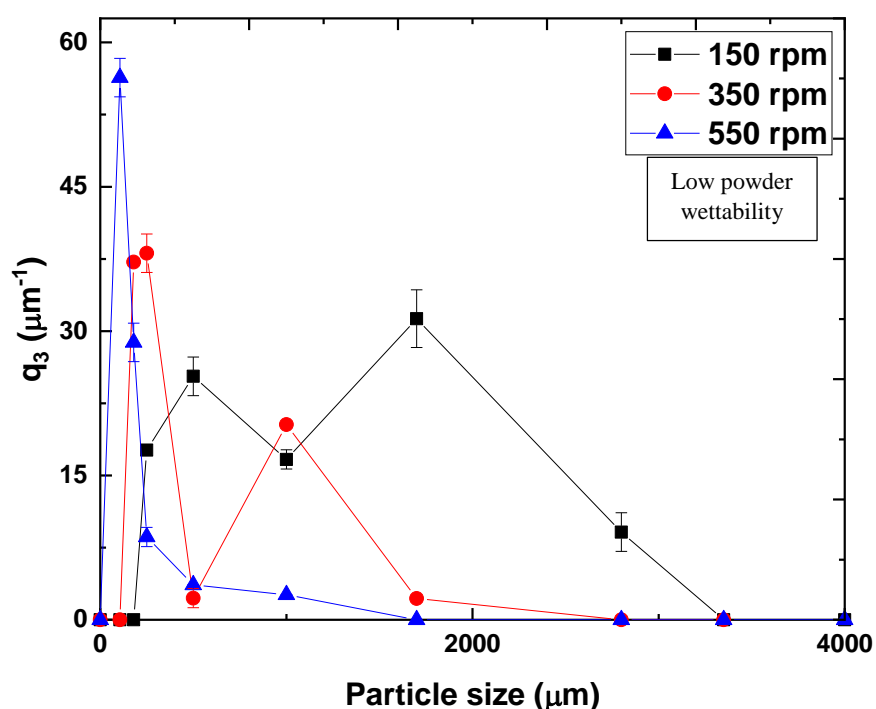


Figure 5.3: Particle size distribution of granules produced using low powder wettability and different impeller speeds, obtained via sieve analysis. Error bars are the standard deviation of two or three measurements.

This result is in agreement with Wade et al. 2015 who investigated the effect of impeller speed on granule physical properties using a reverse phase granulation; here, powder was added to

liquid in a high shear mixer. Pharmaceutical grades of hydroxyapatite powder with polyvinyl pyrrolidone binder were used. A bimodal granule size distribution was observed at lower impeller speed which was indicative of slight granule growth. With an increase in the impeller speed, there was a decrease in the percentage of large granules (1000-2000 μm) and an increase in the percentage of small granules (75-425 μm) signifying that breakage had occurred. When the impeller speed increased further, the collision energy increased until it reached a critical impeller speed in which breakage and attrition of granules took place, and there was a decrease in granule size.

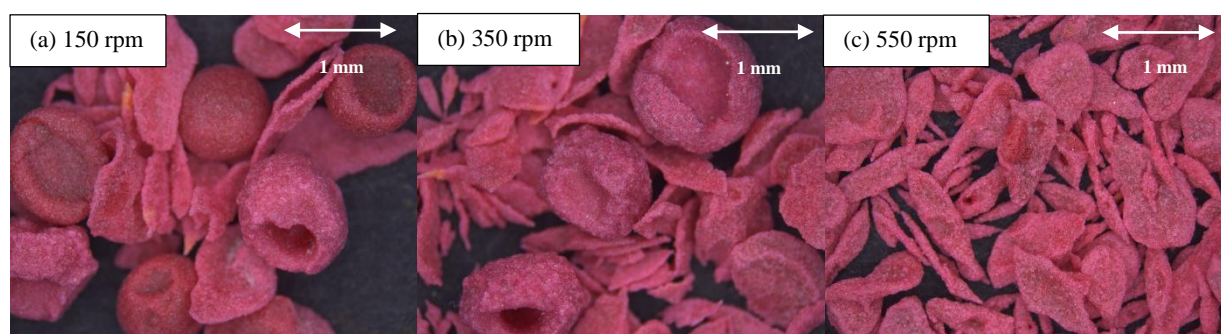


Figure 5.4: Comparison of granules using low powder wettability and different impeller speeds.

5.3.1.1.2 Medium powder wettability

Figure 5.5 shows size distributions of the granule produced using powder of medium wettability at different impeller speeds. The pre-nucleation experiments produced liquid marbles.

Smaller granules were produced using high impeller speed compared ($d_{43} = 863 \mu\text{m}$) to granules produced using low and medium impeller speeds ($d_{43} \approx 1600 \mu\text{m}$). A unimodal granule size distribution was observed using high impeller speed, while, a bimodal size distribution is observed with low impeller speed and a tri-modal size distribution can be seen using medium impeller speed. For more details of q_3 and d_{43} , see Appendix B.1.1.

A combination of semi-spherical and flat granules were observed using low and medium impeller speeds (Figure 5.6 a and b). Only semi-spherical granules were produced using high impeller speed (Figure 5.6 c).

The production of flat shaped granules using low and medium impeller speeds might be due to the effect of shearing forces on the wet liquid marbles. These irregularities of the granule shape using the flat plate impeller might be because of the gap between the underside of the impeller

and the base of the bowl and the gap between the tip of the impeller and the wall of the bowl, leading to trapping of particles between the plate and the bowl, and subsequent deformation will be expected.

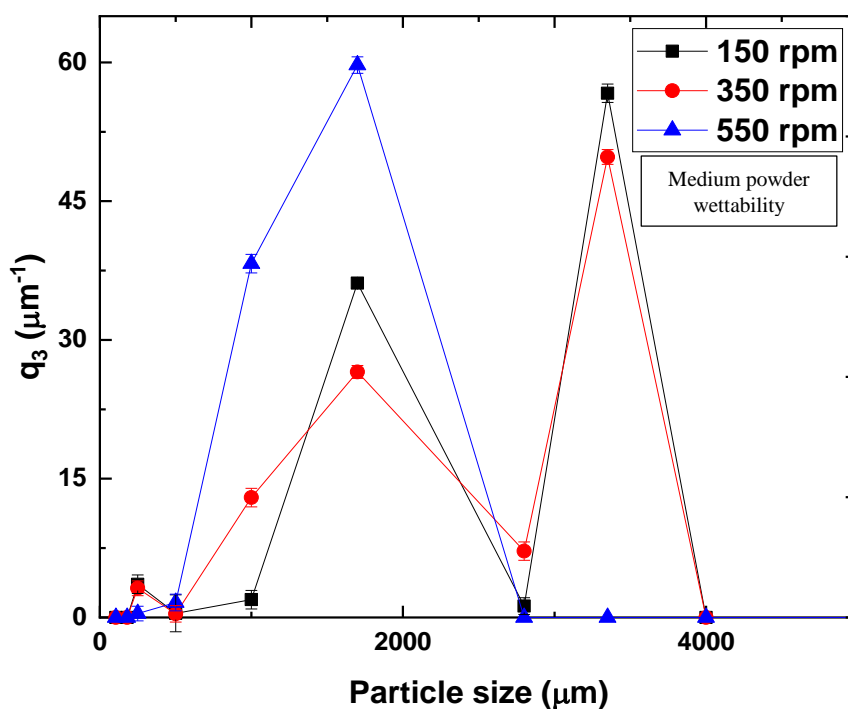


Figure 5.5: Particle size distribution of granules produced using medium powder wettability and different impeller speeds, obtained via sieve analysis. Error bars are the standard deviation of two or three measurements.

The production of spherical shaped granules using high impeller speed is consistent with Schæfer, 2001 who wrote a review featuring the results of many other researchers on the effect of impeller speed on the resultant granule shape. They found that the spherical agglomeration was more pronounced at higher impeller speed because of spheronisation, which was promoted at a high impeller speed. Similarly, Chitu et al. 2011b investigated the effect of impeller speed on granule size and shape using high shear granulation. Microcrystalline cellulose was used as powder and water as binder. Different impeller speeds were studied. They found that the granule roundness increased with increasing impeller speed due to spheronisation.

However, other researchers such as Eliassen, Kristensen and Schæfer, 1999 and Knight et al. 2000 found that the higher impeller speed resulted in less spherical granules. This was partly

because of breakage of wet granules during granulation at high impeller speed due to insufficient bonding forces between the particles. The contradiction might be because of the different powder wettability used in this study and their studies.

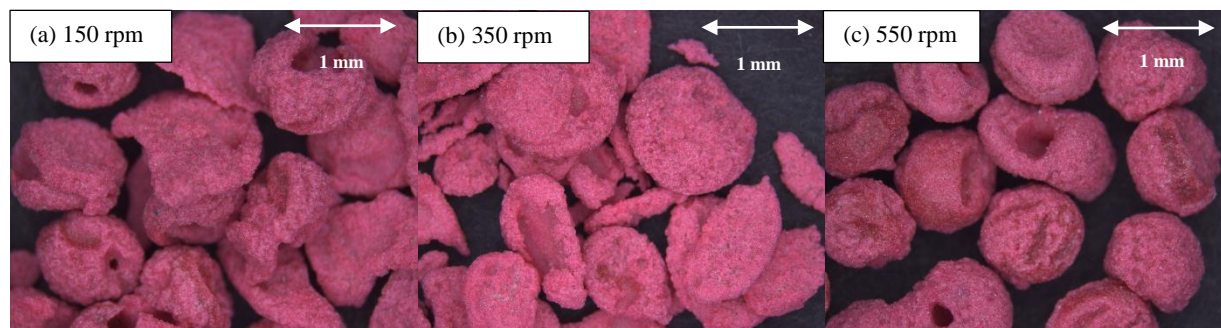


Figure 5.6: Comparison of granules using medium powder wettability and different impeller speeds.

5.3.1.1.2 High powder wettability

Figure 5.7 shows size distributions of the granule produced using powder of high wettability and different impeller speeds. The pre-nucleation experiments produced immersion nuclei. Larger granules can be found using 150 rpm impeller speed ($d_{43} = 3075 \mu\text{m}$) compared to granules produced using 350 and 500 rpm impeller speeds ($d_{43} = 2213 \mu\text{m}$) (Figure 5.7). A unimodal granule size distribution was observed at all impeller speeds. Semi-spherical granules with higher rims were produced using different impeller speeds (Figure 5.8). For more details of q_3 and d_{43} , see Appendix B.1.1.

The shape of the granules produced can be explained by Emady et al. 2011. They found that the spreading/crater formation mechanism was mainly observed for free flowing powder such as the glass beads resulting in flat granules with high rims. For more details of this mechanism, see Section 2.5.1.

The wetting properties of powders with a contact angle of 39° allows for strong binding forces between particles that resist the impeller shearing force resulting in semi-spherical granules with approximately the same size at different impeller speeds. This is probably due to the decrease in granule breakage and attrition.

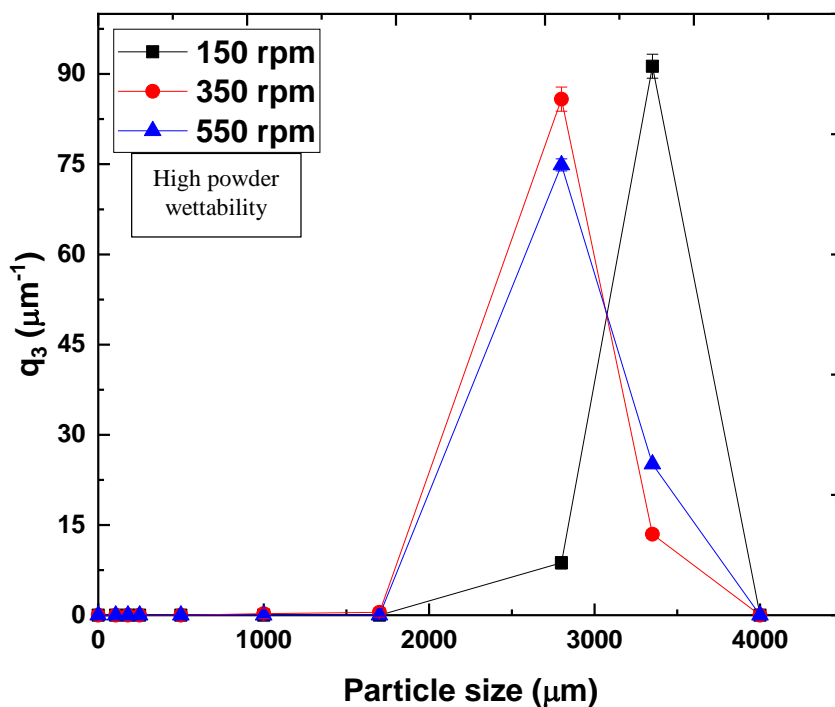


Figure 5.7: Particle size distribution of granules produced using high powder wettability and different impeller speeds, obtained via sieve analysis. Error bars are the standard deviation of two or three measurements.

These results are in accord with Schæfer et al. 1993a, who investigated melt pelletisation in a high shear granulation of lactose powder and PEG 3000. Different impeller speeds were used; 800, 1000 and 1200 rpm. A larger granule size was produced using 800 rpm compared to 1000 and 1200 rpm due to breakage and attrition of granules at higher speeds.

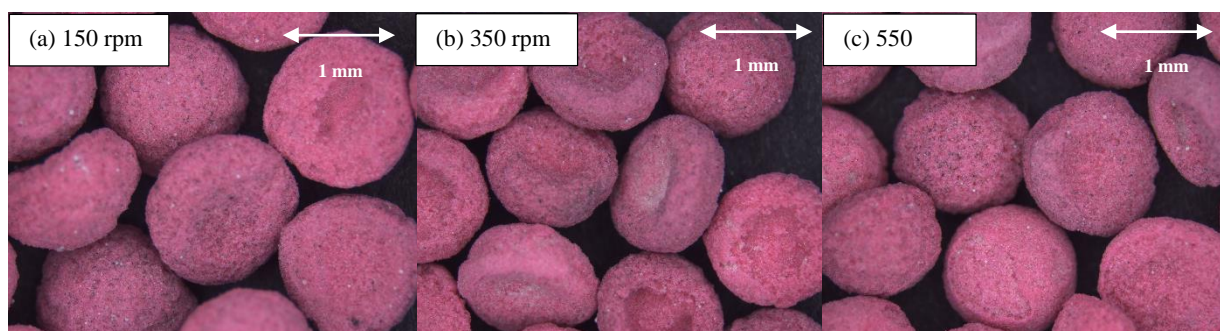


Figure 5.8: Comparison of granules using high powder wettability and different impeller speeds.

5.3.1.2 Internal structural analysis

Figure 5.9 shows XRCT images of granules produced from powders of different wettabilities and different impeller speeds.

For the powder of low wettability, hollow granules were obtained using low and medium impeller speeds. Only flakes were produced using high impeller speed, which were difficult to scan using XRCT. The wall thickness of hollow granules changed slightly from 33.7 μm to 35.9 μm using low and medium impeller speeds respectively (Figure 5.10).

For the powder of medium wettability, hollow granules were obtained using all impeller speeds. The wall thickness of hollow granules increased from 387.4 μm to 724.8 μm using low and high impeller speeds respectively (Figure 5.10).

For the powder of high wettability, hollow granules were obtained using low and medium impeller speeds. Single solid granules were obtained using the high impeller speed. The wall thickness of hollow granules increased from 815.6 μm using low impeller speed to 941.6 μm using medium impeller speed (Figure 5.10). More cross sectional images of the granules can be found in Appendix B.2.1.

Powder of low wettability produced hollow granules with approximately the same size wall thickness using low and medium impeller speeds. This could be because of the formation of a mono-layer of powder around the liquid droplet and the low impact forces applied which limited the penetration of the powder inside the liquid droplet and hollow granules with thin wall thickness are produced.

However, thicker granule wall thicknesses were observed using medium powder wettability than those produced using low powder wettability. This is probably because of improved wetting powder properties. This, in turn, improves the binding force between powder particles and liquid droplets and increases powder particle immersion inside the liquid droplet.

Hollow granules with a thick wall thickness were observed using high powder wettability and at low and medium impeller speeds. This is probably because of decreased shearing and impact forces with the use of the flat plate impeller and this results in less consolidated granules than those obtained at higher impeller speed. Single solid granules were observed at higher impeller speeds using high powder wettability. It is suggested that the wall thickness increased with increasing impeller speed due to an increase in the collisions between the granules and the

powder bed, leading to a greater extent of granule consolidation that squeezed the entrapped air and liquid to the granule surface.

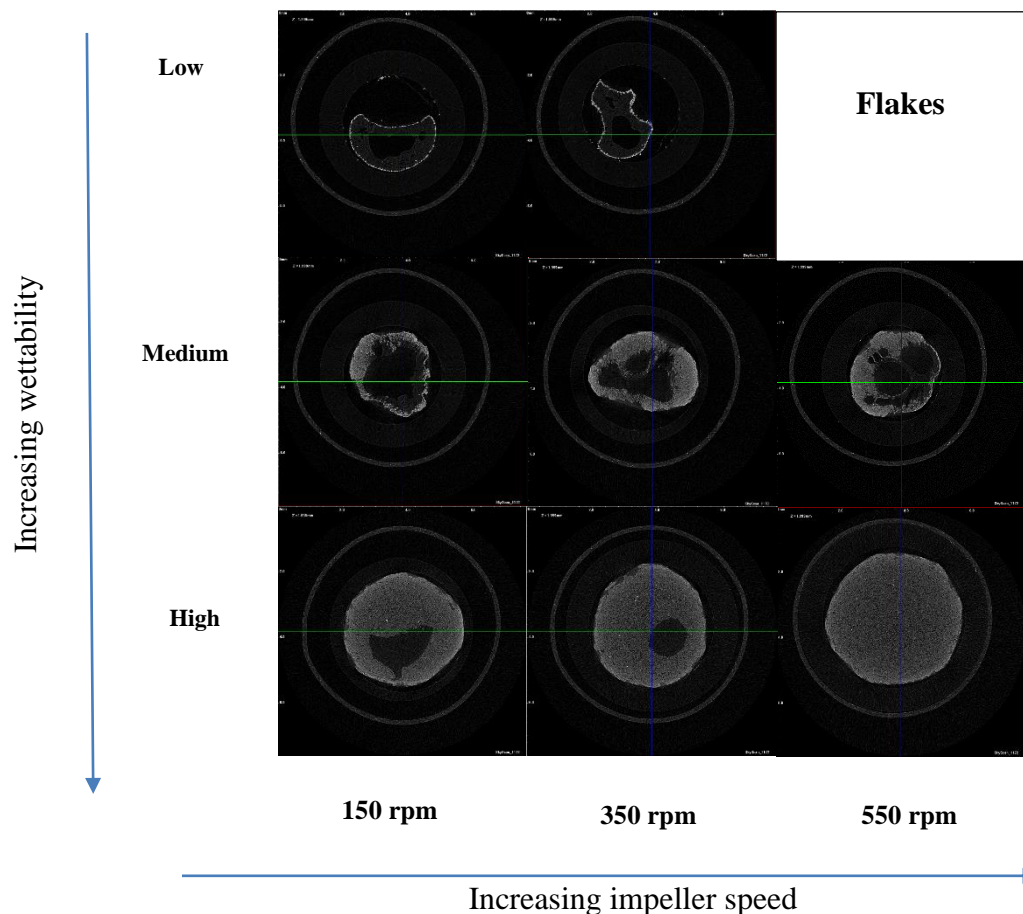


Figure 5.9: Images of granules produced using different powder wettabilities and impeller speeds. The outer rings are part of the sample container. (Reconstructed XRCT images; representative central cross-section).

The results of obtaining hollow granules using low impeller speed are inconsistent with the results obtained by Saleh et al. 2011, probably because they used a large amount of granulating liquid to produce a formulation containing 98 % of water compared to pre-nucleated liquid marbles or immersion nuclei that were used in this work. They developed a regime map that qualitatively outlined the formation of hollow granules in terms of mixing conditions and powder wettability. Hydrophilic fumed silica (Aerosil 200) and hydrophobic fumed silica of different wettabilities (Aerosil R812S and Aerosil R972) as a powder and water as a liquid binder were used. An overhead stirrer with different impeller speeds and designs were used. They found that under severe mixing conditions only highly non-wetting fumed silica powder

produced hollow granules, while medium fumed silica powder wettability produced a mousse and hydrophilic fumed silica produce a suspension. For more details, see Section 2.9.1.

Similarly, Forny et al. 2007 investigated the formation of hollow granules by varying impeller speed and powder wettability. Different wettabilities of fumed silica powder and water were mixed in high shear blender. The final product outcome depended on the energetic contribution by the impeller speed and binding affinity between the solid and the liquid, which was evaluated by the contact angle. Similar findings were observed by Saleh et al. 2011, where hollow granules were produced using higher impeller speed and highly non-wetting powder. A suspension was produced using high powder wettability, while a mousse was produced using medium powder wettability.

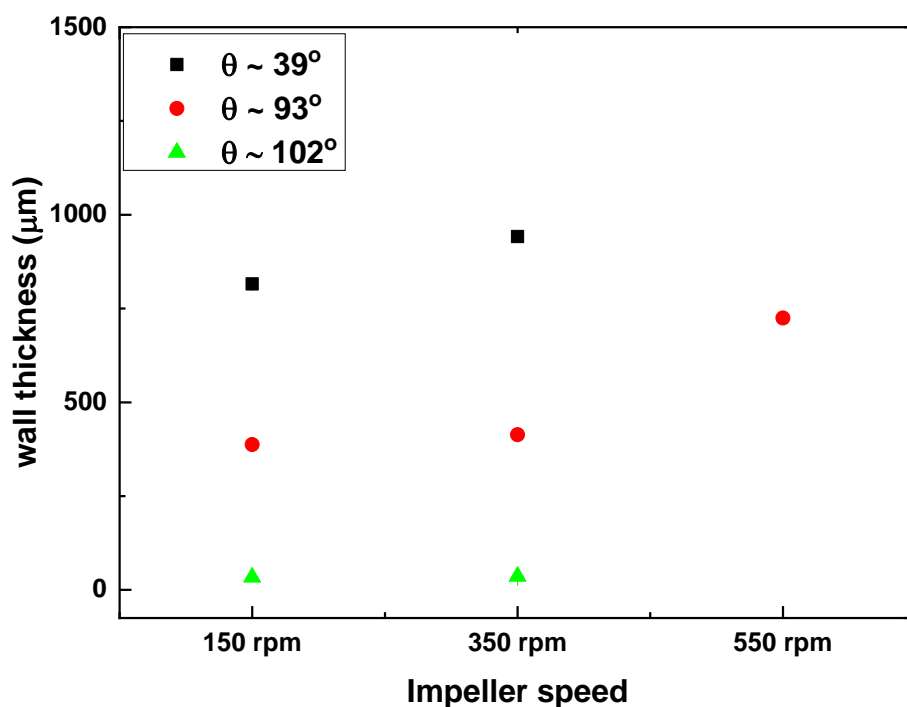


Figure 5.10: Wall thickness as a function of impeller speed and powder wettability. Error bars are the standard deviation of three measurements. θ is liquid powder contact angle.

5.3.1.2.1 Porosity

Figure 5.11 shows the % total porosity of granules as a function of impeller speed and different powder wettabilities.

For low powder wettability, granules produced using low impeller speed showed 87.5 % total porosity, and the granules porosity decreased to 81.6 % using medium impeller speed. For medium powder wettability, there was a decrease in total porosity of granules from 62.9 % using low impeller speed to 50.6 % using high impeller speed. For high powder wettability, the porosity decreased from 34.5 % using low impeller speed to 32.5 % and 26.7 % using medium and high impeller speeds respectively.

The decrease in granule porosity with increasing impeller speed might be due to the increase in shearing forces applied to granules with increasing impeller speed, which contributes to granule consolidation and an increase in granule porosity.

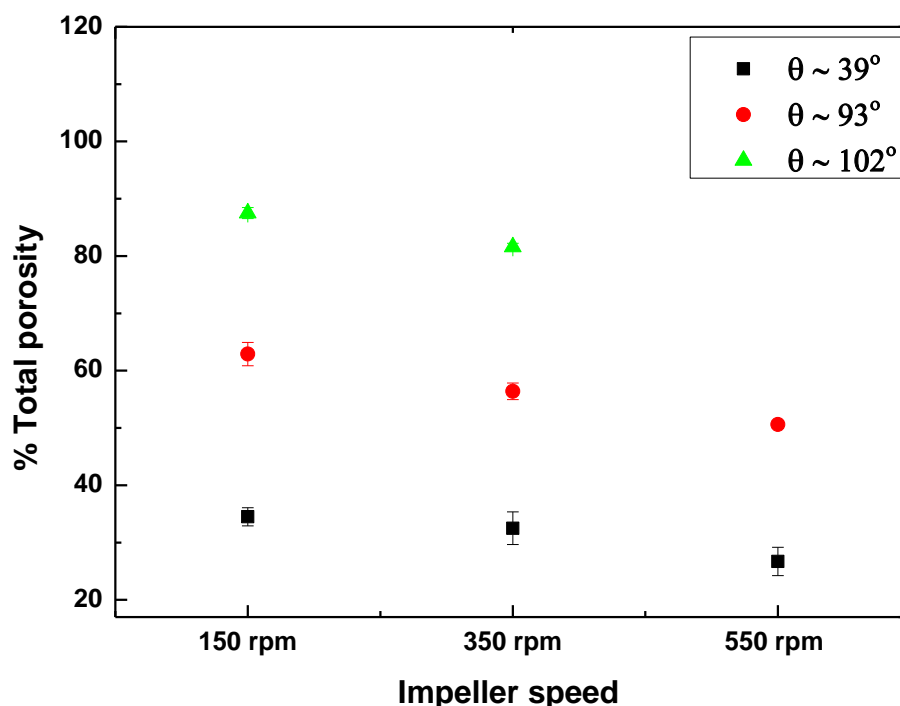


Figure 5.11: Total porosity as a function of impeller speed and powder wettability. Error bars are the standard deviation of three measurements. θ is liquid powder contact angle.

The results of the decrease in granule porosity with increasing impeller speed are in agreement with results found by Saleh et al. 2005, despite the different powder wettability they used from that used in this work. Saleh et al. 2005 studied the effect of impeller speed on granule porosity of alumina powder with aqueous PEG solutions. They reported that the granule porosity decreased and pore saturation increased with increasing impeller speed due to an increase of the frequency and energy of impacts. This contributed to more consolidated granules with low granule porosity.

5.3.2 The effect of impeller design and powder wettability

Granule size and internal microstructure was also studied using different impeller designs and powder wettabilities. An intermediate impeller speed 350 rpm was chosen for these studies because the high shearing forces imposed at high impeller speeds of 500 rpm resulted in destruction of pre-nucleated liquid marbles. Therefore, 500 rpm impeller speed was not investigated for this part of the study. In addition, the powder motion was observed visually for all three impeller speeds and designs, and it was found to have primary rotational motion in the circumferential direction. A secondary, toroidal, motion was also seen. A roping regime was observed with 2-bladed and 3-bladed impeller at 350 rpm and above. However, it was observed with the flat plate at all impeller speeds used in this chapter. For this reason, the use of 150 rpm impeller speed was excluded from this study.

A binder viscosity of 1300 mPa s, primary particle size of 35 μm , impeller speed of 350 rpm and mixing time of 20 s were used throughout this part of the work. A flat plate impeller was used to minimize impact and maximize shear in the granulator. The 2-bladed impeller was used to create both impact and shear in the granulator. The 3-bladed impeller was used to maximise the impact and shear in the high shear granulator.

5.3.2.1 Granule size distribution

The size distribution of the resultant granules produced using different impeller designs and powder wettabilities for 20 s mixing time in high shear mixer are discussed in this section.

5.3.2.1.1 Low powder wettability

Figure 5.12 shows the particle size distributions for low powder wettability using different impeller designs. The pre-nucleation experiments produced liquid marbles. The granule size was larger using the flat plate impeller ($d_{43} = 726 \mu\text{m}$) compared to the 2-bladed and 3-bladed impellers ($d_{43} = 623$ and $407 \mu\text{m}$ respectively). A bimodal distribution was observed with the flat plate impeller, while unimodal granule size distributions were observed using 2-bladed and 3-bladed impellers. For more details of q_3 and d_{43} , see Appendix B.1.2.

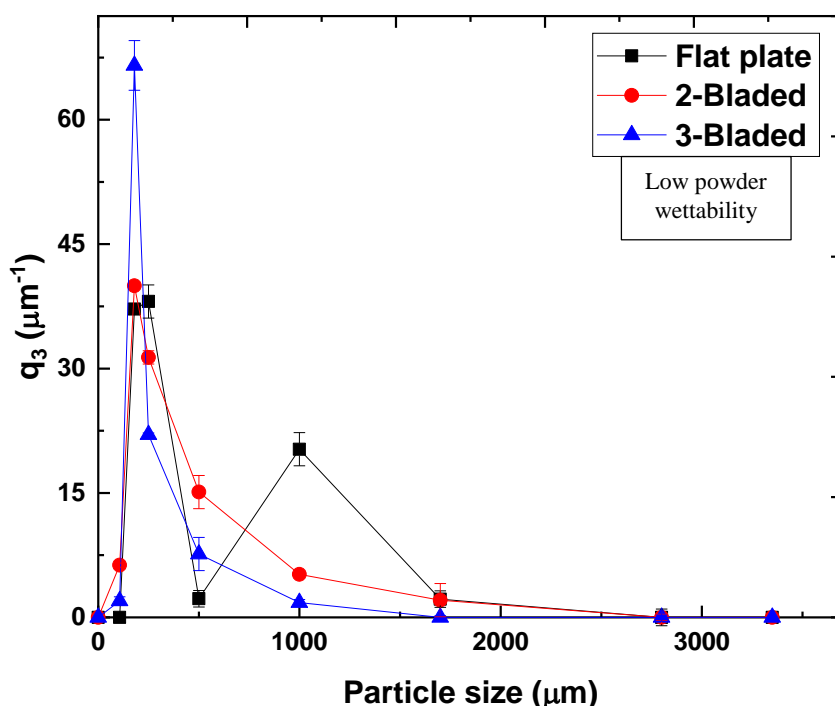


Figure 5.12: Particle size distribution of granules produced using low powder wettability and different impeller designs, obtained via sieve analysis. Error bars are the standard deviation of three measurements.

A mixture of semi-spherical granules and flakes was produced using the flat plate impeller (Figure 5.13 a). However, a mixture of flakes and fine powder was produced using the 2-bladed impeller (Figure 5.13 b). Only fine powder was produced using the 3-bladed impeller (Figure 5.13 c).

The production of fine powder and flakes is probably due to the breakage of the liquid marbles with the high shearing forces applied by the different impeller designs. It is observed that the percentage of flakes increases gradually using flat plate to 2-bladed and 3-bladed impeller. This is most likely due to the effect of the impact and shearing forces applied.

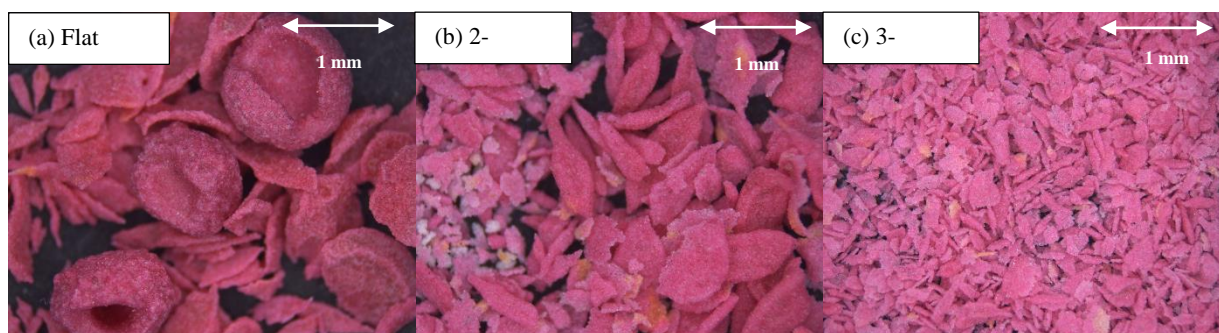


Figure 5.13: Comparison of granules using low powder wettability and different impeller designs.

5.3.2.1.2 Medium powder wettability

Figure 5.14 shows the granule size distributions using powder of medium wettability and different impeller designs. The pre-nucleation experiments produced liquid marbles. A larger granule size was produced using the flat plate impeller ($d_{43} = 1600 \mu\text{m}$), and the granule size decreased using the 2-bladed impeller ($d_{43} = 1072 \mu\text{m}$), while a smaller granule size was produced using the 3-bladed impeller ($d_{43} = 623 \mu\text{m}$). A bimodal size distribution was observed using the flat plate impeller, while unimodal size distributions were observed using 2-bladed and 3-bladed impellers. For more details of q_3 and d_{43} , see Appendix B.1.2.

A mixture of semi-spherical and flat granules were produced using the flat plate impeller (Figure 5.15 a). Semi-spherical granules were produced using the 2-bladed impeller (Figure 5.15 b). Only fine powder and small flakes were produced using the 3-bladed impeller (Figure 5.15 c)

The production of fine powder using 3-bladed impeller might be because the destruction of the pre-nucleated liquid marbles during granulation.

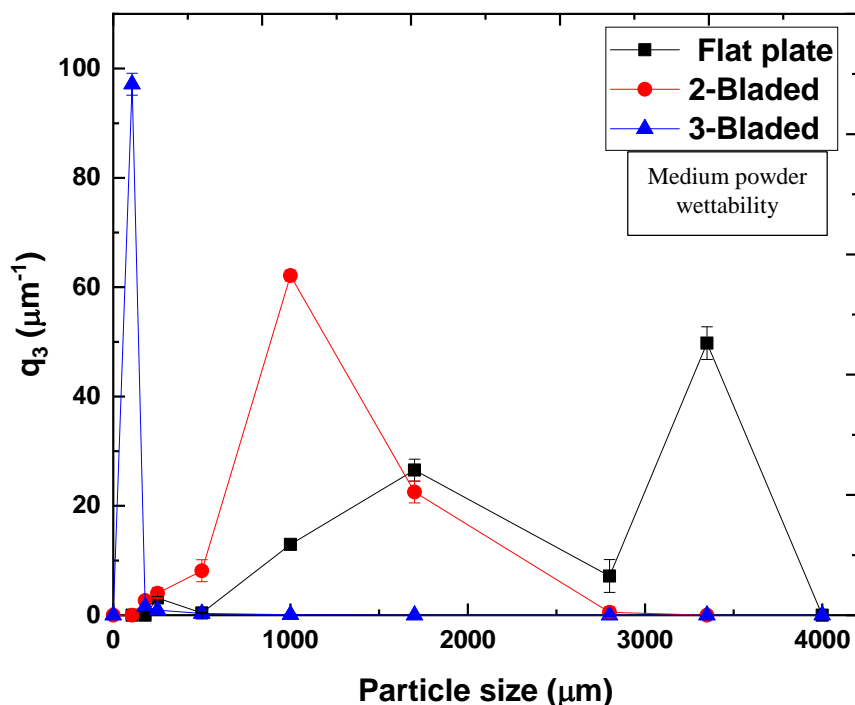


Figure 5.14: Particle size distribution of granules produced using medium powder wettability and different impeller designs, obtained via sieve analysis. Error bars are the standard deviation of three measurements.

The results in this work are also in accord with Schæfer et al. 1993b. They studied the effect of two different impeller designs on granule size using melt pelletisation of lactose as a powder and PEG as a liquid binder in a 50 L high shear mixer. Both flat plate and 2-bladed with 40° inclination impellers were used. They found that a larger and irregular shaped granule size was obtained using flat plate impeller, while small and spherical granules were produced with the 2-bladed impeller. They found that after 17-minute mixing time the energy input was 515 kJ/kg using the 2-bladed impeller, while 198 kJ/kg using the flat plate impeller. The high energy input of the 2-bladed impeller explained the decreased in granule size due to destruction of granules by the high impact forces applied.

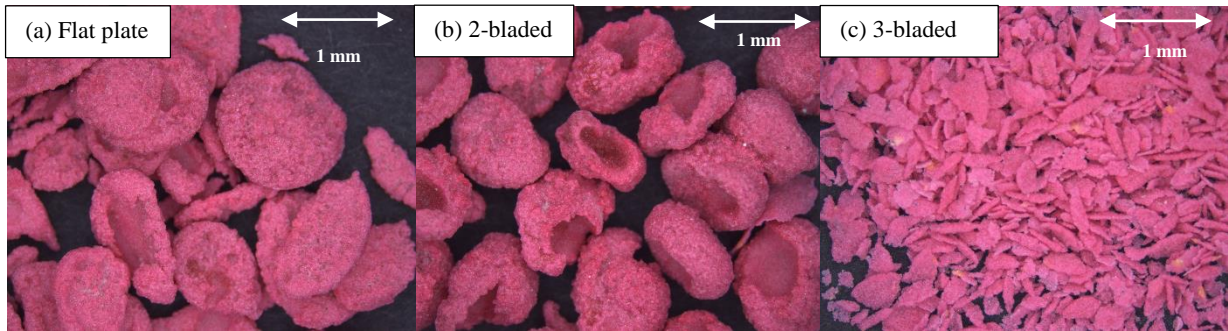


Figure 5.15: Comparison of granules using medium powder wettability and different impeller designs.

5.3.2.1.3 High powder wettability

Figure 5.16 shows the granule size distributions using powder of high wettability and different impeller designs. The pre-nucleation experiments produced immersion nuclei. A larger granule size was produced using the flat plate impeller ($d_{43} = 2213 \mu\text{m}$), and the granule size decrease using the 2-bladed impeller ($d_{43} = 1397 \mu\text{m}$), while a smaller granule size was produced using the 3-bladed impeller ($d_{43} = 1236 \mu\text{m}$). A bimodal size distribution was observed using the 3-bladed impeller, while unimodal size distributions were observed using the flat plate and the 2-bladed impellers. For more details of q_3 and d_{43} , see Appendix B.1.2.

Semi-spherical granules with a high rim were produced using the flat plate and 2-bladed impellers (Figure 5.17 a and b). A mixture of semi-spherical and irregular shaped granules was produced using the 3-bladed impeller (Figure 5.17 c).

The decrease in the size of granules produced using the 2-bladed and 3-bladed impellers is probably due to attrition and breakage of the granules with an increase in the shearing and impact forces using these two impeller designs during granulation. It is hypothesized that the impact and shearing forces increase with these two impeller designs.

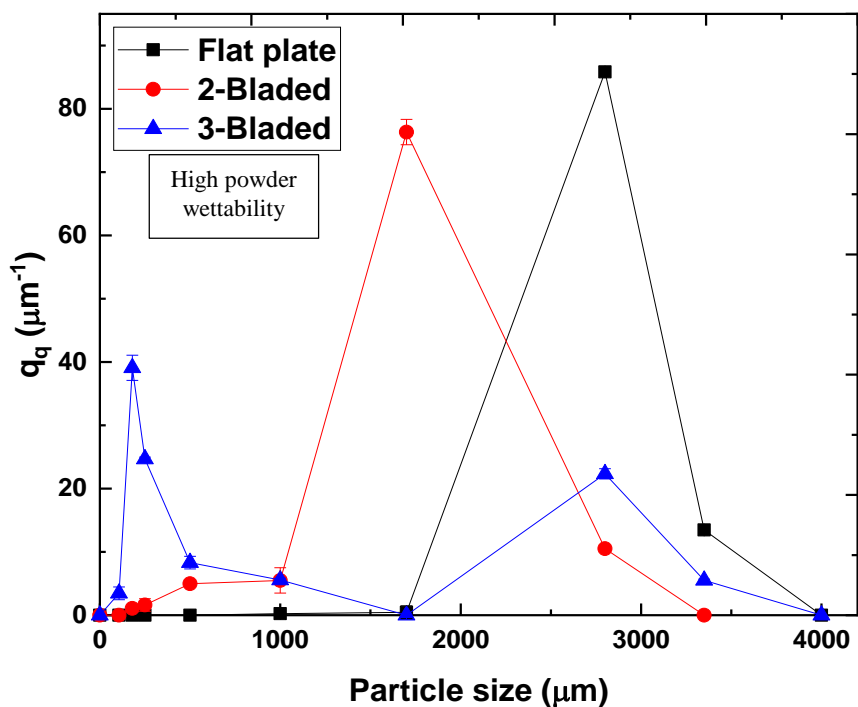


Figure 5.16: Particle size distribution of granules produced using high powder wettability and different impeller designs, obtained via sieve analysis. Error bars are the standard deviation of three measurements.

The difference in granule shapes obtained with different impeller designs in this work can be explained by Voinovich et al. 1999 who suggested that the difference in the appearance of granules can be due to the differences in the movement of powder inside the bowl of different impeller designs.

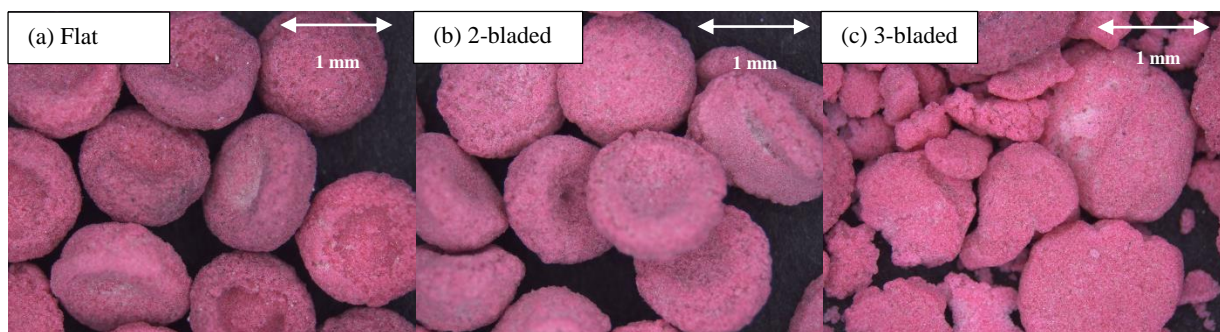


Figure 5.17: Comparison of granules using high powder wettability and different impeller designs.

5.3.2.2 Internal structural analysis

Figure 5.18 shows XRCT images of representative granules produced using different powder wettabilities and impeller designs.

For powder of low wettability, hollow granules were produced using the flat plate impeller. No granules were obtained using 2-bladed and 3-bladed impellers; only fine powder and flakes were produced which were difficult to scan using XRCT. The wall thickness of hollow granules produced using the flat plate impeller was 35.9 μm (Figure 5.19).

For powder of medium wettability, hollow granules were produced using the flat plate and the 2-bladed impeller. Only fine powder was produced using the 3-bladed impeller, which was difficult to scan using XRCT. The hollow granule wall thickness increased from 413.7 μm to 583.7 μm using the flat plate and the 2-bladed impeller respectively (Figure 5.19).

For powder of high wettability, hollow granules were produced using the flat plate impeller, while single solid granules were produced using the 2-bladed and 3-bladed impeller designs. The wall thickness of hollow granules produced using the flat plate impeller was 941.6 μm (Figure 5.19). More XRCT cross sectional images of the granules can be found in Appendix B.2.2.

The liquid marbles produced using powder of low and medium wettabilities are destroyed using 2-bladed and 3-bladed impellers due to the high shearing force applied; it is presumed that there is a specific shearing force that must be exceeded for liquid marbles to survive the impact during granulation.

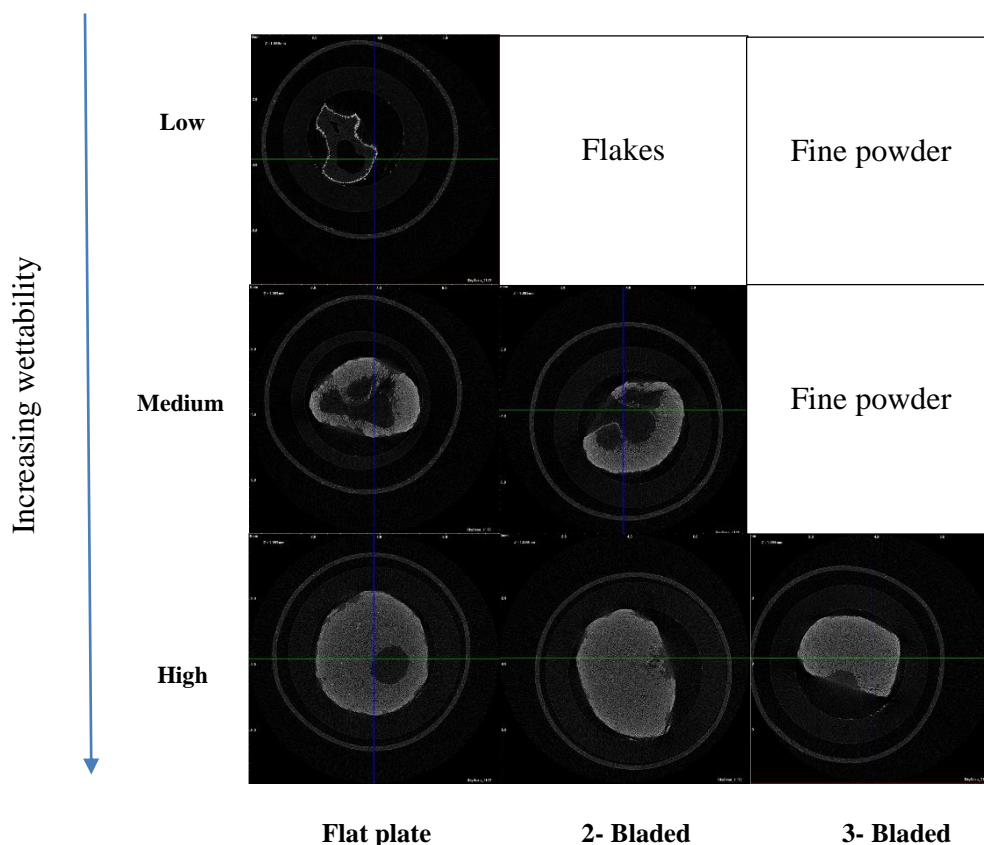


Figure 5.18: Images of granules produced using different powder wettabilities and impeller designs. The outer rings are part of the sample container. (Reconstructed XRCT images; representative central cross-section).

This study showed that hollow granules were produced mostly using the flat plate impeller, which is assumed that it has the lower energy input during granulation and decreased granule deformation. However, Saleh et al. 2011 and Forny et al. 2007, mentioned previously in Section 5.3.1.2. that high energy input during granulation is essential for hollow granule formation. They found that if insufficient energy was applied during mixing, the hydrophobic powder and the binder remains as two phases. The applied energy per unit mass must exceed a minimum limit for liquid marbles to be produced. The difference in the results obtained in this work is probably due to the use of pre-nucleated liquid marbles or immersion nuclei compared to a large amount of liquid used by Saleh et al. 2011 and Forny et al. 2007.

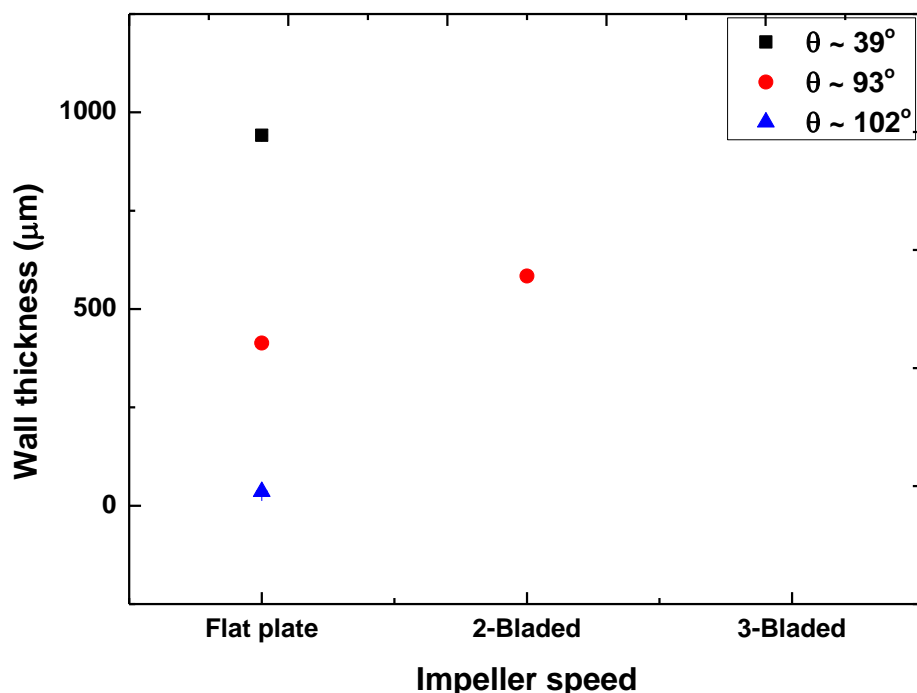


Figure 5.19: Wall thickness as a function of impeller design and powder wettability. Error bars are the standard deviation of three measurements. θ is liquid powder contact angle.

5.3.2.2.1 Porosity

Figure 5.20 illustrates the total porosity by XRCT as a function of powder wettability and impeller design. For powder of low wettability, the total porosity of granules produced using the flat plate impeller was 81.6 %. For powder of medium wettability, the total porosity decreased from 56.4 % to 37.5 % using the flat plate and 2-bladed impellers respectively. Powders of high wettability were not as largely affected by the changes in the impeller design; here, the total porosity decreased from 32.5 % to 24.9 % using flat plate and 3-bladed impellers respectively.

It is assumed that the granules undergo higher collision and compaction using the 2-bladed and 3-bladed impellers. This results in an increase in the collision forces between particles and particle-walls. If the particle survives the impact applied, then it will start to consolidate, and squeeze any entrapped air and liquid from inside to the granule surface.

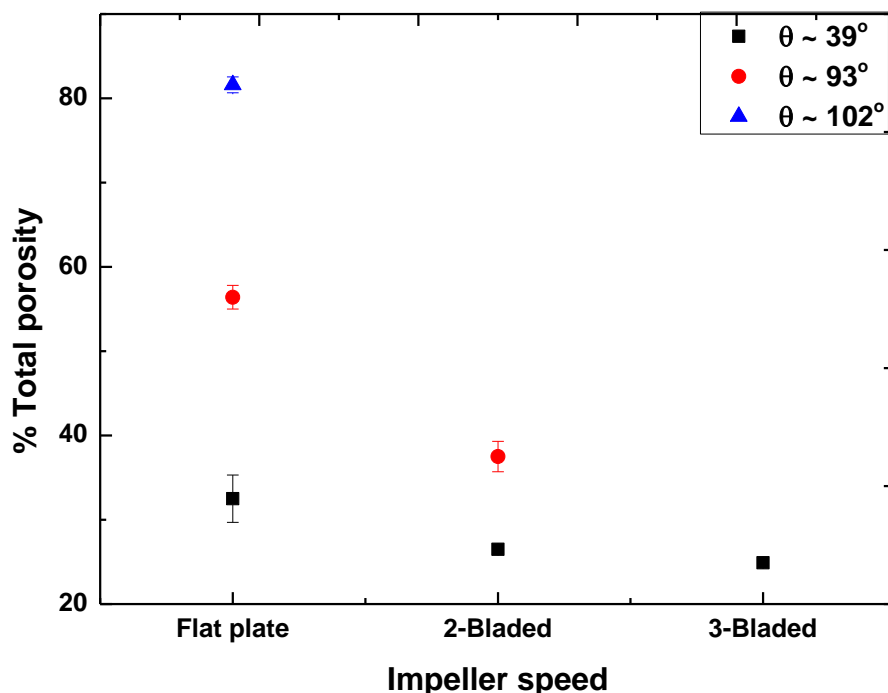


Figure 5.20: Total porosity as a function of impeller design and powder wettability. Error bars are the standard deviation of three measurements. θ is liquid powder contact angle.

The results obtained in this work when the porosity of the granules is higher using the flat plate impeller is consistent with Schæfer et al. 1993b, previously mentioned in Section 3.5.2.1.2. They found that higher intra-granular porosity was obtained using a flat plate impeller. The high energy input of the 2-bladed impeller explained the decrease in granule porosity. This high energy input increased granule collisions which contributed to granule consolidation that squeezed liquid to the granule surface and then decreased granule porosity.

5.3.3 The effect of powder wettability

This section focuses on the effect of powder wettability on granule size and internal microstructure using three different powder wettability mixtures and three different impeller designs. An impeller speed of 350 rpm was used. The high impeller speed is not used because most of the pre-formed liquid marbles, particularly those produced with low powder wettability, were destroyed. This makes it difficult to measure the porosity and wall thickness.

In addition, 150 rpm impeller speed was not used because a roping regime was not produced with the 2-bladed and 3-bladed impellers.

5.3.3.1 Granule size distribution

The size distribution of the resultant granules produced from different powder wettabilities and impeller designs for 20 s mixing time in high shear mixer are discussed in this section.

5.3.3.1.1 Flat plate impeller

Figure 5.21 show granule size distributions using the flat plate impeller and different powder wettabilities. A larger granule size was obtained using high powder wettability ($d_{43} = 2213 \mu\text{m}$), the granule size decreased with decreasing powder wettability ($d_{43} = 1600$ and $726 \mu\text{m}$) using medium and low powder wettabilities respectively (Figure 5.21). Bimodal size distributions were observed using low and medium powder wettabilities. A unimodal size distribution with high frequency peak at 3 mm was observed using the powder of high wettability. For more details of q_3 and d_{43} , see Appendix B.1.2.

A mixture of spherical granules and flakes was observed using low powder wettability (Figure 5.22 a). A mixture of spherical, flat and elongated granules was observed using medium powder wettability (Figure 5.22 b), while using high powder wettability, semi-spherical granules were observed (Figure 5.22 c).

It is concluded that the percentage of flakes decreases gradually with increasing powder wettability. High powder wettability give larger granule sizes compared to the granules produced using medium and low powder wettabilities.

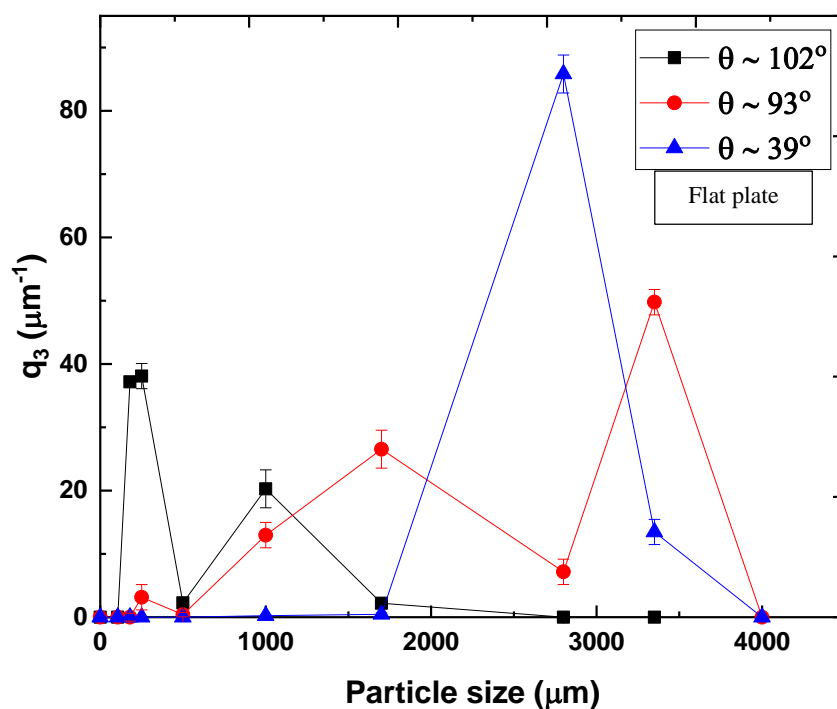


Figure 5.21: Particle size distribution of granules produced using the flat plate impeller and different powder wettabilities, obtained via sieve analysis. Error bars are the standard deviation of three measurements.

The same findings was observed by Yu et al. 2014. Lactose, microcrystalline cellulose, crosscarmellose sodium as a wetting powder and dicalciumphosphate dihydrate as a non-wetting powder were granulated without binder in a twin screw granulator. They studied the granulation behaviour of increasing powder hydrophobicity. They reported that with an increase in the content of wetting powder, the granule size increased. A decrease in powder wettability led to a decrease in the liquid binder distribution leading to a large proportion of un-wetted particles and a decrease in granule size.

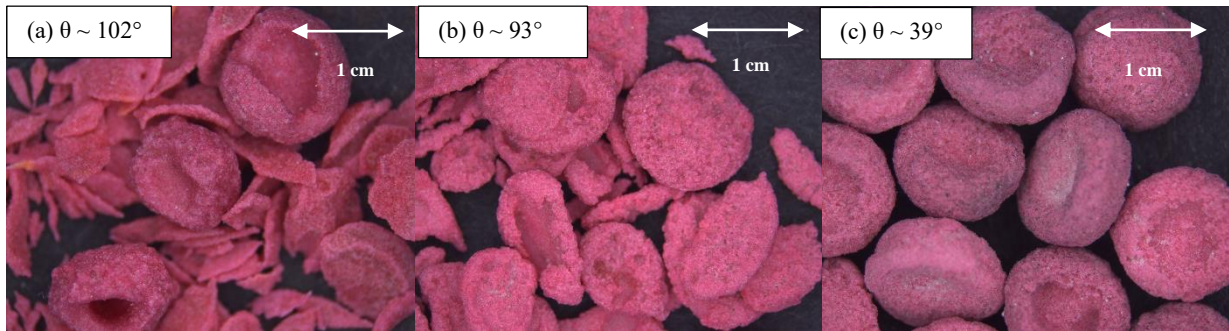


Figure 5.22: Comparison of granules using the flat plate impeller and different powder wettabilities.

5.3.3.1.2 2-Bladed impeller

Figure 5.23 show granule size distributions using the 2-bladed impeller and different powder wettabilities. A larger granule sizes were obtained using high and medium powder wettability ($d_{43} = 1397$ and $1072 \mu\text{m}$ respectively). The granule size decreases using low powder wettability ($d_{43} = 623 \mu\text{m}$). Unimodal granule size distributions were observed for all powder wettabilities, with high granule frequency peak at 3 mm using powder of high wettability. For more details of q_3 and d_{43} , see Appendix B.1.2.

A mixture of fine powder and flakes was obtained using low powder wettability (Figure 5.24 a). However, semi-spherical granules were obtained using medium and high powder wettabilities (Figure 5.24 b and c).

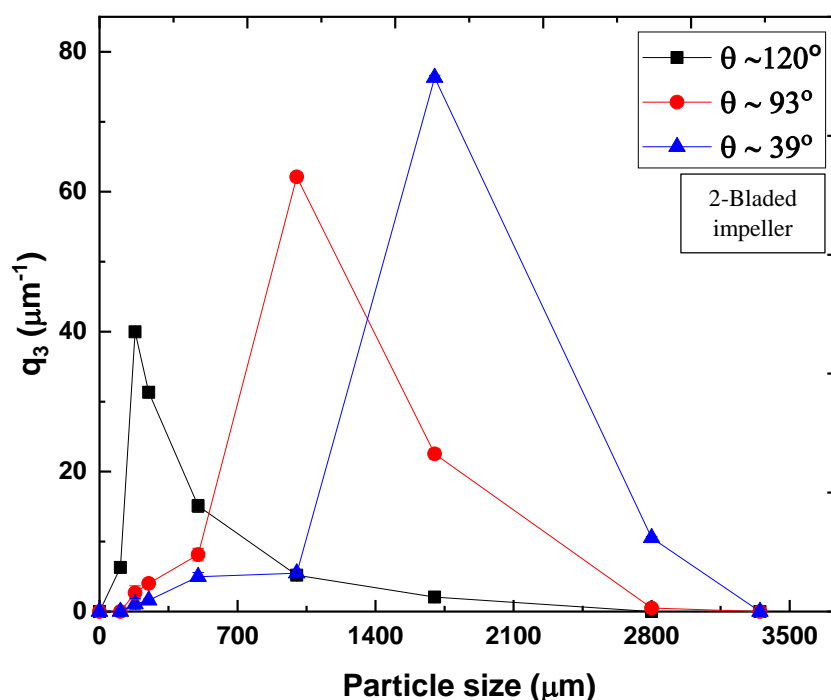


Figure 5.23: Particle size distribution of granules produced using the 2-bladed impeller and different powder wettabilities, obtained via sieve analysis. Error bars are the standard deviation of three measurements. θ is liquid powder contact angle.

The observed increase in the granule size by increasing powder wettability is consistent with Chitu et al. 2011a, who studied the liquid distribution in the granules produced using different powder wettabilities. Microcrystalline cellulose as a non-wetting powder and lactose as wetting powder were granulated with water in a high shear mixer. Two formulations were used; the first had a high amount of non-wetting powder and the second had high amount of wetting powder. They found that the granulation liquid was easily distributed across the wetting powder bed, resulting in larger granules with a high powder wettability.

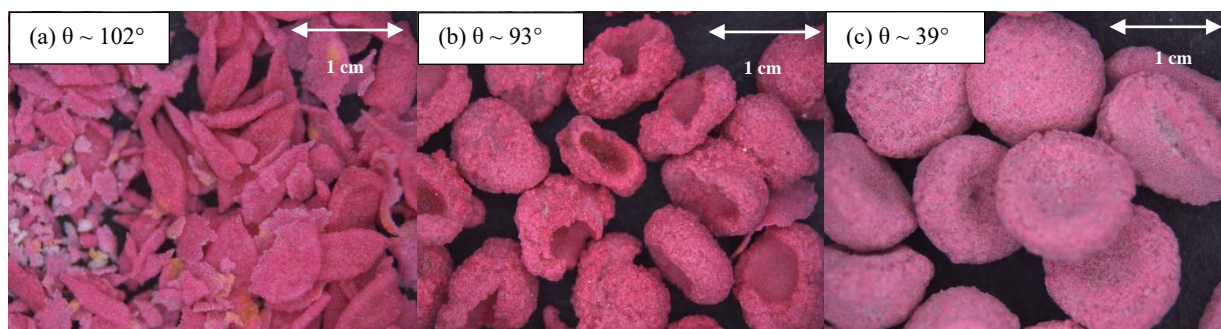


Figure 5.24: Comparison of granules using the 2-bladed impeller and different powder wettabilities.

5.3.3.1.3 3-Bladed impeller

Figure 5.25 show granule size distributions using the 3-bladed impeller and different powder wettabilities. There were minimal changes in the size of granules produced using different powder wettabilities. Fine powders were produced using powder of low and medium powder wettabilities ($d_{43} = 407$ and $623 \mu\text{m}$ respectively) (Figure 5.26 a and b). Irregular shaped granules were produced using high powder wettability ($d_{43} 1236 \mu\text{m}$) (Figure 5.26 c). For more details of q_3 and d_{43} , see Appendix B.1.2.

The production of fine powder and flakes using the 3-bladed impeller with different powder wettabilities is probably due to destruction of the preformed liquid marbles and immersion nuclei during granulation. The destruction is probably due to high shearing and impact forces applied using the 3-bladed impeller.

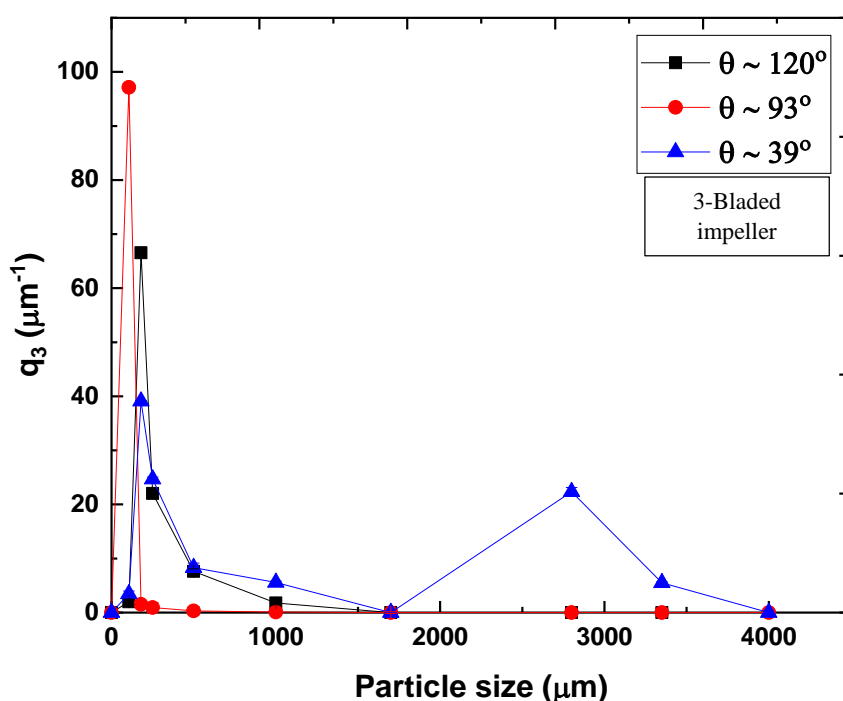


Figure 5.25: Particle size distribution of granules produced using the 3-bladed impeller and different powder wettabilities, obtained via sieve analysis. Error bars are the standard deviation of three measurements. θ is liquid powder contact angle.

These results are in accord with Verstraeten et al. 2017 who studied the effect of impact and shearing forces on granule size applied using conveying and kneading elements in twin screw granulation. Conveying elements are designed to impart low mechanical energy, while kneading elements are designed to impart high mechanical energy. They found that the granule size was unaffected after passing conveying elements for both wetting and non-wetting formulations due to the low impact forces applied. However, a decrease in granule size for both wetting and non-wetting formulations was observed after the granules were passed through the kneading elements. This was probably due to high shearing and compression forces applied by kneading elements that results in either destruction of the granules produced using non-wetting powder or consolidation of granules produced using a wetting formulation. Similarly, within each formulation studied in this section, the granule size is smaller for high shear conditions, and larger for lower shear conditions.

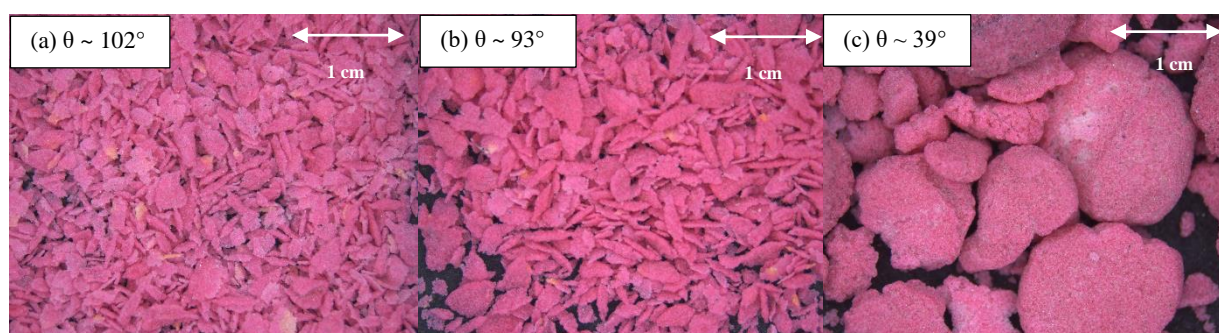


Figure 5.26: Comparison of granules using the 3-bladed impeller and different powder wettabilities.

5.3.3.2 Internal microstructural analysis

XRCT images of granules are presented in Figure 5.27 focusing on the effect of different powder wettabilities and impeller designs. For the flat plate impeller, hollow granules were obtained using different powder wettabilities. The granule wall thickness decreased from 941.6 μm using high powder wettability to 413.7 μm and 35.9 μm using medium and low powder wettabilities respectively (see Figure 5.19, Section 5.3.2.2). For the 2-bladed impeller, single solid granules were obtained using high powder wettability, while hollow granules were obtained using medium powder wettability. Only fine powders were obtained using low powder wettability. The hollow granules wall thickness was 583.7 μm using medium powder wettability (see Figure 5.19, Section 5.3.2.2). For the 3-bladed impeller, single solid granules were obtained using high powder wettability, and fine powders were obtained using medium

and low powder wettabilities. More XRCT cross sectional images of the granules can be found in Appendix B.2.2.

The production of single solid granules using high powder wettability and the increase in granule wall thickness using medium powder wettability, is probably due to increasing immersion of powder particles inside the liquid droplets because of the decrease in powder liquid contact angle. Increasing powder wettability encourages the hydrophilic drainage of liquid droplets through the powder particles.

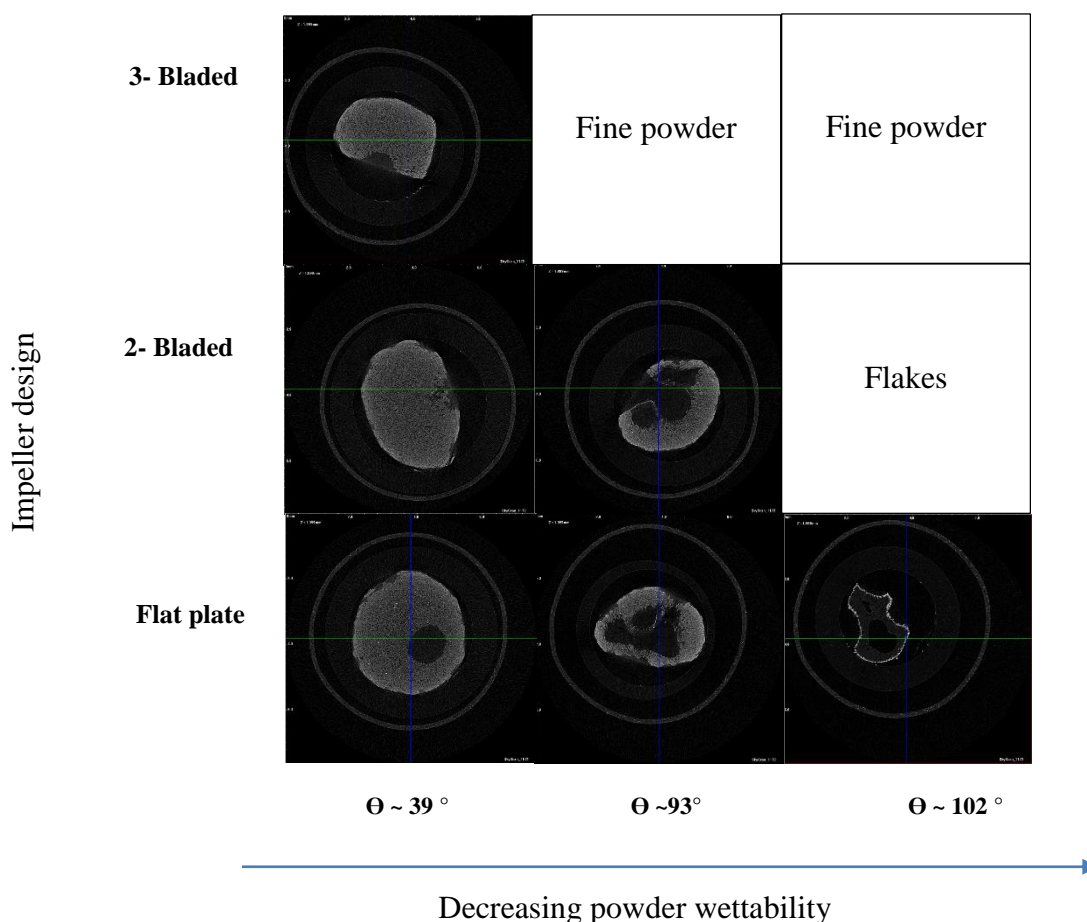


Figure 5.27: Images of granules produced using different powder wettabilities and impeller designs. The outer rings are part of the sample container. (Reconstructed XRCT images; representative central cross-section).

These results are consistent with results of work performed previously by Hapgood and Khanmohammadi, 2009. Non-wetting glass beads, salicylic acid, 2-ethoxybenzamid were used as powders. Water, aqueous solutions of glycerol and PEG 200, 300, 400 and 600 as liquid binders were used. Different liquid droplets were released into different powder beds. The

immersion of liquid droplets into the powder bed or spreading of powder particle around the liquid droplet were investigated. They found that droplet immersion into the powder bed occurred when the liquid powder contact angle $< 90^\circ$. However, liquid marbles were formed when the liquid powder contact angle $> 90^\circ$. Hollow granules were produced after drying of the liquid marbles. For more details of the formation of the immersion nuclei or liquid marbles see Section 3.6.1.

5.3.3.2.1 Porosity

The total porosity of the granules produced using different powder wettabilities and impeller designs were calculated using XRCT.

For the flat plate impeller, the total porosity decreased from 81.6 % using low powder wettability to 56.4 % and 32.5 % using medium and high powder wettabilities respectively (see Figure 5.20, Section 5.3.2.2.1). For the 2-bladed impeller, the porosity decreased from 37.5 % using medium powder wettability to 26.5 % using high powder wettability. Only fine powder was produced using low powder wettability (see Figure 5.20, Section 5.3.2.2.1). For the 3-bladed impeller, the porosity of granules produced using high powder wettability was 24.9 % (see Figure 5.20, Section 5.3.2.2.1). However, only fine powder was produced using medium and low powder wettabilities.

Generally, the porosity decreased with increasing powder wettability. It is hypothesised that the binding force between powder particles and the immersion of the powder inside the liquid droplets increased with increasing powder wettability, giving a relatively thicker wall of powder around the liquid droplet. The granules became denser, more consolidated, less porous, and larger than granules produced from powder of low wettability. The improvement in the wettability of the powder improves the hydrophilic drainage of liquid droplets through the powder particles.

These results are in agreement with Verstraeten et al. 2017, mentioned previously in Section 5.3.3.1.3, who found that the porosity was lower for the wetting formulation. They hypothesized that this was because of higher affinity of wetting particles to the granulation liquid. The particles can immerse quickly into liquid droplets which results in more consolidated granules and higher granule porosity.

5.4 Summary and further discussion

In this chapter, the following main experimental effects were measured and observed:

- Increasing the impeller speed resulted in a decrease in granule size for all powder wettabilities
- Thin walled, hollow granules were promoted by low powder wettability and low impeller speed. Increasing either powder wettability or impeller speed tended to thicken the granule walls, to the point where solid granules are formed.
- Impeller geometry had a strong effect on granule size and structure. Changing from a flat plate, to a 2-bladed impeller, and to a 3-bladed impeller saw a decrease in granule size.
- In the study of impeller geometry, wall thickness of the granules was decreased with decreasing powder wettability. Hollow granules were only produced with flat plate and 2-bladed impellers. Hollow granules were produced over a greater range of powder wettabilities with the flat plate impeller than the 2-bladed impeller.
- Increasing powder wettability increased granule size for all systems

The key results will be discussed in the following sections.

5.4.1 The effect impeller speed on granule size and internal structure

An increase in the impeller speed resulted in a decrease of the granule size for all systems investigated in this chapter. The decrease in granule size is probably due the use of high binder viscosity which decreased the coalescence between wet granule surfaces and the powder bed. In addition, it might be due to the use of high impeller speed that contributed to increased granule deformation to the point that the granules cannot withstand the impact and shearing forces applied leading to granule breakage and a decrease in granule size.

Ennis et al. 1991 concluded that granule size is highly influenced by impact collisional velocity and liquid binder viscosity. They reported that high impeller speed decreases the probability of the coalescence between the two wet particles which results in a decrease in granule size.

Iveson et al. 2001 validated a regime map previously proposed by Iveson and Litster, 1998. They developed a regime map in terms of Stokes deformation number (St_{def}) and maximum pore saturation (S_{max}), for more details see Section 2.5.2.2. St_{def} is increased with increasing process impact velocity and hence an increase in the agitation intensity. According to this regime map, increasing process agitation intensity shifts a system behaviour towards the top right of the regime map, previously mentioned in Section 2.5.2.2.3. The granulation behaviour changed from nucleation to steady or induction growth, from induction to steady or rapid growth, from steady or rapid growth to crumb region. They concluded that Stokes deformation number increased with increasing collision velocity and at some point during granulation reached a critical value of St_{def}^* , above which granules start to deform and break.

Hollow granules were produced at low impeller speed regardless of powder wettability. However, with increasing impeller speed, different granule structures were produced depending on powder wettability. Using powder of low wettability, hollow granules with a thin wall thickness were produced. This wall thickness slightly increased with increasing impeller speed. This is probably due to the wettability effect that inhibits the penetration of powder particles into the liquid droplets. Using powder of medium wettability, hollow granules with a thin wall thickness were produced and this wall thickness increased with increasing impeller speed. Using powder of high wettability, hollow granules with a wall thickness increasing with increasing impeller speed were observed. However, a further increase in impeller speed resulted in the production of granules with a solid internal structure. This was probably due to increasing shearing forces with high impeller speed led to granule consolidation.

5.4.2 Effect of impeller design on granule size

Flat plate impeller produced the highest granule size of all impeller designs. For the bevelled impellers, the 2-bladed impeller produced larger granule size than the 3-bladed impeller. The difference is due to the energy input into the system; 3-bladed > 2-bladed > flat plate. If the granule does not have sufficient strength to resist the energy input due to the weak binding forces between the particles, then destruction of liquid marbles or immersion nuclei is more expected when using 2-bladed and 3-bladed impellers rather than flat plate impeller. The results in this thesis are agreement with many researchers such as Smith, Liu and Litster, 2010

Boonkanokwong et al. 2016. Knight et al. 2001 also reported that the energy input by 3-bladed was more than 2-bladed and flat plate impeller.

Knight et al. 2001, investigated the torque produced using three different impeller designs; flat plate, 2-bladed with 11° bevelled angle and 3-bladed impeller with 17° bevelled angle. Sand was the experimental material. They reported a the 2-bladed impeller gave 25 % less torque than a 3-bladed impeller. In addition, lower energy input was produced using a flat plate impeller. This can explain the results obtained in this work.

Likewise, Boonkanokwong et al. 2016 studied the effect of the number of impeller blades, and the impact of impeller blade on granular mixing kinetics energy using DEM. The energy input to granules was stronger with a 3-bladed impeller than a 2-bladed impellers and a flat plate impeller. It was concluded that the 3-bladed impeller imposes more collision velocities than 2-bladed or flat plate impellers. Granule destruction was expected using 3-bladed impeller, and this agrees with results in this work, in which a smaller granule size was produced using 3-bladed impeller.

In this work, the decrease in granule size using 2-bladed impeller to flat plate impeller can be explained by Smith, Liu and Litster, 2010. They studied the effect of impeller design on granule breakage in a breakage only granulator. Two impeller designs; a 11° bevelled edge 2-bladed and a flat plate were used. Results from the 11° bevelled edge impeller showed an increase in breakage. However, the flat plate impeller showed very little breakage. It was proposed that either impact in the impeller zone was dominant over shear for breakage within the high shear, or that the two impeller designs give considerably different collision velocities in the mixer. An increase of collision velocities with the 11° bevelled edge impeller decreases the rate of granule survival in the granulator.

5.4.3 Effect of powder wettability

In this study, the granule size decreased with increasing the proportion of non-wetting powder in powder mixture. This was observed to happen in all system studied.

According to the dimensionless drop penetration time proposed by Hapgood et al. 2002, explained previously in Section 4.5, the increasing powder wettability led to a decrease in liquid penetration time inside the powder bed and increased binder distribution. Binder distribution

is an important step for granule liquid saturation, deformation and granule growth. In this work, and according to the penetration time theory, an increase of the amount of non-wetting powder leads to an increase in liquid binder penetration time inside the powder, which results in a decrease in binder distribution and then a decrease in granule size.

This was confirmed by Charles-Williams et al. 2013, who reported that the increasing the amount of non-wetting powder led to prolonged drop penetration time inside the powder and then a decrease in the resultant granule size. Lactose as a wetting and limestone as a non-wetting powder were granulated in high shear mixer. Water and saturated lactose solution were used as liquid binder. They found that as the non-wetting component increased, there was a decrease in granule size. On comparison with the penetration time on a static powder bed, the penetration time increased with increasing the percentage of limestone powder in the mixture.

5.4.4 Effect of impeller speed and powder wettability on granule porosity

Granule porosity increased with decreasing impeller speed, impeller blade number, impeller blade bevelled angle and powder wettability. This is probably because the higher impeller speed and the 3-bladed impeller impart high energy to granules during granulation than the lower impeller speed and flat plate impeller. This high energy input resulted in an increase in granule collisions, and then consolidation which decreased granule porosity.

Benali et al. 2009 used a high shear mixer to study the effect of impeller speed on granule porosity. Wet granulation was carried out using microcrystalline cellulose (Avicel PH101) as a powder, and an aqueous solution of polyvinyl pyrrolidone as liquid binder. Using low shear granulation, the formed granules were porous and the porosity decreased with an increase in impeller speed. Dense and rigid granules with low porosity were obtained at higher impeller speed. They suggested that with the increase in impeller speed, high mixing quality between powder and liquid was achieved. This resulted in the reduction of preferential growth and formation of consolidated and strong granules with lower porosity.

5.5 Conclusions

Powders of different wettabilities were granulated in a high shear mixer using aqueous PEG 12000 as the binder. The influence of the impeller speed, impeller design and powder wettability were investigated.

The key conclusions of this chapter are:

d- Granule size increases with:

- Decreased energy input: decreasing impeller speed and use of a flat plate impeller.
- Increasing powder wettability.

e- Hollow granules obtained with:

- Decreased energy input: decreasing impeller speed and use of a flat plate impeller.
- Decreasing powder wettabilities.

f- Granule porosity increase with:

- Decreased energy input: decreasing impeller speed and use of a flat plate impeller.
- Decreasing powder wettability.

The change in impeller speed, impeller design and powder wettability results in a large change in granule size and internal microstructure. For the intention of producing hollow granules, a flat plate impeller at low speed is successful in producing large hollow granules with different powder wettability. However, all these investigations were performed using wet granulation of model wetting and non-wetting powders that might or might not reflect the granule behaviour using pharmaceutical powder. Chapter 6 will investigate the effect of different formulation and process parameters on granule size and internal microstructure using pharmaceutical powders. In addition, the applicability of the data obtained using the model powder into pharmaceutical powder blends will be investigated.

CHAPTER 6. Granulation of pharmaceutical powder

In the study of granulation of non-wetting powders, the literature has largely focused so far on the nucleation mechanisms. The models for nuclei formation and growth in non-wetting powders are not able predict the formation of hollow granule microstructures, and hence academic research has focused on understanding the formation of liquid marbles of single-component powder systems. These researchers have made strides to answer the question “Why are liquid marbles formed?”. The attempt to produce hollow granules with a uniform shell has not been successful so far, and this forms the motivation of this work.

In this chapter an example pharmaceutical formulation has been used, and the effects of blend wettability, binder viscosity, mixing time, and shear forces on granule size and microstructure were assessed by sieving, optical microscopy, X-ray computed tomography (XRCT) and scanning electron microscopy (SEM).

In low shear granulation, the granule size decreased with increasing binder viscosity. In high shear granulation, granule size increased with increasing binder viscosity due to destruction of liquid marbles or immersion nuclei with low binder viscosity. Using both low and high shear mixers, hollow granules were produced using high binder viscosity with porosity increasing with increasing binder viscosity. A non-uniform distribution of the ingredients was most pronounced using the high binder viscosity. However, the wetting powder was mostly found at the surface of the granules regardless the binder viscosity or powder wettability.

Granule size increased with increasing mixing time during low shear granulation. Hollow granules were produced with the porosity reaching a maximum at 5-minute mixing time and then the porosity decreased with increasing mixing time. A more uniform distribution of the ingredients can be seen with increasing mixing time.

For intentional design of hollow granules, this study suggests that medium powder wettability is most favorable and the binder should have high viscosity to reduce shear dispersion and, in wetting systems, to increase the drop wetting time scale to match or exceed the processing time.

6.1 Introduction

In previous chapters, the effect of different formulation and process parameters on granule size and internal microstructure of model powders were investigated. The aim of this chapter is to investigate the effect of powder wettability, binder viscosity, granulation time, and external forces (shear/impact) on granule size and microstructure using real industrial pharmaceutical powders. However, there is a particular focus on intra-granular material distribution performed. Conditions that lead to the formation of hollow granules were of particular interest. Two ingredients were used; non-wetting micron-size pharmaceutical powder (efavirenz) and a wetting excipient (red iron oxide) in order to limit the number of contributing phenomena. Dextran at different aqueous concentrations was used as a liquid binder. Both a tumbling drum (low shear) and a high shear mixer were used.

In granulation, liquid marbles are a promising way to solve the problematic behaviour of non-wetting powders where the powder spreads around the liquid droplet in the nucleation stage and the interior liquid is subsequently evaporated to form hollow granules.

The previous works on the effect of binder viscosity, mixing time and shearing force on non-wetting powder focus on the formation and stability of liquid marbles (Eshtiaghi, Liu, & Hapgood, 2010, K.P. Hapgood, Farber, & Michaels, 2009, Forny, Pezron, Saleh, Guigon, & Komunjer, 2007). Although studies have been conducted into liquid marbles and hollow granules, the granulation mechanism of non-wetting powder remains not well understood. In addition, only a few studies have examined beyond nuclei formation to the entire non-wetting granulation process. There is little work looking at the effect of changing binder viscosity, mixing time and shearing force on the granule size, internal microstructure and ingredients distribution of the formed hollow granules. More investigation is required in this area.

The objective of this chapter is to perform a systematic study of the effect of:

- Binder viscosity
- Mixing time
- Shearing force

with a view to measuring parameters relevant to hollow granule size and formation for range of powder wettabilities. In particular:

- Particle size distribution using Image Pro Premier software.
- Granule internal structure using X-ray tomography (XRCT) and calculation of the % total porosity and wall thickness of hollow granules. This will give an insight into the internal structure of hollow granules.
- Compositional analysis using scanning electron microscopy (SEM) and energy dispersive X-ray spectroscopy (EDX).

6.2 Materials and Methods

A short overview of the materials and methods used is explained in this section. A detailed materials and methods can be found in Chapter 3. Experiments were performed using tumbling a drum (low shear) and a 1L Diosna High Shear Granulator (high shear). In this work, non-wetting micron-size pharmaceutical powder (efavirenz) was blended with a wetting excipient IROX (red iron oxide) in different ratios of 60%-40%, 50%-50% and 30%-70% respectively and granulated using dextran solutions of different viscosity as a binder in both low and high shear mixers.

The first stage of this study involved mixing the two powders, efavirenz and iron oxide, in different proportions. This was performed by using a 2L high shear mixer. Different impeller speeds and mixing times were investigated. Good dispersion of blend colour was observed visually using a 470 rpm impeller speed and a 1000 rpm chopper speed. First, 200 g of the dry mixture was put in the bowl of the high shear mixer and allowed to rotate for 5 minutes. After the first 5 min, significant build-up of efavirenz was typically observed on the walls. The material was scraped manually, placed into the middle of the bowl, and mixing was continued for another 5 min. Almost no build-up was typically observed then, but the scraping and further mixing was repeated every 5 min for up to 20 min of total mixing time. There was no visible difference in color distribution after mixing for 15 and 20 minutes in all blends as shown in Figure 6.1.

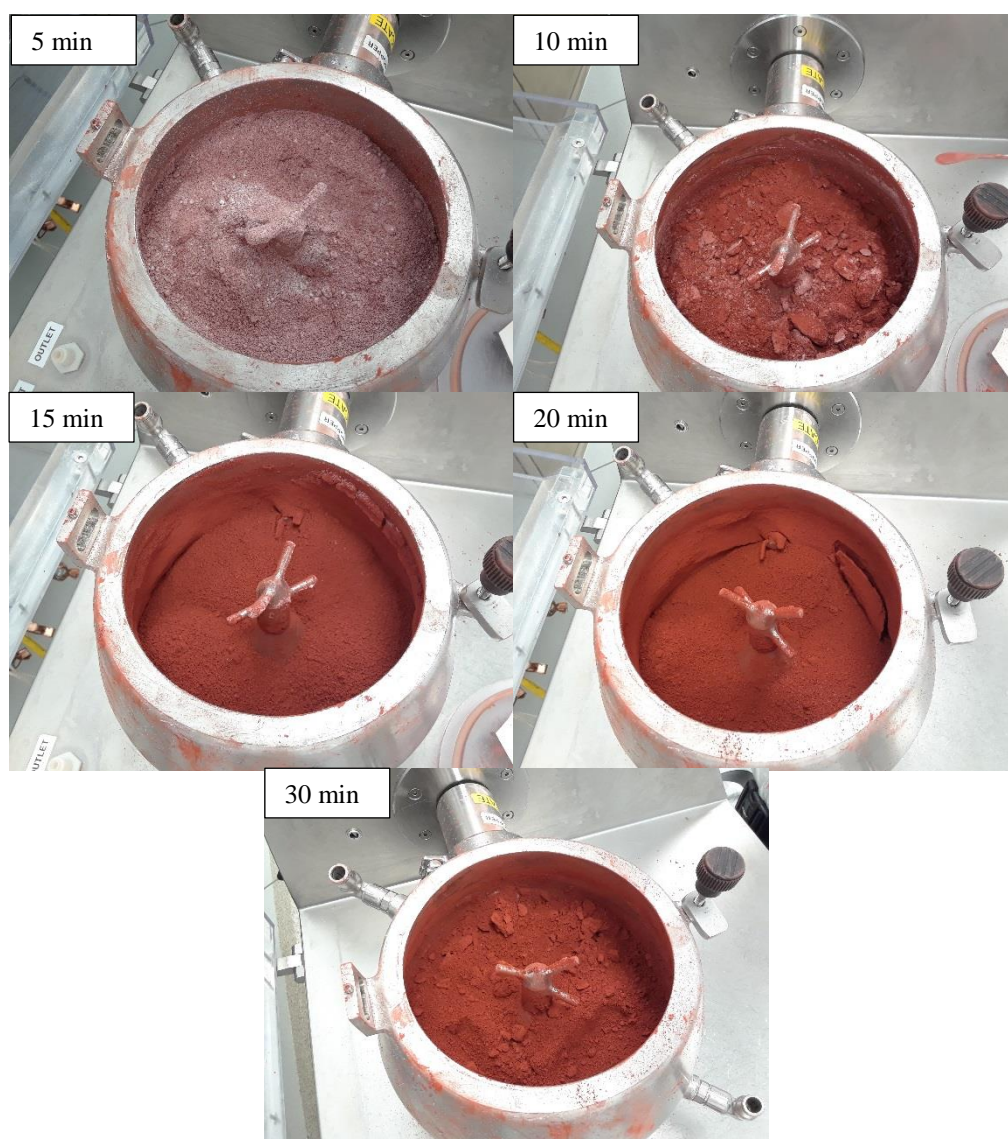


Figure 6.1: Mixing time of the dry mixture using the high shear mixer.

The work performed in this chapter can be divided into four parts. Firstly, liquid marbles or immersion nuclei were made without granulation to form a baseline for comparison with granules formed after granulation in the low and high shear granulators. In this part, three different mixtures of 60%-40%, 50%-50%, and 30%-70% efavirenz – IROX were used, which will simply be denoted as low, medium and high powder wettability respectively or by their contact angle of the liquid over powder. Three binder solutions were used: 10%, 30% and 50% dextran aqueous solutions which will be simply referred to by their viscosities of 1000, 100 and 8 mPa s respectively. An in situ XRCT of powder of 60%-40% efavirenz-IROX and high binder viscosity at three points was performed: (1) after initial liquid marble formation (nucleation in petri dish) and keeping it wet by using small airtight container (2) after granulation (3 minutes of hand rolling by orbital hand motion within the petri dish) and also

by keeping it wet by using small airtight container, and (3) during drying (leaving for 4-24 hr to dry). In addition, XRCT of wet and dry nuclei from the experiment using a powder mixture of 30%-70% efavirenz-IROX with low binder viscosity was carried out at two points: (1) initial liquid marble formation and (2) after drying, and comparing to the first powder mixture mentioned above. These experiments were performed to understand the shape of the resultant granules and at which point segregation happen. In addition, to understand the steps of hollow granules formation.

The second set of experiments involved varying powder wettability and binder viscosity using the low shear mixer. In this part, three different mixtures of 60%-40%, 50%-50%, and 30%-70% efavirenz-IROX were used. Three binder solutions were used: 10%, 30% and 50% aqueous dextran solutions. 20 g of powder mixture was loaded to a 10% fill level. Nuclei were prepared outside the mixer and deposited on the powder surface in the drum immediately after extraction from the petri dish. Tumbling was initiated. The drum ran at 25 rpm for 5 min.

The third set of experiments, investigated varying the mixing time; 60, 300, 900 and 1800 sec, using the low shear mixer. In this part, one powder of 50%-50% efavirenz-IROX and one binder solution; PEG 12000 were used, which will be simply denoted as a medium powder wettability and high binder viscosity respectively. The tumbling speed was set at 25 rpm.

Finally, granulation using the high shear mixer was carried out. Varying powder wettabilities and binder viscosities were investigated. In this part, three different mixtures of 60%-40%, 50%-50%, and 30%-70% efavirenz-IROX and three binder solutions were used: 10%, 30% and 50% dextran solutions. The amounts of powder used were 200 g per experiment. The impeller was operated at 370 rpm for 20 seconds. The experiments were repeated after the end of each of the experiments, using different binder viscosity and powder wettability. Roping flow was observed in all runs.

Table 6.1 shows the binder viscosity and blends of the powders used in this chapter, and the liquid-powder contact angle. Table 6.2 shows all the experiments performed in this chapter.

Table 6.1: Binder viscosity and powder-binder systems and contact angles.

Binder (% w/v Dextran)	Viscosity (mPa s)	Powder Efavirenz-IROX		
		Contact angle° of binder/powder		
		60%-40% (wt/wt)	50%-50% (wt/wt)	30%-70% (wt/wt)
10	8	125	89	63
30	100	130	92	72
50	1000	141	128	94

The images of all granules in this chapter were produced using light microscopy; SZX16 Olympus stereo microscope. Granules were placed on white plastic dishes.

Granule size distributions were measured by sieving with the following mesh sizes: 1000, 500, 300, 180, 150 and 106 μm . Granules were collected from sieve cut + 1000 μm and granule size was analysed using Image Pro Premier software. d_{50} values which is the median of the granule size distribution, are presented. This sieve cut fraction was reserved for microstructural analysis by X-ray tomography (XRCT), SEM and EDX.

Representative granules were chosen for each experiment for XRCT imaging to examine and analyse the internal structure. Images were processed with Skyscan software DataViewer and CTAn. Three representative granules were measured for wall thickness and % total porosity. In addition, compositional analysis using SEM and EDX was carried out to examine the distribution of efavirenz and IROX inside the granules. The granules examined by SEM and EDX were cross sectioned for a better view and understanding of the distribution of liquid binder, wetting and non-wetting powder inside the granules.

Table 6.2: Experimental design.

Formation (Liquid marbles /immersion nuclei)	Powder (efavirenz -IROX)	Binder viscosity (mPa s)			
		10% Dextran	30% Dextran	50 % Dextran	
	60%-40%	8	100	1000	
	50%-50%	8	100	1000	
30%-70%	8	100	1000		
Granulation (Low shear)	Powder (efavirenz -IROX)	Binder viscosity (mPa s)			
		10% Dextran	30% Dextran	50% Dextran	
	60%-40%	8	100	1000	
	50%-50%	8	100	1000	
30%-70%	8	100	1000		
Binder viscosity	Powder (efavirenz- IROX)	Mixing time (sec)			
50 % Dextran					
1000	50%-50%	10	300	900	1800
Granulation (High shear)	Powder (efavirenz -IROX)	Binder viscosity (mPa s)			
		10% Dextran	30% Dextran	50% Dextran	
	60%-40%	8	-	1000	
	50%-50%	-	100	-	
30%-70%	8	-	1000		

Preliminary studies were performed to select the best powder binder combination to produce constant liquid-powder contact angle for least 5 minutes, the expected period of the granulation process in this work. The aim was to select three different mixtures with contact angles; $> 90^\circ$, $\sim 90^\circ$ and $< 90^\circ$. Table 6.3 summarise the powder liquid combination and the resultant contact angle 5 minutes after the liquid droplet touched the powder bed. Some powder produced a powder-liquid contact angle $> 90^\circ$, others produced a contact angle $< 90^\circ$. None of the powder mixtures in Table 6.3 produced a contact angle very close to 90° , however, it was found the efavirenz-red iron oxide mixture produced the desirable range of contact angle and was approximately constant for more than 10 minutes. For more details, see Section 3.5.

Table 6.3: Overview of powder liquid combinations and their contact angle.

Powder 1	Powder 2	Contact angle of liquid - powder				
		Liquid binder				
		water	4% PVP	4% HPC	1% PEG 10000	4% HPMC
Efavirenz	-	124	122	86	12	88
Red iron oxide	-	12	27	-	-	-
Yellow iron oxide	-	64	33	-	-	-
Avisel PH-105	-	Imbibed	-	-	-	-
Hydrochlorothiazide (HCTZ)	-	32	12	Imbibed	-	Imbibed
Estazolam	-	126	87	14	-	-
Talc	-	86	60	-	-	-
50% Efavirenz	50% Yellow iron oxide	32	36	-	-	-
50% Efavirenz	50% PH-105	121	114	-	-	80
25% Efavirenz	75% HCTZ	120	114	-	-	-
50% Efavirenz	50% Zinc oxide	124	120	-	-	-
50% Talc	50% HCTZ	63	45	Imbibed	-	imbibed

6.3 Results and Discussion

The aim of this chapter is to investigate the effect of different formulation and process parameters on granule size and internal microstructure using pharmaceutical powder mixtures.

In this section, a range of binder viscosities and powder wettabilities were used. Some of the mixtures formed immersion nuclei, while others formed liquid marbles, as noted in Table 6.4. Immersion nuclei are formed when the liquid powder contact angle is ~ less than 90°, while liquid marbles are formed when the contact angle is ~ greater than 90°. For more details, see Section 3.6.1.

The measured diameter of initial liquid droplets (ILD) before nucleation and granulation can be seen in Table 6.5. Liquid droplet diameters were measured from the mass, volume and density of the liquid as described in Section 3.2.8. Figure 6.2 show a calibration curve as a function of droplet diameter and binder concentration. From this curve one can predict the diameter of the liquid droplet from binder concentration. As the binder viscosity increase there was an increased in the diameter of the liquid droplets.

Table 6.4: Summary of pre-nucleation experiments.

Conditions			Contact angle ^o	Nucleation product
Non wetting-wetting mixture	Binder viscosity (mPa s)	Binder surface tension mN/m		
60%-40%	8	72.09	125.25	Liquid marbles
60%-40%	100	73.09	130.05	Liquid marbles
60%-40%	1000	73.74	141.35	Liquid marbles
50%-50%	8	72.09	89.43	Liquid marbles
50%-50%	100	73.09	92.83	Liquid marbles
50%-50%	1000	73.74	128.63	Liquid marbles
30%-70%	8	72.09	63.51	Immersion nuclei
30%-70%	100	73.09	72.37	Immersion nuclei
30%-70%	1000	73.74	94.33	Immersion nuclei

The results and discussions section can be divided into five parts: the first part will give an overview of the characteristics of powder blends and ingredients distribution. The second section will explain the nucleation using a range of powder wettabilities and binder viscosities. The third part will give an investigation of the effect of varying binder viscosity and powder wettability on granule size and internal microstructure in a low shear granulator. The fourth part will give details of the increasing mixing time on granule size and structure, using the low shear mixer. Finally, the last section will show the effect of increasing shearing forces, using a high shear mixer, on the size and internal microstructure of the granules produced using range of powder wettabilities and binder viscosities.

Table 6.5: Liquid droplet properties.

Binder viscosity (mPa s)(PEG)	Droplet mass (g)	Density (g/cm ³)	Droplet Volume (cm ³)	Droplet diameter (μm)
8	0.0113 ± 0.0001	1.04 ± 0.023	0.0109	2758
100	0.0161 ± 0.0005	1.13 ± 0.028	0.0143	3024
1000	0.0209 ± 0.0003	1.2 ± 0.014	0.01748	3236

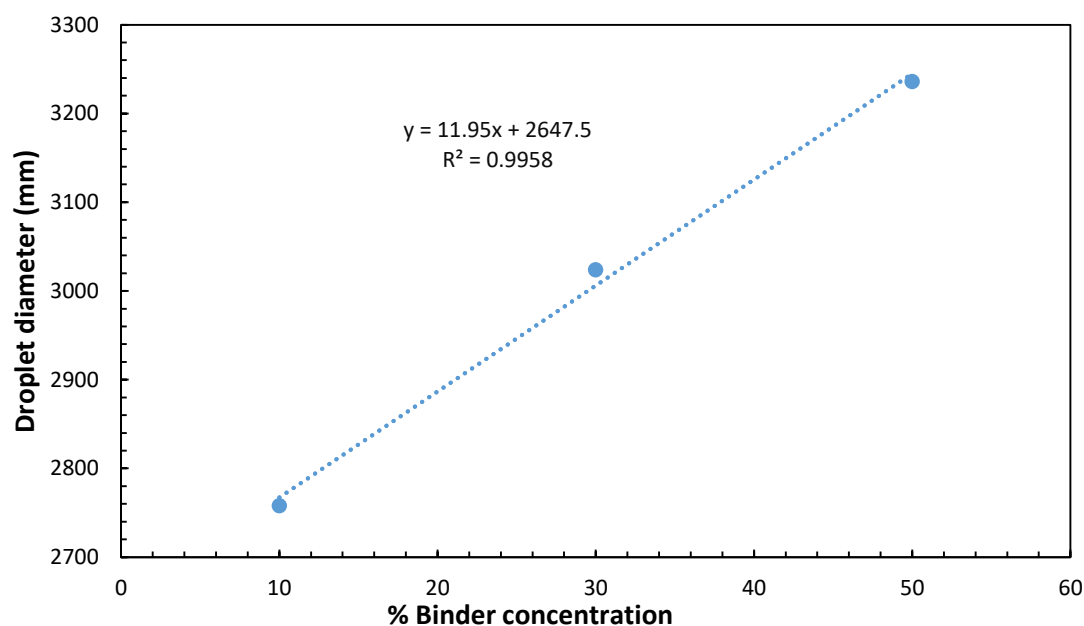


Figure 6.2: Calibration curve of droplet diameter and binder concentration.

The shear forces impacted on liquid marble or immersion nuclei in low and high shear granulation are considered using the Froude number; for more details see Section 4.3. The Froude number is higher using the high shear mixer (Table 6.6).

Table 6.6: Froude number data of low and high shear mixer.

Speed rate (rpm)	Drum internal diameter (m)	Gravitational acceleration (m/s)	Angular velocity (radian/s)	Froude number
25	0.035	9.81	2.61	0.024
370	0.7	9.81	38.70	107.15

6.3.1 Analysis of the powder blends

The dry powder mixtures of efavirenz and IROX were produced by mixing using a high shear mixer, as described in Section 6.2. Three different mixtures were investigated; 60%-40%, 50%-50% and 30%-70% of efavirenz and IROX respectively. The characterisation of dry powder blends was performed to investigate the distribution of efavirenz and IROX throughout the mixture, and later to compare the distribution of the efavirenz and IROX in the granules formed in both low and high shear mixers.

Figure 6.3 shows the particle distribution in different blends. In the 60%-40% efavirenz-IROX mixture, particles were distributed mostly along the edges and corners of efavirenz crystals, so that the sides of the crystals were IROX free (Figure 6.3 c). In the 30%-70% efavirenz-IROX mixture, IROX particles cover both the edges and the sides of the efavirenz crystals (Figure 6.3 d). In the 50%-50% efavirenz-IROX mixture, the sides of the efavirenz crystals were partially covered, in addition to edges and corners (Figure 6.3 e). The change in coverage of efavirenz crystals by IROX is consistent with the difference in mixtures wettability.

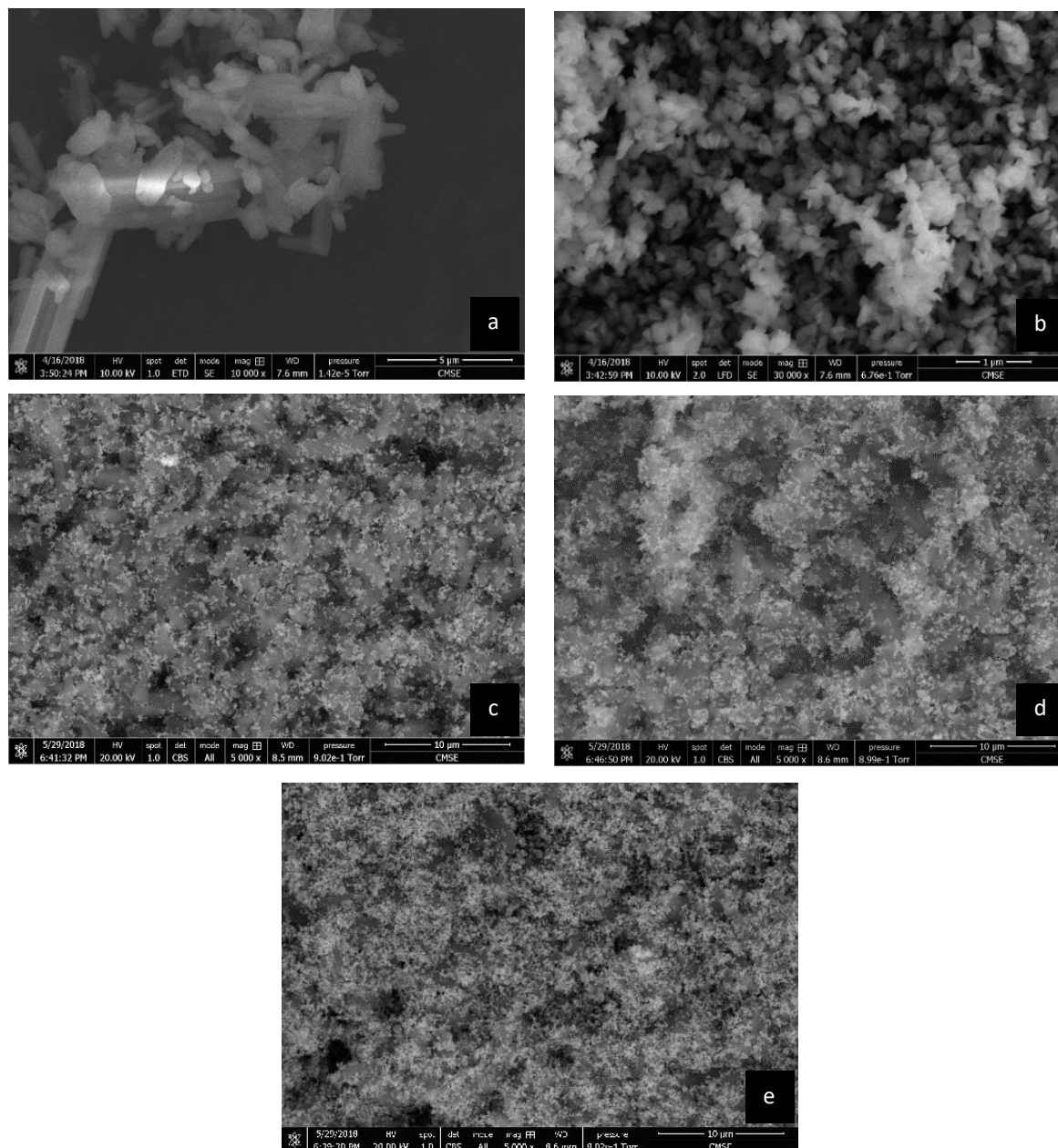


Figure 6.3: SEM images of efavirenz and IROX and the different blends of the two ingredients; (a) efavirenz, (b) Red iron Oxide (IROX), (c) 60% Efavirenz-40% IROX, (d) 50% Efavirenz-50% IROX, (e) 30% Efavirenz-70% IROX.

SEM imaging also revealed that mixtures containing 60%-40% and 50%-50% efavirenz-IROX contained undispersed cohesive agglomerates of iron oxide ranging from microns to tens of microns (Figure 6.4 a and b). It was also found that the powder in all as-prepared blends was partially agglomerated, i.e. consists of both agglomerates and non-agglomerated powder, with agglomerates ranging in size from tens of microns to hundreds of microns. Manipulation showed that the agglomerates were relatively soft and deform easily upon light compression

forming a continuous single powder bed. It was also found that the as-prepared blends have a strong tendency to self-agglomerate during sizing by Ro-Tap, forming dry agglomerates that were distributed on different sieve cuts mostly below 1 mm mesh size. Since the primary focus of the study was on granules formed by wet binder which were typically retained on the top sieve of 1 mm, dry agglomeration has not been investigated.

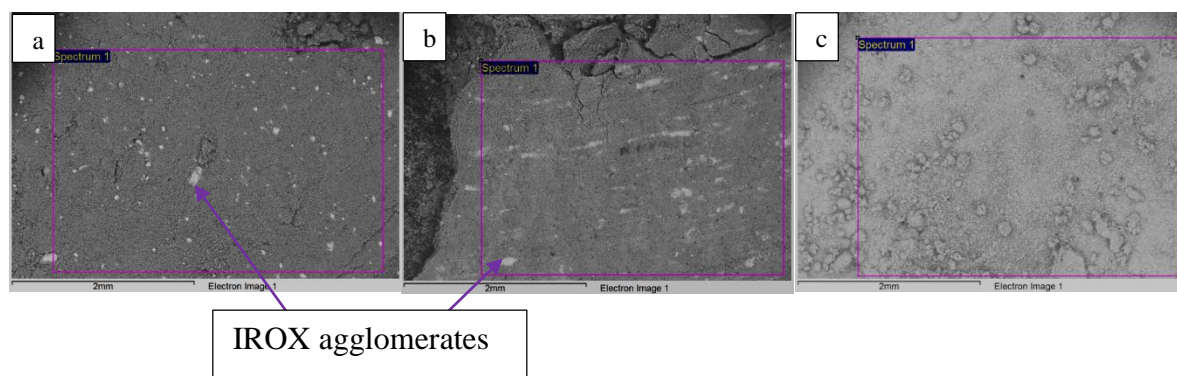


Figure 6.4: SEM images of compressed mixtures of (a) 60%-40% efavirenz-IROX, (b) 50%-50% efavirenz-IROX, (c) 30%-70% efavirenz-IROX.

In order to enable the identification of different components within the granules, EDX quantitative compositional analysis was performed for efavirenz, IROX, dextran and a mixture of different ratios of efavirenz and IROX (Table 6.7). The chlorine (Cl), ferrous (Fe) and carbon (C) ratios are sensitive to the presence of efavirenz, IROX and dextran respectively. The Fe/Cl ratio is sensitive to IROX and efavirenz composition only. For different powder blends, it can be seen that the Fe/Cl ratios increased with increasing the IROX percentage in the mixtures. Cl/C is sensitive to efavirenz and dextran only. The initial value of Cl/C is 0.16 in efavirenz only, while this percentage remained approximately the same in the mixtures of efavirenz and IROX. Fe/C is sensitive to both IROX-efavirenz blend composition and can be sensitive to dextran. The initial value is 11.31 in the IROX only component and this value increased with an increase in the percentage of IROX in the efavirenz-IROX mixtures. Comparative analysis of both Cl/C and Fe/C ratios could be used to elucidate presence of dextran.

Table 6.7: Compositional analysis of efavirenz, IROX, dextran and different mixtures of powder blends.

Elements ratios	Efavirenz	IROX	Dextran	60%-40% Efavirenz-IROX	50%-50% Efavirenz-IROX	30%-70% Efavirenz-IROX
C	54.8	5.5	46.7	35.74	31.62	21.5
N	5.0	0	0	3.53	0	0
O	9.9	32.3	53.3	20.54	22.92	27.51
F	21.4	0	0	13.83	10.47	6.1
Cl	9	0	0	5.22	4.65	2.58
Fe	0	62.2	0	21.14	30.34	42.32
Ratios						
Fe/Cl	0	0	0	4.0	6.5	16.4
Cl/C	0.16	0	0	0.15	0.15	0.15
Fe/C	0	11.31	0	0.59	0.96	1.97

XRCT images of the initial blends, 60%-40%, 50%-50% and 30%-70%, of efavirenz-IROX that were used for the experiments can be seen in Figure 6.5. Bright white contrast indicates agglomerates of IROX. A large volume of each blend exists as agglomerates (size range: tens of microns to hundreds of microns). In addition, compositional inhomogeneity of agglomerates ranges from micro scale to macro scale: from inclusions of undispersed agglomerates of IROX and efavirenz (macro) to efavirenz/IROX ratio deviating from nominal value in the powder blend in different areas of an agglomerate (micro). There were some IROX agglomerates in the 60%-40% and 50%-50% efavirenz-IROX blends (Figure 6.5 a and b). The inhomogeneity decreased with an increase in IROX ratio in the blend (Figure 6.5 c).

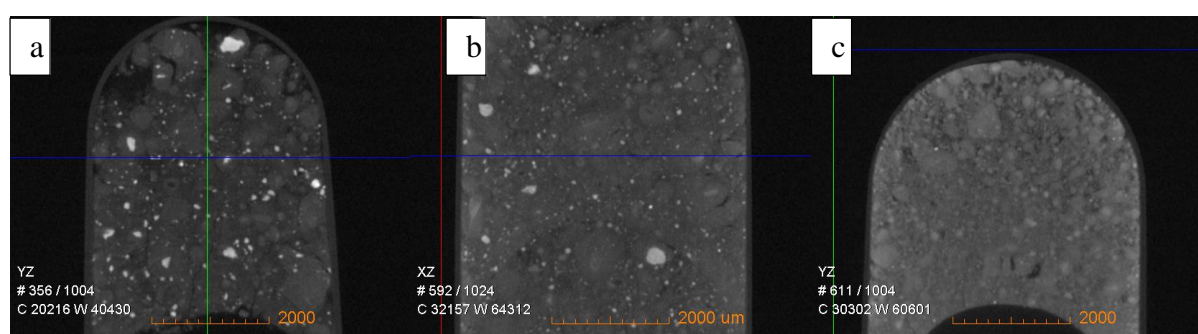


Figure 6.5: Images of primary blends of efavirenz-IROX in different ratios (a) 60%-40%, (b) 50%-50%, (c) 30%-70%. (Reconstructed XRCT images; representative central cross-section).

6.3.2 Single drop nucleation

Experiments initially focused on nucleation of the wetting and non-wetting pharmaceutical powder formulations, prior to granulation in both low and high shear mixers. The main aim of this part of the work is to form a base line for comparison of granule size and internal microstructure of pre-nucleated granules with granules formed after granulation in low and high shear mixers.

Figure 6.6 shows the size of the initial liquid droplets (ILD) and the size of the dried liquid marbles or immersion nuclei, produced using different binder viscosities and powder wettabilities. For low and medium powder wettabilities, smaller granules were produced using low binder viscosity. While, a larger granule size can be seen using higher binder viscosities of 100 and 1000 mPa s. For powder of high wettability, the lower binder viscosity produced granules that were larger in size than those produced using high binder viscosity (Figure 6.6).

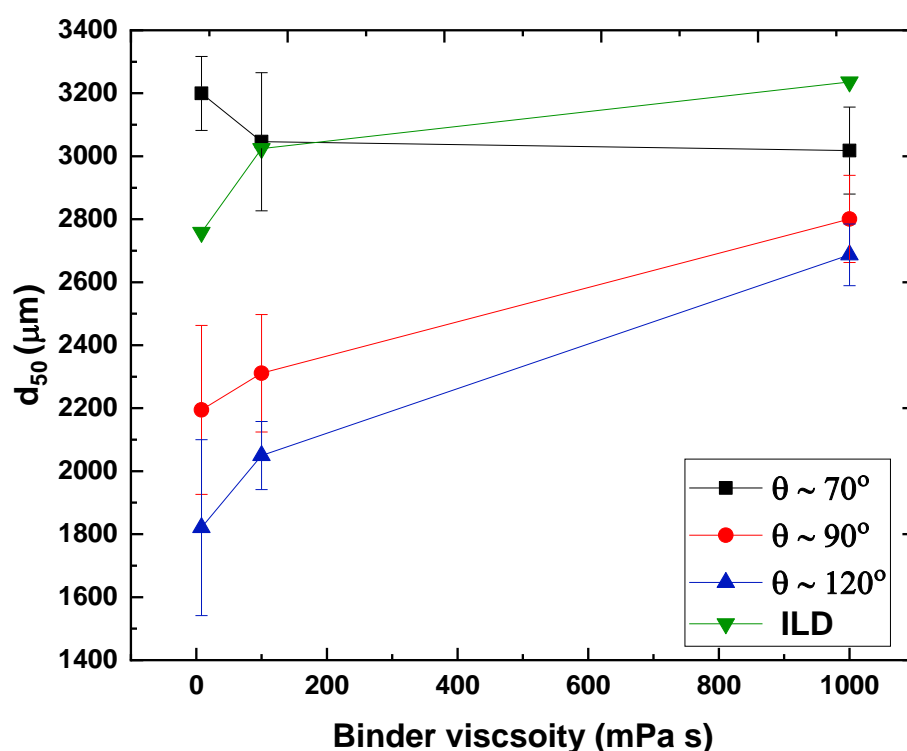


Figure 6.6: Particle size of dried liquid marbles or immersion nuclei of different powder wettabilities and binder viscosities, obtained via image analysis. The error bars are the standard deviation of the ten measurements. θ is liquid powder contact angle.

Figure 6.7 shows images of ILD and the size of the dried liquid marbles or immersion nuclei, produced using different binder viscosities and powder wettabilities. For low powder wettability, buckled granules with one or more depressions were obtained at low binder viscosity. However, spherical granules were obtained at medium and high binder viscosities. For medium powder wettability, at low binder viscosity, the liquid marbles were collapsed into hemispheres upon drying. At medium binder viscosity, buckled hemispherical granules were obtained. However, only spherical granules were obtained using high binder viscosity. For high powder wettability, semi-spherical granules were produced using low and medium binder viscosities, while spherical granules were produced using high binder viscosity.

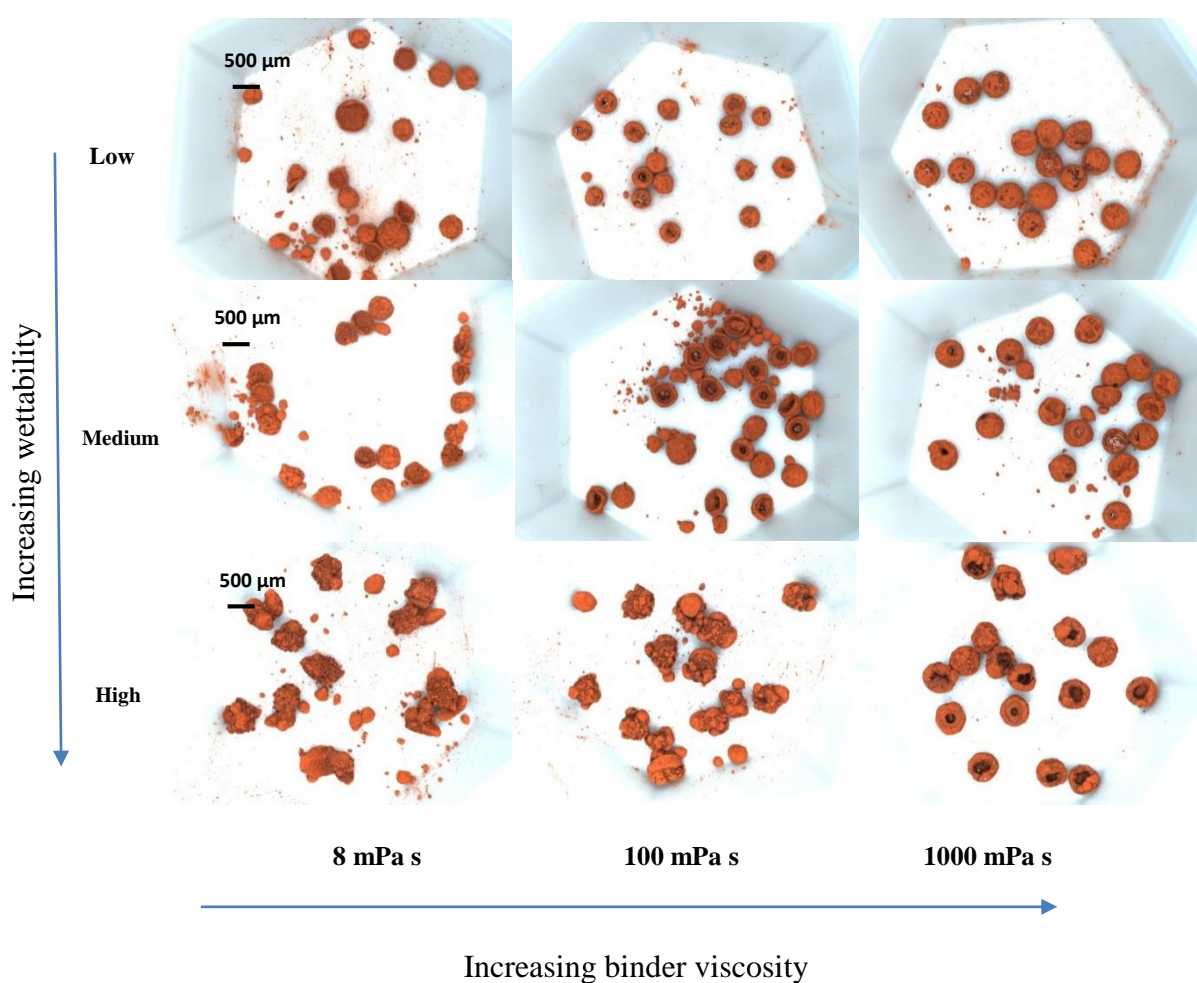


Figure 6.7: Comparison of dried liquid marbles or immersion nuclei of different powder wettabilities and binder viscosities.

Table 6.8 shows the % of change of the size of the dried liquid marbles or immersion nuclei compared to the size of ILD. For powder of low and medium wettability, the final granule size was smaller and decreased monotonically with a decrease in binder viscosity, relative to the

size of ILD. For powder of high wettability, the final granules size was larger using low and medium binder viscosities, while the final granules size was smaller using high binder viscosity, relative to the size of ILD.

Table 6.8: Summary of % change in size of dried liquid marbles or immersion nuclei in relation to the size of initial liquid droplets.

Non wetting – wetting mixture	Binder viscosity (mPa s)	Powder/ liquid contact angle °	Size (µm)		% granule size change
			Initial liquid droplet	Dried liquid marble or immersion nuclei	
60%-40%	8	125.25	2758	1821.0	-33.97
60%-40%	100	130.05	3024	2049.7	-32.21
60%-40%	1000	141.35	3236	2686.7	-16.97
50%-50%	8	89.43	2758	2194.8	-20.42
50%-50%	100	92.83	3024	2310.9	-23.58
50%-50%	1000	128.63	3236	2800.9	-13.44
30%-70%	8	63.51	2758	3199.4	16.0
30%-70%	100	72.37	3024	3046.0	0.72
30%-70%	1000	94.33	3236	3017.9	-6.73

The decrease in granule size with decreasing binder viscosity of low and medium powder wettabilities is probably due to the formation of weak liquid marbles. Liquid marbles were collapsed into hemispheres or buckled granules after drying using low and high binder viscosities respectively.

The increase in granule size with decreasing binder viscosity using high powder wettability is probably due to a low penetration time of low viscous binder through a high wetting powder bed, leading to powder layering at the surface of nuclei.

Spherical granules were produced using high binder viscosity regardless of powder wettability. This is likely due to the viscous force effect, which decreases liquid droplet deformation. This result is in agreement with Hapgood & Khanmohammadi, 2008. They studied the effect of different powder wettabilities and binder viscosities on the formation and stability of liquid marbles using nucleation experiments. Different non-wetting drugs such as salicylic acid and 2-ethoxybenzamide and non-wetting glass beads were used. Binder viscosities, ranging from 1 to 152 mPa s. were used. Stable liquid marbles were formed with low binder viscosity. However, these liquid marbles collapsed into hemispheres after drying due to insufficient binding forces between the particles.

Similarly, Eshtiaghi, Liu, & Hapgood, 2009 investigated the effect of binder viscosity on the stability of liquid marbles and the formation of hollow granules after drying using nucleation drop experiments. Glass beads, polytetra fluoroethylene and fumed silica were used as non-wetting powders. Hydroxypropyl methylcellulose (HPMC) with different concentrations and viscosities were used as liquid binder. They found that as the concentration of HPMC increased there was an increase in the stability and survivability of hollow granules. It was concluded that for the liquid marbles to collapse, the drop must be deforming which requires internal fluid flow. They proposed that at a higher binder viscosity the binder resists the internal fluid flow which therefore increases liquid marbles stability during drying.

6.3.2.1 Internal structural analysis

Figure 6.8 presents XRCT images of representative granules as a function of both powder wettability and binder viscosity. For powder of low wettability, hemispherical granules were observed using low binder viscosity. Hollow granules with a thick wall thickness were observed using medium and high binder viscosities.

For powder of medium wettability, hemispherical granules can be seen using low binder viscosity. Granules with some pores inside were observed using medium binder viscosity. Hollow granules with thin wall thickness can be seen using high binder viscosity.

For powder of a high wettability, the microstructure changed from single solid granules using low and medium binder viscosities to granules with small agglomerates bound together using high binder viscosity. It is expected that the liquid droplets are dried surrounded by the accumulation of powder agglomeration; in another words, inhomogeneous distribution of powder around the liquid droplet. This may be due to that the nuclei formation occurred by a tunneling mechanism.

Emady, Kayrak-Talay, Schwerin, & Litster, 2011 found that a tunneling mechanism was observed with fine cohesive powder; such as the powder used in this work. Cohesive powder formed a large loose aggregate with high powder bed porosity. These dry aggregates were the sucked inside the droplet which tunnels into the powder bed. This leads to collecting up dry

aggregates from the new surface. Therefore, the nucleus has a spherical core with some protrusions on the granule surface. The protrusions were caused by dry agglomerates going into the droplet. For more details, see Section 2.5.1.

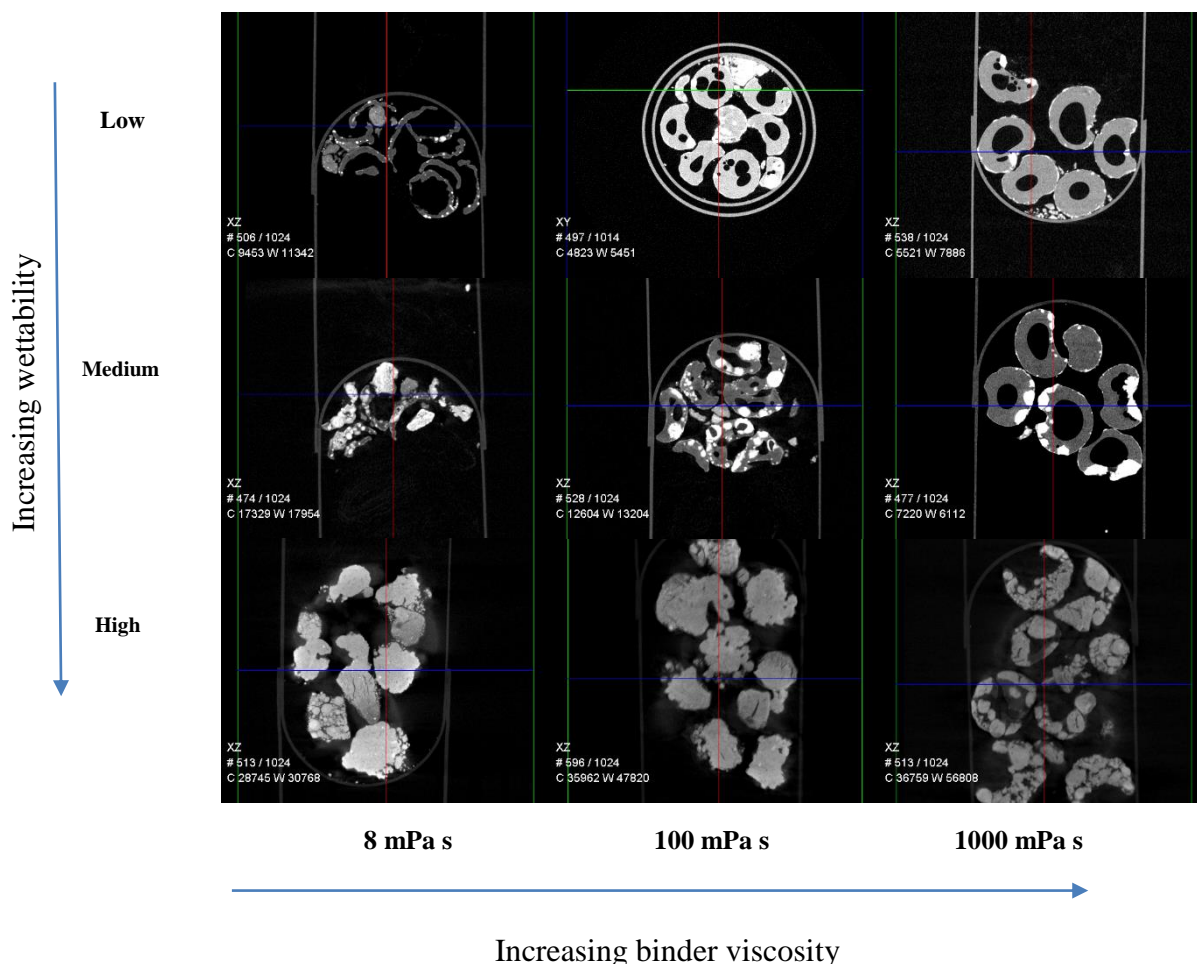


Figure 6.8: Images of dried liquid marbles or immersion nuclei of different powder wettabilities and binder viscosities. (Reconstructed XRCT images; representative central cross-section).

An in situ XRCT was performed for granules produced using high powder wettability and low binder viscosity in order to understand the resultant granule shape. The liquid droplet penetrated the powder bed quickly (within a second) and formed nuclei with a secondary wetted outer shell (Figure 6.9 a). Then, after 15 min of drying the granule kept its shape with a dense core and secondary outer shell (Figure 6.9 b). These images are in accordance with the microscope images, in which there is a shell surrounding the granule core.

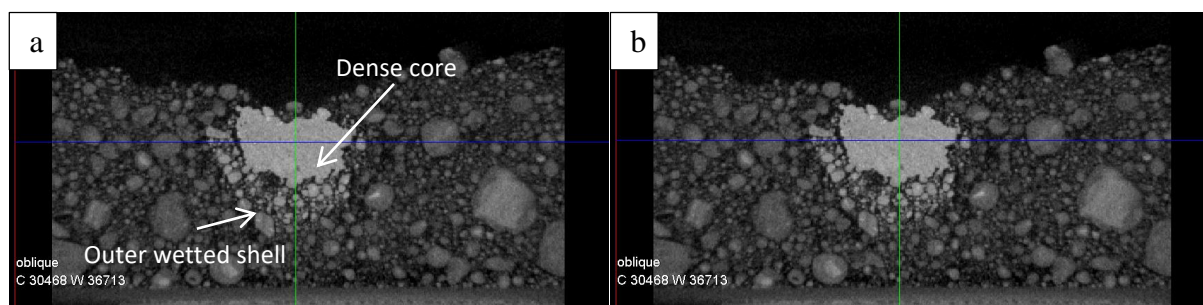


Figure 6.9: Images of immersion nuclei of powder of high wettability and low binder viscosity (a) wet immersion nuclei (b) dry immersion nuclei. (Reconstructed XRCT images, representative central cross-section).

An in-situ XRCT was also performed using powder of low wettability and high binder viscosity in a petri dish. The powder surrounded the liquid droplets during the nucleation stage and formed liquid marbles (Figure 6.10 a). After 2 hours of drying, formation of an interior void was observed, in addition to the formation of a collapsed surface (Figure 6.10 b). The same finding was observed after 14 hours of drying. However, there was an increase in the size of the void at the core of the granule (Figure 6.10 c). It should be noted that during manual granulation (hand rolling by orbital hand motion within the petri dish), see Section 6.2, periodic formation and then breakage of an exterior shell was observed. This confirmed the propensity of dry self-agglomeration of efavirenz or IROX due to the weak binding forces of dry agglomerates. In addition, it can be concluded that voids and an open hole on the surface of some of the granules occurred during the drying stage.

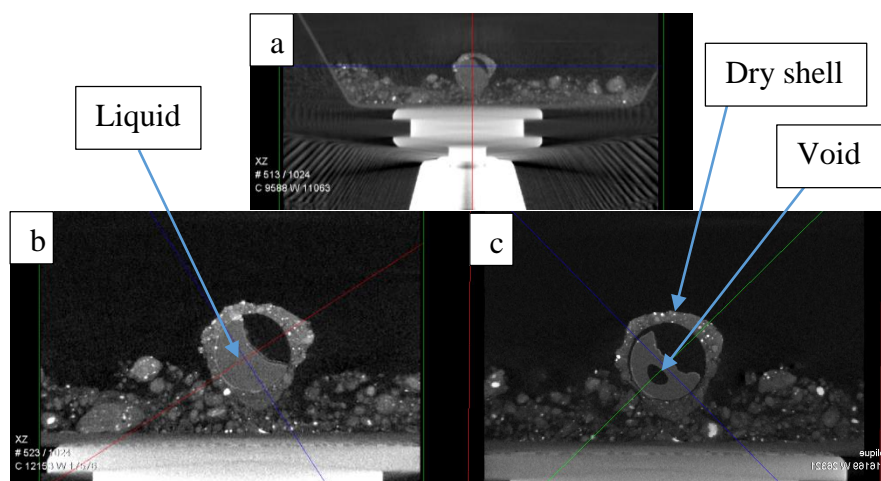


Figure 6.10: Images of a liquid marble of powder of low wettability and high binder viscosity (a) wet liquid marble (b) after drying for 2 hr (c) after drying for 14 hr. (Reconstructed XRCT images; representative central cross-section).

6.3.3 Granulation in a low shear mixer

In this section, experiments focus on the granulation of different powder wettabilities and binder viscosities in a low shear mixer (note that this is the same low shear tumbling mixer as that used throughout Chapter 4). The aim of this part of the research is to investigate the effect of different parameters on granule size, internal microstructure and ingredient distribution. Granulation was performed using 25 rpm tumbling speed and 5 min granulation time.

Figure 6.11 shows the size of initial liquid droplets (ILD) and the size of granules produced using different powder wettabilities with contact angles ranging from 70° to 130° , and different binder viscosities of 8, 100 and 1000 mPa s. For different powder wettabilities, an increase in the size of granules with decreasing binder viscosity was observed.

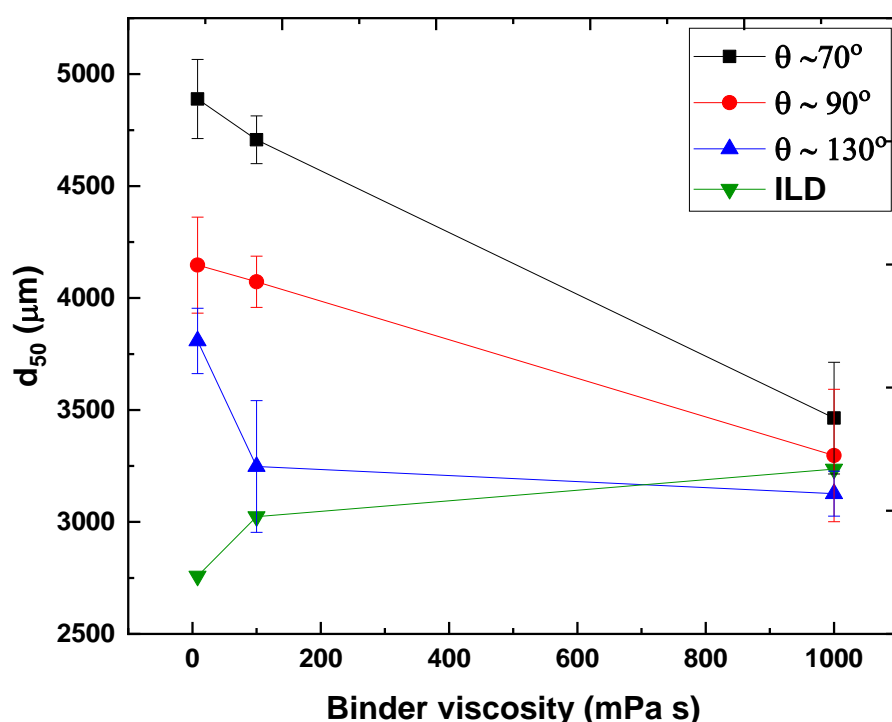


Figure 6.11: Particle size of granules produced using different powder wettabilities and binder viscosities, obtained via image analysis. The error bars are the standard deviation of the ten measurements. θ is liquid powder contact angle.

Figure 6.12 shows microscopy images of granules produced using different powder wettabilities and binder viscosities in low shear mixer. For low powder wettability, a mixture

of semi-spherical and elongated granules was produced using low and medium binder viscosities. Spherical granules were obtained using higher binder viscosity. For medium powder wettability, spherical granules were obtained using low and high binder viscosities, while a mixture of semi-spherical and elongated granules were produced using medium binder viscosity. For high powder wettability, elongated granules were produced using low and medium binder viscosities. Buckled and semi-spherical granules were obtained using high binder viscosity.

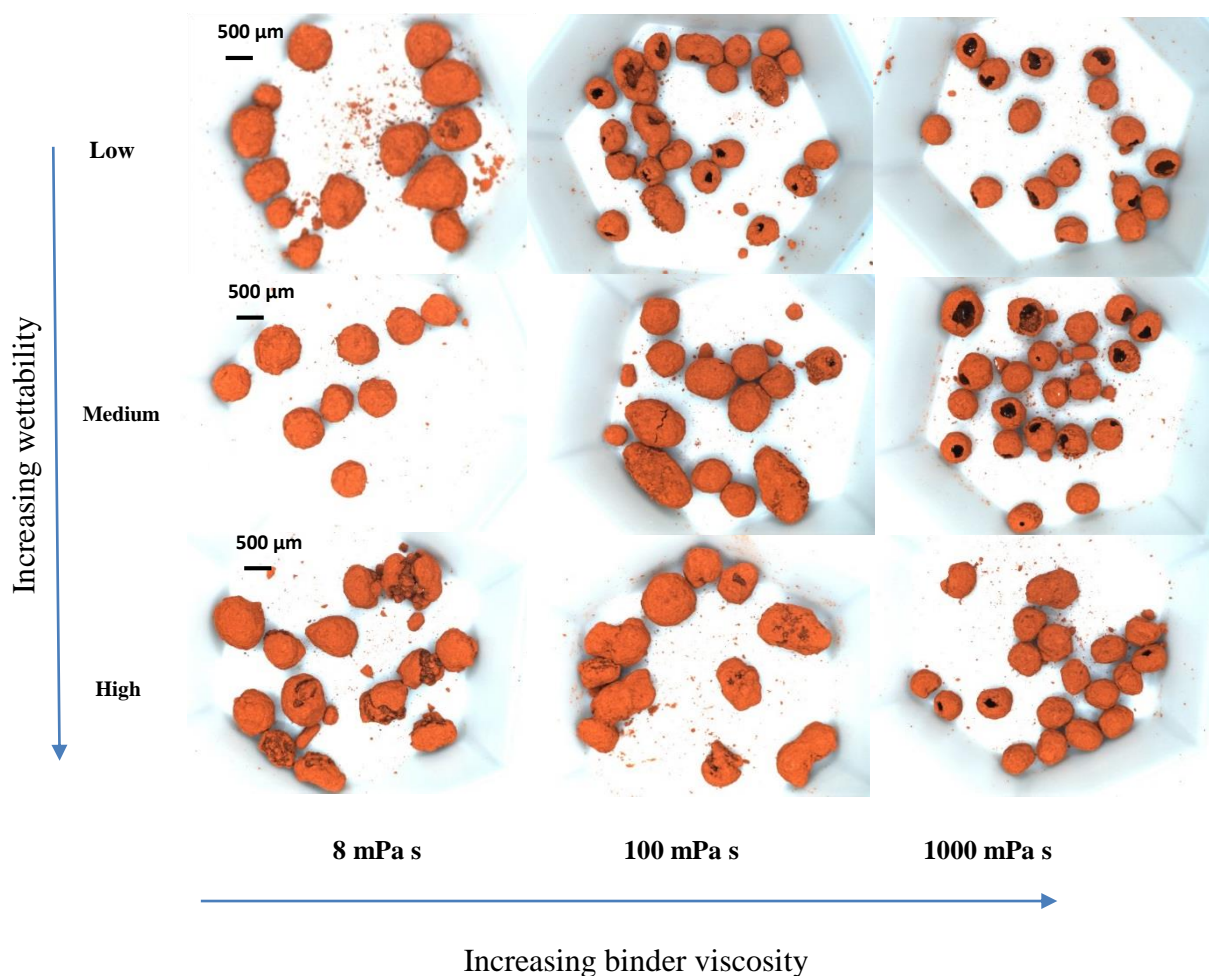


Figure 6.12: Comparison of granules of different powder wettabilities and binder viscosities.

Table 6.9 shows the % of change of the size of granules to the size of the ILD produced using different powder wettabilities and binder viscosities. For powder of low wettability, the final granules size was smaller using high binder viscosity, while the final granule size was larger using medium and low binder viscosities, relative to the size of the ILD. For powder of high

and medium wettabilities, the final granule size was larger and increased monotonically with decreasing binder viscosity, relative to the size of the ILD.

Table 6.9: Summary of % change in size of granule in relation to size of initial liquid droplet.

Non wetting-wetting mixture	Binder viscosity (mPa s)	Powder/liquid contact angle °	Size (µm)		% granule size change
			Initial liquid droplet	Dried granules	
60%-40%	8	125.25	2758	3808.67	38.09
60%-40%	100	130.05	3024	3248.03	7.40
60%-40%	1000	141.35	3236	3126.04	-3.39
50%-50%	8	89.43	2758	4147.21	50.37
50%-50%	100	92.83	3024	4072.7	34.67
50%-50%	1000	128.63	3236	3296.86	1.88
30%-70%	8	63.51	2758	4888.65	77.25
30%-70%	100	72.37	3024	4707.08	55.65
30%-70%	1000	94.33	3236	3463.9	7.04

The increasing granule size with decreasing binder viscosity is probably due to a low penetration time of the low viscous binder. However, using the high binder viscosity prolonged the penetration time and increased the powder liquid contact angle which inhibited granule consolidation and then growth.

This is agreement with Tan, Wong, Lum, & Hapgood, 2009, who studied the effect of binder viscosity on penetration time and nuclei size using foam and drop penetration experiments. Glass beads and lactose monohydrate as powder with different concentrations of HPC and HPMC as liquid binder were used. They found that using low binder viscosity allow a faster penetration of the liquid through the powder pores, which was likely to form larger nuclei and then granules with good liquid distribution. This was unlikely to occur using higher binder viscosity.

Comparing the effect of binder viscosity on granule size using the model powder in Chapter 4, Section 4.3.1 with pharmaceutical powder in this Chapter, it is obvious that there is a difference in granule behaviour. For the pharmaceutical powder, the granule size decreased with increasing binder viscosity using different powder wettabilities. However, for the model powder, the opposite trend was observed using low and high powder wettabilities. For pharmaceutical powders, the binder with low viscosity can penetrate easily through the highly

cohesive powder bed resulting in larger nuclei and then granule size. However, for model particles the weak binding forces between the glass beads powder and low binder viscosity make the liquid marbles unable to resist the impact forces applied during granulation which leads to either fine powder or small granules due to breakage or attrition respectively.

6.3.3.1 Internal structural analysis

Internal granule microstructure was characterised using XRCT and SEM. XRCT was used to investigate the granule internal microstructure behaviour and porosity of the granules produced using different parameters. SEM and EDX were used to investigate ingredients distribution and ingredients ratio within the granules respectively.

6.3.3.1.1 XRCT analysis

Figure 6.13 confirms that hollow granules are produced using medium and high binder viscosities for different powder wettabilities.

For high binder viscosity, the granules consist of two layers: pure binder (inner) and powder-containing layer (outer).

For medium binder viscosity, three different granule internal structures were observed depending on powder wettability. For low powder wettability, granules of two layers; powder and binder were observed. The medium powder wettability produced hollow granules with no binder layer or core. For high powder wettability, there was a distinct void in many of the granules produced. The granules are surrounded by what appears as consolidated original nucleus as the core (with no inner binder layer as for the low powder wettability), surrounded by the distinct exterior layer of granulated powder.

For low binder viscosity, the internal morphologies were core-shell, and the outline of the original agglomerate can still be distinguishable. For the core-shell granules, powder layer thickness was relatively consistent around the granule for the low and medium powder wettabilities, in contrast to those for high powder wettability, where the lumpy interface suggests that pre-existing dry cohesive agglomerates within the initial blend were wetted, captured and pulled into the liquid droplet with limited deformation.

The granulation of low powder wettability with high and medium binder viscosity resulted in the formation and growth of a mixed powder/binder layer on top of the binder droplet surface which indicates a constructive and critical role of both the impact forces and the viscous forces. Immersion of low wettability powder particles into the surface of the liquid droplet by the impact forces resulted in the retention of that material in the liquid droplet due to viscous interactions. The negative contribution from capillary forces is apparently overcome. Reducing impact forces (as in single drop experiments; Section 6.3.2) practically eliminates granule growth. Reducing binder viscosity changes the internal granule structure from hollow granules to core/shell.

The core-shell structure of granules produced using low binder viscosity agrees with Pitt, Smith, de Koster, Litster, & Hounslow, 2018. They proposed that this might be due to the formation of the nuclei from binder and powder and then a secondary migration of the liquid to the surface after nuclei has been formed.

Similarly, Nguyen, Shen, & Hapgood, 2009 proposed the core-shell microstructure produced using low binder viscosity. Salicylic acid and lactose monohydrate as powder and water as liquid binder were used. They suggested that, after the initial formation of a core-saturation region, the immersion of liquid through the powder bed became weaker, but was enough to bind the powder particles together. The immersion of liquid through the particle then led to the formation of semi-saturated shell around the saturated core of the granule. This semi-saturated shell can break away during handling due to the weak binding forces.

The most obvious difference between representative XRCT images of dried nuclei (without tumbling) (Figure 6.8) and tumbled nuclei (Figure 6.13) is that the tumbling allowed more powder incorporation, structured symmetry and reinforcement. A similar prevalence of shell or hollow granules indicates that hollow granules produced from high binder viscosity primarily arise from the classic drying mechanism in which evaporation increase out surface viscosity to the point that droplet shrinkage is too slow to prevent nucleation of gas bubbles.

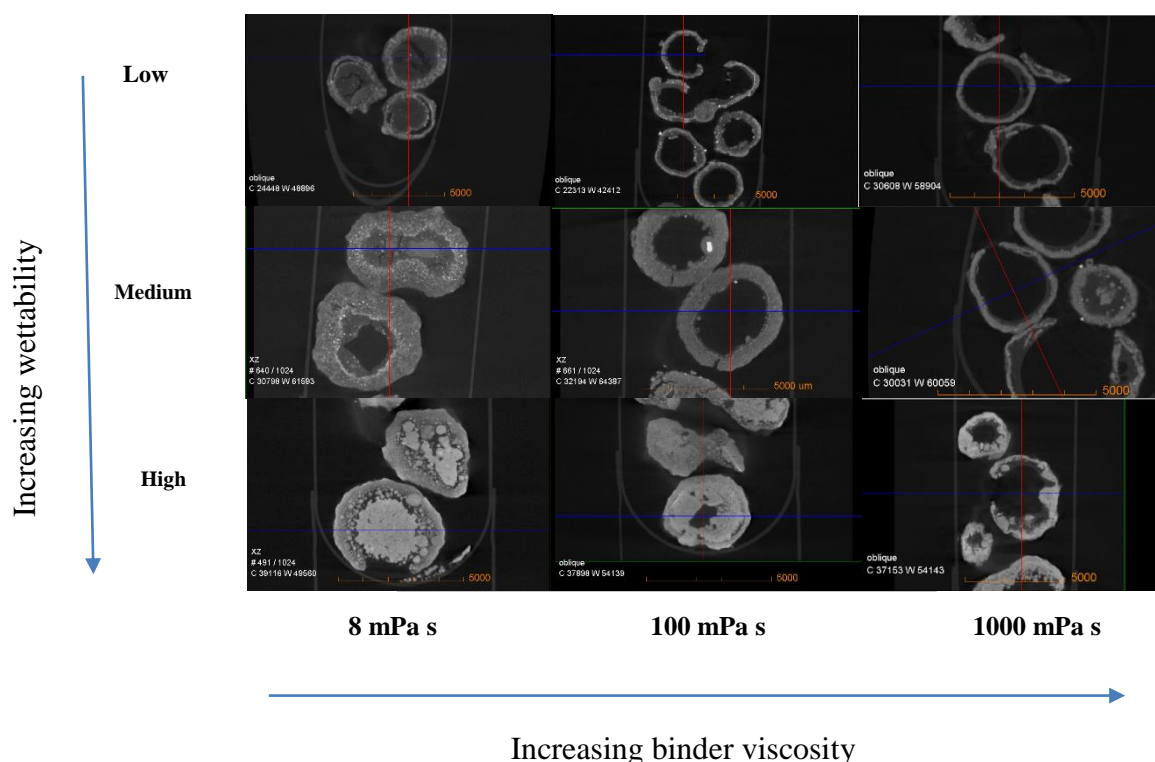


Figure 6.13: Images of granules of different wettabilities and different binder viscosities. The outer rings are part of the sample container. (Reconstructed XRCT images; representative central cross-section).

6.3.3.1.1 Porosity

Figure 6.14 expresses the percentage total porosity as a function of binder viscosity and powder wettability.

For all powder wettabilities, the granule porosity increased with increasing binder viscosity. This is probably because the low binder viscosity penetrates into the powder bed easily, and upon collisions inside the granulator, further powder imbibition occurred leading to the lower granule porosity. However, it is expected that the immersion of the liquid into the powder is decreased using high binder viscosity. In addition, drop deformation is decreased with high binder viscosity leading to an increase in granule porosity. This is in agreement with Ennis, Tardos, & Pfeffer, 1991 and Iveson & Litster, 1998 who proposed that the higher binder viscosity led to low rates of granule consolidation and high granule porosity; for more details see Section 4.3.1.2.1.

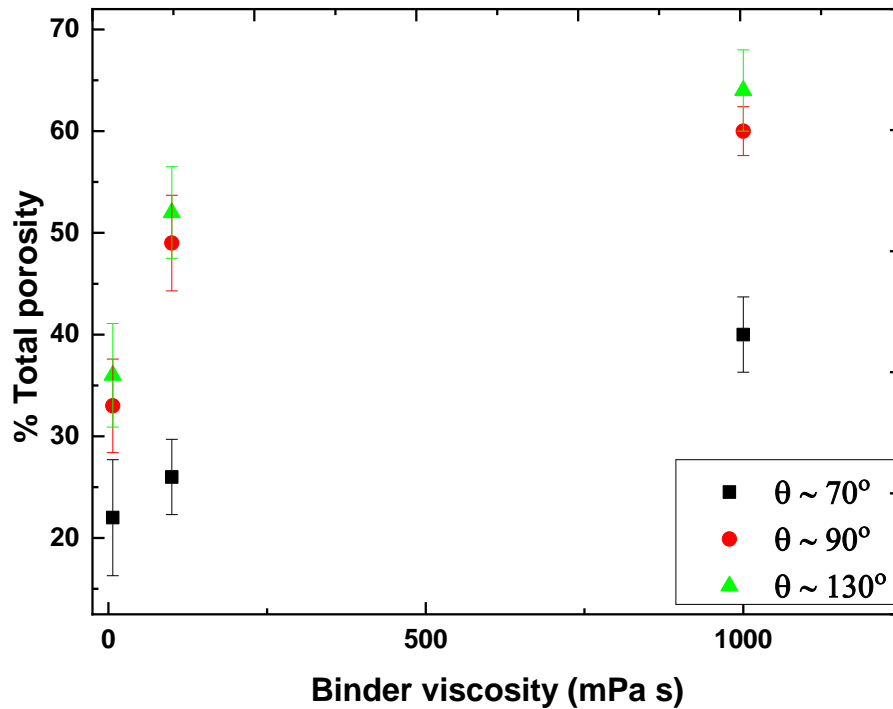


Figure 6.14: Total porosity as a function of binder viscosity and powder wettability. The error bars are the standard deviation of three measurements. θ is liquid powder contact angle.

This is agreement with Johansen & Schafer, 2000, who studied the effect of binder viscosity on granule porosity using melt granulation experiments in a high shear mixer. Lactose was used as a powder and different molecular weight PEGs (2000, 3000, 6000, 8000, 10000 and 20000) were used as a liquid binder. At a higher liquid viscosity, the granule porosity was noticeably higher than with lower binder viscosity. This was because the higher binder viscosity gave rise to a lower liquid saturation and lower granule deformation and high granule porosity.

6.3.3.1.2 SEM analysis

Figure 6.15 shows SEM images of selected granules of different powder wettability and binder viscosity. SEM images of selected granules in Figure 6.15 compares well with the XRCT images in Figure 6.13.

For the high binder viscosity, the granules consist of two layers: pure binder (inner) and powder-containing layer (outer). SEM imaging of low powder wettability and high binder viscosity with higher magnification (1000 X) demonstrated that the outer layer was a powder blend that was infused with binder.

For the medium binder viscosity, it was a balanced condition in which there was no binder layer or core. There were small spherical granules decorating the inner surface that suggest formation in-situ by cleaving and rolling of partially wetted powder from the inner surface during tumbling.

For low binder viscosity, the core shell structure consists of a relatively dense core and a relatively brittle and weak shell.

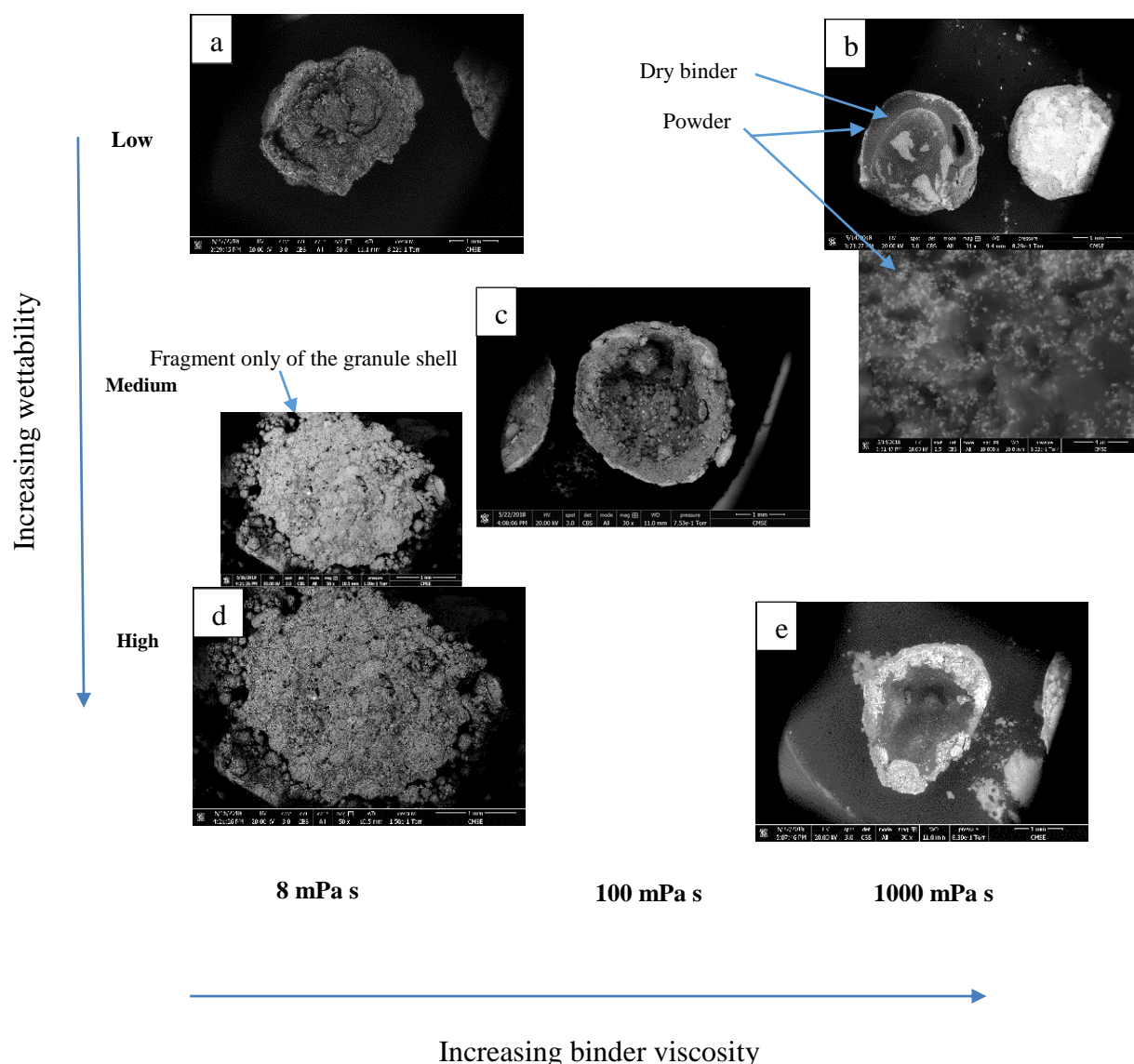


Figure 6.15: SEM images of granules produced using different powder wettabilities and different binder viscosities.

6.3.3.1.2.1 EDX analysis

Figure 6.16 shows composition analysis of granules obtained from powder of low wettability and different binder viscosities. The blue is the IROX rich area, the red is the efavirenz rich area and the green is the binder rich area. For granules produced using low binder viscosity, spectrum 1 (randomly selected area to investigate element distribution) is near the core, spectrum 2 between the core and the shell and spectrum 3 near the shell. For granules produced using high binder viscosity, spectrum 1 is in the core, spectrum 2 in the layer adjacent to the core and spectrum 4 near the shell. In Figure 6.16 a, it can be seen that the granule shell

produced from low binder viscosity is rich in IROX while the granule core is rich in efavirenz. However, Figure 6.16 b, using high binder viscosity, the shell is rich with IROX, the middle layer is rich with efavirenz and the core contains only binder.

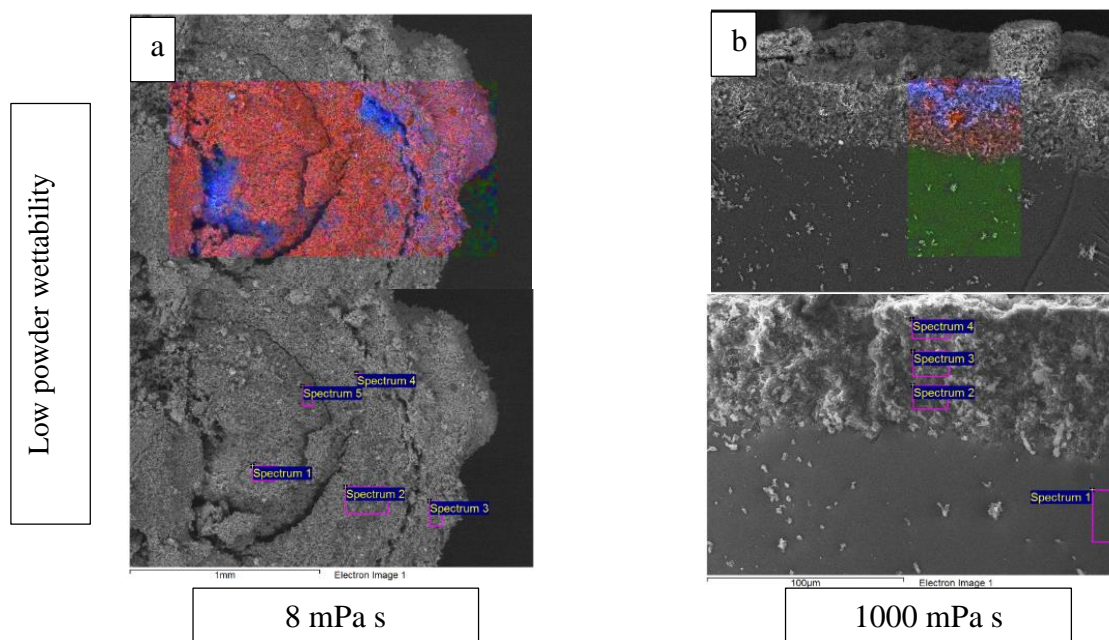


Figure 6.16: Compositional analysis of granules produced using low powder wettability and different binder viscosities.

A comparison of the elemental ratio in the powder blends and granules produced using low powder wettability can be seen in Table 6.10.

For granules produced using low binder viscosity, the Fe/Cl ratio in spectrum 1 and spectrum 2 is 1.6 which is lower than the nominal value in the powder blend. This indicates that the core and the middle of the granule are deficient with IROX and enriched with efavirenz. However, this ratio increased to 3.4 at granule shell which is close to the nominal value in the powder blend and this indicates that this area is rich with IROX. The Cl/C ratio is approximately equal to the nominal value in powder blend; this indicates the presence of binder and efavirenz throughout the granule. Fe/C ratios of 0.21, 0.22 and 0.40 for spectra 1, 2 and 3 respectively are lower than the nominal value in the powder blend of the corresponding composition. This indicates that the binder is distributed inside the granule which is consistent with morphology seen using SEM (Figure 6.15 a).

For granules produced using high binder viscosity, the Fe/Cl and Cl/C ratios in spectrum 1 is zero which indicates that there is no IROX and efavirenz in the core and the core contains only binder.

binder. However, this ratio increased to 1.7 and 5.6 in spectrum 2 and spectrum 4 respectively, which indicates that the ratio of IROX increases towards the shell. The Cl/C ratio of 0.11 in spectrum 2 is close to the nominal value and indicates that this area is enriched with efavirenz. Fe/C ratio of 0.02, 0.18 and 0.43 for spectra 1, 2 and 4 respectively are lower than the nominal value in the powder blend. This indicates that the core and the middle of the granule is deficient with IROX and rich with binder and efavirenz.

Table 6.10: Elemental ratio comparisons in powder blends and granules produced using low powder wettability and different binder viscosities.

Elements	Powder blends (efavirenz-IROX) 60%-40%	Granules 60%-40% (efavirenz-IROX)					
		Binder viscosity (mPa s)					
		8			1000		
		Spectrum 1	Spectrum 2	Spectrum 3	Spectrum 1	Spectrum 2	Spectrum 4
Fe/Cl	4.0	1.6	1.7	3.4	0	1.7	5.6
Cl/C	0.15	0.14	0.13	0.12	0	0.11	0.08
Fe/C	0.59	0.21	0.22	0.40	0.02	0.18	0.43

Figure 6.17 presents compositional analysis of granules obtained from powder of medium wettability and different binder viscosities.

The blue indicates the IROX rich area, the red is the efavirenz rich area and the green is the binder rich area. In Figure 6.17 a, spectrum 1 is near the core and spectrum 3 is near the shell. In Figure 6.17 b, spectrum 2 is near the shell and spectrum 1 is near the core. The granule shell appears be rich in IROX while the granule core is rich with efavirenz using low and medium binder viscosities.

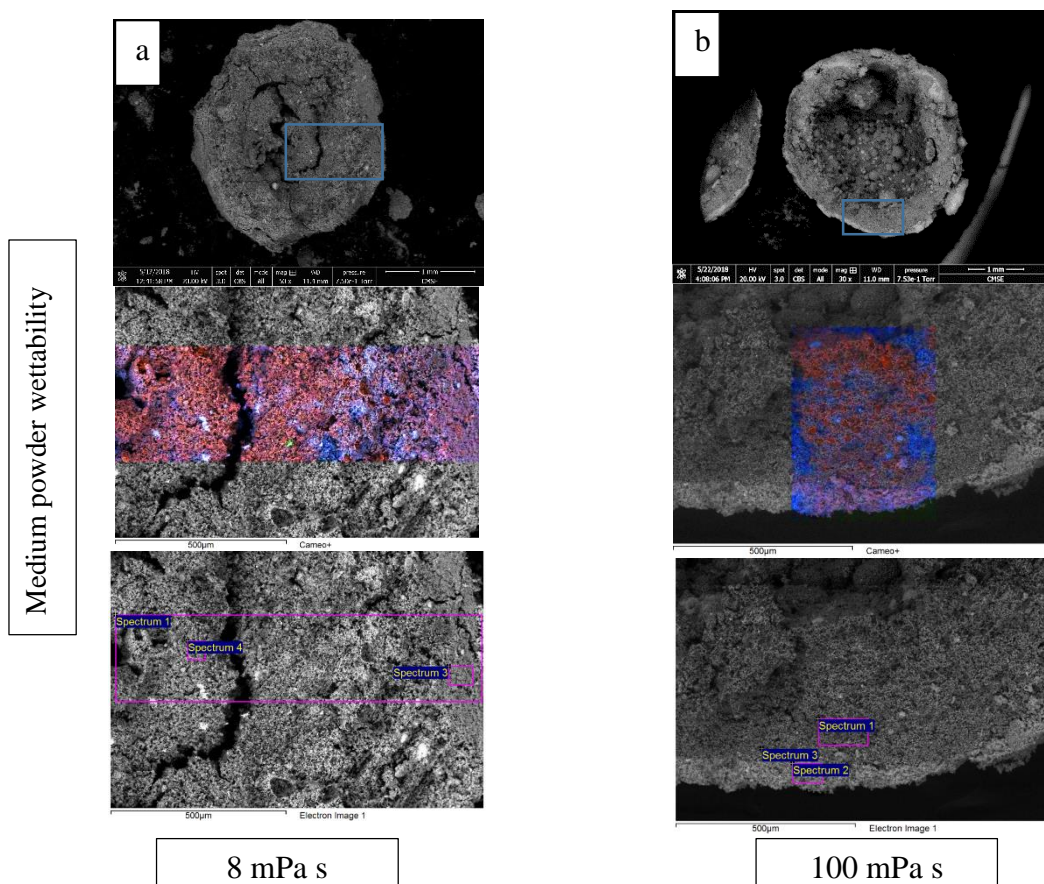


Figure 6.17: Compositional analysis of granules produced from medium powder wettability and different binder viscosities.

A comparison of the elemental ratio in the powder blends and granules produced using medium powder wettability can be seen in Table 6.11.

For granules formed using low binder viscosity, the Fe/Cl ratio in spectrum 3 is 5.1 which is close to the nominal value in the powder blend and this indicates that there is more IROX than efavirenz at the granule shell. However, this ratio decreased to 2.5 in spectrum 4, indicating that the ratio of IROX decreases and efavirenz increases towards the core. Cl/C ratios of 0.11 and 0.13 in spectrum 3 and spectrum 4 respectively are lower than the nominal value which indicates that this area is enriched with binder and efavirenz. Fe/C ratios of 0.58, 0.32 for spectrum 3 and spectrum 4 respectively are lower than the nominal value in a powder blend. This indicates that the binder is distributed throughout the granule. The IROX ratio increased at the granule shell. The shell is enriched in IROX, especially in the region close to core/shell interface. The core part appears to consist of the compressed original blend, with some dry

aggregates. The core has more developed cracks than in the non-wetting powder and potentially some narrow voids.

For granules produced using medium binder viscosity, the Fe/Cl ratio increases from 5.3 in spectrum 1 to 12.8 in spectrum 2. This indicates that the granule shell is enriched with IROX and deficient with efavirenz. The Cl/C ratio is 0.1 in spectrum 1 and 2 which is lower than the nominal value in the powder blend and this indicates that the binder is distributed in this area. The Fe/C ratio is 0.53 in spectrum 1 which is lower than the nominal value in the powder blend. This indicates that the core of the granule is deficient with IROX and rich with binder and efavirenz. This ratio increased to 1.24 which is higher than the nominal value in the powder blend and this means that the shell is enriched with IROX.

Table 6.11: Elemental ratio comparisons in powder blends and granules produced using medium powder wettability and different binder viscosities.

Elements	Powder blends (efavirenz-IROX) 50%-50%	Granules 50%-50% (efavirenz-IROX)			
		Binder viscosity (mPa s)			
		8		100	
		Spectrum 3	Spectrum 4	Spectrum 1	Spectrum 2
Fe/Cl	6.5	5.1	2.5	5.3	12.8
Cl/C	0.15	0.11	0.13	0.10	0.10
Fe/C	0.96	0.58	0.32	0.53	1.24

Figure 6.18 presents the compositional analysis of granules obtained from powder of high wettability and low binder viscosity.

The blue indicates the IROX rich area, the red is the efavirenz rich area and the green is the binder rich area. A core-shell granule structure was produced using low binder viscosity. It should be noted that the spectra are selected in different places on the core and on the shell of the granule. In general, the core and the shell of the granule appear to be rich in IROX, but brighter contrast appears on the shell.

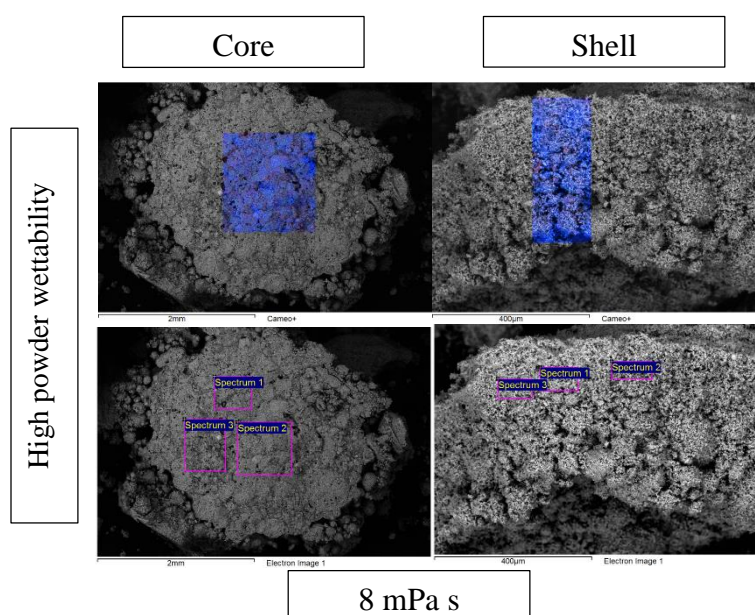


Figure 6.18: Compositional analysis of granules produced from high powder wettability and low binder viscosity.

For the granule core, the Fe/Cl ratio in spectrum 1 is 14.7 which is lower than the nominal value in the powder blend and this indicates that this area is deficient in IROX and rich in efavirenz. However, this ratio increased to 16.2 in spectrum 2 which is close to the nominal value in the powder blend and this indicates a distribution of IROX and efavirenz in this area. The Cl/C ratios of 0.21 and 0.22 in spectrum 1 and spectrum 2 respectively are higher than the nominal value in the powder blend which indicates that these areas are enriched with efavirenz and deficient in binder. Fe/C ratios of 3.11 and 3.53 of spectrum 1 and spectrum 2 respectively are higher than the nominal value in the powder blend. This indicates that the binder is not well distributed throughout the granule and these areas are enriched with IROX.

For the granule shell, the Fe/Cl ratio is higher in spectrum 2 than in spectrum 3 which means that spectrum 2 is richer in IROX. In addition, Cl/C and Fe/C ratios in spectrum 2 and spectrum 3 are higher than the nominal value in the powder blend and this indicates that the binder is not well distributed in this area and these areas are enriched with IROX and efavirenz.

Table 6.12: Elemental ratio comparisons in powder blends and granules produced using high powder wettability and low binder viscosity.

Elements	Powder blends (efavirenz-IROX) 30%-70%	Granules 30%-70% (efavirenz-IROX)			
		Binder viscosity (8 mPa s)			
		Core		Shell	
		Spectrum 1	Spectrum 2	Spectrum 2	Spectrum 3
Fe/Cl	16.4	14.7	16.2	17.5	16.3
Cl/C	0.12	0.21	0.22	0.19	0.20
Fe/C	1.97	3.11	3.53	3.34	3.29

It can be concluded that the spatial distribution of IROX, efavirenz and dextran binder are similar when using the same binder viscosity regardless of the powder wettability.

At low binder viscosity, the bright contrast is not uniformly distributed across the shell; there is a thin bright interface layer between the shell and the core and significant IROX rich inclusion distributed within the shell. This might be due to inhomogeneous distribution of the ingredients in the primary powder blends before granulation.

At medium binder viscosity, the efavirenz and dextran are well distributed at the core and between the core and the shell. However, the shell appeared more enriched with IROX. Nevertheless, still there is some efavirenz and binder at the shell. This is probably due to the ability of the binder to easily penetrate into powder bed of different wettabilities leading to a somewhat uniform ingredient distribution inside the granule.

At high binder viscosity, three distinct layers of IROX, efavirenz and dextran were observed. The core of the granules is dextran rich, between the core and the shell is efavirenz rich and the shell is IROX rich. Low binder deformability is probably one of the causes of non-uniform distribution of the ingredients inside the granule.

These results are in agreement with Warren & Price, 1977 who studied the effect of binder viscosity on intragranular drug migration. Propoxyphene hydrochloride was used as an active ingredient and lactose, starch and magnesium stearate were used as excipients. Various povidone solutions with viscosities ranging from 1 to 1000 mPa s were used as liquid binder. They found that the drug migration to the surface of the granules decreased with increasing binder viscosity. Granules produced using low binder viscosity showed significant migration

of the drug to granule surface and uniform drug content throughout the layers inside the granules.

6.3.4 Granulation as a function of time

In this section, granulation as a function of time will be examined using the medium powder wettability and high binder viscosity in a low shear mixer. This powder wettability was selected because it is neither high nor low and can be easily controlled in term of internal structure. The choice of high binder viscosity was because to allow for an investigation of how the mixing over time will affect the viscous forces in terms of granule size and structure. The aim of this section is to investigate the changes in granule size and internal microstructure using different mixing times.

Figure 6.19 shows the size of granules produced using medium powder wettability and higher binder viscosity (1000 mPa s) as a function of mixing time. There was an increase in granule size with an increase in the mixing time.

At 0 and 1 min mixing time, a mixture of buckled and hemispherical shaped granules were obtained (Figure 6.20). Semi-spherical granules were produced at 5 min mixing time. At 15 and 30 min mixing time, a mixture of elongated and hemispherical granules was produced using these two mixing times.

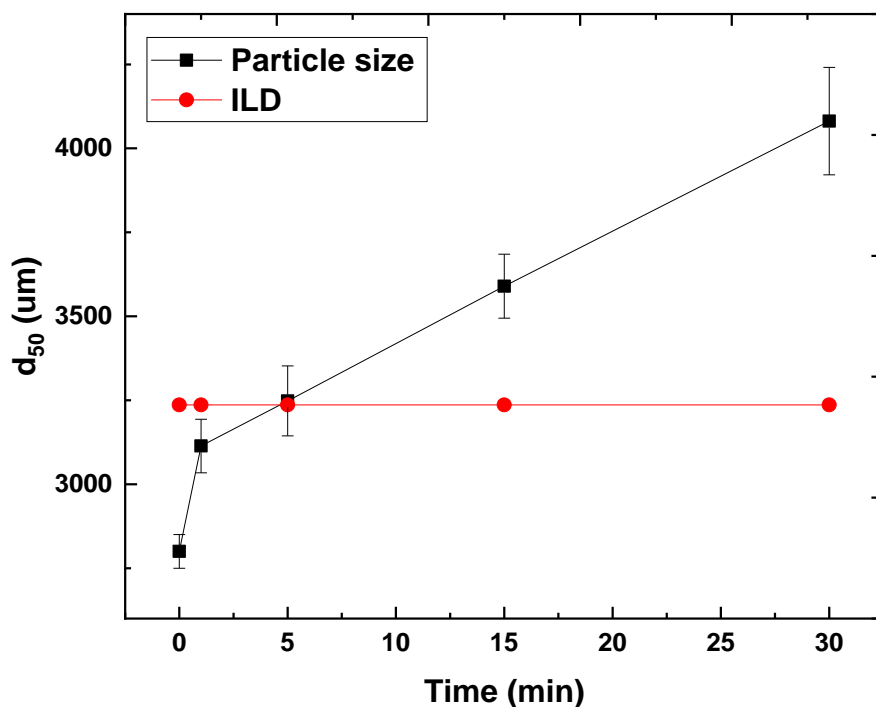


Figure 6.19: Granule size of medium powder wettability and higher binder viscosity as a function of time, obtained via image analysis. The error bars are the standard deviation of the ten measurements.

Table 6.13 presents the change in the size of granules produced over time in low shear mixer relative to the size of initial liquid droplets (ILD). There was a little or no change in the ultimate granule size produced at 5 min mixing time. However, granules started to increase in size with prolonged granulation time up to 30 min. Granule size (d_{50}) changed from 1.85 % at 5 min mixing time to 10.9 % and 26.11 % at 15 and 30 min mixing times respectively, relative to the size of the ILD.

It is expected that at a short mixing time, the low shear force experienced by the granules decreases the penetration of high viscous binder inside the powder bed. This, in turn, decreases the granule consolidation and growth, and an opposite trend is expected with prolonged mixing time.

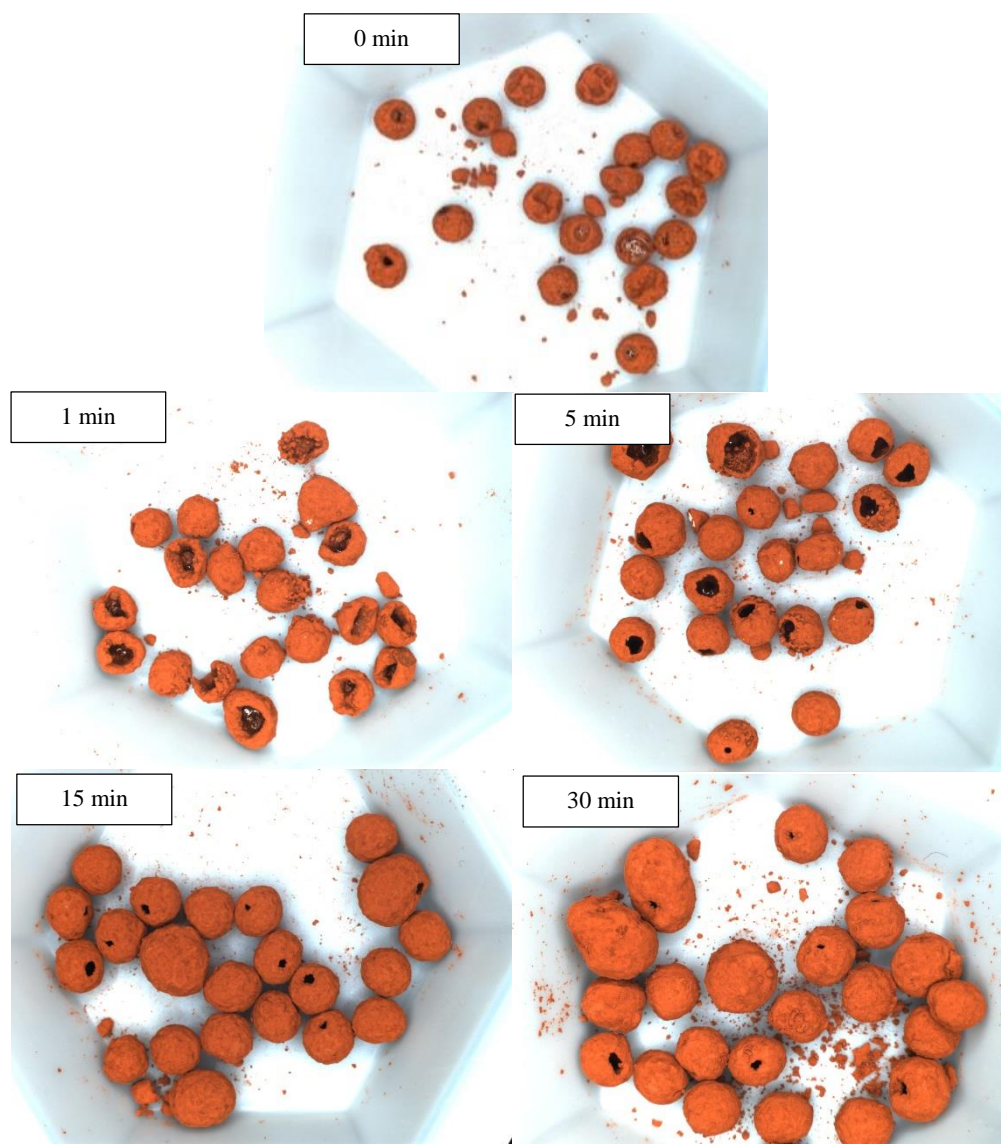


Figure 6.20: Comparison of granules produced using medium powder wettability and different mixing times.

The results are in agreement Oka et al. 2015, who investigated the effect of mixing time on the size of granules produced using a high shear mixer. Microcrystalline cellulose (wetting) and acetaminophen (non-wetting) as powders and water as a liquid binder were used. They hypothesised that the liquid marbles undergo growth by layering of new powder particles with an increase in the mixing time. With increasing mixing time, the deformability of the granules will increase during collisions leading to granule densification. The granule densification will squeeze out more liquid to the liquid marble surfaces and this will promote granule growth.

Table 6.13: Summary of % change in size of granules in relation to size of initial liquid droplet.

Time of granulation (min)	Size (μm)		% granule size change
	Initial liquid droplet	Dried granules	
0	3236	2800	-13.47
1	3236	3113	-3.78
5	3236	3296	1.85
15	3236	3589	10.90
30	3236	4081	26.11

Similarly, Simone, Caccavo, Lamberti, D'Amore, & Barba, 2018 found that increasing the mixing time led to the production of larger granules. They granulated HPMC with water in low shear granulator. With increasing mixing time, the saturation of the granules increases and a higher percentage of void space within the granules was filled with binder, reducing the intergranular voids. More liquid was available on the granule surfaces and granules become easily deformable. The probability of granule growth by layering or coalescence during granulation increased led to an increase in granule mean size.

6.3.4.1 Internal structural analysis

Internal granule microstructure was characterised using XRCT and SEM. XRCT was used to investigate the granule internal microstructure and porosity of the granules produced using different parameters. SEM was used to investigate the ingredients distribution and EDX was used to investigate the ingredients ratio within the granules.

6.3.4.1.1 XRCT analysis

Figure 6.21 shows XRCT images of representative granules as a function of mixing time. The images demonstrate that the granules formed across most mixing times are hollow with a thin or a thick wall thickness. The white outer shell is presumed to be the powder, the dark grey is the dried liquid and dark space in the middle of the granules is air.

Buckled granules with some voids inside can be seen with granules produced at a short mixing time of 1 min. Hollow granules with thin wall thickness can be seen at 5 min mixing time. The

wall thickness of the hollow granules became thicker with increasing mixing time; 5-30 min. The thickness of the powder infused layer steadily increased with tumbling time. At the longest mixing time of 30 min, it appears that drying proceeded to point of rupturing the shell.

It is hypothesized that the increasing mixing time leads to an increase in the granule collisions with the walls of the equipment and with the powder bed resulting in densification of the powder layer. During the densification of the granules, the binder is squeezed to the surface of the granules, increasing the chance for particles sticking to granule surfaces which allows more layering of powder particles around the granules and this is expected to start after 5 minutes mixing time.

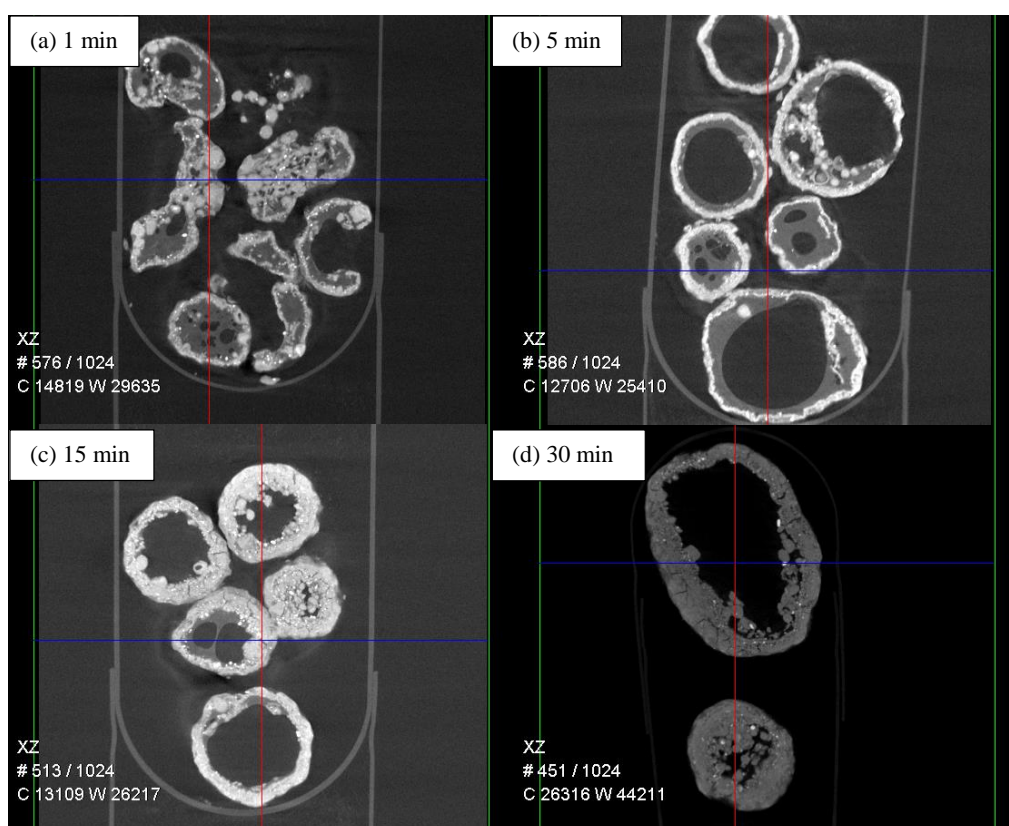


Figure 6.21: Images of granules produced using medium powder wettability and different mixing times. The outer rings are part of the sample container. (Reconstructed XRCT images; representative central cross-section).

Figure 6.22 expresses the percentage total porosity as a function of mixing time. The porosity increased and reached the highest value at 5 min mixing time, and then decreased with increasing mixing time. The lowest granule porosity can be seen at 1 min mixing time; this was because of the collapse of the granules upon drying. The highest granule porosity can be seen

at 5 min mixing time. Then, with increasing mixing time, granule consolidation increased due to prolonged collisions resulting in a reduction in the hollowness inside the granules and an increase in the wall thickness.

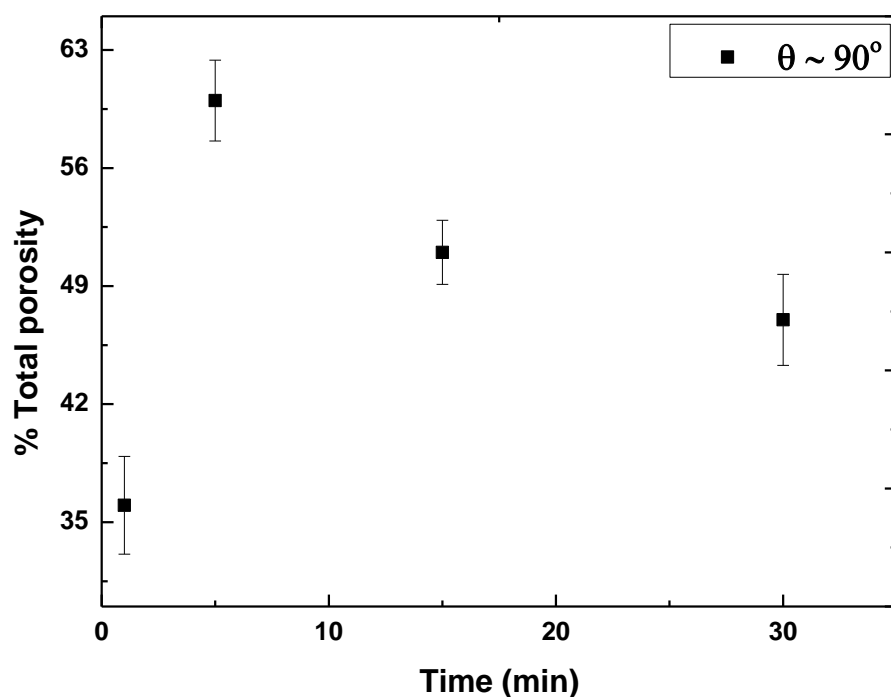


Figure 6.22: Total porosity as a function of mixing time. The error bars are the standard deviation of three measurements. θ is liquid powder contact angle.

These results are in accordance with Levin & Hanover, 2006 and Raj Kumar & Malayalamurthi, 2017. Levin et al. 2006 suggested that the intragranular porosity decreases during the wet massing stage of the granulation process. This was because of granule densification caused by collisions and the shearing action of the drum during prolonged granulation mixing time. Kumar et al. 2017 studied the effect of granulation time on the resultant granule density using sago powder (a staple food in Africa) and water as a liquid binder. The granule porosity decreased with an increase in the granulation time. The number of bowl rotations increases with the prolonged granulation time leading to a higher granule density and lower porosity.

6.3.4.1.2 SEM analysis

Figure 6.23 shows SEM images of the granules produced using different mixing times. The dark contrast is the dried liquid binder while the light contrast is the powder.

At 1 min mixing time, a thick layer of dried liquid binder surrounded by a thin layer of powder particles was observed. It should be noted that there was an uneven thickness of the layer and there were pores in the middle of the layer which indicate localized drop collapse during evaporation. In addition, there was some powder attached on the surface of the cavity which indicates localized flow or deformation of the binder in that location of the initial spherical granule with full powder coverage.

At 5 min mixing time, the dried liquid layer was smaller and the powder layer attached to the liquid binder was thicker compared with the granules produced at 1 min mixing time.

A good distribution of liquid binder with powder particles was observed at 15 min mixing time leaving a very thin layer of liquid droplet surrounded by thick layer of powder particles.

At 30 min mixing time, the dried liquid layer disappeared; instead one layer of thick powder appeared to be distributed well throughout the liquid droplet.

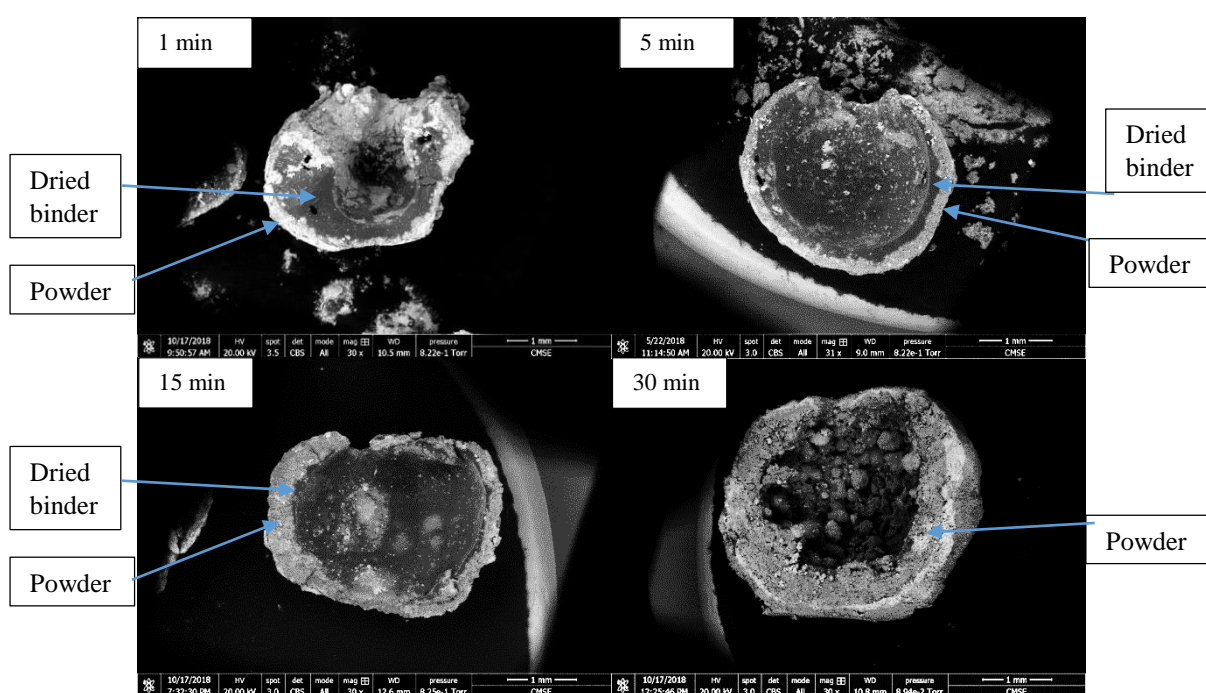


Figure 6.23: SEM images of granules produced using medium powder wettability and different mixing times.

Figure 6.24 shows compositional analysis of granules at two different mixing times (1 and 5 min). The blue is the IROX rich area, the red is the efavirenz rich area and the green is the binder rich area. In Figure 6.24 a, spectrum 1 is near the core, spectrum 3 between the shell and the core and spectrum 5 near the shell. In Figure 6.24 b, spectrum 2 is near the core, spectrum 4 between the shell and the core and spectrum 6 near the shell. Granules produced using 1 min mixing time appeared to have two distinct layers; binder (green) towards the inside of the granule and a mixture of efavirenz (red) and IROX (blue) towards the granule edge. Granules produced from 5 min mixing time show more binder distribution towards the core and distribution of IROX and efavirenz in the shell.

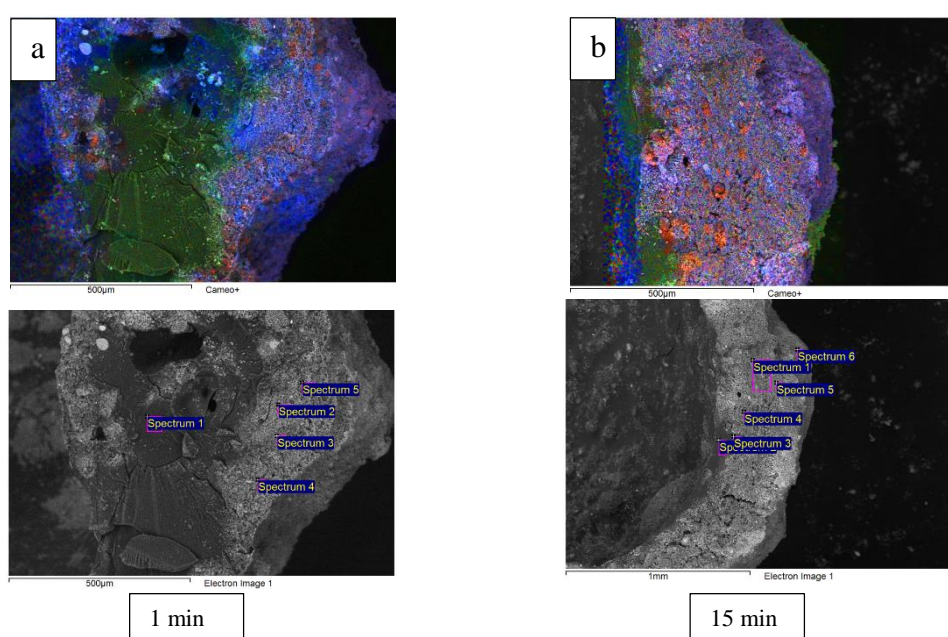


Figure 6.24: Compositional analysis of granules produced using medium powder wettability and high binder viscosity at two different mixing times.

A comparison of the elemental ratio in the powder blends and granules produced using two different mixing times can be seen in Table 6.14.

For granules produced using 1 min mixing time, the Fe/Cl ratio in spectrum 1 is 0; this indicates that this area is a binder pure area. However, this ratio increased to 4.2 in spectrum 2 and is lower than the nominal value in the powder blend which indicates that there is efavirenz and IROX in this area. In spectrum 5, this ratio increased to 8.5 which is higher than the nominal value in the powder blend and indicates an IROX rich area. Cl/C and Fe/C ratios in all spectra are lower than the nominal value in the powder blend which suggested that the binder is distributed throughout these areas.

For granules produced using 5 min mixing time, the Fe/Cl, Cl/C and Fe/C ratios in spectrum 2 are 0 which indicates that this area is a binder enriched area. However, the Fe/Cl ratios in spectrum 4 and spectrum 6 are still lower than the nominal value in the powder blend which indicates that these areas contain binder in addition to efavirenz and IROX. The Cl/C and Fe/C ratios in spectra 4 and 6 are lower than the nominal value in the powder blend which suggests that binder is distributed throughout these areas as well as efavirenz and IROX (Figure 6.12).

Table 6.14: Elemental ratio comparisons in powder blends and granules produced using medium powder wettability and high binder viscosity and at different mixing times.

Elements	Powder blends (efavirenz-IROX) 50%-50%	Granules 50%-50% (efavirenz-IROX)					
		Mixing time (min)					
		1			5		
		Spectrum 1	Spectrum 3	Spectrum 5	Spectrum 2	Spectrum 4	Spectrum 6
Fe/Cl	6.5	0	4.2	8.5	0	3.6	5.5
Cl/C	0.15	0	0.13	0.09	0	0.05	0.06
Fe/C	0.96	0	0.53	0.78	0	0.17	0.36

It is concluded that the granules produced at 1 and 5 min mixing consist of core and shell. The elemental compositional distribution is; binder in the core, layer of efavirenz and IROX at the shell. The distribution of efavirenz and IROX at the shell increased with increasing mixing time from 1 to 5 min.

The results in this work are in accord with Kataria et al. 2018 who quantitatively investigated the intra-granular drug migration under different mixing times in a high shear mixer. Aqueous potassium chloride as a tracer was used to study the drug migration and microcrystalline cellulose (MCC) was used as an excipient. Polyvinyl pyrrolidone was used as a liquid binder. It found that the distribution of potassium chloride varied with granulation mixing time. At a lower mixing time, potassium chloride was found to deposit at the periphery of the granules. With increasing mixing time, potassium chloride was uniformly distributed throughout the granules.

However, these results are not in agreement with Oka et al. 2015 who studied the effect of various powder wettabilities and mixing times (5 and 7 min) on the distribution of active pharmaceutical ingredient (API). Acetaminophen (API) (non-wetting) and MCC (wetting) powders were granulated with water as a binder. It was found the inhomogeneity of the content

of the granules was poorer with increasing mixing time. They suggested that when the nuclei were formed, the liquid droplet preferentially wets MCC particles due to its wetting properties. With increasing mixing time, granules continue to selectively grow with MCC; this results in the increase in content inhomogeneity with increasing mixing time. This contradiction from the result in this study is probably because of the use of the different nucleation and granulation procedure. Pre-nucleation was used in this study compared to dripping of the liquid on the powder bed in high shear mixer used in their study.

6.3.5 Granulation in a high shear mixer

The aim of this part of the study is investigate the effect of higher shearing forces on granule size and internal microstructure using different powder wettabilities and binder viscosities. Here, a study in the granule size and internal microstructure in a high shear granulator is presented and compared to the data obtained using the low shear mixer. Formulations of wetting and non-wetting pharmaceutical powder (in different percentages; 60%-40%, 50%-50%, 30%-70% of efavirenz and IROX respectively), with different binder viscosities ranging from 8 mPa s to 1000 mPa s were investigated. Impeller speed was operated at 370 rpm for 20 seconds.

Figure 6.25 presents the size of granules produced using different powder wettabilities and binder viscosities in the high shear mixer. For powder of low and high wettabilities, the granule size increased with increasing binder viscosity.

Figure 6.26 presents images of granules produced using different powder wettabilities and binder viscosities. For low powder wettability, hemispherical granules were produced using high binder viscosity. The granules obtained using low viscosity were too friable and difficult to extract from the powder batch (Figure 6.26 a and b). For medium powder wettability, hemispherical granules were observed upon drying (Figure 6.26 c). For high powder wettability, a mixture of semi-spherical and elongated granules were produced using low and high binder viscosities (Figure 6.26 d and e).

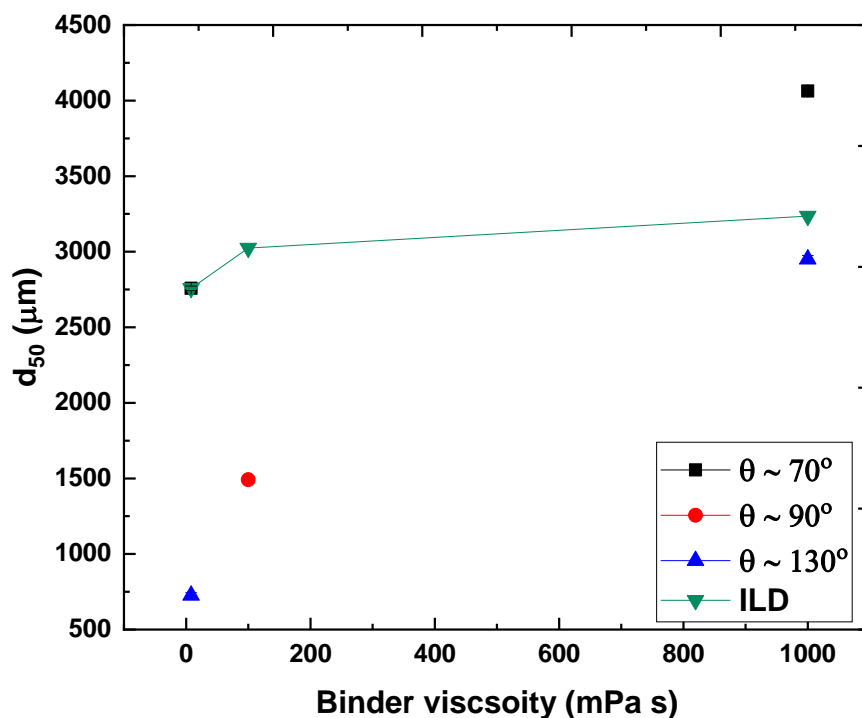


Figure 6.25: Granule size of different powder wettabilities and binder viscosities obtained via image analysis. The error bars are the standard deviation of the ten measurements. θ is liquid powder contact angle.

Table 6.15 shows that there was a change in the ultimate size of granules produced using different binder viscosities relative to size of initial liquid droplets (ILD). For low powder wettability, the percentage changes in granule size were -73.64 % and -8.83 % using low and high binder viscosity respectively, relative to the size of ILD. For medium powder wettability, there was a decrease in the ultimate granule size relative to the size of ILD. The percentage change in granule size was -50.69 %, relative to the size of ILD. For high powder wettability, percentage changes in granule size were 47.31 % and -14.80 % using low and high binder viscosity respectively, relative to the size of ILD.

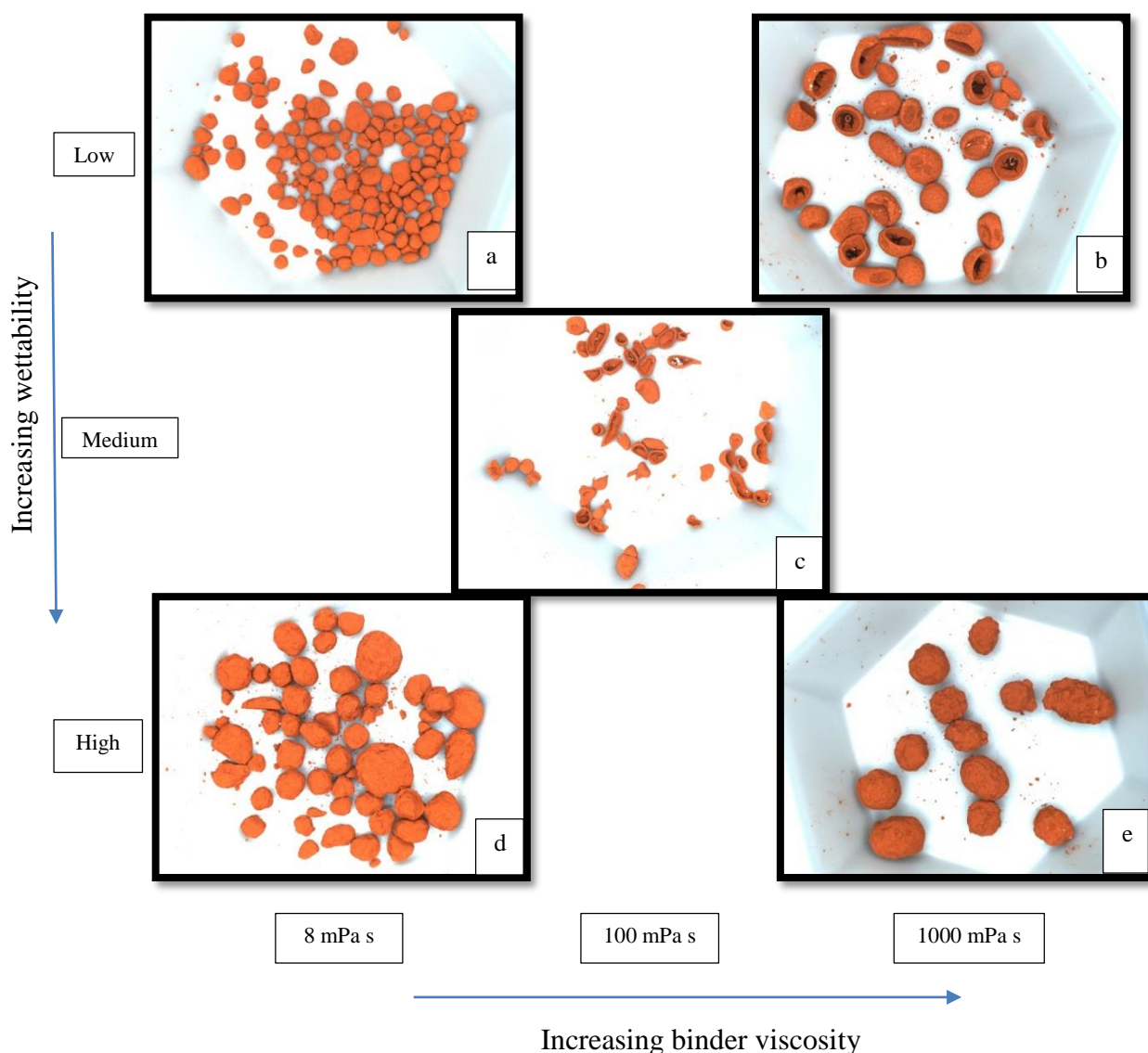


Figure 6.26: Comparison of granules produced using different powder wettabilities and binder viscosities in a high shear.

It is suggested that the use of the higher binder viscosity lead to strong binding forces between the liquid and the powder that is enough to resist the shearing forces applied and forms granules which might increase in size depending on powder wettability. However, using low binder viscosities, the binding forces between powder particles cannot withstand the shearing forces applied, leading to breakage and attrition of the liquid marbles or immersion nuclei respectively. The binding forces between powder of medium wettability and binder of medium viscosity are weak and unable to resist the shearing forces applied. The liquid marbles underwent attrition and breakage leading to the formation of small granules upon drying.

Table 6.15: Summary of % change in size of granules in relation to size of initial liquid droplet.

Non wetting-wetting mixture	Binder viscosity (mPa s)	Powder/liquid contact angle °	Size (µm)		% granule size change
			Initial liquid droplet	Dried granules	
60%-40%	8	125.25	2758	726.8	-73.64
60%-40%	1000	141.35	3236	2950	-8.83
50%-50%	100	92.83	3024	1491	-50.69
30%-70%	8	63.51	2758	4063	47.31
30%-70%	1000	94.33	3236	2757	-14.80

A comparison of granule size produced using low and high shear mixers showed that a smaller granule size was produced under different powder wettabilities and binder viscosities using a high shear mixer. This is probably due to breakage and attrition of granules in the high shear mixer because of the increase in the shearing forces applied.

These results are in accord with Raj Kumar & Malayalamurthi, 2017 who investigated the effect of low and high rotational speed on granule size using cassava (a staple food in Africa and in South America) as a powder and water as a liquid binder. It was observed that the final product quality (size and shape) were dependent on the rotational speed of the mixer. The mean diameter of the granules was larger for low rotational speed and smaller for the highest rotational speed. The reason for this was due to the fact that when using high rotational speed, the particles were tightly packed with high density; hence the granule size was reduced. However, using low rotational speed, the particles were loosely connected with low density which results in a larger granule size.

6.3.5.1 Internal structural analysis

Internal granule microstructure was characterised using XRCT and SEM. XRCT was used to investigate the granule internal microstructure and porosity of the granules produced using different parameters. SEM was used to investigate the ingredients distribution and EDX was used to investigate the ingredients ratio within the granules.

6.3.5.1.1 XRCT analysis

Figure 6.27 shows a comparison of XRCT images of representative granules using the high shear mixer.

For low powder wettability, few granules were obtained at low binder viscosity. However, hemispherical and hollow granules can be seen using high binder viscosity. It is suggested that using low binder viscosity, the liquid binder was distributed throughout the powder bed without granule formation. This is probably due to low binding forces between the powder particles. However, the ability of the high binder viscosity to reduce granule deformation during collisions decreases liquid marble destruction during granulation.

For medium powder wettability, hemispherical granules were obtained. For high powder wettability, the granule microstructure changed from single solid granules using low binder viscosity to hollow granules using high binder viscosity. This is might be due to the penetration of binder with a low viscosity being faster than binder with high viscosity.

It is suggested that destructive high shear deformation within the 20 s mixing time did not occur with high binder viscosity (for wetting and non-wetting powder) or with wetting powder and low binder viscosity. The granules for those extremes are strikingly similar to those produced from the low shear mixer. This demonstrates that deformation resistance by binder viscosity or nuclei strength is critical to produced hollow or layered granules in a high shear mixer. In addition, most observed granules at this condition had an oval shape rather than more spherical in the case of the low shear mixer. This probably due to both deformation and binary aggregation.

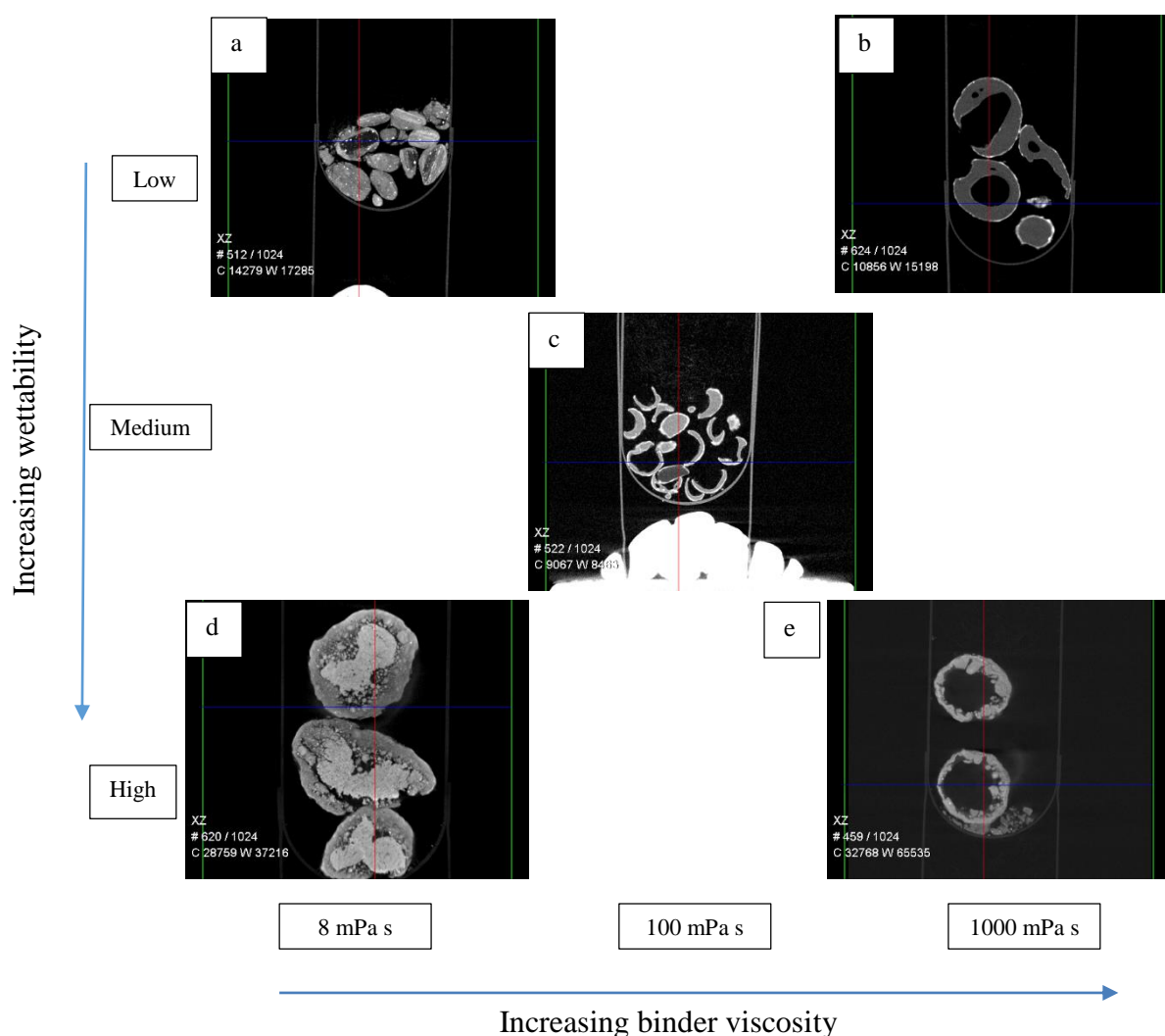


Figure 6.27: Images of granules produced using different powder wettabilities and binder viscosities in a high shear mixer. (Reconstructed XRCT images; representative central cross-section).

Figure 6.28 expresses the percentage total porosity as a function of different powder wettabilities, binder viscosities and shearing forces. The porosity of granules produced using low powder wettability and higher binder viscosity was 63 %. The porosity of granules produced using medium powder wettability was 30 %. For powder of high wettability, the granule porosity increased from 20 % using low binder viscosity to 38 % using high binder viscosity.

In comparison with granules produced using low shear, for powder of low wettability, there is a small decrease in the porosity of the granules produced using the high shear mixer compared with those produced using the low shear mixer. For powder of medium wettability, there is a clear decrease in granule porosity using the high shear mixer compared with granules produced

using the low shear mixer. For powder of high wettability, approximately the same granule porosities were obtained using low and high shear mixers with different binder viscosities.

It is suggested that the granules of low wettability and low binder viscosity have weak binding forces and are unable to keep the liquid marbles intact during granulation in a high shear mixer. This resulted in breakage and shattering of liquid marbles leading to formation of flakes and small friable hollow granules that underwent breakage during handling. However, using high binder viscosity, a strong enough binding force between the powder and the binder can overcome granule breakage and contribute to granule consolidation and growth. These results are in accord with Ennis et al. 1991 who found that higher binder viscosities lead to low rates of granule consolidation and high granule porosity due to less granule deformation.

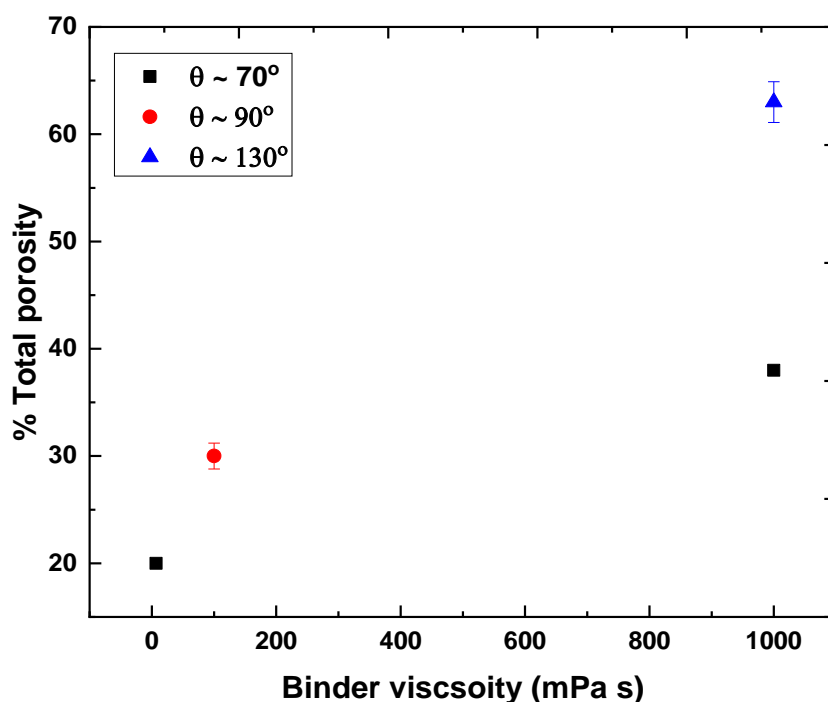


Figure 6.28: Total porosity as a function of powder wettability, binder viscosity and shear force. The error bars are the standard deviation of three measurements. θ is liquid powder contact angle.

6.3.5.1.2 SEM analysis

Figure 6.29 present SEM images of granules produced using different powder wettabilities and binder viscosities. For low powder wettability, the structure changed from no granules obtained using low binder viscosity, to hollow granules with two distinct layers; powder and binder using high binder viscosity

For medium wettability, granules of two layers; a thick dried liquid and a thin powder were observed.

For powder of high wettability, the granule structure changed from single solid granules to hollow granules using low and high binder viscosity respectively.

Granules produced using the low and high shear mixers were compared. For low powder wettability, no granules were obtained using low binder viscosity and the high shear mixer compared to hollow granules obtained using the low shear mixer. Using high binder viscosity, a thinner powder layer surrounded by a dried liquid layer was produced using the high shear mixer. For powder of medium wettability, the granules produced using the high shear mixer showed two layers; core and shell. However, a good distribution of the liquid throughout the powder could be found in the granules using the low shear mixer. For powder of high wettability, no difference in granule structure between granules was observed.

This suggests that the high shear forces lead to attrition of the powder layer surrounding the liquid droplet using medium powder wettability or breakage of liquid marbles using low powder wettability.

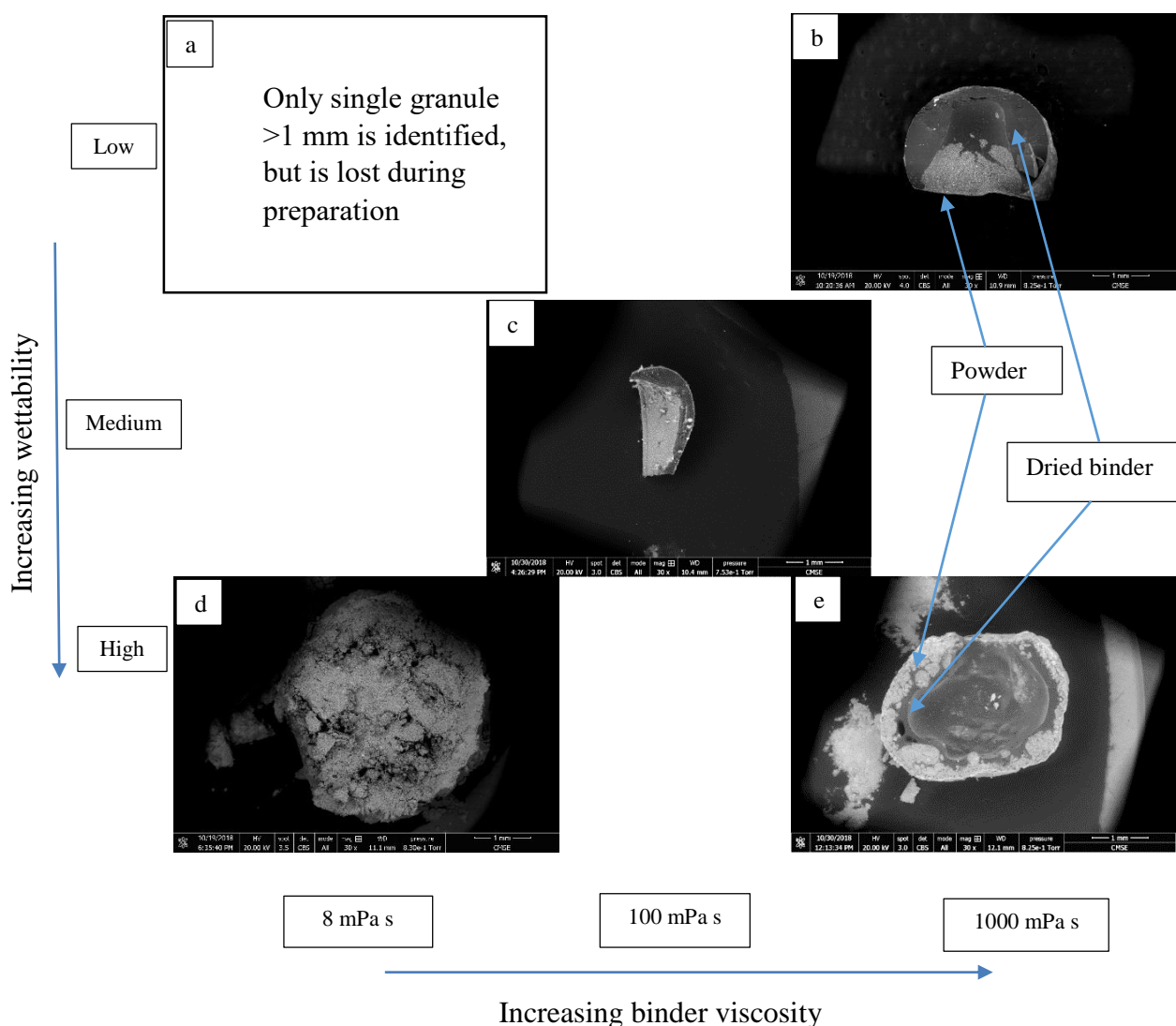


Figure 6.29: Comparison of SEM images of granules of produced using different powder wettabilities and binder viscosities in a high shear mixer.

Figure 6.30 shows the compositional analysis of granules obtained from powder of low wettability and high binder viscosity in the high shear mixer. The blue is the IROX rich area, the red is the efavirenz rich area and the green is the binder rich area. Spectrum 1 is near the core, spectrum 3 is on agglomerates of powder on granule surface and spectrum 4 is near the shell. The surface of the granule appears to be rich with IROX and efavirenz, while the granule core is rich with the binder.

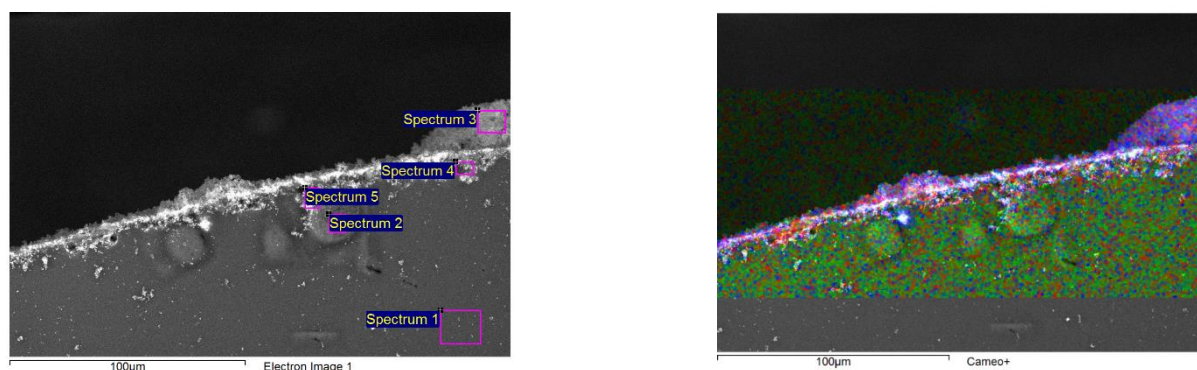


Figure 6.30: Compositional analysis of granules produced from low powder wettability and high binder viscosity using the high shear mixer.

A comparison of the elemental ratio in the powder blends and granules of low wettability can be seen in Table 6.16. The Cl/C ratio in the granule in spectrum 1 is 0 which is much lower than the nominal value in the powder blend. This indicates that the core is deficient with efavirenz and enriched with dried binder. However, this ratio increased to 0.12 in the agglomerates at the surface of the granule which is close to the nominal value in the powder blend and this indicates that the agglomerate is rich with efavirenz. This area may be formed from dry agglomerates attached to the surface of the granule. At the same time, this ratio decreased to 0.04 in spectrum 4 which again indicates an area which is enriched with binder and deficient with efavirenz.

Table 6.16: Elemental ratio comparisons in powder blends and granules produced using low powder wettability in a high shear.

Elements	Powder blends (efavirenz-IROX) 60%-40%	Granules 60%-40% (efavirenz-IROX)		
		Binder viscosity (1000 mPa s)		
		Spectrum 1	Spectrum 3	Spectrum 4
Cl/C	0.15	0.00	0.12	0.04

Figure 6.31 shows the compositional analysis of granules obtained from powder of medium wettability and medium binder viscosity. The blue is the IROX rich area, the red is the efavirenz rich area and the green is the binder rich area. Spectrum 1 is near the core and spectra 2 and 3

are near the shell. The granule shell appears to be rich in IROX and efavirenz, while the granule core is rich with binder.

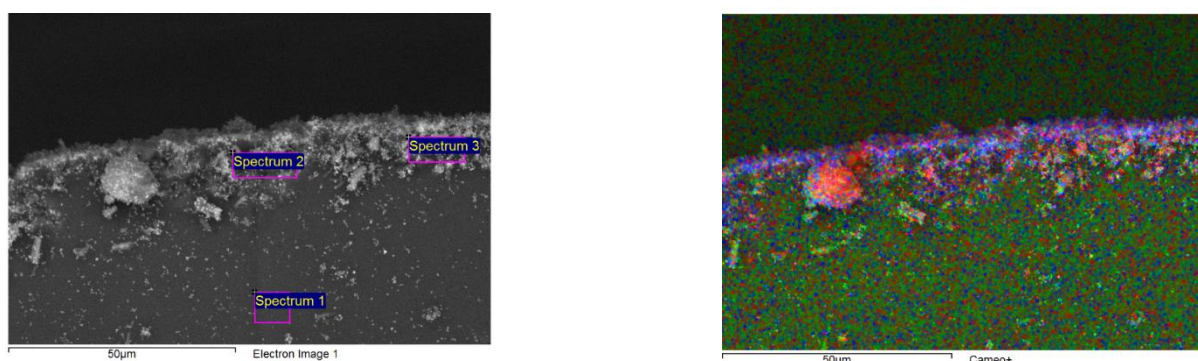


Figure 6.31: Compositional analysis of granules produced from medium powder wettability and medium binder viscosity using a high shear mixer.

Table 6.17 shows the elemental ratio of Cl/C in three different areas in a granule formed from powder of medium wettability and medium binder viscosity. The Cl/C ratios in all three spectra are lower than the nominal values in the powder blend. This indicates that the granule is deficient with efavirenz and the granule is formed mainly of binder. This result is in agreement with the XRCT image (Figure 6.27) which shows granules formed from medium powder wettability and medium binder viscosity have a thin powder wall thickness surrounded by a liquid droplet.

Table 6.17: Elemental ratio comparisons in powder blends and granules produced using medium powder wettability and medium binder viscosity in a high shear mixer.

Elements	Powder blends (efavirenz-IROX) 50%-50%	Granules 50%-50% (efavirenz-IROX)		
		Binder viscosity (100 mPa s)		
		Spectrum 1	Spectrum 2	Spectrum 3
Cl/C	0.15	0	0.04	0.05

In comparison with the elemental distribution of the granules produced in the low shear mixer, the Cl/C ratio is much higher than those obtained using the high shear mixer. This means that granules formed in the low shear mixer have a better distribution of efavirenz and binder than those produced using the high shear mixer. This is probably due to the attrition of the granule surfaces with high shear forces.

Figure 6.32 shows compositional analysis of granules obtained from powder of high wettability and high binder viscosity. The blue is an IROX rich area, the red is the efavirenz rich area and the green is the binder rich area. Spectrum 1 is near the core and spectrum 2 near the shell. IROX and efavirenz appear to be distributed in the granule shell.

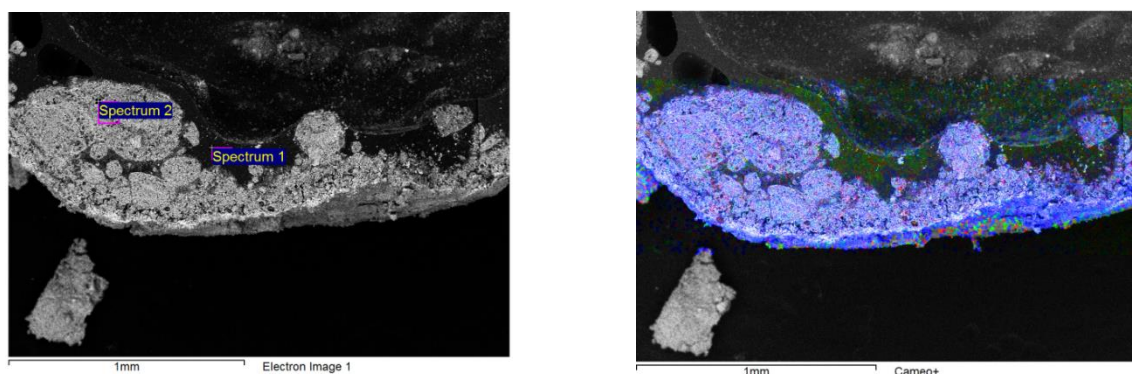


Figure 6.32: Compositional analysis of granules produced from high powder wettability and high binder viscosity using a high shear.

Table 6.18 shows compositional analysis of the powder blends and the granule. In spectrum 1, the ratio of Fe/Cl, Cl/C and Fe/C are 0, this indicating that this area is deficient in IROX and efavirenz and rich in binder. In spectrum 2, the Fe/Cl ratio is 12.1 which is lower than the nominal value in the powder blend and this indicates that this area contains efavirenz as well as IROX. The Cl/C ratio is 0.05 which is lower than the nominal value in the powder blend and this indicates that this area is rich in binder and contains some efavirenz. The Fe/C ratio is 0.64 which is lower than the nominal value in a powder blend. This indicates that the binder is well distributed throughout the granule and this area is enriched with binder and IROX. This probably due to good powder wettability allowing a better distribution of the ingredients throughout the granule.

Table 6.18: Elemental ratio comparisons in powder blends and granules produced using high powder wettability and high binder viscosity in a high shear.

Elements	Powder blends (efavirenz-IROX) 30%-70%	Granules 30%-70% (efavirenz-IROX)	
		Binder viscosity (1000 mPa s)	
		Spectrum 1	Spectrum 2
Fe/Cl	16.4	0	12.1
Cl/C	0.12	0	0.05
Fe/C	1.97	0	0.64

6.4 Summary and further discussion

In this chapter, the following main experimental effects were measured and observed:

- In low shear granulation, increasing binder viscosity resulted in a decrease in granule size for all powder wettabilities
- In high shear granulation, increasing binder viscosity resulted in an increase in granule size for all powder wettabilities
- Spherical granules were produced using high binder viscosity regardless of powder wettability and shearing forces applied
- EDX analysis showed an inhomogeneity in the distributions of the ingredients within the granule. However, a more uniform distribution was observed with decreasing binder viscosity
- Hollow granules were promoted using high binder viscosity regardless of powder wettability and shearing forces applied.

The key results will be discussed in the following sections.

6.4.1 Effect of binder viscosity and shear forces on granule size and shape

In low shear granulation, the production of a large granule size using low binder viscosity is probably due to the short penetration time of liquid droplets into a powder bed. According to the drop penetration time proposed by Hapgood, Litster, Biggs, & Howes, 2002, Equation (5.2) described in Section 5.4, the drop penetration time is directly proportional to binder viscosity. At low binder viscosity, it is faster for powder particles to migrate into the liquid droplet, and it is also faster for the liquid to be drawn to the granule surface leading to further granule growth. It should be noted that the faster drop penetration times promote more uniform binder distribution, liquid saturation, granule deformation and growth.

These results are in agreement with Korteby, Kristó, Sovány, & Regdon, 2018 who studied the effect of binder viscosity on the granule growth mechanism in an in situ fluid bed melt granulation. Lactose monohydrate was used as a powder and two different molecular weight polyethylene glycols (2000 and 6000) were used as a meltable binders. A smaller granule size was produced using high binder viscosity because only a small fraction of the liquid binder

was distributed on the lactose particles which reduced growth by coalescence. The deformation of the granules was higher using the low binder viscosity, leading to a larger granule size. Granule growth occurred after surface wetting generated by granule densification as the liquid binder was squeezed to the granule surface and resulted in a wider size distribution.

In high shear granulation, the production of large granules using high binder viscosity is probably due to strong binding forces between powder particles; see Equation (4.2), Section 4.5. In this equation the liquid viscous bridge strength is directly proportional to binder viscosity. The high binder viscosity produced stronger and less deformable granules which inhibits granule breakage and attrition in high shear granulation or collapse of liquid marbles during drying in single drop nucleation experiments.

The difference in granule size behaviour using low and high shear mixers is in agreement with Schæfer & Mathiesen, 1996. They investigated the effect of binder viscosity and shear force on granule growth in high shear granulation. Lactose monohydrate was used as a powder and polyethylene glycol of different molecular weight as a meltable binder. They found that the granule size decreased with increasing binder viscosity using a low shear mixer. However, the granule size increased with an increase in binder viscosity using a high shear mixer. It was concluded that a higher binder viscosity reduces the granule deformability and increases granule strength and reduces breakage of the granules using high shear granulation.

The production of spherical granules using high binder viscosity and elongated granules using low binder viscosity in this study are in accord with Mašić et al., 2012. They studied the effect of binder viscosity on the granule shape. Aspect ratio and projection sphericity were used to evaluate granule shape. They found that the granules produced using higher binder viscosity were more regular in shape than those produced using low binder viscosity. This was because the growth of the granules using low binder viscosity occurred by coalescence of primary nuclei followed by adherence of un-granulated powder.

However, Schæfer & Mathiesen, 1996b found that more spherical pellets were produced at low binder viscosity when they studied the effect of binder viscosity on granule shape. Anhydrous lactose was melt pelletised in a high shear mixer using different molecular weight polyethylene glycol as a liquid binder. Granule shape was characterised using image analysis software. They suggested that the granule surface plasticity was higher at low binder viscosity, and this made the granule rounding easier. The difference in findings is probably due to the binder viscosity

used. Lower binder viscosity used in the work performed by Schæfer and Mathiesen, 1996 was 100 mPa s compared to 1000 mPa s used in this thesis.

6.4.2 Effect of binder viscosity on intra-granular materials distribution

Using EDX analysis of the granules produced using different conditions, it can be seen that there was inhomogeneity in the distribution of efavirenz, IROX and binder throughout the granules. It is probably due to either the non-uniform drug distribution in the primary powder blends or the difference in powder wettability that leads to preference of nucleation of one ingredient; mostly the wetting one over the non-wetting ingredient. It is expected that the presence of non-wetting ingredients in the formulation can lead to poor wetting of the powder bed by the binder fluid, resulting in a non-uniform distribution of the formulation ingredients that amplifies the challenge of achieving the homogenous granules. Nguyen, Shen, & Hapgood, 2010 concluded that achieving drug uniformity distribution with non-wetting formulations was a difficult criterion because there was competition between wetting and non-wetting components in the formulation.

For low binder viscosity, in low shear granulation, uniform distribution of ingredients was observed in some parts of the granules. However, there was still some non-uniform distribution in another places, with preferences of IROX to be present near the shell.

For medium binder viscosity using medium powder wettability in low shear granulation, resulted in the formation of hollow granule that is “perfect”. The shell is uniform compositionally, the size is significantly larger than the size of initial liquid droplet, the shape is relatively close to spherical, and there is no rupture from the internal gas escape.

For high binder viscosity, granules produced using low shear granulation showed three distinct layers of IROX, efavirenz and dextran: binder rich inclusion distributed within the core, efavirenz rich inclusion distributed between the shell and the core, and IROX rich inclusion distributed within the shell. However, in high shear granulation with high powder wettability, more uniform distribution of IROX and efavirenz was observed within the shell, but binder rich inclusion still distributed within the core. In high shear granulation with low powder wettability, granules mainly consist of a binder layer within the core. This is probably due to the attrition of the granule surfaces with high shear forces.

The distribution of efavirenz and IROX within the shell was more uniform with increasing mixing time. It is expected that with the increasing mixing time the collisions between the granules provide better ingredients distribution. It should be noted that this is not conclusive because ingredients distribution using longer mixing time such as 15 and 30 min was not measured in this thesis.

From all the conditions mentioned above, it can be observed the granule shell was mainly enriched with IROX. The accumulation of IROX (wetting ingredient) at the shell regardless of powder wettability, binder viscosity and mixing time is in agreement with Ojile, Macfarlane, & Selkirk, 1982. They studied the uniformity distribution of wetting and non-wetting ingredients inside the granule. They found that the different ingredient wettabilities were the main cause of distribution inhomogeneity due to migration of binder and, consequently, the wetting ingredients during drying. It was found that the wetting ingredient was leached to the surface of the granules during drying. The binder evaporates, leaving deposits of the wetting ingredient at the granule surface.

Similarly, Warren & Price, 1977 studied the effect of drug solubility on intra-granular drug migration. Propoxyphene hydrochloride, lactose, starch as wetting powder and magnesium stearate as non-wetting powder were used. Water was used as a liquid binder. They found that the wetting powder was depleted from the inner layer and this was probably due to the fact that during drying the drug was transported towards the granule surface and was readily depleted from the inner layers of the granulation bed.

6.4.3 Formation of hollow granules

This study demonstrates that large hollow granules can be formed from powder mixtures ranging from wetting to non-wetting through the use of high binder viscosity, which is beneficial in two respects: preventing significant granule deformation, both from shear (during granulation) and during static drying, despite sometimes very little powder imbibition as for wetting powder, and slowing propagation of wetting in medium and low powder wettability mixtures. Hollow granule produced from medium powder wettability is the most favorable.

Overall, formation of hollow granules in general, consists of several stages:

- Initial drop dispersion

- Formation and growth of the shell
- Final microstructure evolution during drying

From all the results, it is clear that the internal microstructure and growth kinetics of hollow granules are controlled by viscous forces, surface tension, impact and shear forces. A quantitative model that can adequately explain the observed microstructures while taking into account the above experimental conditions is required.

6.5 Conclusions

Nuclei were prepared from wetting, non-wetting and medium wetting binary blends using liquid droplets of different viscosities, and further granulated in low and high shear mixers. The effect of powder wettability, binder viscosity, shearing forces and mixing time on granule size and internal structure were investigated.

The key conclusions are:

a- Granule size:

- Low shear granulation; granule size decreased with increasing binder viscosity
- High shear granulation; granule size increase with increasing binder viscosity
- Granule size increased with increasing mixing time

b- Granule internal structure:

- Hollow granules were produced using high and medium binder viscosities, regardless of powder wettability
- Uniform shells were only observed in granules from medium powder wettability; multi-layered shells were observed otherwise.
- Solid granules with a complex internal microstructure were produced at a low binder viscosity regardless of powder wettability

c- Distribution uniformity:

- Using low binder viscosity regardless of powder wettability, resulted in significant compositional difference between the shell and the core, the shell enriched with IROX relative to the core.
- Using high binder viscosity regardless of powder wettability, there are three distinct layers of binder, efavirenz and IROX; the shell enriched with IROX relative to the core.
- Non-uniform distribution was found at a short mixing time, while the distribution improved with prolonged mixing time.

In order to evaluate the mechanical stability of the forming shell and rationalise the observed microstructure, mathematical equations are needed to account for the difference in properties between the growing powder-binder shell and the pure liquid binder core. Chapter 7 will investigate the mechanism and growth kinetics of the shell by developing dimensionless groups based on mechanistic understanding and physical phenomena occurring during the process.

CHAPTER 7. Mechanistic behaviour of internal granules microstructure

In this study, novel regime maps were developed to understand the mechanistic behaviour of the internal microstructure of granules produced using different powder wettabilities, binder viscosities and impact forces.

The first regime was developed for granules produced using medium and high powder wettabilities. Granulation process in this regime was limited by immersion rate. Granulation number (G_{Nu}) was developed as a dimensionless group to demarcate the boundary between different granule structures. As the binder viscosity increased the immersion time of the powder particles inside the liquid droplet increases. This resulted in the formation of hollow granules upon drying.

The second regime was developed for granules produced using low powder wettability. Three different behaviours were identified in this regime; inertial force dominated, surface tension and viscous forces dominated and combined forces dominated. Weber number multiplied by Reynolds number (WRe) is a dimensionless group used to demarcate the boundary between these different behaviours. As the inertial force increases, the immersion of powder particles inside the liquid droplet increases, leading to the formation of solid internal microstructure upon drying.

These regime maps give a better understanding of the controlling mechanisms of the granule internal microstructure produced using different parameters. This provide a basis on how to mass produce hollow granules to facilitate progress in granulation of heterogeneous-wetting powder blends in pharmaceutical, cosmetics and other advanced materials.

7.1 Introduction

In the work presented in this thesis, nucleation of different powder wettabilities produced either liquid marbles or immersion nuclei. Granulation of these liquid marbles or immersion nuclei in low and high shear mixers produced different granule internal microstructures. Some of the granules produced have a solid internal microstructure, while others have a hollow internal microstructure and with different wall thickness. In Chapter 6 efavirenz as a non-wetting powder, IROX as a wetting powder and different concentrations of dextran as a liquid binder were used to investigate the effect of powder wettability and binder viscosity on granule internal microstructure. In order to understand the mechanistic behaviour of the formation of different internal microstructures of granules, two novel regime maps were developed.

The first regime was developed for powder of medium and high wettabilities, while the second regime for powder of high wettability. In both regime maps, dimensionless groups were developed and used to demarcate the boundary between different behaviour of granule internal microstructure.

Population balance modelling has been used to simulate granule growth and consolidation by many researchers. Granulation rate kernels were developed to model growth by granule-granule collision (Peña et al. 2017). A model of granule layering is previously developed and has been used to quantify and predict the increase in the size of the nuclei produced by immersion nucleation through the attachment of fresh primary particles (Hounslow et al. 2009).

However, no study has specifically looked at the mechanisms involved in the formation of the internal microstructure of granules formed from powder blends of different wettabilities. In this study, the internal microstructure of granules produced in low and high shear mixers were investigated. Dimensionless groups were developed based on mechanistic understanding and physical phenomena occurring during the process. Results were analysed for different formulation and process parameters. These dimensionless groups were used to determine the boundary between different regimes of the change in the granule internal microstructure produced using different parameters. Understanding the mechanisms of the changes of granule internal microstructure produced from powder of different wettabilities will allow a quantitative explanation of the variation in a granulation process. This may provide an opportunity to predict granule internal microstructure and to easily adjust the equipment for further different process and formulation parameters

Section 7.2 will discuss the first regime map. Here, the granules are produced using medium and high powder wettabilities. The immersion rate limited is the only kinetic behaviour identified in this regime.

Section 7.3 will discuss the second regime map. Here the granules are produced using low powder wettability. Three different kinetic behaviour are introduced; inertial force dominated, surface tension and viscous forces dominated and combined forces; inertial, surface tension and viscous forces dominated.

7.2 Granule kinetic behaviour using powder of medium and high wettability

The aim of this part of the study is to understand the kinetic mechanism of granule internal microstructure produced using medium and high powder wettabilities by development of a regime map. The data used in this section is adopted from Chapter 6. Here, efavirenz was used as a non-wetting powder, IROX as a wetting powder and different concentrations of dextran were used as a liquid binder. These were granulated in low and high shear mixers.

7.2.1 Background

In wet granulation, there are two different nuclei formation mechanisms; distribution or immersion, depending on the relative size of the liquid droplets to the primary particles. If the size of the liquid droplets is smaller than that of the primary particle size, then distribution nucleation will occur. In this case, the liquid droplets coat the primary particles which on subsequent collision will combine to form small agglomerates. If the liquid droplet is larger in size than the powder particles, immersion nucleation will occur. In this instance, powder particles spread over the liquid droplet and driven by surface tension and other forces and will enter the droplet. This granule nucleus will increase in size through the attachment of the fresh powder particles to the liquid that is available on the surface of the nucleus. This observation in wet granulation has been recognised and described and it is found that the immersion nucleation is favoured over distribution nucleation because the granules produced by immersion tend to be spherical and consolidated (Iveson et al. 2001).

7.2.3 Kinetic analysis: Theory

In the granulation process described here, granules are formed by the collision between the preformed liquid marbles or immersion nuclei and powder bed in a low and a high shear mixer. According to Arjmandi-tash, Tew, Pitt, Smith, & Litster, 2019, the time of granulation and collisions between the preformed liquid marbles or immersion nuclei and the powder bed depend upon the impact velocity, surface tension and binder viscosity and powder wettability at the liquid droplet-powder interface, and the following scenarios may happen:

- 1- High powder wettability; the powder liquid contact angle is less than 90° ($\theta < 90^\circ$). The penetration of powder particles inside the liquid marbles or immersion nuclei depends on binder viscosity and surface tension forces. However, the kinetics of immersion can be limited by immersion, collision or both of them.
- 2- Low powder wettability; the powder liquid contact angle is more than 90° ($\theta > 90^\circ$). The powder particles can either stay at or rebound away from the liquid droplets due to the surface tension force. However, the powder particles can penetrate inside the liquid droplet due to high impact forces that overcome the surface tension forces.

Arjmandi-tash et al. 2019, presented two dimensionless groups for the kinetics of immersion of powder particles inside the liquid droplets when the powder liquid contact angle is less than 90° depending on surface tension and binder viscosity. This will form the basis of the work presented in this chapter. For developing both dimensional groups, further immersion of powder particles inside the liquid droplets is considered to occur by compressive forces between the contacting particles. Therefore, the shell of the liquid marble or immersion nucleus should have a constant particle packing volume fraction and there is liquid in between them. This is called the critical-packing liquid volume fraction, ϕ_{cp} , and according to this, the centre of the liquid marbles or immersion nuclei should be composed of liquid binder (Arjmandi-tash et al. 2019).

In this instance, the granule internal structure is controlled by the immersion rate of particles inside the liquid droplets, collision rate between the liquid marbles or immersion nuclei and powder bed or by both of them. In the first case, termed the immersion rate limited regime, it assumed that the rate of immersion is controlled by binder viscosity and surface tension if the powder wettability and the droplet diameter are the same. For example, the penetration of the

powder particles inside the liquid droplets occurs fast using low binder viscosity according to the Darcy law and Kozeny Carmen equations. The timescale of granule nucleation in an immersion rate limited regime can be found by Arjmandi-Tash et al. 2019:

$$t_{imm} = \frac{15 \mu_d D_d^2}{4 D_p \gamma \cos \theta} \frac{(1 - \varphi_{cp})}{\varphi_{cp}^3} \quad \text{Equation (7.1)}$$

where μ_d is liquid binder viscosity, D_d is droplet diameter, φ_{cp} is the critical packing liquid volume fraction which has a constant value of 0.36 (Dullien et al. 1992), D_p is the primary powder particle size, γ is liquid surface tension and θ is powder liquid contact angle.

For the second case, the collision rate limited regime, it is assumed that the penetration of powder particles inside the liquid droplets due to the wetting action at the interface is fast, the rate of granulation nucleation is limited by the collision rate and the arrival of particles to the surface of the liquid droplets especially if the collision rate of binder droplets and particles is not sufficiently high. A simplified equation from Arjmandi-Tash et al. 2019 was used, in which the change in relative velocity of primary particles in the powder bed over time was neglected. This was based on the assumption that the volume of powder bed inside the mixer remains constant during granulation.

If it is assumed that the immersion of powder particles inside the liquid droplets is limited by the arrival of crystals at the surface of the growing nucleus. Then, the time scale for complete immersion of powder particles inside the liquid droplet is limited by collision rate and can be calculated by:

$$t_{coll} = \frac{D_d (1 - \varphi_{cp})}{v \varphi_{pb} \varphi_{cp}} \quad \text{Equation (7.2)}$$

where D_d is the droplet diameter, v is the relative velocity between liquid droplet and the particles and it is taken as the wall velocity or drum periphery which is equal to (ωa) in which ω is a mixer velocity and a is a mixer diameter. Parker et al. 1997 tracked similar size particles inside the rotating drum by using positron emission particle tracking. They used 1.5 mm particles in a 0.136 m diameter drum. They found that the free surface particle velocity matched the wall velocity (0.45 m/s). This shows that it is acceptable to use the approximation of particle

velocity as the speed of drum periphery. ϕ_{pb} is a particle volume fraction in the bulk of powder bed and it is constant (0.64) (Dullien et al. 1992).

In some cases, the system can be controlled by both the immersion rate and collision rate. A granulation number (G_{Nu}) is obtained by calculating the ratio between timescales for complete granulation limited by the immersion rate and collision rate. In this instance, one can find the boundary between different behaviour of granule internal microstructure for the process:

$$G_{Nu} = \frac{t_{imm}}{t_{coll}} \quad \text{Equation (7.3)}$$

For systems with a granulation number larger than 1 (e.g. $> 10^2$), the granulation process is limited by the immersion rate, and the kinetic behaviour of granule internal microstructure can be explained using Equation (7.1). For systems with granulation number lower than 1 (e.g. < 0.01), then the collision rate is the controlling rate and is limited by the arrival of powder particles at the surface of the liquid droplets. The behaviour of granule internal microstructure can be explained using Equation (7.2). However, for a system with granulation number close to 1, the granule internal microstructure is limited by both of the immersion and the collision rate and can be explained using both equations; Equation (7.1) and Equation (7.2) (Arjmandi-tash et al. 2019). In the next section, a regime map for the internal granule microstructure will be presented to discuss the effect of immersion and collision kinetic on granule internal microstructure.

7.2.4 Regime maps of granule behaviour of medium and high powder wettabilities

Using the theory developed by Arjmandi-Tash et al. 2019, two different model systems of granules produced using medium and high powder wettabilities were used. Each system was produced using three different binder viscosities, binder surface tension, binder density and binder droplet diameter as can be seen in Table 7.1. All these formulation parameters were used to discuss the conditions for using the developed immersion rate and collision rate equations, and the formation of granule internal microstructure in each model.

According to the results identified in Table 7.1, immersion time, collision time and G_{Nu} increased with increasing binder viscosity and droplet diameter for both medium and high powder wettabilities. The same findings were observed for high powder wettability system, while immersion time is shorter than medium powder wettability model system. This because of improved powder wettability. It can be seen from Table 7.1 that the shortest calculated immersion time was observed using high powder wettability and at low binder viscosity and small droplet diameter. The immersion time increased with increasing binder viscosity and decreasing powder wettability. The longest immersion time was reached using high binder viscosity, and medium powder wettability due to combined effect of binder viscosity and surface tension forces.

There is a difference between collision time using low and high shear mixers. Shorter collision time was obtained using high shear mixer, and this is mean that the immersion of powder particles inside the liquid droplet occurred at shorter time than those in low shear granulation.

It can also be seen that the immersion time is longer than the collision time for all model systems in Table 7.1. This indicate that the granulation process of the all six models system used in this section are limited by the immersion rate. The collision time is far lower than the immersion time. The G_{Nu} showed a wide range of numbers ranging from 6.8 using high powder wettability and low binder viscosity to 21000 using medium powder wettability and high binder viscosity.

Table 7.1: Six different model systems for wet granulation with different formulation and process parameters along with the calculated timescales and dimensionless numbers.

Formulation and process parameters	Model systems					
	Medium powder wettability			High powder wettability		
	1	2	3	4	5	6
θ (radian)	~ 89	~ 89	~ 89	~ 64	~ 64	~ 64
μ_d (Pa s)	0.008	0.1	1	0.008	0.1	1
D_d (m)	27.58E-04	30.24E-04	3236E-04	27.58E-04	30.24E-04	3236E-04
D_p (m)	1.00E-06	1.00E-06	1.00E-06	1.00E-06	1.00E-06	1.00E-06
γ (N/m)	72.09E-03	73.09E-03	73.74E-03	72.09E-03	73.09E-03	73.74E-03
ϕ_{cp} (-)	0.36	0.36	0.36	0.36	0.36	0.36
ω (low shear) (radian/s)	2.61	2.61	2.61	2.61	2.61	2.61
a (low shear) (m)	0.035	0.035	0.035	0.035	0.035	0.035
ω (high shear) (radian/s)	38.74	38.74	38.74	38.74	38.74	38.74
a (high shear) (m)	0.07	0.07	0.07	0.07	0.07	0.07
ϕ_{pb} (-)	0.64	0.64	0.64	0.64	0.64	0.64
Measured parameters						
v low shear (m/s ⁻¹)	91.35 E-03	91.35 E-03	91.35 E-03	91.35 E-03	91.35 E-03	91.35 E-03
v high shear (m/s ⁻¹)	-	2.71	-	2.71	-	2.71
Timescales						
t_{imm} (s)	14.4	195.1	2069	0.574	7.76	82.39
t_{coll} (low shear) (s)	83.86E-03	91.15E-03	98.40E-03	83.86E-03	91.15E-03	98.40E-03
t_{coll} (high shear) (s)	-	30.97 E-04	-	28.25 E-04	-	33.14 E-04
Dimensionless parameter						
G_{Nu} (low shear) (-)	1.72 E+02	2.12 E+03	2.10 E+04	6.85 E+00	8.45 E+01	8.37 E+02
G_{Nu} (high shear) (-)	-	62.9E+03	-	2.03E+02	-	2.48E+04

Timescales for the granulation processes for immersion rate and collision rate were calculated using Equation (7.1) and Equation (7.2). Then, the dimensionless group was calculated using Equation (7.3).

A regime map has been developed. G_{Nu} is not presented in this regime map, and this is because G_{Nu} does not predict granule wall thickness, as viscous forces are not considered in t_{coll} . Viscous

forces have a significant effect on granule microstructure such as wall thickness, previously concluded in Chapters 4, 5 and 6. However, G_{Nu} values give a prediction of internal granule microstructure depending on initial formulation properties stated in Equation (7.1) and Equation (7.2). The powder wettability was plotted against viscous Stokes number. Contact angle was used to reflect the effect of powder wettability on the kinetic of internal microstructure of the granules. On the other hand, viscous Stokes number is a dimensionless group that is used to reflect the effect of the ratio of granule collisional kinetic energy to the viscous dissipation brought about by interstitial binder according to (Ennis et al. 1991):

$$St_v = \frac{8\rho_l v D_g}{9\mu} \quad \text{Equation (7.4)}$$

where ρ is the liquid density, v is the characteristic shear velocity, it is taken as the wall velocity which is equal to (ωa) , a is granule radius and μ is binder viscosity. The data of the viscous Stokes number can be found in Table 7.2. It can be seen in Table 7.2, that as the binder viscosity and density and granule size increased the st_v decreased.

Table 7.2: Six different model systems for wet granulation of different formulation and process parameters along with the calculated viscous Stokes numbers.

Parameters	Model systems					
	Medium powder wettability			High powder wettability		
	$\theta \approx 89^\circ$	$\theta \approx 89^\circ$	$\theta \approx 89^\circ$	$\theta \approx 64^\circ$	$\theta \approx 64^\circ$	$\theta \approx 64^\circ$
ρ_l (kg/m ³)	1040	1130	1200	1040	1130	1200
ω (low shear) (radian/s)	2.61	2.61	2.61	2.61	2.61	2.61
a (low shear) (m)	0.035	0.035	0.035	0.035	0.035	0.035
ω (high shear) (radian/s)	38.74	38.74	38.74	38.74	38.74	38.74
a (high shear) (m)	0.07	0.07	0.07	0.07	0.07	0.07
D_g (m)	13.79E-04	15.12E-04	16.18E-04	13.79E-04	15.12E-04	16.18E-04
μ (Pa s)	0.008	0.1	1	0.008	0.1	1
Measured parameters						
v (low shear) (m/s ⁻¹)	91.35 E-03	91.35 E-03	91.35 E-03	91.35 E-03	91.35 E-03	91.35 E-03
v (high shear) (m/s ⁻¹)	-	2.71	-	2.71	-	2.71
Dimensionless group						
St_v (low shear) (-)	14.55	1.38	0.15	14.55	1.38	0.15
St_v (high shear) (-)	-	41.18	-	4.32 E+02	-	4.68

Figure 7.1 shows a regime map of granule internal microstructure using low shear mixer in terms of contact angle and viscous Stokes number. As mentioned above, all the six model systems used are limited by the immersion rate. However, there is a difference in granule internal microstructure. This suggested that when the G_{Nu} is low, the immersion time is low, leading to the fast penetration of powder particles inside the liquid droplet. This results in the production of granules with solid internal microstructure. This occurred when using low binder viscosity and high powder wettability. When the G_{Nu} is high, the immersion time is longer, and the liquid droplet might evaporate before the powder particles can penetrate inside the liquid droplet. This results in the production of a granule with hollow internal microstructure. This occurred when using high binder viscosity and low powder wettability.

Using a powder of high wettability and low and medium binder viscosities (bottom right corner in Figure 7.1), it can be seen that the G_{Nu} is small. This means that the immersion of powder particles inside the liquid droplet is fast. In this system, the immersion of powder particles inside the liquid droplet happens immediately and spontaneously without the need of any impact to push the powder particles inside the liquid droplet. The granules produced in this regime appeared to have a solid internal microstructure.

In the system using high powder wettability and high binder viscosity (lower left of Figure 7.1), the immersion of powder particles inside the liquid droplet is mostly retarded by the effect of viscous forces. Therefore, the immersion of powder particles inside the liquid droplet takes longer time. Hollow granules are produced in this system is probably because the liquid droplets drying time is faster than the penetration of powder particles inside the liquid droplets, especially as granules were dried in an oven.

For systems using medium powder wettability and different binder viscosities (upper row of Figure 7.1), contact angle at a three face contact line is higher than the system using high powder wettability. The G_{Nu} in the system using medium powder wettability and low binder viscosity is 172, this dimensionless number increases to 2120 and 21000 using medium and higher binder viscosity respectively. Most of granules produced using medium powder wettability and different binder viscosities have a hollow internal microstructure. This is most

probably because of the wettability effect that resists the immersion of powder particles inside the liquid droplets, this effect is enforced by using high binder viscosity.

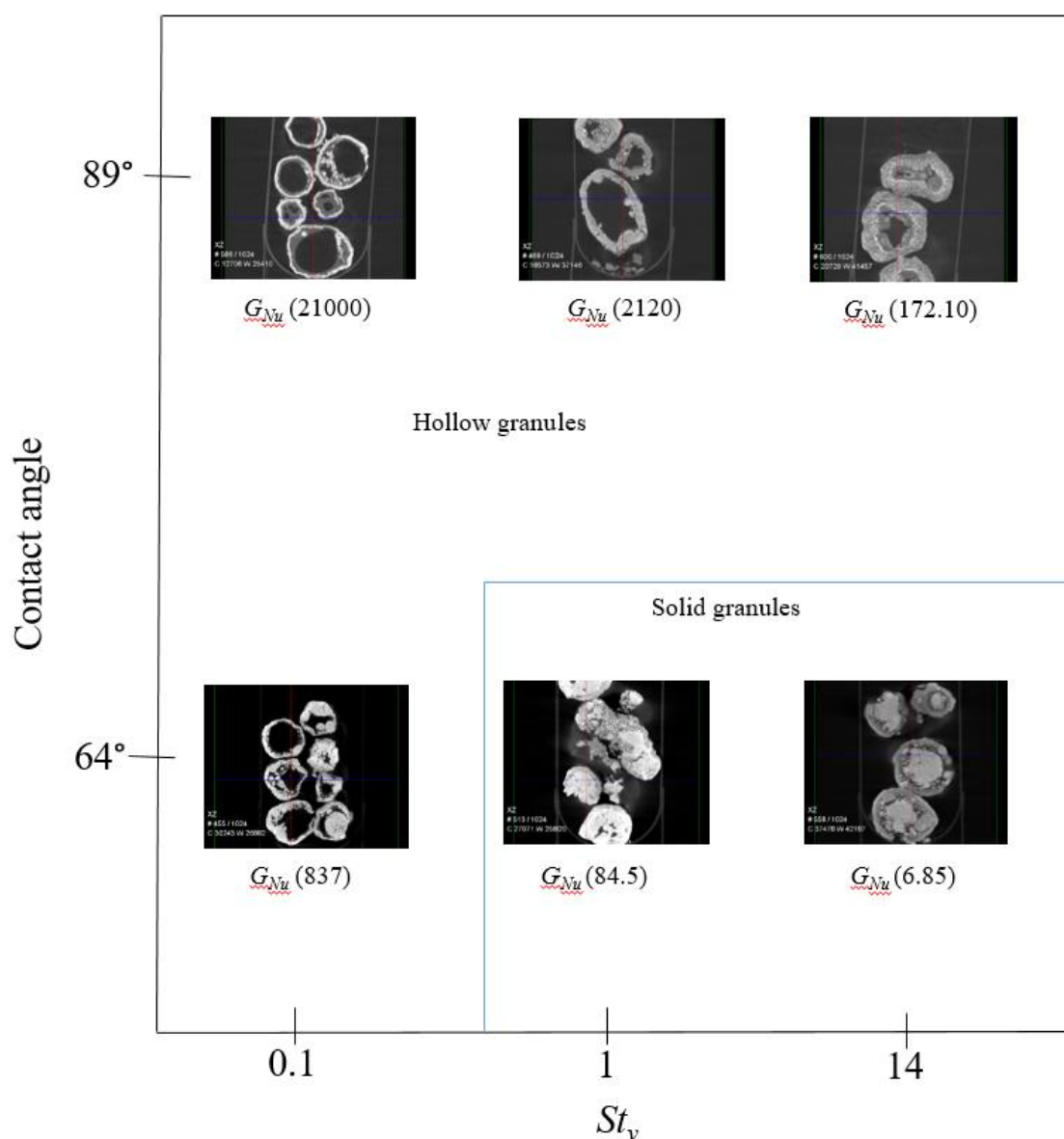


Figure 7.1: Regime map of granule internal microstructure in terms of contact angle and St_v in low shear mixer.

It should be noted that only three granulation experiments in high shear mixer were performed for powder wettability ($\theta < 90^\circ$), and presented as three images in Figure 7.2. The same observation was found compared with granulation in low shear mixer. However, lower collision times and then high G_{Nu} values were obtained, because of high inter-particle velocities in the high shear system compared to the low shear granulation. The immersion time for all three model systems used are longer than the collision time, this means that the all granulation process in these model systems are limited by the immersion rate (Table 7.1). The lower right

corner in Figure 7.2 with system using high powder wettability and low binder viscosity the G_{Nu} has the lowest immersion time, indicating that immersion is fast. The granules produced within this regime appeared to have a solid internal microstructure.

For a system using high powder wettability and high binder viscosity, the immersion time is longer, because using high binder viscosity resists the immersion of powder particles inside the liquid droplet. Hollow granules are produced in this system, including drying in an oven, probably because the liquid droplet drying time is faster than the immersion of powder particles inside the liquid droplets.

For the system using medium powder wettability and medium binder viscosity the G_{Nu} is the highest. This means that the immersion of powder particles inside the liquid droplet will take longer due to the effect of viscous and surface tension forces. These forces resist the penetration of powder particles inside the liquid droplet. Hollow granules are produced in this system due to the effect of surface tension and binder viscosity.

It can be concluded that, hollow granules are produced when the G_{Nu} is approximately larger than 500 in low shear mixer and approximately larger than 10000 in high shear mixer. The discrepancies in the critical values for G_{Nu} between different mixer types is most likely due to inaccuracies in the estimation of particle velocities in these systems. Estimating the inter-particle velocities for these systems is notoriously difficult. This is expected to also give inaccurate estimation of St_v . In this study, the approximate relative velocity was predicted as a wall velocity of the mixer of the low shear or the tip speed of the high shear. To accurately determine the particle velocity, modelling or particle tracking should ideally be employed, but this was not available for this study. Inaccurate estimation of St_v resulted in difficulty to include both systems in one regime map.

It can be concluded that, in this study, the binder viscosity is the most contributing factor in producing hollow granules. High binder viscosity produced hollow granules regardless of powder wettability. The higher binder viscosity increases the immersion time into the powder particles into the liquid droplet.

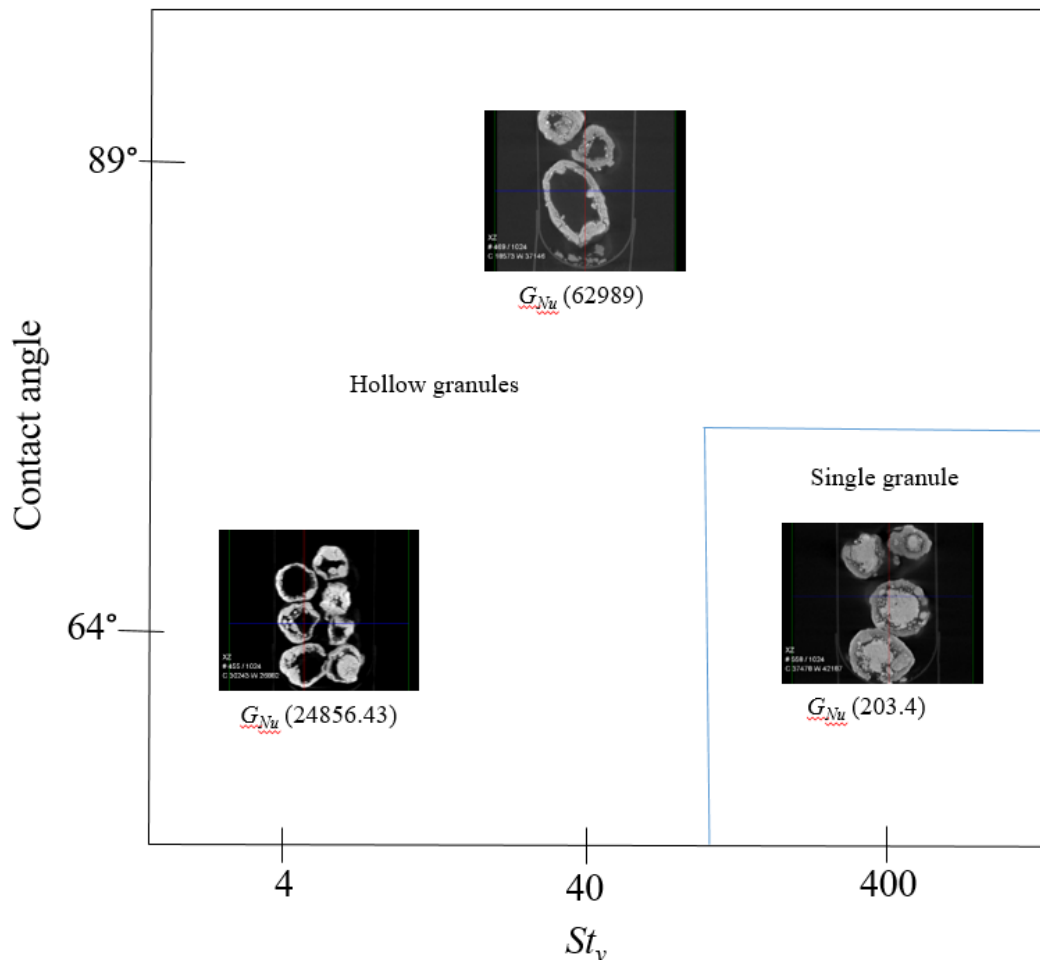


Figure 7.2: Regime map of granule internal microstructure in terms of contact angle and St_v in high shear mixer.

7.3 Granule kinetic behaviour using low powder wettability

In the previous section, the G_{Nu} value of granules was used for wettable powders (contact angle $< 90^\circ$). However, in the case of low powder wettability (contact angle $> 90^\circ$), the G_{Nu} analysis is not applicable and it results in negative values. This means that the immersion time is infinite and the most of powder particles either stay at or rebound from the surface of the liquid droplet. The only way that the non-wetting particles move to droplet surface can be by the high impact forces. However, wetting particles in the mixture can penetrate inside the liquid droplet.

In this case, different influential forces will affect the internal microstructure of the granules. Dimensionless groups will be use to explain the effect of different forces on the granulation of

low powder wettability and the kinetic behaviour of granule internal microstructure. The data used in this section is adopted from Chapter 6, where efavirenz as non-wetting powder, IROX as wetting powder and different concentrations of dextran as a liquid binder, and these were granulated in low and high shear mixers.

7.3.1 Background

It is well known that the motion of small insects on a water surface is an interesting subject of many researchers. The small object has the ability to remain afloat even with a high density on water due to the interfacial forces at a liquid and a gas interface. Although this effect is important for water-walking creatures to avoid drowning (Gao et al. 2004), it is also important on other aspects such as mineral flotation and self-assembly using surface tension forces (Braun et al. 2012).

Researchers have given an attention to understanding and explain the ability of small objects to float on water surface at equilibrium, and the question of when the object will sink if the balance of forces is lost. This can happen if the vertical forces provided by surface tension is decreased or when a portion of meniscus is eliminated, which can be easily achieved by the adding surfactant to the water (Vella et al. 2006).

Wang et al. 2015 reported that hydrophobic powder particles which spread on liquid droplets undergo two stages; movement after impacting on the droplet surface and movement to the droplet surface under the influence of external forces. Particles collide with the droplet surface under the action of impact forces. After collision of the powder particles with the liquid droplets, wetting particles enter the droplets, while non-wetting particles may enter the droplets, remain on the surface or rebound under the action of surface tension.

Wang et al. 2015, described the effect of impact forces, inertial and surface tension, which is important for scrubbing hydrophobic particles by droplets. Scrubber systems are control devices that can be used to purified the industrial exhaust streams. They developed dynamic simulations and showed that the micron sized hydrophobic particles exhibit three motional behaviours; “submergence, oscillation and rebound”, with an increase in the impact velocity applied. The criteria of these three motions were investigated by calculating their critical

velocities with a simplified method. Then, the accuracy of the impact criteria was verified by the results of numerical simulation.

Lee et al. 2008, developed a regime map to explain the impact behaviour of millimetre super hydrophobic spheres onto water. Three distinct impact behaviours were discovered; “damped oscillation, bouncing off and sinking”, depending on impact condition. They defined these three kinds of behaviour by using the Weber number and Bond number. The Weber number (W) describes the relative magnitude of liquid inertial to surface tension forces, while the Bond number (B) describes the relative magnitude of gravitational to surface tension forces.

Lee et al. 2008, concluded that there are three different impact behaviours of hydrophobic particles, with powder/liquid contact angles greater than 120° , onto a liquid droplet. At low velocity, the particles hit the liquid surface and it might oscillate. With increasing impact velocity, the oscillation amplitude first increases. Further increases in impact velocity make the particles rebound off the liquid surface. However, with a further increase in the impact velocity, the particles penetrate the interface and sink.

However, no previous study has specifically looked at the behaviour of granule internal microstructure produced using low powder wettability in low and high shear mixers. In this study, the forces affecting granule internal microstructure using low and high shear mixers were investigated. Then, dimensionless groups were developed based on mechanistic understanding of the process. Results were analysed based on the difference in formulation and process parameters. These dimensionless groups were used to determine the boundary between different regimes of granule internal microstructure produced using different parameters.

7.3.2 Kinetic analysis: Theory

The granulation of non-wetting powder in this study was performed by formation of liquid marbles outside the granulator in a petri dish and then putting inside low and high shear mixers for granulation. Wang et al., 2015, found that the impact behaviour of granules inside the granulator was influenced by surface tension, drag force, buoyancy, viscous force and added inertial forces. Lee et al. 2008 found that the motion of a sphere can be obtained by equating the granule inertia to the sum of the above forces. Dimensionless analysis simplified this

physical phenomenon, in which the impact behaviour of the granules can be determined by Bond number, Weber Number, Reynolds number and contact angle. The Reynolds number describes the relative magnitude of inertial forces to viscous forces (Chetia et al. 2000).

In this study, two impact behaviours only will be considered; oscillation and immersion. This is because Lee et al. 2008 found that the non-wetting particles do not rebound off when the liquid viscosity is higher than 3 mPa s, which is lower than the lowest binder viscosity used in this study.

At the time of granulation, collisions between the preformed liquid marbles and the powder bed can be described by added inertia, surface tension, binder viscosity and powder wettability at the binder-powder interface. In this part of the study, the ratio between the inertial force to surface tension and viscous force will be taken to develop a regime map. Therefore, the Weber number (W) multiplied by the Reynolds number (Re), (WRe), will be used in this regime map and will represent the relative magnitude of inertial forces to surface tension and viscous forces. This will describe the internal microstructure behaviour of non-wetting powder particles on the liquid droplet, with a contact angle higher than 120° .

The following scenarios may happen inside the granulator:

- If the value of WRe is high, immersion of non-wetting powder particles inside the liquid droplets occur due to high inertial force that overcomes the surface tension and viscous forces. The kinetics of immersion is dominated by inertial forces.
- If the value of WRe is low, then there is a combined effect of three forces; inertia, surface tension and viscous forces. There may be a balance effect of these three forces and limited immersion of powder to the droplet surface is expected. The kinetic behaviour is dominated by all three forces.
- If the value of WRe is very low, then the powder particles will stay at the surface of the liquid droplet. The kinetic behaviour is dominated by surface tension and viscous forces. The inertial force cannot overcome the surface tension and viscous forces and it cannot force the powder particles into the liquid droplets.

Here, two dimensionless groups are presented for the immersion kinetics of powder particles onto the surface of the liquid droplets. In this instance, the granule structure is controlled by the immersion of particles into the liquid droplets by the effect of inertial force, or oscillation

of powder particles onto the surface of the liquid droplet by the effect of surface tension and viscous forces. In the first case, it is termed the inertial force dominated regime, and the second case it is termed the surface tension and viscous forces dominated regime. Additionally, it can be dominated by all three forces; inertial, surface tension and viscous forces and it is termed combined forces dominated regime.

In this study, W number was used to show the relationship between inertial forces to surface tension forces according to Equation (7.5) (Lee et al. 2008). Depending on the data obtained, it suggests that these two forces and the powder wettability affect the formation of hollow granules from liquid marbles:

$$W = \frac{(2R_d)\rho_l\ddot{u}^2}{\gamma} \quad \text{Equation (7.5)}$$

where R_d is the liquid droplet radius, ρ_l is the liquid density, \ddot{u} is the particle acceleration and γ is the liquid surface tension.

Acceleration is the rate of change of velocity ($\Delta\ddot{u}$) with respect to time (Δt),

$$\ddot{u} = \frac{\Delta u}{\Delta t} = \frac{v - v_o}{t} \quad \text{Equation (7.6)}$$

where v is the initial velocity, v_o is the final velocity and t is the time. The time of the non-wetting particles to penetrate inside the liquid droplets was calculated according to (Aristoff et al. 2009). Aristoff et al. 2009, used both experimental and theoretical investigations to explain the impact behaviour of hydrophobic particles onto a water surface. A hydrophobic sphere released from a particular height to the water surface and the maximum depth (Z_{max}) the sphere reached before pinch off from the water surface was calculated. Then, the depth at which the sphere was completely separated from the water surface, pinch off depth (Z_{pinch}) was measured according to maximum depth (Figure 7.3). Then, the time at pinch off depth (t_{pinch}) is calculated.

In this study, t_{pinch} was calculated and represents the time required for the non-wetting particles to penetrate inside the liquid droplet.

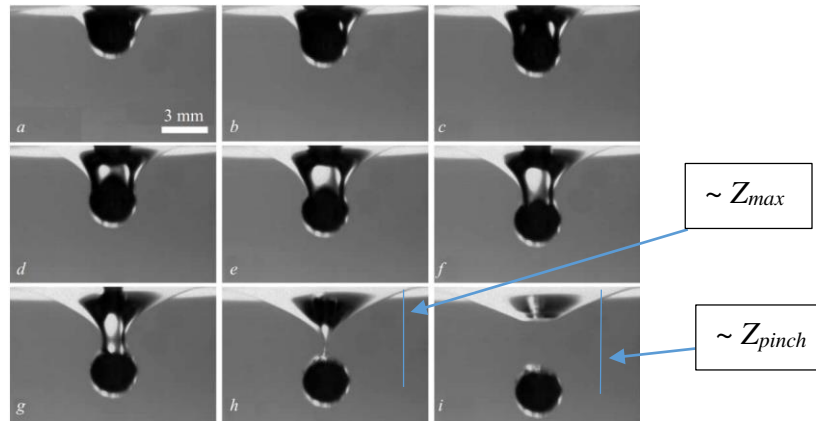


Figure 7.3: Images of video sequence of the water entry of a hydrophobic sphere.

Aristoff & Bush, 2009, Water entry of small hydrophobic spheres, Journal of fluid mechanics, vol. 619, pp. 45-78, reproduced with permission.

According to Aristoff et al. 2009, the penetration depth, Z_{max} , was calculated by experimental trial. They used Bond number (B) and contact angle to calculate Z_{max} according to Equation (7.7).

$$\frac{Z_{max}}{R_p} \sim 0.83 B^{-0.035 \log_{10} B - 0.31} \left(\sin \frac{\theta}{2} \right)^{1.6} + 1 \quad \text{Equation (7.7)}$$

where R_p is the particle radius, B is Bond number and θ is the contact angle. The Bond number is the ratio of gravitational forces to capillary forces (Equation (7.8)) (Lee et al. 2008):

$$B = \frac{\rho_l g (2R_d)^2}{\gamma} \quad \text{Equation (7.8)}$$

where ρ_l is the liquid density, g is the acceleration due to gravity, R_d is the radius of the liquid droplet, γ is the liquid surface tension.

Then, according to geometric relation, the Z_{pinch} is calculated according to the following equations:

$$Z_{pinch} \approx Z_{max} - 1 \quad \text{for } B \gg 1, \quad \text{Equation (7.10)}$$

$$Z_{pinch} \approx Z_{max} + \cos \left(\pi - \frac{\theta}{2} \right) \quad \text{for } B \ll 1, \quad \text{Equation (7.9)}$$

Likewise, the pinch off time can be calculated in term of pinch off depth as:

$$t_{pinch} \frac{\ddot{v}}{R_p} = \frac{Z_{pinch}}{R_p} + 1 \quad \text{Equation (7.11)}$$

The predicted theoretical pinch off time according to Equation (7.11) differs from that proposed by Lee et al. 2008; the pinch off time is assumed to be the time for the capillary-gravity wave to travel the capillary length leading to $t_{pinch} \sim W^{1/2}$.

The Reynolds number (Re), on the other hand, is the ratio between inertial forces to viscous forces and is a convenient parameter to predict the fluid flow behaviour (Chetia et al. 2000). In this study, Re will show the effect of inertial forces relative to viscous forces according to Equation (7.12) (Lee et al. 2008) :

$$Re = \frac{\rho_l v (2R_d)}{\mu} \quad \text{Equation (7.12)}$$

where ρ_l is the liquid density, v is the relative velocity and it is taken as wall velocity (ωa), R_d is the liquid droplet radius and μ is the liquid viscosity.

To include the effects of inertial forces, surface tension and viscous forces, the Weber number can be multiplied by the Reynolds number (WRe). This dimensionless number will be plotted as a function of powder wettability expressed by the contact angle of powder on the liquid droplet. Then, different granule internal behaviour depending on different impact forces will be presented and a regime map for non-wetting powder will be developed.

7.3.3 Regime maps of granule behaviour of low powder wettability

Three different model systems are presented in Table 7.3. Each model consists of granules produced using low powder wettability with different binder viscosities in a low and a high shear mixer. All these formulation parameters are used to discuss the conditions to investigate and understand the behaviour of powder particles with liquid droplets, and the resultant internal granule microstructure.

For the determination of the effect of the three forces; inertial, surface tension and viscous forces on the granule internal microstructure using non-wetting powder, a regime map was developed. Three different regime maps are identified; inertial force dominated regime, surface

tension and viscous forces dominated regime and combined forces dominated regime; inertia, surface tension and viscous forces.

According to the results identified in Table 7.3, time for the powder particle to penetrate to the liquid droplet (t_{pinch}) increased with increasing binder viscosity, droplet diameter and binder surface tension, while, acceleration velocity decreased with increasing these parameters. WRe decreased with increasing binder viscosity and binder surface tension. Smaller values of WRe were observed using low shear mixer than high shear mixer due to the high impact forces applied by the high shear mixer.

Table 7.3: Three different model systems of granules produced using low powder wettability with different formulation and process parameters along with the calculated parameters and dimensionless numbers.

Formulation and process parameters	Model system		
	Low powder wettability		
	1	2	3
θ (radian)	125	125	125
μ (Pa s)	0.008	0.1	1
R_d (m)	13.79E-04	15.12E-04	16.18E-04
R_p (m)	5.00E-07	5.00E-07	5.00E-07
γ (N/m)	72.09E-03	73.09E-03	73.74E-03
ρ_l	1040	1130	1200
$\omega_{low\ shear}$ (radian/s)	2.61	2.61	2.61
$a_{low\ shear}$ (m)	0.035	0.035	0.035
$\omega_{high\ shear}$ (radian/s)	38.74	38.74	37.74
$a_{high\ shear}$ (m/s)	0.07	0.07	0.07
g (ms ⁻²)	9.8	9.8	9.8
Calculated parameters			
$v_{low\ shear}$ (m/s ⁻¹)	91.35E-03	91.35E-03	91.35E-03
$v_{high\ shear}$ (m/s ⁻¹)	2.71	2.71	2.71
B	0.53	0.69	0.83
Z_{max}/R_o	6.37E-01	7.67E-01	8.44E-01
Z_{pinch}/R_o	1.76E-01	3.05E-01	3.38E-01
$t_{pinch(low\ shear)}$	1.91E-01	3.21E-01	4.00E-01
$t_{pinch(high\ shear)}$	1.76E-01		3.83E-01
$\ddot{u}_{low\ shear}$ (m/s)	0.47	0.28	0.22
$\ddot{u}_{high\ shear}$ (m/s)	15.4		7.07
Dimensionless groups			
$W_{(low\ shear)}$	9.13	3.77	2.74
$Re_{(low\ shear)}$	32.75	3.12	0.35
$W_{(high\ shear)}$	9437.02		2635.39
$Re_{(high\ shear)}$	65.50		0.70
$WRe_{(low\ shear)}$	299.12	11.78	0.97
$WRe_{(high\ shear)}$	618174.71		1869.71

Figure 7.4 shows a regime map of internal microstructure of granules produced using low shear mixer in terms of WRe number. It can be seen that there are three regimes; on the left hand, at low WRe number, the effect of surface tension and viscous forces are predominant and acts as a resistant force against the inertial force. The inertial force effect is minimal and cannot overcome the surface tension and viscous forces and cannot force the particles inside the liquid droplet. Therefore, the powder particles stay at the surface of the liquid droplet and the granules produced in this regime have a hollow internal microstructure.

On the right side of Figure 7.4 the value of WRe is high, and this means that the effect of inertial forces is predominant and the effect of surface tension and viscous forces are minimal. For this reason, inertial forces can overcome the surface tension and viscous forces and push the powder particles inside the liquid droplet. This regime is called inertia force dominated regime and granules appeared to have a solid internal microstructure.

However, when the WRe value is between 10-100, there is limited immersion of the powder particles inside the liquid droplets. This is because this system is under the effect of three forces; inertial, surface tension and viscous. The inertial force is not enough to overcome the surface tension and viscous forces and push the powder particles inside the liquid droplet and the surface tension and viscous forces are not enough to overcome the inertial forces. Therefore, the effect of the three forces are comparable and most of the powder particles stay at the surface of the liquid droplets with limited immersion. This regime is called combined forces; inertial, surface tension and viscous forces dominated regime.

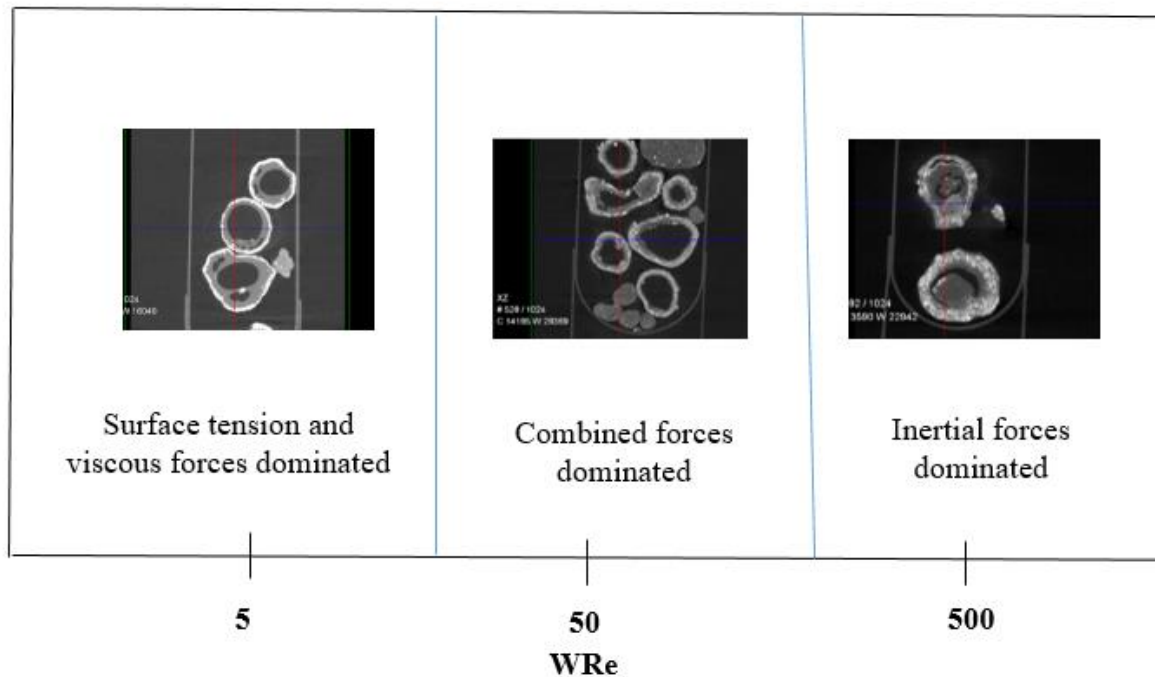


Figure 7.4: Regime map of granule internal microstructure in low shear mixer.

For a system using high shear mixer (Table 7.3), the WRe value is higher than the value of granules produced using low shear mixer and this means that the inertial forces are the predominant forces. The inertial force is high enough to overcome the surface tension and viscous forces and can force the powder particles inside the liquid droplet. However, the preformed liquid marbles were fragile and can be destroyed if they experience high impact forces during granulation.

Figure 7.5 shows a regime map of granule internal microstructure produced in high shear mixer. On the left hand side of Figure 7.5, the WRe value is high, and the inertial force can push the powder particles inside the liquid droplet. However, a deformation of granule shape after drying was observed. On the right hand side of the regime map of Figure 7.5, the WRe is the highest and the inertial forces led to the destruction of the preformed liquid marbles during granulation and no granules were obtained after drying. The surface tension and viscous forces in this regime cannot withstand the inertial forces and therefore, cannot keep the liquid marbles intact during granulation.

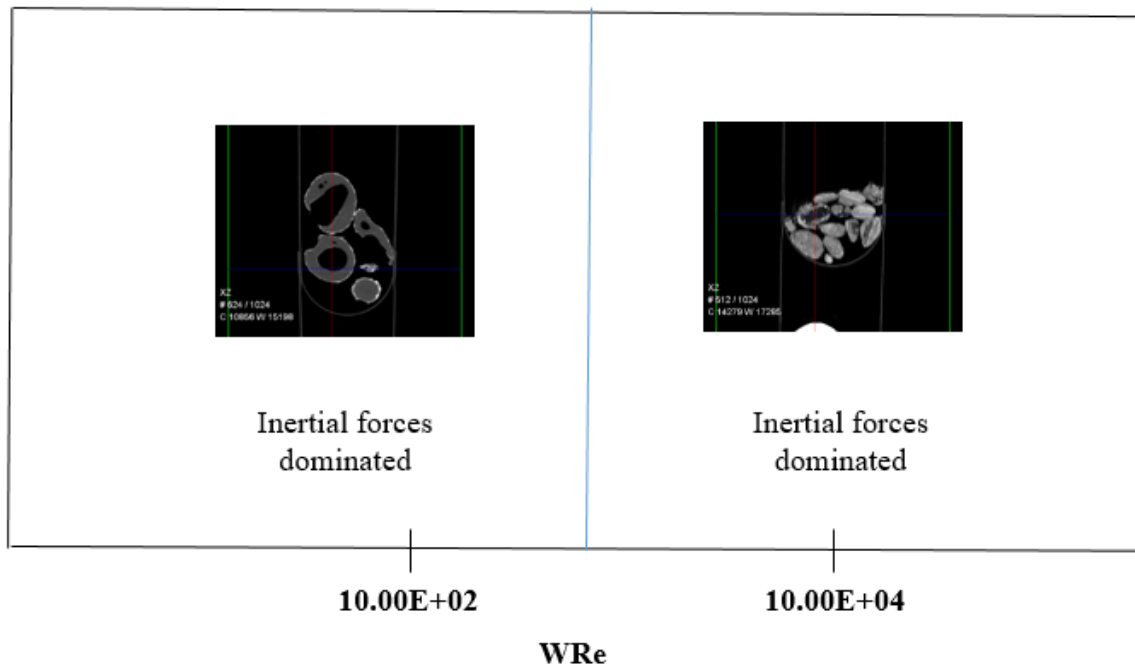


Figure 7.5: Regime map of granule internal microstructure in a high shear mixer.

It can be concluded that:

- If $WRe < 10$, then the surface tension and viscous forces are dominant and the particles cannot penetrate the liquid droplets. The powder particles in this case will stay at the droplet surface forming a powder layer on the surface of the liquid droplet leading to the formation of a hollow granule internal microstructure upon drying.
- If WRe is between 10-100, the effect of the three forces are comparable, in which there is a limited penetration of powder particles inside the liquid droplet. The granules produced in this regime consist of a thicker wall thickness than the previous regime and still have hollow internal microstructure.
- If WRe is > 100 , the inertial force is dominant and this force can push the powder particles inside the liquid droplet and overcome the resistance forces; surface tension and viscous forces. The granules in this regime can have a solid internal microstructure.
- If the WRe value increases further than 1000, such as the granules that produced using high shear mixer, inertial force is still dominant and can force the powder particles inside the liquid droplet with deformation of the granules shape observed upon drying. A further increase of WRe means the inertial force is very high, and the preformed liquid marbles cannot withstand the impact forces applied during granulation, which leads to

the destruction of the preformed liquid marbles during granulation. In this case, no granules were produced. In this regime, surface tension and viscous forces cannot withstand the impact forces and keep the preformed liquid marbles intact.

It should be noted that it is difficult to include the data from both low and high shear granulations in one regime map. This is very likely due to the inaccurate estimation of particle velocity in both low and high shear mixers. Accurate measurements of particle velocity during granulation can be performed by using tracers such as Positron Emission Particle. However, this is an expensive technique and was not available in this study.

The powder wettability measured by contact angle was plotted on the y-axis in Figure 7.1 and Figure 7.2, because there are many industrial powders with these different powder wettabilities. Therefore, these regime maps can give a prediction of internal granule microstructure from primary powder properties. The viscous Stokes number on the x-axis (Figure 7.1 and Figure 7.2), gives an estimation of granule collisional kinetic energy to the viscous dissipation brought about by interstitial binder. This also gives a prediction of granule internal structure from liquid binder fundamental properties and mixer velocity. WRe is used to estimate the impact forces applied on the liquid marbles or immersion nuclei by the mixer and the surface tension and viscosity forces of the liquid binder. This gives a prediction of internal granule microstructure from fundamental formulation and process properties.

For the intentional design of hollow granules, this study suggests that liquid droplet diameter should be larger than the powder particle size $D_d > D_p$, and the liquid binder should have higher viscosity to reduce shear dispersion and, in wetting system, to increase the drop wetting time scale to match or exceed the process time. In addition, the inertial forces should be limited to well below the level that would damage the liquid marble due to impact during granulation. It suggests the WRe should approximately be lower than 100 for the formation of hollow granule. Finally, the powder liquid contact angle should ideally be close (but smaller) to 90° .

Overall, the regime maps presented in this study are successful in predicting granules internal structure from their initial properties. However, a limitation in the estimation of some physical parameters such as particle velocity, which is a recurring problem in granulation research, results in difficulty to include the data from both low and high shear mixers in one regime map.

7.4 Conclusions

Novel regime maps were developed to understand the mechanistic behaviour of internal microstructure of granules produced using different powder wettabilities, binder viscosities and impact forces.

The first regime was developed for granules produced using medium and high powder wettabilities. The key conclusion of the first regime are:

- Immersion rate limited is the only kinetic behaviour of granule internal microstructure
- Binder viscosity, binder surface tension, droplet diameter effects on the immersion time of the powder particles inside the liquid droplet

A second regime map was developed for granules produced using powder of low wettability. The key conclusions of this regime are:

- Three different regime behaviours were developed; inertial force dominated, surface tension and viscous forces dominated and combined forces dominated.
- Binder viscosity, binder surface tension, droplet diameter and inertial force effects granule internal microstructure.

These dimensionless groups are proposed to account for the difference in properties between the growing powder-binder shell and the pure binder core in order to evaluate the mechanical behaviour of the forming shell and rationalise the observed microstructure.

For the intension of producing hollow granules, liquid with high binder viscosity and surface tension should be used. In addition, for the liquid marbles to survive the impact during granulation and become a hollow granule upon drying the WRe should approximately be less than 100.

These dimensionless groups will be beneficial in industry which provide an opportunity to predict granule internal microstructure through its fundamental properties which decrease the number of experimental works needed.

CHAPTER 8. Conclusions and recommendations

8.1 Introduction

This thesis investigation into the fundamentals and mechanisms regarding the granulation of heterogeneous wetting formulations. This thesis has proposed novel regime maps to qualitatively or semi-quantitatively analyse granule internal microstructure. This presents a unique approach to understanding the effect of formulation and process parameters on the granule size and internal microstructure of granules formed from wetting and non-wetting powder blends. The knowledge gained in this thesis can provide a practical insight during formulation and product development of pharmaceutical products in industry based on using different powder wettabilities. The aim of this chapter is to summarise the major conclusions achieved in this thesis and initiate ideas for future work.

8.2 Conclusions

The key objective of this work was to develop a mechanistic understanding of internal microstructure of granules produced using heterogeneous powder wettabilities. To this aim, novel regime maps have been developed for granule internal microstructure behaviour. Experimental data were produced using different formulation and process parameters with model and pharmaceutical powders.

The key findings achieved from this research are:

- A systematic set of experiments employing different types of powders and binders at a range of different tumbling speeds, mixing times and primary particle sizes was performed for the first time to find which conditions resulted in the formation of hollow granules and which ones resulted in the formation of solid granules. Low powder wettability, higher binder viscosity, low shearing forces and small primary particle size tend to promote the formation of hollow granules. Higher binder viscosity, prolonged mixing time and larger primary particle size tend to promote the formation of larger granules. It was found that the use of low binder viscosity and low powder wettability led to the destruction of liquid marbles inside the tumbling drum resulting in fine powder or flakes due to weak binding bridges between the binder and the powder. Different combinations of powder wettability, binder viscosity, tumbling speed, mixing time and primary particle size could result in a large change in granule size and internal

microstructure indicating careful formulation consideration during granule process development.

- A studying of the effect of shearing forces with different powder wettabilities on granule size and internal microstructure was carried out for the first time to find the conditions that result in the formation of spherical and hollow granules. This was accomplished by the use of a high shear mixer which is capable of employing large range of impeller speeds and different impeller designs. Low powder wettability, low shearing forces and a flat plate impeller tended to promote the formation of hollow granules. Low impeller speed, flat plate impeller and higher powder wettability tended to produced large granules. The wall thickness and the porosity of the hollow granules were different using different conditions. It was found that the use of 3-bladed impeller and low powder wettability led to the destruction of the preformed liquid marbles during granulation due to high shearing forces imparted. This study highlighted the importance of material properties as well as the importance of shearing forces with the preformed liquid marbles or immersion nuclei in order to control final granule size and internal microstructure. This implies that different formulations and process conditions may produce different granule size and internal microstructure.
- A systematic set of experiments was performed to investigate the applicability of the results obtained with the previous two studies using model powder blends into industrial pharmaceutical powders. For the first time, the effect of different types of powders and binders at a range of different shearing forces and mixing times was performed to observe what happens beyond liquid marble formation and which conditions result in the formation of a large, hollow granule and uniform ingredients distribution inside the granule. Low binder viscosity in low shear granulation, high binder viscosity in high shear granulation and increasing mixing time produced large granules. High binder viscosity produced hollow granules with different wall thickness and porosity, regardless of powder wettability. This was probably due to the decrease in droplet deformation. Low binder viscosity, prolonged mixing time and higher powder wettability promote more uniform ingredient distribution inside the granules. However, a wetting ingredient was found at the shell for the majority of the granules produced using different formulation and process conditions. This was probably due to migration of wetting ingredients with the binder during drying. It can be concluded that the binder viscosity plays a critical role in the resultant granule microstructure.

Different formulation and process parameters could result in granules with different properties, indicating the importance of the careful choice of materials properties and the equipment to achieve the desired end product.

- This study revealed the importance of using X-ray tomography for measuring granules porosity and investigating granule microstructure. In addition, SEM/EDS proved an important technique for investigating the composition analysis of granules produced using different formulation and process conditions.
- A mechanistic understanding of granule internal microstructure produced using different powder wettabilities, binder viscosities and shear forces was proposed. Two novel regime maps were developed. The first regime was developed for powders of medium and high wettability with a contact angle of $\sim 89^\circ$ and $\sim 70^\circ$ respectively. One limiting behaviour was identified; immersion rate limited. A dimensionless group (G_{Nu}) was developed to demarcate the boundaries between different granule internal microstructure behaviour. Hollow granules were produced with a prolonged immersion time. The second regime map was developed for powder of low wettability with a contact angle $\sim 125^\circ$. Three different regime behaviours were developed; inertial force dominated, surface tension and viscous forces dominated and combined forces dominated. A dimensionless group (WRe) in which Weber number multiplied by Reynolds number was used to demarcate the boundary between these different regimes. A solid internal microstructure was produced with increasing the inertial force which led to an increase in the immersion of powder particles inside the liquid droplet. Difficulty in the estimation of inter-particle velocity is expected to result in inaccurate estimation of the dimensionless groups. However, this study strongly demonstrates that large (> 1 mm) hollow granules can be formed in blends ranging from wetting to non-wetting through the use of: (1) high binder viscosity (> 100 mPa s) which is beneficial in two respects; decreased granule deformation and prolonged immersion time which was obvious for powder of high and medium wettabilities. (2) a combined effect of viscous force, surface tension and inertial forces represented by WRe which should not exceed 100 for the liquid marbles to survive the impact during granulation, and form hollow granules upon drying.

8.3 Recommendation for future work

Further investigation is recommended in the following areas:

- The nucleation of liquid marbles and immersion nuclei has been performed outside the granulator to reduce the complexity of the process. Further studies to produce liquid marbles and immersion nuclei in the granulator by dripping and spraying atomisation are required to investigate whether similar results will be obtained in producing spherical hollow granules.
- A scale up study for the granulation of different powder wettabilities and binder viscosities is essential for many industries such as pharmaceutical, food, chemicals and detergents.
- Granule porosity and wall thickness has so far been reported mostly for the whole granule, but not for local parts of the granule. A more detailed study of intra-granular porosity and wall thickness would provide an interesting avenue of research.
- Quantitative calculations of energy for predicting the optimum tumbling or impeller speed that is required to prevent liquid marbles breakage inside the mixer would be beneficial. This might be helpful for predicting the speed required without performing experimental works, although this is currently a challenging task in all granulation processes.
- In the pharmaceutical industry, the content uniformity distribution is essential to meet the criteria of good quality control and content uniformity from the Food and Drug Administration (FDA) for granulated material and tablets. Good mixing quality is therefore an important area for research. Research of quantitative mixing analysis of powders of different wettabilities, primary particle size and density would benefit from the use of quantitative techniques such as laser Particle Image Velocimetry, X-ray image analysis and Positron Emission Particle Tracking (PEPT).
- Accurate measurement of particle velocity using tracers such as; Positron Emission Particles, modelling or video image should ideally be employed. This would enable more accurate calculation of dimensionless groups will be obtained.
- It is possible to use the regime maps developed in this work to semi-quantitatively explain variations in granulation behaviour, and they provide an opportunity to adjust

conditions to achieve required granules structures. Further experiments and validation studies are recommended to further verify the regime maps developed in this study.

Appendix

Appendix A.1: The volume moment mean diameter d_{43} (μm) of all granules produced in Chapter 4:

A.1.1 The effect of binder viscosity and powder wettability

Table A.1.1: Granule size distribution, q_3 in each size fraction for granule produced using low powder wettability and different binder viscosity.

Binder viscosity (mPa s)	q_3						
	Sieve size (μm)						
	180	250	500	1000	1700	2800	3500
60	62.15	23.45	9.83	3.51	1.06	0	0
300	57.01	21.62	11.23	6.34	0	3.8	0.98
1300	69.17	0	0	20.49	5.76	3.82	0.76
3000	0	4.65	90.34	5.01	0	0	0

Table A.1.2: Granule size distribution, q_3 in each size fraction for granule produced using medium powder wettability and different binder viscosity.

Binder viscosity (mPa s)	q_3						
	Sieve size (μm)						
	500	1000	1700	2800	3350	4000	5600
60	29.81	56.78	2.258	2.28	7.64	1.24	0
300	48.27	7.83	39.89	4.01	0	0	0
1300	0	97.73	0.52	0.03	1.42	0.26	0.04
3000	100	0	0	0	0	0	0

Table A.1.3: Granule size distribution, q_3 in each size fraction for granule produced using high powder wettability and different binder viscosity.

Binder viscosity (mPa s)	q_3			
	Sieve size (μm)			
	2800	3350	4000	5000
60	72.65	27.35	0	0
300	82.54	17.46	0	0
1300	100	0	0	0
3000	0	70.55	24.20	5.25

Table A.1.4: d_{43} of granules produced using different binder viscosity and powder wettability.

Binder viscosity (mPa s)	d_{43}		
	Low powder wettability	Medium powder wettability	High powder wettability
60	726	3075	2800
300	1346	2225	3075
1300	1356	1500	3075
3000	1365	500	4116

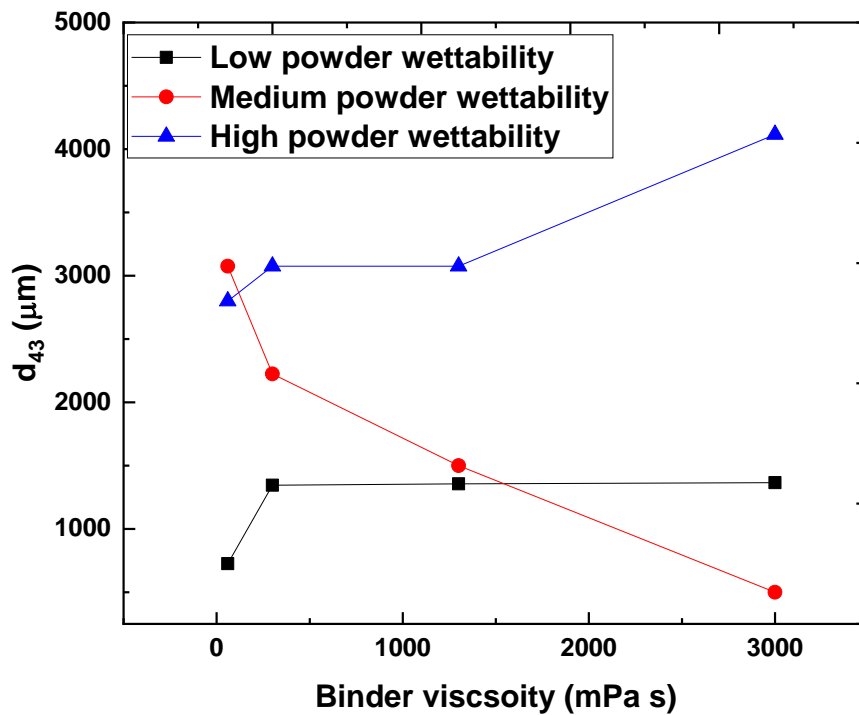


Figure A.1.1: Granules volume moment mean diameter (d_{43}) produced using different binder viscosity and powder wettability.

A.1.2 The effect of powder particle size and wettability

Table A.1.5: Granule size distribution, q_3 in each size fraction for granule produced using low powder wettability and different primary particle size.

Particle size (μm)	q_3							
	Sieve size (μm)							
	180	250	500	1000	1700	2800	3350	4000
35	69.17	0	0	21.67	6.32	2.08	0.76	0
70	0	0	0.05	99.61	0.14	0.11	0.09	0
115	0	0	1.18	1.77	2.96	21.59	59.28	13.22

Table A.1.6: Granule size distribution, q_3 in each size fraction for granule produced using medium powder wettability and different primary particle size.

Particle size (μm)	q_3							
	Sieve size (μm)							
	250	500	1000	1700	2800	3350	4000	5600
35	0	0	97.73	0.52	0.03	1.42	0.26	0.04
70	0	0	0	75.53	24.47	0	0	0
115	2.03	1.01	1.81	3.48	83.48	8.19	0	0

Table A.1.7: Granule size distribution, q_3 in each size fraction for granule produced using high powder wettability and different primary particle size.

Particle size (μm)	q_3					
	Sieve size (μm)					
	250	500	1000	1700	2800	3350
35	4.74	0	0	0	100	0
70	0	0	0	0	0	100
115	0	1.33	1.33	6.17	6.64	79.77

Table A.1.8: d_{43} of granules produced using different powder particle size and powder wettability.

Powder particle size (μm)	d_{43}		
	Low powder wettability	Medium powder wettability	High powder wettability
35	1532	2002	2516
70	2225	2454	2800
115	2570	3075	3350

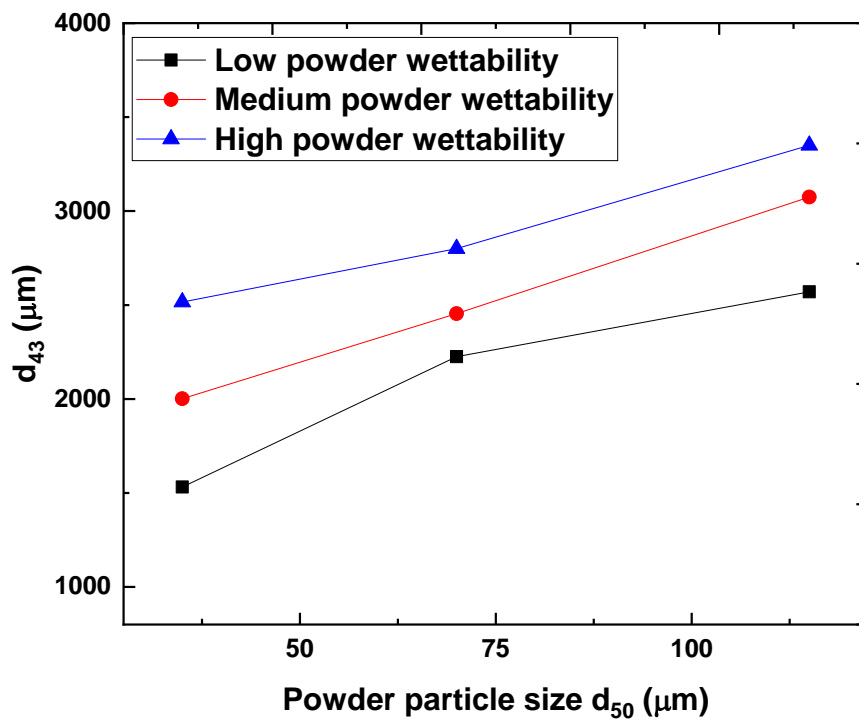


Figure A.1.2: Granules volume moment mean diameter (d_{43}) produced using different powder particle size and powder wettability.

A.1.3 The effect of mixing time

Table A.1.9: Granule size distribution, q_3 in each size fraction for granule produced using low powder wettability and different mixing time..

Mixing time (s)	q_3						
	Sieve size (μm)						
	106	180	250	500	1000	1700	2800
10	15.39	15.39	21.98	47.24	0	0	0
300	69.17	0	0	21.67	4.58	3.82	0.76
900	0	0	0	50.26	26.45	9.47	13.82
1800	0	0	0	12.14	50.60	23.16	14.10

Table A.1.10: d_{43} of granules produced using different mixing times and low powder wettability.

Mixing time (s)	d_{43}
10	259
300	1221
900	1500
1800	1500

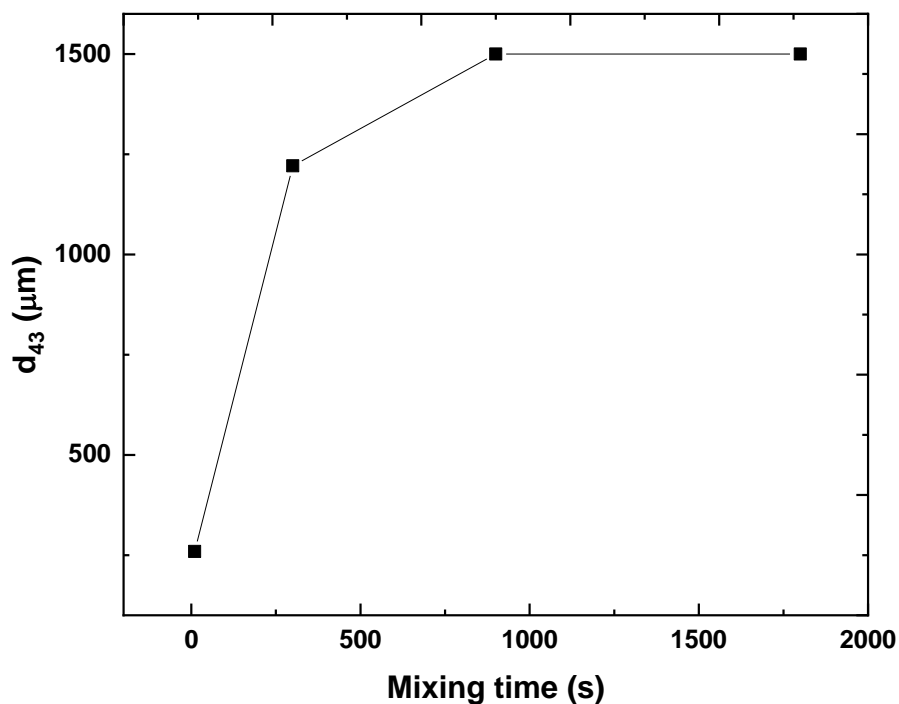
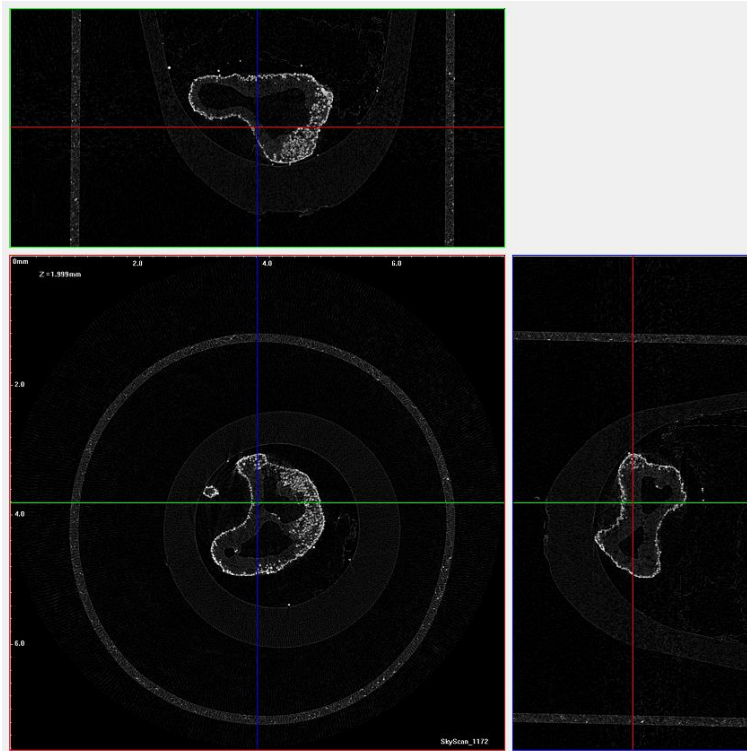


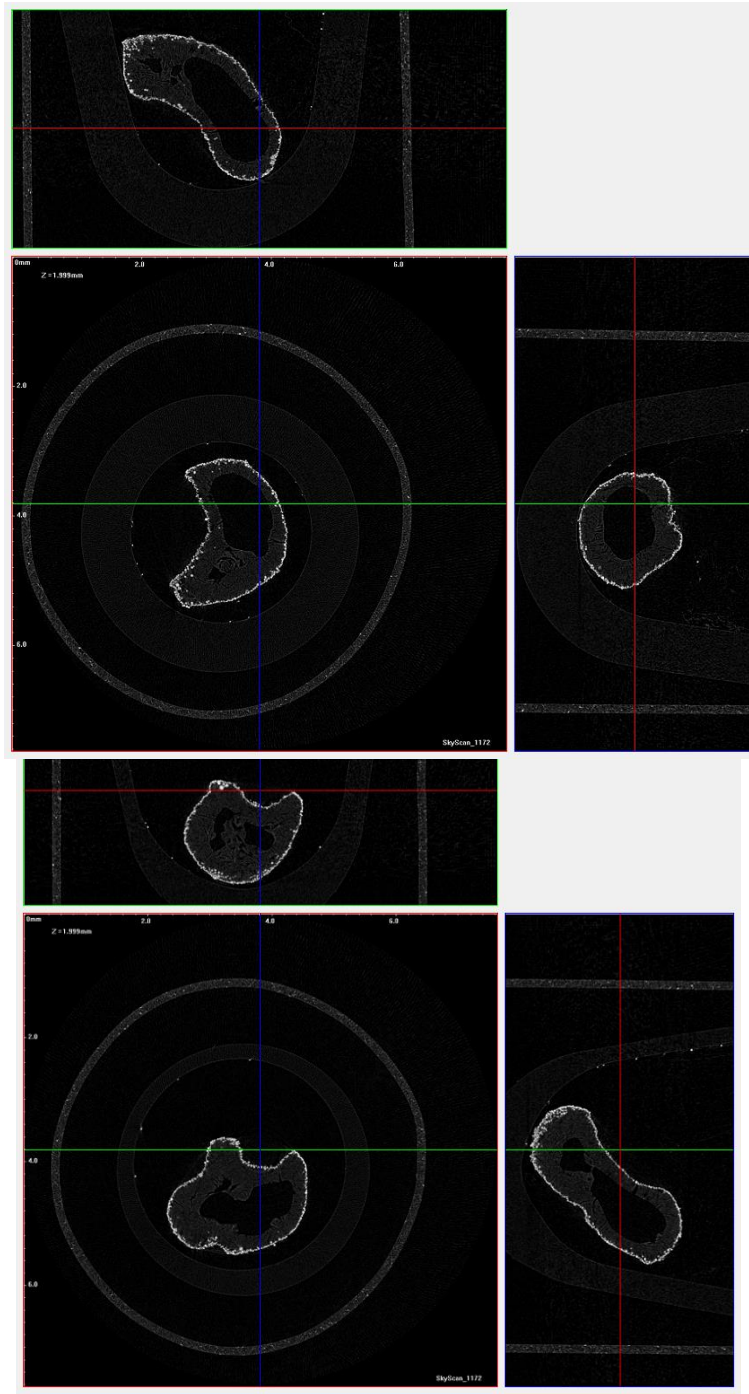
Figure A.1.3: Granules volume moment mean diameter (d_{43}) produced using different mixing time and low powder wettability.

Appendix A.2: XRCT cross sectional images

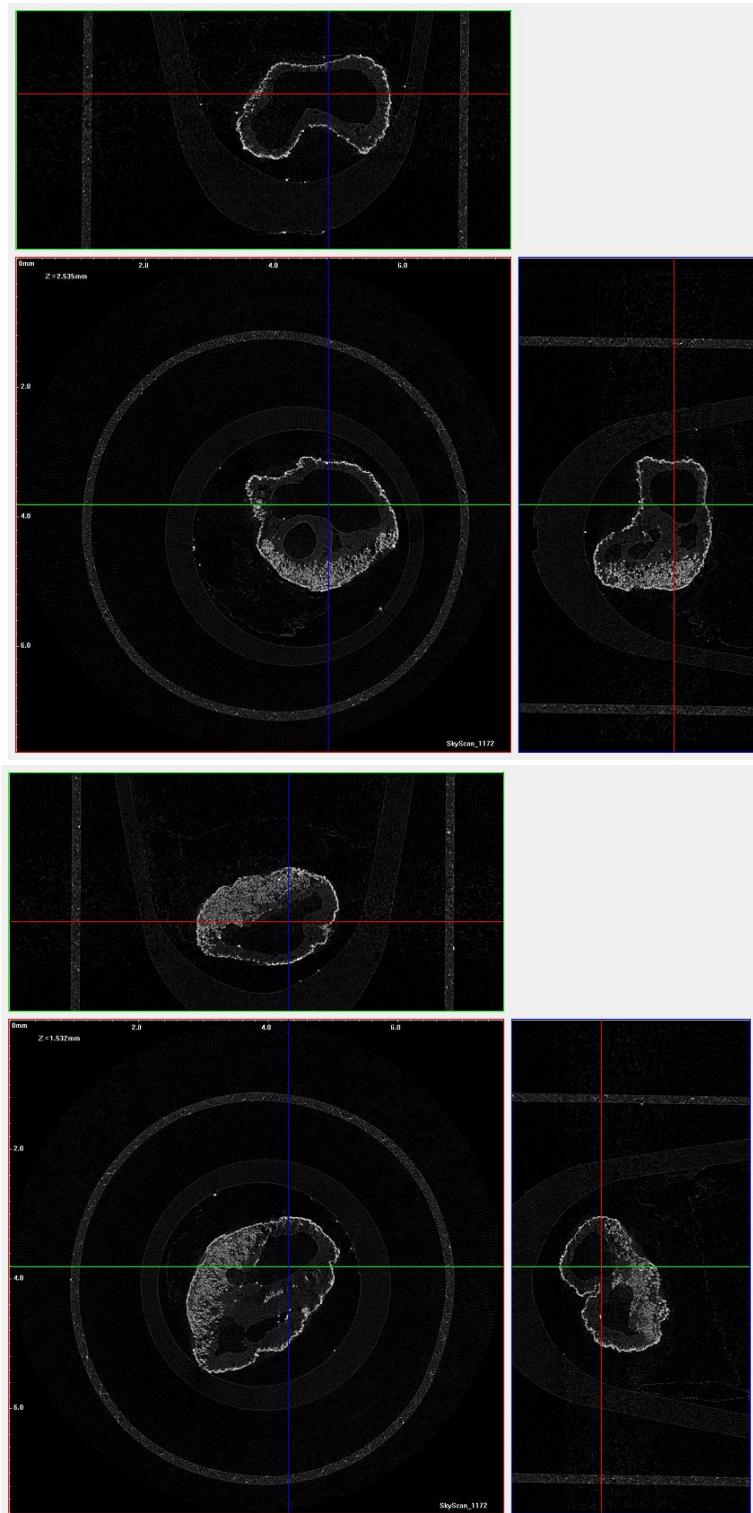
A.2.1: Effect of binder viscosity and powder wettability

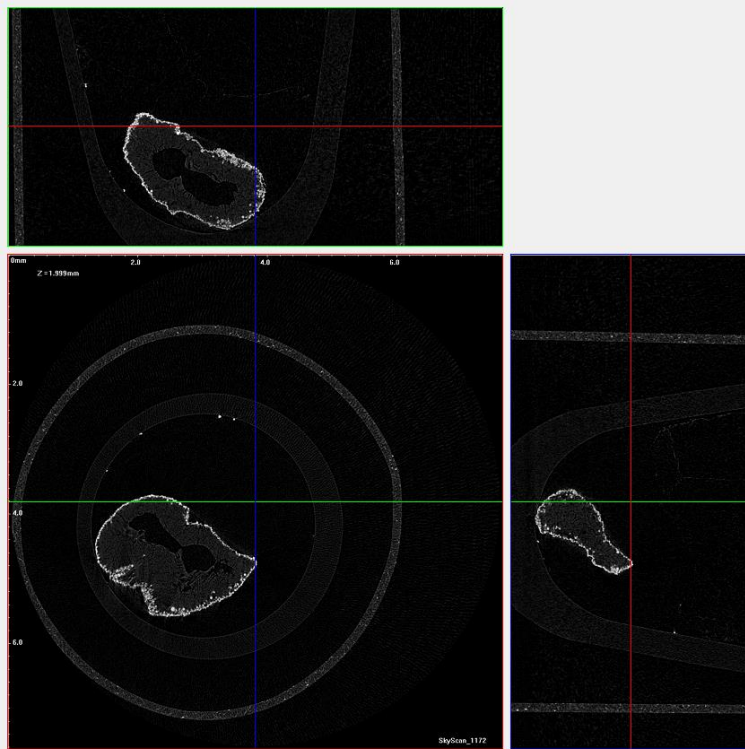
- 100%-0% Non-wetting–wetting beads, 300 mPa s, 25 rpm tumbling speed, 5 minutes mixing time, 35 μm primary particle size.



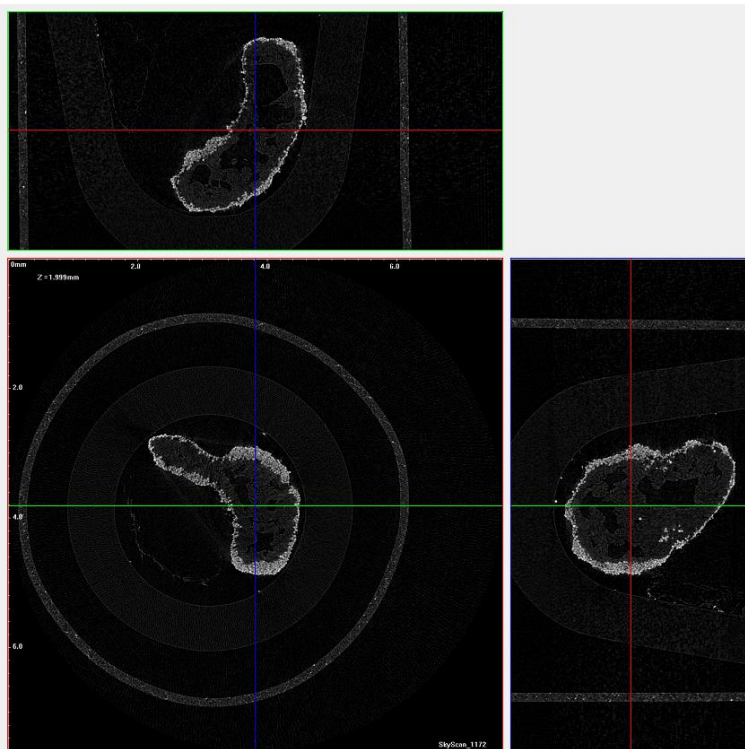


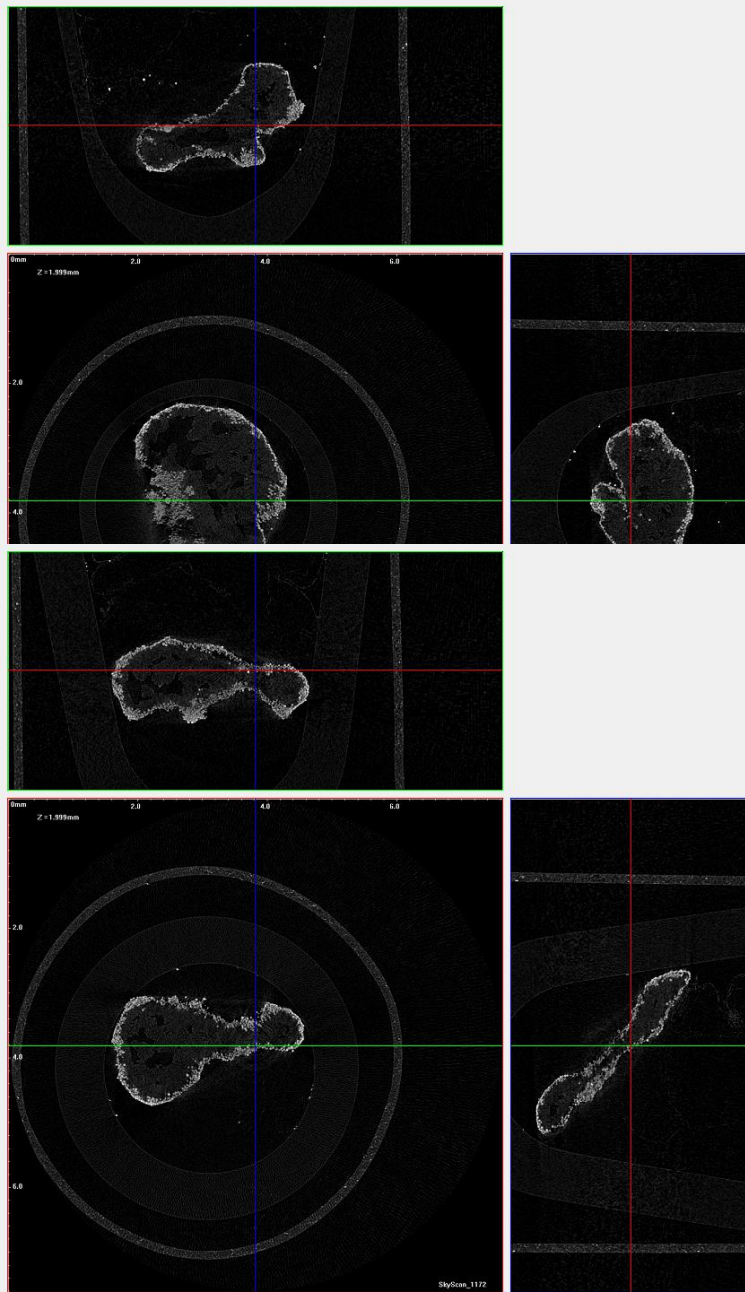
- **100%-0%** Non wetting–wetting beads, **1300 mP a s**, 25 rpm tumbling speed, 5 minutes mixing time, 35 μm primary particle size.



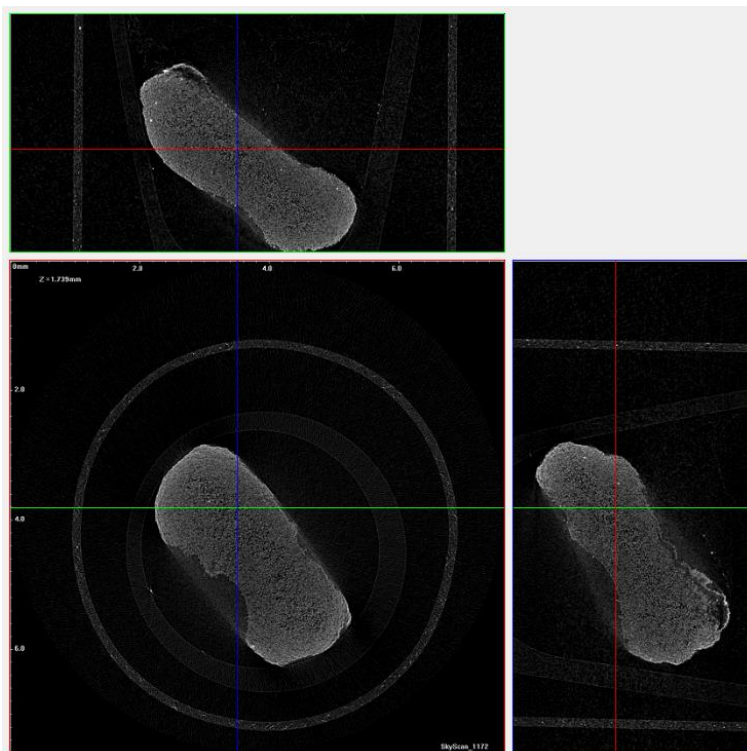
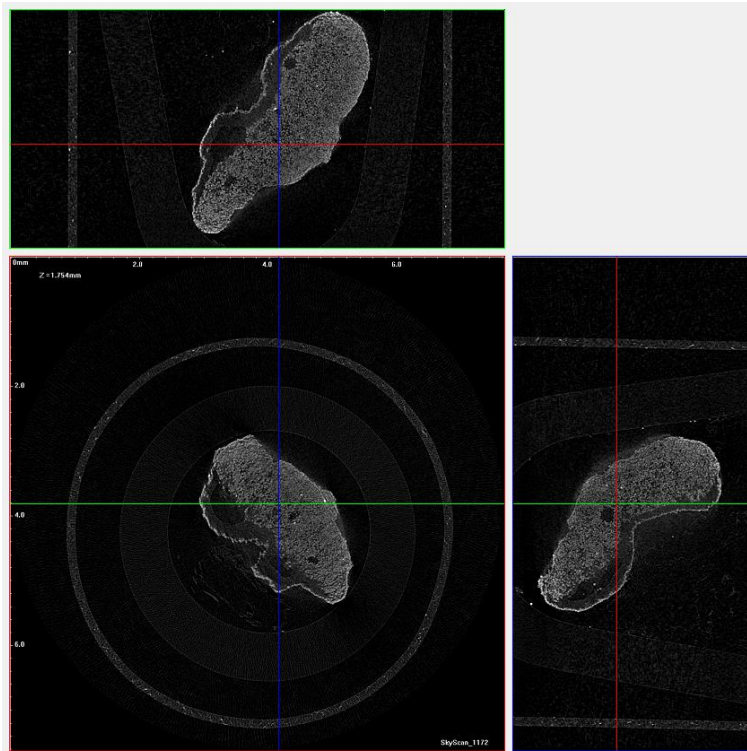


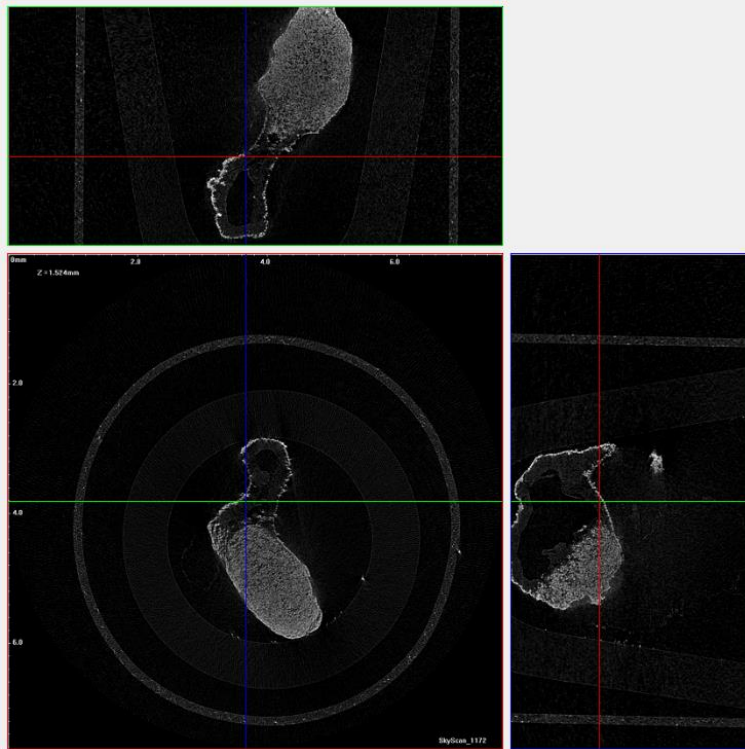
- **100%-0%** Non wetting–wetting beads, **3000 mPa s**, 25 rpm tumbling speed, 5 minutes mixing time, 35 μm primary particle size.



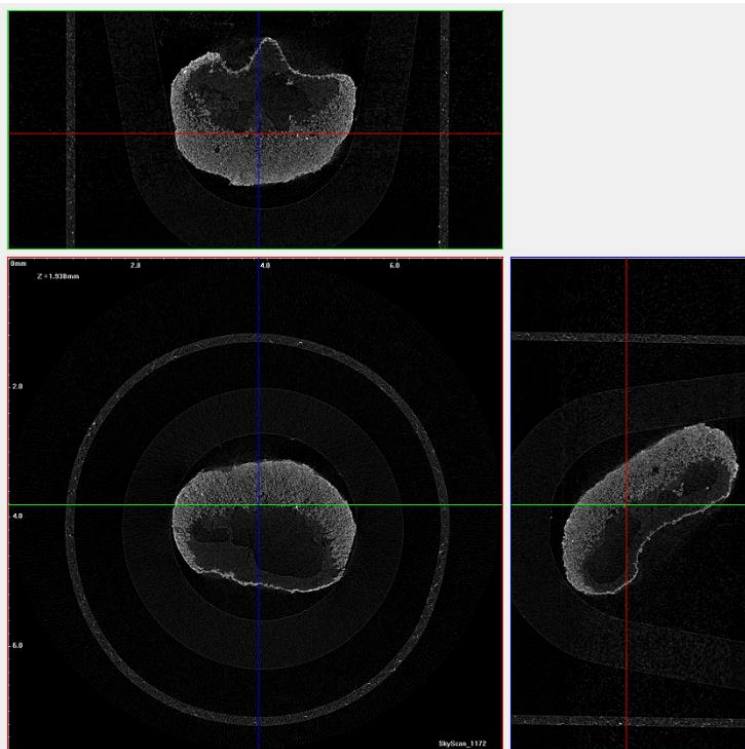


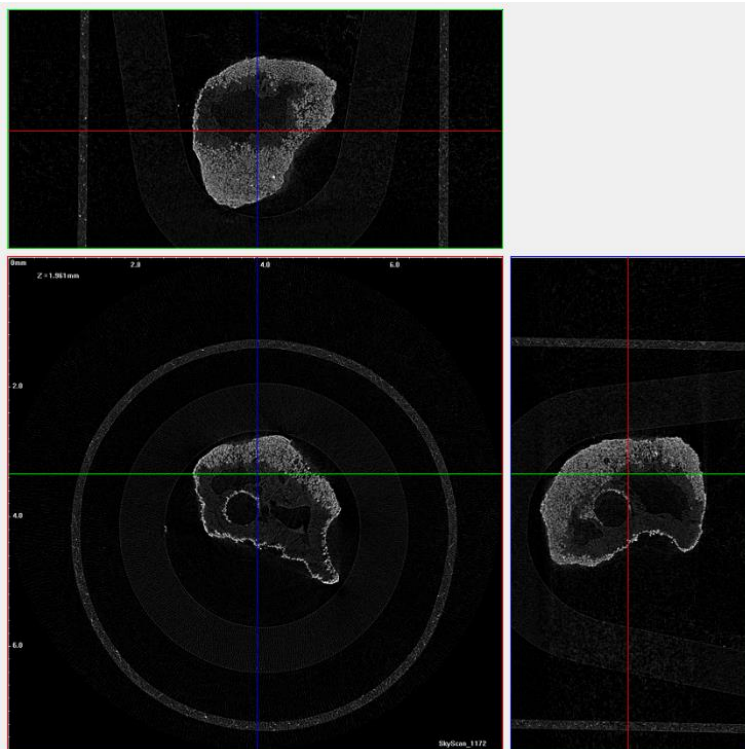
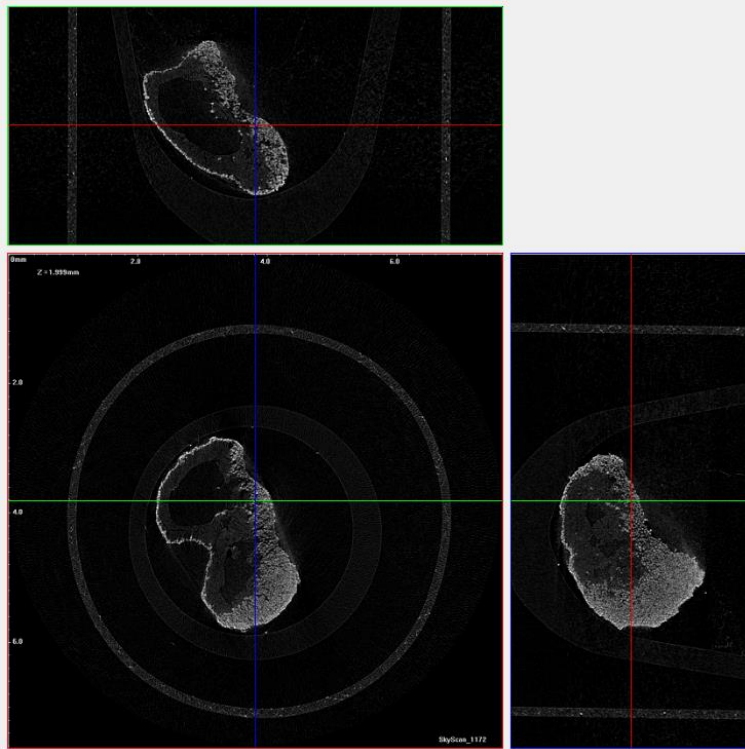
- **65%-35%** Non wetting–wetting beads, **300 mPa s**, 25 rpm tumbling speed, 5 minutes mixing time, 35 μm primary particle size.



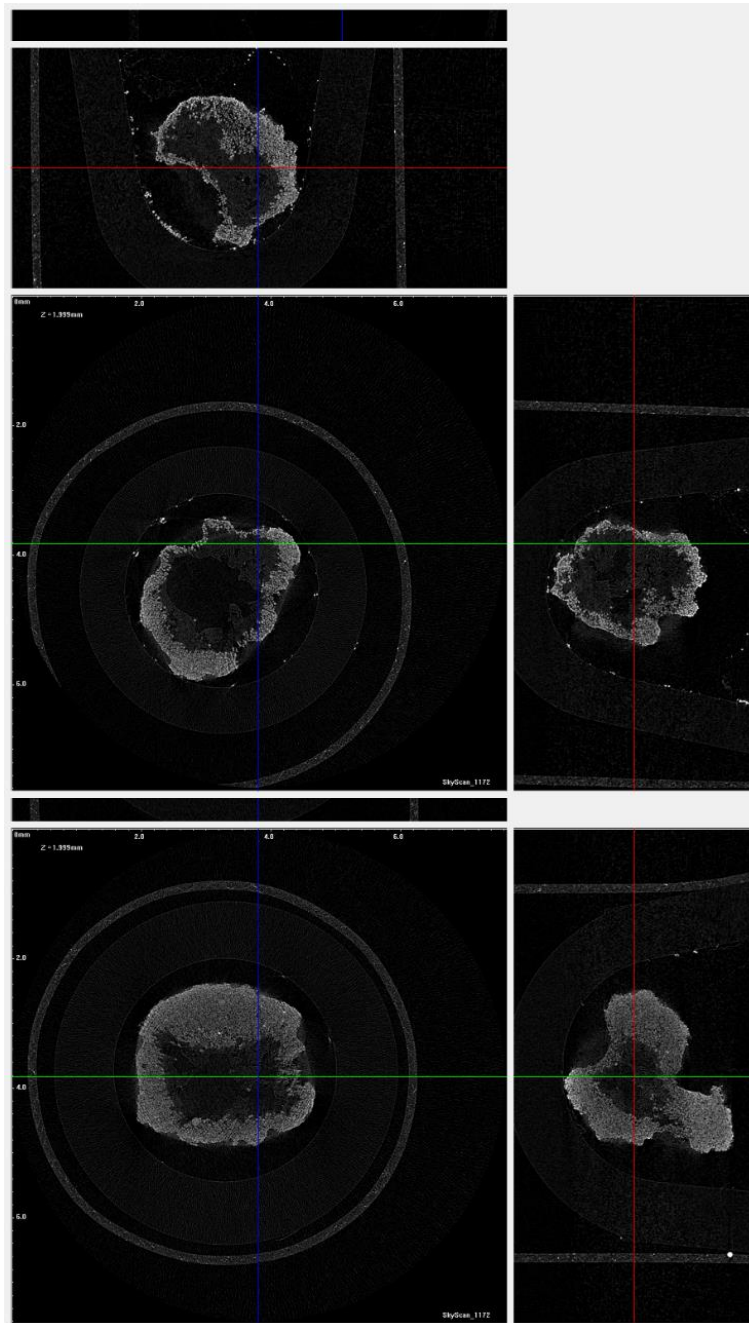


- **65%-35%** Non wetting–wetting beads, **1300 mPa s**, 25 rpm tumbling speed, 5 minutes mixing time, 35 μm primary particle size.

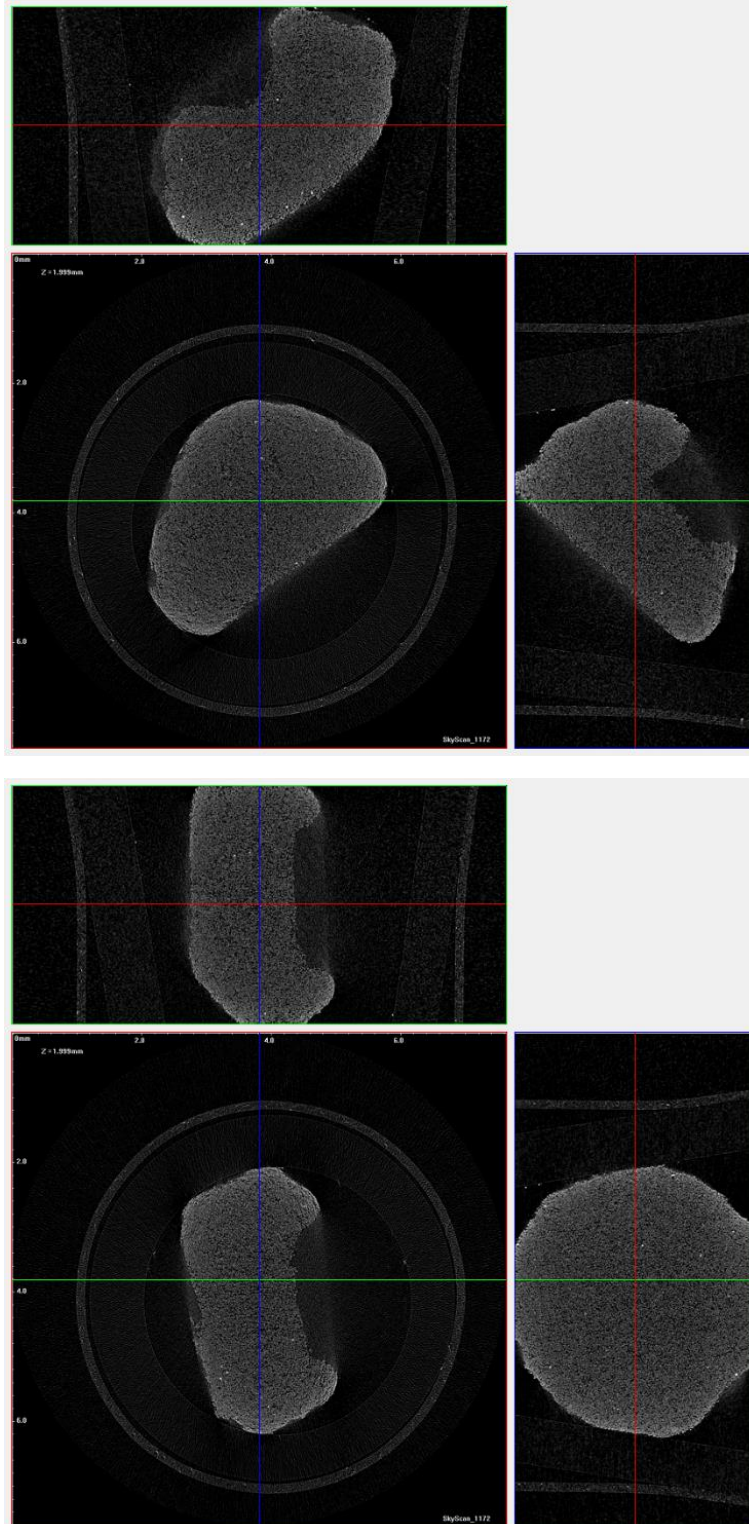


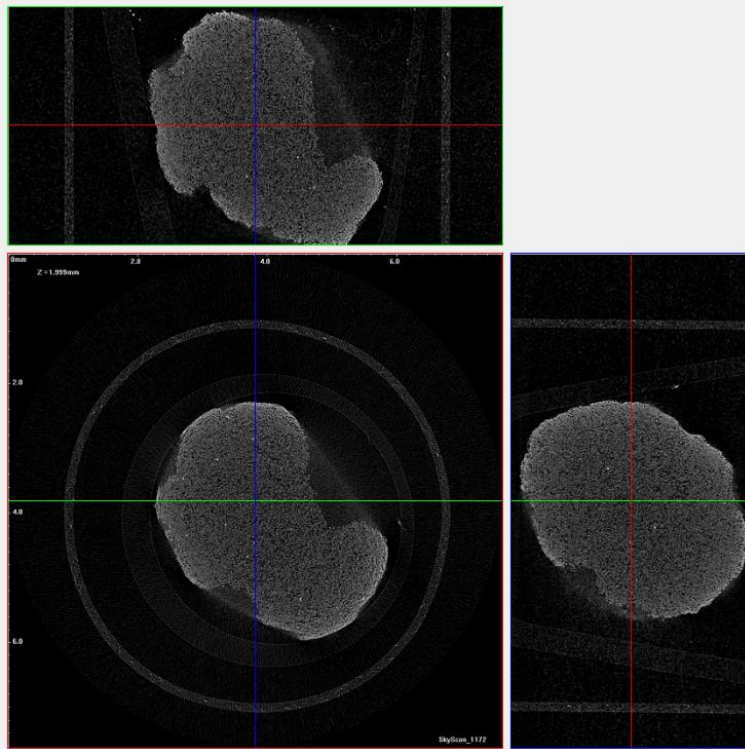


- **65%-35%** Non wetting–wetting beads, **3000 mPa s**, 25 rpm tumbling speed, 5 minutes mixing time, 35 μm primary particle size.

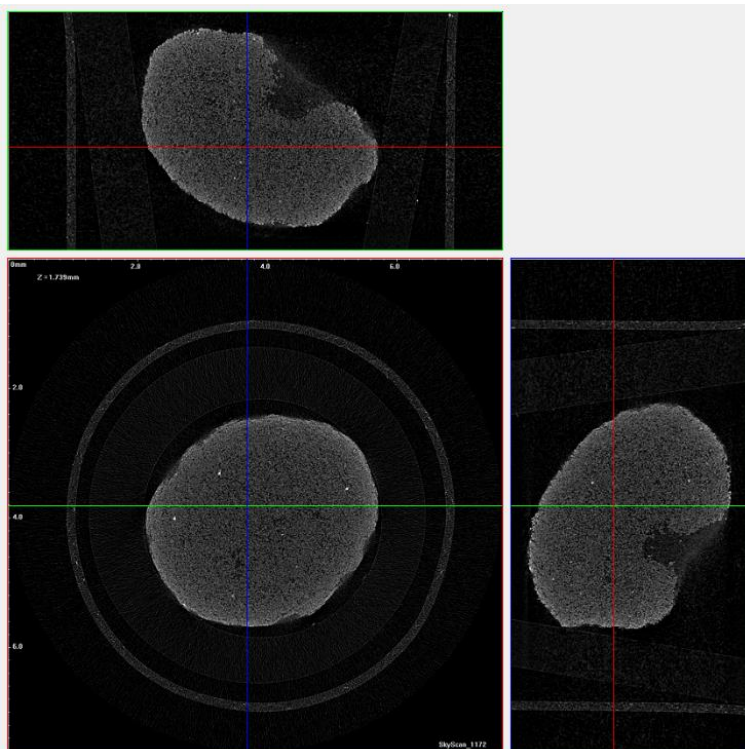


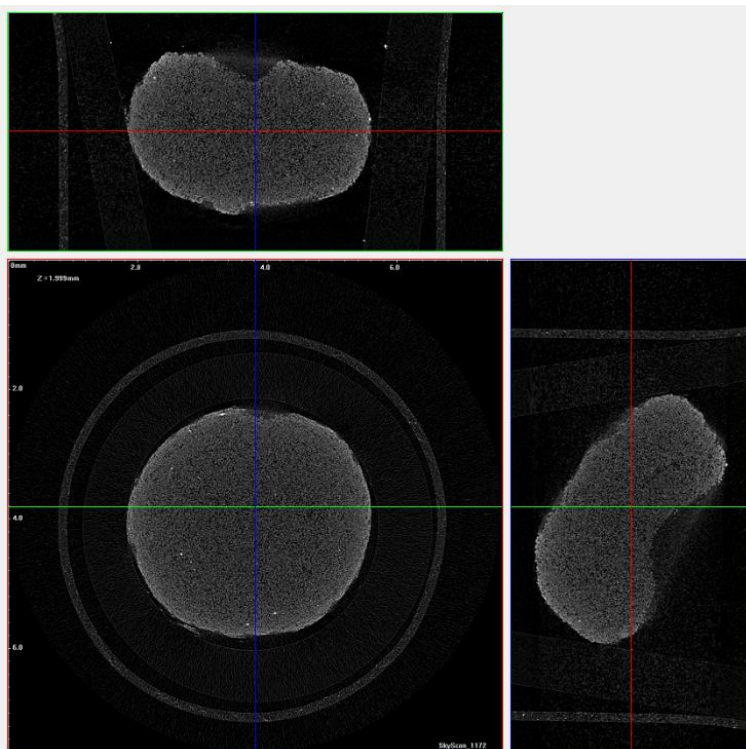
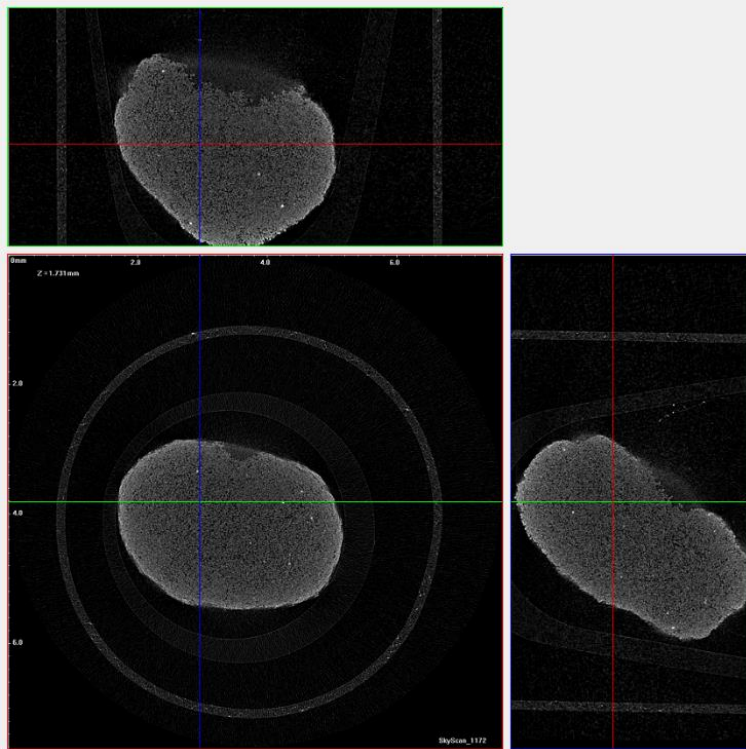
- **25%-75%** Non wetting–wetting beads, **60 mPa s**, 25 rpm tumbling speed, 5 minutes mixing time, 35 μm primary particle size.



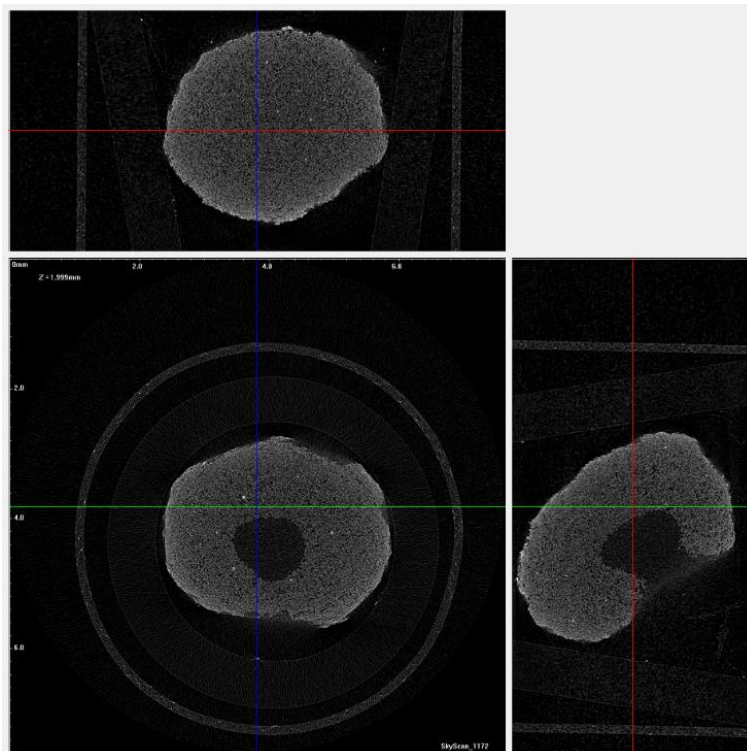
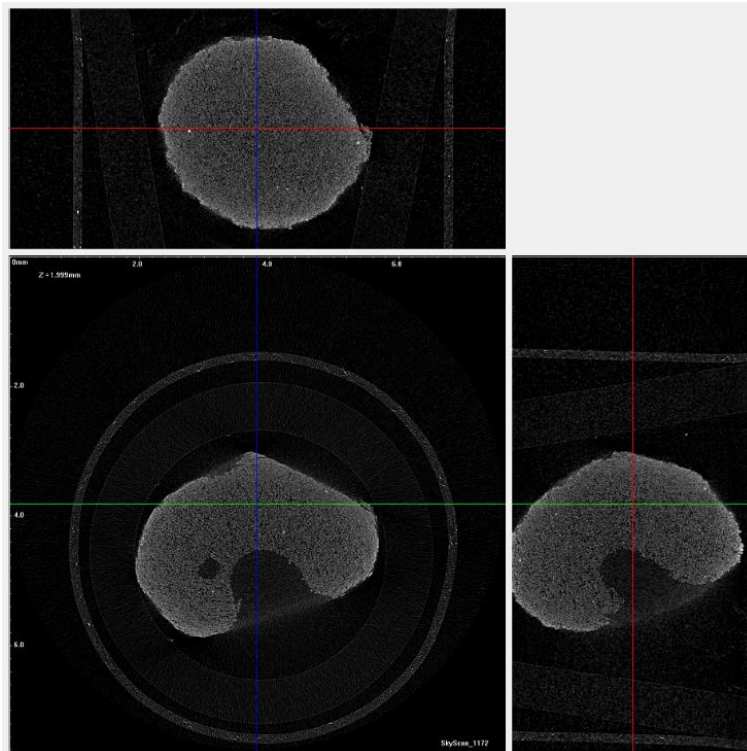


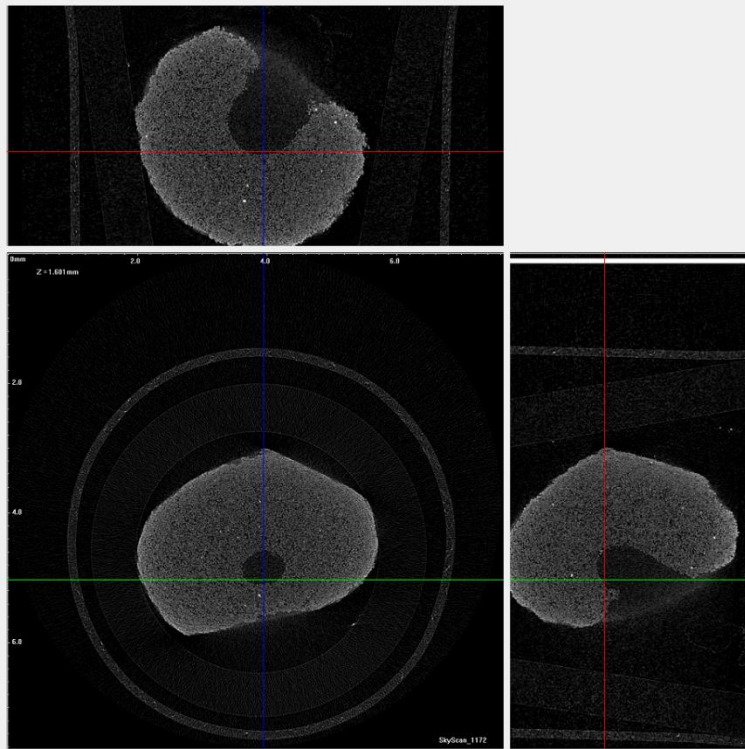
- **25%-75%** Non wetting–wetting beads, **300 mPa s**, 25 rpm tumbling speed, 5 minutes mixing time, 35 μm primary particle size.



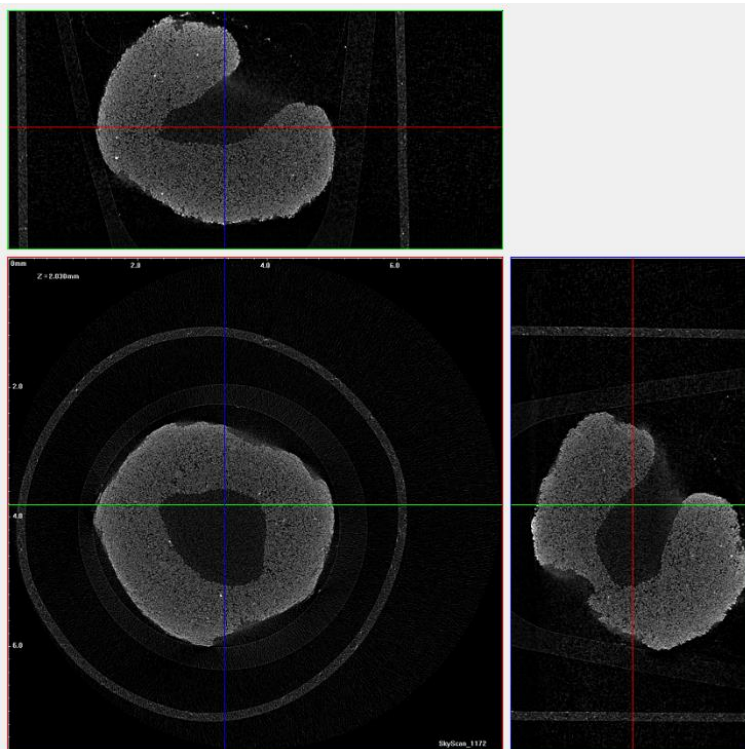


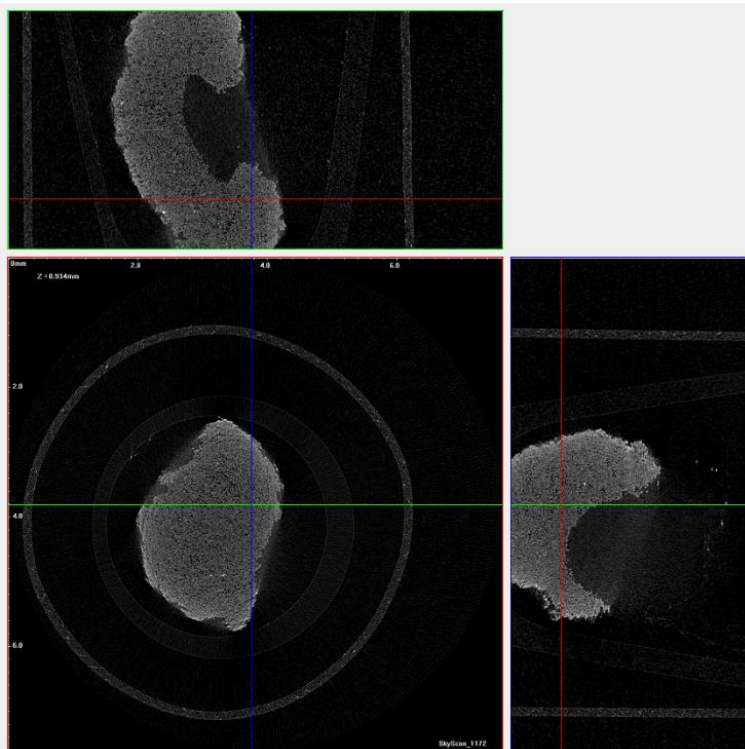
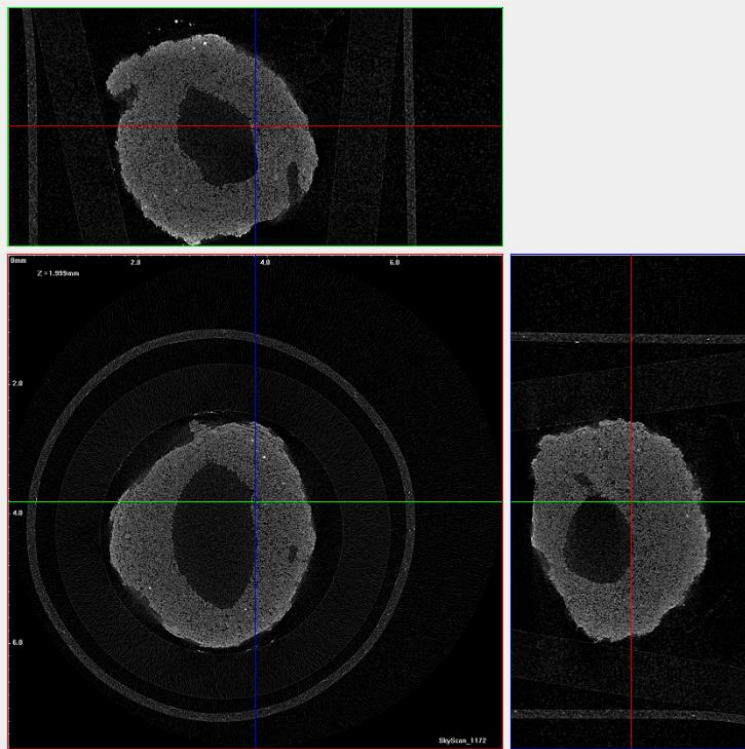
- **25%-75%** Non wetting–wetting beads, **1300**, 25 rpm tumbling speed, 5 minutes mixing time, 35 μm primary particle size.





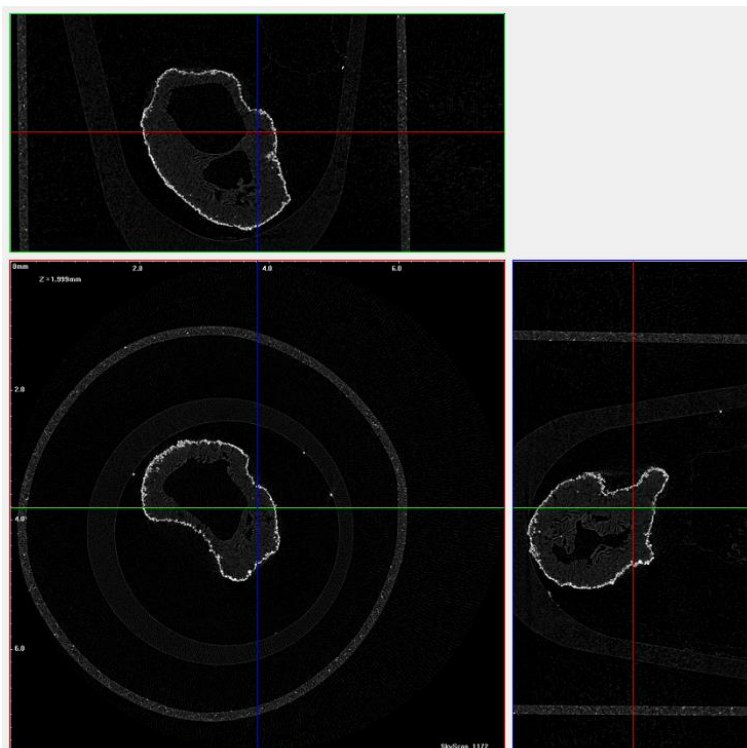
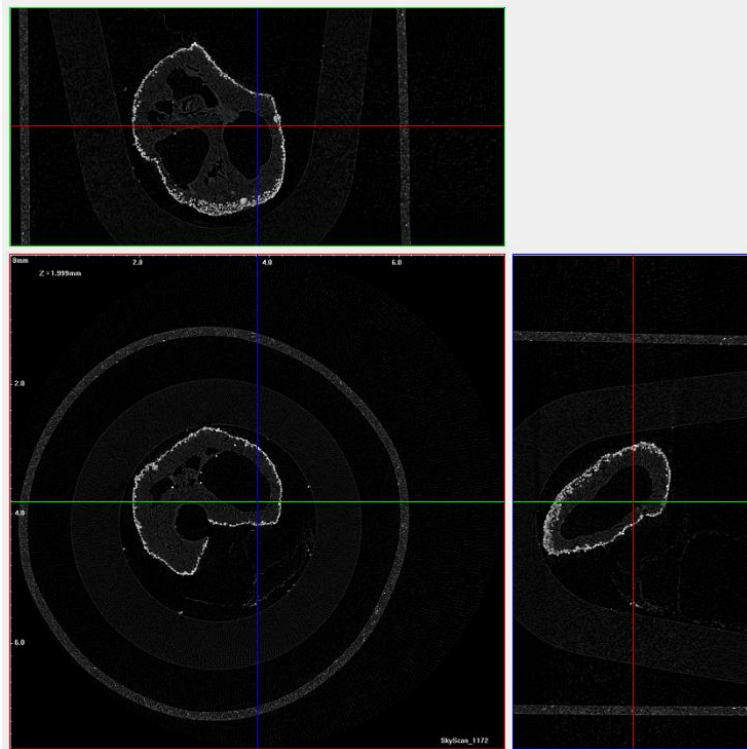
- **25%-75%** Non wetting–wetting beads, **3000 mPa s**, 25 rpm tumbling speed, 5 minutes mixing time, 35 μm primary particle size.

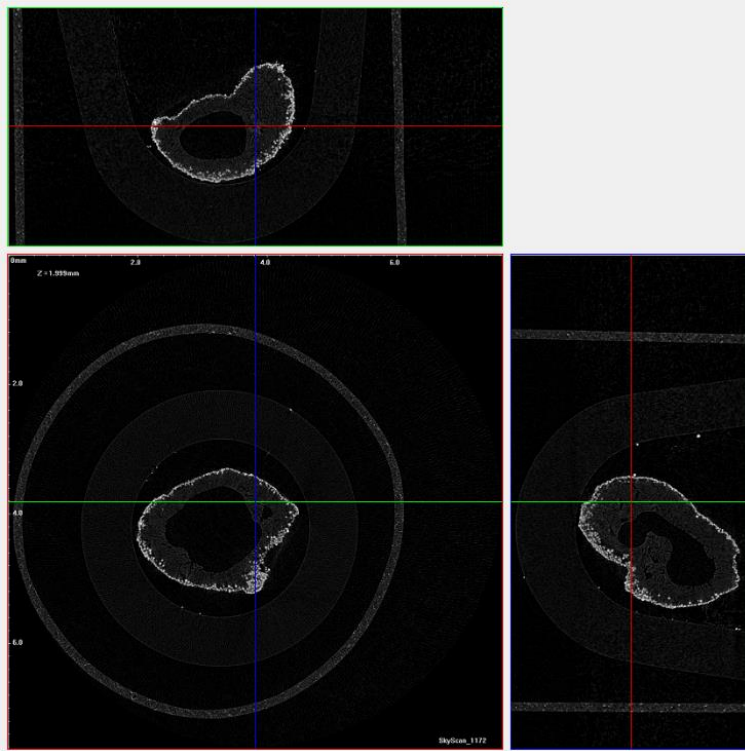




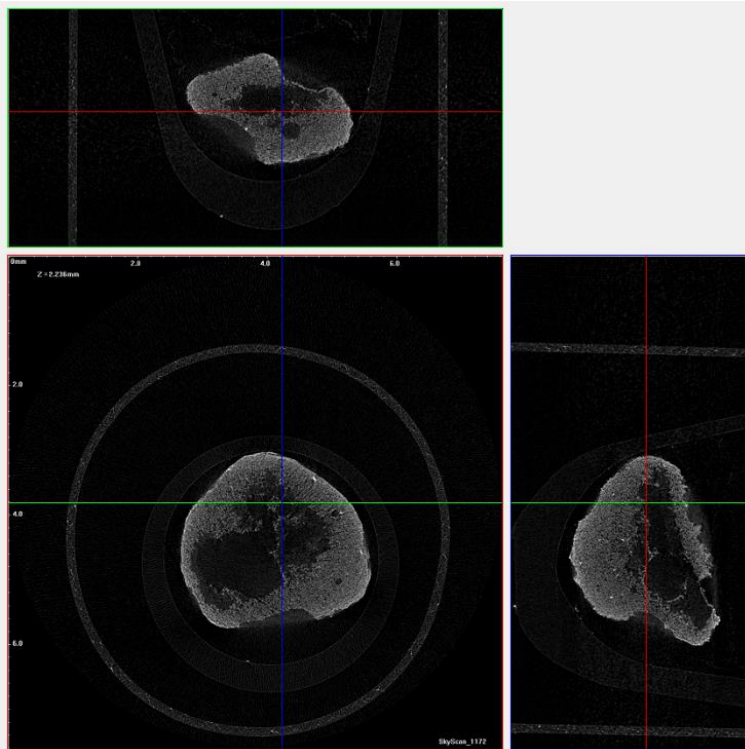
A.2.2: Effect of tumbling speed and powder wettability

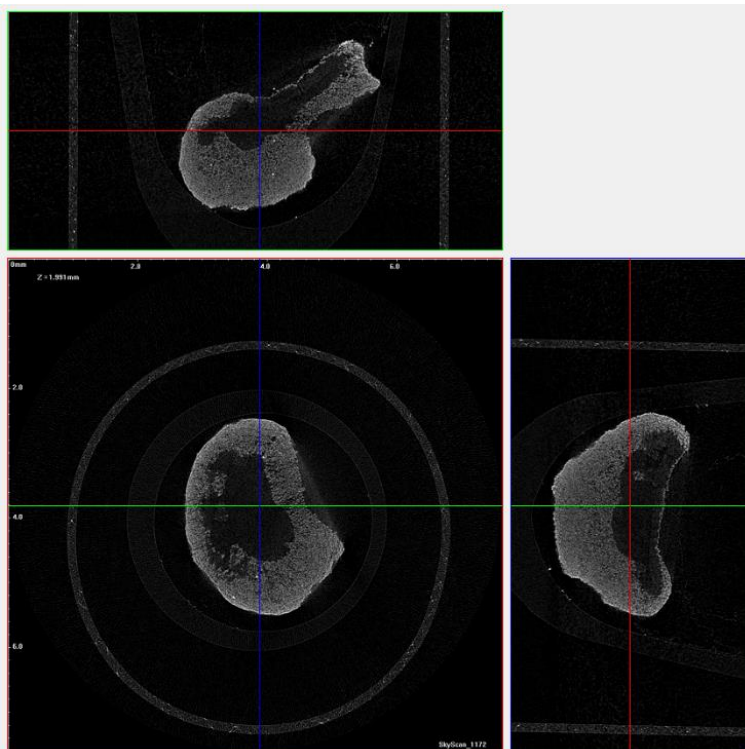
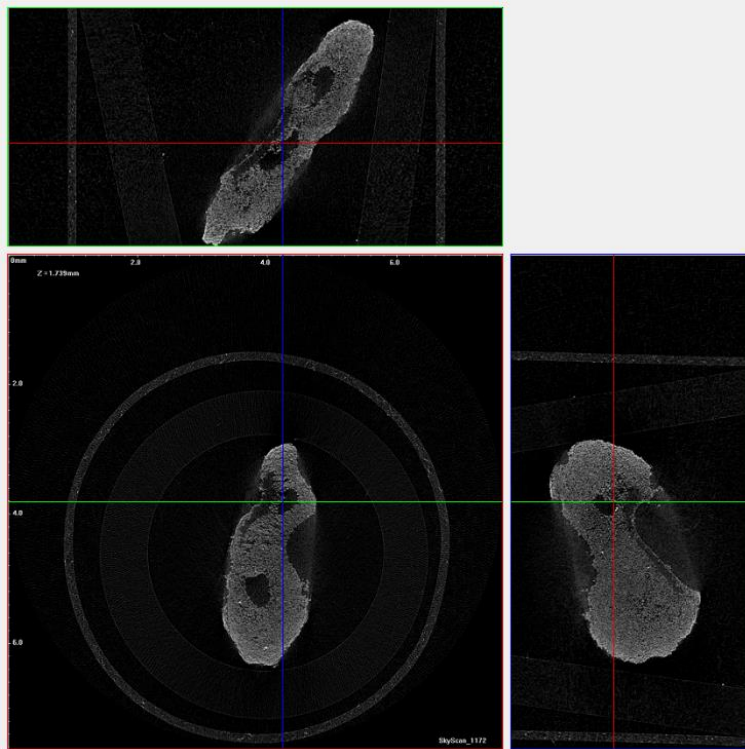
- 100%-0% Non wetting–wetting beads, 1300 mPa s, 60 rpm tumbling speed, 5 minutes mixing time, 35 μm primary particle size.



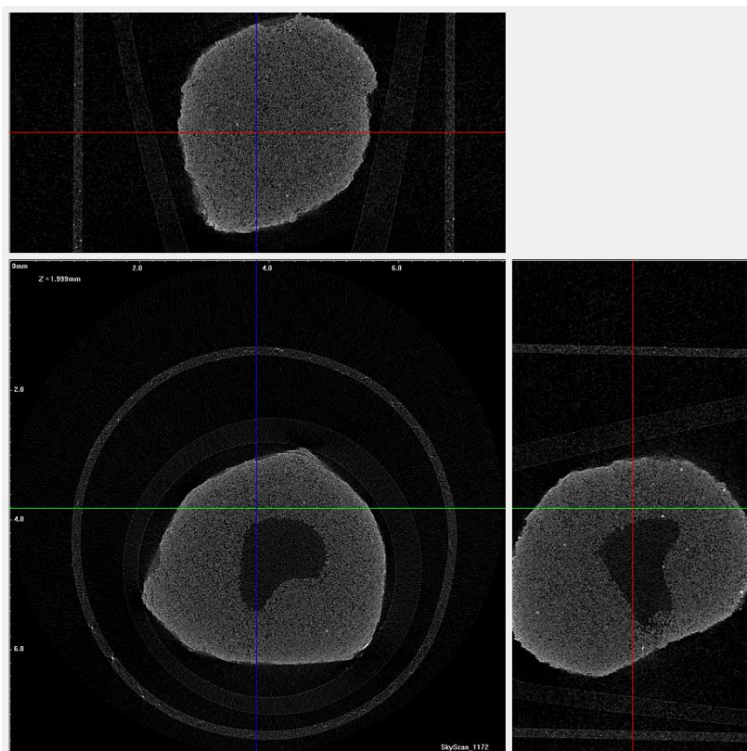
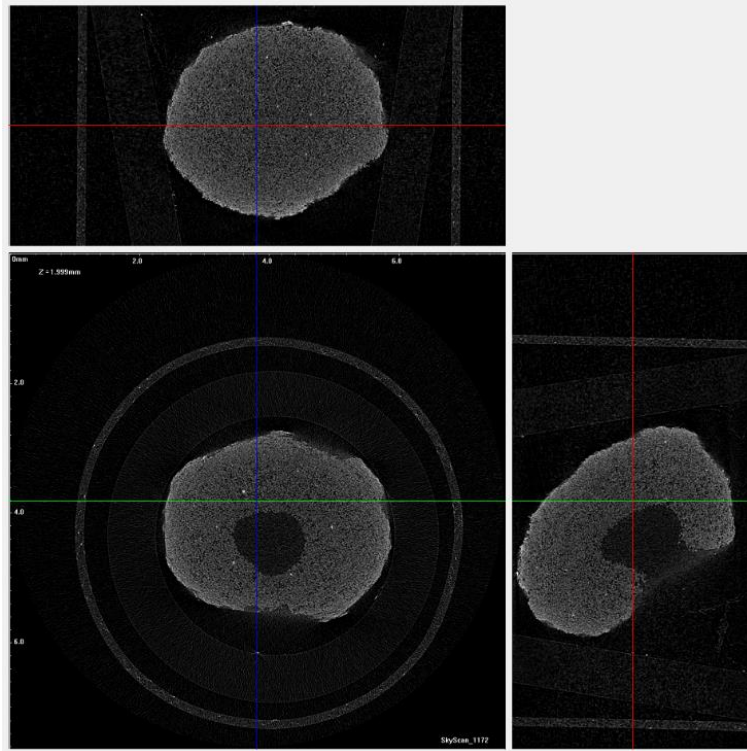


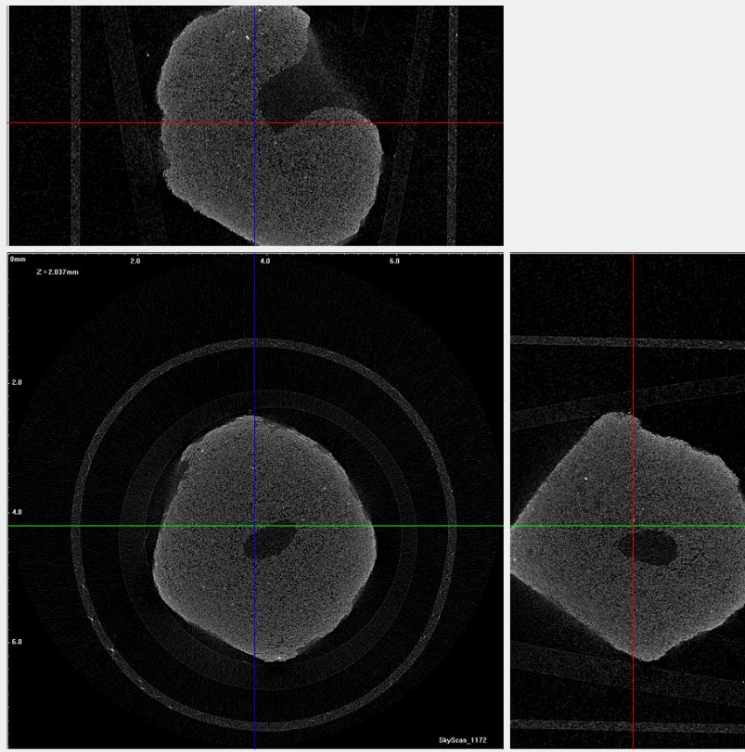
- **65%-35%** Non wetting–wetting beads, 1300 mPa s, **60 rpm tumbling speed**, 5 minutes mixing time, 35 μm primary particle size.





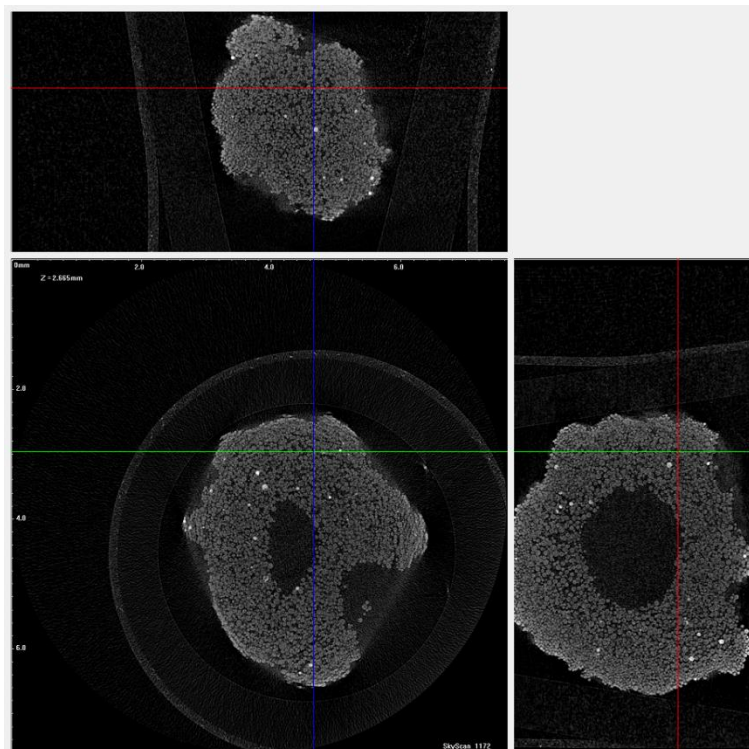
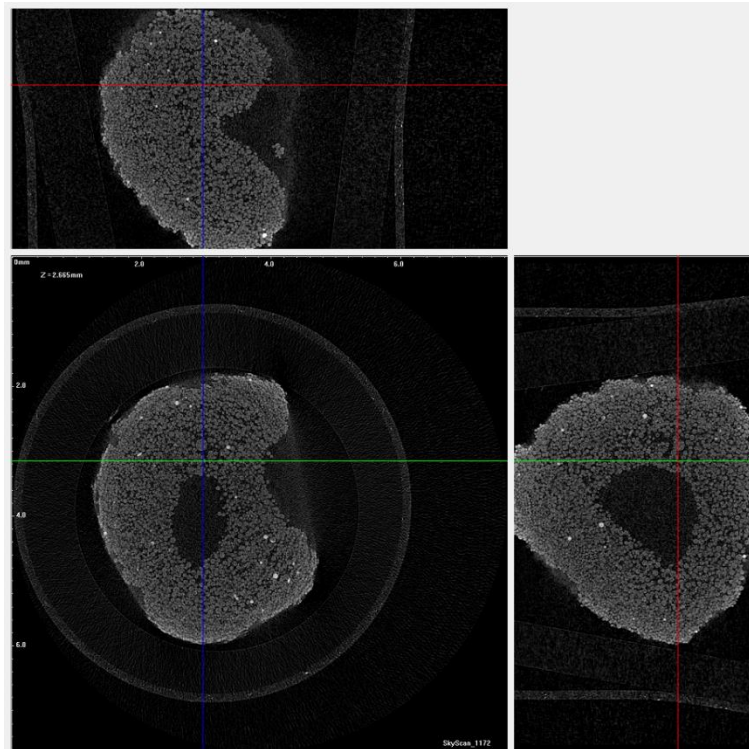
- **25%-75%** Non wetting–wetting beads, 1300 mPa s, **60 rpm tumbling speed**, 5 minutes mixing time, 35 μm primary particle size.

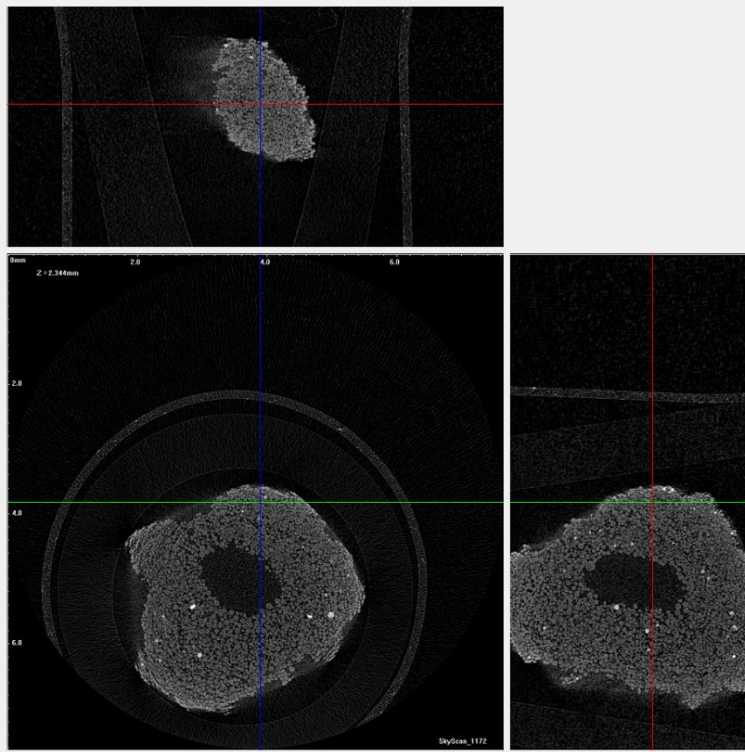




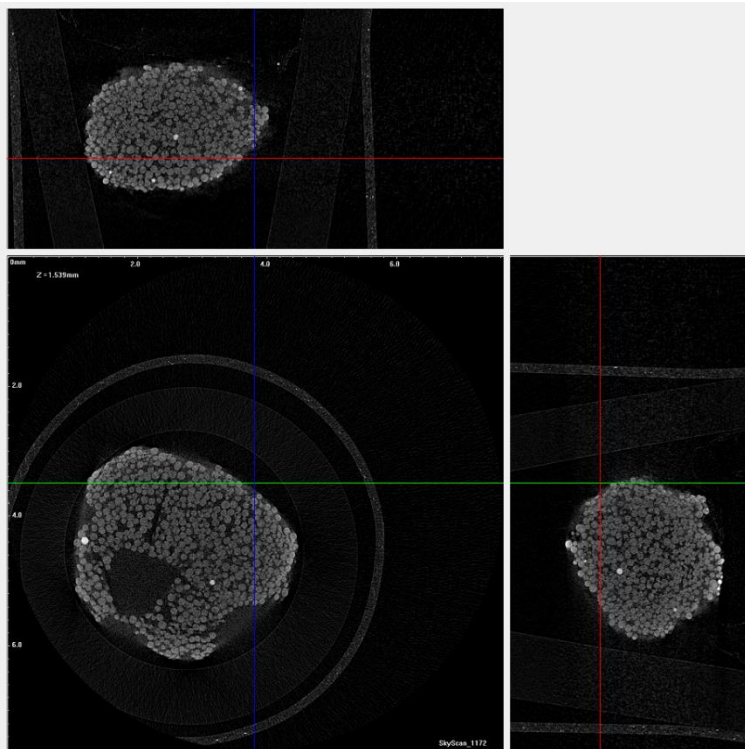
A.2.3: Effect of powder particle size and powder wettability

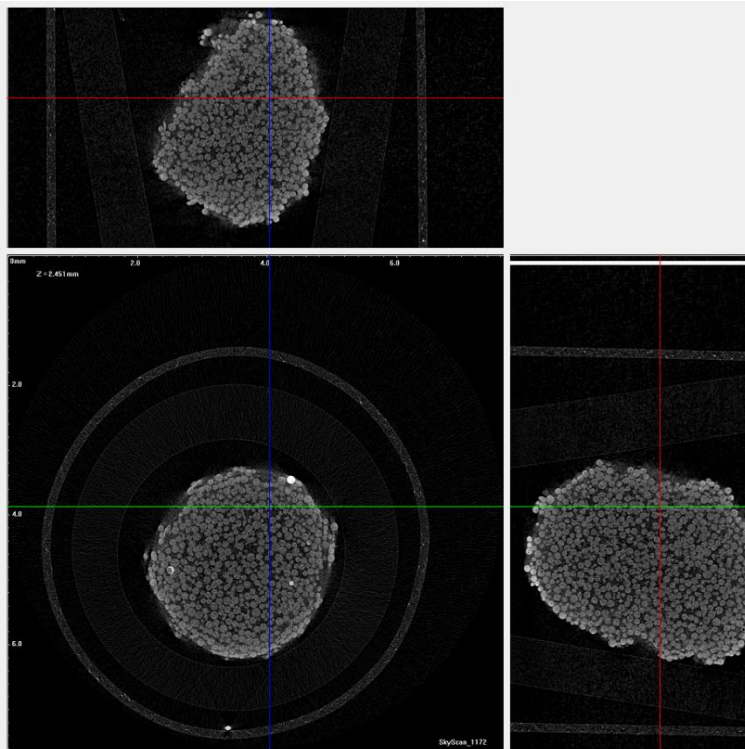
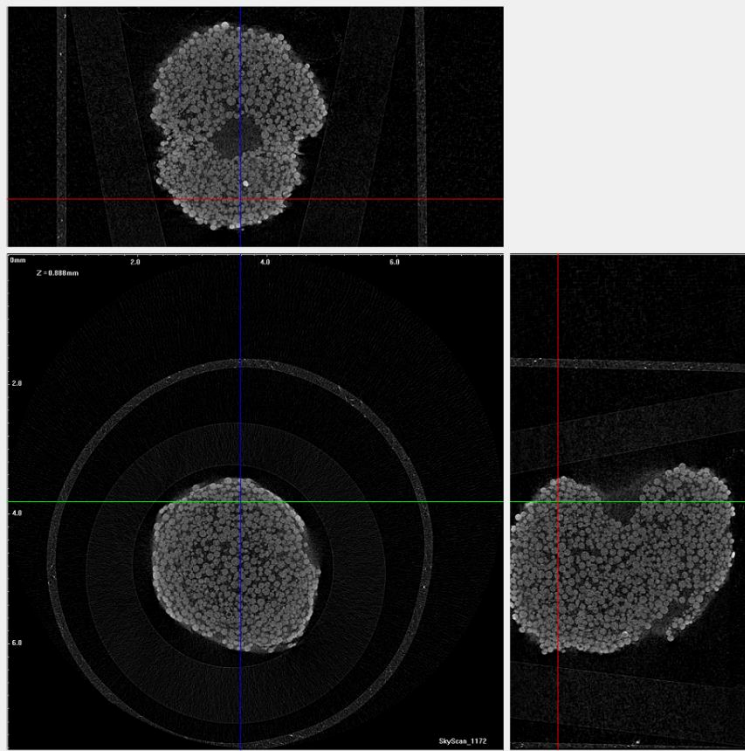
- 100%-0% Non wetting–wetting beads, d_{50} 70 μm , 1300 mPa s, 25 rpm tumbling speed, 5 minutes mixing time.



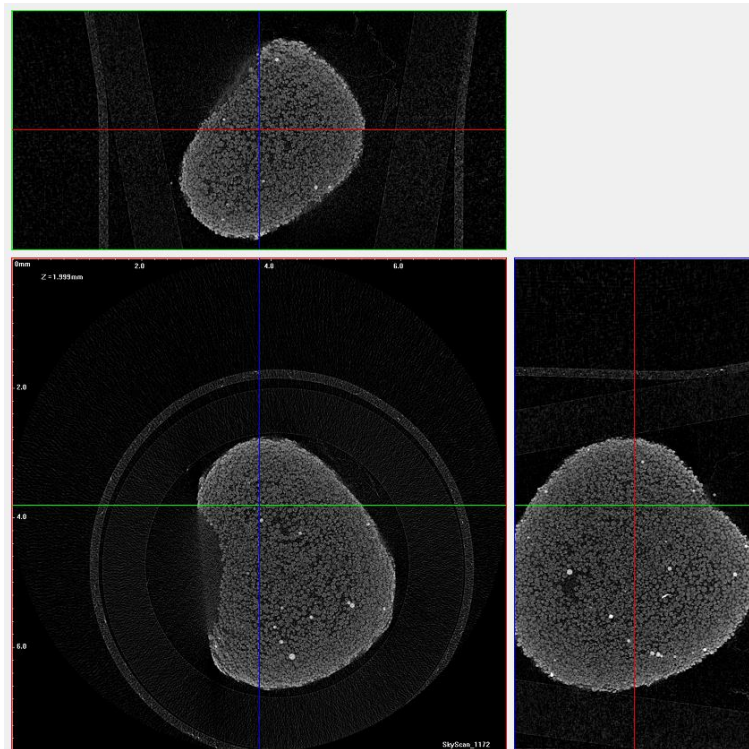
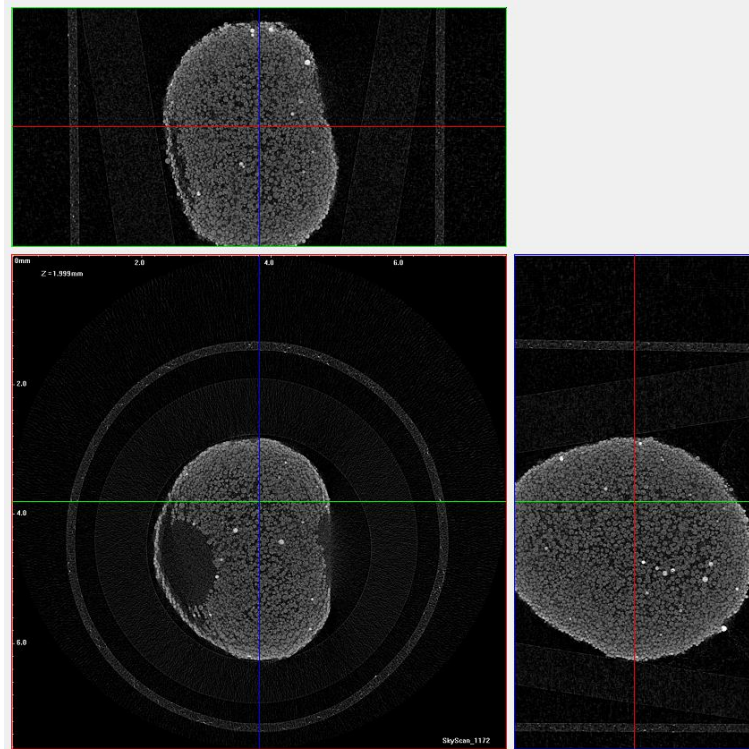


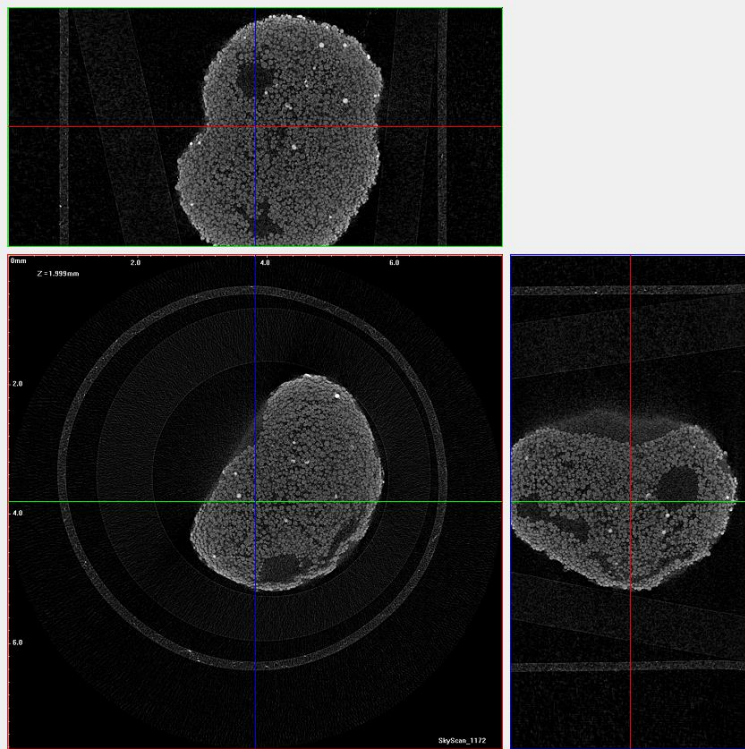
- **100%-0%** Non wetting–wetting beads, d_{50} **115 μ m**, 1300 mPa s, 25 rpm tumbling speed, 5 minutes mixing time.



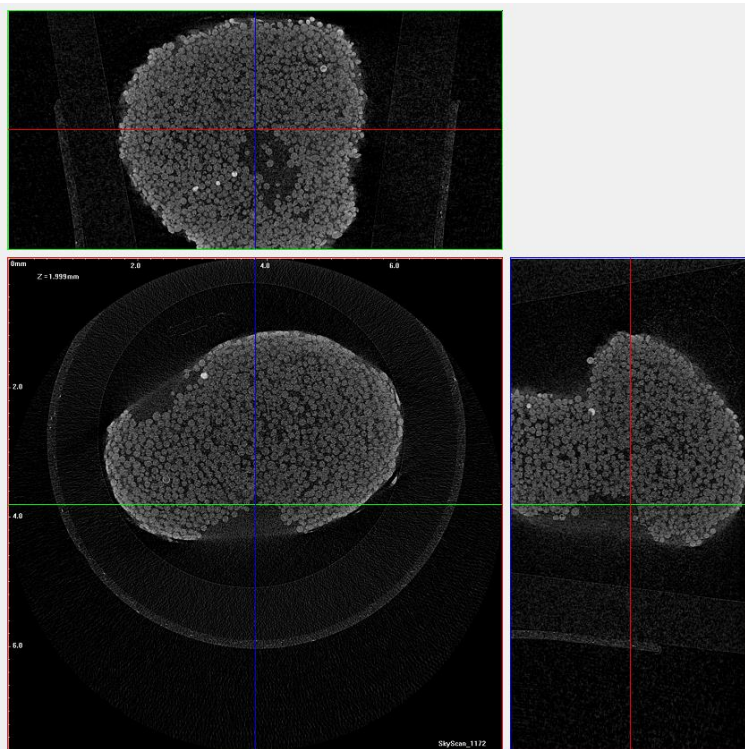


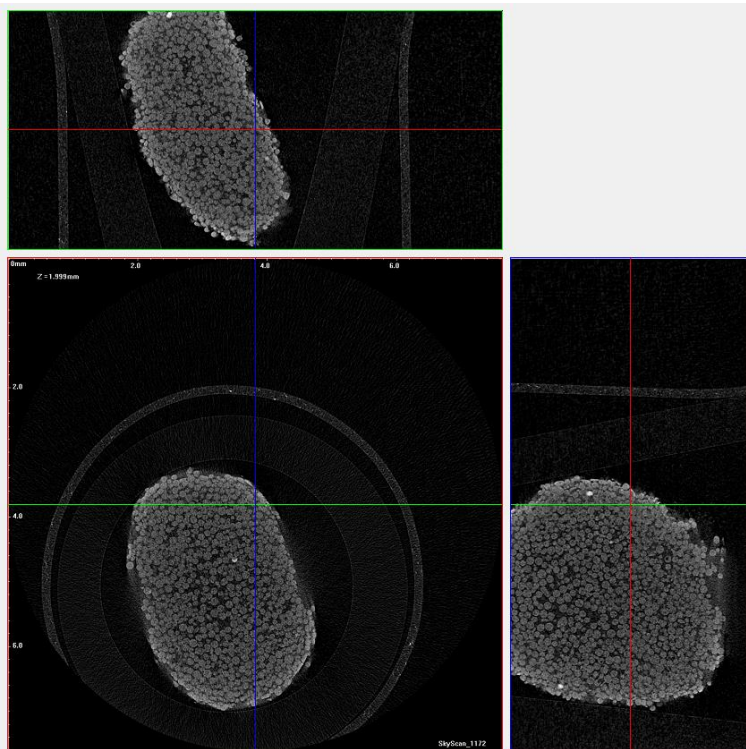
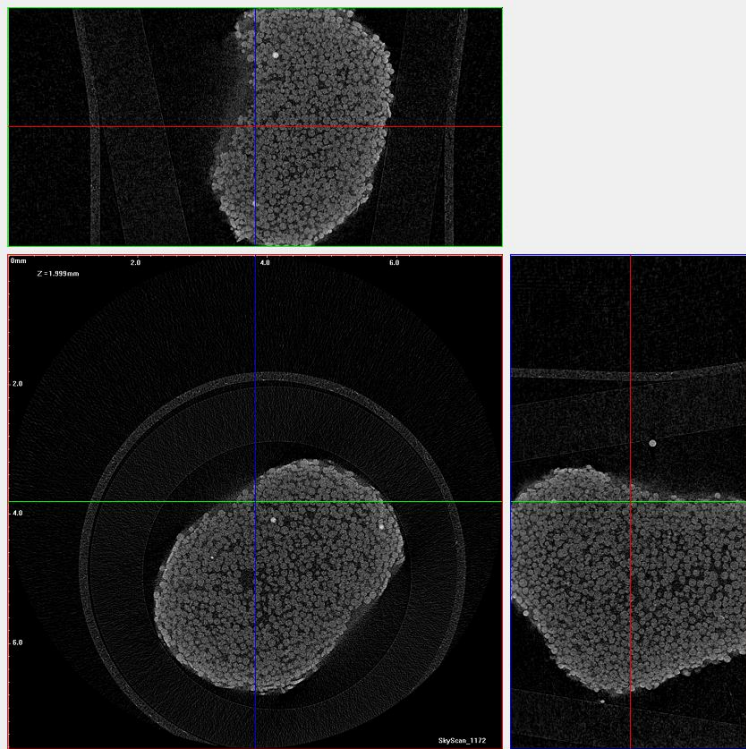
- **65%-35%** Non wetting–wetting beads, **d₅₀ 70μm**, 1300 mPa s, 25 rpm tumbling speed, 5 minutes mixing time.



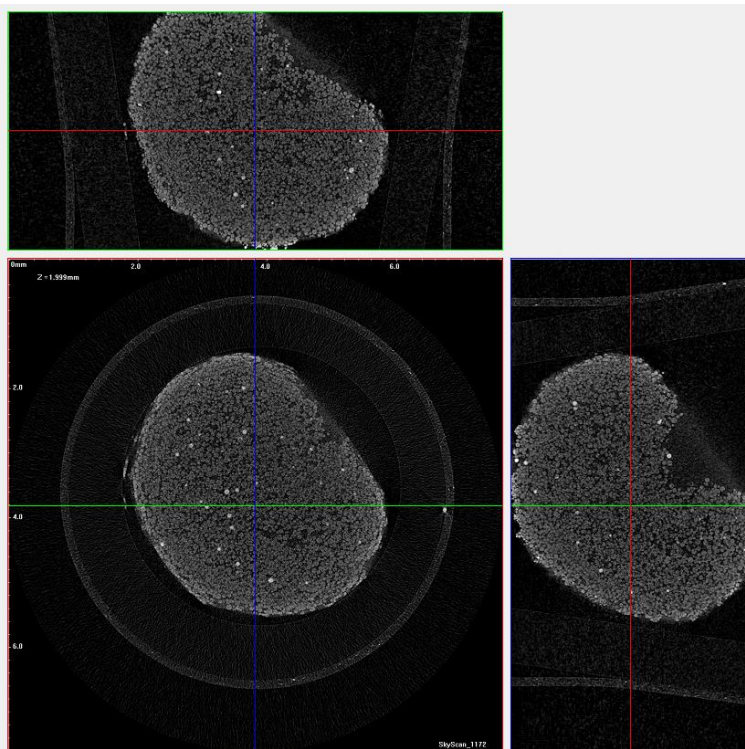
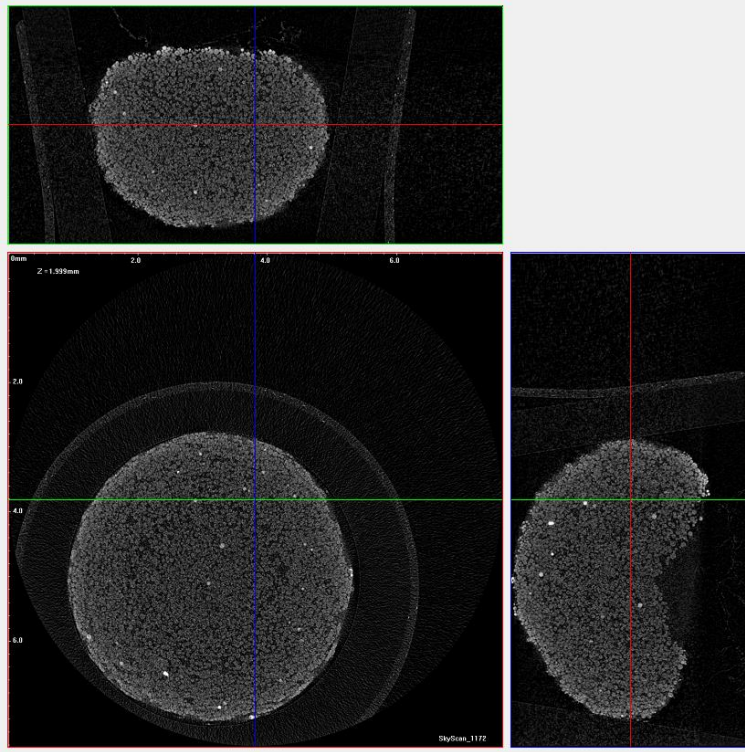


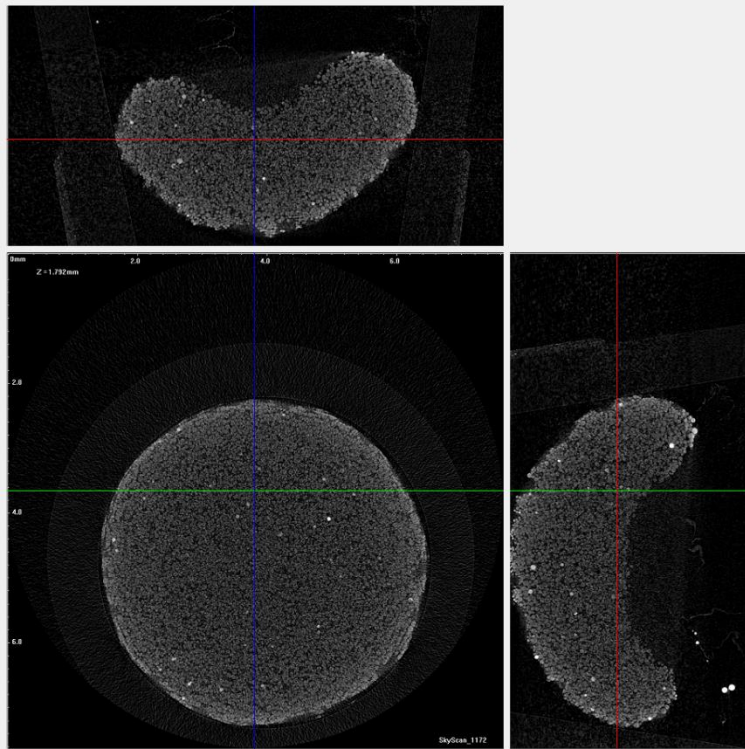
- **65%-35%** Non wetting–wetting beads, d_{50} **115 μ m**, **1300**, 25 rpm tumbling speed, 5 minutes mixing time.



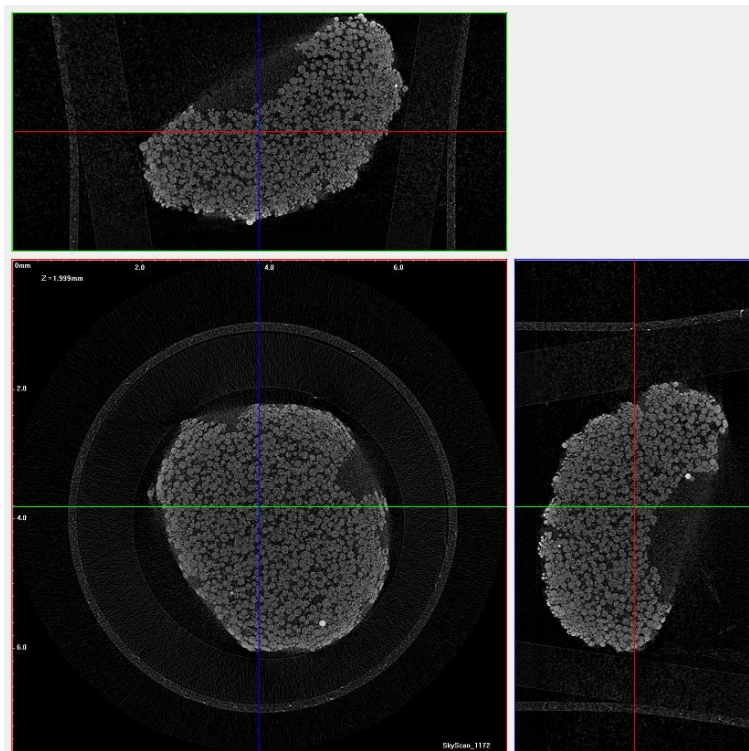


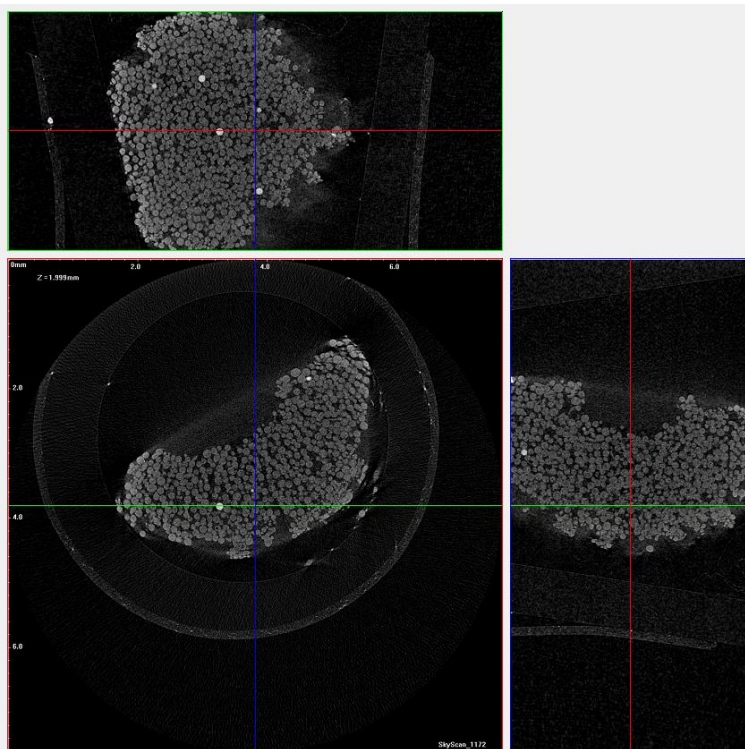
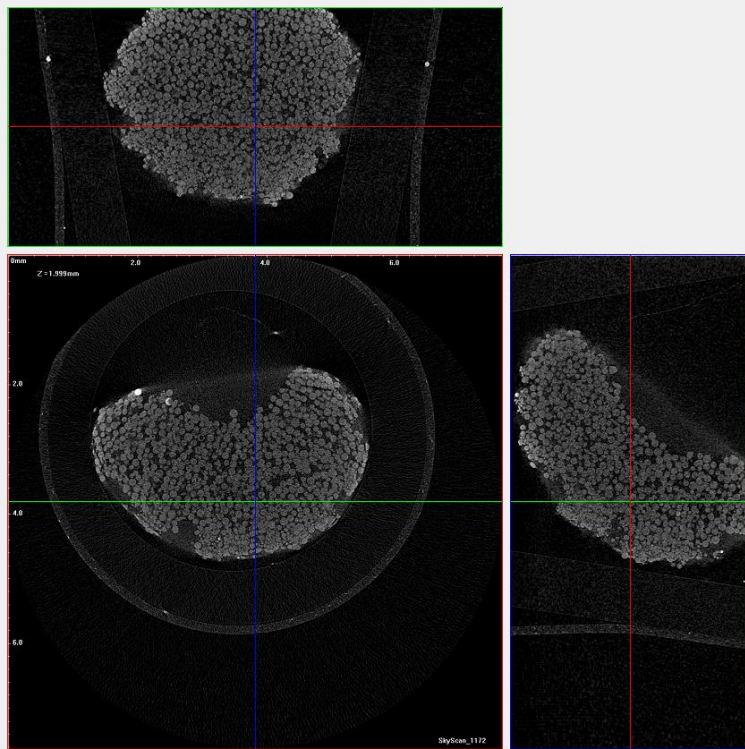
- **0%-100%** Non wetting–wetting beads, **d₅₀ 70μm**, 1300 mPa s, 25 rpm tumbling speed, 5 minutes mixing time.





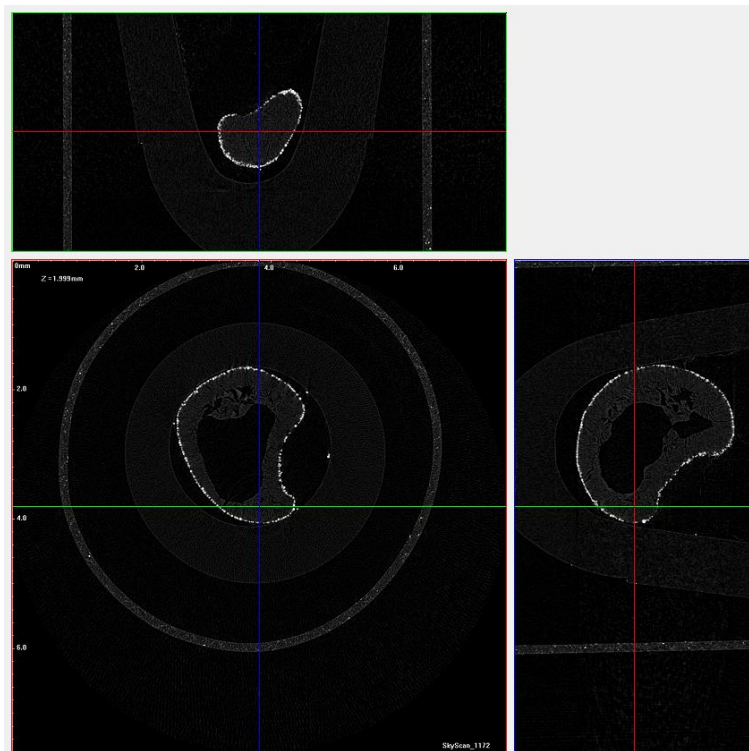
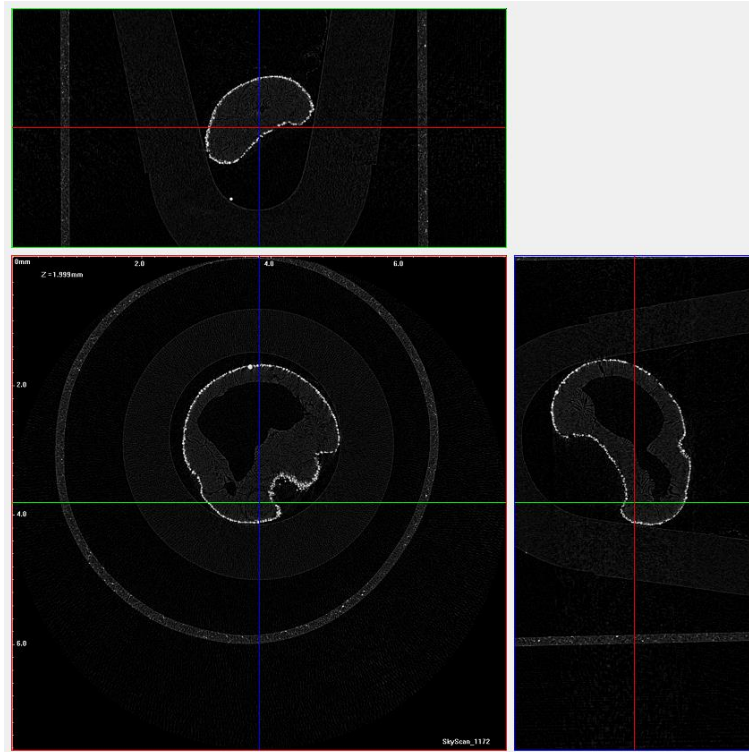
- **0%-100%** Non wetting–wetting beads, d_{50} **115 μ m**, 1300 mPa s, 25 rpm tumbling speed, 5 minutes mixing time.

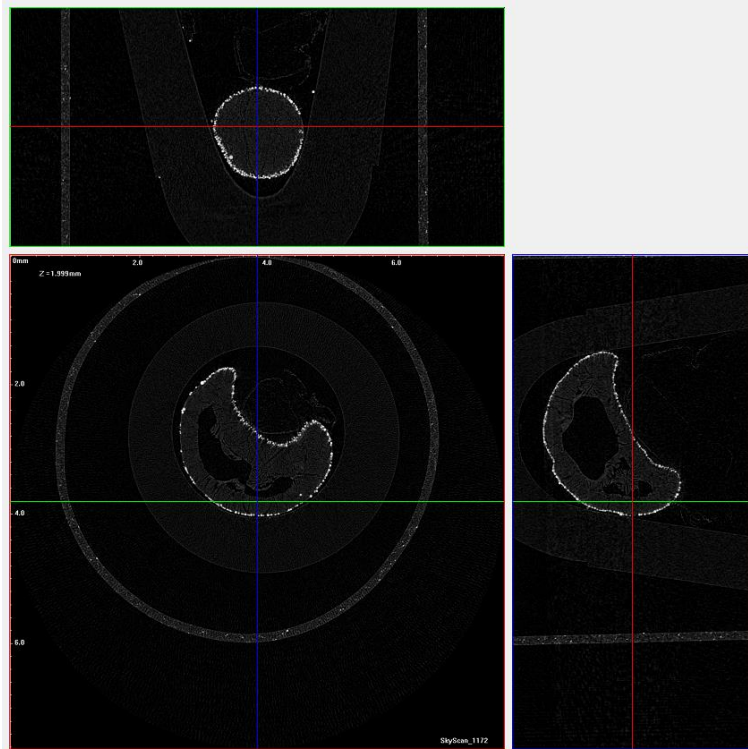




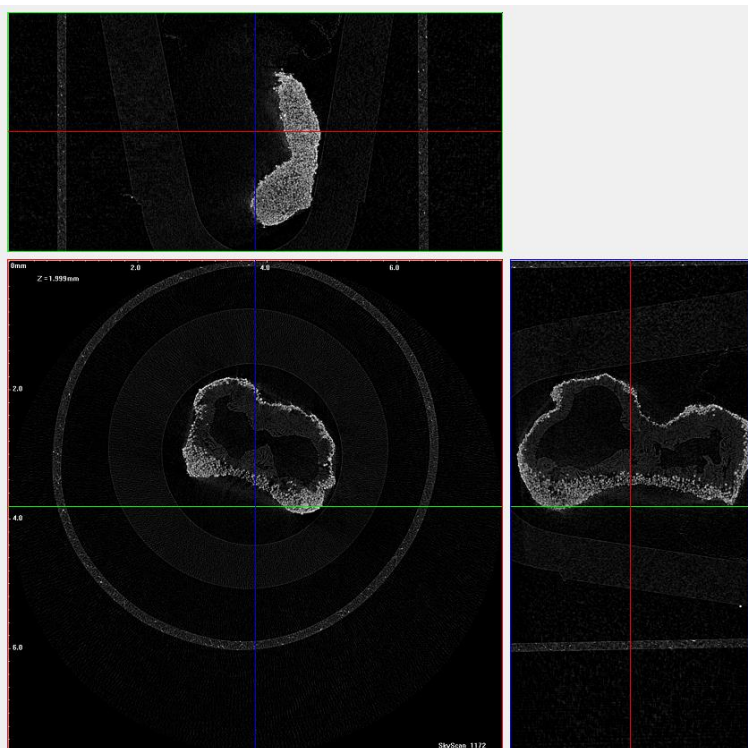
A.2.4: Effect of mixing time

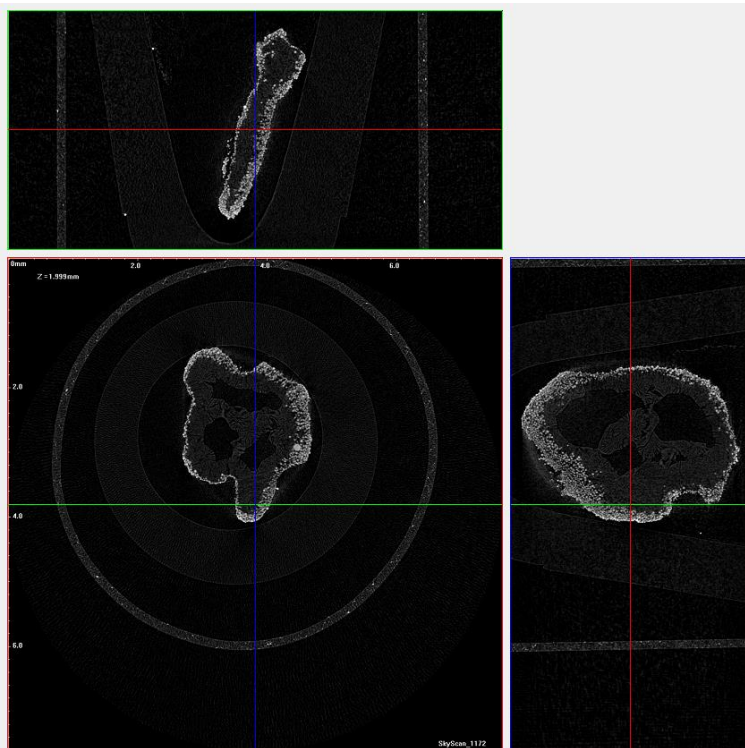
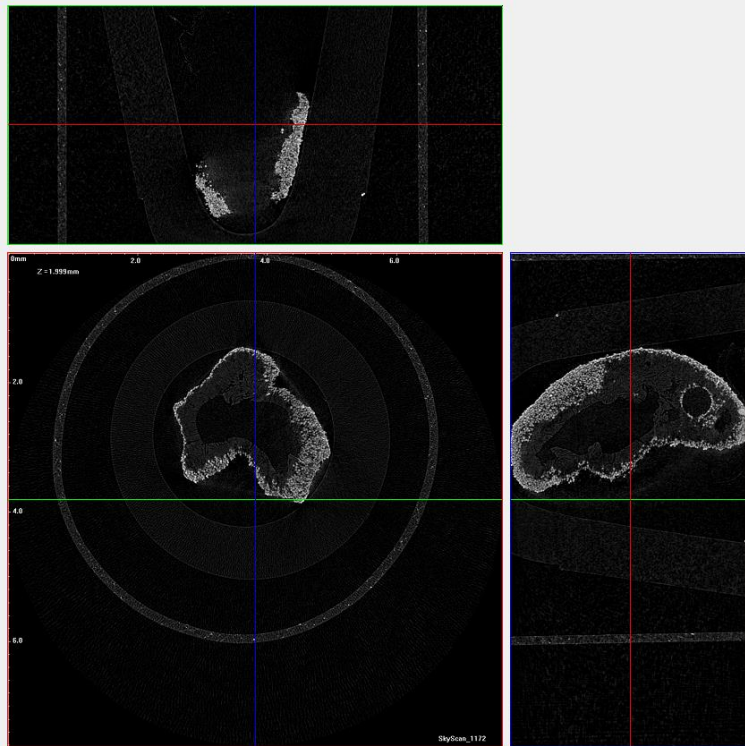
- 100%-0% Non wetting–wetting beads, **mixing time 10 sec**, 1300 mPa s, 25 rpm tumbling speed, 35 μm primary particle size.



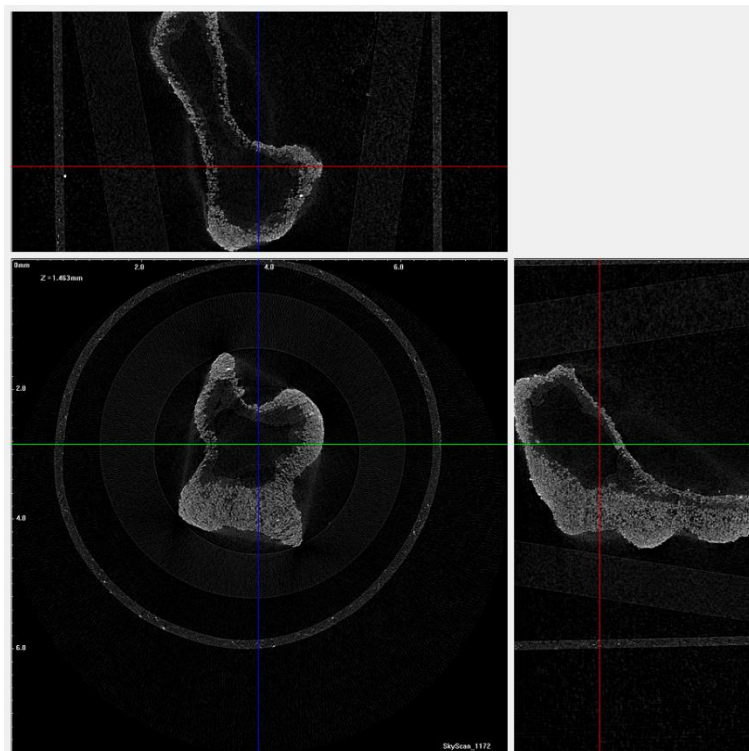
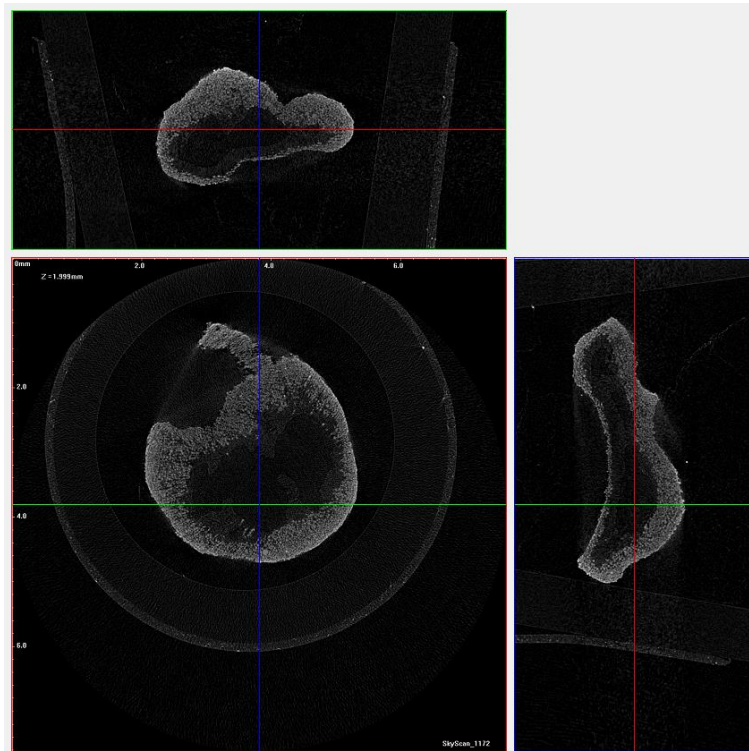


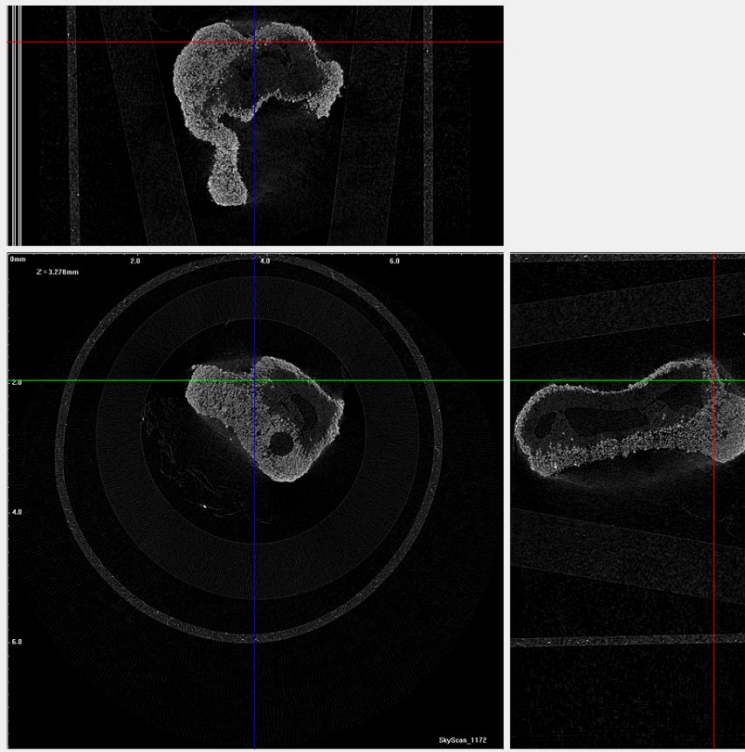
- 100%-0% Non wetting-wetting beads, **mixing time 900 sec**, 1300 mPa s, 25 rpm tumbling speed, 35 μm primary particle size.





- 100%-0% Non wetting–wetting beads, **mixing time 1800 sec**, 1300 mPa s, 25 rpm tumbling speed, 35 μm primary particle size.





Appendix B.1: the volume moment mean diameter d_{43} (μm) of all granules produced in Chapter 5:

B.1.1 The effect of impeller speed and powder wettability

Table B.1.1: Granule size distribution, q_3 in each size fraction for granule produced using low powder wettability and different impeller speed.

Impeller speed (rpm)	q_3						
	Sieve size (μm)						
	106	180	250	500	1000	1700	2800
150	0	0	17.65	25.3	16.66	31.29	9.1
350	0	37.17	38.09	2.27	20.27	2.20	0
550	56.34	28.82	8.60	3.65	2.59	0	0

Table B.1.2: Granule size distribution, q_3 in each size fraction for granule produced using medium powder wettability and different impeller speed.

Impeller speed (rpm)	q_3					
	Sieve size (μm)					
	250	500	1000	1700	2800	3350
150	3.59	0.44	1.92	36.17	1.22	56.66
350	3.15	0.39	12.96	26.56	7.17	49.77
550	0.42	1.61	38.26	59.71	0	0

Table B.1.3: Granule size distribution, q_3 in each size fraction for granule produced using medium powder wettability and different impeller speed.

Impeller speed (rpm)	q_3			
	Sieve size (μm)			
	1000	1700	2800	3350
150	0	0	8.71	91.29
350	0.24	0.48	85.82	13.46
550	0	0	74.88	25.12

Table B.1.4: The volume moment mean diameter (d_{43}) of granules produced using different impeller speed and powder wettability.

Impeller speed (rpm)	d_{43}		
	Low powder wettability	Medium powder wettability	High powder wettability
150	1250	1610	3075
350	726	1600	2213
550	407	863	2213

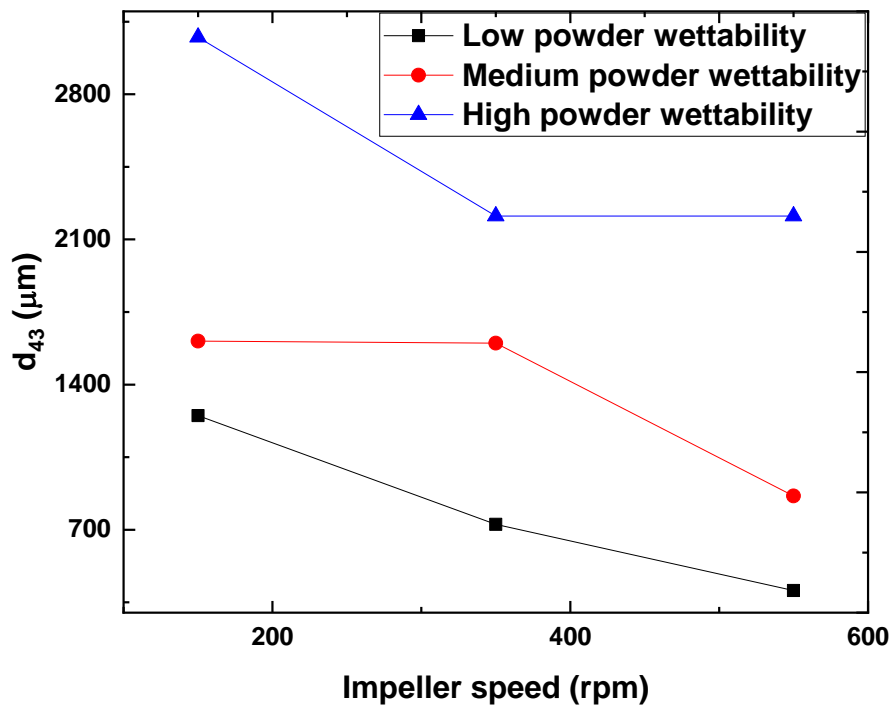


Figure B.1.1: The volume moment mean diameter (d_{43}) of granules produced using different impeller speed and powder wettability.

B.1.2 The effect of impeller design and powder wettability

Table B.1.5: Granule size distribution, q_3 in each size fraction for granule produced using low powder wettability and different impeller design.

Impeller design	q_3						
	Sieve size (μm)						
	106	180	250	500	1000	1700	2800
Flat plate	0	37.17	38.09	2.27	20.27	2.20	0
2-bladed	6.30	39.97	31.34	15.13	5.19	2.07	0
3-bladed	1.98	66.54	22.04	7.66	1.78	0	0

Table B.1.6: Granule size distribution, q_3 in each size fraction for granule produced using medium powder wettability and different impeller design.

Impeller design	q_3							
	Sieve size (μm)							
	106	180	250	500	1000	1700	2800	3350
Flat plate	0	0	3.15	0.39	12.96	26.52	7.17	49.77
2-bladed	0	2.68	4.01	8.13	62.14	22.53	0.51	0
3-bladed	97.13	1.52	0.91	0.35	0.09	0	0	0

Table B.1.7: Granule size distribution, q_3 in each size fraction for granule produced using high powder wettability and different impeller design.

Impeller design	q_3							
	Sieve size (μm)							
	106	180	250	500	1000	1700	2800	3350
Flat plate	0	0	0	0	0.24	0.46	85.84	13.46
2-bladed	0	1.07	1.60	4.98	5.48	76.35	10.52	0
3-bladed	2.45	38.08	22.58	7.31	3.73	0	21.34	4.51

Table B.1.8: The volume moment mean diameter (d_{43}) of granules produced using different impeller speed and powder wettability.

Impeller design	d_{43}		
	Low powder wettability	Medium powder wettability	High powder wettability
Flat plate	726	1600	2213
2-Bladed	623	1072	1397
3-Bladed	407	623	1236

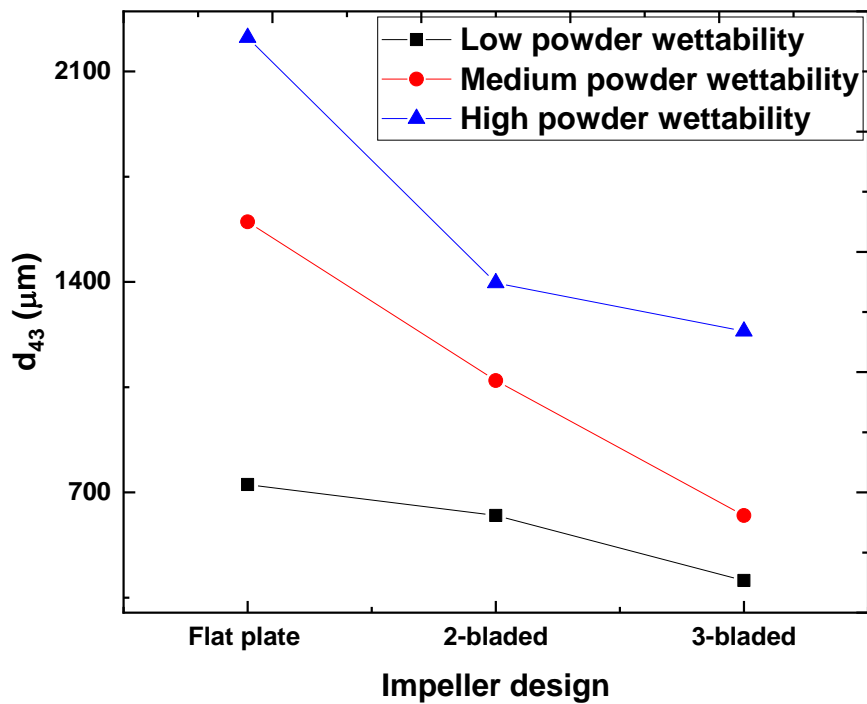
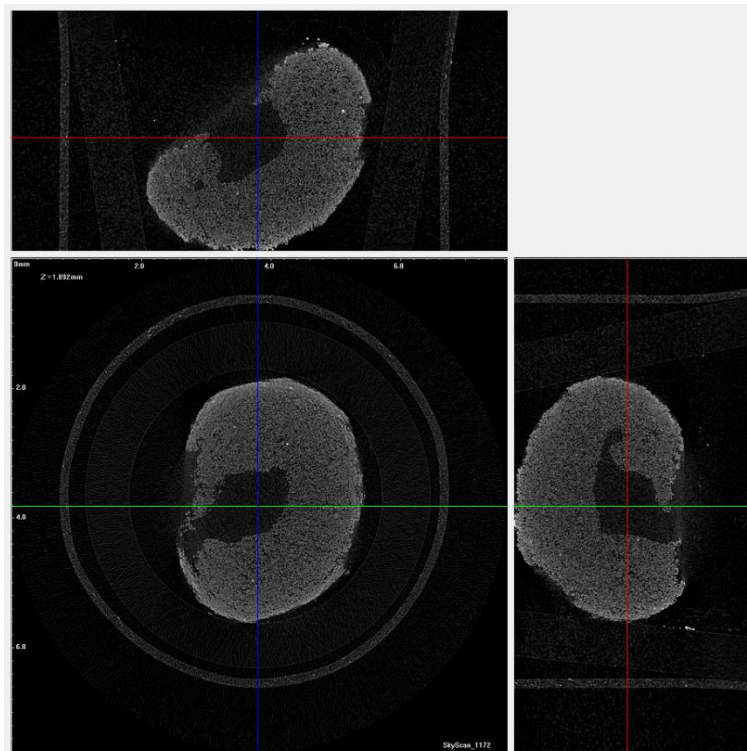


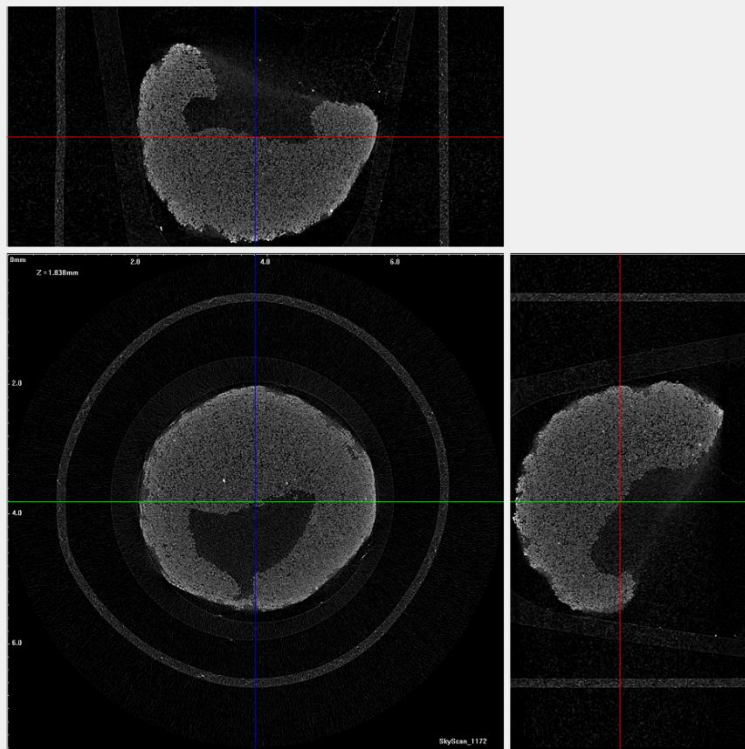
Figure B.1.2: The volume moment mean diameter (d_{43}) of granules produced using different impeller speed and powder wettability.

Appendix B.2: XRCT-3D images

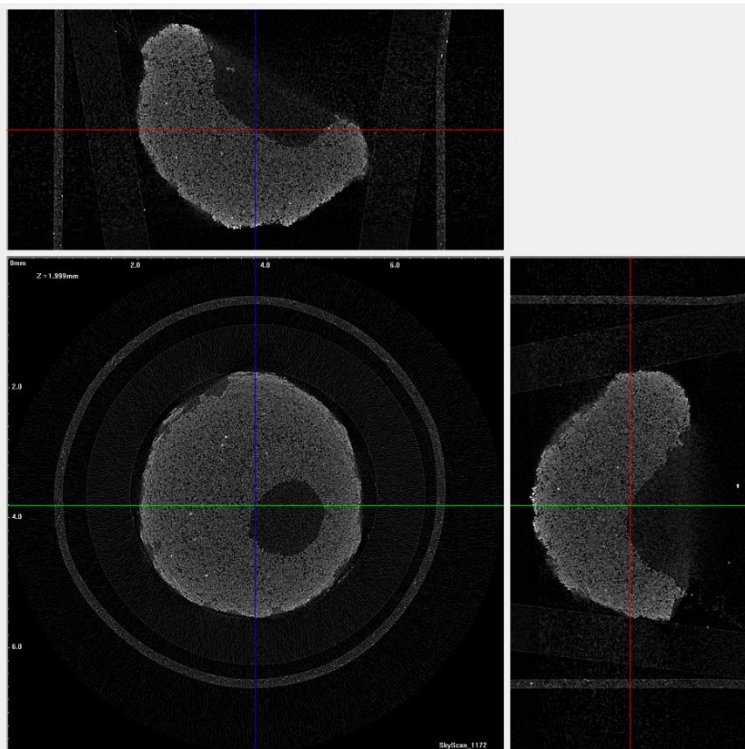
B.2.1. Effect of impeller speed and powder wettability

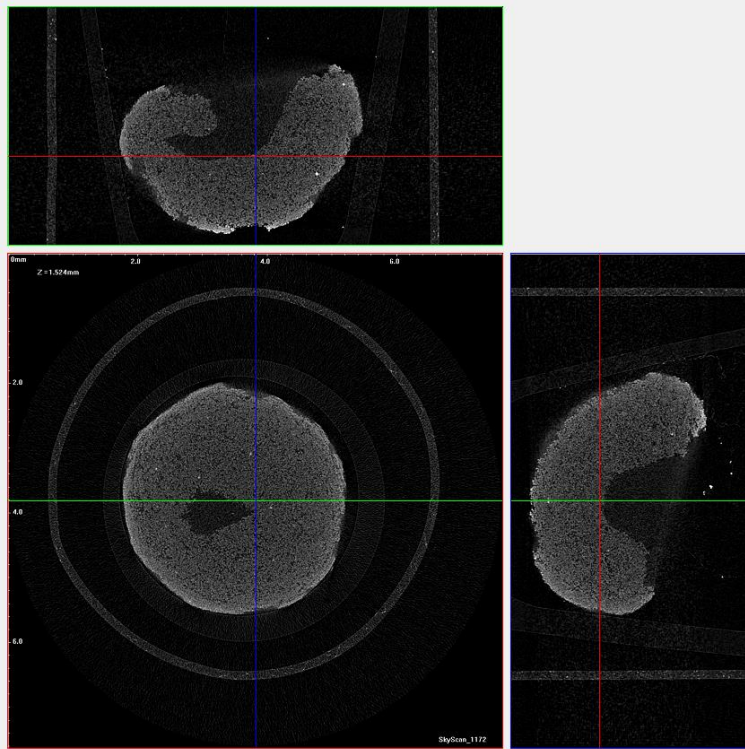
- **0%-100%** Non wetting–wetting beads, **150 rpm speed**, flat plate, 1300 mPa s, 20 s mixing time, 35 μm primary particle size.



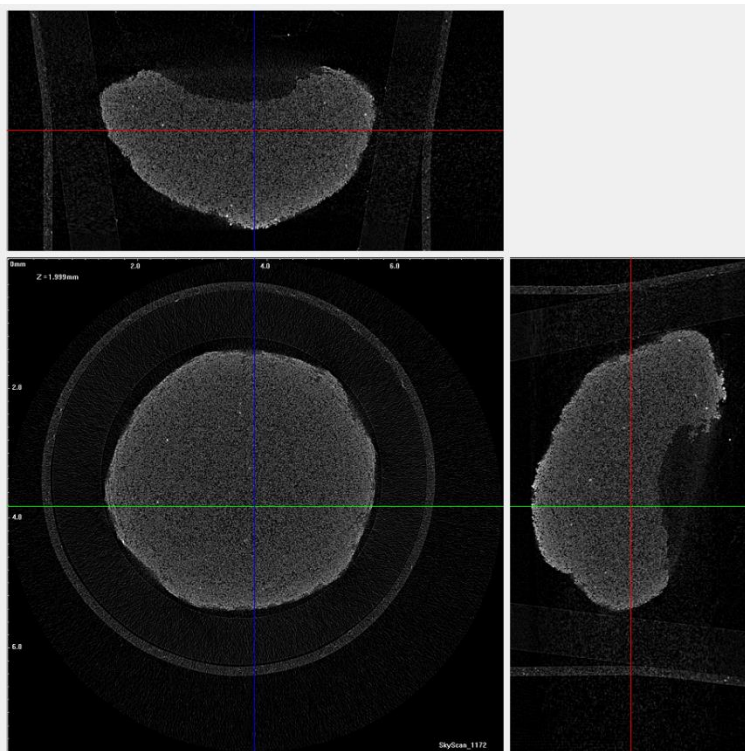


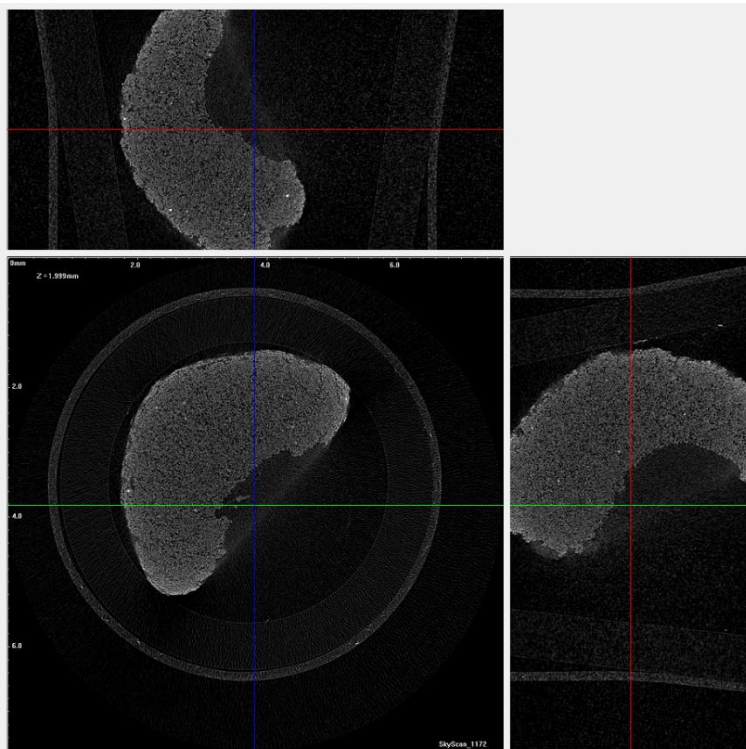
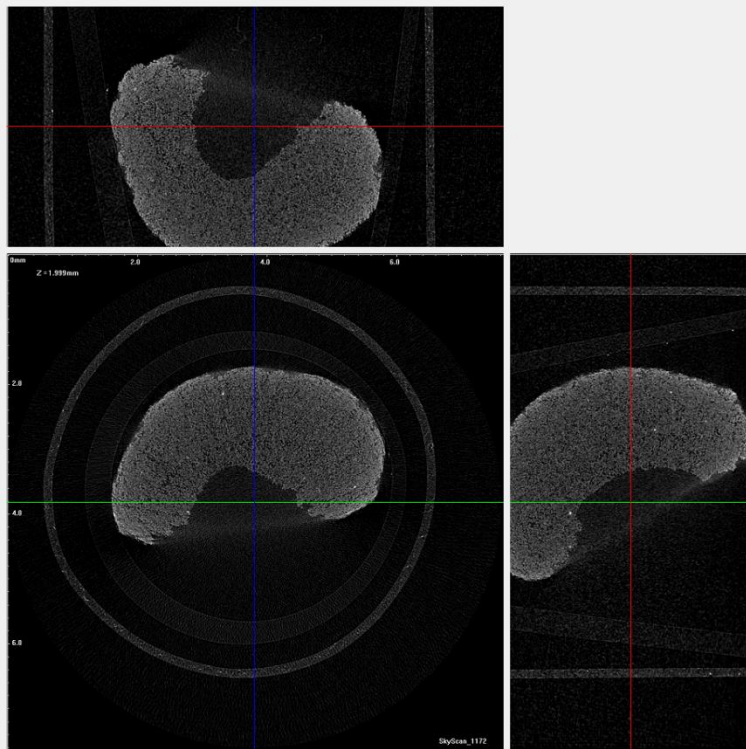
- **0%-100%** Non wetting–wetting beads, **350 rpm speed**, flat plate, 1300 mPa s, 20 s mixing time, 35 μm primary particle size.



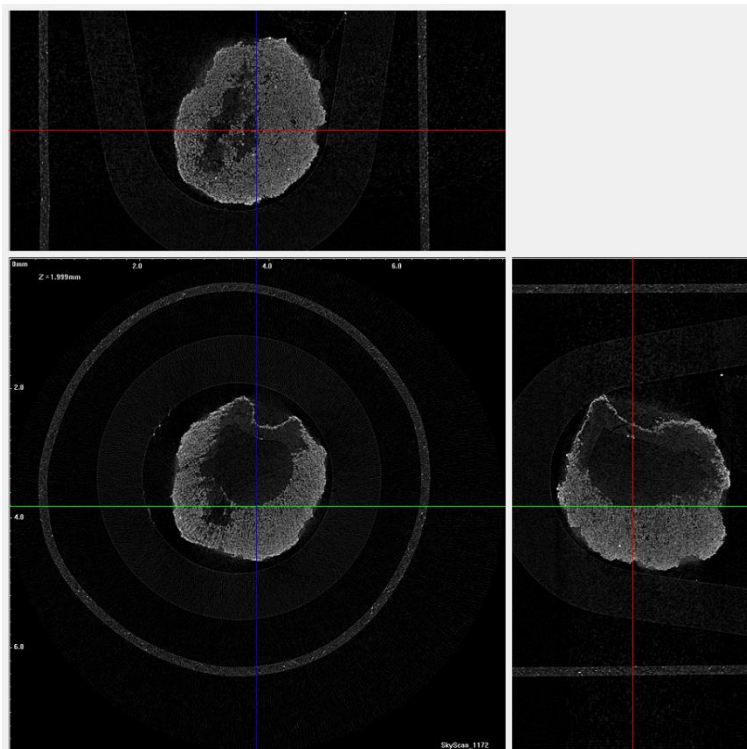
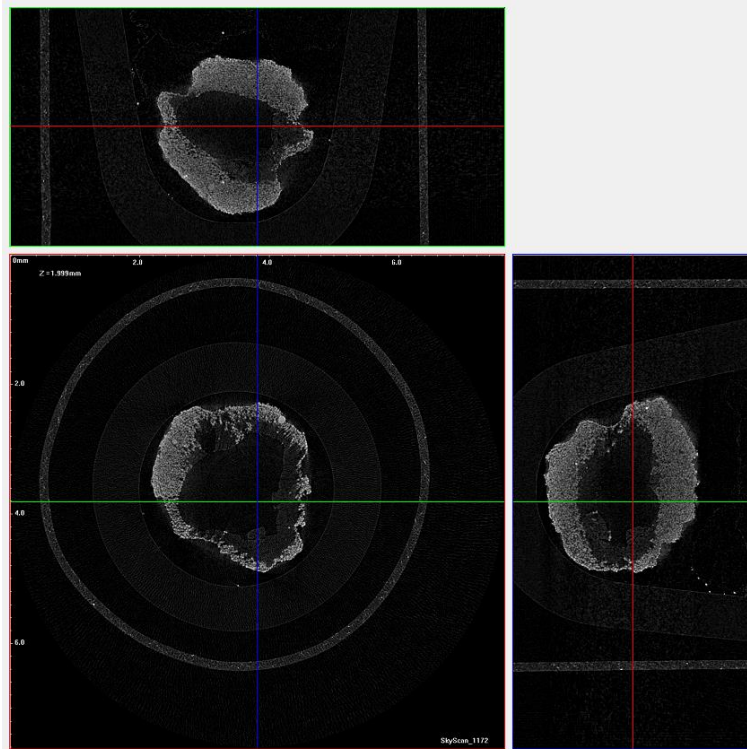


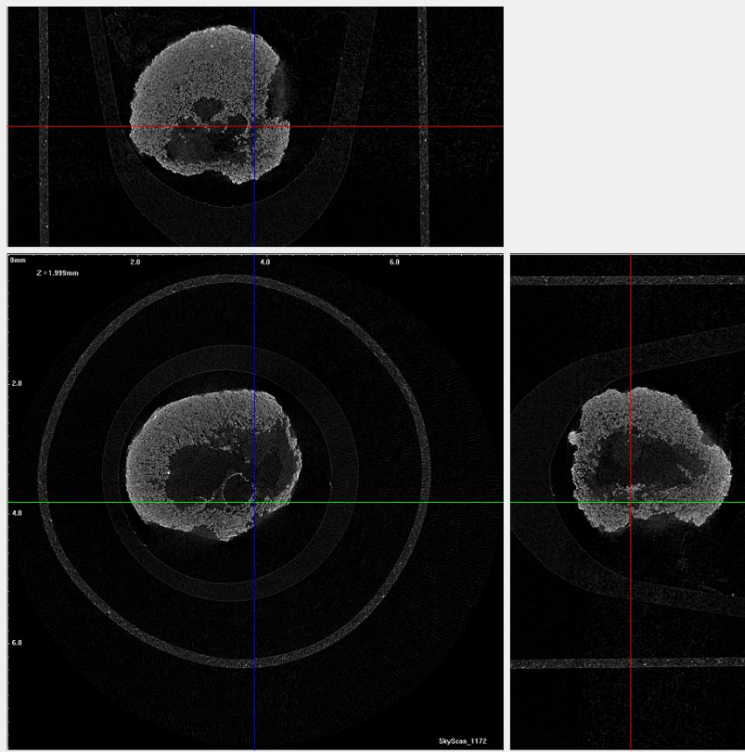
- **0%-100%** Non wetting–wetting beads, **550 rpm speed**, flat plate, 1300 mPa s, 20 s mixing time, 35 μm primary particle size.



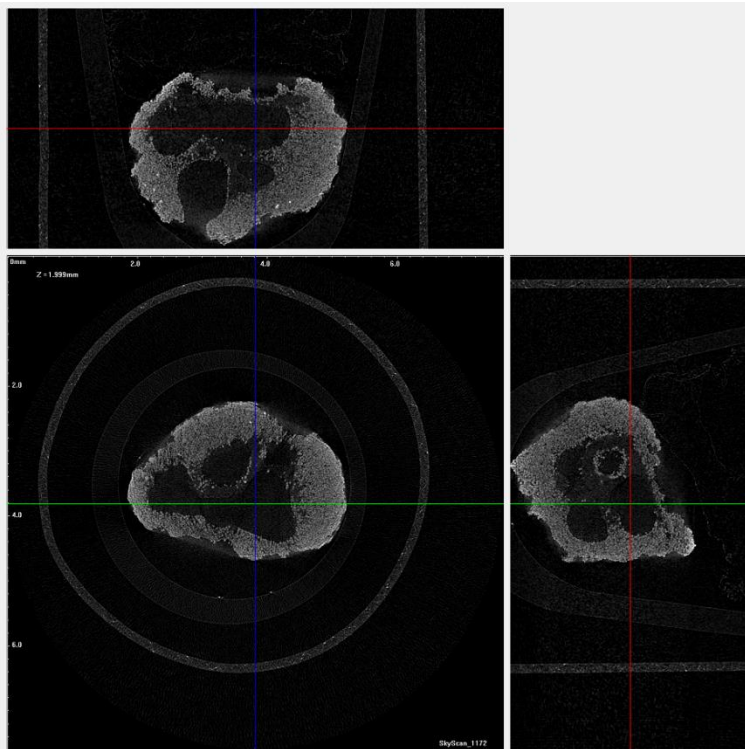


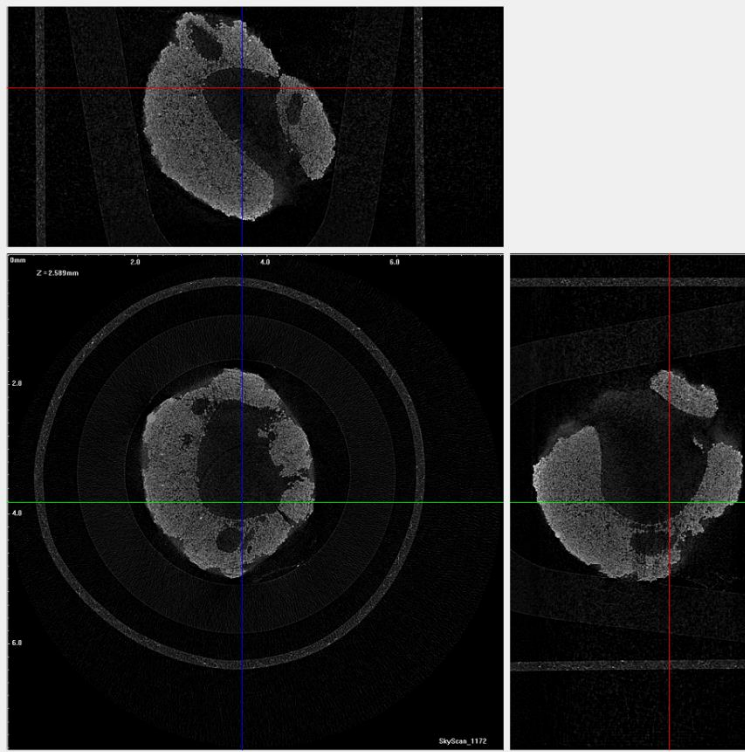
- **65%-35%** Non wetting–wetting beads, **150 rpm speed**, flat plate, 1300 mPa s, 20 s mixing time, 35 μm primary particle size.



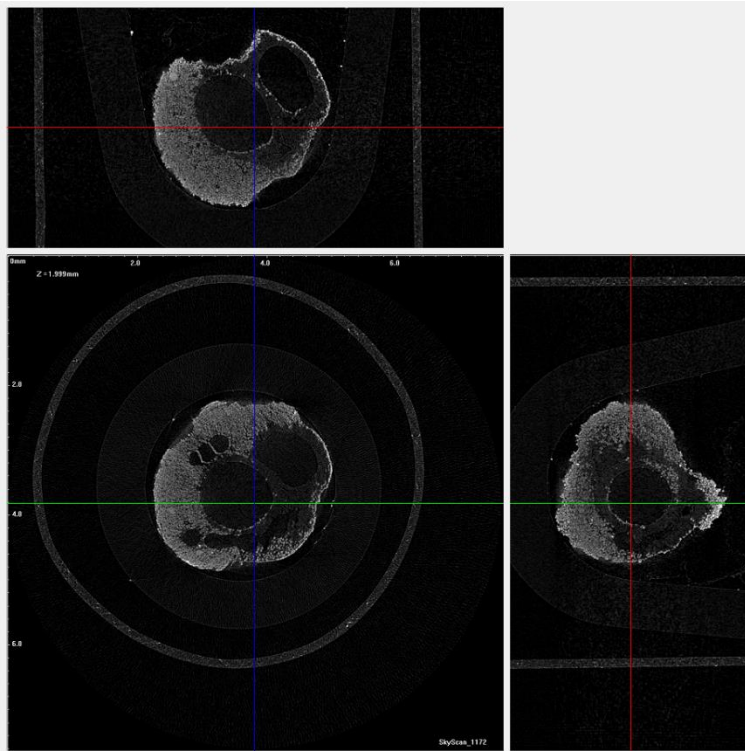


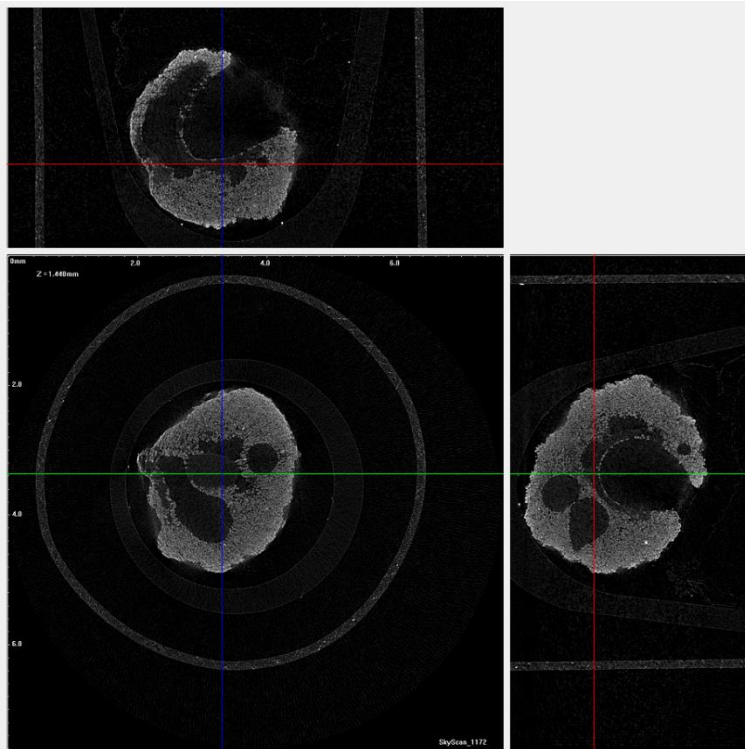
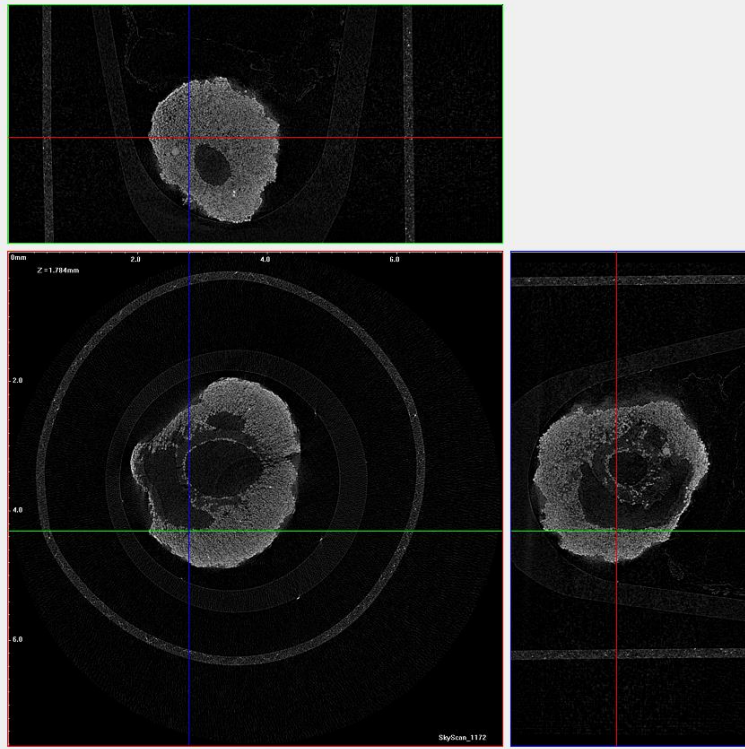
- **65%-35%** Non wetting–wetting beads, **350 rpm speed**, flat plate, 1300 mPa s, 20 s mixing time, 35 μm primary particle size.



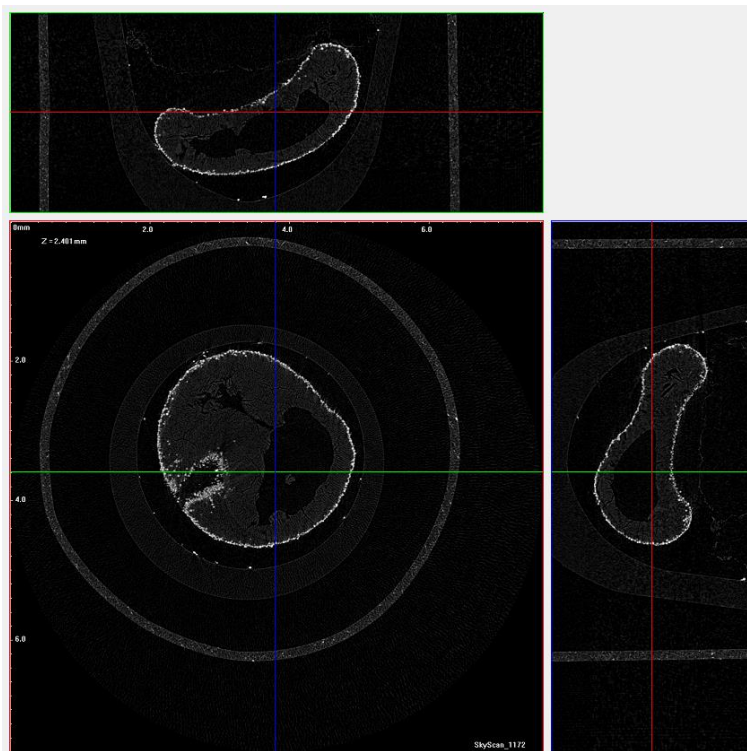
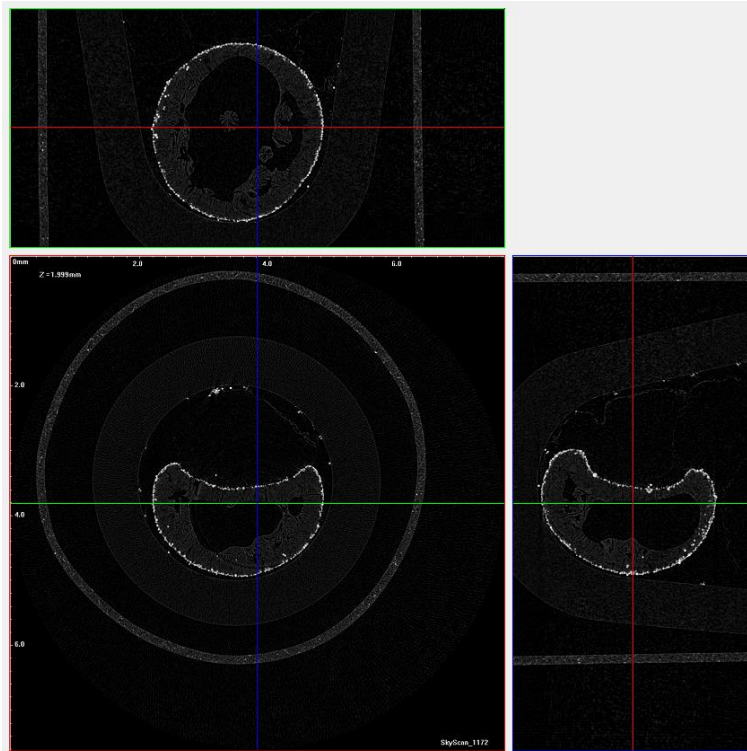


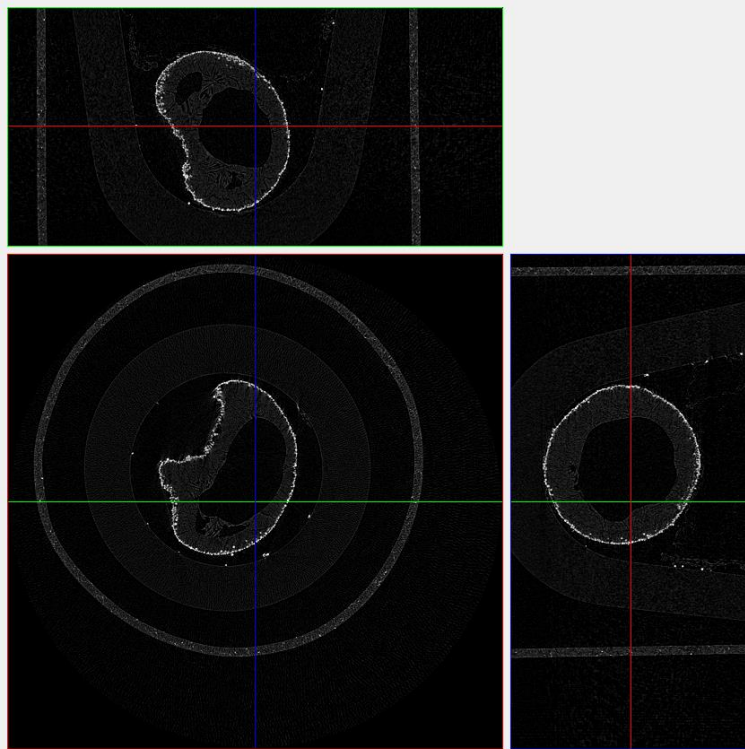
- **65%-35%** Non wetting–wetting beads, **550 rpm speed**, flat plate, 1300 mPa s, 20 s mixing time, 35 μm primary particle size.



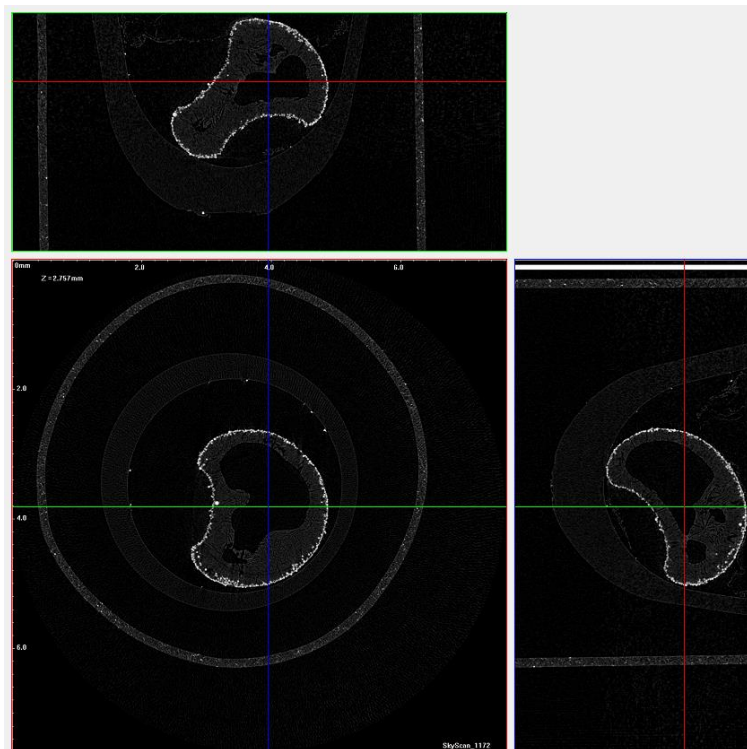


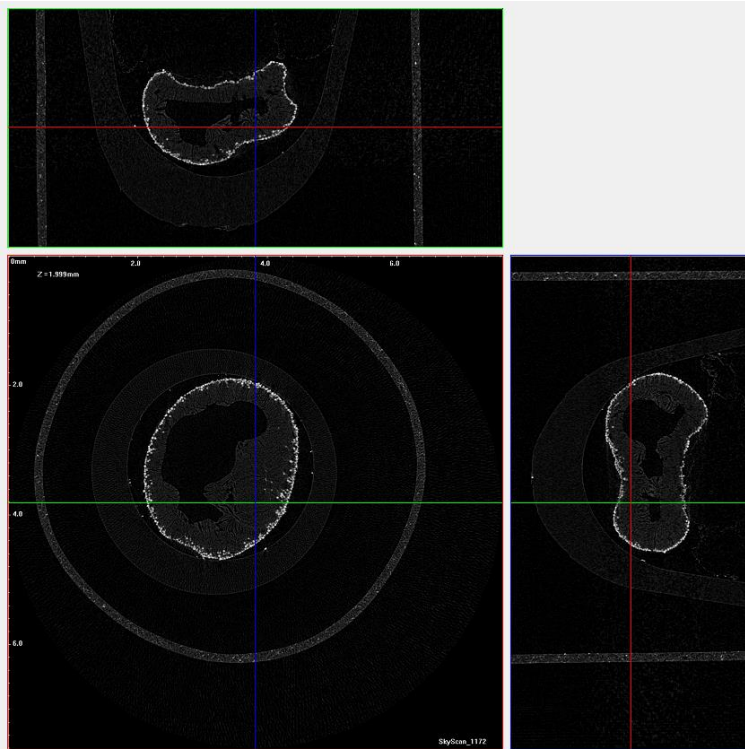
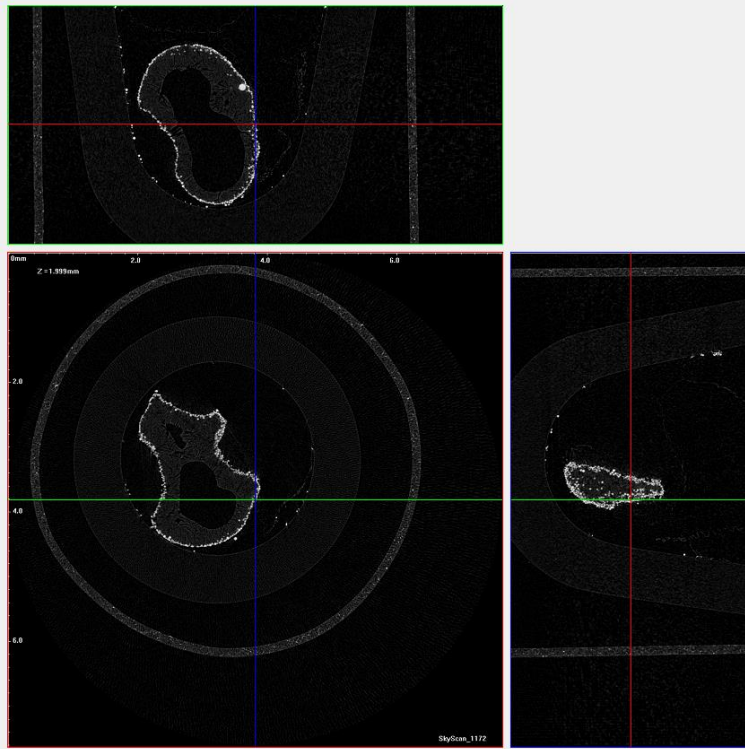
- **100%-0%** Non wetting–wetting beads, **150 rpm speed**, flat plate, 1300 mPa s, 20 s mixing time, 35 μm primary particle size.





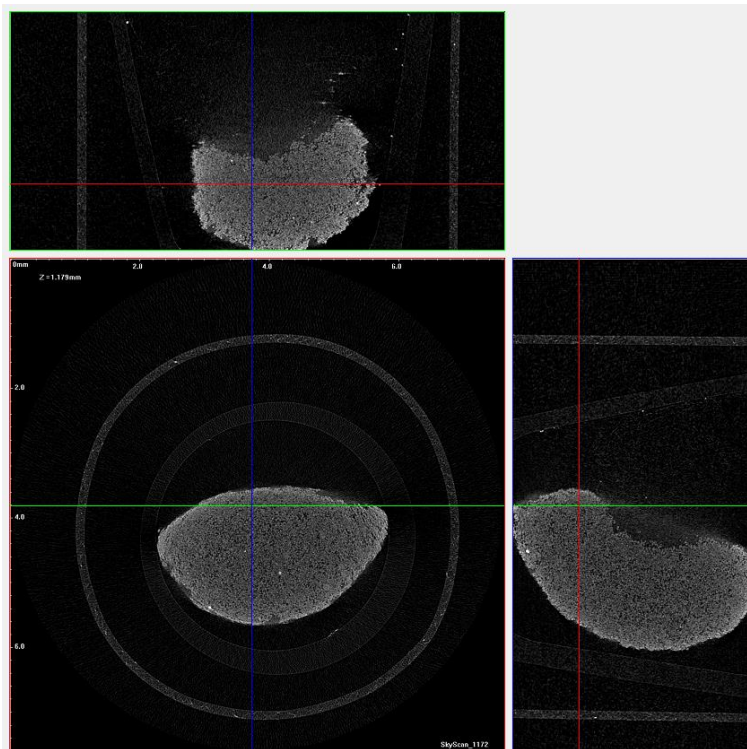
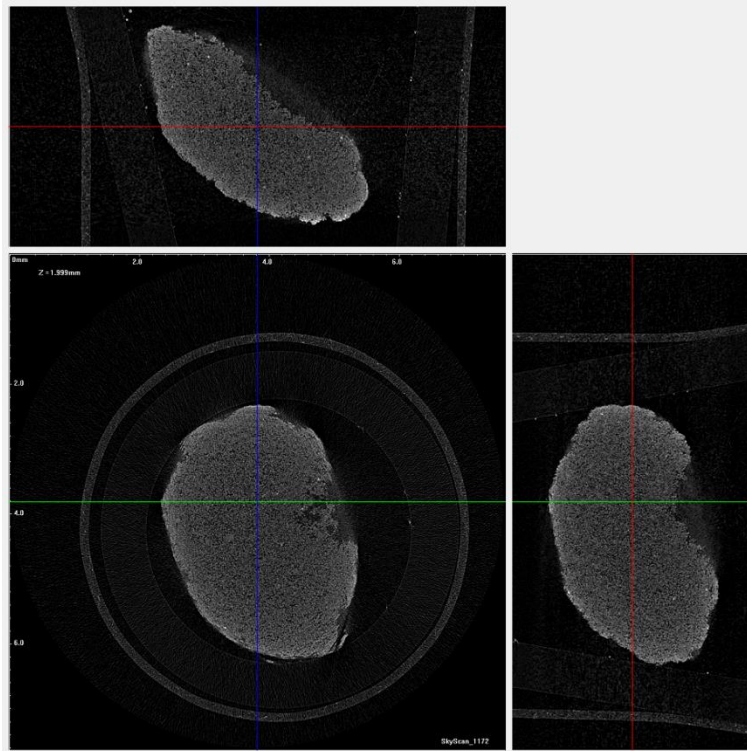
- **100%-0%** Non wetting–wetting beads, **350 rpm speed**, flat plate, 1300 mPa s, 20 s mixing time, 35 μm primary particle size.

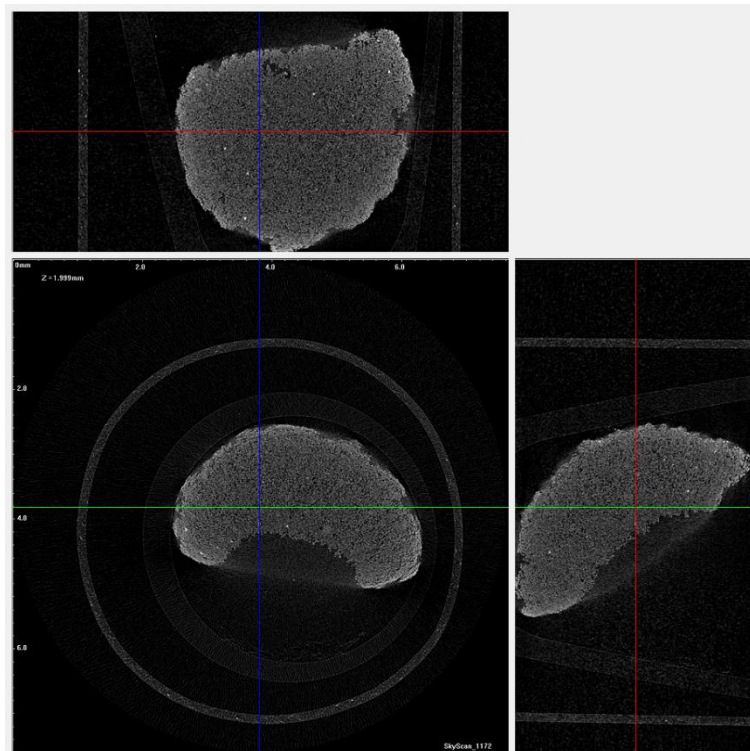
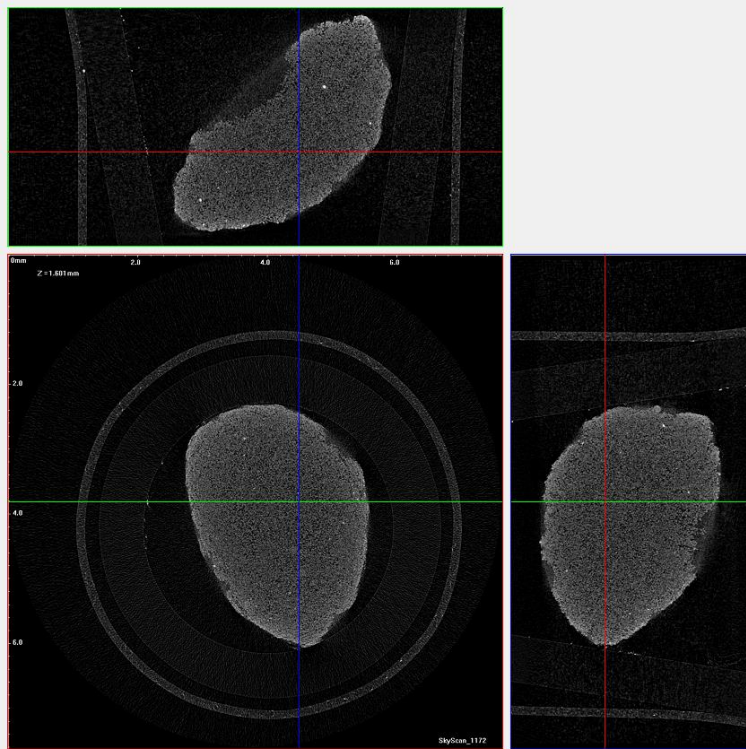




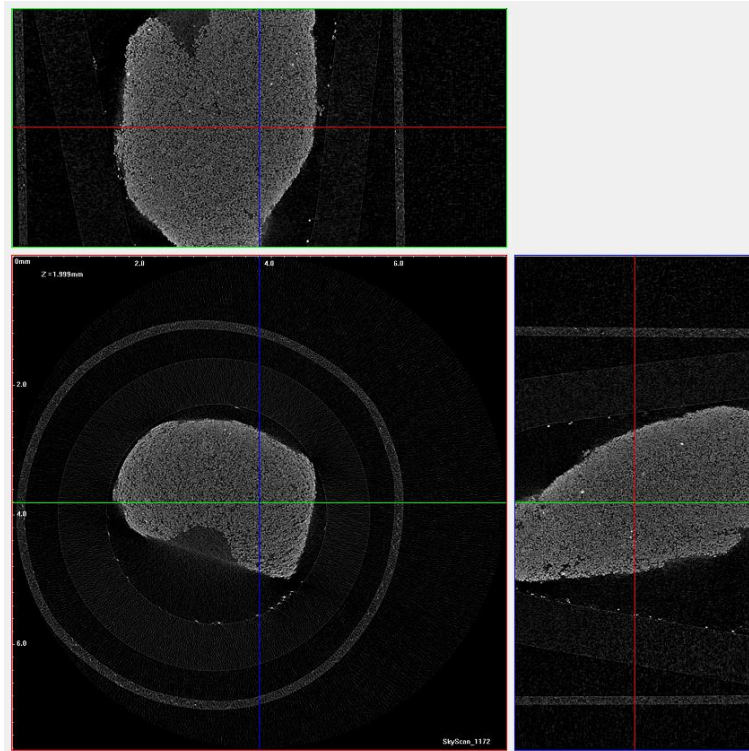
B.2.2 Effect of impeller design and powder wettability

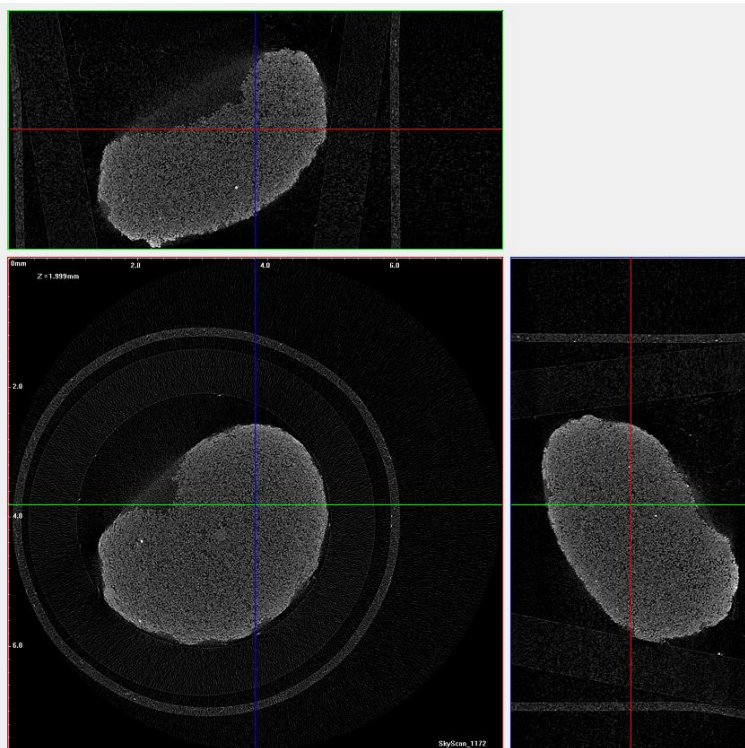
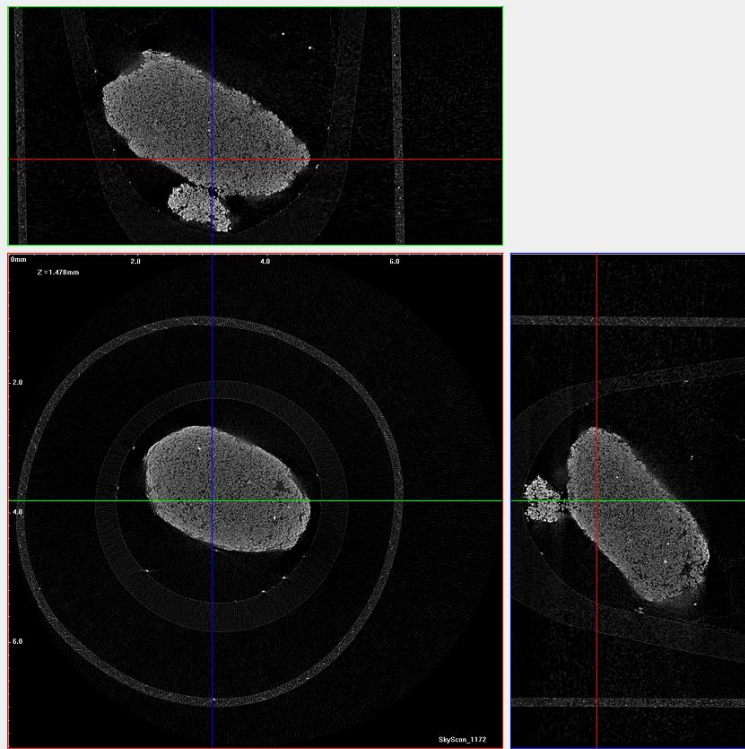
- **0%-100%** Non wetting–wetting beads, **2-bladed impeller**, 350 rpm, 1300 mPa s, 20 s mixing time, 35 μm primary particle size.





- **0%-100%** Non wetting–wetting beads, **3-bladed impeller**, 350 rpm, 1300 mPa s, 20 s mixing time, 35 μm primary particle size.





References

1. A.D. Salman, M.J. Hounslow, and J.P.K. Seville. (2007) 'High shear granulation Granulation, in Handbook of Powder Technology', Elsevier Science, 11, pp. 3-19.
2. Alghunaim, A., Kirdponpattara, S. and Newby, B. M. Z. (2016) 'Techniques for determining contact angle and wettability of powders', Powder Technology. Elsevier, 287, pp. 201–215.
3. Allen, T. (2003). Powder Sampling and Particle Size Detremination . Elsevier Science.
4. Ansari, M. A. and Stepanek, F. (2006) 'Formation of hollow core granules by fluid bed in situ melt granulation: Modelling and experiments', International Journal of Pharmaceutics, 321(1–2), pp. 108–116.
5. Ansari, M. A. and Stepanek, F. (2008) 'The effect of granule microstructure on dissolution rate', Powder Technology, 181(2), pp. 104–114.
6. Arbatan, Tina et al. (2012) 'Liquid Marbles as Micro-bioreactors for Rapid Blood Typing', Advanced Healthcare Mater, 1, pp. 80–83.
7. Asada, T. et al. (2018) 'Mechanism of the formation of hollow spherical granules using a high shear granulator', European Journal of Pharmaceutical Sciences. Elsevier, 117, pp. 371–378.
8. Aristoff, J. M., & Bush, J. W. M. (2009) 'Water entry of small hydrophobic spheres', Journal of Fluid Mechanics, 619, 45–78.
9. Arjmandi-tash, O., Tew, J. D., Pitt, K., Smith, R., & Litster, J. D. (2019). 'A new mathematical model for nucleation of spherical agglomeration by the immersion mechanism', Chemical Engineering Science, 4, pp. 1-16.
10. Aulton, M. E. (2007) Aulton's Pharmaceutics: The Design and Manufacture of Medicine. Elsevier.
11. Aussillous, P. and Quere D. (2001) 'Properties of liquid marbles', Nature 411, 924-927.
12. Balashanmugam, M. et al. (2015) 'Semi-solid paste binder dispersion in a moving powder bed', Procedia Engineering, 102, pp. 626–633.
13. Benali, M., Gerbaud, V. and Hemati, M. (2009) 'Effect of operating conditions and physico-chemical properties on the wet granulation kinetics in high shear mixer', Powder Technology. Elsevier, 190(1–2), pp. 160–169.
14. Bhosale, P. S., Panchagnula, M. V and Stretz, H. A. (2008) 'Mechanically robust nanoparticle stabilized transparent liquid marbles', Citation: Applied Physics Letters, 93(034109).
15. Binks, B. P. and Murakami, R. (2006) 'Phase inversion of particle-stabilized materials from foams to dry water', Nature Materials, 5(11), pp. 865–869.

16. Boonkanokwong, V. et al. (2016) 'The effect of the number of impeller blades on granular flow in a bladed mixer', *Powder Technology*. Elsevier B.V., 302, pp. 333–349.
17. Bormashenko, E. (2011) 'Liquid marbles: Properties and applications', *Current Opinion in Colloid & Interface Science*, 16, pp. 266–271.
18. Bowden-Green, B. and Briens, L. (2016) 'An investigation of drum granulation of biochar powder', *Powder Technology*. Elsevier B.V., 288, pp. 249–254.
19. Braun, H.-G., & Cardoso, A. Z. (2012). Self-assembly of Fmoc-diphenylalanine inside liquid marbles. *Colloids and Surfaces B: Biointerfaces*, 97, 43–50.
20. Briens, L. and Bowden-Green, B. (2019) 'A comparison of drum granulation of biochars', *Powder Technology*, 343, pp. 723-732.
21. Buckton, G. (1990) 'Contact angle, adsorption and wettability - a review with respect to powders', *Powder Technology*, 61(3), pp. 237–249.
22. Campbell, G. A. et al. (2011) 'Closing the gap in series scale up of high shear wet granulation process using impeller power and blade design', *Powder Technology*. Elsevier B.V., 205(1–3), pp. 184–192.
23. Cassie, A. B. D. and Baxter S. (1944) 'Wettability of porous surfaces', *Transactions of Faraday society*, (5), pp. 546–551.
24. Cavinato, M. et al. (2011) 'Combining formulation and process aspects for optimizing the high-shear wet granulation of common drugs', *International Journal of Pharmaceutics*. Elsevier B.V., 416(1), pp. 229–241.
25. Chang, F. et al. (2014) 'Preparation and characterization of modified starch granules with high hydrophobicity and flowability', *Food Chemistry*. Elsevier Ltd, 152, pp. 177–183.
26. Charles-Williams, H. R. et al. (2011) 'Granule nucleation and growth: Competing drop spreading and infiltration processes', *Powder Technology*. Elsevier B.V., 206(1–2), pp. 63–71.
27. Charles-Williams, H., Wengeler, R., et al. (2013) 'Granulation behaviour of increasingly hydrophobic mixtures', *Powder Technology*, 238, pp. 64–76.
28. Chau, T. T. (2009) 'A review of techniques for measurement of contact angles and their applicability on mineral surfaces', *Minerals Engineering*. Elsevier Ltd, 22(3), pp. 213–219.
29. Chetia, B. C., & Hazarika, G. C. (2000) 'Effects of fuzziness on dynamical similarity and Reynold's number', *Fuzzy Sets and Systems*, 115(3), 463–469.
30. Chitu, T. M., Oulahna, D. and Hemati, M. (2011a) 'Rheology, granule growth and granule strength: Application to the wet granulation of lactose-MCC mixtures', *Powder Technology*. Elsevier B.V., 208(2), pp. 441–453.

31. Chitu, T. M., Oulahna, D. and Hemati, M. (2011b) 'Wet granulation in laboratory-scale high shear mixers: Effect of chopper presence, design and impeller speed', *Powder Technology*. Elsevier B.V., 206(1–2), pp. 34–43.
32. Dandan, M. and Erbil, H. Y. (2009) 'Evaporation rate of graphite liquid marbles: Comparison with water droplets', *Langmuir*, 25(14), pp. 8362–8367.
33. Davis, N. B. et al. (2017) 'Microstructure of single-droplet granules formed from ultra-fine powders', *Powder Technology*. Elsevier B.V., 305, pp. 19–26.
34. Dengxin, L. et al. (2008) 'Preparation of nano-iron oxide red pigment powders by use of cyanided tailings', *Journal of Hazardous Materials*, 155(1–2), pp. 369–377.
35. D. M. Parikh, (2005) 'Introduction, in Handbook of Pharmaceutical Granulation Theory', Taylor & Francis Group, LLC: Boca Raton, USA.
36. D. Salman, M.J. Hounslow, and J.P.K. Seville, (2007) 'Granulation rate processes, in Handbook of Powder Technology', Elsevier Science, 11, pp. 898-962.
37. D, V. et al. (1999) 'Screening of high shear mixer melt granulation process variables using an asymmetrical factorial design', *International Journal of Pharmaceutics*, 190, pp. 73–81.
38. Dullien, F. (1992). *Porous Media: Fluid transport and pore structure* (2nd edition). Academic Press, INC.
39. Eliassen, H., Kristensen, H. G. and Schæfer, T. (1999) 'Growth mechanisms in melt agglomeration with a low viscosity binder', *International Journal of Pharmaceutics*, 186(2), pp. 149–159.
40. Emady, H. N., Kayrak-Talay, D., Schwerin, W. C., & Litster, J. D. (2011) 'Granule formation mechanisms and morphology from single drop impact on powder beds', *Powder Technology*, 212(1), 69–79.
41. Ende, D. J. (2011). *Chemical Engineering in Pharmaceutical Industry: R& D to Manufacturing*. Hoboken, New Jersey: John Wiley & Sons, Inc.
42. Ennis, B. J., Tardos, G. and Pfeffer, R. (1991) 'A microlevel-based characterization of granulation phenomena', *Powder Technology*, 65(1–3), pp. 257–272.
43. Eshtiaghi, N., Arhatari, B. and Hapgood, K. P. (2009) 'Producing hollow granules from hydrophobic powders in high-shear mixer granulators', *Advanced Powder Technology*. The Society of Powder Technology Japan., 20(6), pp. 558–566.
44. Eshtiaghi, N. and Hapgood, K. P. (2012) 'A quantitative framework for the formation of liquid marbles and hollow granules from hydrophobic powders', *Powder Technology*. Elsevier, 223, pp. 65–76.
45. Eshtiaghi, N., Liu, Jacques S, et al. (2009) 'Liquid marble formation: Spreading coefficients or kinetic energy?', *Powder Technology*, 196, pp. 126–132.

46. Eshtiaghi, N., Liu, J. J. S. and Hapgood, K. P. (2010) 'Formation of hollow granules from liquid marbles: Small scale experiments', *Powder Technology*. Elsevier B.V., 197(3), pp. 184–195.
47. Fandaruff, C. et al. (2015) 'Correlation between microstructure and bioequivalence in Anti-HIV Drug Efavirenz', *European Journal of Pharmaceutics and Biopharmaceutics*. Elsevier B.V., 91, pp. 52–58.
48. Farber, L., Tardos, G. and Michaels, J. N. (2003) 'Use of X-ray tomography to study the porosity and morphology of granules', 132, pp. 57–63.
49. Forny, L. et al. (2007) 'Storing water in powder form by self-assembling hydrophobic silica nanoparticles', *Powder Technology*, 171(1), pp. 15–24.
50. Forny, L. et al. (2009) 'Influence of mixing characteristics for water encapsulation by self-assembling hydrophobic silica nanoparticles', *Powder Technology*. Elsevier B.V., 189(2), pp. 263–269.
51. Gao, L. and McCarthy, T. J. (2007) 'Ionic liquid marbles', *Langmuir*, 23(21), pp. 10445–10447.
52. Gao, X., & Jiang, L. (2004) 'Water-repellent legs of water striders' *Nature*, 432(7013), 36.
53. Gmbh, R. (2014) 'The Basic Principles of Sieve Analysis', *Online Magazine for Analytic Laboratories*, pp. 1–4.
54. Hapgood, K. P. (2000). *Nucleation and Binder Dispersion in Wet Granulation*. PhD Thesis, 2-1.
55. Hapgood, K. P. et al. (2002) 'Drop penetration into porous powder beds', *Journal of Colloid and Interface Science*, 253(2), pp. 353–366.
56. Hapgood, K.P., Farber, L. and Michaels, J. N. (2009) 'Agglomeration of hydrophobic powders via solid spreading nucleation', *Powder Technology*, 188(3), pp. 248–254.
57. Hapgood, K. P. and Khanmohammadi, B. (2009) 'Granulation of hydrophobic powders', *Powder Technology*. Elsevier B.V, 189(2), pp. 253–262.
58. Hapgood, K. P., Litster, J. D. and Smith, R. (2003) 'Nucleation regime map for liquid bound granules', *AIChE Journal*, 49(2), pp. 350–361.
59. Hassanpour, A. et al. (2009) 'Effect of granulation scale-up on the strength of granules', *Powder Technology*. Elsevier B.V., 189(2), pp. 304–312.
60. Hemati, M. et al. (2003) 'Fluidized bed coating and granulation: Influence of process-related variables and physicochemical properties on the growth kinetics', *Powder Technology*, 130(1–3), pp. 18–34.
61. Hounslow, M. J., Oullion, M., & Reynolds, G. K. (2009) 'Kinetic models for granule nucleation by the immersion mechanism' *Powder Technology*, 189(2), 177–189.

62. Iveson, S. M. et al. (2001) 'Nucleation, growth and breakage phenomena in agitated wet granulation processes: a review', *Powder Technology*, 117(1–2), pp. 3–39.
63. Iveson, S. M. and Litster, J. D. (1998) 'Growth regime map for liquid-bound granules', *AIChE Journal*, 44(Compendex), pp. 1510–1518.
64. Iveson, S. M. and Litster, J. D. (1998a) 'Fundamental studies of granule consolidation. Part 2: Quantifying the effects of particle and binder properties', *Powder Technology*, 99(3), pp. 243–250.
65. Iveson, S. M. and Litster, J. D. (1998b) 'Liquid-bound granule impact deformation and coefficient of restitution', *Powder Technology*, 99(3), pp. 234–242.
66. Iveson, S. M., Litster, J. D. and Ennis, B. J. (1996) 'Fundamental studies of granule consolidation part 1: Effects of binder content and binder viscosity', *Powder Technology*, 88(1), pp. 15–20.
67. Iveson, S. M., Wauters, P. a L., et al. (2001) 'Growth regime map for liquid-bound granules: Further development and experimental validation', *Powder Technology*, 117(1–2), pp. 83–97.
68. Jiang, M.L. (2017). Chapter 2 Porosity, Pore Size Distribution,. University of Bath: Springer.
69. Johansen, A. and Schafer, T. (2000) 'Effects of interactions between powder particle size and binder viscosity on agglomerate growth mechanisms in a high shear mixer', *European Journal of Pharmaceutical Sciences*, 12(3), pp. 297–309.
70. Kataria, A., Oka, S., Smrčka, D., Grof, Z., Štěpánek, F., & Ramachandran, R. (2018) 'A quantitative analysis of drug migration during granule drying', *Chemical Engineering Research and Design*, 136, 199–206.
71. Keleb, E. I. et al. (2004) 'Twin screw granulation as a simple and efficient tool for continuous wet granulation', *International Journal of Pharmaceutics*, 273(1–2), pp. 183–194.
72. Knight, P. C. et al. (2000) 'An investigation of the effects on agglomeration of changing the speed of a mechanical mixer', *Powder Technology*, 110(3), pp. 204–209.
73. Knight, P. C. et al. (1998) 'An investigation into the kinetics of liquid distribution and growth in high shear mixer agglomeration', *Powder Technology*, 97(3), pp. 246–257.
74. Knight, P. C. (2001) 'Structuring agglomerated products for improved performance', *Powder Technology*, 119(1), pp. 14–25.
75. Knight, P. C. et al. (2001) 'Prediction of impeller torque in high shear powder mixers', *Chemical Engineering Science*, 56(15), pp. 4457–4471.
76. Korteby, Y., Kristó, K., Sovány, T., & Regdon, G. (2018) 'Use of machine learning tool to elucidate and characterize the growth mechanism of an in-situ fluid bed melt granulation' *Powder Technology*, 331, 286–295.

77. Kumar, A. et al. (2016) 'Development of a process map: A step towards a regime map for steady-state high shear wet twin screw granulation', *Powder Technology*, 300, pp. 73-82.
78. Kwok, D. Y. and Neumann, A. W. (1999) 'Contact angle measurement and contact angle interpretation', *Advances in Colloid and Interface Science*, 81(3), pp. 167-249.
79. Lackman, L., & Liebermann, H. A. (2013). *The Theory and Practice of Industrial Pharmacy*. New Delhi: CBS publishers and distributors pvt. Ltd.
80. Lazghab, M. et al. (2005) 'Wettability assessment of finely divided solids', *Powder Technology*, 157(1-3), pp. 79-91.
81. Lee, D. G., & Kim, H. Y. (2008) 'Impact of a superhydrophobic sphere onto water', *Langmuir*, 24(1), 142-145.
82. Levin, M., & Hanover, E. (2006) 'Wet granulation: End-point determination and scale-up', *Encyclopedia of Pharmaceutical Technology*, pp. 4078-4098.
83. Litster, J. D. et al. (2002) 'Scale-up of mixer granulators for effective liquid distribution', *Powder Technology*, 124(3), pp. 272-280.
84. Litster, J., Ennis, B., & Liu, L. (2004). *The Science and Engineering of Granulation Processes*. USA: Kluwer Academic Publishers.
85. Liu, L. X. et al. (2000) 'Coalescence of deformable granules in wet granulation processes', *AIChE Journal*, 46(3), pp. 529-539.
86. Mašić, I., Ilić, I., Dreu, R., Ibrić, S., Parojčić, J., & Durić, Z. (2012) 'An investigation into the effect of formulation variables and process parameters on characteristics of granules obtained by in situ fluidized hot melt granulation', *International Journal of Pharmaceutics*, 423(2), 202-212.
87. MacKaplou, M. B., Rosen, L. a. and Michaels, J. N. (2000) 'Effect of primary particle size on granule growth and endpoint determination in high-shear wet granulation', *Powder Technology*, 108(1), pp. 32-45.
88. McEleney, P. et al. (2009) 'Liquid marble formation using hydrophobic powders', *Chemical Engineering Journal*, 147(2-3), pp. 373-382.
89. McHale, G. et al. (2007) 'Electrowetting of nonwetting liquids and liquid marbles', *Langmuir*, 23(2), pp. 918-924.
90. McHale, G. et al. (2009) 'Levitation-free vibrated droplets: Resonant oscillations of liquid marbles', *Langmuir*, 25(1), pp. 529-533.
91. McHale, G. and Newton, M. I. (2011) 'Liquid marbles: principles and applications', *Journal of Soft Matter*, 7, pp. 5473-5481.
92. Mellmann, J. (2001) 'The transverse motion of solids in rotating cylinders-forms of motion and transition behavior', *Powder Technology*, 118(3), pp. 251-270.

93. Mirza, Z. et al. (2015) 'Effect of impeller design on homogeneity, size and strength of pharmaceutical granules produced by high-shear wet granulation', *Particuology*. Chinese Society of Particuology, 23, pp. 31–39.
94. Mohammad Karim, A. and Kavehpour, H. P. (2018) 'Effect of viscous force on dynamic contact angle measurement using Wilhelmy plate method', *Colloids and Surfaces A: Physicochemical and Engineering Aspects*. Elsevier, 548, pp. 54–60.
95. Morrison, A. J. et al. (2016) 'The shape and behaviour of a granular bed in a rotating drum using Eulerian flow fields obtained from PEPT', *Chemical Engineering Science*. Elsevier, 152, pp. 186–198.
96. Nguyen, T. H. (2009). *Fundamental Effects of Hydrophobic Powders on Nucleation and Wet Granulation*. MSc thesis, Monash : Monash University.
97. Nguyen, T. H. et al. (2010) 'An analysis of the thermodynamic conditions for solid powder particles spreading over liquid surface', *Powder Technology*. Elsevier B.V., 201(3), pp. 306–310.
98. Nguyen, T., Shen, W., & Hapgood, K. (2009) 'Drop penetration time in heterogeneous powder beds', *Chemical Engineering Science*, 64(24), 5210–5221.
99. Nguyen, T. H., Shen, W. and Hapgood, K. (2010) 'Effect of formulation hydrophobicity on drug distribution in wet granulation', *Chemical Engineering Journal*. Elsevier B.V., 164(2–3), pp. 330–339.
100. Nordström, J. and Alderborn, G. (2015) 'The granule porosity controls the loss of compactibility for both dry- and wet-processed cellulose granules but at different rate', *Journal of Pharmaceutical Sciences*, 104(6), pp. 2029–2039.
101. Nowak, E. et al. (2013) 'A comparison of contact angle measurement techniques applied to highly porous catalyst supports', *Powder Technology*, 233, pp. 52–64.
102. Oka, S. et al. (2015) 'A quantitative study of the effect of process parameters on key granule characteristics in a high shear wet granulation process involving a two component pharmaceutical blend', *Advanced Powder Technology*, 26(1), pp. 315–322.
103. Oka, S., Emady, H., Kašpar, O., Tokárová, V., Muzzio, F., Štěpánek, F., & Ramachandran, R. (2015) 'The effects of improper mixing and preferential wetting of active and excipient ingredients on content uniformity in high shear wet granulation', *Powder Technology*, 278, 266–277.
104. Öner, D. and McCarthy, T. J. (2000) 'Ultrahydrophobic surfaces. Effects of topography length scales on wettability', *Langmuir*, 16(20), pp. 7777–7782.
105. Oostveen, M. L. M., Meesters, G. M. H. and van Ommen, J. R. (2015) 'Quantification of powder wetting by drop penetration time', *Powder Technology*. Elsevier B.V., 274, pp. 62–66.
106. Ojile, J. E., Macfarlane, C. B., & Selkirk, A. B. (1982) 'Drug distribution during massing and its effect on dose uniformity in granules', *International Journal of Pharmaceutics*, 10(2), 99–107.

107. Parker, D. J., Dijkstra, A. E., Martin, T. W., & Seville, J. P. K. (1997) 'Positron emission particle tracking studies of spherical particle motion in rotating drums', *Chemical Engineering Science*, 52(13), 2011–2022.
108. Patil, H. et al. (2015) 'Formulation and development of pH-independent/dependent sustained release matrix tablets of ondansetron HCl by a continuous twin-screw melt granulation process', *International Journal of Pharmaceutics*. Elsevier B.V., 496(1), pp. 33-41.
109. Pawar Jaywant, N. and Amin Purnima, D. (2016) 'Development of efavirenz cocrystals from stoichiometric solutions by spray drying technology', *Materials Today: Proceedings*. Elsevier Ltd, 3(6), pp. 1742–1751
110. Peña, R., Burcham, C. L., Jarmer, D. J., Ramkrishna, D., & Nagy, Z. K. (2017) 'Modeling and optimization of spherical agglomeration in suspension through a coupled population balance model', *Chemical Engineering Science*, 167, 66–77.
111. Pepin, X., Blanchon, S. and Couarraze, G. (1997) 'A new approach for determination of powder wettability', *International Journal of Pharmaceutics*, 152(1), pp. 1–5.
112. Perfetti, G. et al. (2010) 'X-ray micro tomography and image analysis as complementary methods for morphological characterization and coating thickness measurement of coated particles', *Advanced Powder Technology*. The Society of Powder Technology Japan, 21(6), pp. 663–675.
113. Pimparade, M. B. et al. (2015) 'Development of taste masked caffeine citrate formulations utilizing hot melt extrusion technology and in vitro–in vivo evaluations', *International Journal of Pharmaceutics*, 487(1–2), pp. 167–176.
114. Pitt, K., Smith, R. M., de Koster, S. A. L., Litster, J. D., & Hounslow, M. J. (2018) 'Kinetics of immersion nucleation driven by surface tension', *Powder Technology*, 335, 62–69.
115. Planinsek, O. et al. (2000) 'The utilization of surface free-energy parameters for the selection of a suitable binder in fluidized bed granulation', *International Journal of Pharmaceutics*, 207(1–2), pp. 77–88.
116. Pohlman, D. a and Litster, J. D. (2015) 'Coalescence model for induction growth behaviour in high shear granulation', *Powder Technology*. Elsevier B.V., 270, pp. 435–444.
117. Puri, V. et al. (2010) 'Wettability and surface chemistry of crystalline and amorphous forms of a poorly water soluble drug', *European Journal of Pharmaceutical Sciences*. Elsevier B.V., 40(2), pp. 84–93.
118. Rahmanian, N., Naji, A. and Ghadiri, M. (2011) 'Effects of process parameters on granules properties produced in a high shear granulator', *Chemical Engineering Research and Design*, 89(5), pp. 512–518.
119. Raj Kumar, S. M. and Malayalamurthi, R. (2017) 'Agglomeration and sizing of rolling particles in the sago sizing mechanism', *Powder Technology*. Elsevier B.V., 320, pp. 428–444.

120. Realpe, A. and Velázquez, C. (2008) 'Growth kinetics and mechanism of wet granulation in a laboratory-scale high shear mixer: Effect of initial polydispersity of particle size', *Chemical Engineering Science*, 63(6), pp. 1602–1611.
121. Rhodes, M. (1998). *Introduction to Particle Technology*. John Wiley & Sons.
122. Rodrigues, R. F. et al. (2017) 'Drum granulation of single super phosphate fertilizer: Effect of process variables and optimization', *Powder Technology*. Elsevier B.V., 321, pp. 251–258.
123. Ryzak, M. and Bieganowski, A. (2011) 'Methodological aspects of determining soil particle-size distribution using the laser diffraction method', *Journal of Plant Nutrition and Soil Science*, 174(4), pp. 624–633.
124. Rumpf H. (1962), 'The strength of granules and agglomerates', W.A Knepper (Ed.), *Agglomeration*, Wiley, New York, pp. 379-418.
125. Saleh, K. et al. (2011) 'Dry water: From physico-chemical aspects to process-related parameters', *Chemical Engineering Research and Design*, 89(5), pp. 537–544.
126. Saleh, K. and Guigon, P. (2007) 'Influence of wetting parameters on particle growth in fluidized-bed coating and agglomeration processes', *Particle and Particle Systems Characterization*, 24(2), pp. 136–143.
127. Saleh, K., Vialatte, L. and Guigon, P. (2005) 'Wet granulation in a batch high shear mixer', *Chemical Engineering Science*, 60(14), pp. 3763–3775.
128. Schæfer, T. (2001) 'Growth mechanisms in melt agglomeration in high shear mixers', *Powder Technology*, 117(1–2), pp. 68–82.
129. Schæfer, T. et al. (1993a) 'Melt pelletization in a high shear mixer. IV. Effects of process variables in a laboratory scale mixer', *European Journal of Pharmaceutical Sciences*, 1(3), pp. 125–131.
130. Schæfer, T. et al. (1993b) 'Melt pelletization in a high shear mixer. V. Effects of apparatus variables', *European Journal of Pharmaceutical Sciences*, 1(3), pp. 133–141.
131. Schæfer, T. (1996) 'Melt pelletization in a high shear mixer. X. Agglomeration of binary mixtures', *International Journal of Pharmaceutics*, 139(1–2), pp. 149–159.
132. Schæfer, T. and Mathiesen, C. (1996a) 'Melt pelletization in a high shear mixer. IX. Effects of binder particle size', *International Journal of Pharmaceutics*, 139(1–2), pp. 139–148.
133. Schæfer, T. and Mathiesen, C. (1996a) 'Melt pelletization in a high shear mixer. VII. Effects of product temperature', *International Journal of Pharmaceutics*, 134(1–2), pp. 105–117.
134. Schæfer, T. and Mathiesen, C. (1996b) 'Melt pelletization in a high shear mixer. VIII. Effects of binder viscosity', *International Journal of Pharmaceutics*, 139(1–2), pp. 125–138.

135. Schuster, J. M., Schvezov, C. E. and Rosenberger, M. R. (2015) 'Influence of Experimental Variables on the Measure of Contact Angle in Metals Using the Sessile Drop Method', *Procedia Materials Science*. Elsevier B.V., 8(2009), pp. 742–751.
136. Seem, T. C. et al. (2015) 'Twin Screw Granulation – A Literature Review', *Powder Technology*. Elsevier B.V., 276, pp. 89–102.
137. Shang, J. et al. (2008) 'Comparison of different methods to measure contact angles of soil colloids', *Journal of Colloid and Interface Science*. Elsevier Inc., 328(2), pp. 299–307.
138. Shi, S. Q. and Gardner, D. J. (2000) 'A new model to determine contact angles on swelling polymer particles by the column wicking method', *Adhesion Science and Technology*, 14(2), pp. 301–314.
139. Simone, V. De, Caccavo, D., Lamberti, G., D'Amore, M., & Barba, A. A. (2018) 'Wet-granulation process: phenomenological analysis and process parameters optimization', *Powder Technology*, 340, pp. 411-419.
140. Smith, R. M., Liu, L. X. and Litster, J. D. (2010) 'Breakage of drop nucleated granules in a breakage only high shear mixer', *Chemical Engineering Science*. Elsevier, 65(21), pp. 5651–5657.
141. Sondej, F. et al. (2015) 'Investigation of coating layer morphology by micro-computed X-ray tomography', *Powder Technology*. Elsevier B.V., 273, pp. 165–175.
142. Snoeijer, J. H. and Andreotti, B. (2008) 'A microscopic view on contact angle selection', *Physics of Fluids*, 20(5), pp. 1–11.
143. Tan, M. X. L., Wong, L. S., Lum, K. H., & Hapgood, K. P. (2009) 'Foam and drop penetration kinetics into loosely packed powder beds', *Chemical Engineering Science*, 64(12), 2826–2836.
144. Timmons, C. . and Zisman, W. . (1966) 'The effect of liquid structure on contact angle hysteresis', *Journal of Colloid and Interface Science*, 22(2), pp. 165–171.
145. Tu, W. (2009) 'Regime map development for co-rotating twin screw granulation', MSc. thesis, University of Brimigham.
146. Tu, W. Da et al. (2009) 'Exploring the regime map for high-shear mixer granulation', *Chemical Engineering Journal*, 145(3), pp. 505–513.
147. Tu, W. Da, Ingram, A. and Seville, J. (2013) 'Regime map development for continuous twin screw granulation', *Chemical Engineering Science*. Elsevier, 87, pp. 315–326.
148. Torkkeli, A. (2003) 'Droplet microfluidics on a planar surface', *VTT Publications*, 55(504), pp. 3–194.
149. Van Den Dries, K. et al. (2003) 'Granule breakage phenomena in a high shear mixer; influence of process and formulation variables and consequences on granule homogeneity', *Powder Technology*, 133(1–3), pp. 228–236.

150. Vella, D., Metcalfe, P. D., & Whittaker, R. J. (2006) 'Equilibrium conditions for the floating of multiple interfacial objects', *Journal of Fluid Mechanics*, 549, 215–224.
151. Verstraeten, M. et al. (2017) 'In-depth experimental analysis of pharmaceutical twin-screw wet granulation in view of detailed process understanding', *International Journal of Pharmaceutics*. Elsevier B.V., 529(1–2), pp. 678–693.
152. Wade, J. B., Martin, G. P. and Long, D. F. (2014) 'Feasibility assessment for a novel reverse-phase wet granulation process: The effect of liquid saturation and binder liquid viscosity', *International Journal of Pharmaceutics*. Elsevier B.V., 475(1), pp. 450–461.
153. Wade, J. B., Martin, G. P. and Long, D. F. (2015) 'An assessment of powder pycnometry as a means of determining granule porosity', *Pharmaceutical Development and Technology*, 20(3), pp. 257–265.
154. Wade, J. B., Martin, G. P. and Long, D. F. (2015) 'Controlling granule size through breakage in a novel reverse-phase wet granulation process; The effect of impeller speed and binder liquid viscosity', *International Journal of Pharmaceutics*. Elsevier B.V., 478(2), pp. 439–446.
155. Walker, G. M. et al. (2000) 'Drum granulation of NPK fertilizers', *Powder Technology*, 107(3), pp. 282–288.
156. Wang, S. et al. (2008) 'Investigation of high shear wet granulation processes using different parameters and formulations', *Chemical & pharmaceutical bulletin*, 56(1), pp. 22–27.
157. Wang, A., Song, Q., & Yao, Q. (2015) 'Behavior of hydrophobic micron particles impacting on dropletsurface', *Atmospheric Environment*, 115, pp. 1–8.
158. Warren, J. W., & Price, J. C. (1977) 'Drug migration during drying of tablet granulations II: Effect of binder solution viscosity and drying temperature', *Journal of Pharmaceutical Sciences*, 66(10), 1409–1412.
159. Weatherley, S. et al. (2013) 'Hot-melt granulation in a twin screw extruder: Effects of processing on formulations with caffeine and ibuprofen', *Journal of Pharmaceutical Sciences*, 102(12), pp. 4330–4336.
160. Wenzel, R. N. (1936) 'Resistance of solid surfaces to wetting by water.', *Journal of Industrial and Engineering Chemistry (Washington, D. C.)*, 28, pp. 988–994.
161. Whitby, Catherine P., Bian, X. and Sedev, R. (2013) 'Rolling, penetration and evaporation of alcohol-water drops on coarse and fine hydrophobic powders', *Colloids and Surfaces A: Physicochemical and Engineering Aspects*. Elsevier B.V., 436, pp. 639–649.
162. Yu, S. et al. (2014) 'Granulation of increasingly hydrophobic formulations using a twin screw granulator.', *International journal of pharmaceutics*. Elsevier B.V., 475(1–2), pp.
163. Yuan Y., Lee T.R. (2013) Contact Angle and Wetting Properties. In: Bracco G., Holst B. (eds) *Surface Science Techniques*. Springer Series in Surface Sciences, vol 51. Springer, Berlin, Heidelberg.

164. Zeitler, J. A. and Gladden, L. F. (2009) 'In-vitro tomography and non-destructive imaging at depth of pharmaceutical solid dosage forms', *European Journal of Pharmaceutics and Biopharmaceutics*. Elsevier B.V., 71(1), pp. 2–22.
165. Zhang, D. et al. (2002) 'Wettability of pharmaceutical solids: Its measurement and influence on wet granulation', *Colloids and Surfaces A: Physicochemical and Engineering Aspects*, 206(1–3), pp. 547–554.
166. Zhenyu, S. et al. (2015) 'Prediction of contact angle for hydrophobic surface fabricated with micro-machining based on minimum Gibbs free energy', *Applied Surface Science*. Elsevier B.V., 364, pp. 597-603.

